ISSN 0386-5878
Technical Memorandum
of PWRI No.3481

PROCEEDINGS OF THE THIRD U.S.-JAPAN WORKSHOP ON SEISMIC RETROFIT OF BRIDGES

by

**Shigeki Unjoh, Toru Terayama,
Yukio Adachi, Jun-ichi Hoshikuma,
Kazuhiro Nagaya, Michio Ohsumi and Takashi Sato**

Synopsis:

The proceedings document the results of the third U.S.-Japan Workshop on Seismic Retrofit of Bridges which was held at Osaka, Japan, on December 10 and 11, 1996, under the auspices of the Panel on Wind and Seismic Effects, UJNR. The Workshop was organized by Task Committee J "Wind and Earthquake Engineering for Transportation Systems" (U.S. side chairman: Mr. J. D. Cooper, FHWA, Japan side chairman: Mr. Y. Fujishiro, PWRI) of the Panel.

Key words: Bridge Seismic Retrofit, Evaluation of Existing Bridges, Retrofit Method, Reinforced Concrete Column, Steel Column, Foundation, Loading History, UJNR

FOREWARD

The proceedings include the results of the Third U.S.-Japan Workshop on Seismic Retrofit of Bridges which was held at Osaka, Japan, on December 10 and 11, 1996 under the auspices of the UJNR Panel on Wind and Seismic Effects. The workshop was organized by the Task Committee J "Wind and Earthquake Engineering for Transportation Systems" (Japan-side chair : Mr. Yasuyuki Fujishiro, Director of Structure and Bridge Department, Public Works Research Institute, U.S.-side chair : Mr. James D. Cooper, Chief of Structures Division, Turner-Fairbank Highway Research Center, Federal Highway Administration) of the Panel. The workshop was jointly coordinated by Dr. Shigeki Unjoh, Head of Earthquake Engineering Division of the Public Works Research Institute (PWRI) and Dr. Ian G. Buckle, Deputy Director of the National Center for Earthquake Engineering Research (NCEER). The staff of the Earthquake Engineering Division of PWRI, consisting of Messrs. Toru Terayama, Yukio Adachi, Jun-ichi Hoshikuma, Kazuhiro Nagaya, Michio Ohsumi and Takashi Sato arranged the workshop on behalf of the Japan side. The U.S.-side steering committee for this workshop, consisting of Dr. Ian G. Buckle and Mr. Ian M. Friedland of NCEER, Dr. Frieder Seible of University of California, San Diego and Dr. Gregory L. Fenves of University of California, Berkeley, organized the workshop on behalf of the U.S.-side. The U.S.-side financial support was provided by the National Science Foundation and the Federal Highway Administration.

The aims of the workshop were: (1) to bring together experts from both countries to exchange technical information on current research and practical efforts being made in the area of seismic retrofit of bridges, and (2) to identify future needs and opportunities between the two countries for cooperative research.

A broad range of technical topics were presented at the workshop. These included:

- Damage to Bridges in the Hyogo-ken-Nanbu Earthquake
- Assessment and Prioritization of Vulnerable Bridges
- Inspection and Strengthening Methods for Reinforced Concrete Bridge Piers
- Research on Seismic Retrofit and Strengthening of Reinforced Concrete Bridge Piers
- Research on Seismic Retrofit of Steel Piers, Restrainers, Bearings, and Foundations
- Effects of Loading History

The workshop was attended by 20 U.S. and 66 Japanese participants. In total, 26 papers were presented ; 15 papers from Japan, 11 papers from the United States. The material in the proceedings includes (1) all technical papers in the order in which they were presented during the workshop, (2) resolutions that were unanimously approved by the participants

during the closing session of the workshop, and (3) the workshop program and the list of participants.

A special session was prepared by the agreement between the coordinators of both countries. The topic of the special session was "Effects of Loading History", which is considered to be a major issue to be studied and examined in the future.

We wish to express our profound gratitude and sincere appreciation to all participants in the workshop for supporting the workshop by active presentations and discussion. In particular, we would like to thank Dr. K. Kawashima, Dr. H. Otsuka, Dr. I. G. Buckle and Dr. H.S. Lew for leading the discussions.

Grateful thanks are also extended to the Japan side members. Special appreciation also goes to the Kinki Construction Bureau of the Ministry of Construction, Hanshin Expressway Public Corporation, Metropolitan Expressway Public Corporation, Trans-Tokyo Bay Highway Corporation, Bridgestone Corporation for the generous cooperation in the workshop and during the study-tour. We also would like to thank the assisting staff members, Messrs. M. Takahashi, K. Murai and K. Tasaki of PWRI, for the smooth progress of the schedule.

Shigeki UNJOH,
Toru TERAYAMA,
Yukio ADACHI,
Jun-ichi
HOSHIKUMA,
Kazuhiro NAGAYA,
Michio OHSUMI, and
Takashi SATO
Earthquake Engineering Division
Earthquake Disaster Prevention Research Center
Public Works Research Institute

February, 1997





保 存 用

TABLE OF CONTENTS

PAPERS

Session 1: State of the Art

(Co-Chairs: S. Unjoh, M. Shinozuka)

"Damage to Highway Bridges by the 1995 Hyogoken Nanbu Earthquake and the Retrofit of Highway Bridges in Japan" 3
by H. Otsuka, T. Terayama, J. Hoshikuma, K. Kosa
Presented by: Hisanori Otsuka

"Innovative Seismic Retrofit of California Highway Structures" 17
by S. El-Azazy
Presented by: Saad El-Azazy

Session 2: Screening and Prioritization of Bridges for Retrofitting

(Co-Chairs: H. Mutsuyoshi, J. Mander)

"Seismic Retrofitting Manuals for Highway Systems: System Assessment, Screening, Evaluation, and Retrofitting" 35
by I. Buckle, I. Friedland
Presented by: Ian Friedland

"Use of Transportation Network Systems for Bridge Retrofit Prioritization and Emergency Response" 51
by A. Kiremidjian, N. Basöz
Presented by: Anne Kiremidjian

Session 3: Evaluation of Existing Bridges

(Co-Chairs: J. Hoshikuma, N. Makris)

"Analytical Methods for the Seismic Evaluation of Existing Bridges" 67
by R. Imbsen, F. Nobari
Presented by: Roy Imbsen

"Seismic Evaluation and Retrofit of Existing Multi-column Bents" 87
by T. Terayama, H. Otsuka
Presented by: Toru Terayama

"Queensboro Bridge: Seismic Condition Assessment and Retrofit of a Landmark Bridge" 103
by S. Arzoumanidis, R. Gajer, A. Malik
Presented by: Serafim Arzoumanidis

Session 4: Retrofit Methods for RC Columns 1

(Co-Chairs: Y. Kimura, R. Imbsen)

"Seismic Retrofit of Square RC Columns by Steel Jacketing" 125
by J. Hoshikuma, H. Otsuka, K. Nagaya
Presented by: Jun-ichi Hoshikuma

"An Experimental Study on Seismic Retrofit of Reinforced Concrete Bridge Piers" . 141
by H. Ikeda, N. Wada, K. Osada, Y. Igase, Y. Tamura
Presented by: Yoshinori Igase

"Retrofits of Reinforced Concrete Bridge Columns with Prestressing Steel Ties" 159
by T. Yoshioka
Presented by: Tamio Yoshioka

Session 5: Retrofit Methods for RC Columns 2
(Co-Chairs: Y. Adachi, P. Clark)

"Development of Base Isolation System of Existing Bridges" 175
by Y. Hishiki, T. Takeda, H. Nagumo, T. Ichinomiya, Y. Okimi
Presented by: Hiroyuki Nagumo

"An Experimental Study on Ductility of RC Pier Models Winded with FRP Tape" .. 189
by H. Mikami, M. Sato, H. Konno, N. Kishi
Presented by: Hiroshi Mikami

"Seismic Retrofit of Bridge Columns using Prefabricated Composite Jackets" 201
by Y. Xiao
Presented by: Yan Xiao

"Seismic Retrofit of Reinforced Concrete Bridge Piers by Carbon Fiber Sheet" 217
by M. Hosotani, K. Kawashima, J. Hoshikuma
Presented by: Manabu Hosotani

"Experimental Study Concerning Retrofit of RC Column by CFRP Sheet" 243
by F. Hakamada, Y. Maekawa, J. Hoshikuma
Presented by: Fumio Hakamada

Session 6: Retrofit Methods for Steel Columns, Superstructure and Restrainers
(Co-Chairs: K. Tamura, Y. Xiao)

"Cyclic Behavior of Shear Links in Retrofitted Richmond-San Rafael Bridge Towers" 261
by A. Itani
Presented by: Ahmad Itani

"An Experimental Study on Seismic Retrofit of Steel Bridge Piers" 269
by K. Nishikawa, J. Murakoshi, Y. Josen, M. Takahashi
Presented by: Jun Murakoshi

"Intermediate Hinge Restrainers for Bridges: Performance, Design, and Retrofit" 289
by R. DesRoches, G. Fenves

Presented by: Gregory Fenves

"Seismic Vulnerability Analysis of Steel Bridge Bearings" 309

by J. Mander, D-K Kim, I. Buckle

Presented by: John Mander

Session 7: Retrofit Methods for Foundations and Geotechnical Considerations

(Co-Chairs: J. Murakoshi, K. Almand)

"Inspection and Restoration of Damaged Foundations due to the Great Hanshin Earthquake 1995" 327

by H. Ishizaki, A. Nanjo, J. Kawakami, N. Egawa, Y. Adachi

Presented by: Yukio Adachi

"Seismic Design of Pile Foundations" 343

by M. Nakano, Y. Kimura

Presented by: Yoshitomi Kimura

"Site Remediation and Seismic Response Mechanisms" 357

by K.Adalier, A. Elgamal

Presented by: Ahmed Elgamal

"Seismic Design Treatment of Liquefaction-Induced Ground Flow" 371

by K. Tamura, T. Hamada, T. Azuma

Presented by: Kei-ichi Tamura

"A Study on Measures against Ground Flow Using The Finite Element Method" 383

by M. Ogasawara, H. Tsunoda, T. Makita, S. Gose

Presented by: Hiroshi Tsunoda

Special Session: Effects of Loading History

(Co-Chairs: K. Kawashima, A. Whittaker)

"Effect of Loading Hysteresis on Ductility of Reinforced Concrete Columns" 401

by J. Hoshikuma, S. Unjoh, K. Nagaya

Presented by: Jun-ichi Hoshikuma

"Testing Methodologies for the Seismic Performance of Reinforced Concrete Bridge Piers" 413

by A. Taylor

Presented by: Andrew Taylor

RESOLUTIONS 427

(Co-Chairs: S. Unjoh, H. S. Lew)

APPENDICES

WORKSHOP PROGRAMS 431

PARTICIPANTS 439

Session 1

State of the Art

(Co-Chairs: S. Unjoh, M. Shinozuka)

"Damage to Highway Bridges by the 1995 Hyogokén Nanbu Earthquake And the Retrofit of Highway Bridges in Japan"
by H. Otsuka, T. Terayama, J. Hoshikuma, K. Kosa
Presented by: Hisanori Otsuka

"Innovative Seismic Retrofit of California Highway Structures"
by S. El-Azazy
Presented by: Saad El-Azazy

DAMAGE TO HIGHWAY BRIDGES BY THE 1995 HYOGOKEN NANBU EARTHQUAKE AND THE RETROFIT OF HIGHWAY BRIDGES IN JAPAN

Hisanori OTSUKA
Professor of Civil Engineering, Kyushu University
(Former Head of Eartquake Eng. Division, PWRI)
Toru TERAYAMA and Jun-ichi Hoshikuma
Senior Researcher and Researcher,
Earthquake Eng. Division, Eartquake Disaster Prevention Research Center, PWRI
Kenji KOSA
Senior Engineer, Kobe Route Reconstruction Division,
Hanshin Expressway Public Corporation

Abstract

This paper describes the nature of the ground motion induced by the 1995 Hyogoken Nanbu Earthquake, the features of the damage of highway bridges, lessons learned from this earthquake, and the basic policy and design concept of seismic retrofit of the highway bridges. Furthermore design example for seismic retrofit and performance of strengthened model piers are described.

1. Introduction

The Hyogoken Nanbu Earthquake occurred at 5:46 a.m. on January 17, 1995. Its hypocenter was close to the northern tip of Awaji Island located in south of Hyogo Prefecture. The Japan Meteorological Agency (JMA) announced that the depth of the hypocenter was 14km and that its magnitude was 7.2 on the Richter Scale.

This earthquake is not extremely large when compared with past large earthquakes in Japan, as long as they are compared in terms of magnitude. However, because this earthquake had its epicenter closer to an urbanized and densely populated area than three recent earthquakes occurred in near Hokkaido, it caused, besides loss in human life, severe damage on numerous structures and a massive financial loss. In this earthquake, 5,502 people lost their lives, 2 people are still missing, 41,648 people were injured. 101,233 residential houses were totally destroyed, and 107,269 were partially destroyed. The maximum number of refugee reached more than 316,000 at peak time, and 48,000 refugee are still staying at the temporarily builted houses on April 23, 1995.

Economical loss to all facilities has reached approximately 9.9 thousands billion yen. Major part of economic loss is buildings, and it reaches 5.8 thousands billion yen. The economic loss of highways amounts 550 billion yen (1 billion yen = 9.5 million USD).

2 Damage to Highway Bridges due to the 1995 Hyogoken Nanbu Earthquake

2-1 The nature of the earthquake and Observation Records

Aftershocks lie along some active faults located in Awaji island and Hanshin area as shown in Fig. 1. The active faults in the disaster region are dominated by Rokko Fault System running south-west to north-east from the hypocenter region of Awaji Island to Kobe. The principal part of the earthquake fault which appeared on Awaji Island was revealed at the

location of the existing Nojima Active Fault. The hills of Awaji Island rose along the existing Nojima Active Fault, while the sea coast side of the fault has settled. The Nojima Active Fault includes right lateral components. The Rokko Fault System on the Kobe side on the other hand, under the south-east foothills of the Rokko Range, is a dip-slip fault (Rokko mountains rise relatively) and includes right lateral components.

Many acceleration records were obtained in the most seriously damaged area, by the JMA, the Ministry of Construction, and other several organizations. Fig. 2 shows the distribution of the maximum acceleration observed by these organizations. At six different recording sites, the maximum horizontal accelerationexceeding 600gal(cm/s ^{2}) was recorded.

At the JMA Kobe station in particular, extremely strong ground motion was recorded and its maximum acceleration reached 818gal in the north-south compo- nent as shown in Fig. 3. The response acceleration spectra obtained by assuming a damping ratio of 5% reached 2G for the natural period between 0.4 second and 1 second as shown in Fig. 4, indicating that the ground motion contained large components over an extremely broad frequency range. Furthermore, the maximum velocity and maximum displacement of the earthquake motion recorded at the JMA Kobe station were 90cm/sec and 21cm, respectively. These are extremely high values compared to records obtained by other earthquake.

As the natural period of a structure is generally prolonged when it is damaged, earthquake motion with a large response spectrum in the long natural period range has a significant effect on the behavior of the structure. Such characteristics of the ground motion, as described above, therefore, may be partially the reason for the severe damage by the 1995 Hyogo-ken Nanbu Earthquake.

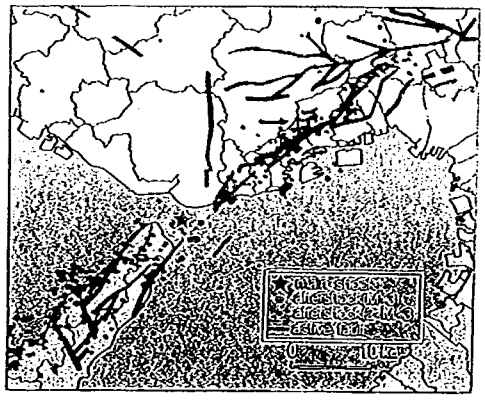


Fig.1 Main Shock and Aftershocks

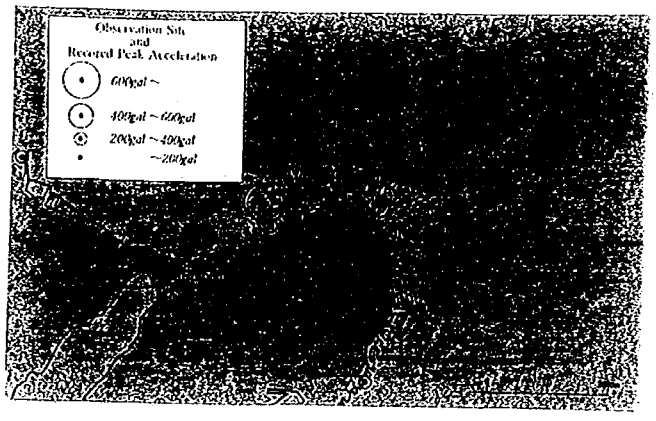


Fig.2 Distribution of Peak Ground Acceleration

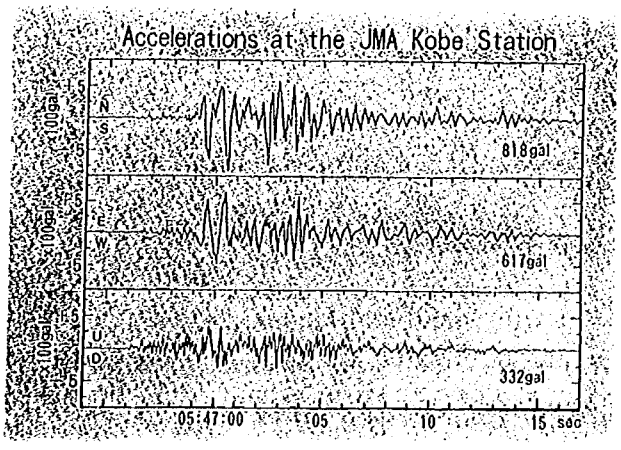


Fig. 3 Accelerations at the JMA Kobe

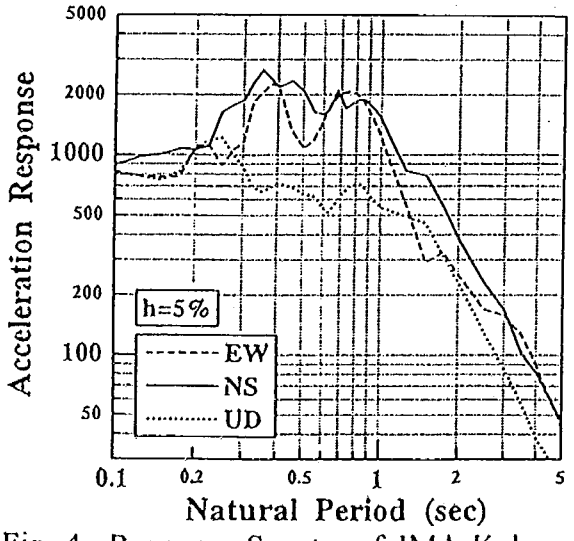


Fig. 4 Response Spectra of JMA Kobe

2-2 Classification of Damage to Highway Bridges

Fig. 5 shows the locations of severely damaged highway bridges. The earthquake caused damage to elevated highway bridges on National Highway Route(NHR) 2, 43, and 171, the Meishin Expressway(JHM), Chugoku Expressway(JHC), and the Route 3 Kobe Highway and Route 5 Harbor Highway of the Hanshin Expressway (HER3 and HER5). Inspected region contains seven cities located on this map. Road bridges located in these region are accumulated to classify the extent of their damages

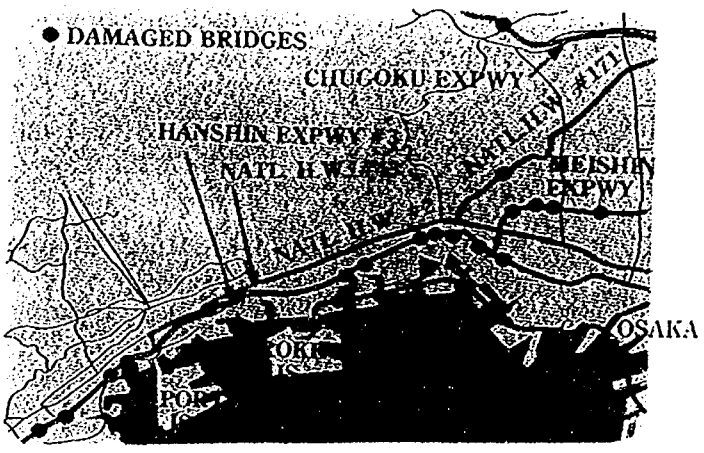


Fig. 5 Locations of Severely Damaged Bridges

Damage are classified from class As to class D for piers and superstructures, and from A to D for bearing supports. Class As is categolized for falling off or collapse, A is major damage, B is moderate damage, C is minor damage and D is very slight or no damage. Table 1 shows the definition of class B.

46 spans in 9 different places fell down by this earthquake, but the percentage of this number for the total number of spans is about 1%. The percentage of spans of superstructures judged to be class B or higher than is about 19%.

The number of steel piers and reinforced concrete(RC) piers inspected are 355 and 3041, respectively. Among them, the percentages of the piers judged to be class B or higher are about 14% for steel piers and 13% for RC piers.

Table 1 Definition of Class B

Component	Definition
Steel Pier	local buckling or deformation occurred partially
RC Pier	fracture or buckling of reinforcement occurred partially crack and falling out of concrete occurred partially
Steel girder	deformation of lower flange or local buckling of web
Concrete girder	large crack or falling out of concrete
Supports	fracture of pin or stopper, slipping out of roller, pulling out of anchor bolt

Single column-type of pier had severe damage regardless the used materials. Piers damaged to be class B and higher are about 28% among the total number of the single column-type of piers in HER3.

The percentage of metal bearing supports lines judged to be class B or higher is about 34%. In those supporting lines, pin support for fix condition and roller support for movable condition show the highest percentage in class A, respectively. The number of damaged rubber bearings were very small, i.e. 0% for class A and 2% for class B, therefore the rubber bearing seems to have good performance for seismic effects.

According to the survey to clarify which edition of specifications for highway bridges were used to design the piers, a very large proportion of about 81% among total number of piers were designed by the 1964 edition or before, and only 9%, 9% and 2% are designed by the 1971, 1980 and 1990 editions, respectively. All piers designed by 1980 edition are

the 1971, 1980 and 1990 editions, respectively. All piers designed by 1980 edition are located in HER5 only. In the 1980 edition of the specification, the anchoring of reinforcement in axial direction of the pier was extended to the cross section where tensile stress of the reinforcement is equal or less than one second of allowable stress. Among piers designed by the 1971 edition or before, about 15% piers were judged to be class B or higher, on the other hand among piers designed by 1980 edition or after, about only 4% piers were judged to be class B or higher.

Table 2 Percentage of Damaged Components Ranked Higher than Class B

Component	Percentage(Higher than B)
Superstructure	19%
Pier	14% (Steel), 13% (RC)
Bearing Support	34% (Metal), 2% (Rubber)

Table 3 Number of Piers Designed by Different Specifications

Routes	Edition of Specifications			
	1964 or before	1971	1980	1990
National Highways	366	74	5	
Hanshin Expressway Route 3	890	216		
Route 5			289	56
Meishin & Chugoku Expressway	1500			
Total	2756(81%)	290(9%)	294(9%)	56(2%)

2-3 Features of Damage

(1) Reinforced Concrete Piers

Collapse of seventeen RC piers sustaining rigidly RC decks occurred continuously along 18 spans in HER3 as shown Fig. 6. The most of piers fractured at the base of the columns, where the reinforcement bar cut off. One pier was broken into three parts, because the failure of RC pier occurred at the location of the bar cut-off in the pier. Fig. 7 shows the middle part of broken pier and fallen superstructure.

Shear failure of RC pier with large rectangular cross section occurred in HER3 are shown in Fig.8. The amount of the vertical reinforcements and hoop tie in the pier with large cross sections are rather small.

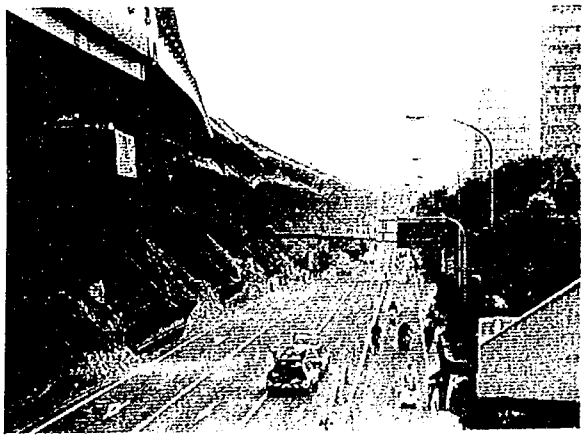


Fig.6 Collapsed 17 RC Piers

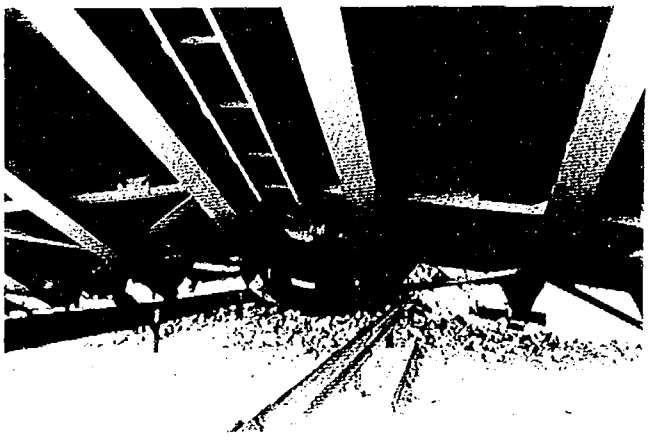


Fig.7 RC Piers broken into 3 parts



Fig.8 Shear Failured RC Pier

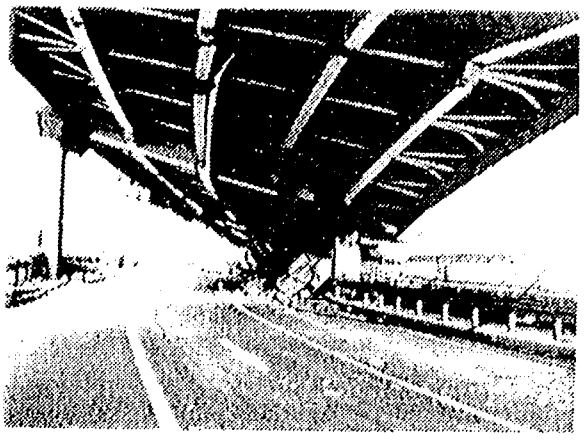


Fig.9 Failured Independent Single Pier

The RC pier which sustain independently the cross beams of the superstructure failured in HER3 as shown in Fig 9. Steel bearings were used on the top of the pier.

Failure of RC wall-type pier sustaining five-span continuous RC hollow slab occurred in JHM as shown in Fig. 10. This type of pier in JHM, which were constructed according to the bridge specification enacted in 1964 or before, has no horizontal shear reinforcement (hoop tie) except the assemble reinforcement in the wall type pier.

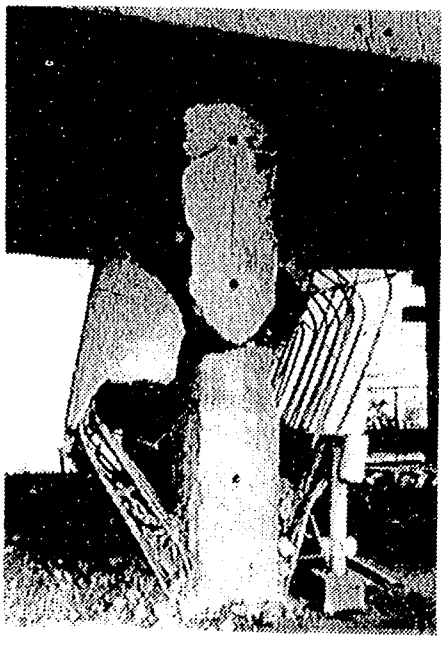


Fig.10 Shear Failured Wall Type Pier

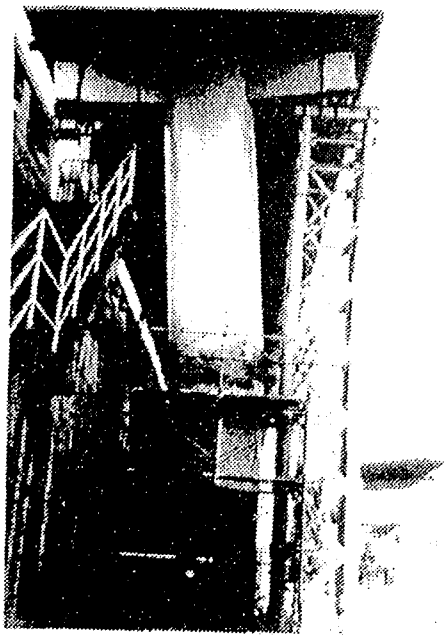


Fig.11 Buckled Circular Steel Pier

(2) Steel Piers

Buckling of circular columns occurred in HER3 as shown in Fig.11. The residual displacement is remarkable in this pier.

Steel piers with rectangular cross section which were rigidly connected to horizontal box girder collapsed in HER3. This pier sustained the very wide superstructure. Four stiffened plates composing rectangular cross section of the pier failured from the corner in the vicinity of weld lines after the local buckling of the stiffened plates at the bottom of the column. Figs. 12 and 13 shows the collapse steel piers. Fig. 14 shows a typical local buckling in the midheight of rectangular pier. Many stiffened plates in piers with rectangular cross sections buckled and an out-of plane deformation occurred in the midheight of the pier.

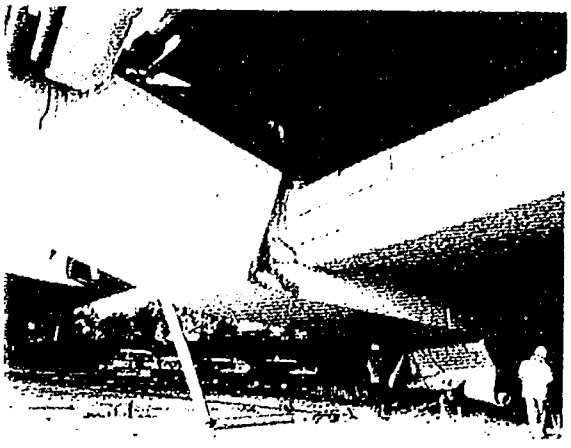


Fig.12 Collapse of Rectangular Steel Pier



Fig.13 Zoomed View of Collapsed Pier



Fig.14 Local Buckling of Rectangular Steel Pier

(3) Superstructures

One simple-span box girder fell off from the steel pier sustaining the bearing supports of box girder and adjacent long span arch bridge in HER5 as shown in Fig. 15. The evidence of liquefaction and lateral spreading of soils near revetment works occurring at the site of this pier is clearly shown in this figure.

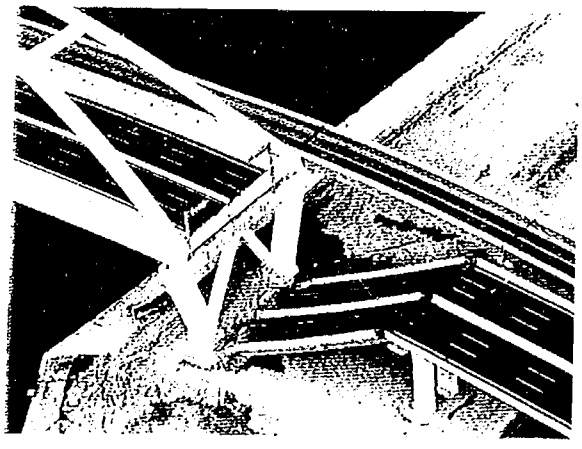


Fig.15 Fell down Simple-span Box Girder



Fig.16 Two Fell down Box Girders

Two adjacent simple-span box girders fell down from RC single column type pier in HER3 as shown in Fig. 16. Including two unseated spans, four simple-span girders were

seated on RC piers, and these four simple girders were put between three-span continuous girder and five-span gerber girder. Substantial horizontal movement also appeared in the girders adjacent to the fallen girders. Failure of the falling prevention devices connecting the girders allowed the falling down of the girders.

Simple span box girder skew bridge dropped off from both abutments to the railway in NHR171 as shown in Fig. 17. Three-span continuous hollow slab skew bridge also fell down because of the unseating of side span in JHM. Simple-span curved and skew bridges, after the fracture of bearing supports and restriction of displacement by abutment or adjecent bridges, tend to rotate by the ground vibration and fall down from outer girder in curved bridges and the corner with acute angle in skew bridges.

Lateral offset of superstructure occurred between the upper deck with a three-span and a two-span continuous steel box girders in NHR2. Superstructures were sustained by steel bearing supports set on the frame type substructure. Fig. 18 shows the transverse movements in the upper deck, and the relative displacement reached to 3.5m.

Although displacement of girders in transverse direction caused severe damages to bridges, falling down of superstructure was fortunately prevented.

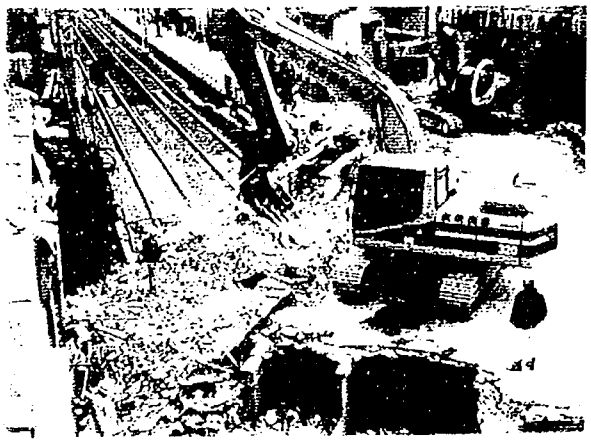


Fig. 17 Fell down Skew Girder Bridge

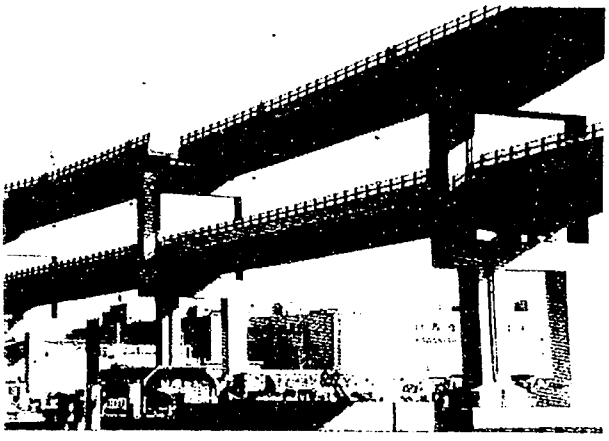


Fig.18 Lateral Offset of Girders

3. Lessons Learned from the Earthquake

In this earthquake, the peak ground motion of more than 800gal(cm/sec 2) was observed. When such strong ground vibrations strike the structures designed by allowable stress design method with seismic horizontal coefficients basically equal to 0.2, it becomes evident that the structural members have the possibility to be suffered from severe damages.

In Japan from 1990 edition of bridge design specification, reinforced concrete pier has been designed by dual-level performance criteria. It means RC piers had been checked the ductility for the maximum response acceleration spectrum of 1G.

Although the maximum response acceleration spectrum of 2G is proposed to check the ductility of piers for the tentative bridge design specification. Fig. 19 shows the proposed response acceleration spectrum. These spectrum was decided in accordance with the observed records in this earthquake.

Steel piers and foundations are also recommended to be designed by dual-level performance criteria.

Single column-type of piers had significant damage especially at the location of the bar cut-off. Therefore except the very tall piers, the bar cut-off in the pier was basically forbidden.

Considering the falling-off of the superstructures would cause the severe disasters, couplers should be designed in order to prevent the falling-off of the superstructure. In addition to couplers, the device which can prevent the displacement of the superstructure is recommend to be added on the top of piers and abutments.

Rubber bearing showed a good performance in this earthquake. Especially bridges with hysteretic damping-type rubber bearing could reduce response accelerations compared to bridges with ordinal steel bearing supports. Therefore the construction of base isolated bridges is recommended.

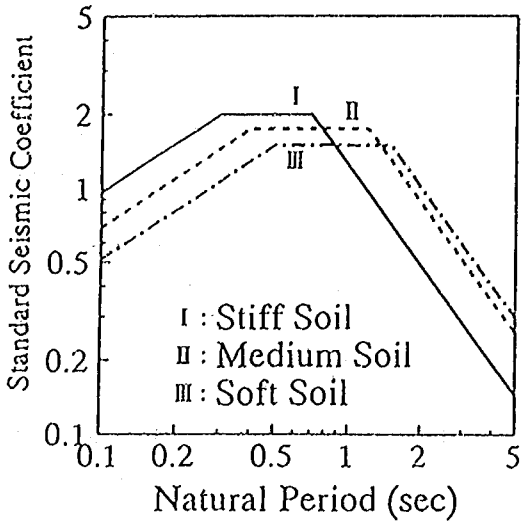


Fig. 19 Standard Seismic Coefficient

Liquefactions occurred in the gravelly granite fill materials. Therefore soil layers to check the liquefactions is spreaded for materials in which diameter of soil in accumulated curve lies between 2mm and 20 mm.

Lateral spreading of soils near revetment works seems to have some influence on the bridge foundation movement. Therefore the effect of lateral spreading on the behaviour of foundations is expected to consider in the design procedure.

4. Seismic retrofit of highway bridges

4. 1 Basic policy for the restoration of highway bridges

The restoration work has been carried out in accordance with "Specifications for the Restoration of Highway Bridges Damaged by the 1995 Hyogoken Nanbu Earthquake"(SRHB) prepared by Ministry of Construction. The basic policies are as follows.

Firstly, improving the deformation performance and strength of individual components, so that the entire bridge can withstand seismic force caused by the near source earthquake such as the 1995 Hyogokenn Nanbu Earthquake. Therefore the ductility and lateral force bearing capacity of substructures have been increased. Furthermore, to reduce the seismic force acting on substructures, superstructures have been improved by connecting girders or making them continuous,installing isolation or horizontal reaction-dispersing bearings, and employing light-weight steel decks for bridge floors.

Secondly, as many components as possible have been reused by repairing and reinforcing existing structures depending on the results of damage investigation. Foundations were reused since they received relatively minor damage. Piers and girders with light damage were repaired and reinforced to improve their seismic performance.

4.2 Design Concept for Seismic Retrofit of Highway bridges

Designs and checks for the three different levels as shown below were demanded.

Level 1: Design of the allowable stress,using a seismic coefficient method in accordance with the 1990 edition of the Specifications for the Design of Highway Bridges(SDHB). The ground on which the HER3(Kobe Route) stands is largely classified as Group II (alluvium and diluvium). The design horizontal seismic coefficient for ground of this class was previously 0.20 but was increased to 0.25 to satisfy the 1990 SDHB.

Level 2: Check on the lateral force bearing capacity, in accordance with the 1990 SDHB. The lateral force bearing capacity had not been taken into account in the previous Specifications before 1990. The seismic coefficient to be used in the check for Group II ground is 0.85.

Level 3a: Check on the lateral force bearing capacity using the response spectrum in accordance with the SRHB.

The 1990 SDHB were used, except for the stress- strain curve of concrete and seismic coefficient which were based on the "Reference for Application of the SRHB". The reference proposes that the shape of the stress-strain curve and the ultimate strain depend on the confinement effect of hoop ties, and that the seismic coefficient for checking the lateral force bearing capacity constructed on Group II ground is 1.75.

Level 3b: Nonlinear dynamic analysis using the seismic records of those areas where the maximum acceleration was observed during the 1995 Hyogoken Nanbu Earthquake. Time histories of ground motion adopted in SRHB are those records obtained on the Kobe Marine Meteorological Observatory, the Takatori Station of West Japan Railways, and Higashi Kobe Cable-stayed Bridge. These three records correspond to the ground group I , II , and III respectively

4.3 Design Example of Seismic Retrofit of Reinforced Concrete Piers

Results of seismic design of an existing reinforced concrete pier for levels 1 and 2 are shown in Fig. 20, comparing the existing pier, reconstruction pier, and strengthened pier. The cross-sectional width of a rectangular pier for reconstruction and retrofit was increased by 0.4 m from 3.2 m to 3.6 m. The cross-section satisfying the requirements on levels 1 and 2 was checked at level 3. Since the SRHB permits the confinement effect to be taken into account in the stress- strain curve in concrete, a reconstructed pier installed hoop ties 22mm in diameter and intervals of 12.5cm can also satisfy the level 3a seismic force. This pier also requires four intermediate hoop ties in a cross-sectional plane. On the other hand a strengthened pier must have hoop ties 25 mm indiameter and intervals of 12.5cm, and also 6mm thick steel Jacket.

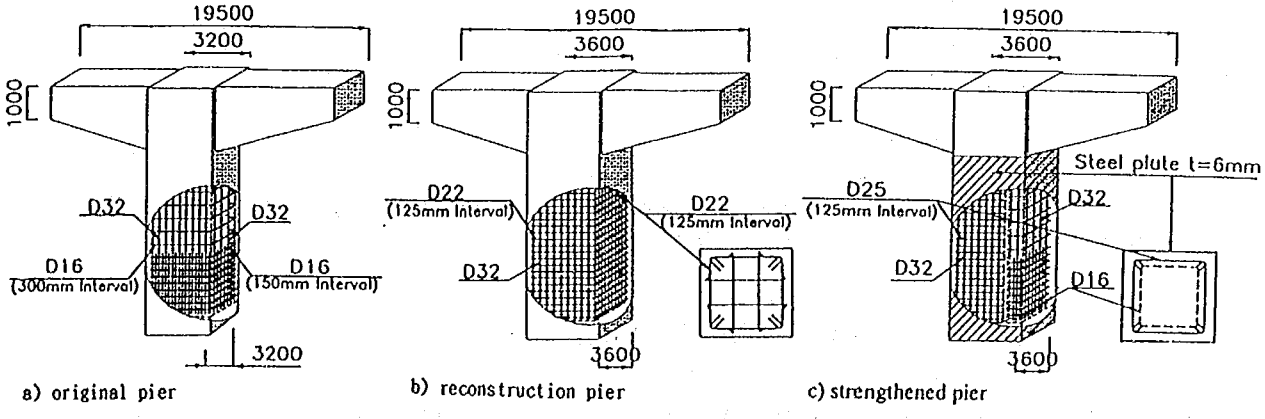


Fig. 20 Results of Checks on Reinforced Concrete Piers

After that the performance of these piers were checked by dynamic response analysis. As an input seismic wave, the north-south time history(maximum acceleration 818 gal) recorded by the JMA Kobe station was used. The time history is shown in Fig 3.

The analysis conditions were determined as follows. The analysis model consisted of only

a pier, and the horizontal component of mass was given as the concentrated mass. The footing and beam were regarded as rigid elements, while the pile foundation was regarded as a spring element. The Takeda model, which takes into account the decline in rigidity due to cracks in concrete and yielding of reinforcement bars, was used to derive the characteristics of the restoring forces of columns. The relationship between the bending moment and curvature of the cross-section followed the SRHB. The damping constant of the beam-column system was set to 2 % and that of the foundation-ground system was set to 20 %. The Newmark β method (β =0.25) was used for numerical integration, with calculation time increments of 0.001 seconds.

The results of the analysis are shown in Table 4. The results were as follows.

a) The response acceleration at the top was almost equal to the input acceleration both in reconstructed piers and in strengthened piers.

b) The response displacement at the top was smaller than the allowable plastic displacement calculated in accordance with the SRHB.

c) The maximum response bending moment and maximum shear force of the pier were below the values calculated in accordance with the SRHB.

As detailed above, firstly the cross-sectional shape was determined on levels 1 and 2, and then hoop tie configuration was determined on level 3a, and finally they were checked on level 3b.

Table 4 Dynamic Response Analysis Results

				Proposal for reconstruction	Proposal for strengthening by a combination of steel places and reinforced concrete
Dynamic analysis	Pier top	Response acceleration (gal)		860	875
		Response displacement (cm)		16.7 (1.17)	17.5 (1.47)
	Pier base	Response bending moment converted as lateral force (tf)		535 (1.11)	602 (1.07)
		Response shear force converted as lateral force (tf)		936 (2.90)	949 (2.25)
Static analysis	Lateral force bearing capacity	Converted flexural failure lateral force (tf)		591	645
		Converted shear failure lateral force (tf)		2715	2139
	P-δ relationship	Yielding	Lateral force (tf)	461	504
			Displacement (cm)	2.6	3.4
		Ultimate	Lateral force (tf)	657	716
			Displacement (cm)	28.1 (19.6)	36.8 (25.7)

Notes: Numbers in parentheses ( ) indicate lateral force bearing capacity/maximum response, allowable plastic displacement/maximum response, or allowable plastic displacement.

4.4 Performance of Strengthened Model Piers

Four types of strengthening methods for reinforced concrete piers were investigated by laboratory tests.

a) Steel plate jacketing: No. 5 is a model to increase the bearing capacity due to bar anchoring, and No. 6 and 7 are the models without bar anchoring, therefore these are expected the confinement effect only. Model No. 5 was attached by H-shape beam at the bottom of the steel jacket to increase the confinement effect of steel jacket, but models No.6 and 7 do not have any stiffner at the bottom of steel jacket.

b) Reinforced concrete jacketing: No. 8 and 9 are expected to improve both the bearing capacity and confinement effect by the reinforced concrete jacket. To investigate the effect of the extent of damage on the pier's bearing capacity, test models No. 8 and 9 were damaged in advance to the rank C or B.

c) A combination of steel plate and reinforced concrete jacketing: the reinforced concrete jacket increases the bearing capacity, while the steel jacket installed around it but not anchored to the footing only increases the confinement effect. Models No.10 and 11 were prepared for this type
of retrofit. To investigate the effect of the extent of damage on the pier's bearing capacity, test models No. 10 and 11 were damaged in advance to the rank C and B respectively.

d) Reconstruction of reinforced concrete piers: In models No.12 and 12', concrete of pier and footing was poured at the same time. The hoop tie in model 12' is double as much as the hoop tie in model No. 12. The pier of models No. 13 and 14 were made by means of post-installed anchors to investigate the degree of unity of a new constructed pier.

All test pieces were one-sixth scale models of a real bridge with square cross-sections.

Table 5 Experimental Conditions and Parameters

Test model No.	Reinforcement technique	Existing pier cross-section	Cross-section after reinforcement	Reinforcement ratio	Hoop tie	Design horizontal seismic coefficient (Kheo)	Reinforcing steel anchorage	Anchorage length	Remarks
1	Existing	Square, 60 cm × 60 cm	—	P – 0.51%	Pw – 0.11%	0.78			Damage rank C
2	Existing								Damage rank C
3	Existing								Damage rank B
4	Existing								Damage rank B
5	Steel plate jacket		Square, 60 cm × 60 cm	P – 0.85%	Pw – 0.64%	1.50	Post-installed resin anchor	To the footing bottom bar*	The bottom ends of the steel plates are anchored.
6	Steel plate jacket			P – 0.61%		1.41			Vg – 0 cm (Vg: clearance between the steel plate and the footing)
7	Steel plate jacket								Vg – 5 cm
8	Reinforced concrete jacket		Square, 70 cm × 70 cm	P – 0.61%	Pw – 0.70%	2.17	Post-installed resin anchor	To the footing bottom bar*	Test model No. 1 reused after the experiment
9	Reinforced concrete jacket						Post-installed resin anchor	To the footing bottom bar*	Test model No. 3 reused after the experiment
10	Steel plate + reinforced concrete				Pw – 0.65%	1.97	Post-installed resin anchor	To the footing bottom bar*	Test model No. 2 reused after the experiment; Vg – 5 cm
11	Steel plate + reinforced concrete						Post-installed resin anchor	To the footing bottom bar*	Test model No. 4 reused after the experiment; Vg – 5 cm
12	Reinforced concrete rebuilding			P – 0.61%	Pw – 0.27%	1.42	Before concrete casting	To the footing bottom bar*	Standard test model
13	Reinforced concrete rebuilding						Post-installed resin anchor	To the footing bottom bar*	
14	Reinforced concrete rebuilding						Post-installed resin anchor	Length required from the top bar**	
12'	Reinforced concrete rebuilding				Pw – 0.58%	2.21	Before concrete casting	To the footing bottom bar*	2G-resistant test model

* One half the thickness of the footing plus the anchorage length needed for calculation
** The thickness of the covering on top of the footing plus the anchorage length needed for calculation

Figure 21 shows the setup of the specimen. Constant axial load and lateral cyclic load were applied to them.

Fig. 22 shows the typical relationship between the load applied to a test model and horizontal displacement. Fig. 23 is a typical load-displacement envelope linking every first applied load under the reversed cyclic lateral loading. In the experiments the maximum bearing capacities of the standard model were about 24.5 tf and those of the strengthened models were around 36 tf, suggesting an increase of about 1.5 times in bearing capacity.The experimental maximum bearing capacities closely agreed with the corresponding analysis values.

Fig. 24 shows the ductility factors of the test models. In this figure, the displacement when the load had dropped to 80 % of its maximum was taken as the ultimate displacement. The experimental values, even after modification for the loss due to the pull-out of

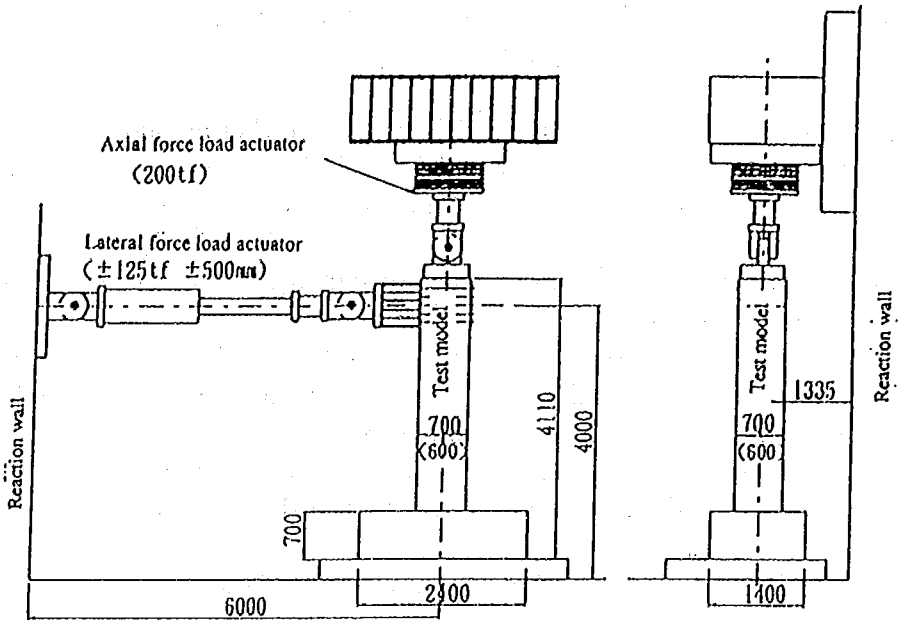


Fig. 21 The Test Model Setup

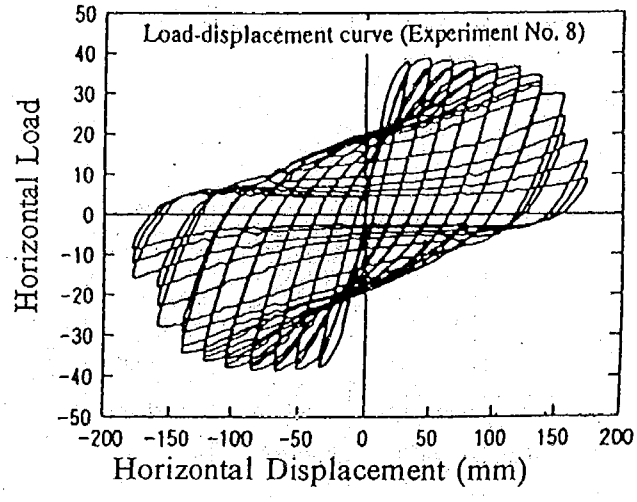


Fig. 22 Load and Horizontal Displacement

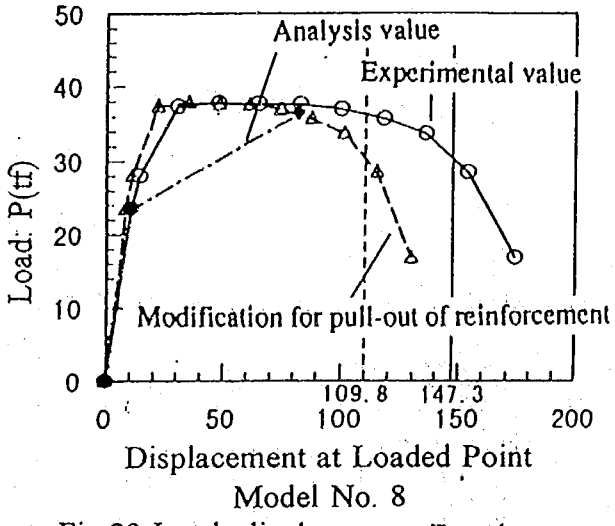


Fig.23 Load- displacement Envelope

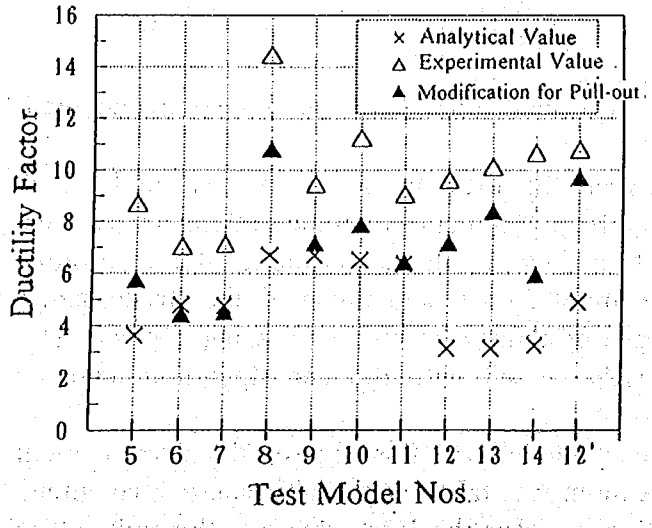


Fig. 24 Ductility Factors for All Models

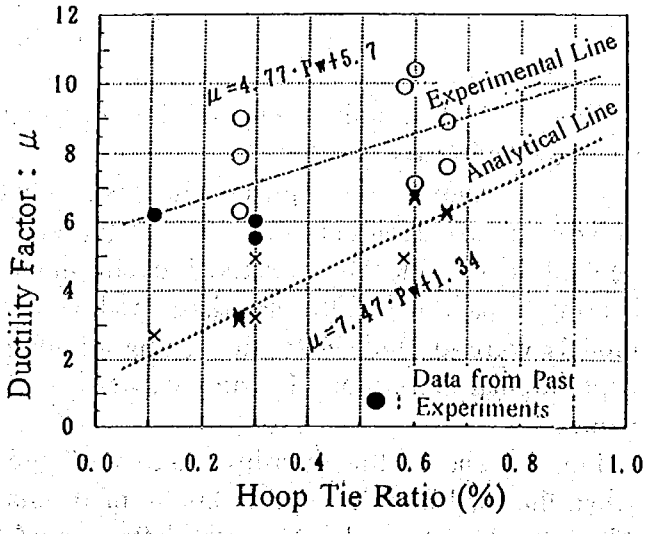


Fig. 25 Hoop Tie Ratio and Ductility Factor

reinforcements, satisfied the analysis values derived from the SRHB. The ductility factor exceeded 8 for some of the reinforced concrete jacket models (No. 8, 13 and 12') , well above the analysis values. In models No. 6 and 7, ductility factors obtained by the test are almost equal to the calculated values, because these models have no stiffner at the bottom of the steel jackets. On the other hand, model No. 5 with stiffner at the bottom of the steel jacket showed the larger ductilities compared to models No. 6 and 7. Models No. 9 and 11, which were made after the rank B damage, showed the small ductility compared to model No. 8 and 10, which were damaged in advance to rank C.

Fig. 25 shows the relationship between the ductility factor and the hoop tie ratio in the reinforced concrete jacket models. With the higher hoop tie ratio, the ductility factor increased from 6 to around 9, suggesting that the increased number of hoop ties contributes to the improvement of ductility. Taking into account that the hoop tie ratio is usually limited to about 0.7 % to 0.9 % in actual structures,the ductility factor of 10 might be a reasonable upper limit for normal reinforcement with reinforced concrete.

4.5 Improvement of the Surrounding of the Bearing Supports

Figure 26 shows the retrofit of the surrounding of the bearing supports located on the steel box beam in a 2-story frame type pier. Enlargement of the width of the box beam of the pier to prevent the falling off the superstructures, set up the steel block to prevent the over displacement of bearing supports, and connectors of the adjacent girders by the cables with damper are adopted in this pier.

Furthermore making the change of ordinal iron made bearing support to high damping rubber bearing support were conducted for the piers in HER3. Fig. 27 shows the high damping rubber bearing support adopted on the reconstructed piers in HER3.

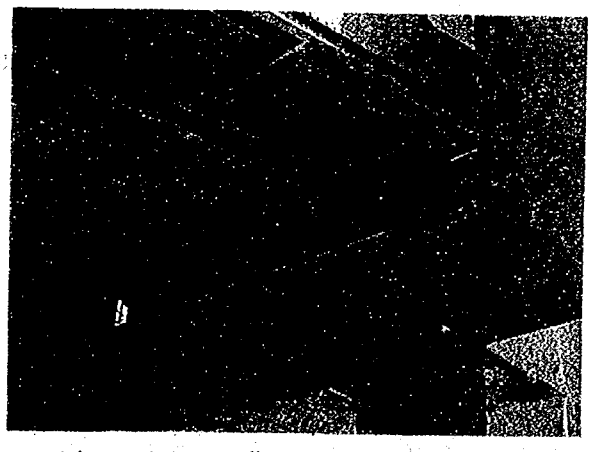


Fig. 26 Retrofit on the Pier Beam

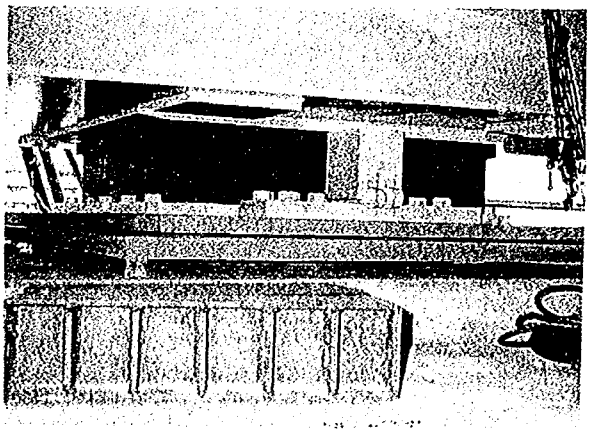


Fig. 27 The High Damping Rubber Bearing

5. Conclusions

Although the magnitude of the earthquake of 7.2 on the JMA scale was not so large, the violent ground motion was very destructive, because the epicenter was very shallow and close to the highly integrated area. Elevated highway bridges suffered extensive damage. The damage included collapse of piers, falling off of a simple supported girder, breakage of bearings and falling prevention devices. Bridge piers constructed based on the highway bridge specifications enacted in 1980 showed better performance than the older ones, but the necessity of increasing the design seismic force was recognized.

According to the design example calculated by the Specifications for the Restoration of Highway Bridges, reinforced concrete jacketing, steel plate jacketing, and their combination method are expected to use successfully for the seismic retrofit of reinforced concrete piers. The seismic performance of the piers constructed according to SRHB were proved by model tests.

6. References

1. Ministry of Construction: Specifications for Restorationcons of Highway Bridges Suffered damage due to the 1995 Hyogo-ken Nanbu Earthquake, February 1995.
2. M. O. C.: Final Report on the Damage to Highway Bridges by the 1995 Hyogoken Nanbu Earthquake.

INNOVATIVE SEISMIC RETROFIT OF CALIFORNIA HIGHWAY STRUCTURES

Saad EL-Azazy, Ph.D., P.E.
California Department of Transportation
Sacramento, California

ABSTRACT

Seismic retrofit of California highway structures presented engineers at the California Department of Transportation (Caltrans) with numerous challenges. Many projects contained unusual structural or construction constraints which required the development of innovative retrofit strategies. The Bixby Creek Bridge, a reinforced concrete arch bridge built in 1932, is located on a scenic portion of State Route 1 south of Carmel. The historical nature of the bridge, environmental impact concerns, architectural considerations, accessibility, construction staging and traffic concerns had a major impact on the seismic retrofit scheme selected. The seismic retrofit of the Alameda/Oakland Posey Tube, a historical structure built in 1928, and the Webster Street Tube, built in 1963, presented unusual challenges because of their location in liquefiable soil. The Oakland 24/580/980 Interchange contained numerous seismic vulnerable details. The presence of the Bay Area Transit System (BART) running north-south through the interchange, limitations on pile driving to preserve historical structures and to prevent BART track settlement, the unknown location of numerous utilities and the resulting limitations in the construction area increased the complexity of this seismic retrofit project. This paper discusses the performance criteria, analysis, seismic vulnerabilities and innovative seismic retrofit scheme planned for each of these projects.

INTRODUCTION

The 1971 San Fernando earthquake provided graphic evidence that bridges in California were vulnerable to earthquakes. This vulnerability represented an unacceptable danger to California residents, the economy and the lifestyle of the State. In response, the California Department of Transportation (Caltrans) initiated a seismic retrofit program to mitigate this risk.

Many of the structures presented engineers with unusual structural or construction constraints. To meet these challenges, innovative strategies were developed to retrofit these structures. This paper presents three types of structures which required innovative approaches: a concrete arch bridge with historical significance, a tunnel structure built in liquefiable soil, and a large complex interchange with many site constraints. Structural details, design constraints, seismic vulnerabilities, performance criteria, analysis used and innovative aspects of the planned seismic retrofit schemes will be presented.

SEISMIC RETROFIT OF REINFORCED CONCRETE ARCH BRIDGE BIXBY CREEK BRIDGE

The Bixby Creek Bridge is a reinforced concrete arch bridge built in 1932. It is located on State Route 1 in the Monterey Bay National Marine Sanctuary, 29 km (18 miles) south of Carmel

and 1.6 km (one mile) from the Palo-Colorado-San Gregorio fault. The historical nature of the bridge, environmental impact concerns, architectural considerations, accessibility, construction staging and traffic concerns had a major impact on the retrofit scheme selected. General views of the Bixby Creek Bridge are shown in Figure 1 and 2.

As Built Condition

This bridge is a 218 m (714 ft) long structure with two approaches and an arch spanning 97.5 m (320 ft) with an arch rise of 73 m (240 ft). The north approach is a 73 m (240 ft) long six span structure. The south approach is a 36.5 m (120 ft) three span structure. Approaches are supported on two column bents founded on 2.40x 2.40 m (8.0 x 8.0 ft) spread footing with a bottom mat of steel only. Columns are slender, lacking confinement with transverse reinforcement of 13M @300 mm (#4 @ 12 inches) and inadequate lap splice at the base of the columns. The arch and the approaches are supported on two pylons with hollow section and shear walls.

The superstructure is a T-beam cross section. The deck has expansion joints and it is simply supported at all bents. Abutments are tall cantilever diaphragm type. Spandrel bent members are slender section with inadequate seismic details. The bridge is founded on rock. Figure 2 shows the bridge components described above.

Seismic Retrofit Performance Criteria

The Caltrans performance criteria for arch bridges states that the bridge should not collapse either globally or locally during the maximum credible earthquake. This can be achieved when:

- Arch ribs remain essentially elastic, i.e. displacement ductility demand, $u_D < 2.0$.

  u_D = Displacement demand / Yield displacement,
  where displacement is obtained at the arch rib crown.

- Bent frame columns and spandrel columns may have inelastic deformation providing displacement capacity > displacement demand.
- Arch rib struts plastic hinging is acceptable providing that the stability of the arch is maintained.
- Deck is to remain elastic in order to provide lateral support.

Analysis

The analysis and seismic retrofit strategy for the bridge were developed by Buckland & Taylor Ltd. Bridge Engineering Consultants in collaboration with the Caltrans Engineering Service Center.

Seismic Loading

A site specific response spectrum was developed by Caltrans (Figure 3).

Seismic Demands

To evaluate seismic demand on the bridge elements, three dimensional elastic dynamic analysis using SAP90 were performed on the "As Built" then later on the retrofitted model. To account for the nonlinear behavior of the arch structure under seismic loading, a series of elastic analyses were performed on secant stiffness models of the bridge. In this series, over stressed members were given a reduced effective inertia to simulate yielding condition at maximum relative displacement. The final retrofit model represents the configuration for which the displacements of the preceding runs have converged indicating the ultimate displacement demands under inelastic action.

Structural Elements Capacity

To evaluate the structural elements capacity, two dimensional pushover analyses were performed in both longitudinal and transverse directions to determine yield displacement of various elements of the bridge. Demands were compared with capacities. As demands exceeded capacities, retrofit strategies were selected. Analyses were repeated until design criteria were satisfied.

In addition, analyses were performed to study the effect of lateral support at the arch crown and arch base condition on the stability of the arch. These analyses showed that arch structures become less stable during a seismic event if arch struts at the crown fail and if the base of the arch yield.

As Built Structural Seismic Vulnerabilities

- Large ductility demands on transverse arch rib struts (flexural D/C ratio ranging from 3 at the arch crown to 14 at the base)
- Large ductility demands on approach bent columns (flexural D/C ratio ranging from 2-6).
- Insufficient shear capacity in the shorter spandrel columns and approach bent columns
- Tower base hollow sections have limited capacity for inelastic deformations (flexural D/C ratios are > 6)
- Damage is expected in the footing/column connections due to lap splicing and lack of confinement
- Arch rib displacement demands are within the elastic range as long as stability of the arch is maintained
- Potential instability of arch ribs after rib strut hinging or failure

Innovative Seismic Retrofit Scheme

A lateral load path is required to minimize lateral displacement and to restrain the arch rib system. This will be achieved by:

- Creating continuity of the deck
- Linking the arch crown to the continuous deck
- Restraining the continuous deck at strengthened towers and restrained abutments

Deck continuity will be obtained through post tensioning. The towers will be strengthened by prestressing and tie downs at the foundations level. Abutments are to be restrained through use of large diameter CIDH piles. The detailed retrofit scheme is shown in Figure 4.

With these measures implemented analyses showed that design criteria were met. Since most of the required work will be away from the arch, the historical nature of the structure will be preserved and traffic interruption during construction will be minimal.

SEISMIC RETROFIT OF TUNNEL STRUCTURE: ALAMEDA/OAKLAND POSEY & WEBSTER ST. TUBES

The seismic retrofit of tunnel structures is illustrated by the planned retrofit of the Posey and Webster St. Tubes. The Posey Tube, a historical structure constructed in 1928, is a 1372 m (4500 ft) long structure including approach sections, immersed sections and portal buildings housing ventilation fans. The tunnel roadway is about 20.7 m (68 ft) below sea level at its lowest crossing under the estuary.

The Webster Street tube, added in 1963, has similar structural details. It is 1341 m (4400 ft) long structure, similar to the Posey Tube. The tube roadway is about 21.6 m (71 ft) below sea level at its lowest crossing under the estuary. Each tube carries two lanes of traffic between Alameda and Oakland, California. The plan view and cross section of the tubes is shown in Figure 5.

As Built Site Condition

The Hayward fault is located about six kilometers (four miles) east of the project site. The maximum earthquake magnitude of 7.25 is postulated on the fault. The bedrock is at about 183 m (600 ft) deep.

Both tubes consist of precast and cast in place reinforced concrete segments with locked up joints. Portal buildings are connected to the tunnels at each side. Because of the presence of bay mud, the tubes on the Alameda side were built on reinforced concrete slabs supported on piles.

Soil at the site is mostly stiff to hard clays, dense sands and mixtures of sand, silts and

clays. The backfill around the Webster Street tube consists of fine to coarse sand, loose to medium density. Backfill around the Posey Tube consists of soft clay with some layers of sand.

During the 1989 Loma Prieta earthquake liquefaction occurred on the Alameda side. Damage was reported as a result of estimated ground acceleration of 0.2g.

Seismic Performance Criteria

These tubes were evaluated for the maximum credible earthquake to satisfy two Caltrans performance criteria:

- Minimum performance level (survivability, no collapse)
- Limited performance level (repairable damage within a year)

Analysis

The analysis and seismic retrofit strategy for these tubes were developed by Parsons Brinckerhoff Quade and Douglas, Inc. Consultants, in collaboration with the Caltrans Engineering Service Center.

Soil and tunnel were analyzed as one system because buried structures that experience seismic excitation are affected by shear deformations of the surrounding soil. Structure forces and deformations being a function of soil deformation and tunnel rigidity.

Seismic Loading

Site-specific response spectra were developed at the bedrock level then a displacement time history was established at the tunnel level. (Figure 6)

Seismic Demands

A soil characterization and soil liquefaction study established the dynamic soil characterization and liquefaction potential.

Soil structure interaction analysis using 3-D ADINA model (Figure 7) was used to evaluate forces, moments, and displacements induced on the tunnel. The tunnel was modeled as an elastic beam supported by springs representing the surrounding soil. The model was continuous to simulate the existing locked up joints. Time history ground displacements were imposed as an input at the free end of springs. Forces and displacements were obtained along the tunnel. Then 2-D plain cross section finite element analysis of the tunnel/soil system was analyzed. (Figure 8) Ground deformations were applied at the boundaries of the finite element model. Cross section stresses and strains were obtained.

Structural Elements Capacity

Tunnel cross section capacities were obtained using the Caltrans, in-house developed, X-section computer program. Then the seismic retrofit scheme was developed to satisfy the design criteria.

As Built Seismic Vulnerabilities

- Liquefaction of sand backfill around the Webster St. tube, sand layer underlying both tubes, and bay mud on the Alameda side
- Tunnel floating as a result of massive liquefaction
- Potential lateral spreading of weak, soft soil surrounding the rigid tunnel
- Joint failure resulting from the build up of internal stresses in the continuous rigid tunnel structure surrounded by soft soil
- Cracking of over stressed concrete tunnel wall
- Potential risk to the structural integrity of ceiling connection, and roadway slab due to large deformations
- Potential risk of tunnel flooding and collapse caused by joint failures
- Potential risk for failure of piles with large soil deformation
- Risk to ventilation, plumbing, and electrical systems secondary to large displacement

Innovative Seismic Retrofit Scheme

- Make ground improvement using stone columns and jet grouting of the backfill surrounding the tunnels
  - -Stone columns reduce the liquefaction potential by providing a relief path for excessive pore pressure and reduce settlement
  - -Jet grouting improves overall soil characteristics by replacing the existing ground with a mixture of cement and natural soil
- Revise existing joints between tunnels segments to allow joints expansion
- Provide post-tensioning of tube section to limit open concrete cracking and water leakage
- Placement of stone columns at pile locations to stiffen the existing soft soil in order to reduce shear demand on these piles
- Add support hangers to ceiling slab to prevent collapse

The proposed seismic retrofit strategy is shown in Figure 9.

In this strategy, seismic demands on the structure will be reduced by understanding the soil-structure interaction problem and then making improvements in the soil condition and changing the structure rigidity.

SEISMIC RETROFIT WITH COMPLICATED SITE CONSTRAINTS: OAKLAND 24/580/980 INTERCHANGE

24/580/980 Interchange was built in the late 1960's in Oakland, California. It is located 4.3 km (2.7 miles) from the Hayward fault and 26 km (16.2 miles) from the San Andreas Fault. The interchange is composed of four "Y" shaped connectors. (Figure 10)

As Built Condition

The interchange contains numerous seismic vulnerable details. The retrofit project consists of work on nine ramps containing 61130 square meter (658,000 square ft) of elevated concrete deck. The Bay Area Rapid Transit District Rail System runs at grade north-south through the interchange parallel to route 24/980. All main lines meet at the McArthur Station just north of route 580 with a daily ridership of approximately 270,000 persons. The Bart System is particularly vulnerable if any ramp structure would collapse.

This structure contains 156 bents. Five different types exist : T bents, C-bents, multi-column bents, outriggers, and double deck bents. Column details were found to be inadequate with transverse steel of 13M@300mm (#4 @12 inches), and lap splices at the column footing connections. Footings were deficient with only a bottom mat of steel. Pile footing connections were found to be inadequate. Piles were found under-reinforced and lacking tensile capacity. Hinges with insufficient seat width were in sixty different locations in this project.

A major feature of this project is the presence of BART and the requirement of having uninterrupted service. Four sets of rails are located directly on the top of the footings. Relocation is required on hundreds of communication and power lines while retrofit work is performed on columns that actually support many of the BART system wireways.

Design Constrains

- The existing Bay Area Transit (BART) system running north-south through the interchange
- Pile driving not allowed to preserve historical structures in the area and to prevent BART track settlement
- Difficulty determining the exact number and location of utilities at site
- Limited construction area due to the BART rails, freeways, local streets, and businesses
- High average daily traffic
- 18-C bents, most with inaccessible footings
- Low overhead clearance in several locations
- Lead contaminated fill material
- Many foundations located under BART tracks and adjacent structures

Design Criteria

- The bridge should stand a maximum credible earthquake with no collapse.
- Seismic load combinations, material properties, design parameters, and design code should

follow Caltrans bridge design specifications.

Analysis

The analysis and seismic retrofit strategy for this interchange were developed by engineers in the Caltrans Engineering Service Center, Ron Bromenschenkel, P.E., Project Engineer, Imbsen and Associates, and The Lawrence Livermore National Laboratory.

Seismic Loading

Two site specific response spectra were developed by Caltrans, one for the interchange with peak spectra acceleration of 1.2 g and the other for the BART viaduct with peak spectra acceleration of 2.0g.

Seismic Demands

Initial dynamic analysis of this bridge was based on Caltrans procedures using STRUDL computer code with several models. Later, nonlinear analysis was conducted by Imbsen and Associates using NEABS computer program. In addition, the Lawrence Livermore National Laboratory conducted nonlinear analysis for south connectors using the NIKE3D computer program. Earthquake demand for each element of this structure was obtained through these analyses.

Structural Elements Capacity

Element capacities were obtained through pushover analysis utilizing the Caltrans in-house-developed computer program, X-section and W-frame.

Then demands on the structure elements during a seismic event were compared to the capacity of the structure elements. Elements with demand exceeding the capacity were identified. Planned retrofit measures were then applied to the model. Analyses were repeated until design criteria were satisfied.

As Built Structure Seismic Vulnerabilities

- C-bents and T-bents share deficient columns and footings
- Multi-column bents with weak bent caps
- Insufficient shear capacity in shorter columns
- Outrigger bents have weak bent caps combined with high torsion and joint shear demands
- Double-deck bents analyses demonstrated that out of phase motion produced high demands on columns.

Innovative Seismic Retrofit Scheme

After considering the site limitations and structural seismic vulnerabilities, the following innovative seismic retrofit design was selected.

- Construct a new permanent BART utility viaduct aerial structure to relocate wireways away from the construction area
- Add new companion bents next to the inaccessible C- bents to carry load away from weak existing bents (Figure 11)
- Construct a new raised link beam at multi-column bents with weak bent cap (Figure 12) Link beam will force plastic hinging in the column, protecting the weak bent cap
- Prestress bent caps to increase their capacities
- Provide double deck separation into independent bents to account for out of phase motion (Figure 13)
- Use drilled micropiles to accommodate the specification of no vibration allowed, the confined work space, and the issue of unknown location of utilities (Figure 14)

The use of micropiles will enhanced the design and constructability of the project. The micropile provides high tension and compression pile capacity while occupying a very small area. Construction space will be reduced because of the small, often hydraulically driven installation equipment. This operation produces lower noise level than the conventional pile driving equipment.

SUMMARY

This paper presents innovative seismic retrofit schemes proposed for three types of highway structures which presented engineers with unique challenges. The seismic retrofit scheme for the Bixby Creek Bridge, a concrete arch bridge, was directed at controlling seismic demands while finding a logical way to preserve the historical and architectural value of the bridge. The Posey and Webster St. Tubes required an innovative retrofit approach because these tunnel structures were built in liquefiable soft soil. An understanding of the interaction between soft soil and rigid structures in an earthquake led to a seismic retrofit scheme in which the soil was improved and the tunnel rigidity was decreased. The 24/580/980 Interchange required an innovative approach because of the presence of BART tracks, numerous utilities, historical structures, and limited construction space. These constraints were overcome by using innovative, viable alternatives to mitigate the seismic risk at that site. The complex nature of the earthquake event combined with the complex site-specific nature of every structure makes innovation a necessity for seismic retrofit engineering.

ACKNOWLEDGMENTS

The author wishes to acknowledge James Gates, Chief, Office of Earthquake Engineering, and Ray Zelinski, Senior Bridge Engineer, Seismic Technology Section, for their valuable suggestions and Ron Bromenschenkel, Project Engineer and designer of 24/580/980 interchange, for providing information related to this project. Special thanks are extended to David Pajouhesh Randy Anderson, Annie Chen, Sam Ataya, and James Mason for their contributions which made this paper possible.

REFERENCES

Buckland & Taylor, Ltd. Bridge Engineering. Bixby Creek Bridge No:44-019 Seismic Retrofit Strategy Report. 1995 Nov. 30.

Parsons Brinckerhoff Quade & Douglas, Inc. Posey and Webster St. Tubes Seismic Draft Retrofit Strategy Report No. SR722 EA No. 04-440101. July 11, 1996.

U.S. Department of Transportation, Federal Highway Administration. Seismic Retrofitting Manual for Highway Bridges. Publication No. FHWA-RN-94-052. May, 1995.

Zelinski, Ray. Caltrans Bridge Seismic Design. United States-Japan Workshop. Lake Tahoe, Nevada. May, 1994.

California Department of Transportation, Caltrans Memo to Designers 20-4.

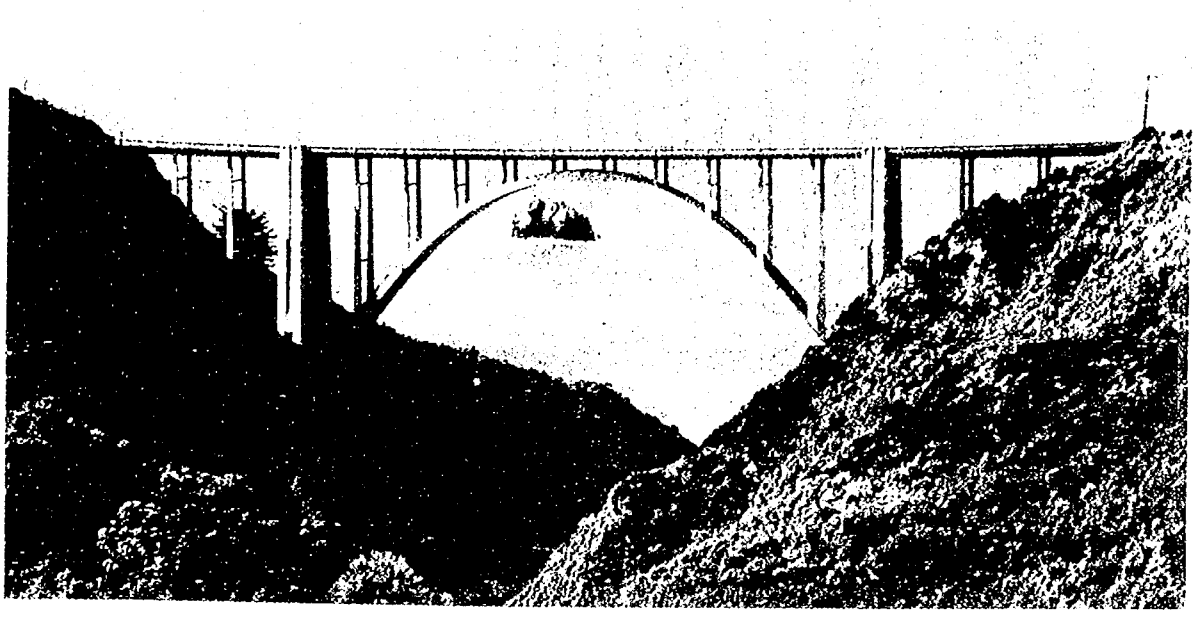


Fig. 1: Overall view of Bixby Creek looking west.

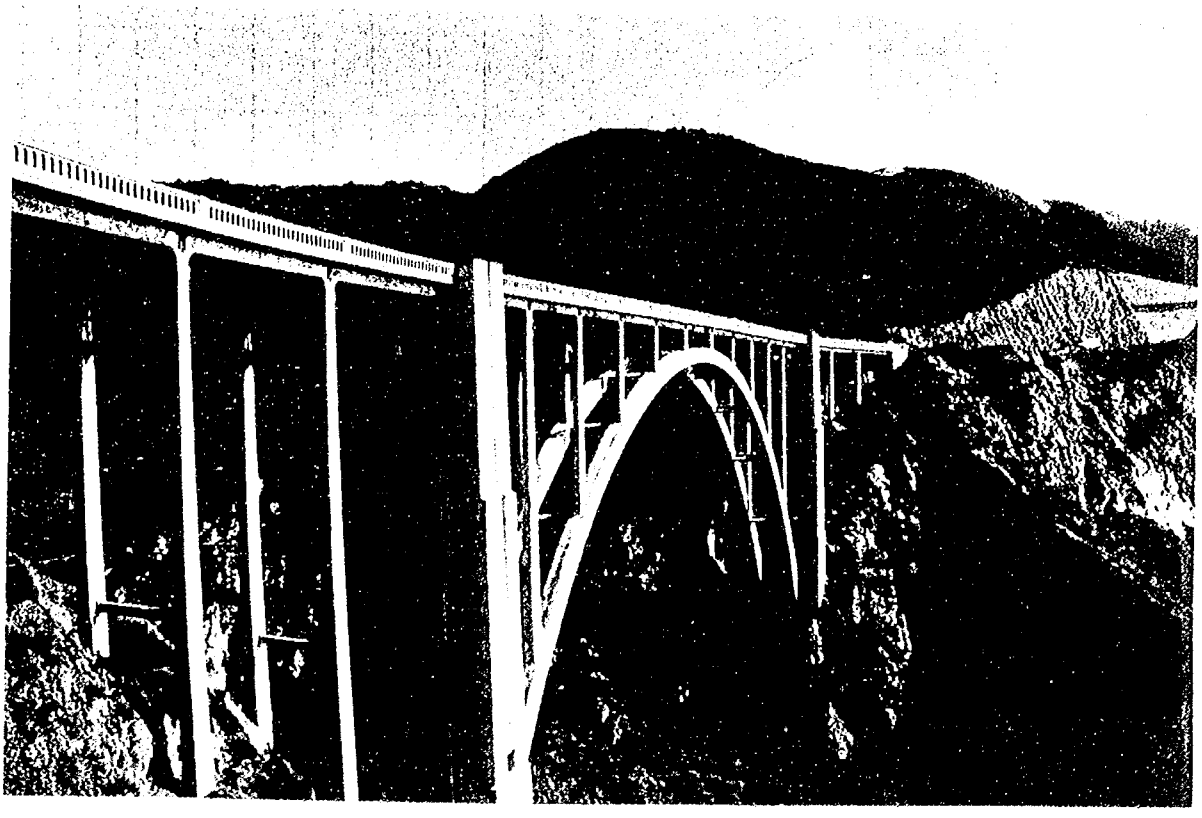


Fig. 2: Overall view of Bixby Creek Bridge Looking N-E

Fig. 4: Detailed retrofit scheme for Bixby Creek Bridge.

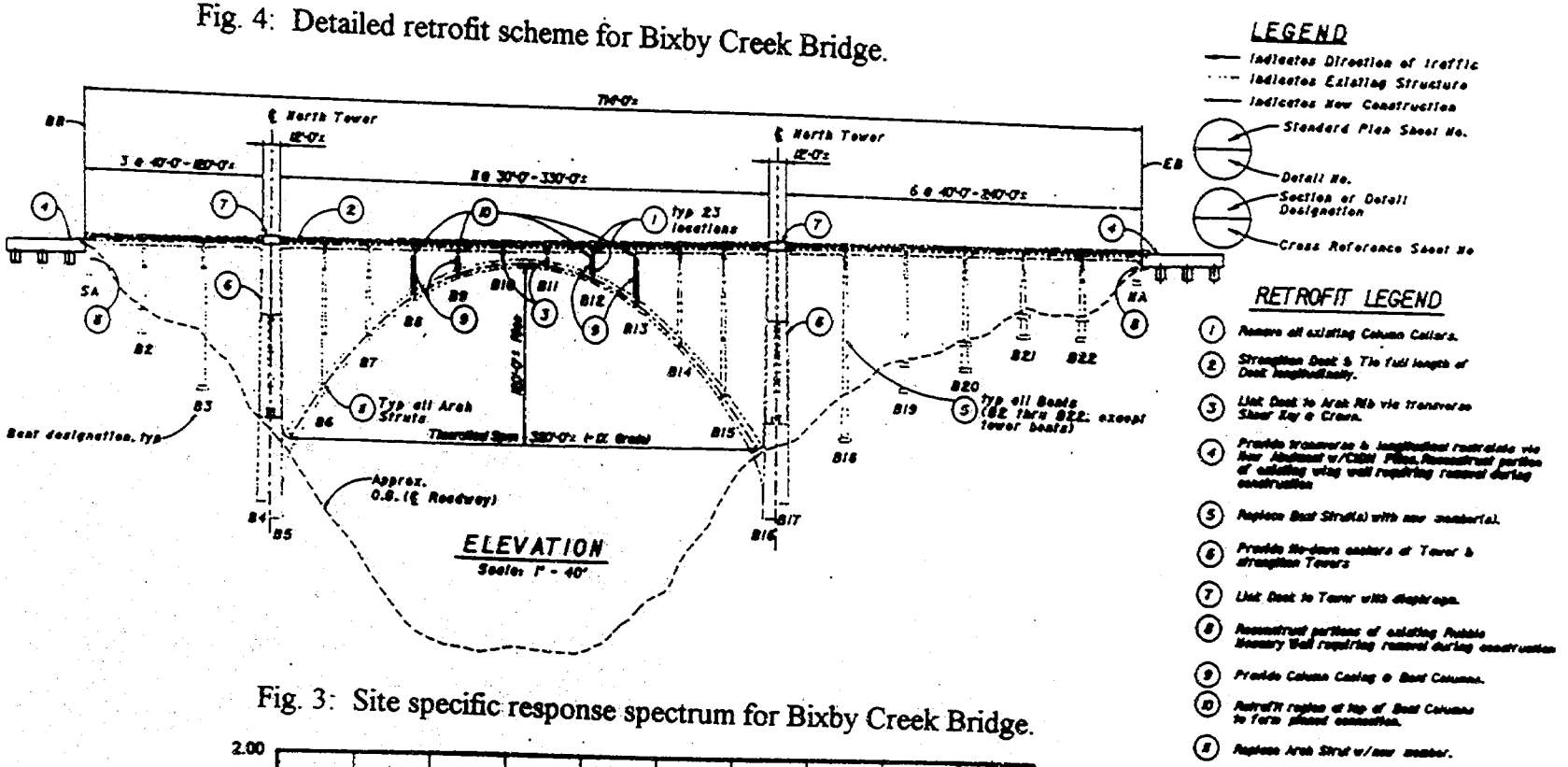
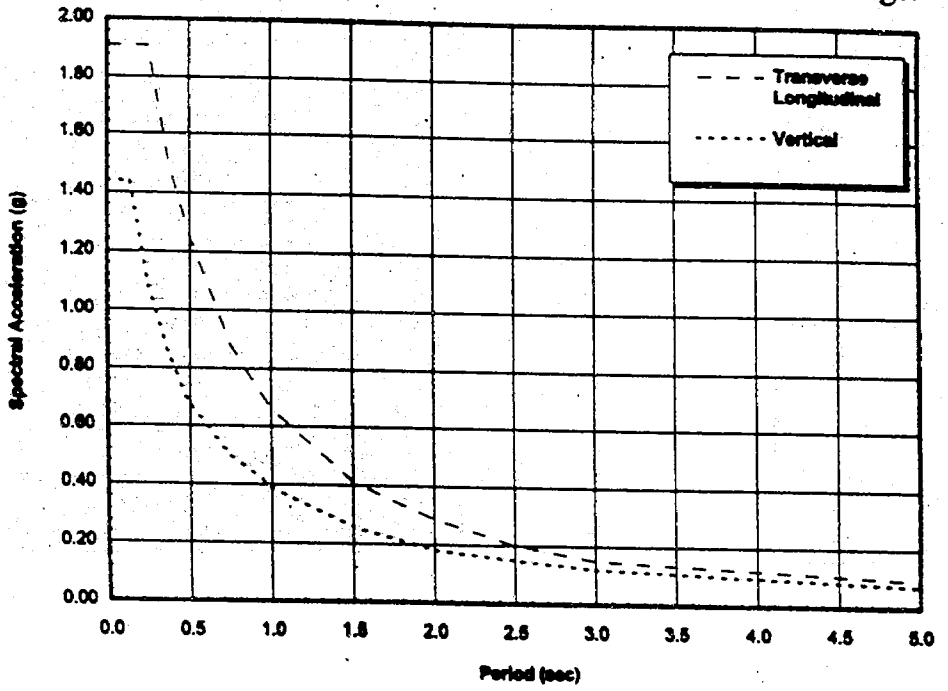


Fig. 3: Site specific response spectrum for Bixby Creek Bridge.



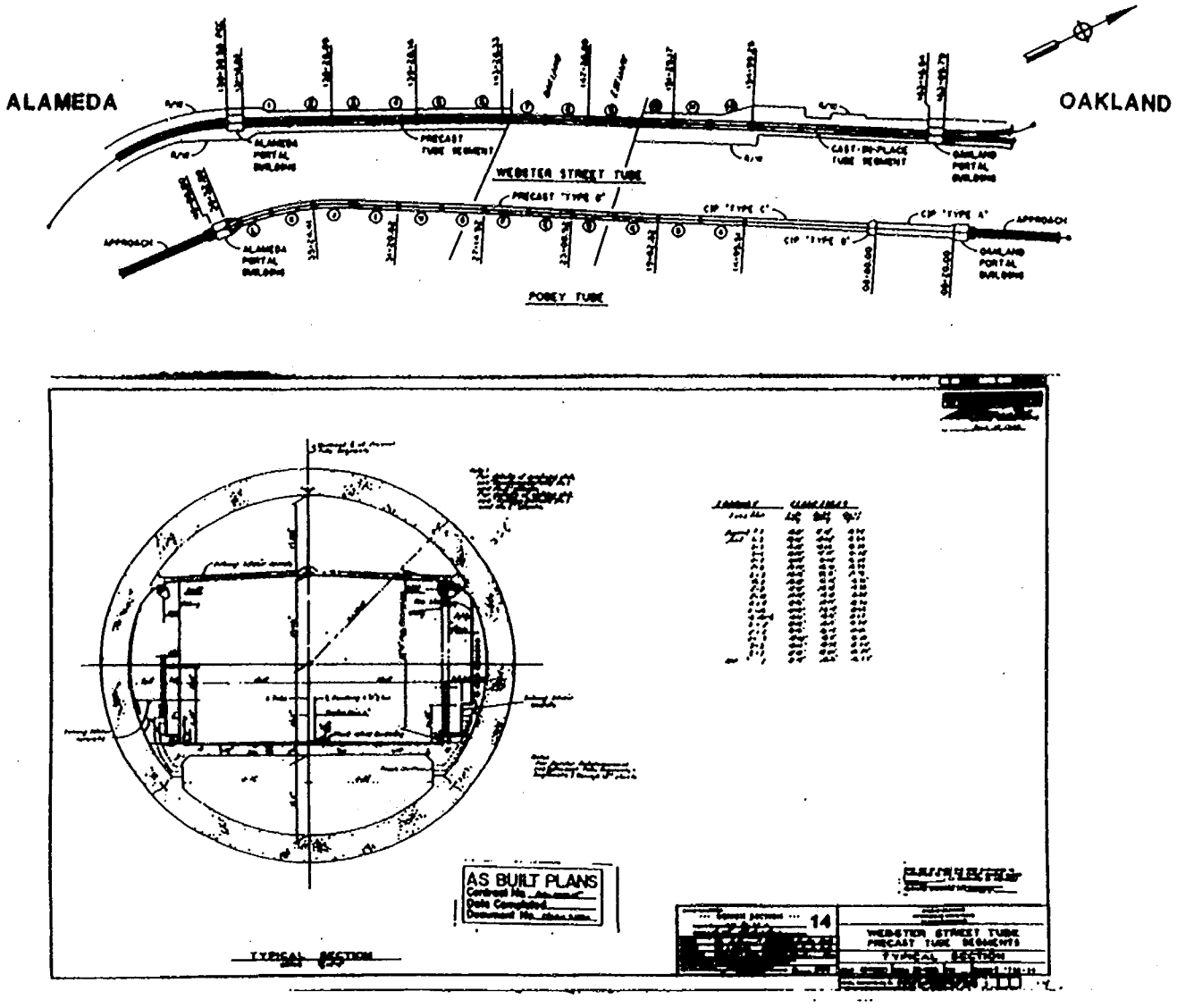


Fig. 5: Plan view and cross section of Posey and Webster St. tubes.

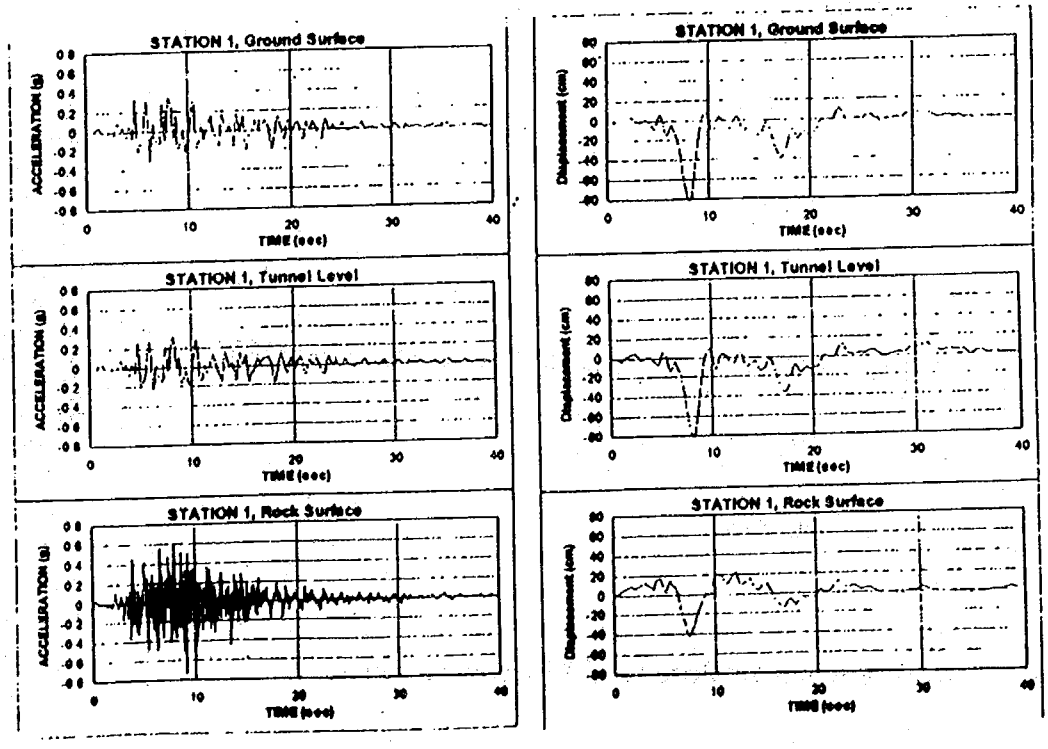
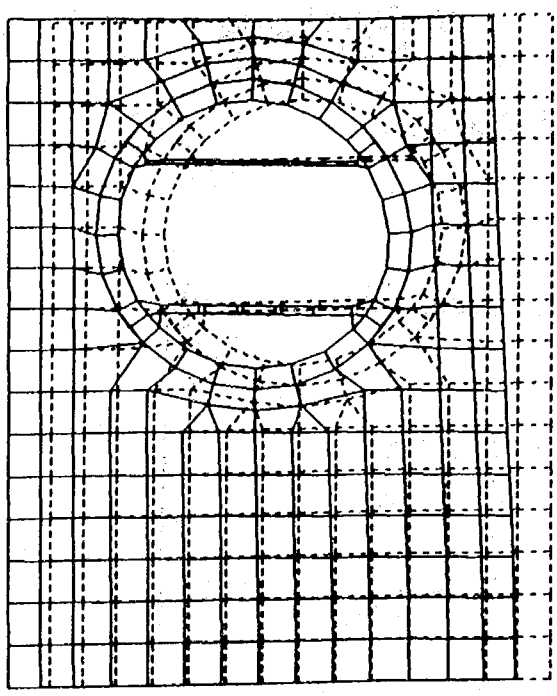


Fig. 6: Propagated acceleration and displacement time histories for Posey and Webster St. tubes.



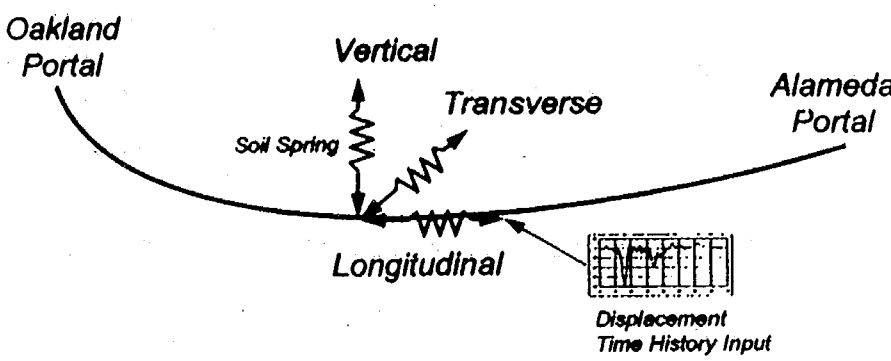


Fig. 7: Global dynamic soil-tunnel interaction model.

Fig. 8: 2-D finite element analysis for Posey and Webster St. tubes.

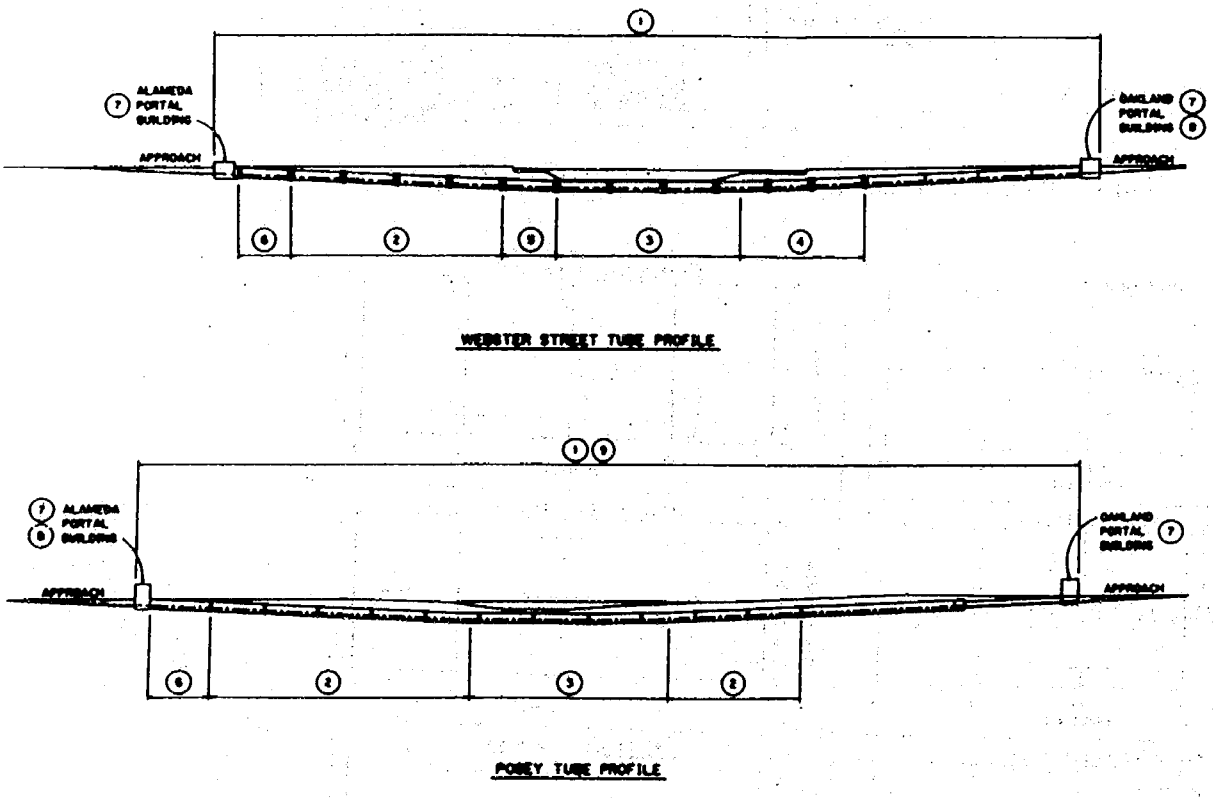


Fig. 9: Seismic retrofit scheme for Posey and Webster St. tubes.

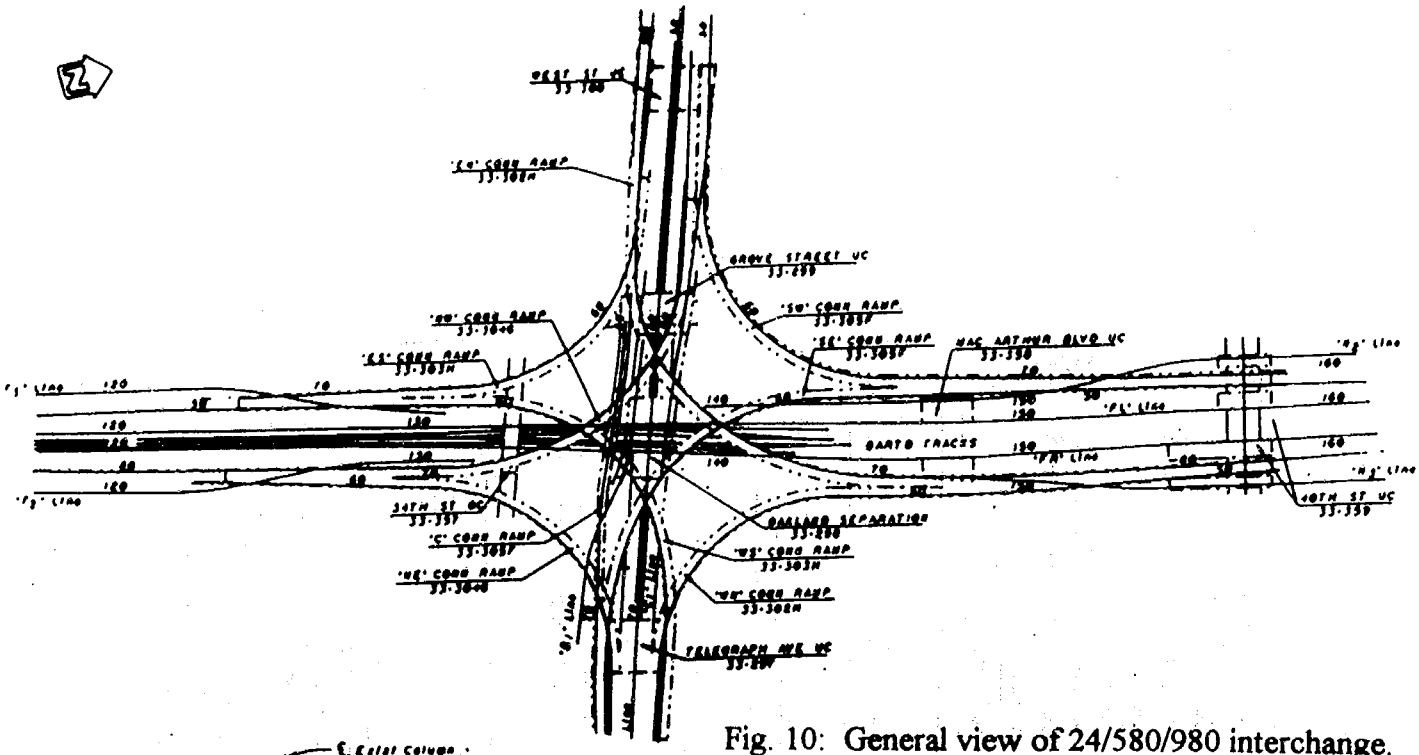


Fig. 10: General view of 24/580/980 interchange.

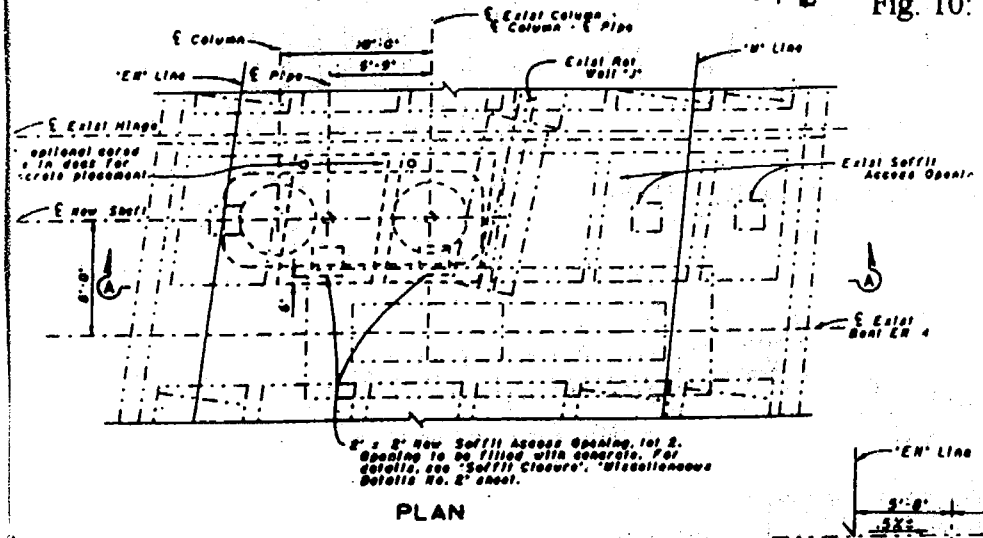


Fig. 11: Companion bents.

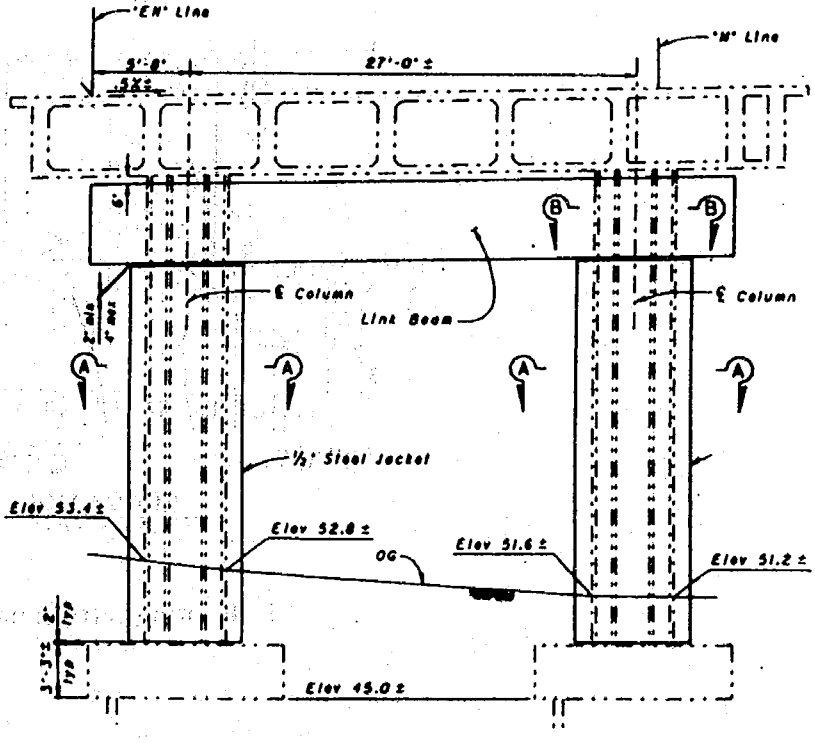


Fig. 12: Raised link beam.

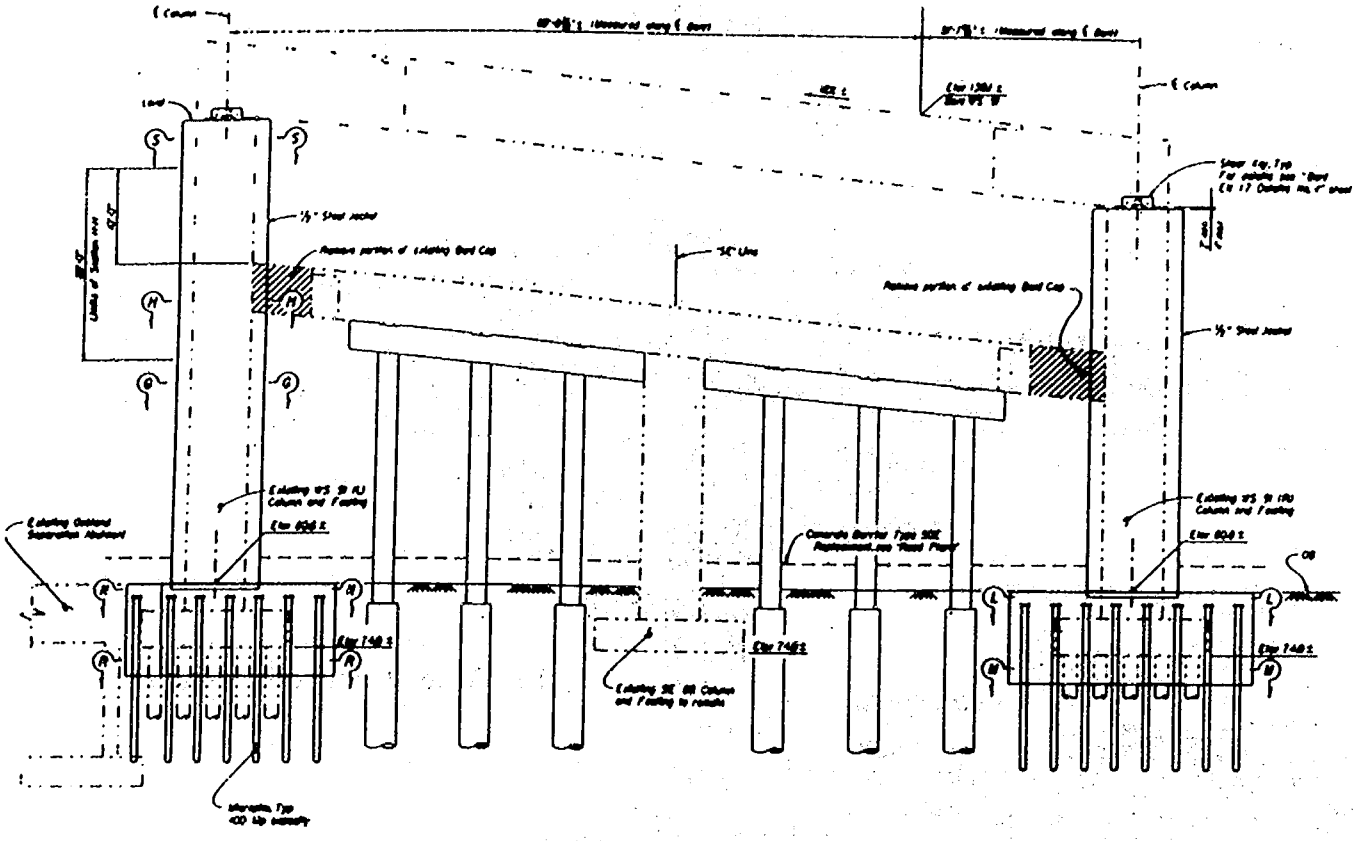


Fig. 13: Double deck separation.

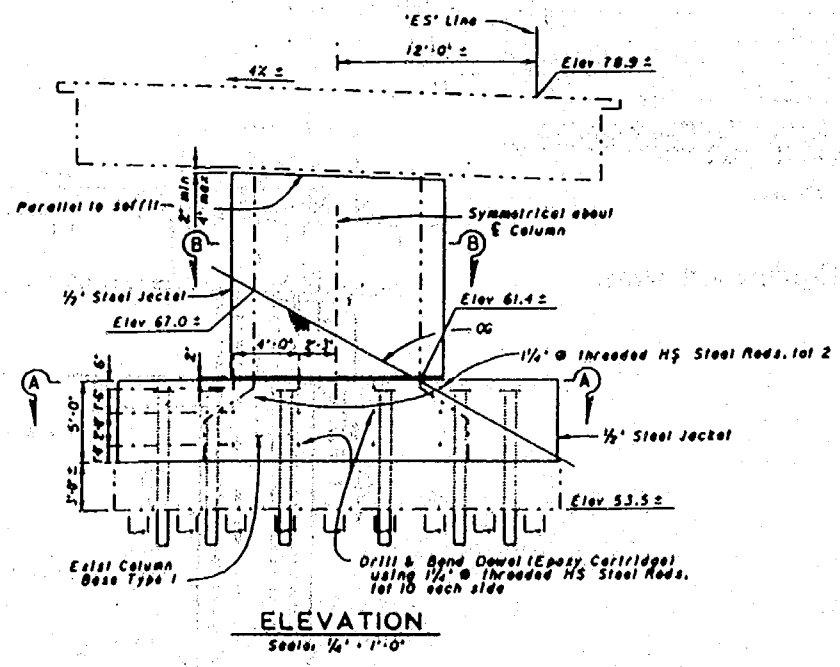


Fig. 14: Footing retrofit using micropiles.

Session 2

Screening and Prioritization of Bridges for Retrofitting

(Co-Chairs: H. Mutsuyoshi, J. Mander)

"Seismic Retrofitting Manuals for Highway Systems: System Assessment, Screening, Evaluation, and Retrofitting"
by I. Buckle, I. Friedland
Presented by: Ian Friedland

"Use of Transportation Network Systems for Bridge Retrofit Prioritization and Emergency Response"
by A. Kiremidjian, N. Basöz
Presented by: Anne Kiremidjian

SEISMIC RETROFITTING MANUALS FOR HIGHWAY SYSTEMS: SYSTEM ASSESSMENT, SCREENING, EVALUATION, AND RETROFITTING

Ian G. Buckle and Ian M. Friedland
National Center for Earthquake Engineering Research
State University of New York at Buffalo, Buffalo, New York

ABSTRACT

Under the sponsorship of the Federal Highway Administration, the National Center for Earthquake Engineering Research (NCEER) is developing a set of guidelines for conducting seismic hazard evaluations and retrofitting of complete highway systems.

These guidelines will be based on current knowledge and the results of ongoing research at NCEER and elsewhere. The intent is to produce state-of-the-art guidance on the seismic assessment, screening, evaluation and retrofitting of not only the structural components of highway systems (bridges, tunnels, retaining walls and the like) but also the system itself as a network of transportation corridors. This six-year effort is currently at the beginning of its fourth year and in addition to an active research program, a draft set of guidelines has been prepared. These guidelines are in three volumes as follows: I – seismic risk assessment of highway systems; II – screening, evaluation and retrofitting of bridges; III – screening, evaluation and retrofitting of retaining structures, slopes, tunnels, culverts and pavements.

These three volumes are called "strawmen" reports because they have been prepared for review and critical comment before final versions are published towards the end of 1998. Furthermore, their preparation has enabled knowledge gaps to be identified which may now be studied and the results obtained used to improve the final edition of these manuals.

INTRODUCTION

General

In the fall of 1992, the National Center for Earthquake Engineering Research (NCEER) initiated work on a comprehensive research program to develop tools to evaluate the seismic vulnerability of the national highway system in the United States. This program is sponsored by the Federal Highway Administration (FHWA) of the U.S. Department of Transportation. The research being conducted includes a series of tasks which will develop an improved understanding of the seismic hazard in the eastern and central United States, the behavior and response of soils, foundations and structures during earthquakes, and the overall impacts on highway systems resulting from earthquakes. In addition, the program is developing appropriate retrofit technologies for those highway system components deemed vulnerable to earthquake damage.

One of the primary objectives of this program is to develop a seismic evaluation and retrofitting manual for existing highway systems which will have national applicability. This manual is being prepared in three parts. The first part (Volume I) will contain the methodologies, procedures, and examples for conducting a seismic risk assessment of highway networks and systems; the second part (Volume II) will contain guidance on seismic vulnerability screening, analysis, and retrofitting of highway bridges; and the third part (Volume III) will contain guidance on screening, analysis, and retrofitting of other major highway system components, including retaining structures, tunnels, culverts, slopes, and pavements.

The three parts and their coordinating authors are as follows:

Volume I	Seismic Vulnerability Assessment of Highway Systems (Coordinator: S. Werner)
Volume II	Seismic Retrofitting Manual for Highway Bridges (Coordinator: I. Buckle)
Volume III	Seismic Retrofitting Manual for Retaining Structures, Slopes, Tunnels, Culverts, and Pavements (Coordinator: M. Power)

As a first step towards the completion of each of these volumes, a "strawman" has been recently developed for each volume which (a) summarizes the current state-of-practice in highway system assessment and component evaluation, and retrofitting; (b) incorporates current research results; and (c) identifies important gaps in knowledge which must be addressed before these three volumes can be completed.

The following sections of this paper provide an overview on the objectives and content of each strawman volume, and, as an example, presents the results of a seismic risk assessment of the highway network in the city of Memphis and surrounding Shelby County, Tennessee.

SEISMIC VULNERABILITY ASSESSMENT OF HIGHWAY SYSTEMS

Background

Past experience has shown that the direct impact of earthquake damage to highway components (e.g., bridges, retaining structures, and tunnels) is both a life-safety issue and a repair and replacement cost issue. Furthermore, the indirect impact can be almost as severe due to closed routes, disrupted access and delayed post-earthquake emergency response, repair, and reconstruction operations. In addition, highway system damage can directly impact the economy of a region, as experienced in Costa Rica in 1991.

The extent of these impacts depends not only on the seismic performance characteristics of the individual components, but also on the characteristics of the highway system that contains these components. For example, studies of highway system performance in the San Francisco Bay area after the Loma Prieta earthquake have shown that post-earthquake traffic flows may strongly depend on (a) the configuration of the highway system, (b) the locations, redundancy, and traffic capacities and volumes of the links within the system

between key origins and destinations, and (c) the locations of the individual components within these links and the overall system (Hobeika et. al., 1991; Wakabayashi and Kameda, 1992).

When one considers these system characteristics, it is evident that earthquake damage to certain components (e.g., those along important and non-redundant links within the system) will have a greater impact on overall system performance than will other components. Currently, such system issues are not considered when specifying seismic performance requirements and design or strengthening criteria for new or existing components, due primarily to the lack of adequate systems-based evaluation tools. Instead, each component type is usually evaluated individually, with screening and ranking criteria applied specifically to the inventory of structures of the same type. For example, formal screening and ranking guidelines for highway bridges have existed since the early 1980s (FHWA, 1983). However, this procedure treats each individual component independently, without regard to how the extent of its damage may impact overall highway performance.

Consideration of each component's importance to system performance can provide a much more rational basis for (a) establishing seismic strengthening priorities, (b) defining seismic design and strengthening criteria, and (c) estimating economic impacts due to component damage. It is important to remember that system performance issues are important to all regions of the U.S. that are at risk due to earthquakes. In recognition of this, system issues are now being incorporated into emerging methods for prioritizing bridge for seismic retrofit (Basöz and Kiremidjian, 1995; Moore et. al., 1995).

Volume I Strawman

The Volume I strawman contains the draft procedures for conducting a seismic risk assessment of highway networks and systems (Werner et. al., 1996). The procedures contained in this strawman provide a basis for addressing the above seismic performance issues. The procedures incorporate data and methodologies pertaining to engineering issues (structural, geotechnical, and transportation), repair and reconstruction, system network and risk analysis, and socio-economic considerations for impacts from system damage. They provide a mechanism to estimate system-wide direct losses (i.e., costs for repair of damaged components) and indirect losses due to reduced traffic flows and/or increased travel times (economic impacts).

The strawman provides (a) a detailed framework for carrying out deterministic and probabilistic evaluations of seismic risks to highway system; (b) the types of data needed to characterize the system, hazards, and components, together with the form of structural, geotechnical, and transportation engineering analysis results needed for these characterizations; (c) a rapid procedure for analysis of post-earthquake traffic flows based on artificial intelligence concepts and the current state of knowledge for traffic flow modeling; and (d) a socioeconomic module for characterizing economic, emergency response, and societal impacts of earthquake damage to highway systems. Key to the seismic risk analysis procedure are four GIS-based modules that act as pre-processors to the procedure in order to model the system, hazards, components, and socio-economics for the system. This modeling comprises the bulk of the effort in the application of the risk analysis procedure.

The strawman is organized into eight chapters, as follows:

Chapter 1 – Introduction (background and overview)
Chapter 2 – Seismic Risk Analysis Procedure (GIS data base, analysis procedure and treatment of uncertainties)
Chapter 3 – System Module (inventory and data, traffic management and system analysis procedures)
Chapter 4 – Hazards Module (earthquake ground motions, geologic hazard evaluation, liquefaction, landslides, and surface fault rupture)
Chapter 5 – Component Module (model development, seismic response evaluation, repair and reconstruction procedures)
Chapter 6 – Socio-Economic Module
Chapter 7 – Demonstration Seismic Risk Analysis
Chapter 8 – Conclusions (future viability of seismic risk analysis procedures and additional research needs)

The report also provides a brief appendix describing the requirements for, and necessary capabilities of, GIS as conceived for this highway system seismic risk analysis methodology.

Analysis Procedure

As described in the Volume I strawman, the analysis procedure consists of four primary steps: (1) initialization of the analysis; (2) development of simulations for the various scenario earthquakes; (3) incrementing the simulations and scenario earthquakes; and (4) aggregating the system analysis results.

Step 1 (initialization of the analysis procedure) is carried out in two parts. First, earthquake source models for the region are used to define an ensemble of scenario earthquakes that could affect the highway system being analyzed. Each earthquake is most commonly defined in terms of its magnitude, location, and frequency of occurrence. In some cases, additional seismo-tectonic parameters, such as orientation of the rupture surface or directivity of the rupture propagation, may also be estimated. Uncertainties in defining the values of the various earthquake inputs are also modeled at this stage. The second part of Step 1 involves identification of an adequate number of simulations for each scenario earthquake. In this procedure, "simulation" corresponds to one estimate of direct losses, traffic flows at various times after the earthquake, and any corresponding socio-economic impacts for the scenario earthquake.

Steps 2 and 3 provide the methodology for determining the n_i^{th} simulation for i^{th} scenario earthquake and uses it for each scenario earthquake. This methodology is based on evaluations of the hazard, direct loss and system state, traffic flows, and socio-economic impacts.

Step 4 is carried out after the system analyses for all simulations and scenario earthquakes have been completed. In this step, the results from all simulations and

earthquakes are aggregated and displayed. Depending on user needs, these aggregations can focus on the seismic risks associated with the total system or with individual components.

Example

A trial demonstration of the proposed seismic risk analysis procedure was conducted on the highway system in Memphis, Tennessee and the surrounding Shelby County (Werner and Taylor, 1995). The city of Memphis is located in the southwestern corner of Tennessee, bounded on the west by the Mississippi River. Because of its proximity to the New Madrid seismic zone, the potential seismic risks to the Memphis area are well recognized and have been studied extensively. The highway system evaluated under this demonstration includes the "beltway" system of interstate highways that surround the city, two crossings of the Mississippi River, major roads within the beltway, and roadways just outside the beltway that extend to important transportation, residential, and commercial centers to the south, east, and north. For example, just south of this roadway network is the Memphis Airport, which is the headquarters and principal transfer point for Federal Express. Figure 1a shows the overall highway network considered in this analysis, while figure 1b is an expanded view of the southern portion of this network. Figures 1a and 1b demonstrate the current state of traffic flows within the system, as designated by the number of traffic lanes open and available to traffic.

Four scenario earthquakes were used in this demonstration, representing a range of different moment magnitude levels and locations in the region. The system performance under each of these earthquakes is described in Werner and Taylor (1995). The results from one of these scenario earthquakes, showing the condition of the partial highway system 3 days and 6 months after the earthquake, is shown in figures 2a and 2b, respectively. A comparison of figures 2a and 2b with figure 1b shows that there was some reduction in traffic flow capacity immediately following the earthquake (i.e., at 3 days), but that most of the capacity was restored within 6 months.

Figures 3a and 3b expand a northeastern portion of the highway system. Figures 4a and 4b again provide the condition of this portion of the highway system 3 days and 6 months following the earthquake. In this region of the network, system damage is extensive and includes segments of highways completely closed following the earthquake. The analysis demonstrates that even after 6 months, there is still a substantial reduction in traffic capacity. There are two possible explanations for this higher level of damage and longer restoration time: first, this area is closer to the source earthquake, and second, the ground in this region may be more susceptible to liquefaction.

This example demonstrates the potential of a risk analysis procedure which includes the setting of priorities on rehabilitation and estimating future losses. The methodology used here has since been revised to improve both the accuracy and efficiency of the procedure. Further improvements, particularly to the bridge vulnerability models, are currently being implemented.

SCREENING, EVALUATION, AND RETROFITTING OF HIGHWAY BRIDGES

Background

In the late 1970s, the Applied Technology Council developed a set guidelines for the seismic retrofitting of highway bridges under FHWA sponsorship. These guidelines were published by the FHWA as the *Seismic Retrofitting Guidelines for Highway Bridges* in 1983 (FHWA, 1983). The guidelines represented what was then the state-of-the-art for screening, evaluating, and retrofitting seismically deficient bridges. At the time the guidelines were issued, the experience with highway bridge retrofitting was limited and many of the proposed techniques had not actually been demonstrated in the field. In the 10 - 15 years since that time, there has been significant progress in understanding the seismic response of bridges and the development of new and improved retrofitting technologies for bridge columns and footings, methods to stabilize soils to prevent liquefaction, and to ensure adequate connections between the bridge superstructure and substructure. Many of these advances in the state-of-the-art are the result of an aggressive research program which was started by the California Department of Transportation (Caltrans) following the Loma Prieta earthquake.

Current Retrofitting Guidelines

In order to capture these advances in seismic retrofitting and to make the current state-of-the-art available to bridge owners and engineers across the United States, the FHWA initiated a project to update the 1983 guidelines. This effort resulted in a new report titled *Seismic Retrofitting Manual for Highway Bridges*, which was published by the FHWA in 1995 (FHWA, 1995). The development of the new manual was conducted by NCEER as part of this overall seismic research program.

The new manual offers procedures for evaluating and upgrading the seismic resistance of existing highway bridges. Specifically, it contains:

- a preliminary screening process to identify and prioritize bridges that need to be evaluated for seismic retrofitting;
- a methodology for quantitatively evaluating the seismic capacity of an existing bridge and determining the overall effectiveness of alternative seismic retrofitting measures; and
- retrofit measures and design requirements for increasing the seismic resistance of existing bridges.

The manual does not prescribe requirements dictating when and how bridges are to be retrofitted. The decision to retrofit depends on a number of factors, several of which are outside the scope of the manual. These include, but are not limited to, the availability of funding and political, social, and other economic considerations. The primary focus of the manual is directed towards providing guidance on the engineering factors for seismic retrofitting.

In effect, the 1995 FHWA manual is the strawman for the second part of the three-volume seismic retrofitting manual. At the current time, a number of studies are being conducted within the NCEER seismic research program and by others including Caltrans and

FHWA to improve evaluation and retrofit methods for highway bridges. The final version of Volume II will be based on this 1995 FHWA manual and the results of these ongoing studies.

SCREENING, EVALUATION, AND RETROFITTING OF RETAINING STRUCTURES, SLOPES, TUNNELS, CULVERTS, AND PAVEMENTS

Background

Current national seismic standards in the United States are primarily limited to design and retrofitting provisions for highway bridges. However, the typical highway system is composed of a number of major structural and geotechnical components, which include retaining structures, slopes (cuts and fills), tunnels, culverts, and pavements. In addition, a typical highway system also contains other functional structural elements such as sound walls, sign and light structures (on towers or sign bridges), and motorist service facilities. While these other functional elements are widespread, the potential impact on traffic flow from their failure during an earthquake is expected to be limited. However, traffic flow impacts from the failure of the other major structural and geotechnical components during an earthquake could be as severe as that shown historically by the failure of highway bridges.

As a result, the third part of the seismic retrofitting manual (Volume III) will focus on the development of screening, evaluation, and retrofitting methods and technologies for retaining structures, slopes, tunnels, culverts, and pavements. Over time, individual structures have been evaluated and retrofitted on a case-by-case basis. Much of this experience, however, is fragmented and not well-documented. This volume is expected to be the first major effort to capture the necessary aspects of screening, evaluation, and retrofitting and present the results in a formal, procedural manner.

Volume III Strawman

Unlike highway bridges, there is no precedent for a manual for screening, evaluation, and retrofitting of retaining structures, slopes, tunnels, culverts, and pavements. The first step, then, in such a development was the preparation of a strawman or draft document. As noted earlier, the strawman is intended to summarize the current state of knowledge and practice for these highway system components, incorporate current research results, and identify important gaps in knowledge or the need for additional research necessary to complete Volume III.

The draft strawman is composed of five sections (one for each highway component covered in the document)(NCEER, 1996). Topics covered within each section are the classification of the component, and the seismic vulnerability screening, evaluation, and retrofitting of each component. Material common to multiple components is contained within the section for that component. In the final version of Volume III, such common material may be moved to an introductory section of the manual.

Screening, Evaluation, and Retrofitting of Tunnels

An example of the coverage for one highway component is that for highway tunnels, in Section V of the Volume III strawman. Tunnels can be classified into two broad categories, bored tunnels or cut-and-cover tunnels. Each category of tunnel exhibits distinctly different design features and construction methods.

Bored tunnels are constructed by excavating the opening and constructing the support system below ground. They may be constructed in a variety of geologic environments, ranging from hard rock to soft soils. Construction techniques involve the use of tunneling machines or other underground excavation methods such as drilling and blasting. The lining/support system is usually constructed as the tunnel is excavated. The cross-sectional shape of these tunnels is usually circular or semi-circular. Bored tunnels are constructed in soft ground by either a two-pass or one-pass lining method, while tunnels bored in rock use methods of support that vary from none (in massive hard rock) to the installation of temporary ribs and lagging liners, followed by cast-in-place final concrete liners.

Cut-and-cover tunnels, meanwhile, are constructed by excavating the opening from the ground surface, constructing the tunnel structure within the excavated opening, and backfilling above the top of the structure and adjacent to the sides of it, if it has not been constructed immediately against the excavation face. This method of construction is used for shallow tunnels. The structure shape in this case is typically rectangular and is constructed of reinforced concrete.

Screening, evaluation, and retrofitting of these two types of tunnels will, by their nature, need to reflect the different excavation and construction methods, and construction materials. The objectives of screening tunnels is to identify those that have a substantial risk of poor performance during an earthquake. For tunnels identified by the screening process as having a significant risk, and either requiring further evaluation to assess the degree of deficiencies or obviously in need of retrofitting, the decision as to whether to conduct further evaluations and retrofit design and the priority for such actions will depend on the importance of the tunnel as established by the owning agency.

In terms of screening, the strawman identified a number of factors which could influence seismic performance, including:

- seismic hazard – considers the intensity of ground shaking, fault rupture, landsliding, and soil liquefaction.
- geological conditions – considers soft soils, rocks with weak planes intersecting a tunnel, failures encountered during tunnel construction that may have weakened geologic formations, and squeezing ground.
- tunnel design, construction, and condition – whether seismic loadings were considered in its design, the nature of the tunnel lining and support system, the history of static tunnel performance (failures, cracking, or distortion), and the current condition of the lining and support system.

It has been noted that the seismic performance of shallow cut-and-cover and box-like tunnels has been relative poor, in comparison to the performance of bored tunnels. As a result, additional guidelines and provisions are provided for these tunnel types.

Evaluation procedures are provided for vibratory ground shaking, fault rupture displacement, landsliding, and liquefaction. Analytical procedures include closed-form equations and numerical analysis techniques, depending on the type and form of the tunnel. For example, figure 5 shows the various approaches that can be used for seismic analysis based on tunnel cross-section.

Retrofitting strategies are provided for tunnels likely to fail by ground shaking, fault displacement, and landsliding or liquefaction. However, the retrofit measures are dependant on the type of tunnel (bored or cut-and-cover), and on the damage mode identified by the screening and evaluation procedures. Among the retrofitting strategies discussed are the following:

- addition of grout behind a concrete lining, if it is in poor shape or in poor contact with the geologic media behind the lining.
- strengthening or stiffening the lining for cases where excessive ovaling and expected failure of the tunnel cross-section may occur.
- providing additional flexibility and circumferential joints in the lining for situations where excessive axial or bending stresses are predicted.
- addition of reinforcement to existing linings or steel plate jackets to linings and columns for cut-and-cover tunnels.
- enlarging the tunnel opening in situations where large fault displacements are anticipated, or adding articulation of the tunnel liner with ductile joints if the expected displacements are small.
- stabilizing the soil around the tunnel if landslides or liquefaction are expected to affect the tunnel.

SUMMARY

The development of the "Seismic Retrofitting Manual for Highway Systems" is a major component of the NCEER research program being conducted for the FHWA. It is expected that a draft of the complete manual will be prepared in mid-1998 and that the final version will be available in mid-1999.

However, in the interim, the three-volume strawman for the seismic retrofitting manual will provide the basis for focussing additional research in areas where current knowledge is considered insufficient, and can act as a guide for agencies embarking on a program to evaluate the seismic vulnerability of highway systems today.

ACKNOWLEDGEMENTS

Work on the Volume I strawman was conducted under the coordination and direction of Stuart D. Werner, with assistance from Craig E. Taylor, James E. Moore II, and Masanobu

Shinozuka. The Volume III strawman was coordinated by Maurice S. Power with the assistance of Geoffrey R. Martin, and sections of the strawman were prepared by Rowland Richards, Kenneth Fishman, Faiz Makdisi, Maurice S. Power, Dario Rosidi, Jon Kaneshiro, Samuel C. Musser, and T. Leslie Youd.

REFERENCES

Basöz, N. and Kiremidjian, A. (1995). *Prioritization of Bridges for Seismic Retrofitting*, Technical Report NCEER-95-0007, National Center for Earthquake Engineering Research, Buffalo, New York.

FHWA (1983). *Seismic Retrofitting Guidelines for Highway Bridges*, Report No. FHWA/RD-83/007, U.S. Department of Transportation, Federal Highway Administration, McLean, Virginia.

FHWA (1995). *Seismic Retrofitting Manual for Highway Bridges*, Publication No. FHWA-RD-94-052, U.S. Department of Transportation, Federal Highway Administration, McLean, Virginia.

Hobeika, A.G., Manchikalapudi, L.N., and Kim, S. (1991). *Transportation Problems Faced after Big Earthquakes: A Case Study of the Loma Prieta Earthquake*, the Center for Transportation Research, Virginia Polytechnic Institute and State University, Blacksburg, Virginia.

Moore, J.E., Kim, G., Xu, R.X., and Cho, S. (1995). *Evaluating System ATMIS Technologies via Rapid Estimation of Network Flows*, MOU-120 Draft Interim Report, California PATH Program, University of California Research Report Nos. VKC-351 and MC-0042, University of Southern California, Los Angeles, California.

NCEER (1996). *Seismic Retrofitting Manual for Highway Systems: Volume III Strawman – Screening, Evaluation, and Retrofitting of Retaining Structures, Slopes, Tunnels, Culverts, and Pavements*, sections contributed by R. Richards, K. Fishman, F. Makdisi, M. Power, D. Rosidi, J. Kaneshiro, S. Musser, and T.L. Youd, National Center for Earthquake Engineering Research, Buffalo, New York.

Wakabayashi, H. and Kameda, H. (1992). "Network Performance of Highway Systems Under Earthquake Effects: A Case Study of the 1989 Loma Prieta Earthquake," *Proceedings of the U.S.-Japan Workshop on Earthquake Disaster Prevention for Lifeline Systems*, Public Works Research Institute, Tsukuba Science City, Japan.

Werner, S.D. and Taylor, C.E. (1995). *Demonstration Seismic Risk Analysis of Highway/Roadway System in Memphis, Tennessee*, Interim Year 2 Report for Task 106-E-7.3.1, National Center for Earthquake Engineering Research, Buffalo, New York.

Werner, S.D., Taylor, C.E., and Moore, J.E. (1996). *Seismic Risk Analysis of Highway/Roadway Systems*, Volume I Strawman Report, prepared for National Center for Earthquake Engineering Research, Buffalo, New York.

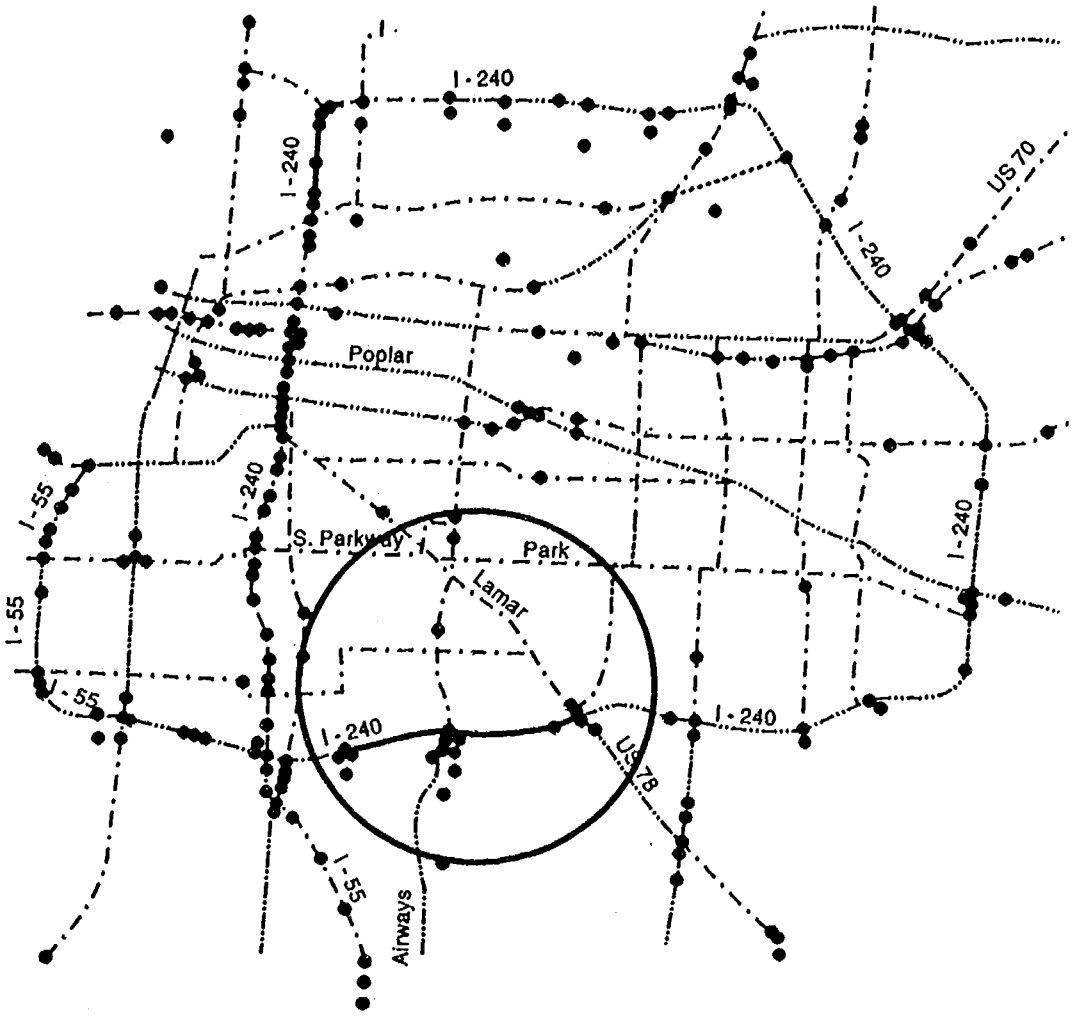


Figure 1a. Memphis and Shelby County Tennessee - Current Highway Network and Traffic Capacity (based on Werner and Taylor, 1995)

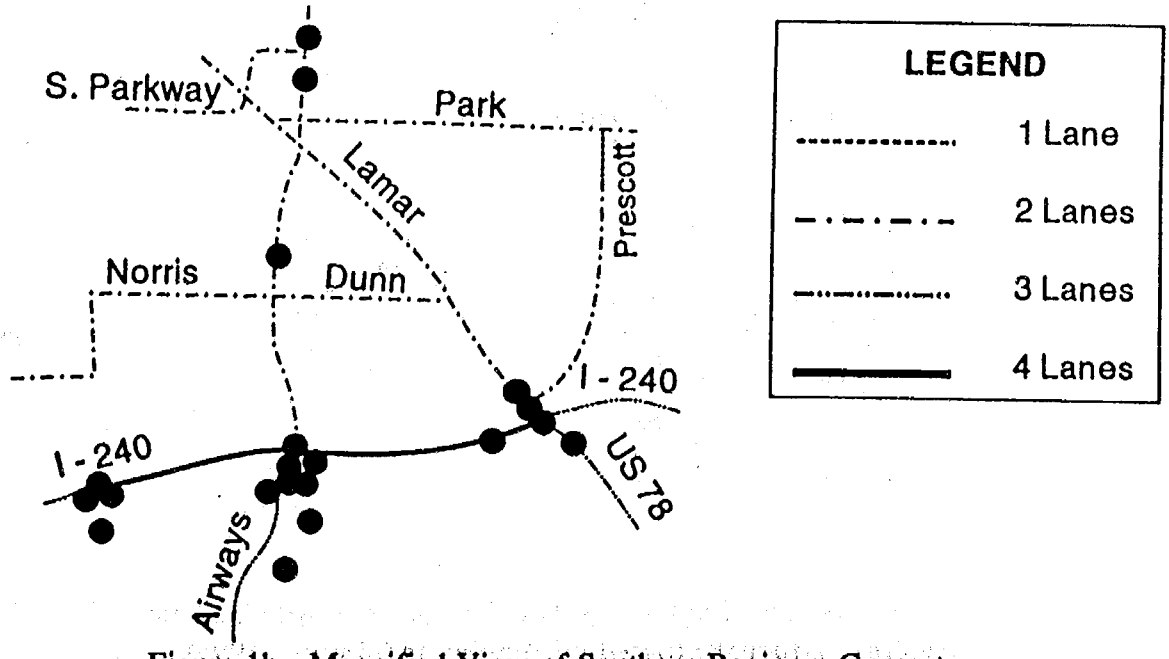


Figure 1b. Magnified View of Southern Region - Current Network Capacity (based on Werner and Taylor, 1995)

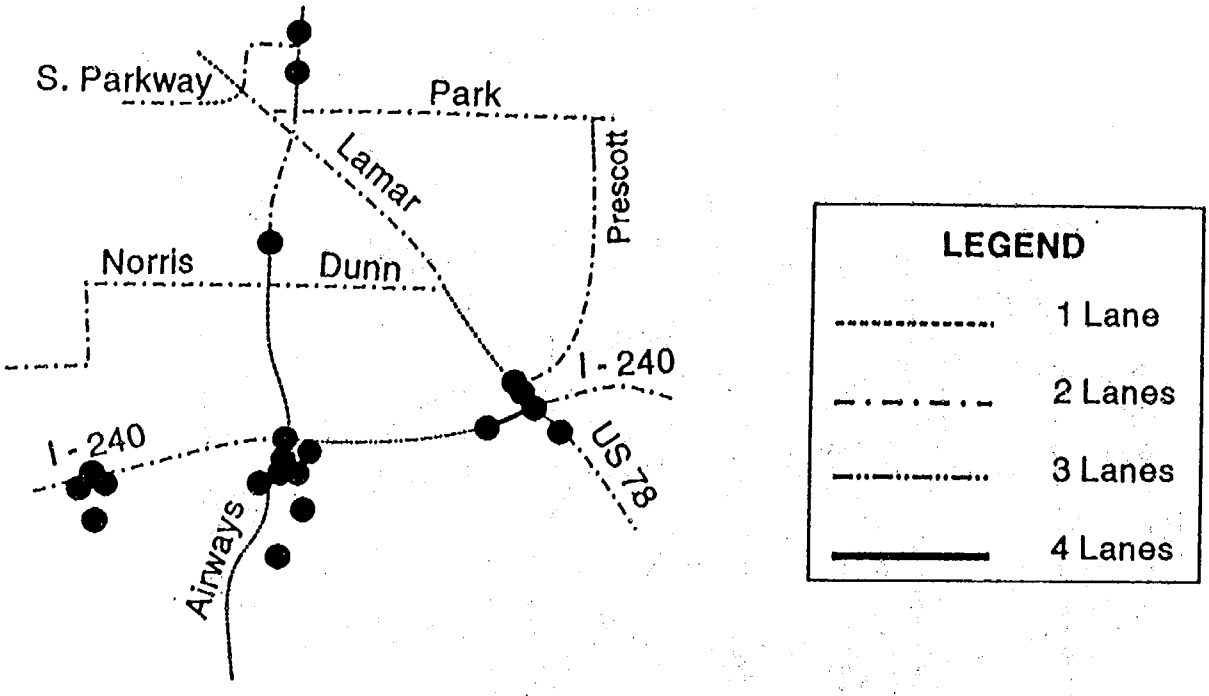


Figure 2a. Southern Region – Network Capacity 3 Days After Scenario Earthquake (based on Werner and Taylor, 1995)

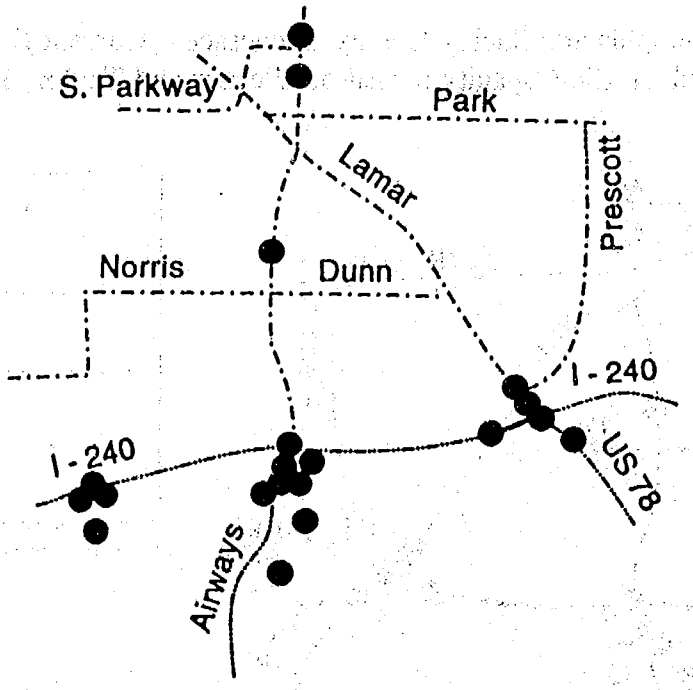


Figure 2b. Southern Region – Network Capacity 6 Months After Scenario Earthquake (based on Werner and Taylor, 1995)

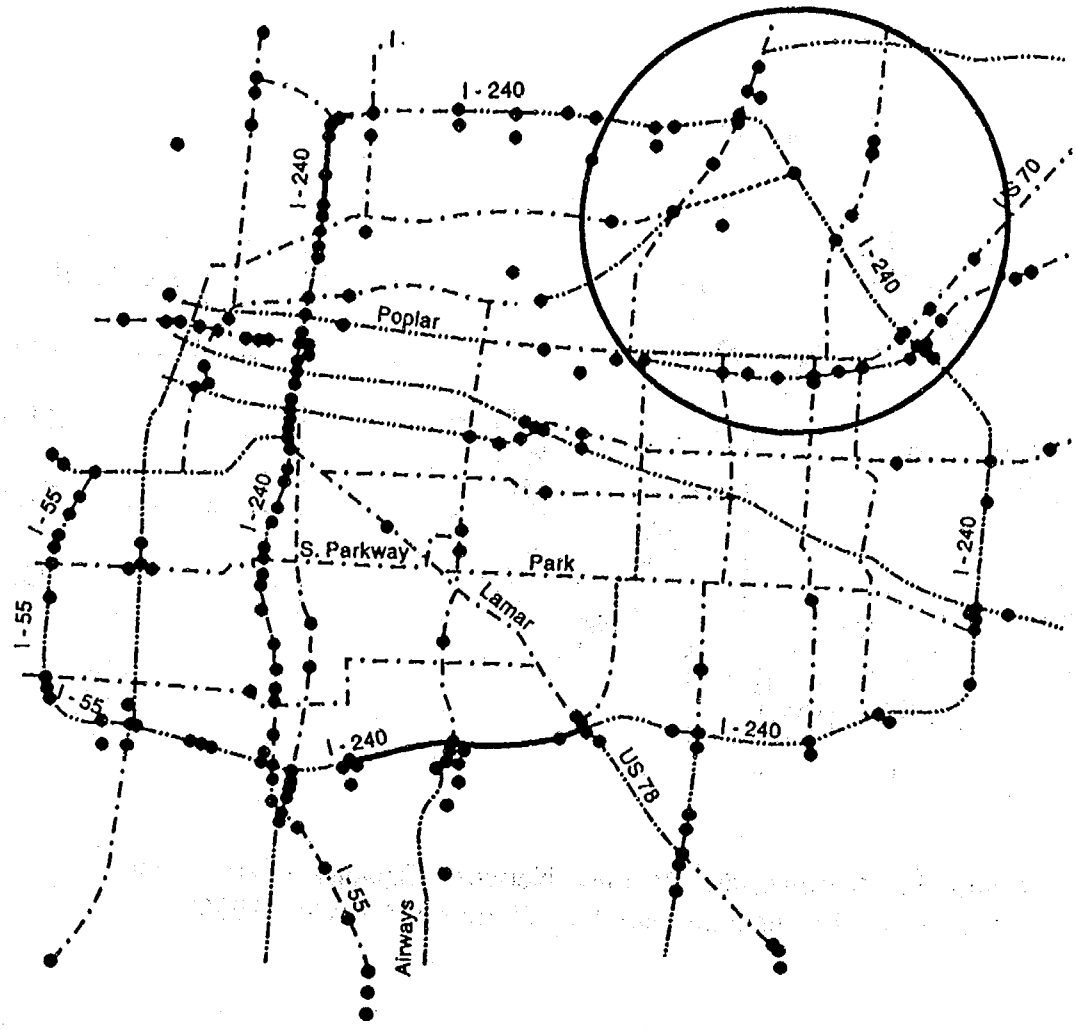


Figure 3a. Memphis and Shelby County Tennessee - Current Highway Network and Traffic Capacity (based on Werner and Taylor, 1995)

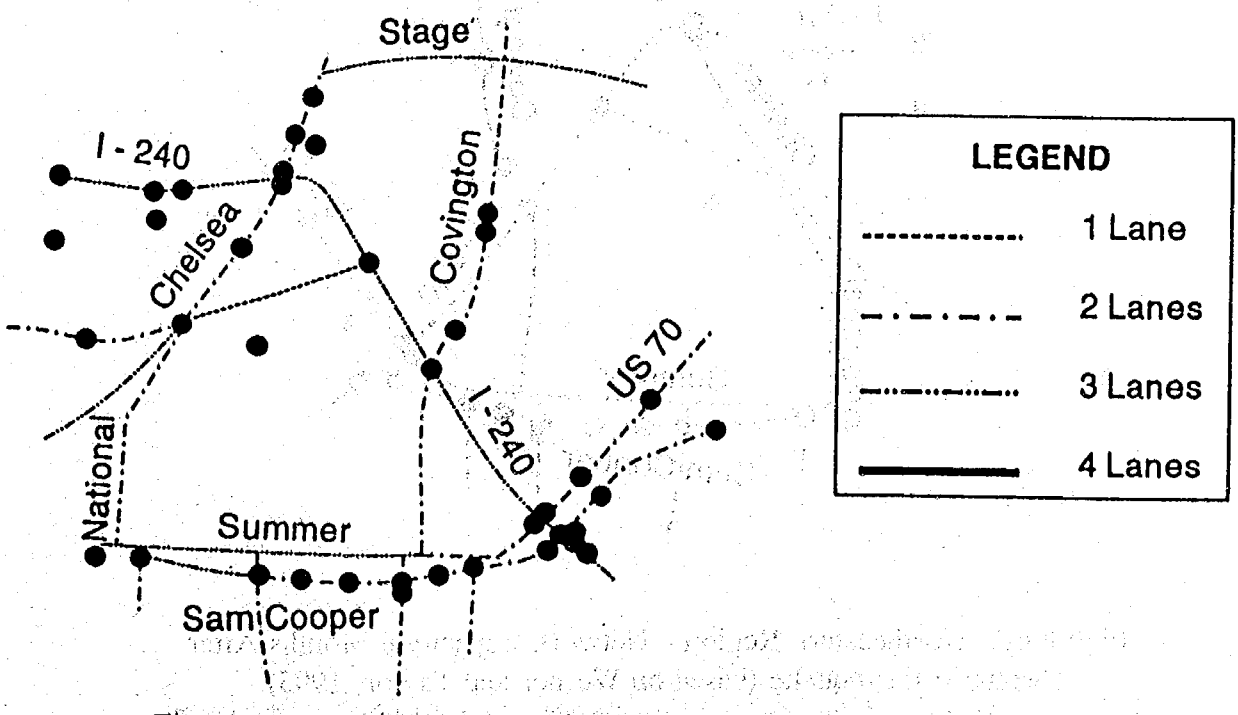


Figure 3b. Magnified View of Northeastern Region - Current Network Capacity (based on Werner and Taylor, 1995)

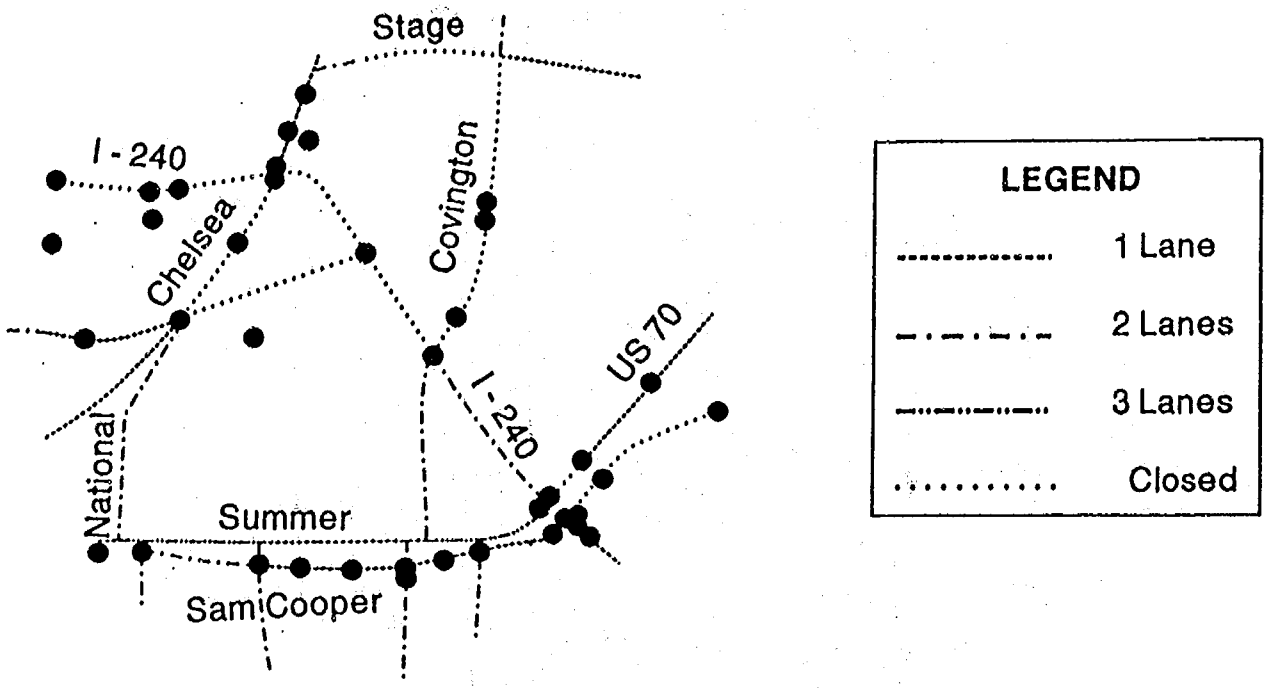


Figure 4a. Northeastern Region - Network Capacity 3 Days After Scenario Earthquake (based on Werner and Taylor, 1995)

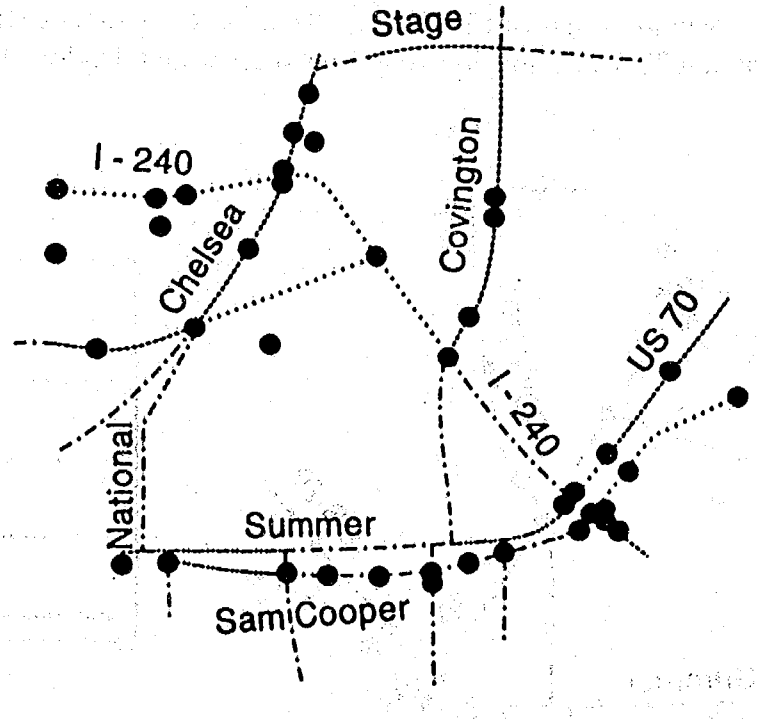


Figure 4b. Northeastern Region - Network Capacity 6 Months After Scenario Earthquake (based on Werner and Taylor, 1995)

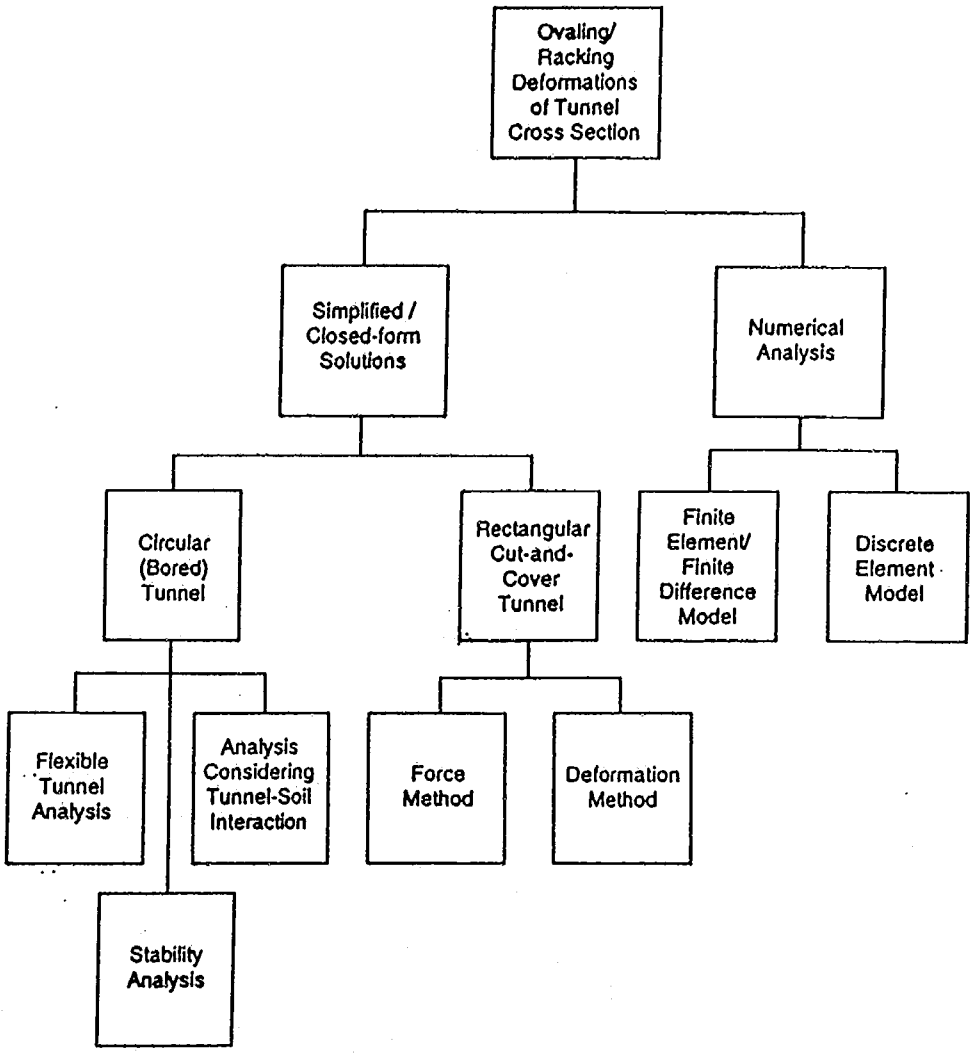


Figure 5. Recommended Seismic Analysis Methods Based on Tunnel Cross-section (from NCEER, 1996)



USE OF TRANSPORTATION NETWORK SYSTEMS FOR BRIDGE RETROFIT PRIORITIZATION AND EMERGENCY RESPONSE

Anne S. Kiremidjian and Nesrin I. Basöz
The John A. Blume Earthquake engineering Center
Stanford University
Stanford, CA 94305

ABSTRACT

Complex transportation systems analysis methods are imbedded in a general seismic risk analysis methodology to develop an approach for prioritizing the seismic retrofit of large number of bridges and for an emergency response system. The prioritization and emergency response methods are applied to the Palo Alto, California area. The prioritization of the bridges is consistent with their seismic exposure and their importance within the transportation system. Critical routes within the system are identified and minimal paths are delineated for hypothetical earthquake events affecting the study region.

INTRODUCTION

Seismic risk assessment methods are particularly suitable tools for scheduling the retrofit of large number of bridges and for the development of emergency response strategies immediately following major earthquake events. Most currently available prioritization schemes consider the seismic exposure, the vulnerability and the importance of a bridge in ranking for seismic retrofitting decisions. General seismic risk analysis methods can be used for the seismic exposure and vulnerability analysis components of prioritization. Most currently available bridge retrofit prioritization methods consider these components (e.g., Buckle [1]; Maffei [2]; Gilbert[3]). The importance of a bridge is defined in terms of several parameters such as the average daily traffic, route type, lifeline, multi-level structure, and detour length. While most of the prioritization methods consider these parameters to assess the importance of a bridge, they do not reflect how important is a bridge for emergency response purposes or for long-term economic recovery following a major earthquake event.

A new method for bridge prioritization was proposed by Basöz [4], which utilizes transportation network systems analysis to quantify the importance of a bridge for bridge prioritization purposes. Geographic information systems (GIS) are used in the methodology to determine the seismic hazard and vulnerability of bridges. Multi-attribute decision theory is used to combine the seismic vulnerability and importance of each bridge.

As part of the transportation network analysis system, a new multiple origin-multiple destination emergency routing algorithm is developed that can be utilized for

emergency response purposes. Most currently available network algorithms used in emergency response applications consider only single origin-single destination networks. Multiple origin-multiple destination network systems are a critical component in any resource allocation decisions and are particularly important for allocation of emergency vehicles and crews following a major earthquake or other disaster.

In order to illustrate the prioritization method and the network analysis for emergency response purposes, the methodology presented in this paper is applied to the City of Palo Alto in California. The bridges in the city are prioritized according to their seismic vulnerability and importance within the transportation network system. In addition the potential damage to bridges in the area is estimated for a scenario event on the San Andreas fault and emergency routes are identified based on the availability of bridges that remain functional following the event.

RISK ASSESSMENT METHODOLOGY

A risk assessment and mitigation methodology for highway transportation systems can be performed for the purpose of (Basöz [4]):

- retrofit of existing bridges and other components of the systems;
- pre-disaster emergency response planning;
- emergency response management immediately following a disaster.

Figure 1 shows the main components of a bridge risk assessment and mitigation system. These include (a) vulnerability analysis, (b) consequence (importance) analysis and (c) decision support systems. The consequence analysis will vary depending on the mitigation strategy being considered. The focus of this paper is on bridge prioritization and emergency response methods as they apply to highway transportation systems. It should be noted, however, the methodology is general and can be applied to other lifeline systems and with some modifications to complex industrial systems.

Bridge Prioritization Methodology

A bridge prioritization scheme is an ordering of a set of bridges $B = \{B_1, B_2, \ldots, B_N\}$, where B_i is the ith bridge and N is the total number of bridges in the system. The bridges in the set B are ranked in decreasing order $R_1 > R_2 > \ldots > R_N$ where the bridge B_1 is the highest ranking bridge and should be retrofitted first. The ranking depends on the vulnerability and importance of each bridge given by

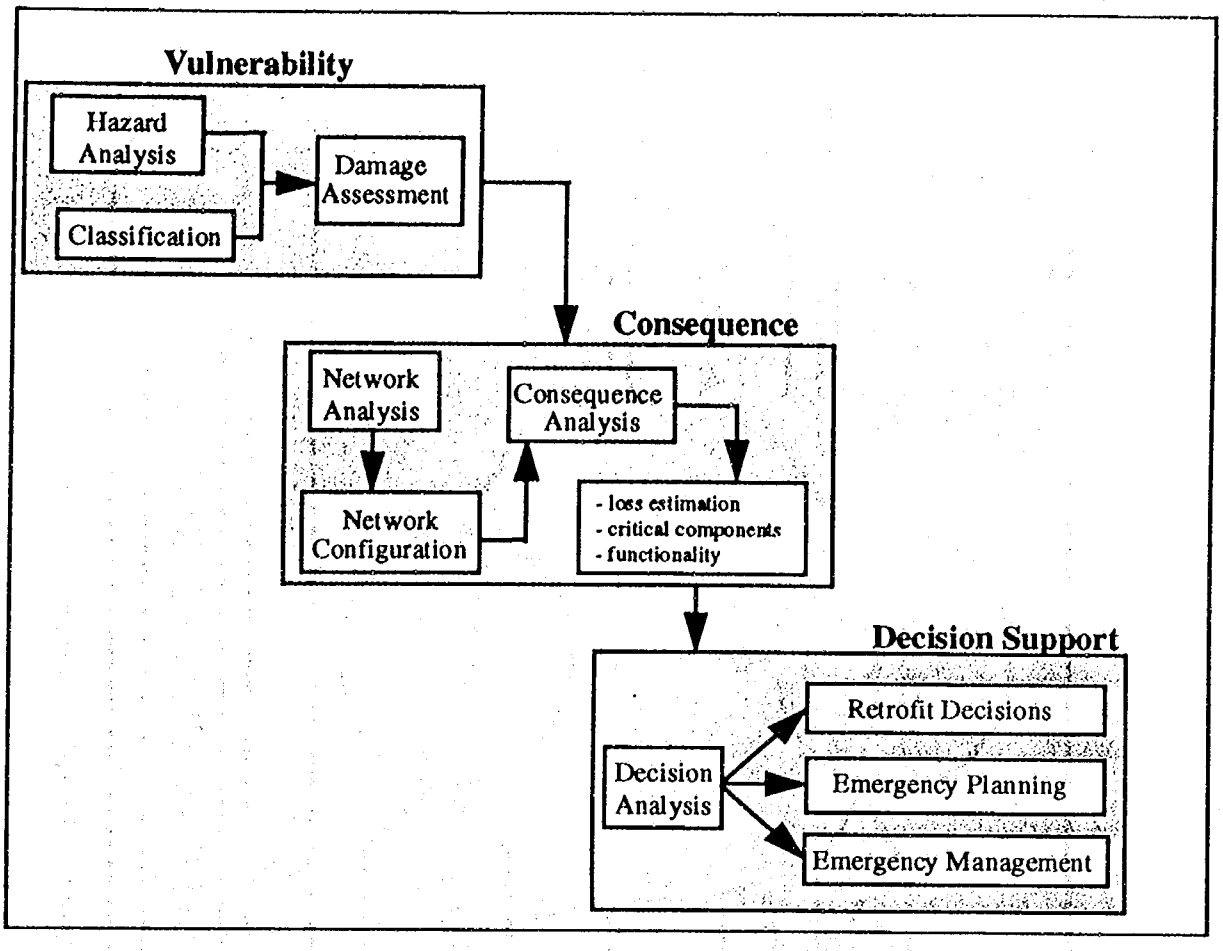


Figure 1. Components of a Risk Analysis and Mitigation System.

$$R_i = f(V_i, I_i) \tag{1}$$

where V_i and I_i denote respectively the vulnerability and importance of bridge i. Figure 2 shows the main components of the bridge prioritization methodology and the steps in vulnerability and importance assessment.

The vulnerability of a bridge is a function of the seismic hazard at the site and the earthquake resistance of the bridge. The seismic hazard at the site will depend on the seismo-tectonic characteristics of the region, the frequency of earthquake events, the largest magnitude of earthquakes on each fault, the distance from each fault to the site of the bridge and the local soil and topographic conditions.

The vulnerability of bridges will depend on several bridge attributes such as material, structural system, and year of construction. The vulnerability of a bridge is most frequently expressed in the form of a fragility function defined as the probability of exceeding a specified damage state as a function of different earthquake ground motion

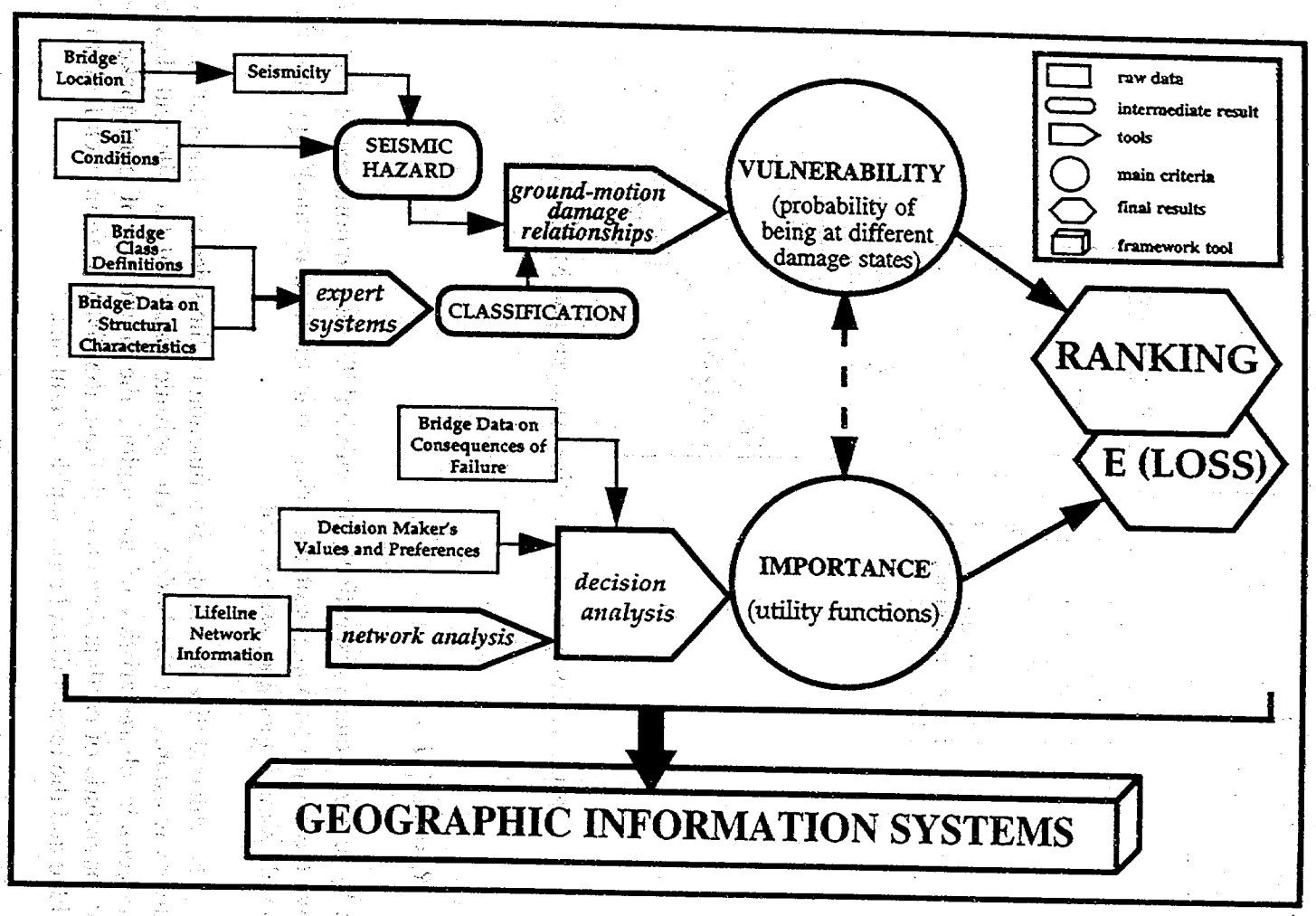


Figure 2. Components of the Prioritization Methodology

severity levels. Alternatively, the vulnerability can also be expressed as the probability of being in a particular damage state as a function of the ground motion severity. For prioritization purposes, it is necessary to obtain fragility functions for all the bridges within the transportation system. A more frequent approach, however, is to classify bridges into a finite set of categories and then develop fragility curves for these generic categories. Simple bridge classifications are included in ATC-13 [5] and NIBS [6]. A comprehensive bridge classification category was developed by Basöz and Kiremidjian [7]. In their classification a hierarchical scheme is used for the bridge attributes and bridges are grouped into categories according to their component and systems properties.

In general the vulnerability of a bridge is given in terms of the expected damage to the bridge due to all possible events over the life of the transportation system. The expected damage of the bridge is given by:

$$E_i[D] = \sum_D \int_A d_r \cdot P[D = d_r | a] \cdot \frac{d}{da}[1 - P[A > a,(0,t)]] \cdot da \tag{2}$$

where

$$\begin{aligned} P[A > a,(0,t)] &= P[\text{seismic hazard parameter } A \text{ will exceed level } a \text{ at least once in time } (0,t)] \\ &= \iiint_{\varepsilon R M} \nu_M \cdot f_{\hat{\varepsilon}|R,M}(\varepsilon|R,M) \cdot f_{R|M}(r|M) \cdot f_M(m) \cdot dm \cdot dr \cdot d\varepsilon \end{aligned} \tag{3}$$

The importance criterion for a bridge B_i is expressed as follows:

$$I_i = f_3(S_i, E_i, G_i, L_i, Q_i, H_i) \tag{4}$$

where:

S_i = life safety factor for bridge B_i
E_i = emergency response factor for bridge B_i
G_i = long-term economic factor bridge B_i
L_i = interaction with other lifelines carried on bridge B_i
Q_i = location of bridge B_i with respect to defense routes
H_i = historical significance of bridge B_i.

A decision model is developed to combine these factors into a multi-attribute importance criterion. The value model used to quantify the consequences from each factor considered in the decision model is expressed as follows:

$$u(I) = \sum_x k_X u_X(x) \tag{5}$$

where:

$u(I)$ = utility function of the importance criterion,

x = one of the importance criterion factors: S, E, G, L, Q and H as defined in equation (4),

k_X = scaling constant for the importance criterion factor X, and $\sum_X k_X = 1$,

$u_X(x)$ = utility function for the importance criterion factor X.

The value and risk preferences of the decision maker are assessed through utility functions and scaling constants defined for each of the importance factors. For the life safety attribute S, the defense route factor Q, and the historical significance factor H, single attribute utility functions are developed. The utility values for each bridge are obtained from these utility functions. The higher the utility value (u-value) assigned, the more important is the bridge with respect to the given factor X.

For the emergency response factor, E, the utility value is calculated on two levels. In level one, critical bridge sets are defined as the set of bridges that would interrupt the connectivity between a disaster area and available resource location. Such critical bridge sets are identified for bridges within a system and a u-value is assigned to each set. A rank order is then assigned to each bridge set. Then the bridges within each critical bridge set are ranked. For this second level ranking travel times and spatial importance attributes are used in the prioritization.

A connectivity network analysis algorithm, **CAFER**, was developed by Basöz [4] for (a) identifying critical bridge sets, (b) determining time delays due to bridge damage, and (c) calculate the spatial importance of bridges in a system.

The vulnerability and importance criteria are combined through their respective utility functions as follows:

$$\hat{U}_{B_i} = k_V u_V(V_i) + k_I u(I_i) \tag{6}$$

where:

$\hat{U}_{B_i}$ = u-value for bridge B_i to be used in obtaining R_i,

k_V = scaling constant for vulnerability,

k_I = scaling constant for importance,

$u_V(V_i)$ = u-value for vulnerability of bridge B_i, and

$u(I_i)$ = u-value for importance of bridge B_i.

Network Analysis For Emergency Response

Immediately following an earthquake, it is important to determine the connectivity of a transportation system, to identify all routes that are available and to estimate time delays. Such information is of critical importance for emergency response and for developing optimal resource allocation strategies. As part of the overall risk mitigation program a network analysis method is developed that addresses the issues of system connectivity, availability of different routes and time delay estimation.

For this purpose, the system is modeled as a directed network with nodes and arcs and specified origin and destination points. The arc and path length in a highway system network might, in general, represent distance or travel time between nodes. For emergency response applications travel time rather than travel distance is used to describe both the arc and the path lengths, since the shortest distance from any origin to a destination does not necessarily constitute the fastest route after a major event. The arc can represent roads or bridges in the system.

The state of the system immediately following an earthquake event is evaluated using the information from the vulnerability analysis. For emergency response purposes, only two states for each arc are possible functional or nonfunctional. Thus, bridges that are severely damaged or have collapsed are considered to be functional. Bridges with minor or moderate damage are considered functional. Basöz [4] developed a network analysis algorithm for connectivity analysis for emergency response (**CAFER**). The **CAFER** model (a) identifies critical arc sets or cut sets in a network, (b) determines the fastest paths and the associated travel times, and (c) determines the spatial importance of each arc in the network.

A set of arcs is defined as critical if the origin and destination points are disconnected when all the arcs in the set are removed from the network. Well known shortest path algorithms are utilized to determine the connectivity of the system. In addition, the shortest path is used to define a directed path from an origin to a destination with minimum total length or travel time. Critical arcs are determined by removing successively arcs until all the paths that initially existed cease to exist. In contrast, if the connectivity between the origin-destination points is retained after removing a set of arcs from the network, then the algorithm finds the fastest path and calculates the travel time. The frequency of observing different critical sets and different fastest paths in all possible configurations of the network are calculated from the results of the shortest path algorithm.

EXAMPLE APPLICATION

The risk assessment and mitigation methodology was applied to several regions in California. In this paper the application to the City of Palo Alto is included for illustrative purposes. There are 11 state and 36 local bridges within the city limits of Palo Alto, California. Four of these bridges are either pedestrian or railroad bridges thus they are excluded from the analysis. The CALTRANS database on structural attributes was used to classify the bridges into NIBS [6] bridge classes. Several earthquake scenarios were considered and the results from a hypothetical earthquake of magnitude 8.0 on the San Andreas fault are included in this paper. Figure 3 shows the horizontal ground surface peak ground accelerations throughout the City of Palo Alto (from Kiremidjian et al, [8]). In addition a probabilistic seismic hazard analysis is performed which considers the contribution of all faults and all possible magnitude events on each fault.

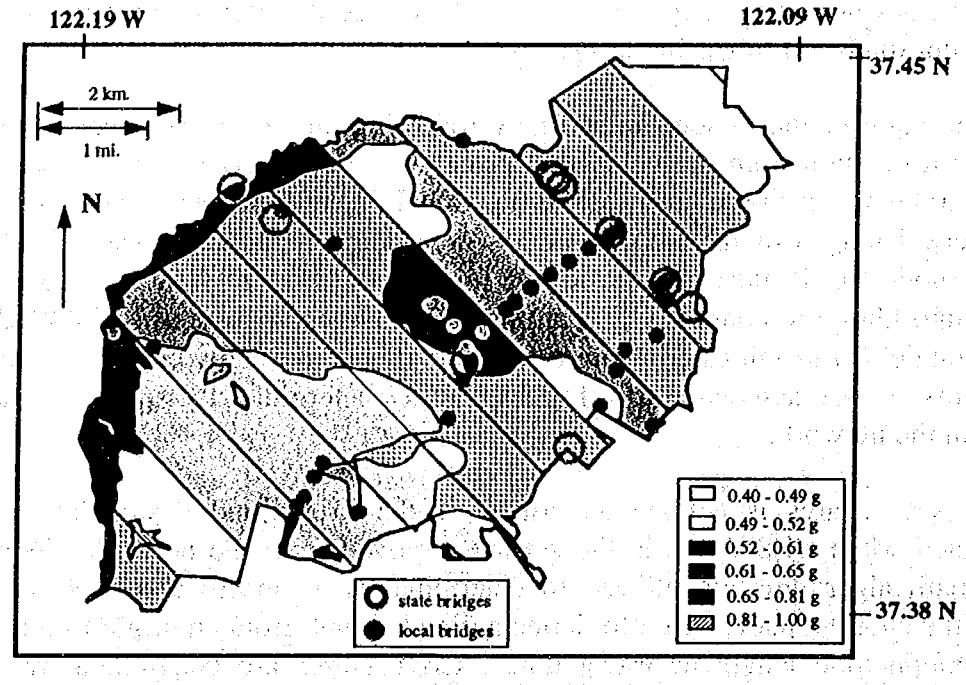


Figure 3. Surface Peak Ground Acceleration in Palo Alto for Magnitude 8.0 Earthquake on the San Andreas Fault (Kiremidjian et al. [8])

Table 1 shows the prioritization of the bridges in Palo Alto for the scenario event and the probabilistic seismic hazard analysis. In addition the critical paths following the scenario event are shown with a single origin-destination pairs and with multiple origin single destination combinations. Figures 4 and 5 show Stanford Hospital as the origin, and Palo Alto Airport as the destination. The original route and two alternate routes are identified on each of these figures where the alternate routes are determined after critical bridges in the system fail under a magnitude 8.0 event on the San Andreas fault. Figures 6 and 7 show the available emergency routes from two origins (Stanford Hospital and the Veterans Administration Hospital) to a hypothetical high damage area in the city.

Table 1. The u-values and Rank Order for Bridges in the City of Palo Alto, California

	Probabilistic		*Scenario*	
Bridge No. *i*	$\hat{U}_{B_i}$	**rank no**	$\hat{U}_{B_i}$	**rank no**
37 0150	0.8452	1	0.7865	1
37 0149	0.7962	2	0.7172	2
37 0146	0.7935	3	0.7146	3
37 0040	0.7178	4	0.6867	4
37 0174	0.6928	5	0.6618	5
37 0092	0.5927	6	0.5716	6
37C0001	0.4951	7	0.4602	8
37 0017	0.4782	8	0.4629	7
37C0189	0.4521	9	0.4429	9
37 0018	0.4467	10	0.4351	10
37C0005	0.4390	11	0.3742	22
37 0016	0.4356	12	0.4039	15
37C0151	0.4344	13	0.4274	11
37C0179	0.4321	14	0.4251	12
37C0188	0.4309	15	0.4238	13
37C0224	0.4261	16	0.4139	14
37C0346	0.4096	17	0.3911	17
37C0072	0.3970	18	0.3759	21
37C0766	0.3947	19	0.3916	16
37C0073	0.3906	20	0.3694	25
37C0226	0.3888	21	0.3765	20
37C0767	0.3886	22	0.3624	27
37C0225	0.3859	23	0.3788	18
37C0152	0.3858	24	0.3787	19
37C0223	0.3856	25	0.3707	23
37 0155K	0.3854	26	0.3065	37
37C0771	0.3853	27	0.3704	24
37C0187	0.3841	28	0.3638	26
37C0369	0.3792	29	0.3529	28
37C0371	0.3731	30	0.3492	29
37C0370	0.3581	31	0.3223	30
37C0059	0.3555	32	0.3069	36
37C0060	0.3500	33	0.3013	38
37C0770	0.3485	34	0.3103	35
37C0769	0.3481	35	0.3218	31
37C0768	0.3471	36	0.3207	32
37C0372	0.3469	37	0.3111	33
37C0222	0.3466	38	0.3108	34
37C0221	0.3463	39	0.2976	39
37C0560	0.2846	40	0.2196	41
37C0561	0.2846	41	0.2196	42
37C0558	0.2846	42	0.2544	40
37C0559	0.2846	43	0.2196	43

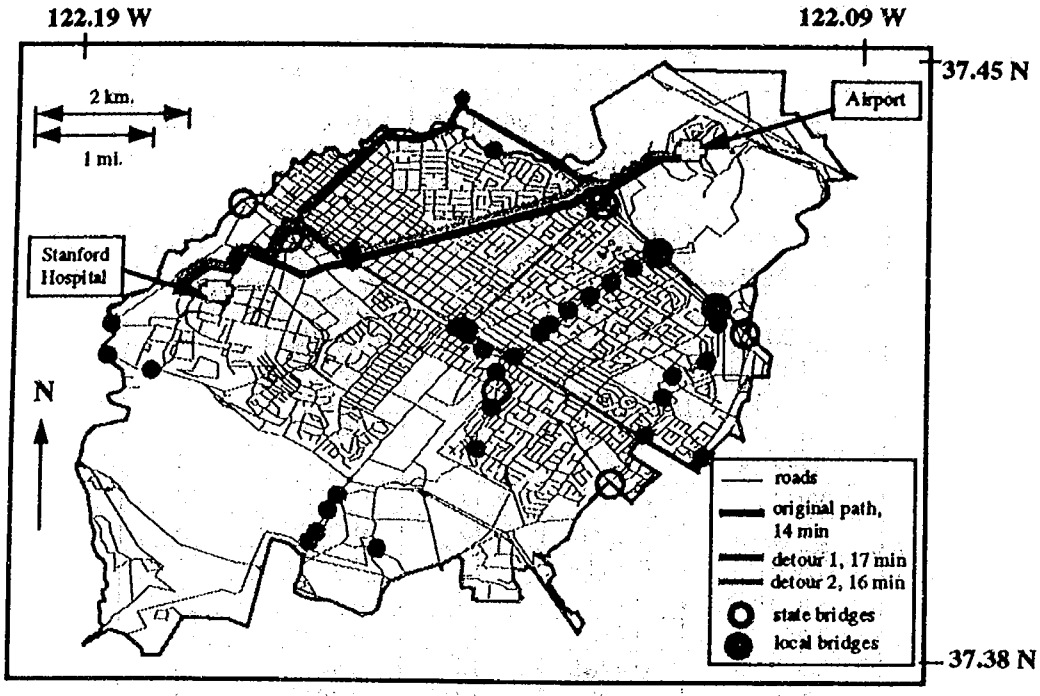


Figure 4. Fastest Paths and Travel Times in Minutes for *OD* Set 1

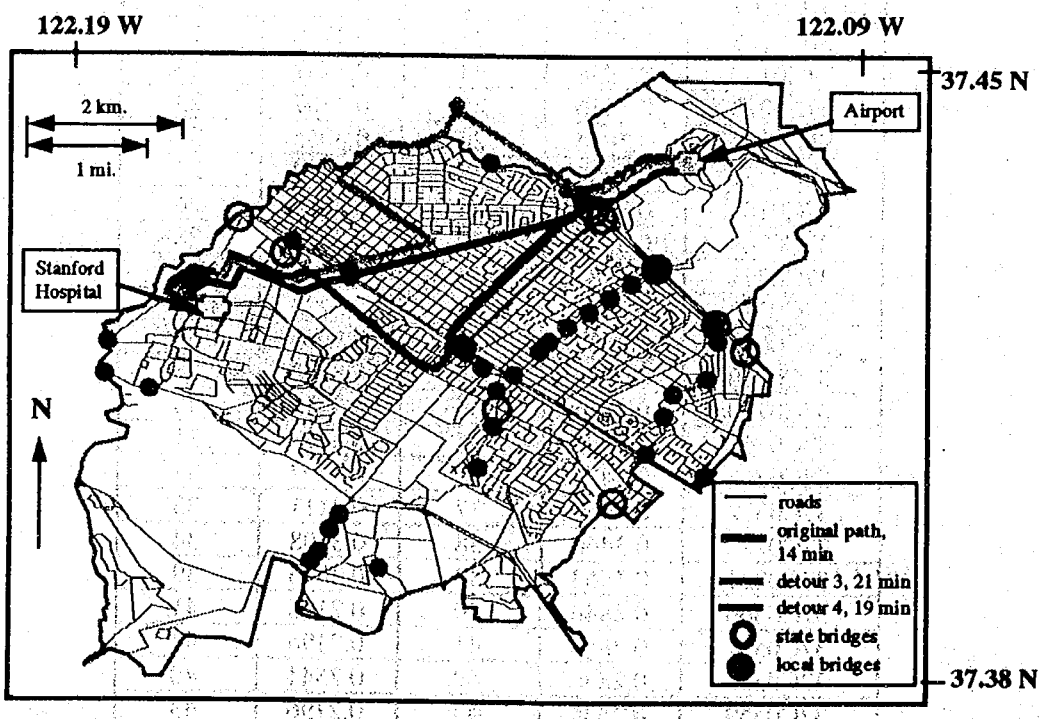


Figure 5. Fastest Paths and Travel Times in Minutes for *OD* Set 1 (continued)

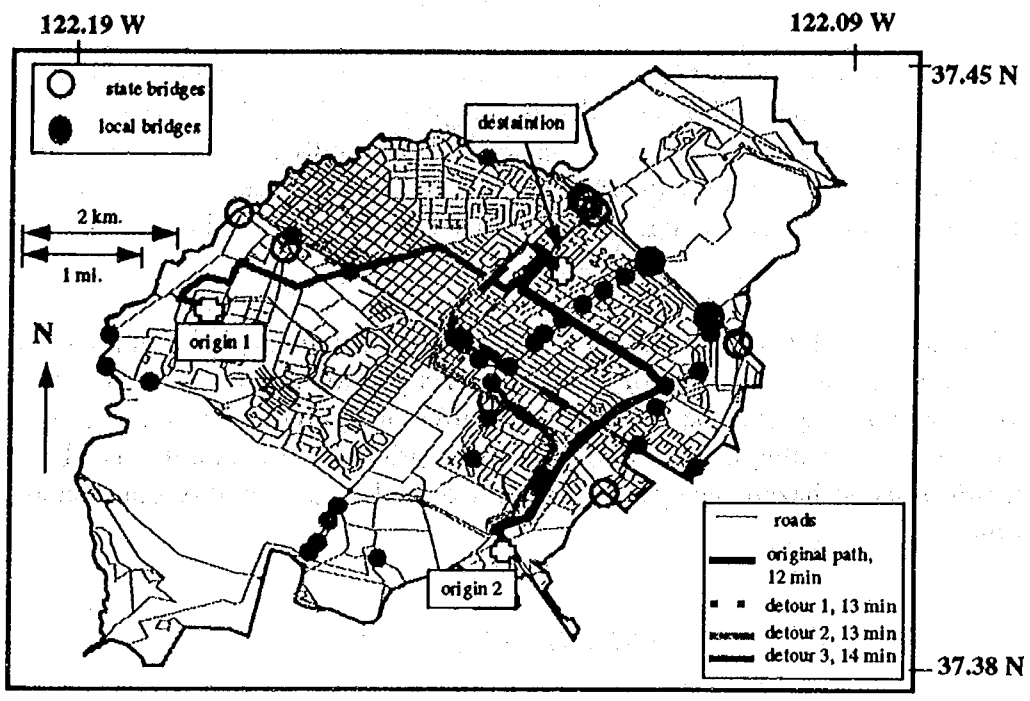


Figure 6. Fastest Paths and Travel Times in Minutes for *OD* Set 2

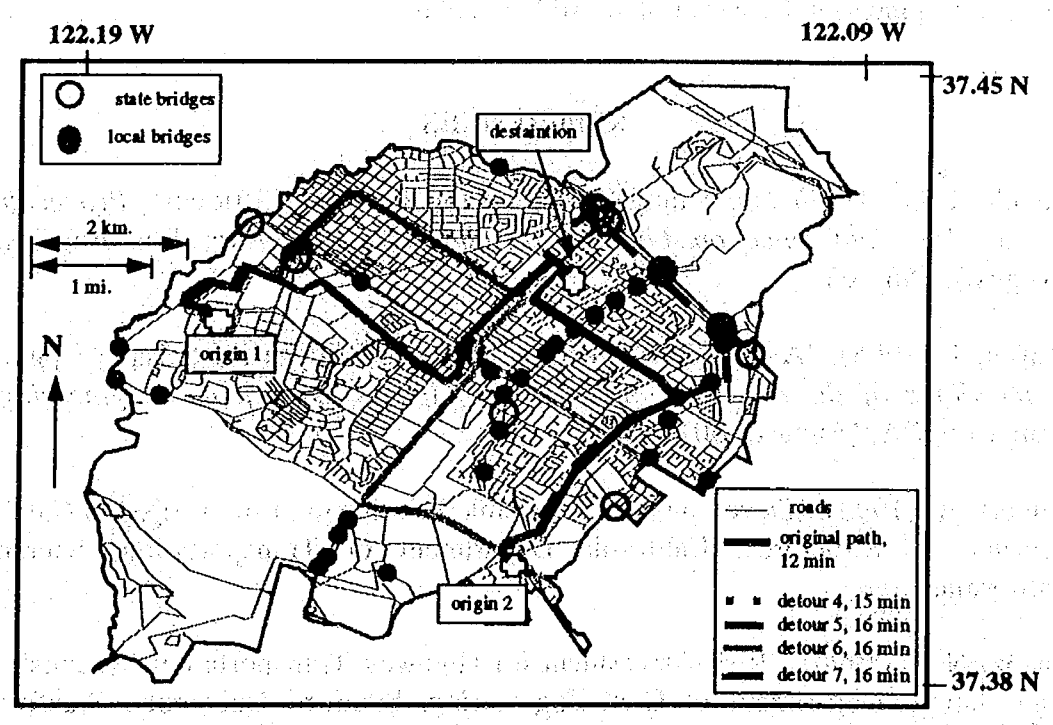


Figure 7. Fastest Paths and Travel Times in Minutes for *OD* Set 2 (continued)

CONCLUSIONS

A bridge prioritization ranking that is consistent with the vulnerability of a bridge to the seismicity of the region and the importance of the bridge with respect to its functionality for emergency response is presented. A multi-attribute utility approach is considered for the combination of vulnerability and importance criteria and a network analysis module is included for the purposes of identifying critical bridges for emergency response routing.

The applicability of the model was demonstrated through its application to the transportation system of the City of Palo Alto. As part of this analysis, it was observed that different ranking can be obtained if different scenario earthquake events are considered for the analysis. A more consistent prioritization ranking is obtained if a probabilistic seismic hazard analysis is performed in the vulnerability components of the methodology.

ACKNOWLEDGMENTS

The authors would like to express their gratitude to Dr. Ian Buckle for the many fruitful discussions and suggestions. In additions, James Gates, Brian Maroney and Ann Gilbert of CALTRANS provided valuable input. We gratefully acknowledge the partial support of NSF Grants EID 9021032 and CMS-9416420, and the John A. Blume Earthquake Engineering Center at Stanford University.

REFERENCES

1. Buckle, I. G. (1991). "Screening Procedure for Retrofit of Bridges", *Proceedings of the 3rd US Conference on Lifeline Earthquake Engineering*, Los Angeles, CA, (August): 156-165.

2. Maffei, J. (1995). "A New Method for Prioritizing Bridges for Seismic Upgrading", *Proceedings of the 4th US Conference on Lifeline Earthquake Engineering*, San Francisco, CA, (August): 501-508.

3. Gilbert, A. (1993). "Developments in Seismic Prioritization of Bridges in California." Division of Structures, California Department of Transportation, Sacramento, California.

4. Basöz, N. I. (1996). "Risk Assessment for Highway Transportation Systems", Ph.D. Dissertation, Department of Civil Engineering, Stanford University, Stanford, CA 94304-4020, 358p.

5. ATC-13 (1985). *Earthquake Damage Evaluation Data for California*, Report ATC-13, Applied Technology Council, Redwood City, California.

6. NIBS (1995). *Development of a Standardized Earthquake Loss Estimation Methodology.* Prepared for the National Institute of Building Sciences by Risk Management Solutions, Inc., Menlo Park, California.

7. Basöz, N. I., and A. S. Kiremidjian. [1996]. *Prioritization of Bridges for Seismic Retrofitting. Technical Report No. 118.* John A. Blume Earthquake Engineering Center, Civil Engineering Department, Stanford University, Stanford, California.

8. Kiremidjian, A. S., S. A. King, N. I. Basöz, and K. H. Law. [1996]. "Methodologies for Evaluating the Socio-Economic Consequences of Large Earthquakes." *Final report for the CUREe/Kajima Joint Project.*

Session 3

Evaluation of Existing Bridges

(Co-Chairs: J. Hoshikuma, N. Makris)

"Analytical Methods for the Seismic Evaluation of Existing Bridges"
by R. Imbsen, F. Nobari
Presented by: Roy Imbsen

"Seismic Evaluation and Retrofit of Existing Multi-column Bents"
by T. Terayama, H. Otsuka
Presented by: Toru Terayama

"Queensboro Bridge: Seismic Condition Assessment and Retrofit of a Landmark Bridge"
by S. Arzoumanidis, R. Gajer, A. Malik
Presented by: Serafim Arzoumanidis

ANALYTICAL METHODS FOR THE SEISMIC EVALUATION OF EXISTING BRIDGES

Roy A. Imbsen, P.E., D.Eng.
Wen David Liu, P.E., Ph.D.
Farid S. Nobari, P.E.
Imbsen & Associates, Inc.
Sacramento, California

ABSTRACT

In recent years, seismic retrofitting of bridges has progressed in the United States. An important aspect of the seismic retrofitting process is the determination of the seismic load path and forces in the individual members of a bridge being upgraded to resist estimated seismic demands as known today and to meet the required bridge performance. The AASHTO Design Specifications and the FHWA Guidelines for the retrofitting include recommendations for the traditional elastic methods using the response spectrum method. Recently the Specifications have recognized the importance of including the effect of yielding elements, expansion joint closure and buckling of members; thus, have added time history nonlinear response analysis.

The conventional method for seismic evaluation of bridge structures has been "Force Based" approach which includes the use of a reduction factor, R, to obtain retrofit design force levels. The deficiency in this practice is the inability to predict component deformation demands and the subsequent force redistribution throughout the bridge substructure system. General force reduction factor approach can not capture critical weak links which may affect stability of the structure. The push-over method and nonlinear time history analysis methods can significantly improve the current evaluation procedure. This paper describes the improved analytical methods which will eventually be incorporated in the Specifications and used for the seismic evaluation and retrofitting of the more routine bridge structures.

INTRODUCTION

An important aspect of the seismic retrofitting process is the determination of the seismic component forces. The American Association of State Highway Transportation Official (AASHTO) Design Specifications (1) and the Federal Highway Administration (FHWA) Seismic Retrofitting Manual for Highway Bridges (2) include recommendations for the traditional elastic response analysis using the response spectrum method. Recently the Specifications have recognized the importance of including the effect of yielding elements, expansion joint discontinuity and buckling of members; thus, have included time history nonlinear response analysis in the recommended procedures. Additionally, the FHWA retrofitting manual has also included an alternative approach to better define the load deformation curve for the individual frames in a bridge.

The conventional method for seismic evaluation of bridge structures has been "force based" approach. Using the elastic response spectrum as ground motion input, elastic structural responses and component forces are obtained. It is recognized that under the strong design earthquake event, it is unrealistic to expect the structure to act elastically and/or remain undamaged. To account for expected inelastic behavior, a structural damping corresponding to 5% of the critical value is used; further, load-reduction factors are used to reduce the predicted elastic member forces as shown in Figure 1.

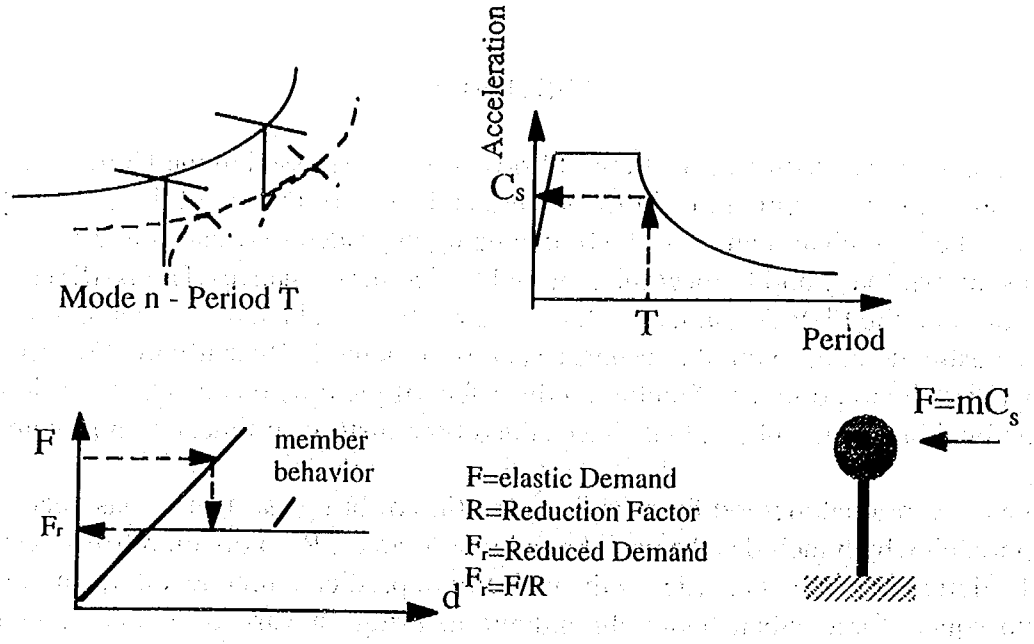


Figure 1 Conventional Force Based Approach

The reduced demand, F_r, is obtained from the elastic demand, F, and a reduction for ductility, R, as follows:

$$F_r = F/R$$

Many factors should be considered before reduced elastic force approach can be justified for a given structure, including:

> For intermediate to long period bridge systems (e.g., T > 0.5 Sec.), the maximum displacements caused by the earthquake excitations are the same regardless of whether a linear elastic model or a nonlinear inelastic model was used in the analytical prediction.

For new constructions, this approach is reasonable because the component capacities can be proportioned to assure a desirable load path. Concentration of inelastic deformation should be avoided if possible; if not, ductile reinforcement details should be provided to assure sufficient deformation capacity.

For existing constructions, the overall displacement response may be estimated within reasonable accuracy by the elastic analysis; however, the distribution of deformation within the structure system could be grossly in error as it is usually dominated by the weakest links (e.g., members, connections, supports, etc.) caused by inadequate design details and/or evaluation practices.

The deficiency in the current practice is the inability to predict component deformation demands and the subsequent force redistribution throughout the bridge substructure system. The general force reduction factor approach can not capture critical weak links which may affect the stability of the structure.

The recent earthquakes of Whittier (1987), Loma Prieta (1989), Northridge (1994), and Kobe (1995) clearly illustrated the need for further improvement of the seismic design procedures and implementation of the most recent research findings. Many research efforts, support "deformation-based" evaluation methods for more accurate assessment of component inelastic response. Furthermore, simplified methods have been developed to characterize inelastic response and lateral strength of substructure systems through push-over analyses of stand-alone local models.

A truly performance-based seismic evaluation can only be accomplished if component inelastic deformations can be realistically estimated. Following the 1989 Loma Prieta earthquake, a deformation-based approach has been gradually incorporated in the current retrofitting practice for some bridges.

As discussed in this paper, the lateral push-over analysis by itself is not intended to accurately predict the seismic demand (force or deformation). It is known to be an effective step in the overall iterative process to gradually fine tune the seismic retrofit strategy. The process produces ductile structure systems with sufficient deformation capacities in all the components and in the overall systems.

This paper describes the analytical methods currently being used in the more complicated bridges which will eventually be incorporated in the Specifications and used for the evaluation of the more routine bridges.

OBJECTIVE

It is generally uneconomical to retrofit bridges to respond elastically under the maximum credible earthquake. The conventional method estimate the expected inelastic response of components by reducing elastic predictions. The reduction factors used are based mostly on empirical studies. The "deformation-based" evaluation method is an improvement for component behavior assessments. Furthermore, simplified methodologies have been developed which take into account member inelastic force-deformation relationships in local lateral push-over analyses of stand-alone bents and frames. The capacity design procedure can better represent the overall response of the substructure, take into account redistributions of component

internal forces following yielding of ductile members, identify strength limit states, and estimate lateral strength of substructures prior to reaching a collapse mechanism.

Simplified single degree-of-freedom models of bents and frames can be of great value in estimating seismic displacement demands for most typical bridges. Geometric complexities such as highly curved alignment and/or highly skewed bents or span hinges require three-dimensional dynamic analyses. However, for most typical bridges, the global responses are dominated by transverse response of individual bents and longitudinal response of individual frames.

The nonlinear characterization of bents and frames can be used to represent inelastic single degree of freedom systems in dynamic inelastic response spectra analyses, from which displacement demands can be estimated. Comparison of the displacement demands from these analyses with limiting capacities established in local push-over analyses can be used to effectively assess the seismic performance of substructure response.

An overall lateral strength evaluation procedure for seismic evaluation of bridges is shown schematically in Figure 2. Tools and methodologies available to evaluate component behavior (strength and stiffness) will be discussed. Levels of refinement required for development of local models will be identified. A procedure to establish substructure inelastic deformation capacity and collapse mechanisms will be discussed. Guidelines for seismic response assessment based on local models will be presented which can be utilized as an effective tool in the iterative retrofit process.

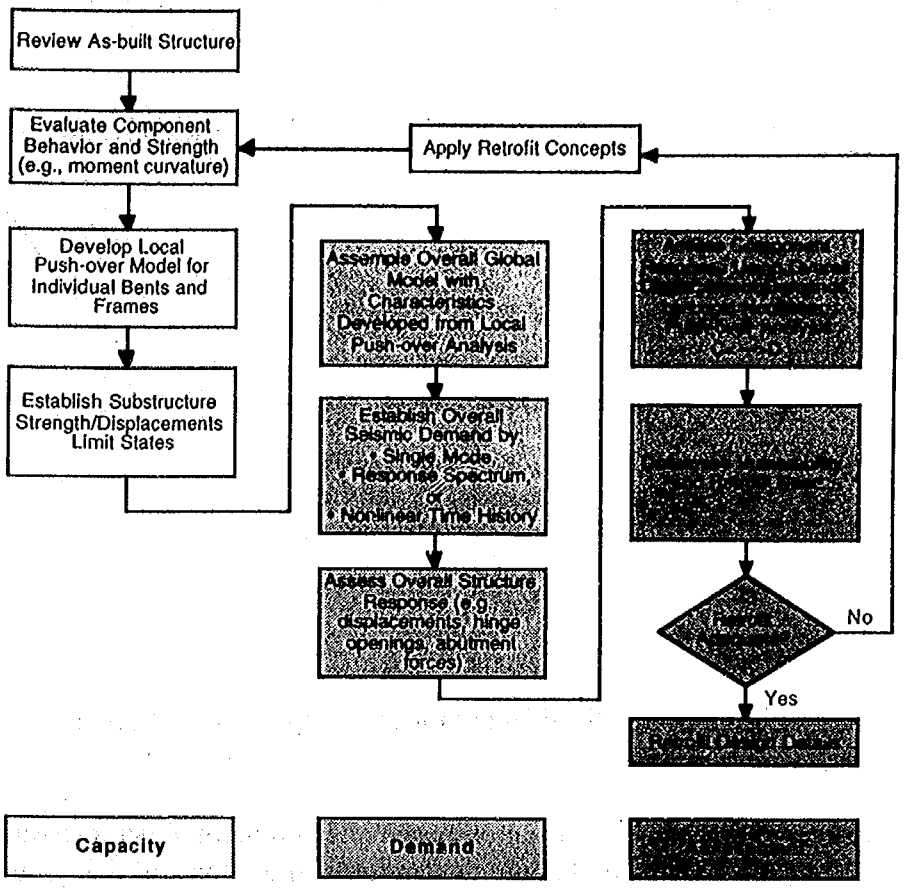


Figure 2 Lateral Strength Evaluation Procedure for Seismic Retrofitting

COMPONENT EVALUATION

The current seismic evaluation procedures recognize the fact that it is not economically feasible to design bridges elastically under seismic loads. Therefore, inelastic deformations and damage are anticipated. To assure satisfactory seismic performance, the following are critical:

- ensure sufficient strength capacity for brittle failure modes,
- limit localized nonlinear deformation to ductile members only,
- ensure adequate deformation capacity in the ductile components, and
- prevent stiffness and strength degradation which can lead to collapse.

The overall deformations capacity of the structure is based on expected behavior of its components. Detailed evaluations of all critical members (in terms of stiffness, strength and ductility) are, therefore, essential. The critical aspects of the expected component performance under cyclic loading can be characterized as:

- Inelastic – ductile
- Stiffness degradation
- Elastic Brittle

Figure 3 shows the schematic force-deformation relationship for each of the above categories.

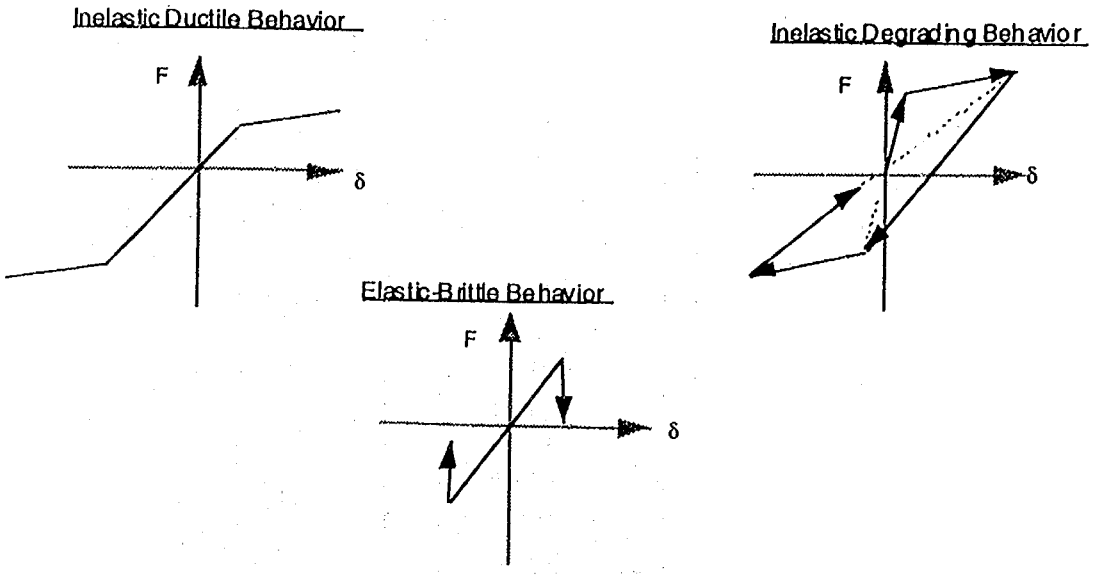


Figure 3 Idealized Behavior of Component Performance

It is recognized that the "deformation based" design method is more rational. The procedures are being established and many design tools in the form of design guidelines and computer programs are available to characterize component responses for different design details. The strength of brittle and degrading components will require careful evaluation to assure an acceptable performance of the seismic response. It is the design objective to fully utilize the deformation capacity of ductile members and to prevent any brittle failure mode.

Material Properties

In evaluation and retrofit design of existing structures, the uncertainty of material properties are typically higher due to lack of construction data, deterioration and aging effects. Nondestructive testing of reinforced concrete can quantify the in-situ material properties. For example, the compressive strength of aged concrete (f_c') is typically much higher than the specified design values (e.g., 50% higher). Design and evaluation criteria for seismic evaluation and retrofit design of existing bridges should specify the material properties to be used based on actual tests, or other experimental findings.

Columns

The capacity design method for bridges depends on the ductile, inelastic deformation of column members during seismic lateral loads. It is essential to represent this inelastic behavior in the local push-over analyses to allow for the force redistribution. The current trend of seismic design is toward the deformation-based approach using various ductility measures to asses the performance. Ductility can be expressed as ratio of the "Ultimate" deformation to "Idealized

Yield" deformation. The basis of comparison can be strain, curvature, displacement, or other measures of deformation.

Moment-curvature section analysis is fundamental in assessing inelastic deformation of column members. Theoretical developments are based on:

- Plane section remain plane
- Steel stress-strain relationship including strain hardening effects
- Concrete compressive and tensile stress-strain relations
- Confinement effects on concrete performance

Figure 4 shows a typical moment-curvature relationship for reinforced-concrete column sections. It is important to represent the member effective stiffness realistically in the local push-over analyses. As shown in Figure 4, concrete cracks at a very low moment level. The initial uncracked stiffness does not represent the overall behavior at high lateral loads or even at the service load level. An "effective" stiffness must be used, which is defined by the "Effective Cracked Moment of Inertia, I_{cr}". Values of "I_{cr}" range from 25% to 70% of gross moment of inertia (I_g) depending on reinforcement ratio and column axial load levels.

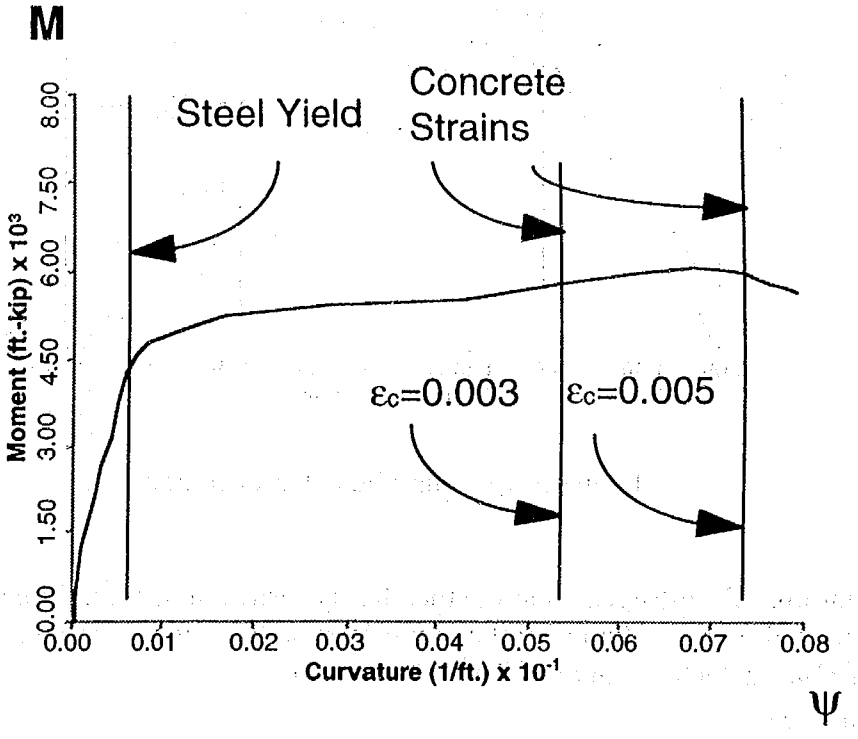


Figure 4 Column Moment-Curvature Relation

Local stand-alone analyses should use the "Effective Stiffness" of the section obtained from the moment-curvature analyses. Since the nonlinear relationship must be idealized (e.g. bilinear), some judgment may be required in defining the effective stiffness. Shown in Figure 4 is a common approach in evaluating effective rotational stiffness (i.e. E I_{cr}) by defining the initial slope of idealized curve to pass through the first yield point of steel reinforcement.

The other important aspect of section moment-curvature analysis results is the ability to determine curvature capacity of the section based on limiting steel or concrete strains. Much research has been conducted to quantify the limiting strains for steel and reinforced concrete columns. Many issues (such as buckling of steel reinforcement, concrete confinement, reinforcement ratio) have to be considered in selecting the limiting strain criteria for the structure. Figure 4 shows the section curvature at concrete strain of 0.003 and 0.005.

Figure 5 shows the results of typical shear-deformation analysis conducted for a cantilever column. The procedure can keep track of the development of curvature and strain during the force-deformation analyses to report column deformations at given strain levels, such as limiting strains for concrete or steel. Concrete strain levels at 0.003 and 0.005 are shown in the figure.

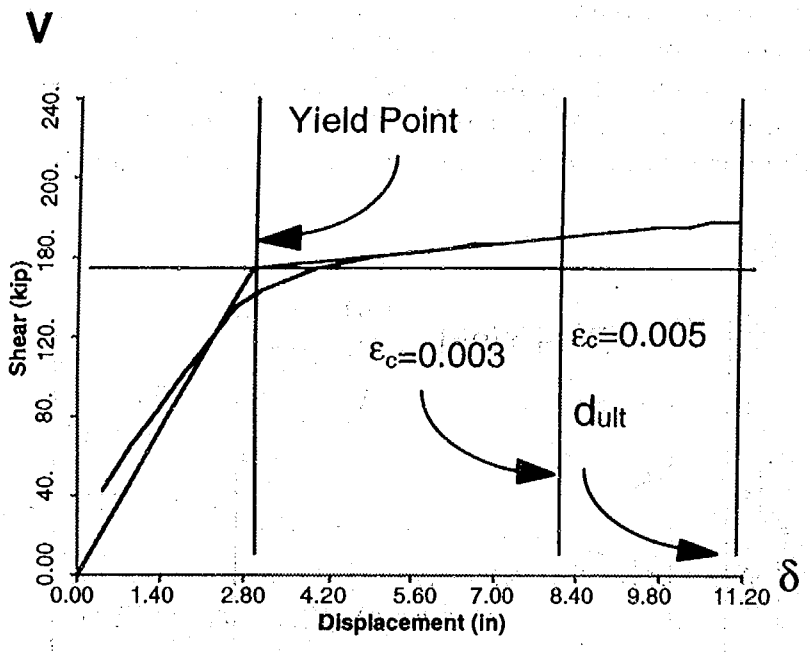


Figure 5 Column Shear-Deformation

Shear failure of reinforced concrete members is brittle in nature. The column shear capacity is enhanced by the column axial compression, and is reduced at higher flexure ductility demands. Variables affecting column shear capacity are:

- Section Area
- Column Axial Force
- Transverse Steel Contribution
- Flexure Ductility Demand

Figure 6 shows the dependence of column shear capacity on flexure ductility demands. The comparison of section shear capacity with shear-deformation relation can establish the governing mode of failure at different ductility demand levels.

The torsional strength of columns depends highly on compressive stress of the section, section dimensions, and "Closed" hoop reinforcement throughout the length of the member. Theoretical procedures have been developed, and implemented in many computer programs. Since torsional response of most existing reinforced concrete columns behave as elastic-degrading members, it is essential to carefully estimate the elastic capacities to assess the seismic performance.

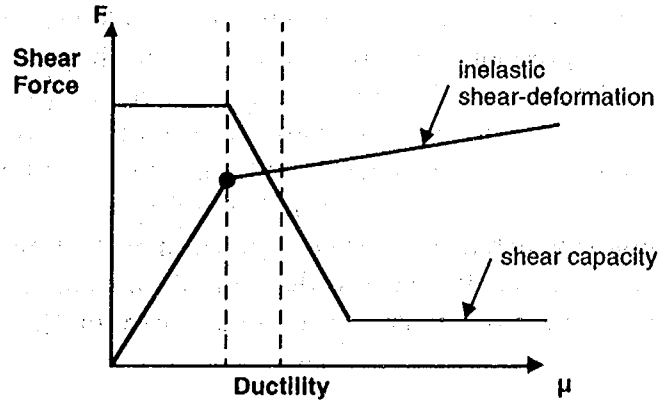


Figure 6

Bent Caps

Bent caps are mostly designed for gravity and live loads. The reinforcement details of bent caps in older bridges are generally deficient in flexural strength to resist expected seismic cyclic loads. Unique issues for these cap members are:

- Unsymmetrical top and bottom reinforcement details resulting in different response characteristics for negative and positive moment demands.
- Distributed weight of superstructure along the length of the bent cap which should be considered for more accurate state of dead load moments.
- Transverse steel reinforcements are commonly designed for cap shear strength and are often open "U" shaped. Open reinforcement details do not enhance inelastic deformation capacity levels.

Well established procedures are available to determine appropriate modeling of the cap member in the local push-over analyses.

Torsional behavior of bent caps, particularly outrigger caps, has been a major concern due to the longitudinal frame response. Many outrigger caps in older structures lack sufficient closed hoop reinforcements to resist torsion. Since these members are normally non-redundant

load carrying elements in the substructure framing system, their capacity should be evaluated carefully.

Joints and Connections

Within the overall inelastic evaluation and design procedure for bridge structures, joints and connections must be stronger than the connecting members. The observed response of highway bridges during the recent earthquakes, and the knowledge gained from experimental testing, indicate the need for better assessment of existing joints, as well as additional considerations for new or retrofit designs.

Reinforced concrete joints connecting column members to bent caps and foundations require reliable concrete compression struts to transfer the loads beyond elastic limits and during penetration of flexure yielding in plastic hinging regions. In current practice, this is assured by providing shear reinforcement in both horizontal and vertical directions throughout the joint core. Simplified methodologies have been developed using strut-and-tie procedure to quantify stress demands at the core of the joints under applied boundary forces and moment. Figure 7 shows the loading conditions which need to be considered in evaluating joint core stresses for typical bent configurations. The analytical consideration of joints in the local push-over studies should include true representation of geometry (i.e., Finite Size Joint).

Foundations

The effects of foundation flexibility and strength must be taken into account in the seismic evaluation process to assess deformation demands in columns and foundation elements. Based on the soil profile and engineering characterization of soil behavior, stiffness and strength of foundations can be developed. Rotational response of foundation is probably the most significant characteristic which interacts with column flexural yielding. The overall rotational resistance of pile-group foundations is mostly provided by axial pile-soil interaction. In addition, shear and flexural behaviors of pile caps should be investigated to finalize the foundation model. Figure 8 shows typical results of pile-group moment rotation evaluation.

Foundation rocking due to compressive pile settlement or tensile pile pull out is possible during lateral response of bents. As shown in Figure 8, the extent of compressive settlement or pull out capacities of piles can be monitored for individual rows of pile at given moment or rotation demands. Since excessive rocking of foundation systems can lead to higher P-Δ moments and potential for instability of the bents, rocking limits should be selected based on the lateral stability consideration and the allowable pile settlement values.

Foundation properties in the local push-over model should reflect the behavior as determined in the force-displacement and moment-rotation analyses of the foundations. The nonlinear relationship, strength, stability limits, and brittle component failure will have to be considered in the local lateral push-over studies.

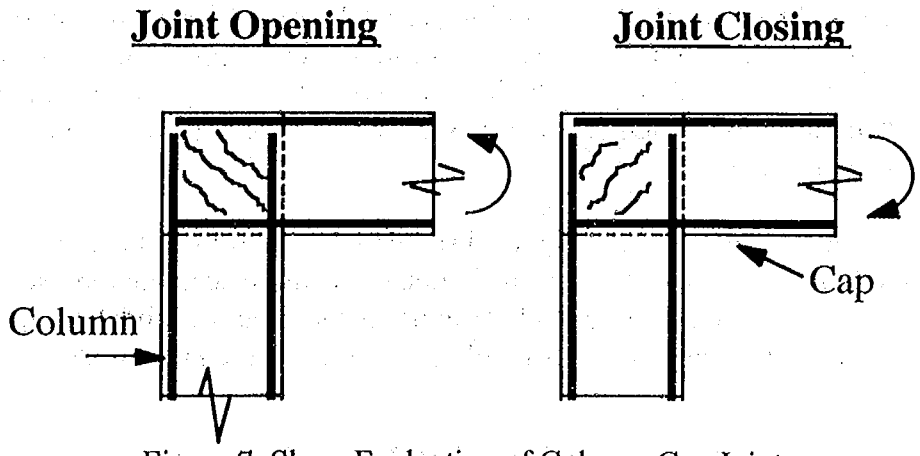


Figure 7 Shear Evaluation of Column-Cap Joints

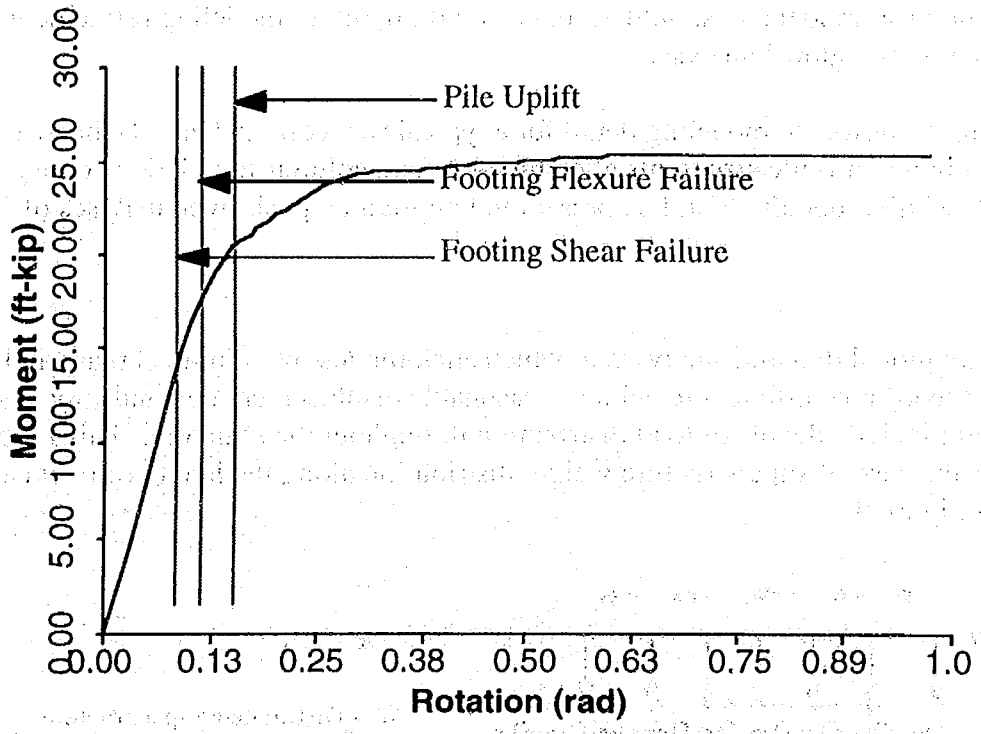


Figure 8 Nonlinear Foundation Analysis

LATERAL PUSH-OVER ANALYSIS TO ESTABLISH LIMIT STATES

The underlying philosophy behind local stand-alone evaluation of a substructure framing system is to develop a better understanding of behavior, deformation distribution and capacities on a bent-by-bent basis. The general procedure also assists designers to provide minimum lateral strength levels for each bent prior to development of any collapse mechanism.

The procedure by itself does not replace the need for global dynamic analyses, particularly for complex structures. However, the results of lateral push-over analyses can provide the understanding required for identifying critical areas and potential retrofit concepts. Furthermore, this understanding of the behavior and strength of supporting frames when used in conjunction with displacement demands obtained from dynamic analyses, can lead to a comprehensive "Deformation-Based" response assessment of the structure and components under a given earthquake.

The analytical model for the local model should be more refined than those generally used in the global dynamic analyses. Since the emphasis is more accurate representation of the overall frame response, a better gravity load distribution and accurate modeling of component behavior in terms of stiffness and strength should be adopted in the local models.

Geometry

The purpose of the local push-over studies is to gain a better understanding of bent resistance mechanism during seismic lateral loads. The modeling and analysis must be more focused in the local model and should account for all important modeling refinements which may be impractical in the global analyses.

Figure 9 shows the modeling detail for a typical two-column bent. Geometric data such as column height and finite size joints at column-cap and column-foundation connections may be represented. Similar details should be present in longitudinal push-over analyses of frames.

Loads

Unlike global dynamic analyses in which stick models with lumped mass and concentrated loads are sufficient to achieve reasonable displacement demands, local stand-alone models should include details of load distribution throughout the structure. This is particularly important in the case of superstructure weight distribution along the length of bent cap members, as shown in Figure 9.

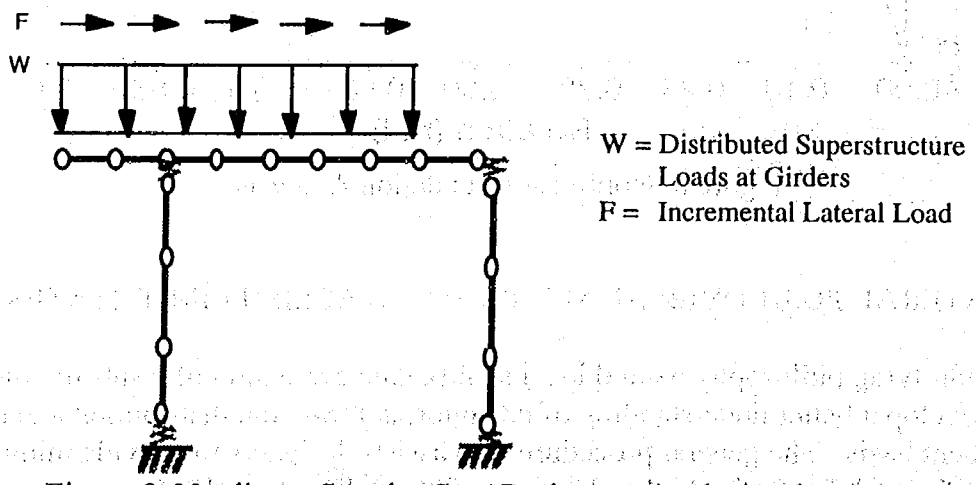


Figure 9 Nonlinear Step-by-Step Push-over Analysis of Local Model

Members

Realistic representation of member stiffness, strength and behavior are essential in the lateral push-over analyses of local models. Issues such as cracked section properties, elastic strengths, ductile, brittle, or degrading member behaviors should be accounted for in assessing frame response and strength by the local analyses. Figure 10 shows possible modeling details which may be used for different members of bents and frames.

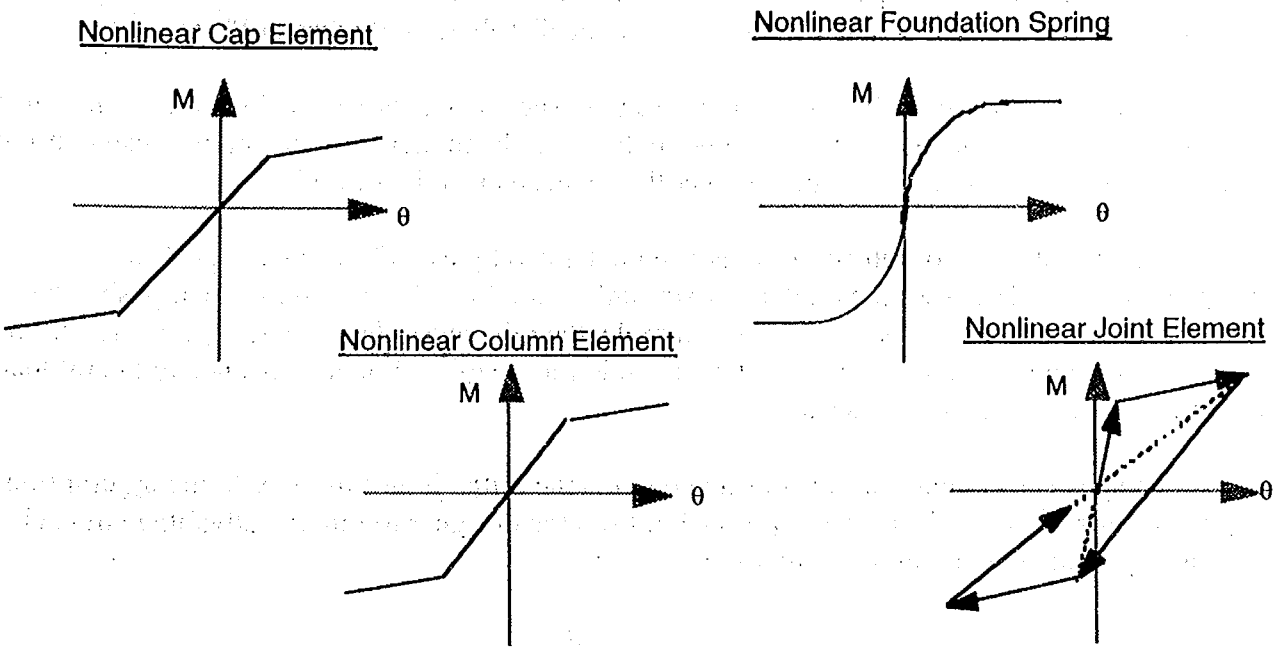


Figure 10 Nonlinear Component Modeling

Loading

The three dimensional nature of seismic loading, and the complexities of 3D dynamic response due to curved geometry, impacting at hinges, skewed bent orientation, and other factors make it impossible to develop general guidelines on the primary mode of response for all bridge structures. However, based on the general philosophy of tributary mass distribution and strength requirements of individual bents and frames, local stand-alone models should be used to evaluate the transverse response of individual bents and longitudinal response of individual frames.

These modes of response are believed to be the most significant components of the global structure response for most bridge structures and will, at the least, ensure a uniform distribution of strength and deformation capacity throughout the structure. The more complex features of structure dynamic characteristics and displacement responses can be captured in the dynamic

analyses from which demands in the longitudinal and transverse directions can be obtained and compared to the established behavior of frames and bents, respectively.

Analysis

Having defined individual component behavior in the local models, push over analyses can be conducted in a step-by-step application of lateral loads along the bent cap (transverse bent analyses) or at the C.G. of superstructure (longitudinal frame analyses). As shown in Figure 11a the distribution of loading should closely relate to the distribution of inertia effect.

Using a nonlinear analysis computer program such as IAI-NEABS (5), realistic nonlinear representation of individual members can be included in the model, and the analysis can continue up to the point of maximum strength when collapse mechanism is formed.

The initial phase of retrofit designs can be iterated by use of these local push-over analyses. Figure 11a shows the joint shear strength as the first "Event" in the local push-over analysis of a typical bent. As seen in this example, the joint shear deficiencies occur first, prior to any inelastic deformation. This is not acceptable for the overall bent resistance to lateral loads and must be strengthened at this stage.

The push-over analysis can continue beyond the initial joint failure with the assumption of joint shear retrofit in place. This approach allows the designer to rate the advantage of each retrofit step in the overall strength increase.

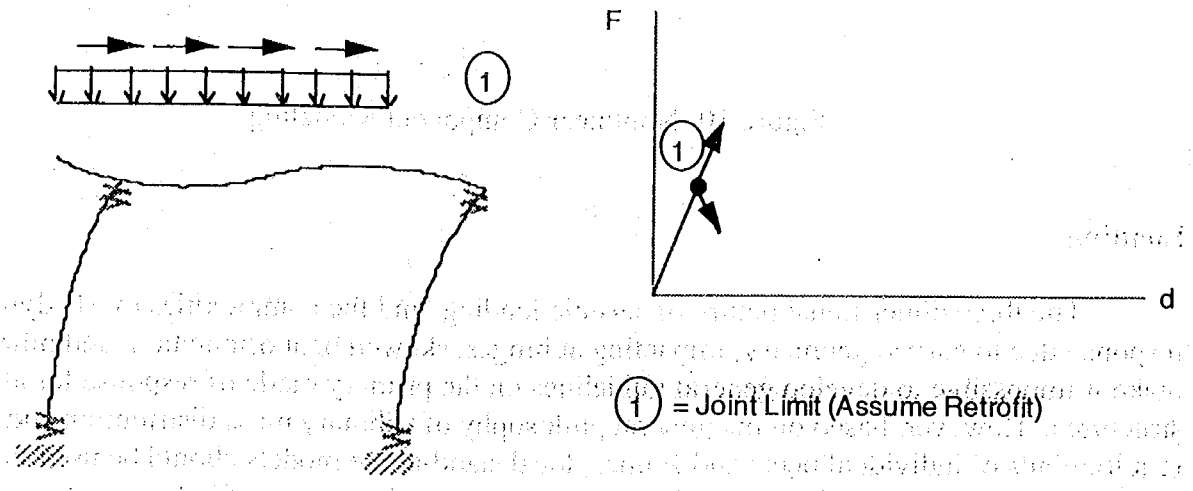


Figure 11a Event 1 – Local Push-over Analysis

Figure 11b shows the final stage of the lateral push-over analysis. The example shows intermediate events of cap and column yielding prior to reading the ultimate strength of the bent system. Each event and corresponding component capacity can indicate adequacy of the existing condition or requirement for applicable retrofit measures.

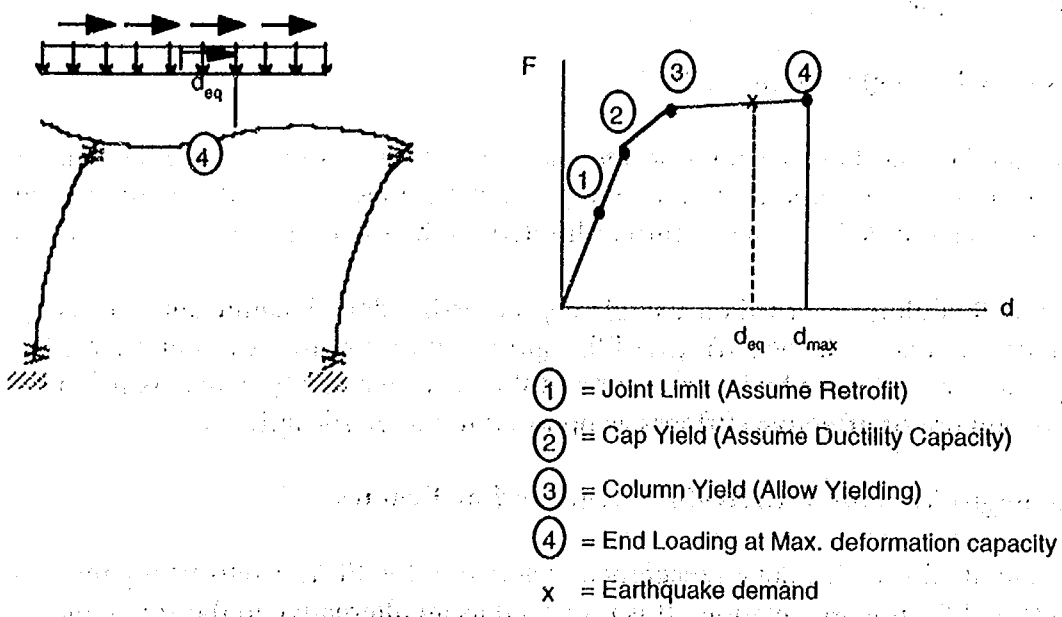


Figure 11b Limit State – Local Push-over Analysis

As demonstrated above, the push-over study of local bent models can identify many details of individual component response, as well as the lateral strength of the overall framing system. Additionally, as shown, the maximum capacity, can be compared to seismic demands (d_{eq}) for an overall performance assessment. The following section discuss various procedures in establishing seismic demands.

DEVELOPMENT OF ANALYTICAL MODEL AND ESTABLISHMENT OF SEISMIC DEMANDS

Having established the stiffness characteristics and capacities of the individual bents and/or frames the next step is to determine the seismic demands. There are several methods available depending on the complexity of the bridge, the purpose of the evaluation, and the given level of performance requirement. The methods include:

1. Simplified Elastic Single Mode Method (i.e., AASHTO Procedure 1 or Procedure 2, and Simplified Method, Seismic Retrofitting Manual for Highway Bridges, FHWA)
2. Lateral Strength Method of Individual Bents and/or Frames (i.e., Alternative Method, Seismic Retrofitting Manual for Highway Bridges, FHWA)
3. Global Multi-mode Response Spectrum Method (i.e., AASHTO Procedure 3) with or without interactive substructure properties
4. Global Nonlinear Time History Analysis (i.e., AASHTO Procedure 4)
5. Simplified Nonlinear Analysis Using Inelastic Design Spectra

The first four methods have been used to varying degrees in seismic retrofitting. The fifth method has been used to some degree in building design but is still at the research level for

bridges. The second method recently proposed in the FHWA retrofitting manual is undergoing testing and verification.

Simplified Elastic Single Mode Method

This method has been used for design and retrofitting of bridges since the San Fernando earthquake in 1971. It is somewhat limited to particular bridge types and structural geometry. It is usually used on a force basis and is further limited by the use of the reductive factor, R.

The methodology is based on a single degree-of-freedom dynamic analysis using tributary mass and linear elastic stiffness of the substructure system. An improvement in the use of this approach can be made by incorporation of the push-over analysis results for the substructure and use of effective stiffness as opposed to the elastic stiffness.

Lateral Strength Method of Individual Bents and/or Frames

This method was developed recently and added to the FHWA retrofitting manual and is now being tested for implementation. It is proposed as an alternative to the single mode force method which has traditionally been used. This method attempts to combine the push-over method with the single mode method and is consistent with the procedure outlined in Figure 2. It is, however, somewhat limited in its application when applied to individual frames and bents in that true superstructure interaction may not be represented.

Global Multi-mode Response Spectrum Method

This method, used since the San Fernando earthquake, is intended for use on the more complicated bridges which have more than a primary single mode of response in the transverse and longitudinal directions. It also has the same problem as the single mode method when used on a reduced force basis.

This method can be valuable to estimate displacement demands which can then be used in conjunction with the push-over method to characterize the substructure stiffness and capacity as shown in Figure 2. This approach is, however, may be limited in that the nonlinearities in the superstructure is still ignored.

Global Nonlinear Time History Analysis

Based on the complexity of the geometry and/or nonlinearities within the structure, step-by-step nonlinear time history analysis of the global model may be required to evaluate the overall dynamic responses. All important nonlinear effects of the superstructure and substructure should be incorporated into this model. The nonlinear behavior in superstructure discontinuities of abutments, intermediate supports and hinges, as well as flexure yielding of the columns, should be represented.

The substructure can be modeled in its entirety composed of yielding ductile columns and nonlinear soil-structure interaction of the foundations. The model can be extended to include the

piles and surrounding soil effects. An alternative approach is to use the substructuring technique to develop an equivalent impedance function which accounts for the nonlinear and damping effects of the foundation. This approach is generally used and has the advantage in that the size of the computer model may be reduced while important aspects of soil structure interaction are accounted for. Other nonlinearities, such as sliding friction at the abutments and hinge seats, buckling of steel truss members should be studied to determine their importance with respect to the global response. The primary function of the global nonlinear analysis is to ensure the key component behavior are represented in the analysis to establish accurate displacement response of the overall structure.

Simplified Nonlinear Analysis Using Inelastic Design Spectra

The local push-over analyses of stand alone bent and frame models can considerably improve the designers' understanding of structure response during seismic lateral loads. The force-displacement relations, such as those shown in Figure 12, contain important information on component strength limit states which influence the overall behavior of the substructure system to lateral load. Additionally, it is possible to idealize the relationship by a bilinear representation and simplify the substructure behavior to nonlinear single degree of freedom systems as shown in Figure 12.

The idealized single degree of freedom systems representing bents and frames in transverse and longitudinal directions, respectively, can be used in "Inelastic Response spectra" analyses which can take into account:

- System elastic stiffness
- System elastic strength
- Post-elastic stiffness
- Effects of successive cyclic response

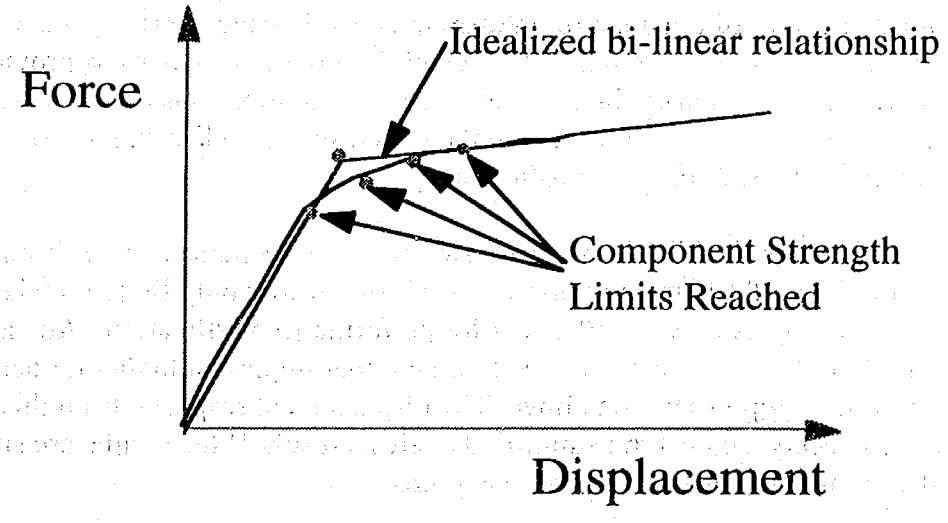


Figure 12 Idealized Bent Transverse Response

The procedure involves generation of representative ground motion time history records, conducting nonlinear (single degree of freedom) time history analyses by varying mass, periods of vibration, ductility level, and establishing the inelastic response spectra.

The theoretical development of inelastic response spectra method have been implemented in computer program NONSPEC (6) which take into account inelastic response and effects of multiple cyclic loading. The expected inelastic displacement demand for the idealized single degree of freedom system can be established within reasonable accuracy.

Recommended Analysis Procedure

The objectives of seismic evaluation in a retrofit project can be classified into the following three categories:

- Analysis to identify vulnerability and to develop preliminary retrofit concept;
- Analysis to establish the response variability to certain parameter uncertainties;
- Analysis to confirm expected structural performance of final design

As a first step in the retrofit project, component behavior assessments are conducted as described earlier. The **lateral push-over analysis** of bents and frames are carried out to establish a basic understanding of the nonlinear force-displacement relationships for the structural system as a whole. This analysis established the deformation capacity existed or can be made available by retrofitting. The next critical question is what is the seismic demand? How much inelastic deformation can be tolerated for the given seismic performance requirement.

Using the push-over analysis result, a **substitute inelastic single-degree-of-freedom structure** can be constructed which has the same overall nonlinear lateral force characteristics. Using the **inelastic response spectrum concept**, the **maximum (inelastic) displacement demand** and **the maximum total hysteretic energy demand** can be established for the structure and for the given earthquake input. Based on these results, we can approximately establish the equivalent number of cycles of this maximum displacement demand. This will be used as the basis to develop retrofit concept such that a sufficient deformation capacity is provided which is also adequate under the expected cyclic load reversals. In addition, this analysis can be conducted for a variety of scenarios to establish the response variability due to parameter uncertainties, and to evaluate alternate retrofit concepts.

Once the concept is established, the next step is the performance verification. After appropriate retrofit, the performance requirement typically allows only limited inelastic behavior, the **elastic dynamic analysis** may be sufficient for performance verification. An elastic global dynamic analysis should always be conducted to assure that important higher modes are not ignored in the simplified representation above. The displacement response from this global analysis should be checked against the simplified analysis result. If the results are similar, it can be concluded that dominant behavior has been captured.

For complicated structures where higher mode contributions are important or the performance requirement is such that a detailed assessment of behavior is necessary, a nonlinear

global model can be developed and **inelastic dynamic time history analysis** carried out to quantify the inelastic deformation demands.

ASSESSMENT OF COMPONENT RESPONSE VULNERABILITY AND RETROFIT NEEDS

Having obtained demands of the overall structure response (d_{cq}), the push-over analysis models established for (d_{max}) the individual bents may be used to determine the individual component capacity/demand ratios, and to determine the vulnerability and retrofit need as graphically shown in Figure 11b.

As noted in Figure 2, this consistent approach to seismic evaluation and retrofit design of bridge structure is equally dependent on accurate estimation of both capacities, as well as demands. The deficient traditional approaches which independently evaluated demands and capacities are now replaced by more logical methods which recognize interdependence of strength, stiffness, and demands for more realistic response assessment of individual components, as well as substructure systems.

SUMMARY

The objective of this paper is to discuss the newly developed analysis procedures used for the seismic retrofitting of bridges.

Based on a review of the existing practices of conducting lateral push-over analysis (essentially the nonlinear capacity analysis) and the evolution of the deformation-based seismic resistance design, we have identified several alternative analytical procedures that can be incorporated into seismic evaluation and retrofit design process. In a way, one can treat this as an extension of the procedure included in the current AASHTO codes for seismic retrofitting.

1. American Association of State Highway and Transportation Officials (AASHTO) Interim Specifications 16, 1996.
2. Federal Highway Administration (FHWA), Seismic Retrofitting Manual for Highway Bridges, May 1995.
3. Imbsen & Associates, Inc., IAI-NEABS – Computer Program for Nonlinear Earthquake Analysis of Bridge Systems, 1986.

Seismic Evaluation and Retrofit of Existing Multi-Column Bents

Toru Terayama[1], Hisanori Otsuka[2]

Abstract

This paper describes mainly four topics. The damaged multi-column bents during Kobe Earthquake are shown first. Secondly, the history of design codes for the multi-column bents for highway bridges in Japan are discussed and a number of the existing multi-column bents are evaluated using a kind of push-over analysis, which is newly introduced in the "Design Specifications for Highway Bridges, 1996". Thirdly, the results of the cyclic loading tests of the as-built and the steel jacketed multi-column bents are shown and compared. Lastly, the retrofit proposal for the multi-column bents are introduced, but the study of this retrofit method is still on-going.

Introduction

Recently, three large destructive earthquakes have occurred in the United States and Japan. These earthquakes, the Lama Prieta earthquake in 1989, the Northridge earthquake in 1994, and the Kobe earthquake in 1995, have severely damaged a number of highway bridges, and have cost many lives and billions of dollars. In the Kobe earthquake, not only the single-column bents but also the multi-column bents are damaged. The major reason of the damage is considered to be insufficient ductility and inadequate shear reinforcement. After 1990, the single-column bents for highway bridges in Japan basically must to be checked by the horizontal dynamic capacity, which is a kind of limited stage design, in the Design Specifications for Highway Bridges Part V. Seismic Design, 1990[1], but multi-column bents need not be checked. In other words, the multi-column bents had been designed by allowable stress design method until the Kobe earthquake.

In the United States, especially in California, the multi-column bents tends to be integral cap beam/superstructure type rather than bearing supported superstructure type. In order to analyze these structure, the push-over analysis method has been already developed, such as DRAIN-3D[2]. Taking the fact into the account that some of the multi-column bents damaged during the Kobe earthquake and that most of the multi-column bents in Japan are bearing

[1] Senior Research Engineer, Earthquake Engineering Division, Earthquake Disaster Prevention Research Center, Public Works Research Institute, Ministry of Construction

[2] Professor, Department of Civil Engineering, Kyushu University
(Former, Head of Earthquake Engineering Division, Earthquake Disaster Prevention Research Center, Public Works Research Institute, Ministry of Construction)

supported superstructure type as can be seen in Fig. 1, the intensive work has been done in Public Work Research Institute to develop the similar type of analysis method to check the horizontal dynamic capacity for the multi-column bents. Using this method, the fact revealed that the most of the existing multi-column bents in Japan are seismically vulnerable due to the insufficient transverse reinforcement.

In this paper, the damaged multi-column bents during the Kobe earthquake are shown first. Then, the history of design codes for the multi-column bents for highway bridges in Japan are discussed. A number of existing multi-column bents are evaluated using the newly developed analysis method. The results of the cyclic loading tests of the as-built and the steel jacketed multi-column bents are also shown and compared. Lastly, the retrofit method for the multi-column bents are proposed.

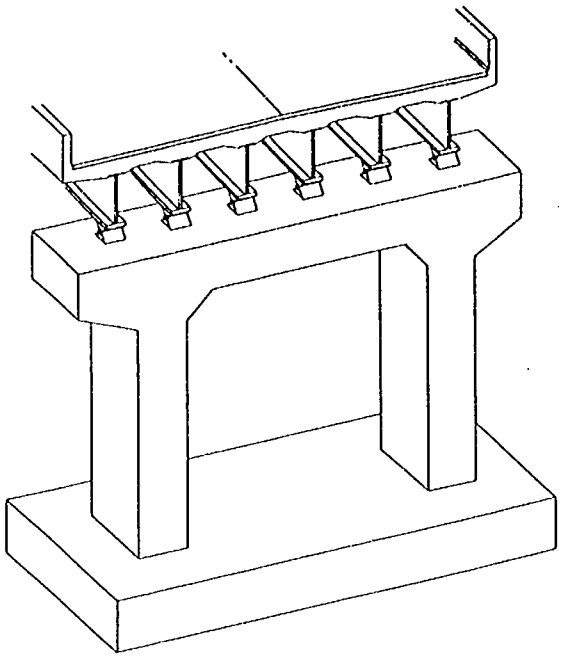


Fig. 1 Typicl Multi-Column Bents in Japan

Damages during Kobe Earthquake

Photo 1 and Photo 2 show the damages of multi-column bents in the transverse direction caused by the Kobe earthquake. Both are located at Iwaya district where is very close to the area recording an intensity of 7 in the JMA seismic intensity scale. These columns are designed by the Design Specifications for Highway Bridges, 1964[3]. The transverse reinforcement of both columns are D16 with a spacing of 300 mm. The spall-off of cover concrete at the top of the right column can be seen in Photo 1. It is not clear in the photo, but the cover concrete is spalling off at the bottom of the left column and the small cracks are observed at the cap beam. The damages of these parts are mainly caused by the inadequate ductility capacity due to the insufficient transverse reinforcement. Photo 2 shows the shear failure occurred at the column of another Multi-column bent. As can be seen, this shear failure is mainly caused by the seismic force

of transverse direction. This damage is mainly caused by the insufficient shear reinforcement.

It can be said that the sufficient transverse reinforcement and the adequate reinforcement details are needed to design the ductile multi-column bents, which is the very same as the single-column bent.

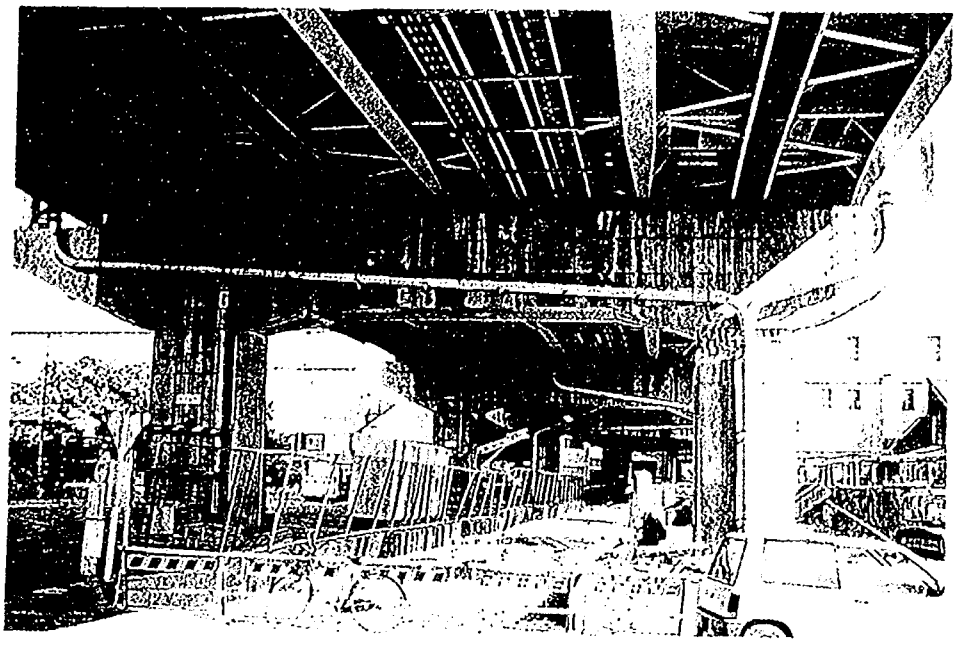


Photo 1 Damages of Multi-Column Bents

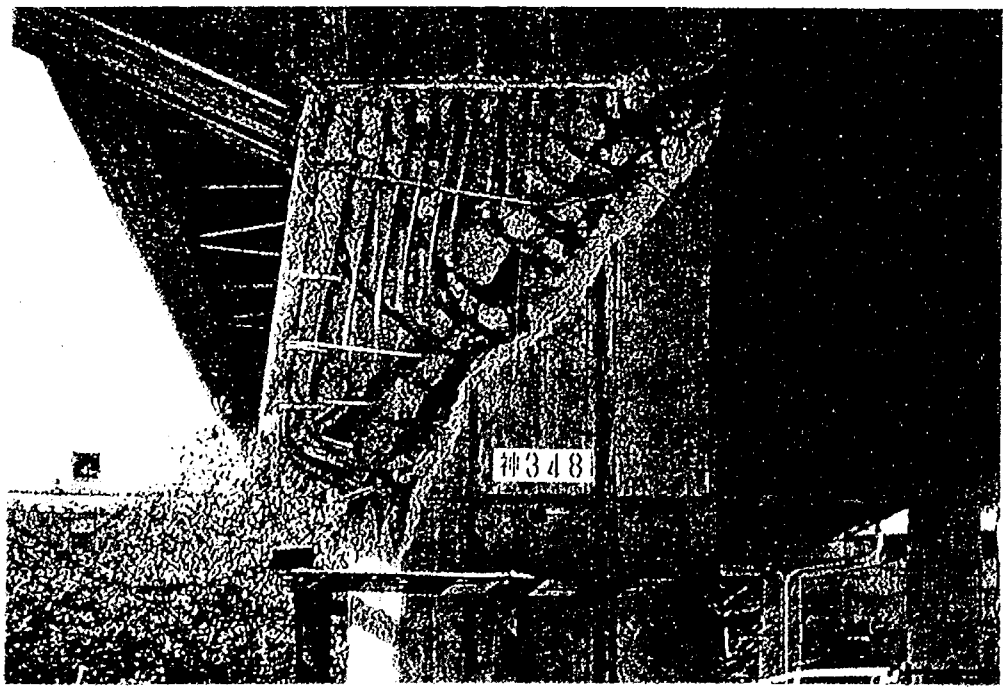


Photo 2 Shear Failure of Multi-Column Bents

Evaluation of Existing Multi-Column Bents

History of Codes for Multi-Column Bents

History of the specifications and the codes for the design of concrete columns in Japan have been already discussed by K. Kawashima, et al. [4][5] Although the checking method of the ductility, namely the check of the horizontal dynamic capacity, was introduced in the specifications of 1990 [1] for the single-column bent, the multi-column bent has been designed by the allowable stress design and the seismic coefficient method until the new Design Specification for Highway Brides, 1996 [6] was issued. In the new specifications, the checking method of the horizontal dynamic capacity for the multi-column bents was introduced, and with that the transverse reinforcement should be arranged adequately preventing from the shear failure or the brittle failure due to the insufficient ductility.

Reinforcement details were specified in the past specifications for highway bridges. In the Design Specifications for Highway Bridges Part IV Substructure, 1980[7], the minimum diameter of transverse reinforcement was specified as 13mm and the spacing should be less than 300mm, less than the twelve times of the diameter of the longitudinal reinforcement and also less than the half of the diameter or the shorter dimension of the column. In the Design Specifications for Highway Bridges Part IV Substructure, 1990[1], the appropriate ratio of the transverse reinforcement was suggested. The ratio of transverse reinforcement should be 0.15% for the column with a longitudinal tensile reinforcement ratio from 0% to 0.5%, 0.2% for the column with a longitudinal tensile reinforcement ratio from 0.5% to 1.0% and 0.25% for the column with a longitudinal tensile reinforcement ratio bigger than 1.0%. The ratio of the transverse reinforcement is calculated by dividing the area of the transverse reinforcement by width of the column and the spacing of the transverse reinforcement. The Design Specifications for Highway Bridges, Part III Concrete Bridges, 1990 [1] specifies the reinforcement details for the frame structure as shown in Fig.2. For the frame structure, the ratio of the transverse reinforcement is specified as 0.2% for the part A and the part B, 0.25% for the part C and 0.15% for the part D.

Evaluation Method

To obtain the ultimate flexural strength and the shear capacity, the multi-column bents are modeled to the frame model with plastic hinges, as can be seen in Fig. 3. Each elastic frame member has the yield stiffness which is based on the axial load by the dead load of the superstructure and the column itself. The plastic hinge is placed at the end part of a cap beam and the top and bottom part of each column. The location of the plastic hinge is a half distance of the plastic hinge length off from the end edge of each member, where plastic hinge length Lp is assumed to be the following equation.

$$Lp = 0.2h - 0.1D \quad and \quad 0.1D \le Lp \le 0.5D$$

where h is a half distance of the member and D is the dimension of the column or the cap beam.

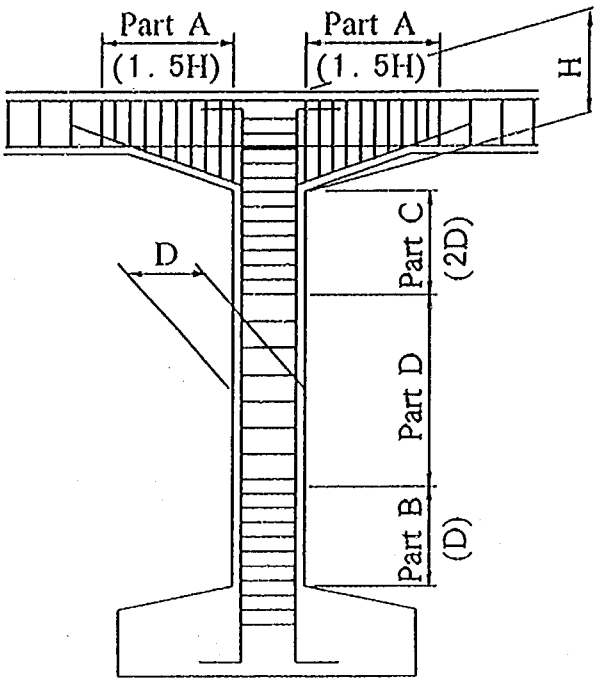


Fig. 2 Reinforcement Details specified in 1990

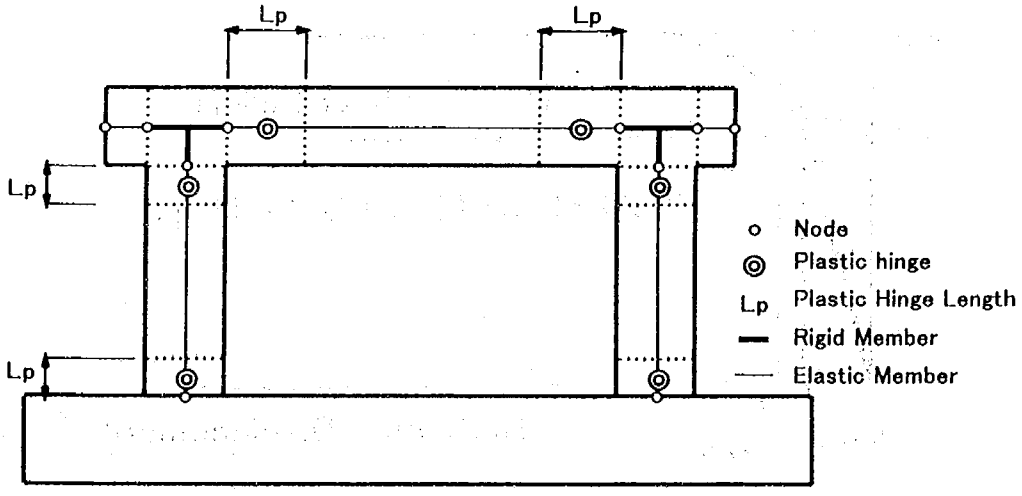


Fig. 3 Model for the Multi-Column Bent

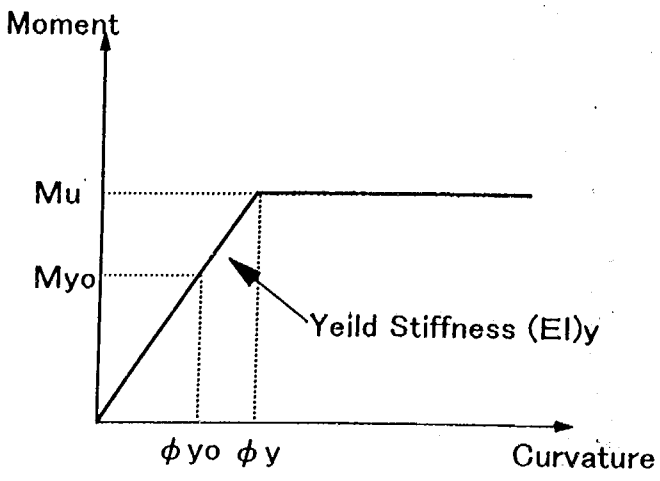


Fig. 4 Moment-Curvature Relation

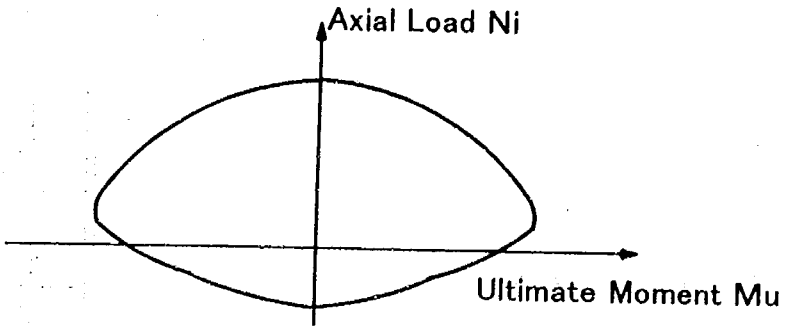


Fig. 5 Axial Load-Moment Interaction

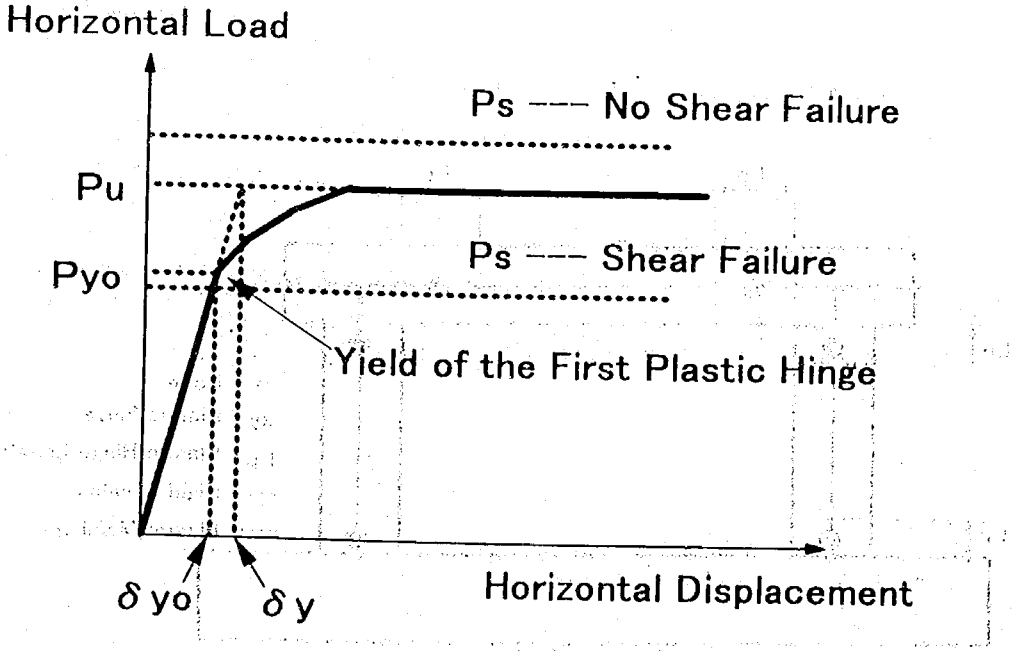


Fig. 6 Horizontal Load-Horizontal Displacement Relation

Fig. 4 shows the moment and curvature relationship, which is based on the stress- strain relationship developed by Hoshikuma et al.[8] Using the model depicted in Fig. 3, the horizontal load is statically increased, which is simulating the inertia force. As the horizontal load increases, the axial load of the column changes. Consequently, the moment-curvature relationship of the column changes, which is considered by N-M interaction curve, see Fig. 5. By increasing the horizontal load statically, the horizontal load-horizontal displacement relationship is obtained, as can be seen in Fig. 6. Shear failures are not expected if the shear capacity of each plastic hinge is larger than the shear force occurring at the stage of the ultimate horizontal flexural strength Pu. On the other hand, shear failures are expected in the case that the shear force of a plastic hinge reached to its shear capacity during the increase of the static horizontal load. The ultimate horizontal shear force Ps is specified as the minimum horizontal load where the shear force of a plastic hinge reached its shear capacity. Here, shear capacity is calculated as follows by the method introduced to the new specifications [6].

$$Ps = Cs + Cc$$

where Cs is a steel contribution and Cc is a concrete contribution to the shear force. Cc is calculated by the effects of the type of the ground motion, the height of the dimension, the ratio of the tensile reinforcement and the concrete strength.

Evaluation

Thirty-three multi-column bents are chosen arbitrary from all over Japan and the ultimate flexural strength Pu and the ultimate shear strength Ps were calculated for each structure. If the Ps is larger than Pu, Ps is specified as the same value as the Pu. Fig. 7 shows the Pu versus Ps for thirty three multi-column bents. As can be seen, Ps is smaller than Pu for most of the chosen multi-column bents. This means that existing multi-column bents possibly cause shear failure once the major earthquake occurs. As mentioned in the previous section, the multi-column bents in Japan were designed with a careful considerations for the reinforcement details, but this analytical results revealed that those details were not sufficient to prevent from a brittle shear failure.

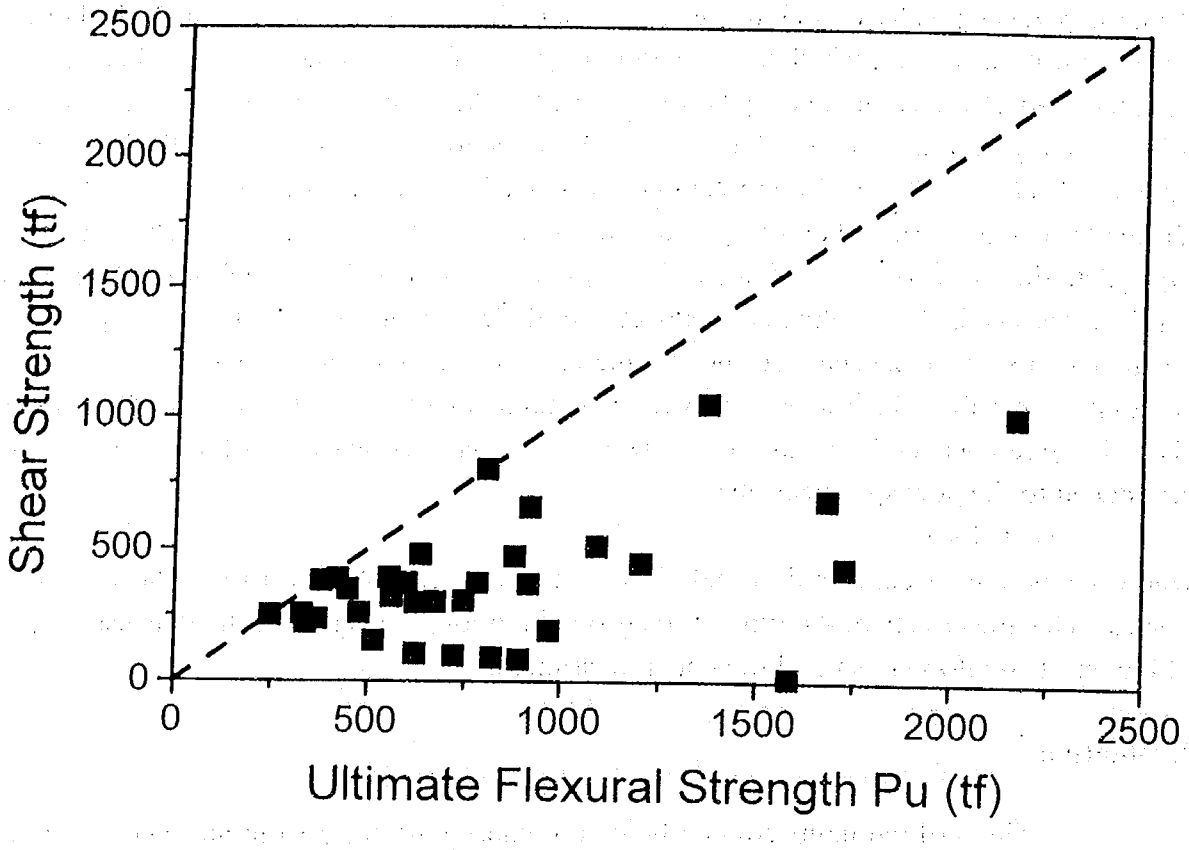


Fig. 7 Ultimate Flexural Strength versus Shear Capacity

Cyclic Loading Tests

Test Setup

Cyclic loading tests were carried out to examine the seismic behavior of an as-built and a retrofitted multi-column bent. As-built specimen represents the multi-column bents designed after 1990, which means the specimen was designed by using the codes shown in Fig. 2. Fig.8 and Fig. 9 show the test specimen of the as-built and the retrofitted multi-column bents. The specimen is set in the horizontal position , as shown in Photo 3. The simulated seismic load was applied using hydraulic actuator acting against the reaction strong wall. To simulate selfweight of superstructure and the column, an additional axial load was applied by means of an axial load apparatus. The axial stress of the simulated deadload was determined as 10kg/cm^2. The test sequence consisted of three cycles of 1δy, 2δy, 3δy and so on in displacement control. The displacement was continued to increase until the test specimen caused the serious damage such as a fracture of the longitudinal reinforcement.

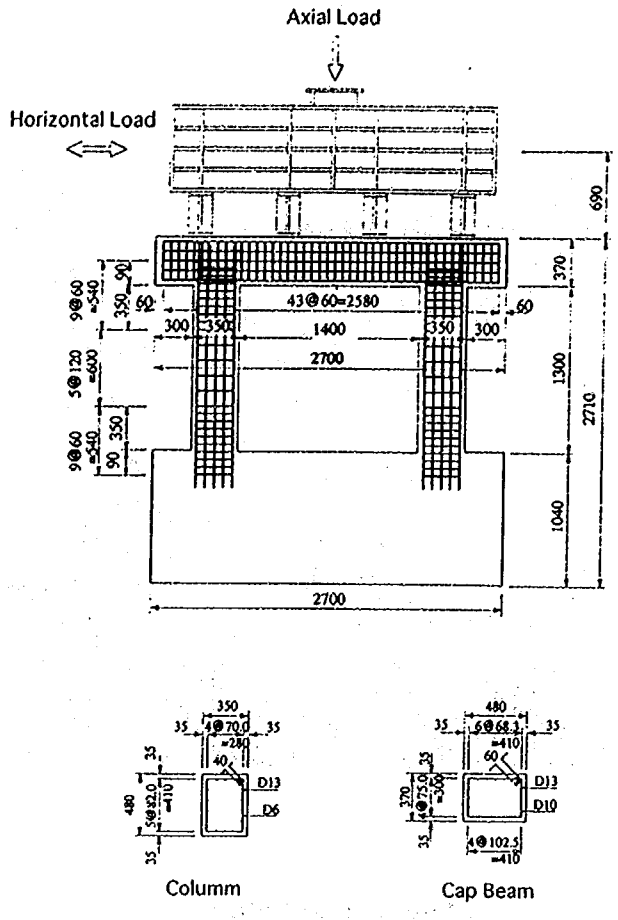


Fig. 8 As-Built Specimen

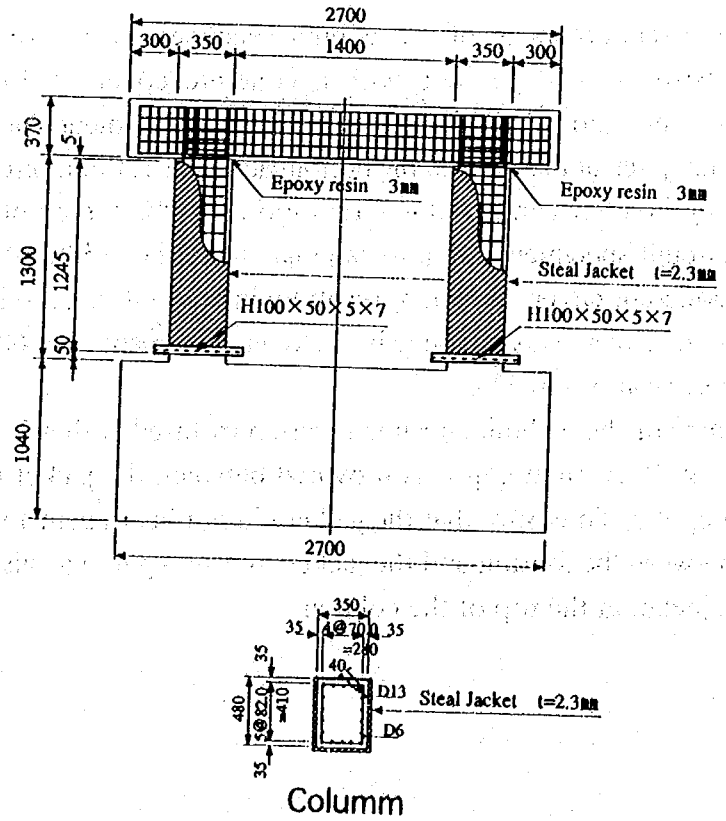


Fig. 9 Retrofitted Specimen

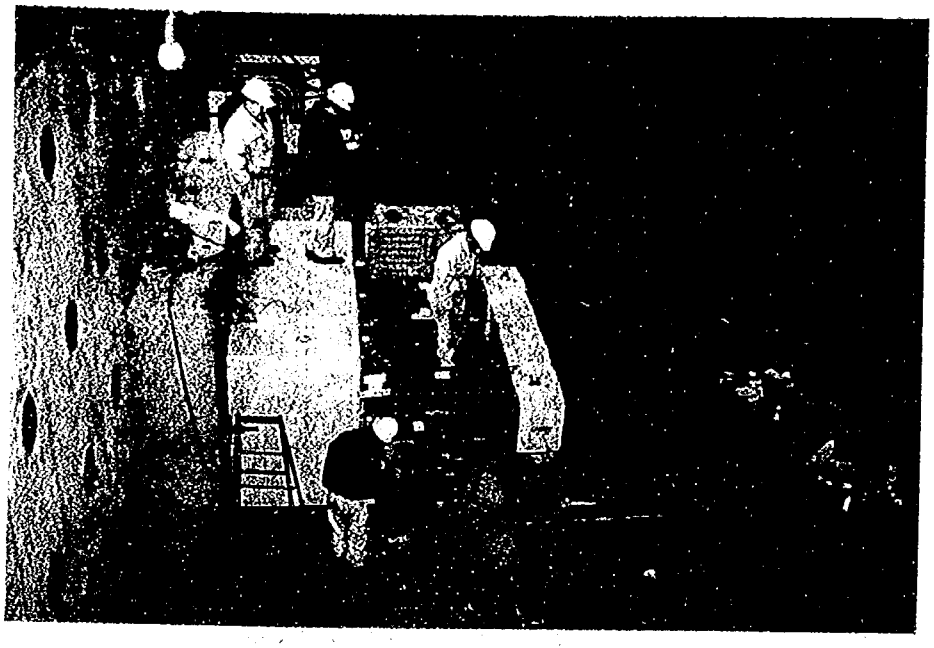


Photo 3 Test Setup

The column reinforcement of the as-built specimen, with a rectangular section of 350mm*480mm, consists of 18-D13 bars with a concrete cover of 35mm, resulting in a longitudinal reinforcement ratio of 1.4%. The horizontal confinement was provided by a D6 reinforcement on a 60mm pitch at the top and the bottom and on a 120mm pitch at the middle part of the column, resulting in a horizontal volumetric ratio of 0.5% at the bottom. The cap-beam reinforcement of the as-built specimen with a rectangular section of 350mm*480mm, consists of 18-D13 bars with a concrete cover of 35mm, resulting in a longitudinal reinforcement ratio of 1.3%. The horizontal confinement was provided by a D6 reinforcement on a 60mm pitch, resulting in a horizontal volumetric ratio of 0.5%.

The columns of the as-built specimen were retrofitted with a 2.3mm-thickness steel jacket, as shown in Fig. 9. A 3mm gap was provided between the jacket and the column and pressure filled with an epoxy. To ensure that the jacket did not bear against the footing, a gap of 50mm was provided between the footing and the jacket. A 5 mm gap was also provided between the cap-beam and the jacket at the top of the column.

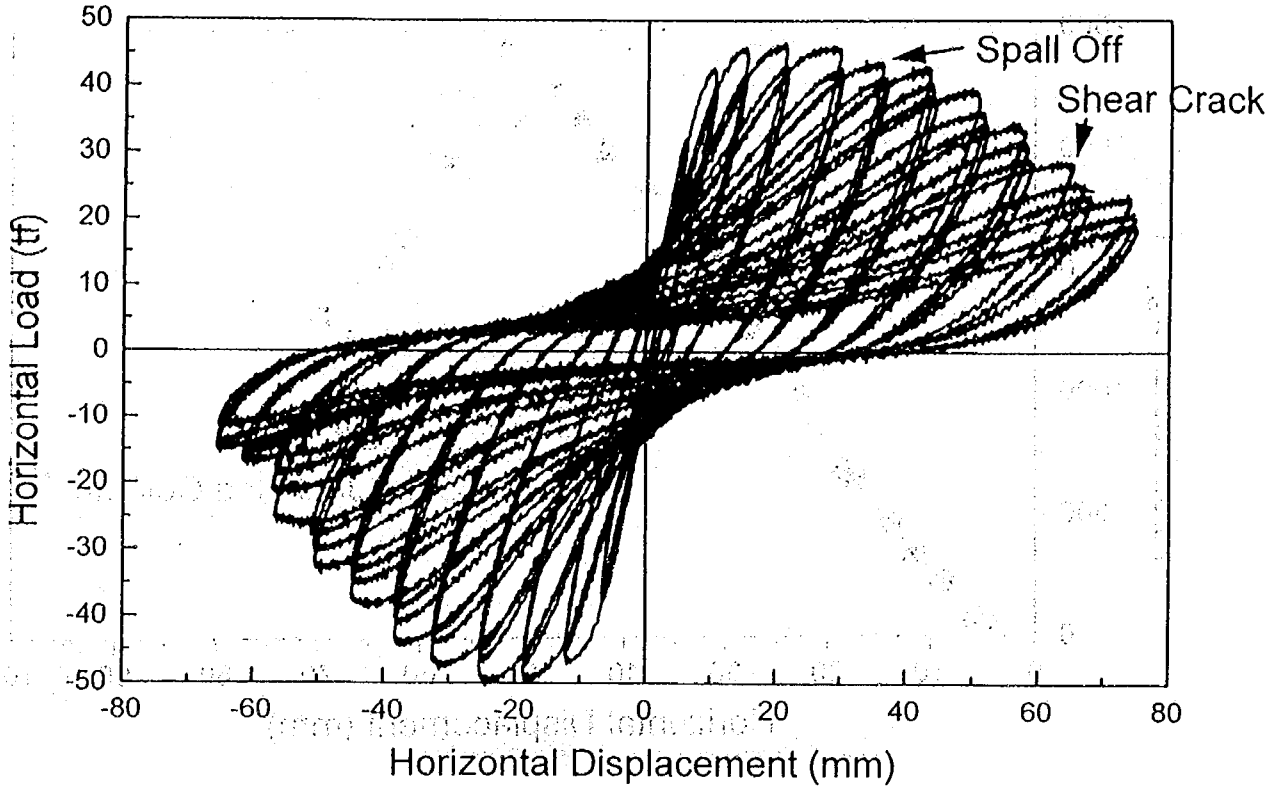


Fig. 10 Hysteresis Loop (As-Built)

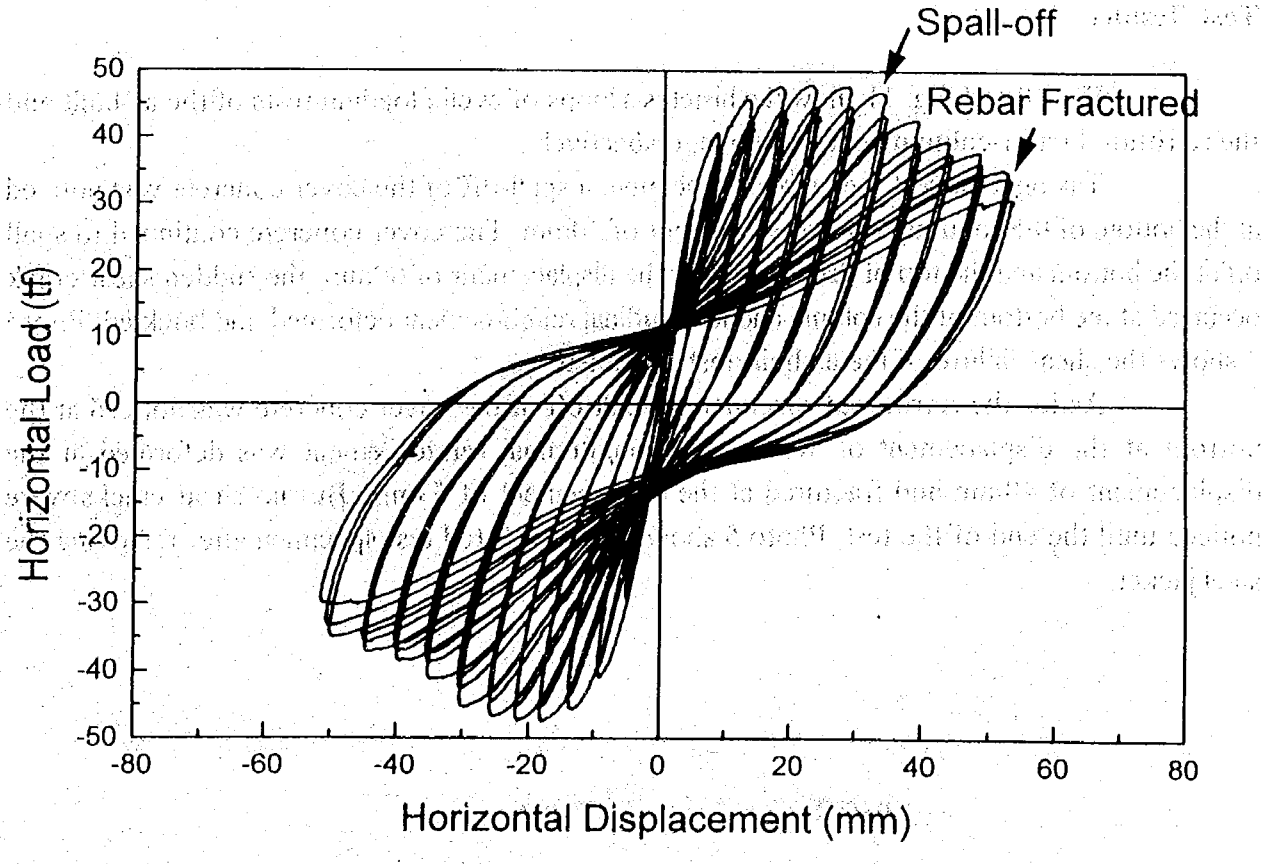


Fig. 11 Hysteresis Loop (Retrofit)

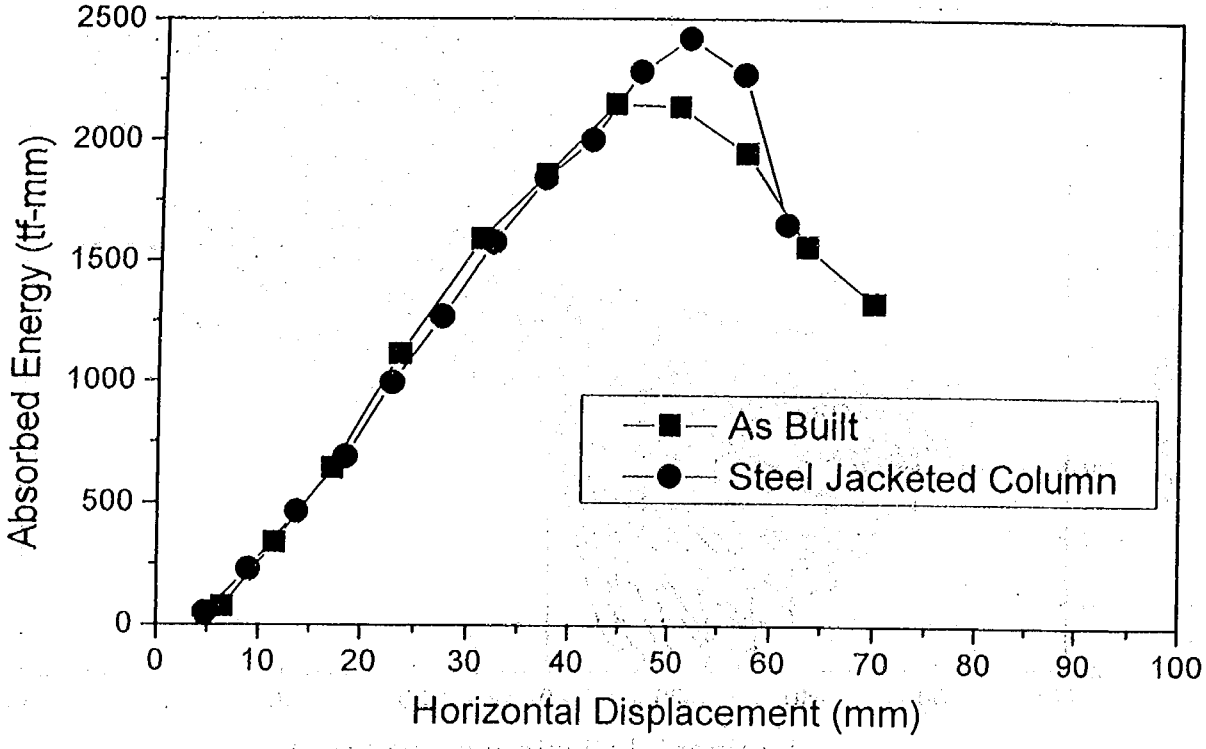


Fig. 12 Absorbed Energy

Test Results

Fig. 10 and Fig. 11 show the histeresis loops of cyclic loading tests of the as-built and the retrofitted multi-column bent specimen, respectively.

Taking a look at the as-built specimen, a spall-off of the cover concrete was noticed at the bottom of the column at the displacement of 30mm. The cover concrete continued to spall off at the bottom and the top of the column. At the displacement of 60mm, the sudden shear crack occurred at the bottom of the column and longitudinal reinforcement deformed and buckled. Photo 4 shows the shear failure of the as-built test specimen.

As for the retrofitted specimen, a spall-off of the cover concrete was noticed at the bottom at the displacement of 30mm. The longitudinal reinforcement was deformed at the displacement of 48mm and fractured at the displacement of 53mm. But no shear cracks were noticed until the end of the test. Photo 5 shows the retrofitted test specimen after removing the steel jacket.

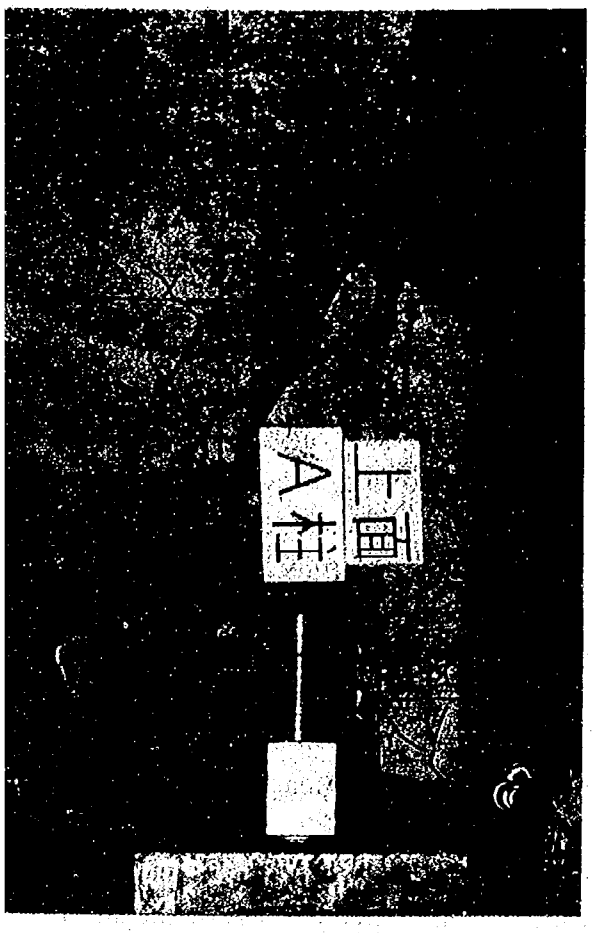


Photo 4 Shear Failure

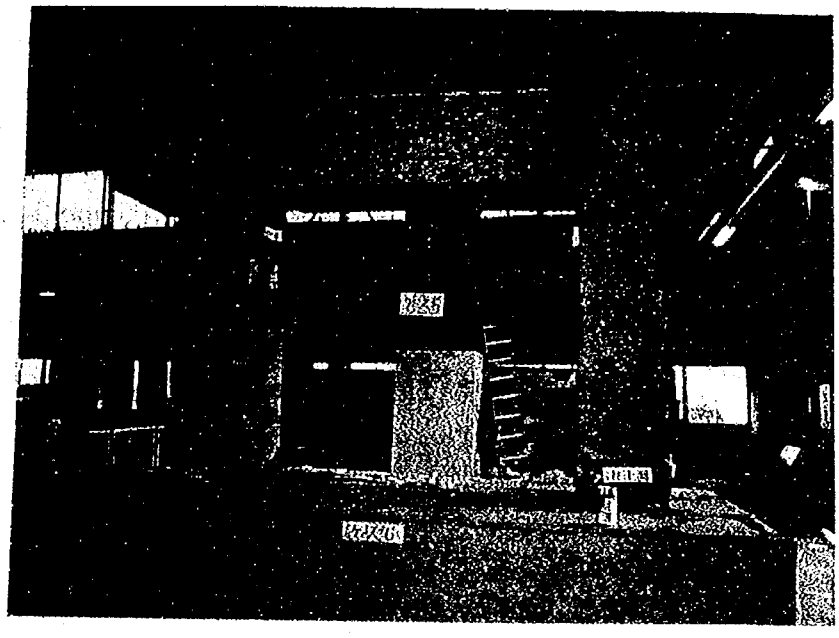


Photo 5 Specimen after the Test

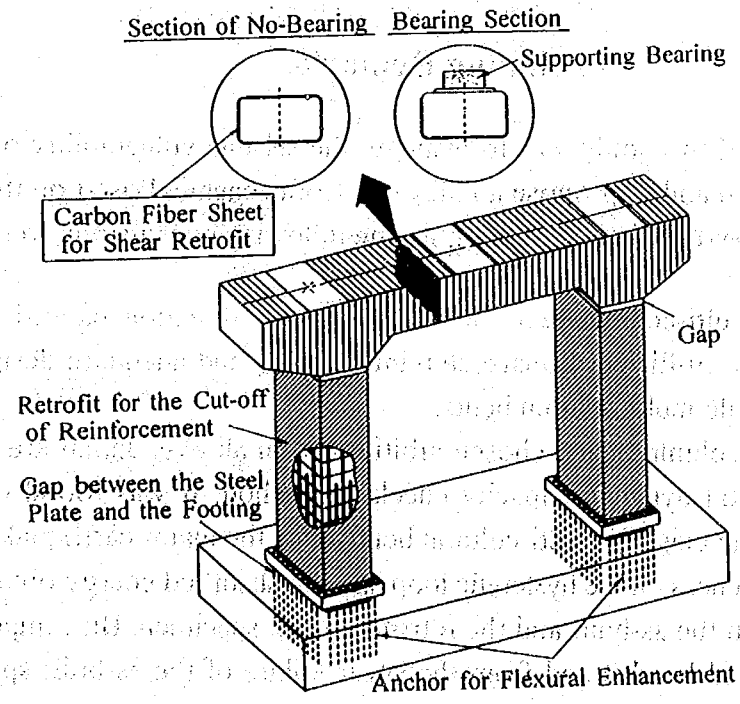


Fig. 13 Proposed Scheme

Fig. 12 shows the comparison of the absorbed energy between the as-built and the retrofitted specimen. As can be seen, there is a few difference between the two specimen. It can be said that the as-built specimen behaved quite well until the shear crack occurred. The general results of the two tests show that only the failure mode could be changed from the shear failure of the as-built specimen to the flexural failure of the retrofitted specimen. But important thing is that the brittle shear failure can be avoided by the steel jacket.

Proposed Retrofit Scheme

In the United States, the extensive work has been done for the retrofit of the multi-column bents[9] such as a link beam or prestressing of the cap-beam. Here, to avoid the shear failure of both the columns and the cap-beams for the multi-column bents and to bear against the major earthquake such as the Kobe earthquake, a seismic retrtofit scheme is proposed, see Fig.13. This approach aims at increasing both the flexural strength and ductility of the columns. The use of well bonded steel jackets are to increase the flexural capacity of columns at sections where premature termination of longitudinal reinforcement at one-half or one-third height was commonly practiced in the older design (Kawashima, 1990[10]). For flexural strength enhancement at the base of the column, longitudinal reinforcement are added outside of the steel jacket and anchored in footing with epoxy grout. The cap-beam is wrapped with carbon-fiber sheet and shear enhancement is expected.

However, there exists considerable controversy about the ductility of the joint region with a reinforcement detail designed by Japan specifications or the effectiveness of the shear enhancement of the carbon-fiber-wrapped cap-beam. Much more study and research are needed and being planned to specify the better retrofit scheme for the multi-column bents.

Concluding Remarks

The purpose of this study was to evaluate the seismic vulnerability of the existing multi-column bents in Japan and to propose a realistic retrofit scheme. Based on the field study, experimental observation and preliminary research , the following conclusions were reached.

1. The damages of multi-column bents in the transverse direction caused by the Kobe earthquake were observed. Sufficient transverse reinforcement and adequate design details are needed to design the ductile multi-column bents.
2. Thirty three multi-column bents, chosen arbitrary from all over Japan are checked by a newly developed horizontal dynamic capacity checking method. It was found out that shear failures are expected on the existing multi-column bents once the major earthquake occurs.
3. There is a few differences on the hysteretic loop and the absorbed energy obtained from the cyclic loading tests between the as-built and the retrofitted test specimen. But, important thing is that the failure mode could be changed from the shear failure of the as-built specimen to the flexural failure of the retrofitted specimen.

4. A seismic retrofit scheme was proposed for the multi-column bents, which aims at the increase of the flexural enhancement, shear enhancement of the column and the cap-beam and the retrofit of the cut-off of the longitudinal reinforcement of the column. But, much more study and research are needed to clarify the ductility of the joint region with a reinforcement detail designed by Japan specifications or the effectiveness of the shear enhancement of the carbon-fiber wrapped cap-beam.

Acknowledgements

Checking method of horizontal dynamic capacity for the muti-column bents were developed through the beneficial and fruitful discussions in the "Special Sub-Committe for Seismic Countermeasures for Highway Bridges"chaired by Dr. K. Kawashima. A significant part of the cyclic loading tests were assisted by Mr. K. Nagaya of PWRI. Assistance from Messers K. Tasaki, T. Sato of PWRI is also gratefully acknowledged.

References

[1] Japan Road Association, Design Specifications for Highway Bridges, Part III Concrete Bridges, Part IV Substructure, Part V Seismic Design, 1990.

[2] V. Prakash, G.H. Powell, S. Campbell, DRAIN-3D, Base Program Description and User Guide, Report No. UCB/SEMM-94/07, University of California, August 1994.

[3] Japan Road Association, Design Specifications for Highway Bridges, 1964.

[4] K. Kawashima, Seismic Design, Seismic Strengthening and Repair of Highway Bridges in Japan, Proceedings of the First U.S.-Japan Workshop on Seismic Retrofit of Bridges, Tsukuba, December 1990.

[5] T. Akimoto, Design Details of Reinforced Concrete Bridges in Japan, Proceedings of the First U.S.-Japan Workshop on Sesismic Retrofit of Bridges, Tsukuba, December 1990.

[6] Japan Road Association, Design Specifications for Highway Bridges, Part V Seismic Design, 1996.

[7] Japan Road Association, Design Specifications for Highway Bridges, Part IV Substructure, 1980.

[8] Hoshikuma, J., Kawashima K., Nagaya K.,"A Stress-Strain Model for Reinforced Concrete Bridge Piers Confined by Hoop Reinforcement," Proceedings of 2nd International Workshop on Seismic Design and Retrofitting of Reinforced Concrete Bridges, 365-385, Edited by R. Park, University of Canterbury, New Zealand, 1994

[9] M.J.N. Priestley, F. Seible, G. M. Calvi, Seismic Design and Retrofit of Bridges, John Wiley & Sons, Inc., 1996

[10] Kawashima, K. "Seismic Design, Seismic Strengthening and Repair of Highway Bridges in Japan", Proceedings of the First U.S.-Japan Workshop on Seismic Retrofit of Bridges, Public Works Research Institute, Tsukuba Science City, Japan, December 17 and 18, 1990.

QUEENSBORO BRIDGE: SEISMIC CONDITION ASSESSMENT AND RETROFIT OF A LANDMARK BRIDGE

S. G. Arzoumanidis
Steinman Boynton Gronquist and Birdsall
New York, New York, 10038

R. B. Gajer
New York City Department of Transportation, Bureau of Bridges
New York, New York, 10006

A. H. Malik
New York State Department of Transportation, Structures Division
Albany, New York, 12232

ABSTRACT

The Queensboro Bridge connecting the boroughs of Manhattan and Queens is a critical transportation link in New York City. It is a two-level, five span truss bridge with extensive approaches and approach ramps. The total length of the Main Bridge spanning the East River is 1135,3 m. The structure, a registered US landmark, opened to traffic in 1909 and carries a daily volume of approximately 147.000 vehicles. An in-depth seismic condition assessment was conducted and retrofit measures were recommended for this major east coast bridge. The study, which combined the efforts of seismologists, geotechnical, and structural engineers, served as a prototype for understanding the seismic response and retrofit needs of bridges at the moderate seismicity environment of the east coast of North America. This paper reports on the issues of condition assessment, retrofit measures, and other findings regarding the expected seismic response of this bridge, which represents the design practice of another era.

BRIDGE DESCRIPTION

The Queensboro Bridge, Figs 1 and 2, consists of four different riveted steel structures with a variety of structural systems and forms resulting in distinct responses:

- *The Manhattan Approach*, a two-level stringer and multiple column bent structure with extensive masonry encasements.
- *The Main Bridge*, a two-level double cantilever span truss structure, supported on masonry piers.
- *The Queens Approach*, a two-level parallel chord truss structure supported on steel four-leg towers and two-leg bents.
- *The Approach Ramps*, a one and two levels system of viaduct structures from stringers, floorbeams, and columns.

The Manhattan Approach has a total length of 329,5 m. The lower roadway framing is enclosed by a facade of granite stones and terra cota tiles forming masonry arches and infill walls,

Fig. 3. Underneath the lower roadway, the enclosed space has a ceiling of historic tiled Guastavino shells, bearing the name of the engineer who invented the method of construction of shells with tiles. The columns of the lower level are encased in concrete and masonry veneers, Fig. 4. They are supported on foundations consisting of 2,44 m x 2,44 m square unreinforced concrete pedestals bearing on hardpan or rock at various levels up to 7,6 m below the ground surface.

The Main Bridge includes towers and trusses passing through the towers, which are features of suspension bridges, showing the influence from the nearby Williamsburg and Manhattan Bridges, constructed about the same time. The Main Bridge consists of the Manhattan, Queens, and the Roosevelt Island portions, which are connected at the middle of the two channels of the East River with vertical links and transverse shear keys. The tension members of the trusses are made of eyebars and the compression members of plates and lacing bars. The four towers, Fig. 5, are about 61 m tall, 29 m wide at the bottom, and 18,3 m wide at the top, where they are connected with the truss diagonals and top chords.

At each end, the bridge is supported on links that allow longitudinal displacements. At Piers 1, 2, and 4, the supports are fixed bearings, and at Pier 3 sliding bearings. Transverse loads are resisted at all piers through shear keys. The arch-shaped piers, Fig. 6, consist of a 4,9 m thick spandrel beam from unreinforced concrete and steel I-beams supported on two legs from unreinforced concrete or limestone. The height of the piers varies between 18,3 m and 42,7 m. These massive structures have a veneer from large granite blocks and are founded on rock.

The Queens Approach is a 681,5 m long through truss structure consisting of simply supported and continuous spans varying in length from 29,6 m to approximately 50,6 m. All members consist of plates and angles connected with lacing bars. As in the Manhattan Approach, each column is founded on 2,44 m x 2,44 m square unreinforced concrete pedestals bearing on rock at various levels up to 15,2 m below the ground surface. Thus, for many columns, the concrete portion embedded in the ground is longer than the steel portion above ground.

The Approach Ramps were constructed at different times and consist of an extensive system of viaducts connecting the upper roadways of the Queens and Manhattan Approaches with local streets. The viaducts are mostly founded on concrete filled steel pipe piles, or H-piles.

GROUND MOTIONS

A seismic hazard analysis was performed by the team of Dr. K. Jacob at Lamont-Doherty Earth Observatory, [1], [2], based on the seismicity of the Manhattan Prong and portions of the adjacent Newark Basin and Hudson Highlands. Straight line fits to the observed seismicity were made using the Gutenberg-Richter frequency of occurence-magnitude relation

$$\log n = a - bM$$

where M is magnitude of earthquakes, n is the rate of events normalized to number of events per year per km^2, and a and b are parameters. This relation allows the representation of magnitude-distance combinations of events consistent with the established hazard levels as follows:

- A low to moderate hazard level, the Operation Basis Earthquake (OBE), established as a seismic event with a 10% probability of exceedance in 50 years or approximately 500 years return period. This is similar to the hazard level of the AASHTO Specifications.
- A high hazard level, the Structural Safety Earthquake (SSE), established as a seismic event with a 10% probability of exceedance in 250 years or approximately 2,500 years return period.

Magnitudes 5, 6, and 7 were used to establish envelope spectra for the above hazard levels and subsequently synthesize ground motions [3]. The rock level envelope spectra for the Queensboro Bridge site are shown in Fig. 7. These spectra are characterized by a significant peak at low periods and by fast reduction in the spectral values with the increase of period, both features of the earthquakes on the east coast of North America.

It should be emphasized that the spectra in Fig. 7 represent earthquake events for which only a handful of recordings are available and even those do not represent the higher magnitude of the considered motions. These spectral accelerations were questioned by some. For this reason, the New York City and State Departments of Transportation in cooperation with the Federal Highway Administration have undertaken the initiative to organize a meeting of well known seismologists to discuss the issues and reach a consensus on the proper ground motions for the New York City Metropolitan area.

GEOTECHNICAL STUDIES

The soil profile of the bridge is shown in Fig. 1. This profile was developed on the basis of old borings obtained at various times and on seventeen new borings as shown in Fig. 8. Quantitative information on the soils was obtained using

1. Standard Penetration Tests (SPT).
2. Water content, gradation, and classification tests.
3. Resonant column and cyclic torsional shear tests on undisturbed samples of peat.
4. In situ shear and compressional wave velocity measurements in the soil and rock using crosshole, surface analysis of surface waves (SASW) and refraction techniques.

Testing of the above items 3 and 4 was conducted by Prof. K. Stokoe. The overall geotechnical work was performed by Prof. R. Dobry, [2], [4]. He determined the soil and foundation conditions along the bridge, developed site-specific free-field elastic design response spectra and compatible time histories for the OBE and SSE earthquakes, performed simplified soil-structure interaction analysis for foundations of the Manhattan and Queens Approaches, and evaluated the liquefaction potential of the granular soils predominant at the project site.

The project site was divided in five areas of similar soil conditions labeled sites 1 through 5, Fig. 8. Site 3 in Queens is the most interesting because it contains a layer of fibrous peat of nearly constant thickness of 1,8 m. Crosshole shear (V_s) and compressional (V_p) wave velocity

measurements at the different soil layers and the top of the rock were conducted at borings NB6/NB6A, Fig. 9, and showed that the shear wave velocity of the peat is 65,2 to 78,9 m/sec., which is much less than the velocity of the soils above and below. A low total unit weight γ_t=10,68 kN/m^3 was measured in the laboratory for the undisturbed peat samples. Fig. 10 presents the shear modulus reduction and material damping curves measured on the undisturbed peat samples in the dynamic soil tests. They are compared with standard curves for sands showing that the peat has an extremely linear cyclic stress-strain behavior.

Ground motions were developed at the top of the foundations for each site and both OBE and SSE events. One-dimensional analyses with the equivalent linear method of the program SHAKE, [6], were used. This method was considered a satisfactory approach , since the seismic shear strains of the soil remained below 0,3%. More elaborate studies, especially for site 3, may be necessary for the design of the retrofit measures.

PERFORMANCE CRITERIA

The bridge performance goals were set as follows:

- For the OBE, the goal is for the bridge to remain functional after an earthquake. The bridge shall be capable to carry normal traffic almost immediately after an earthquake, with minimal or no damage to structural elements.
- For the SSE, the goal is for the bridge to be capable to carry limited traffic within days and full traffic within months after an earthquake. Any damage shall be repairable without complete closure for extended periods.

The performance of structural components was determined on the basis of the capacity over demand ratio *(C/D)* for all potential modes of failure [7]. *C/D* ratios greater than one indicate adequate capacity. The lowest *C/D* ratio value of each component, if it is less than one, indicates the controlling mode of failure. This *C/D* ratio is defined as follows:

$$C/D = \frac{R_c - \sum Q_l}{Q_{EQ}}$$

where R_c the nominal ultimate displacement or force capacity of a component for the mode of failure under consideration,

$\sum Q_l$ is the sum of displacement or force demand for loads other than earthquakes such as dead and live loads, and

Q_{EQ} is the earthquake displacement and force demand.

For a multi-axial stress state, the C/D ratio for a component can be expressed as

$$C/D = \frac{1 - \sum Q_l / R_c}{Q_{EQ} / R_c} = \frac{1 - \sum SR_l}{SR_{EQ}}$$

where $\sum SR_l$ is the sum of stress ratios of force demands, e.g. as per AASHTO Specifications, for other than earthquake loads to the capacity of the component,

SR_{EQ} is the stress ratio for earthquake force or deformation demand to the capacity of the component.

Decisions on which components are to be retrofitted were based on the likely consequences from their damage, especially on the performance of entire structural systems with damaged components. The structural members were classified as primary with no redundant load path, primary with redundant load path, and secondary as follows:

- Primary members with no redundant load path are those members resisting gravity loads and selected members resisting primarily lateral loads. This is a group of members whose failure would result in serious consequences on the integrity of the bridge. These members are subject to the strictest requirements: Under compression or bending, they are required to be capable of developing a full plastic stress distribution before buckling, while under tension, are required not to yield. These requirements are fulfilled by compact members with appropriate lateral supports.
- Primary members with redundant load path are most members resisting primarily lateral loads. Failure of these members would result in less serious consequences on the integrity of the bridge than the primary members with no redundant load path. Under compression or bending, these members are required to be capable of developing their yield stress in compression before buckling, but are not required to be capable of developing their full plastic stress distribution. Under tension, they may yield. These requirements are fulfilled by non-compact members with proper lateral supports.
- Secondary members are those serving as bracings of primary members. Under compression, these members may buckle elastically before their yield stress is reached. Under tension, they may yield. Slender members which may buckle globally or locally belong in this category.

AMBIENT VIBRATION MEASUREMENTS

Ambient vibrations were measured by Lamont-Doherty Earth Observatory (LDEO) using three-component sensors at a number of locations on the bridge and the foundations, [1], [2]. The data were recorded digitally by individual data loggers, whose internal clocks were synchronized to run simultaneously to within a millisecond. Sampling was achieved without cumbersome cabling between each sensor and a recording device. Results of the measurements were used for calibration of the computer models developed for the analysis of the bridge.

Three different portions of the bridge were tested. Samples were taken at the rate of 50 per second. Comparative data for the analytical predictions of periods and those identified by measurements are given in [8], and an excerpt is shown in Fig. 11.

Twelve instruments were deployed near the eastern end of the Manhattan Approach. Only five modes and their periods ranging from 0,36 sec. to 0,25 sec. could be positively identified. It was understood later that the mode shapes in this type of stiff structure involve many small length scales that are hard to identify when only sparse instrumentation is used. It took the assistance of the analytical model to identify further modes and frequencies.

The Main Bridge is a relatively flexible structure and includes many modes of large scale (involving long portions of the bridge). Measurements over the entire Main Bridge were

conducted with twelve instruments placed successively in two separate locations with some instruments common to both locations. All instruments on the superstructure were placed at the lower chord below the deck level. The measurements were taken during four 20-minute time windows.

Twenty four modes and their periods ranging from 2,87 to 0,53 sec. were identified. Unlike the Manhattan Approach, Fig. 11 shows that the comparison between analytical predictions and measurements is very satisfactory, both in the shape of modes as well as value of the respective periods. Longitudinal modes could not be determined from the measurements. With the help of the computer model, these modes were later identified in the measurement records. They are very weak modes, whose amplitude is very small, appearing as tiny peaks in the power spectral logs derived from the measurements.

At the Queens Approach, eleven instruments were used for measurements at the twenty panel western portion of the structure. For this structure of intermediate stiffness, nine modes and their periods were positively identified with a range of periods between 0,90 and 0,28 sec. Analytical predictions for modes involving large length scales agreed well with those obtained by measurements. For modes of smaller length scale, a good match was harder to achieve. Oscillations with periods lower than 0,30 sec. was not straightforward to associate with specific modes. The computer model was used to assist in this identification.

For all portions of the Queensboro Bridge, the computer model was found to give better results with the supports assumed fixed. For the Manhattan Approach model, the concrete and masonry components were assumed without cracking, participating with their full stiffness in the response of the structure. Both of these conditions are reasonable for the low level amplitude vibrations.

ANALYSIS

The Queensboro Bridge seismic condition assessment was performed using the multi-mode response spectrum method with uniform excitation. This procedure of course has its limitations, and a time history approach could have produced more accurate results. However, it is believed that in this phase of identification of vulnerabilities the response spectrum procedure was generally sufficient.

While most structural components have adequate strength to resist the seismic demands, several others are considerably vulnerable, expected to be damaged even at seismic forces of low intensity. This is typical behavior for bridges that were not designed for seismic loads. Examples of vulnerable components at low levels of seismic forces are as follows:

- *Manhattan Approach.* The masonry elements, which provide significant stiffness to the steel components but have limited strength in bending. The unreinforced concrete foundations of columns which were designed as compression members only.
- *Main Bridge.* The masonry piers, which have no reinforcement and resist lateral loads through their own weight and the weight of the superstructure.
- *Queens Approach.* The truss bearings, which have limited shear capacity. The anchor bolts of the column base anchorages, which could yield under the bending moment demands. The

unreinforced concrete foundations of columns, which are similar to those of the Manhattan Approach.

- *Approach Ramps.* The floorbeam connections to columns, which are a part of the framing system resisting lateral loads. The anchor bolts of column base anchorages, which could yield like those of the Queens Approach.

The effect of early damage of key components was accounted for in the analysis as follows:

1. All components whose vulnerability could cause loss of stability of the structure were assumed retrofitted prior to the initiation of the analysis.
2. If early damage would only induce strong nonlinear response, several iterations of analysis and evaluation were performed to determine the secant stiffness for final analysis.

Three large computer models were prepared, one each for the Main Bridge, Manhattan and Queens Approaches. Eighteen smaller size models were necessary for an equal number of portions of the Approach Ramps. Numerous other variations of these models were used for the needs of the analyses. Portions of the Queens Approach Ramps were not analyzed and the assessment of their condition was based on interpolation of the results of adjacent segments.

SEISMIC RESPONSE AND RETROFIT MEASURES

The Manhattan Approach is a stiff structure, particularly at the lower level, where the masonry components contribute significantly to the overall stiffness. Cracking of the masonry due to an earthquake changes significantly the frequencies of the approach. This effect occurs due to the reduction in flexural rigidity at critical locations as shown in Fig. 12. The flexural rigidity is strongly affected by the size of bending moments, Fig. 13. Cracking of the masonry occurs at low levels of seismic loads. At the initiation of cracking, there is a considerable drop in flexural rigidity, which is followed by a more gradual reduction as the bending moment increases further.

The recommended retrofit of this approach is for ductility of the steel components. It consists of local strengthening of floorbeam connections and bracings, elimination of expansion joints, and installation of restraining cables. It allows damage of the masonry, which in itself does not constitute a safety risk for the structure. On the down side, damage of the masonry may hide damage of the underlying steel structure as well, which will not be visible. A strategy for preventing damage of the brittle masonry components would require retrofitting for strength. This could be achieved by providing added stiffness to the flexible steel frames in the form of extensive bracings of the columns at the lower level. This work would interfere with the existing masonry components and would be very expensive.

The unreinforced concrete pedestals of the numerous columns of this approach need further study of their interaction with the soil to determine the exact nature of the soil pressure. Measures for strengthening these embedded in the ground structures, by drilling along their height to install reinforcement, are expensive and due to their large number any excavation would cause disruption to traffic.

Although the Main Bridge truss shows no serious vulnerabilities, its support system, especially for the center Roosevelt Island portion of the bridge, requires major retrofitting. The

support system includes the bearings and the tall arch-shaped masonry piers resisting the seismic demands of this 670 kN heavy superstructure. The bearings were found to be vulnerable in the longitudinal direction due to insufficient shear capacity and the piers due to insufficient bending moment capacity.

The piers require retrofit for strength as ductility and redundancy are non-existent. The envisioned retrofit consists of encasing them with new concrete walls, including embedded steel frames anchored in the existing sound rock, Fig. 14. Two alternative retrofit strategies are considered for other components of the bridge. First, strengthening of the base of the towers and installing dampers to reduce the loads on the piers, Fig. 15. Second, retrofitting of the fixed bearings combined with restoring force and damping devices. Considerable further study is required to identify the best alternative considering performance, constructability, maintenance of traffic requirements, cost, long term maintenance, etc.

The Queens Approach is greatly affected by the response of the underlying soft layers, especially those of site 3. Resonance conditions appear to develop, since the soft soils help shift the peak of the response spectrum towards the important structural periods of the superstructure. This superstructure is stiff, but it is supported on flexible substructure (towers and bents). As mentioned before, the main vulnerabilities concern the support system: Bearings, towers, bents, and the reinforced concrete pedestals. Solutions to these vulnerabilities include strengthening of the towers and bents by providing new members, and replacing existing members with stronger new ones. The work includes reconfiguration of the support system with isolation bearings, and installation of shear transfer keys between adjacent portions of the structure. In lieu of isolation bearings, damping devices were considered and were found in preliminary studies to be beneficial for the response of the bridge, [9].

The Queens and Manhattan Approach Ramps are quite flexible, especially in the longitudinal direction. Most columns and their connections with the foundations, floorbeams, and stringers are vulnerable and cannot resist bending moments to provide frame action for lateral stability. Strengthening of the connections between columns and stringers to improve the longitudinal frame action provides only limited help due to the flexibility of the stringers. Thus, it appears that considerable longitudinal loads must be resisted by cantilever action of the columns fixed at the foundations.

SUMMARY

The Queensboro Bridge, which is a major transportation link in New York City, underwent a seismic condition assessment in order to understand the seismic response and retrofit needs of older bridges at the east coast of USA, a region of moderate seismicity. This effort integrated the knowledge in the fields of seismology, geotechnical, and structural engineering. The project demonstrated that older bridges of the east coast, which were not designed for seismic loads, have many vulnerabilities. It was also demonstrated that the current seismic provisions of specifications, retrofitting guidelines, etc. do not adequately reflect the realities of the east coast.

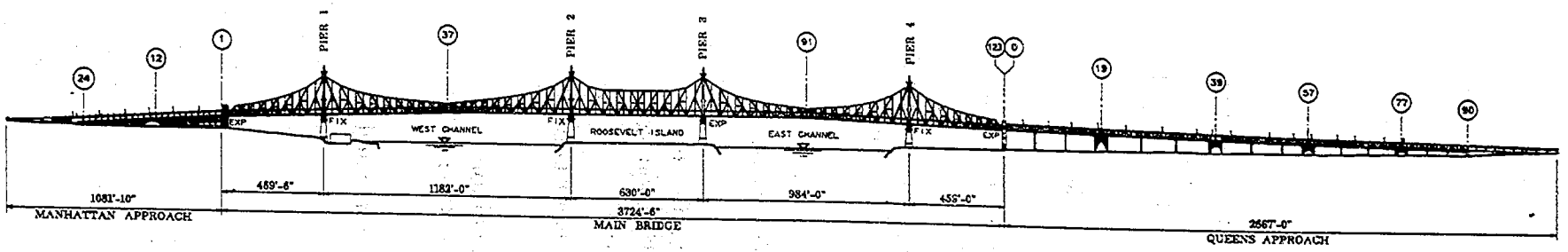
ACKNOWLEDGMENTS

The seismic investigation of the Queensboro Bridge was conducted for the New York City and the New York State Departments of Transportation. Their support in conducting this work is gratefully acknowledged. The authors also want to acknowledge Dr. Ian Buckle and Mr. Ian Friedland of the National Center for Earthquake Engineering Research (NCEER), who organized and coordinated the team of seismologists, geotechnical engineers, and peer reviewers (Mr. M. Power and Prof. M. Shinozuka) for this project.

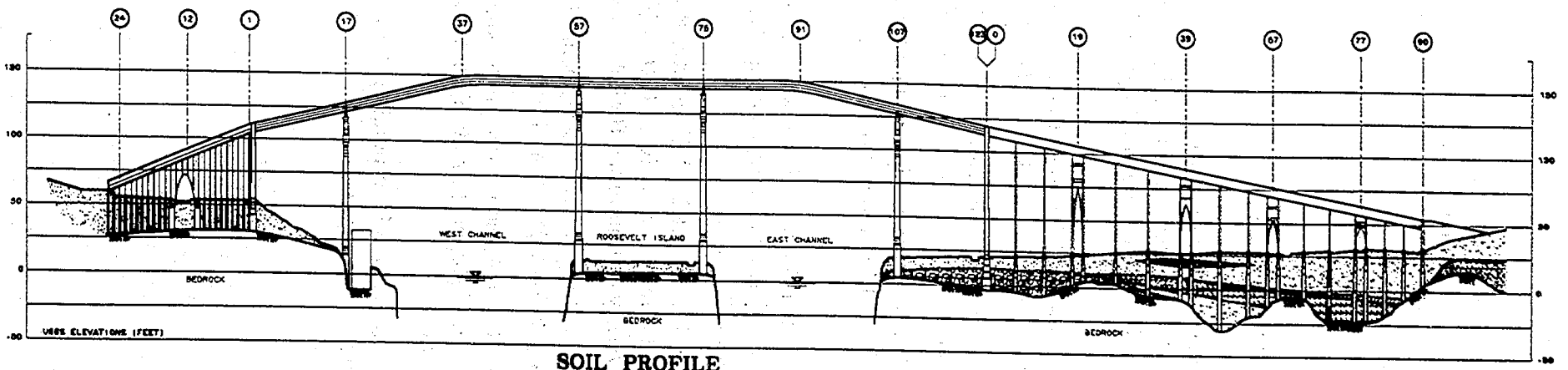
REFERENCES

1. Jacob Klaus H., Horton Steve, Armbruster John and Barstow Noel, "Seismic Retrofit Study of the Queensboro Bridge, N.Y.: Rock Motions and Mode Identification by Ambient Vibration Measurements," Eleventh World Conference on Earthquake Engineering, Acapulco, Mexico, Jun. 1996.
2. "Queensboro Bridge Seismic Hazard Assessment," National Center for Earthquake Engineering Research, State University of New York at Buffalo, Jan. 1995.
3. Horton, S.P., "Simulation of Strong Ground Motion in Eastern North America," Proceedings of the 5th National Conference on Earthquake Engineering, Vol. III, Jul. 1994.
4. Dobry R., Liu L. and Stokoe II K. H., "Queensboro Bridge in New York City: Geotechnical Seismic Hazard Assessment," Eleventh World Conference on Earthquake Engineering, Acapulco, Mexico, Jun. 1996.
5. Seed, H.B. and Idriss, I.M., "Soil Moduli and Damping Factors for Dynamic Response Analysis," Report No. UCB/EERC-70-10, Earthquake Engineering Research Center, University of California, Berkeley, Dec. 1970.
6. Schnabel, P. B., Lysmer, J., and Seed, H. B., "SHAKE: A Computer Program for the Response Analysis of Horizontal Layered Sites," Report No. EERC 72/12, Earthquake Engineering Research Center, The University of California, Berkeley, CA., 1972.
7. "Seismic Retrofitting Manual for Highway Bridges," US Department of Transportation, Federal Highway Administration, FHWA-RD-94-052, May 1995.
8. Steinman Boynton Gronquist and Birdsall, "Queensboro Bridge, Seismic Condition Assessment and Retrofit Recommendations," Report to New York City Department of Transportation, Bridge Design, Jan. 1996.
9. Constantinou, M., "Seismic Rehabilitation Scheme Incorporating Restoring Force and Damping Devices for Queensboro Bridge," Sep. 1994.

K:\cadd\849100\fig1.dgn Nov. 26, 1996 12:23:48



ELEVATION

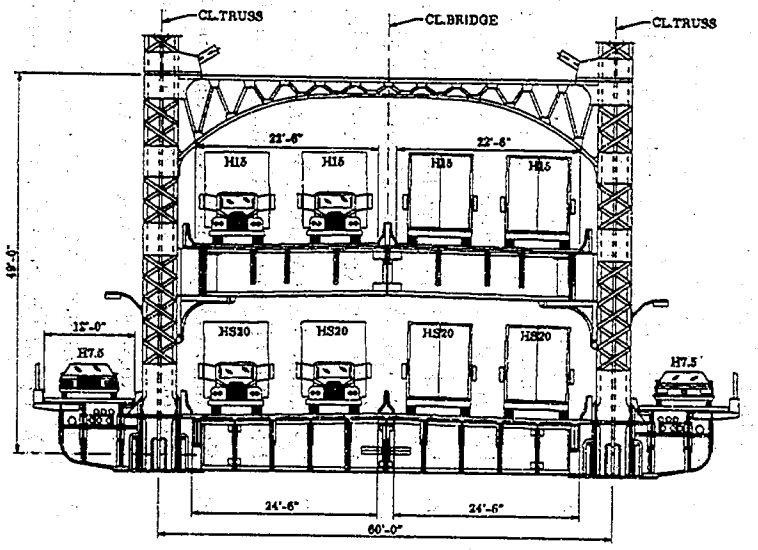


SOIL PROFILE

SCALE: 1"=500' HORIZONTAL
1"= 75' VERTICAL

LEGEND:

- LOOSE TO DENSE SILTY SAND
  LOOSE SAND AND GRAVEL
- MEDIUM DENSE TO DENSE SAND AND SILT
- COBBLES
- SANDY GRAVEL
- SOFT ORGANIC PEAT



CROSS SECTION

Fig.1 Elevation, Soil Profile and Cross Section

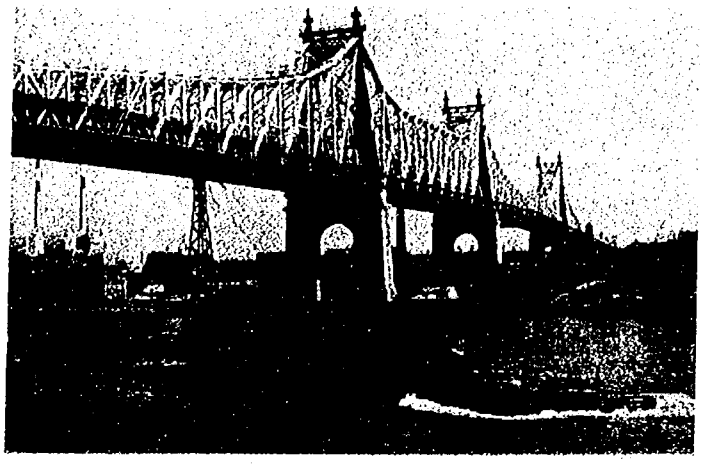


Fig. 2 Queensboro Bridge

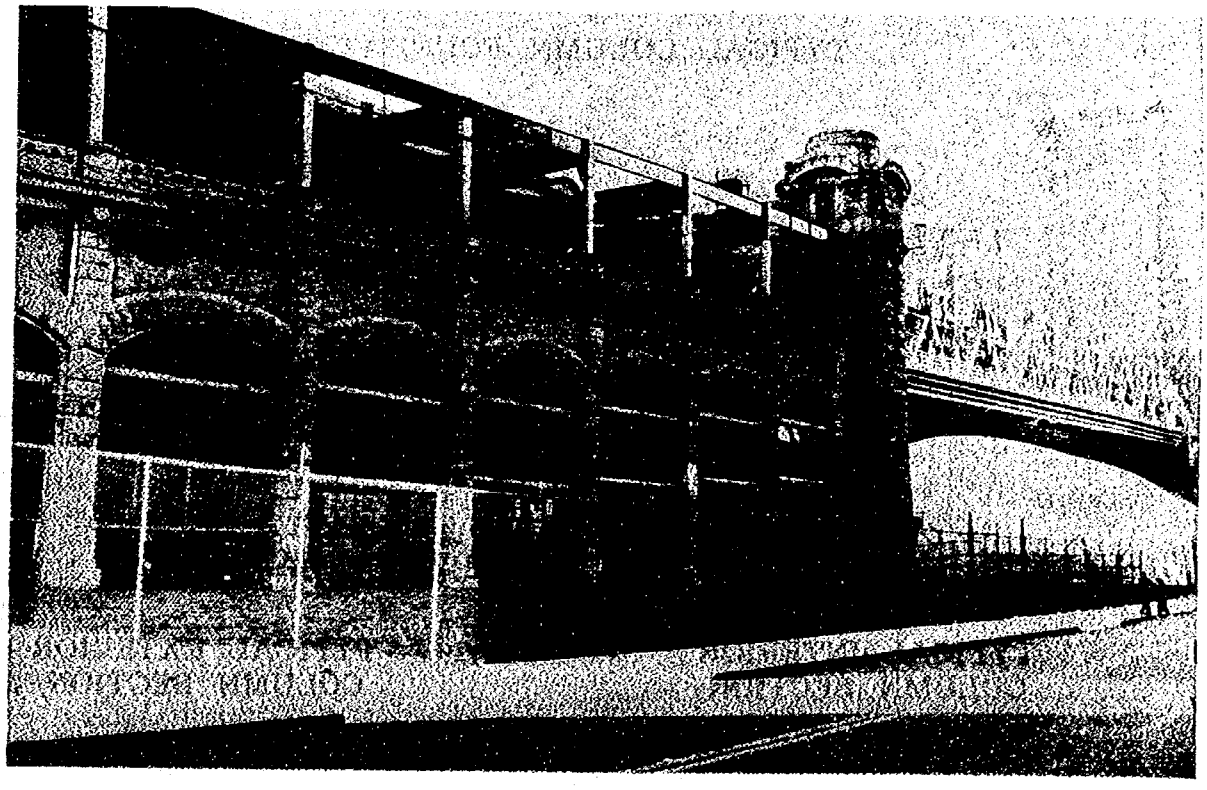
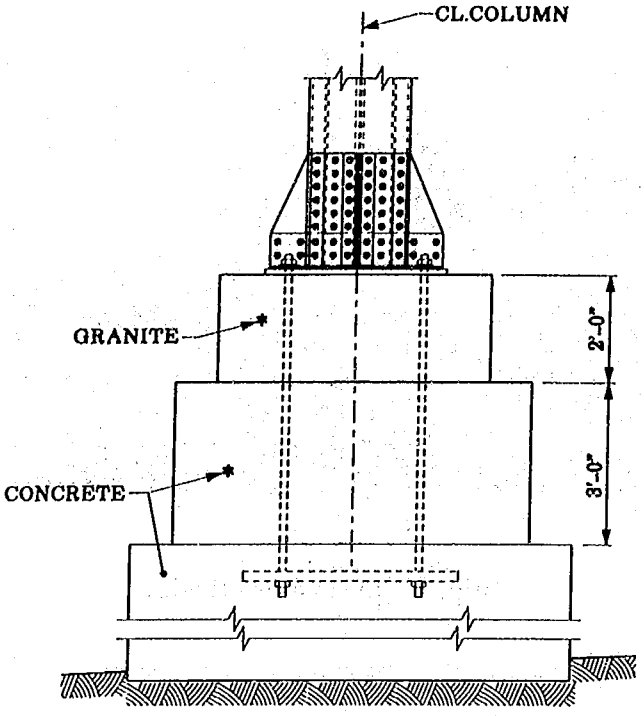
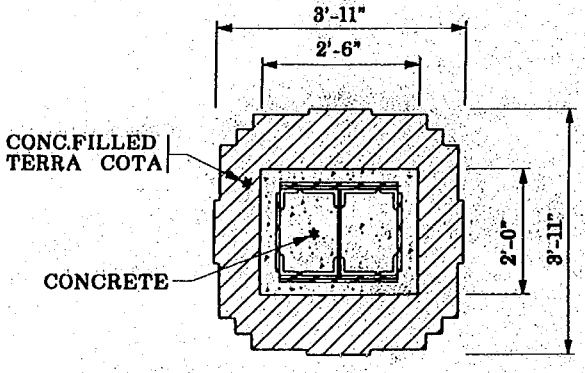


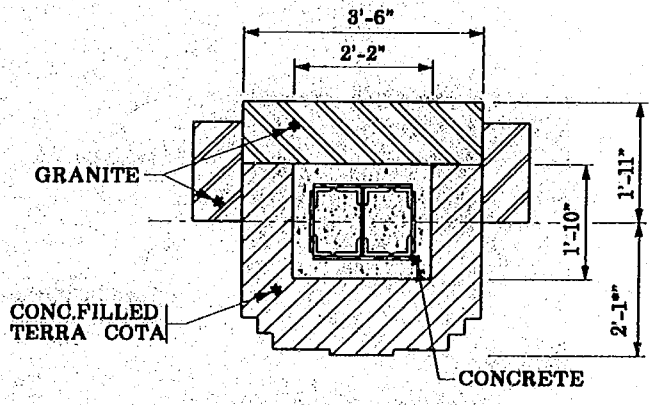
Fig. 3 Manhattan Approach



TYPICAL COLUMN FOUNDATION



TYPICAL INTERIOR
COLUMN SECTION



TYPICAL EXTERIOR
COLUMN SECTION

Fig.4 Typical Column and Foundation Details in Manhattan Approach

k: \cadd\849100\fig4.dgn Nov. 26, 1996 12:54:45

k:\cadd\849100\fig5-6.dgn Nov. 26, 1996 12:49:26

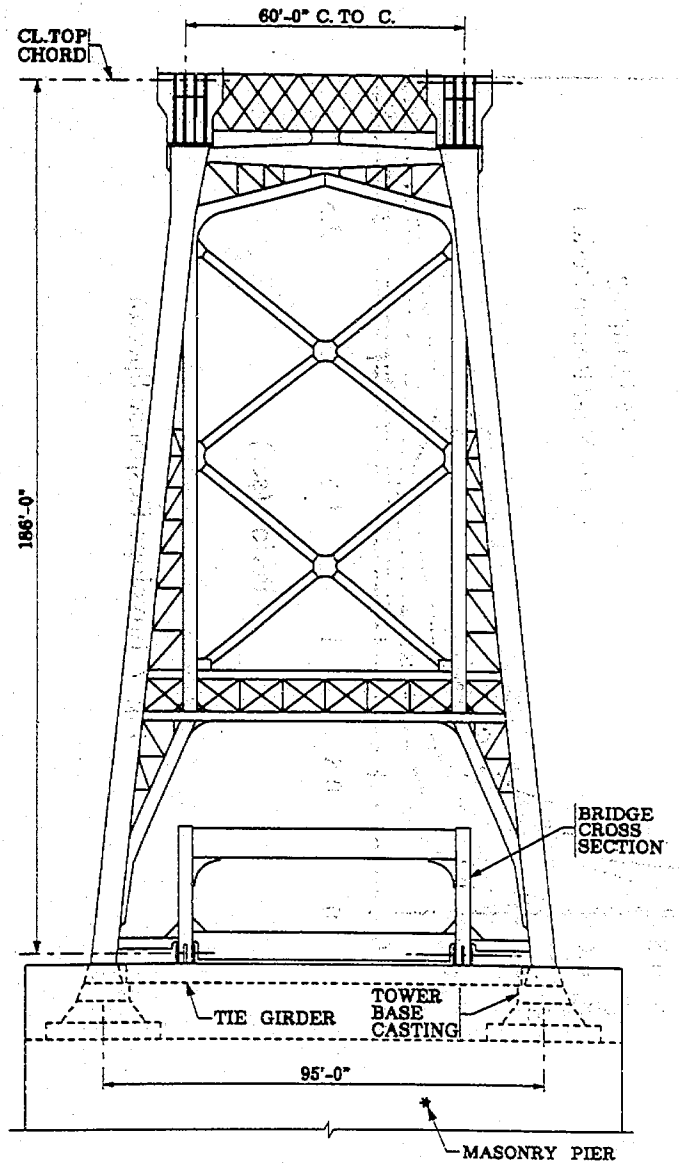


Fig.5 Tower Elevation

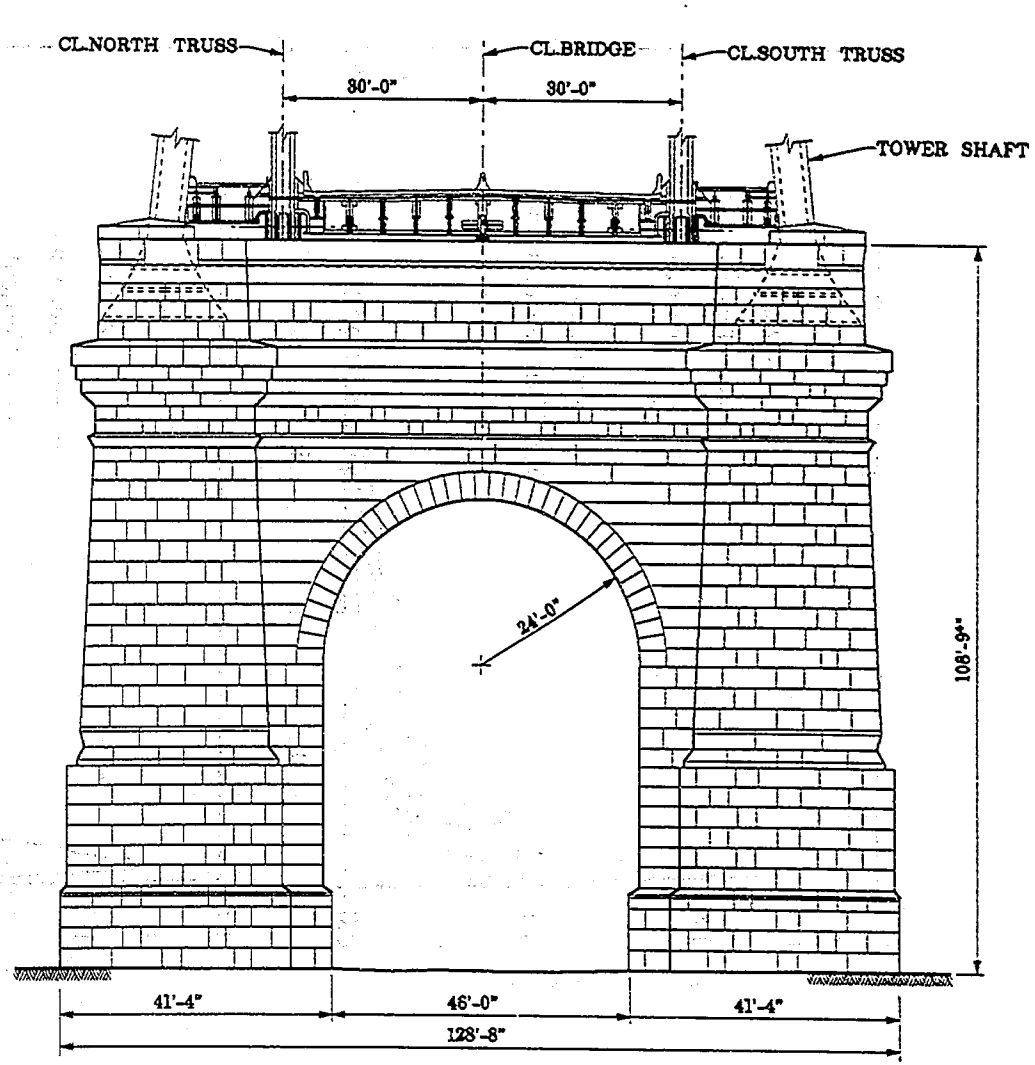


Fig.6 Pier 1 Elevation

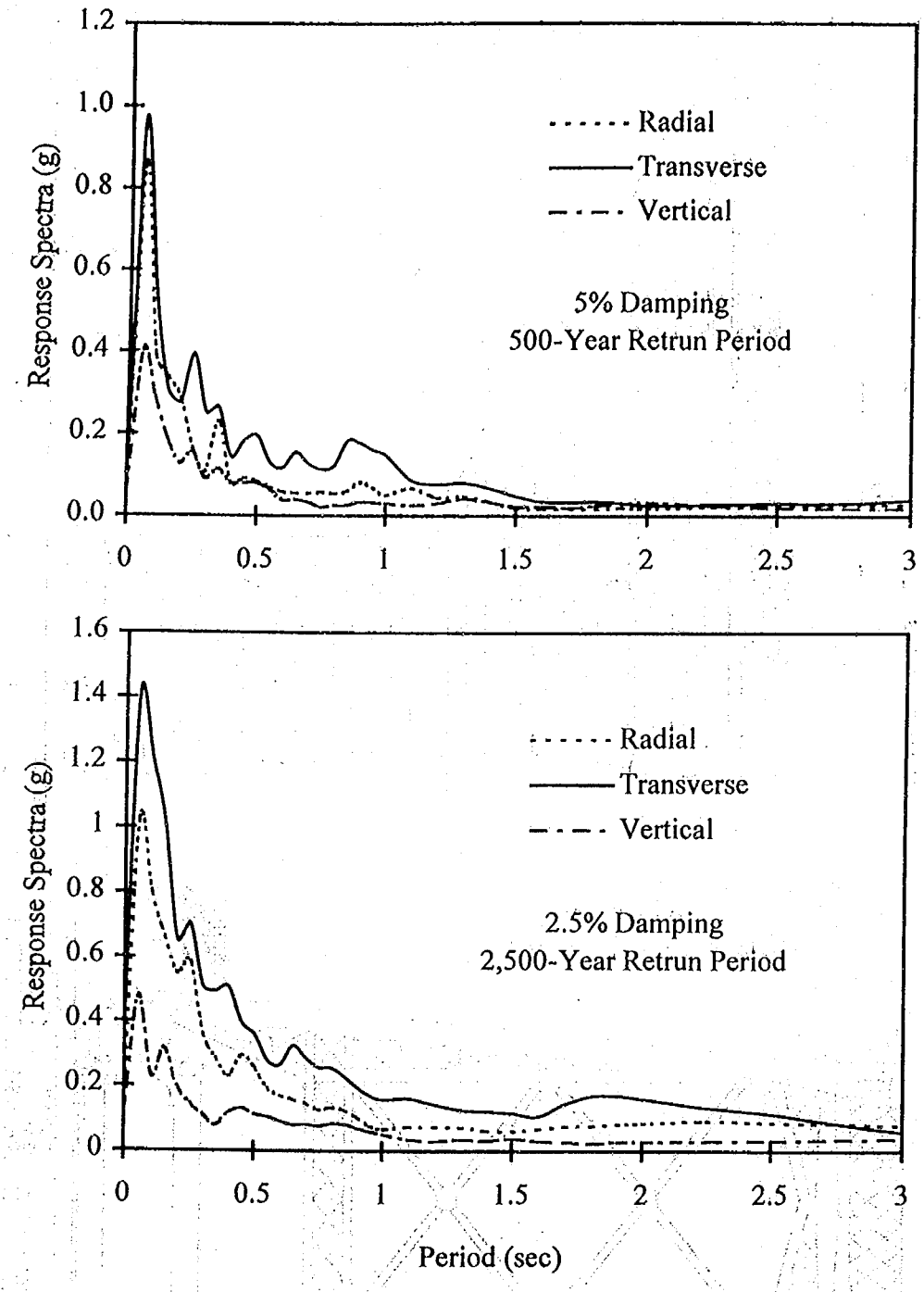


Fig. 7 Envelope Response Spectra

K:\cadd\849100\fig8.dgn Nov. 26, 1996 12:29:29

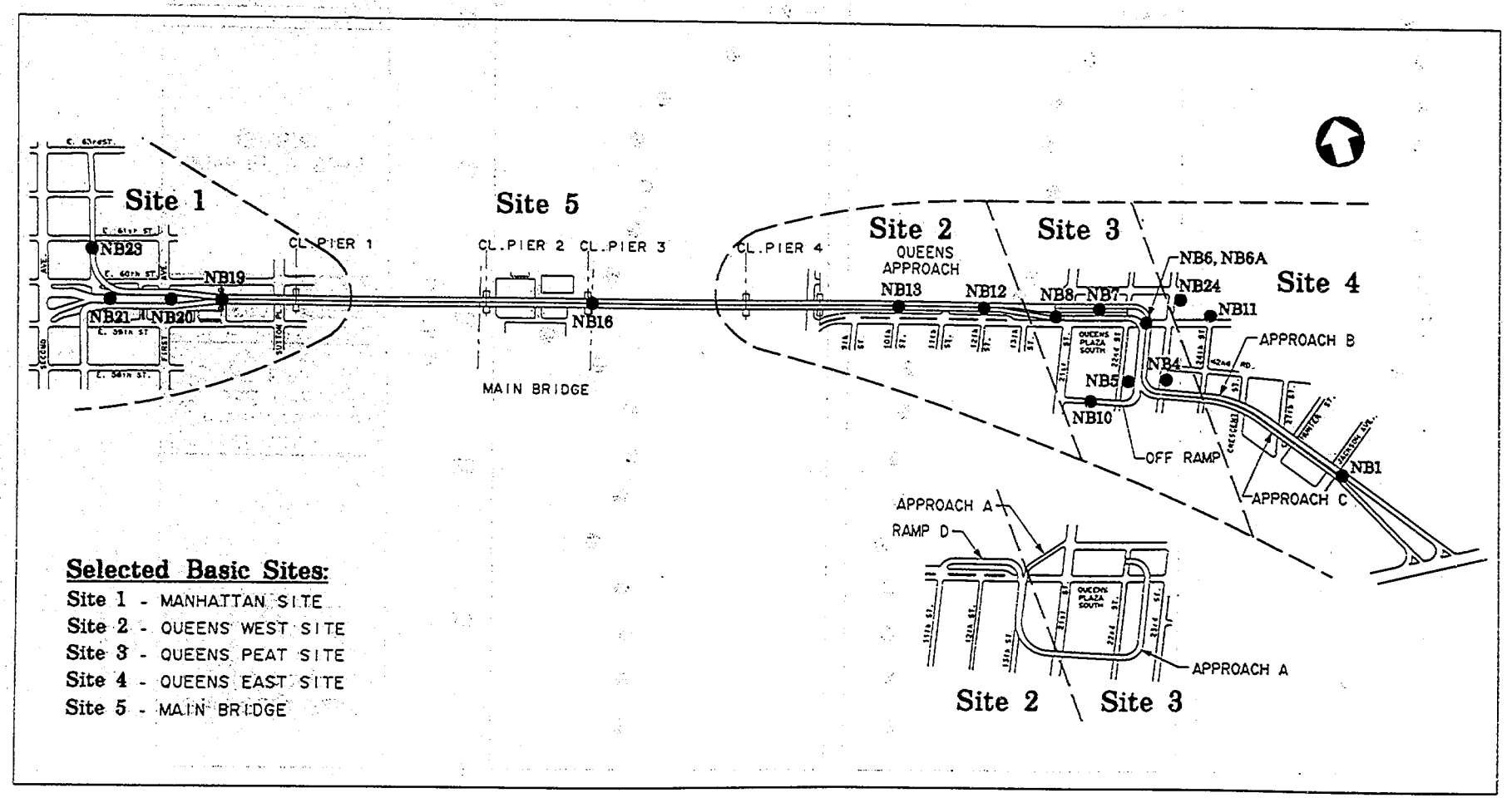


Fig.8 Locations of Borings

K:\cadd\849100\fig9.dgn Nov. 26, 1996 12:30:40

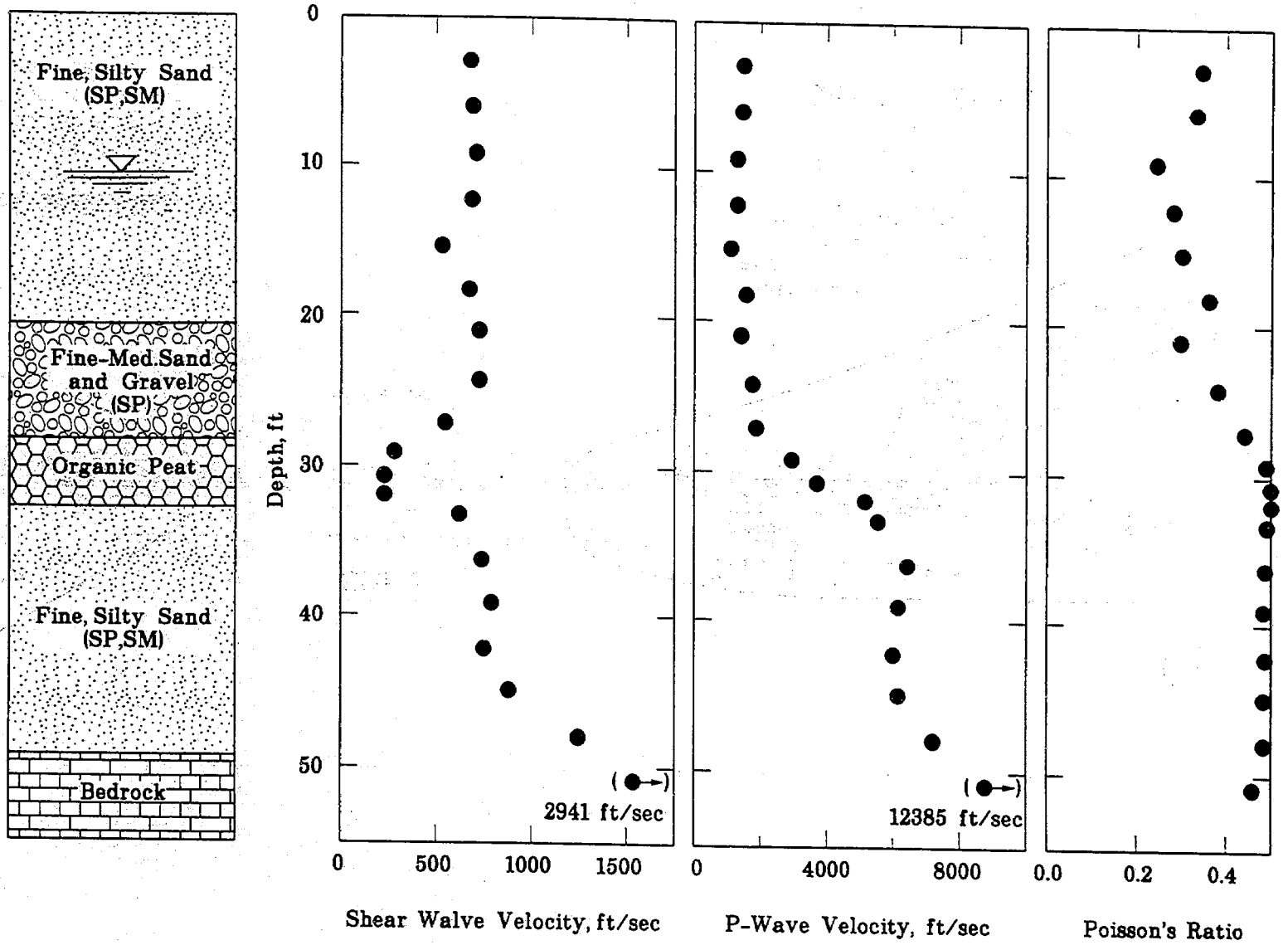
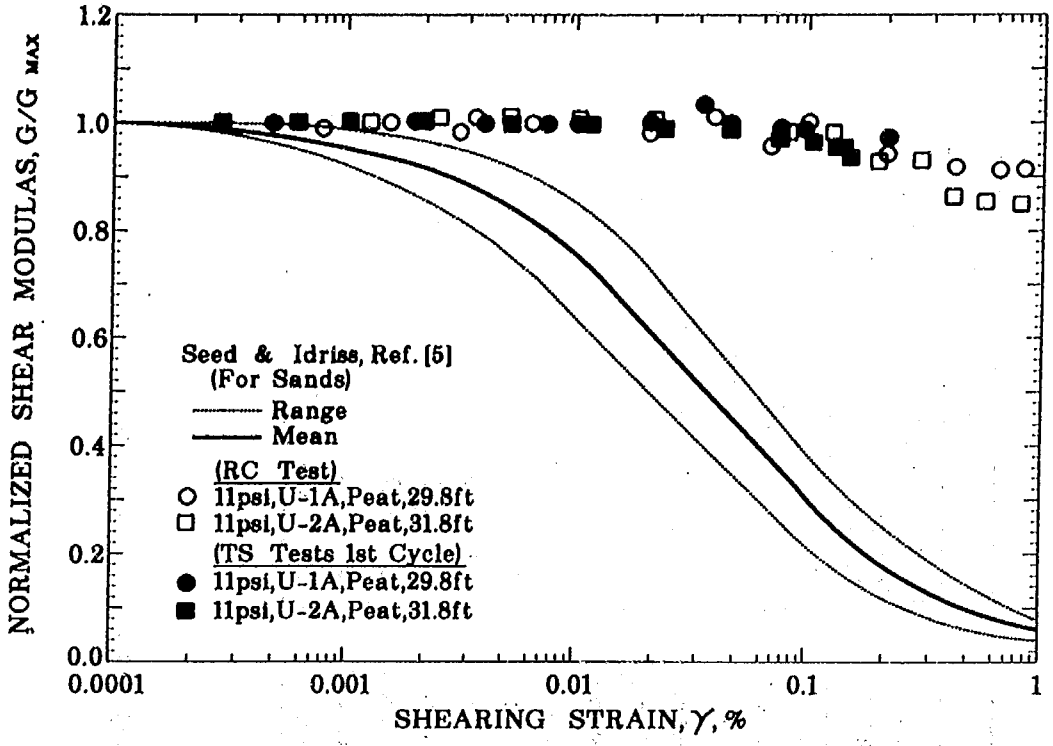
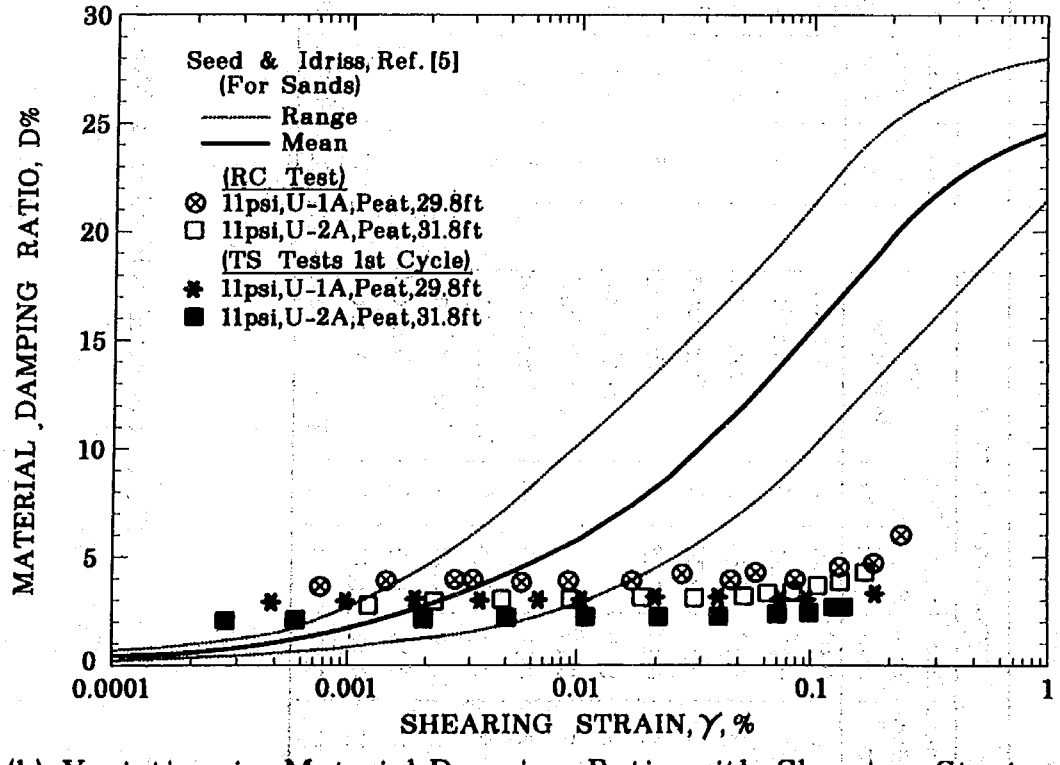


Fig.9 Shear and Compessional Wave Velocity Profiles Obtained from Crosshole Seismic Testing at Location NB6/NB6a



(a) Variation in Normalized Shear Modulus with Shearing Strain

NOTES: 1. Only Results at the Estimated in Situ Mean Effective Stress for Each Sample are Plotted.
2. Shearing Strains in RC Test Were Corrected to the Average of the First 3 Free-Vibration Cycles.



(b) Variation in Material Damping Ratio with Shearing Strain

Fig.10 Results from Resonant Column and Torsional Shear Tests of Undisturbed Peat Sample from the Qeensboro Bridge Site

Manhattan Approach				
Comp. Mode No.	Comp. Period (sec)	Meas. Period (sec)	Perc. Diff. %	Mode Description
1	0.39	0.36	8	Transverse
2	0.37	0.35	6	Vertical
3	0.28	0.30	8	Transverse
4	0.27	0.26	3	Transverse
5	0.25	0.25	0	Vertical
6	0.19			Longitudinal
7	0.19			Longitudinal
8	0.18	0.19	10	Transverse
9	0.15	0.15	0	Trans. & Long.
10	0.14	0.14	1	Vert. & Long.
11	0.14	0.13	7	Vertical
12	0.12	0.11	7	Vertical
13	0.11	0.11	1	Trans. & Vert.

Main Bridge				
Comp. Mode No.	Comp. Period (sec)	Meas. Period (sec)	Perc. Diff. %	Mode Description
1	2.87	2.63	8	Transverse
2	2.24	2.17	3	Vertical
3	2.06	2.08	1	Transverse
4	1.85	1.79	3	Vertical
5	1.35			Local
6	1.24	1.27	2	Transverse
7	1.22	1.18	3	Vertical
8	1.16			Local
9	1.14	1.14	0	Transverse
10	1.09	1.10	0	Torsional
		1.02		Transverse
11	1.05	1.01	4	Vertical
12	0.92	0.92	0	Transverse

Queens Approach				
Comp. Mode No.	Comp. Period (sec)	Meas. Period (sec)	Perc. Diff. %	Mode Description
1	0.89	0.91	2	Transverse
2	0.79	0.75	5	Transverse
3	0.74	0.59	20	Longitudinal
4	0.69	0.65	6	Transverse
5	0.63	0.59	7	Transverse
7	0.50	0.55	8	Transverse
8	0.50	0.40	20	Longitudinal
18	0.36	0.31	13	Longitudinal
20	0.33	0.37	10	Transverse
21	0.32	0.33	4	Trans. & Tor.
23	0.29	0.29	2	Vertical
24	0.28	0.28	1	Vertical
25	0.27	0.26	6	Torsional

Fig. 11 Computed vs Identified by Measurements Modal Response of Queensboro Bridge

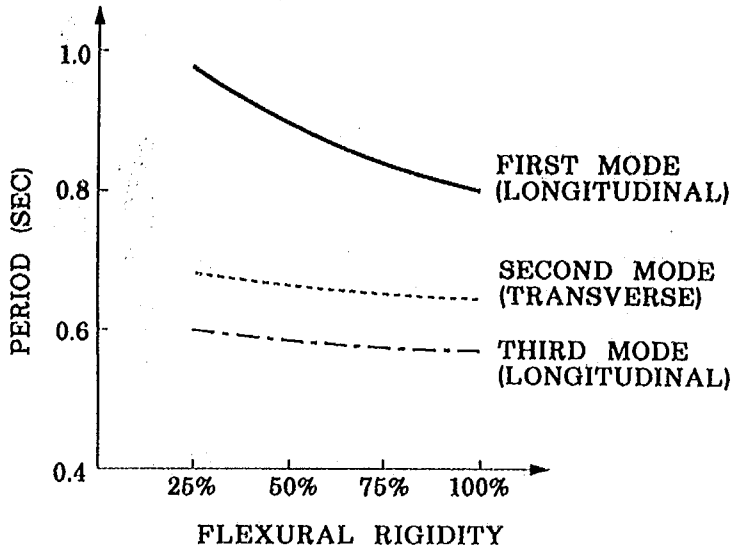


Fig.12 Period of Vibrations vs Flexural Rigidity at Column Bases

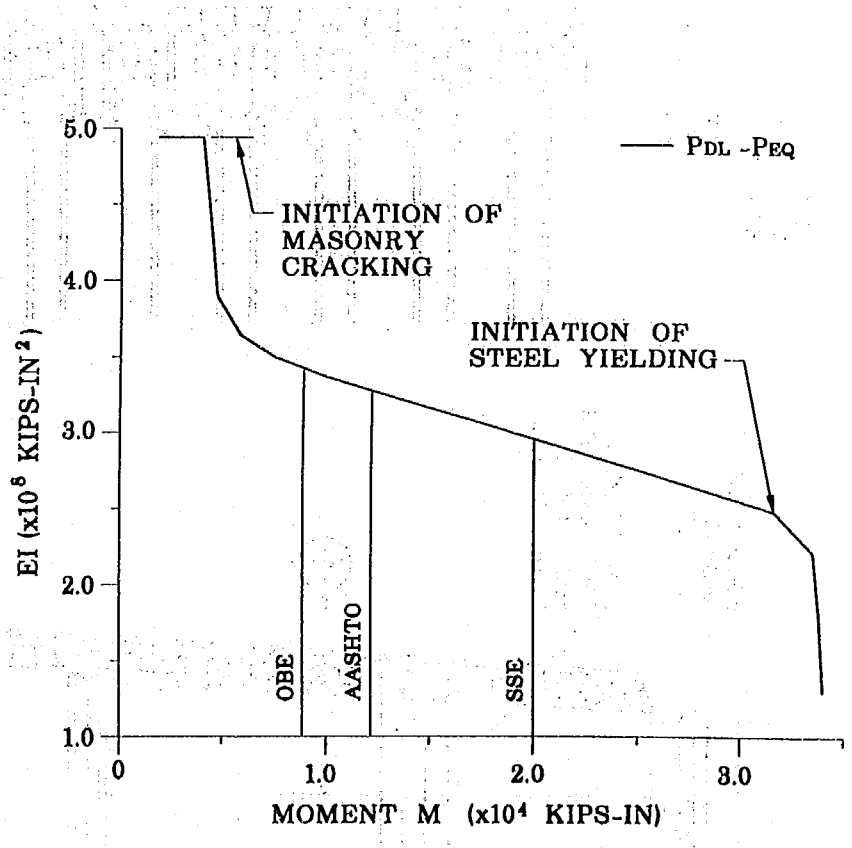


Fig.13 Effect of Bending Moment on Flexural Rigidity of Columns

k:\cadd\849100\fig12-13.dgn Nov. 26, 1996 12:34:51

k:\cadd\849100\fig14-15.dgn Nov. 26, 1996 13:36:41

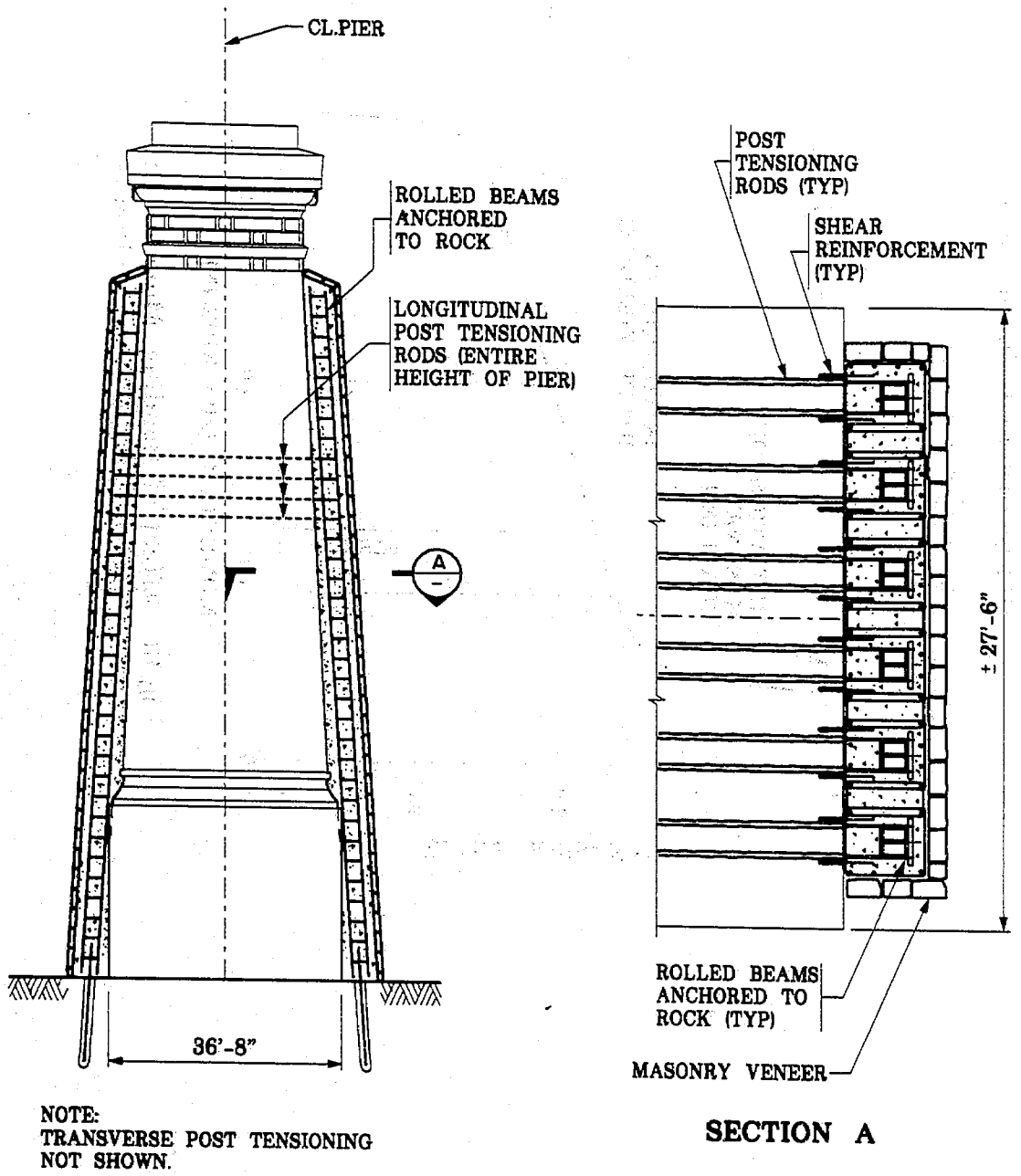


Fig. 14 Schematic of the Recommended Retrofit of Piers

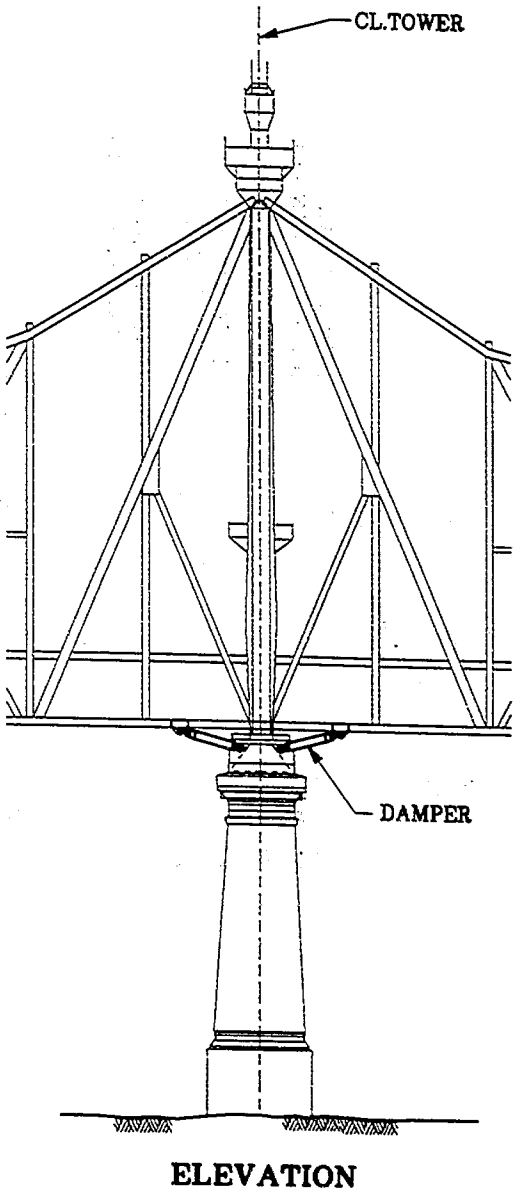


Fig. 15 Schematic of the Application of Dampers

Session 4

Retrofit Methods for RC Columns 1

(Co-Chairs: Y. Kimura, R. Imbsen)

"Seismic Retrofit of Square RC columns by Steel Jacketing"
by J. Hoshikuma, H. Otsuka, K. Nagaya
Presented by: Jun-ichi Hoshikuma

"An Experimental Study on Seismic Retrofit of Reinforced Concrete Bridge Piers"
by H. Ikeda, N. Wada, K. Osada, Y. Igase, Y. Tamura,
Presented by: Yoshinori Igase

"Retrofits of Reinforced Concrete Bridge Columns with Prestressing Steel Ties"
by T. Yoshioka
Presented by: Tamio Yoshioka

SEISMIC RETROFIT OF SQUARE RC COLUMNS BY STEEL JACKETING

Jun-ichi Hoshikuma
Research Engineer, Earthquake Engineering Division, Public Works Research Institute
Ministry of Construction

Hisanori Otsuka
Professor, Department of Civil Engineering, Kyushu University

Kazuhiro Nagaya
Research Engineer, Earthquake Engineering Division, Public Works Research Institute
Ministry of Construction

ABSTRACT

A new steel-jacketing strengthening method for enhanced flexural performance of existing reinforce concrete bridge piers with square section was proposed in this paper. A series of large-scale specimens were cyclic-loaded, to examine the strengthening effect. Test results showed that the strengthening method was effective in enhancing both the flexural strength and the ductility. Also, effects of steel-jacket details were studied based on the loading tests. Furthermore, an analytical model for the steel-jacketing reinforced concrete piers was proposed. The flexural strength and the ductility analyzed by the model showed good agreements with the test results.

INTRODUCTION

When the Hyogo-ken Nambu Earthquake hit the Hanshin and Awaji districts in the early morning of January 17, 1995, civil engineering structures, including highway bridges, were severely damaged that had never been seen in past earthquakes. With regard to damage to highway bridges, it was noted that the piers of some bridges that had been designed in accordance with the 1964 or 1971 seismic specifications suffered severe damage; the provisions in those standards for the cut-off of longitudinal reinforcement required for piers were revised in 1980(1). The reason for the damage was that the ground motion had properties that produced greater effects on highway bridges than had previously been observed. It has been estimated that severely damaged bridges received seismic forces larger than had been assumed in their design (1).

To make a bridge sufficiently resistant to earthquakes such as this one, its structure has to be made tougher by increasing the strength and ductility of the bridge as a total system (2). The philosophy of seismic design for a bridge also applies to the seismic retrofitting of existing bridges: it is necessary to adopt a retrofitting method that can be expected to enhance both the

flexural strength and the ductility of the piers. However, when the flexural strength of piers is enhanced, the seismic forces propagated into the foundation are increased all the more. Therefore, if the calculated strength of the foundation of a bridge is smaller than the expected of its retrofitted piers, it is necessary to carry out more wide-ranging retrofitting of the bridge by retrofitting its foundation as well. On the other hand, if the ductility of the piers alone is enhanced, while their flexural strength is left as it is, this may lead to substantial plastic deformation during a major earthquake, which would cause a residual deformation that could not be repaired (3). It is therefore important to work out a retrofitting design that is capable of enhancing the flexural strength of the piers as required, within the range that can be supported by existing foundation, and to make this enhancement match the improvement in the ductility.

This paper proposes the steel jacketing method, with a controlled increase in flexural strength allowing well-balanced enhancement of both the flexural strength and the ductility of each pier in a reinforced concrete bridge. It also describes the results of a cyclic loading test using large-scale models constructed in order to examine the effects of enhancing the strength and ductility of bridge piers using this retrofitting method. Furthermore, the analytical method considering the confinement of concrete is checked the validness by comparing the test results.

SEISMIC RETROFITTING OF REINFORCED CONCRETE PIERS USING A STEEL JACKET WITH ANCHOR BARS

The steel jacket method, providing a controlled increase in flexural strength, involves steel plates around the reinforced concrete bridge piers, and bonding the steel jacket to the pier with epoxy resin or non-shrinkage mortar, while anchoring the jacket to the footing with anchor bars, as shown in Figure 1. This retrofitting method mainly aims to compensate for the inadequate cut-off of the longitudinal reinforcement and, at the same time, to enhance the flexural strength and ductility of the pier. The structure has several important characteristics, including the anchoring of the steel jacket to the footing with anchor bars, the vertical gap between the lower end of steel jacket and the top of the footing, and the use of H-beams fastened at the lower end of the jacket. These characteristics are described below.

First, the anchor bars play a part in enhancing the flexural strength of the pier, as well as in controlling the seismic forces propagated into the footing. This is because the increase in the flexural strength of the pier resulting from the retrofitting method can be controlled by adjusting the number and diameter of the anchor bars installed. The vertical gap between the lower end of the steel jacket and the top of the footing is provided because it is expected that, when it receives a large seismic force, the steel jacket may come into contact with the footing, which may then buckle under the unexpectedly large compressive force and receive damage. However, when the length of the vertical gap is too large, the confining effect of the jacket at the bottom of pier is reduced. The length should therefore be as small as possible.

Piers with a rectangular section also have H-beams installed around them at the lower end of the jacket. The reason for this is that, when the base of the pier suffers from a deformation with a large curvature, the jacket at the plastic hinge zone swells out, and the confining effect of the jacket is liable to be lost. When the lower end of the jacket is attached with the H-beams, however, then even under large deformations it still functions as a lateral reinforcement.

CYCLIC LOADING TEST FOR MODELS OF RETROFITTED REINFORCED CONCRETE PIERS

Specimens

The specimens used are shown in Figure 2. Their section was a square of 60 cm x 60 cm. The height from the base to the loading point was 3.01 m. The shear span ratio was 5.0. As longitudinal reinforcements, SD295/D10 bars were arranged, and the ratio of longitudinal reinforcement was 1.58% (the ratio of tensile reinforcement was 0.55%). As hoop reinforcements, SD295/D6 hoops were arranged at intervals of 20 cm. In the specimens used in the test, the longitudinal reinforcement was not cut off at mid-height. This was because previous studies (4) had found that the steel jacket method can prevent damage to the cut-off sections of longitudinal reinforcement, thus it was decided that effect of this method in retrofitting the cut-off sections was not to be examined in this test.

When the steel jacket was applied to the specimen to be retrofitted, two steel plates with a thickness of 1.6 mm (SS400) were each bent into a channel -shape, and then welded into a jacket. Finally, the jacket was slipped from above over the specimen. As described above, however, a vertical gap of 5-15 cm was set between the lower end of steel jacket and the top of the footing (see Photo 1). In addition, H-beams (100 x 100 x 6 x 8, SS400) were used to strengthen the lower end of the jacket. Epoxy resin was poured in between the reinforced concrete pier and the steel jacket, with a thickness of 4 mm, to bond them.

The numbers and diameters of the anchor bars were set in such a way that the flexural strength of the specimen could increase by approximately 30%. As described above, with this retrofitting method, any increase in the strength of the pier has to be set so that its resulting strength will not exceed that of the foundation. In this test, it was arbitrarily decided that the pier strength should be increased by about 30%. It was found that, using the calculation method described later, when anchor bars equivalent to about 60% of the total strength of the steel jacket were used, the pier strength increased by approximately 30%. Consequently, it was decided that twenty anchor bars, made by processing SD345 /D13 reinforcements into an M12 screw bolt (effective section area: 0.843 cm ^{2}), should be arranged at intervals of 12 cm. The bars were anchored with resin anchors 55.6 mm outside the external edge of the concrete. The upper ends of the anchor bars were fastened to the webs of the H-beams by double nuts, as shown in Photo 2. In this structure, the axial force produced in the anchor bars must be propagated smoothly via the H-beams to the steel jacket. In the specimens for the test, therefore, the H-beams and the steel jacket were joined with six rib plates (thickness: 6 mm) per side, as shown in Figure 2b and Photo 1. The anchor bars were anchored to the footing for a length of 65 cm.

In order to examine the retrofitting effect produced by the steel jacket, and the effect of vertical gaps of varying length between the lower end of jacket and the top of the footing, one as-built specimen (P-1) and three retrofitted specimens (P-2 - P-4) were used in this test. The vertical gap length in specimen P-2 was 10 cm, while those of specimens P-3 and P-4 were 5 cm and 15 cm, respectively.

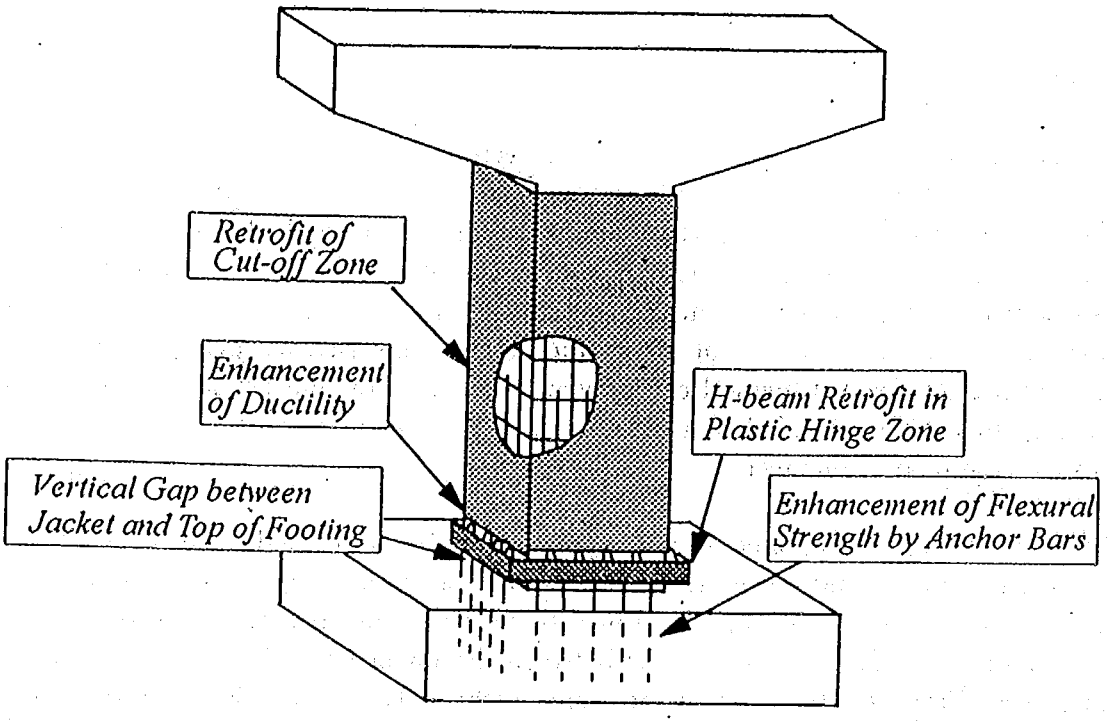


Fig. 1 Illustraion of Retrofit by Steel-Jacketing with Anchor Bars

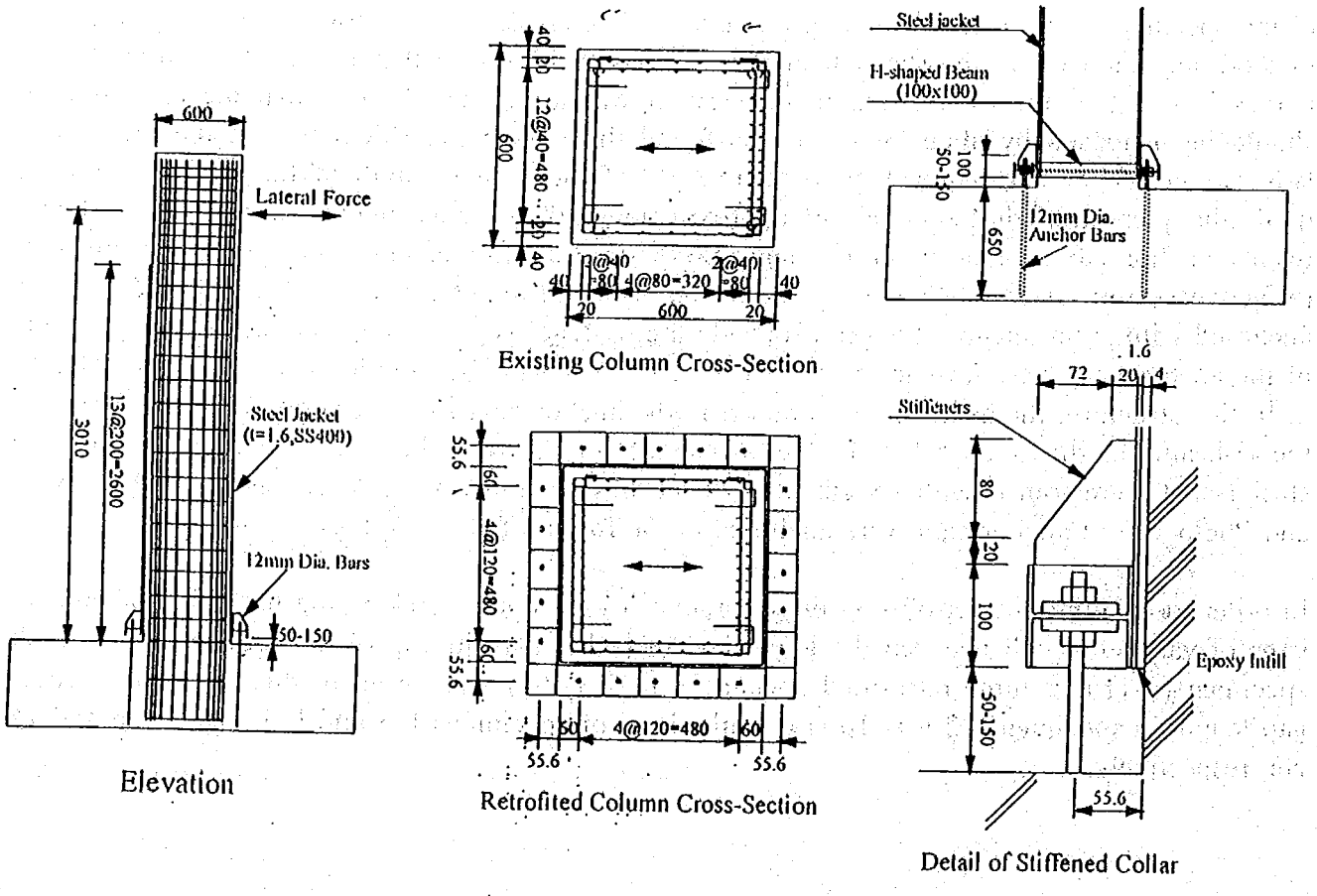


Fig. 2 Details of Test Specimens (unit: mm)

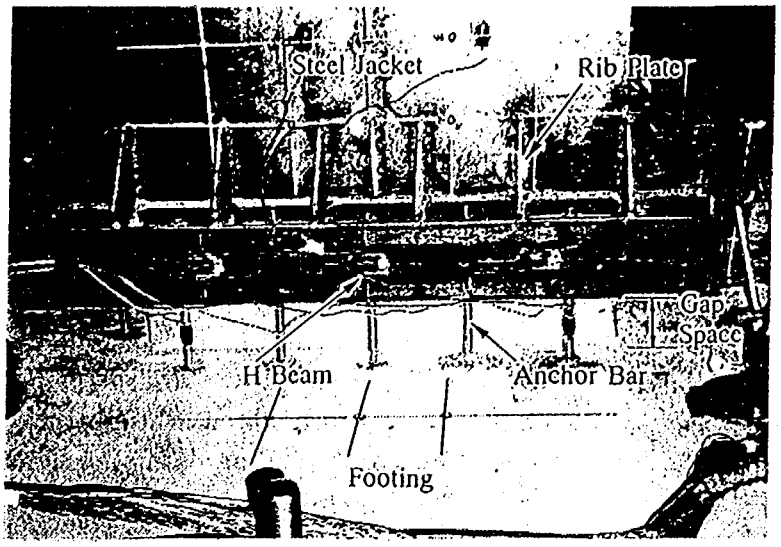


Photo 1 Detail around Base

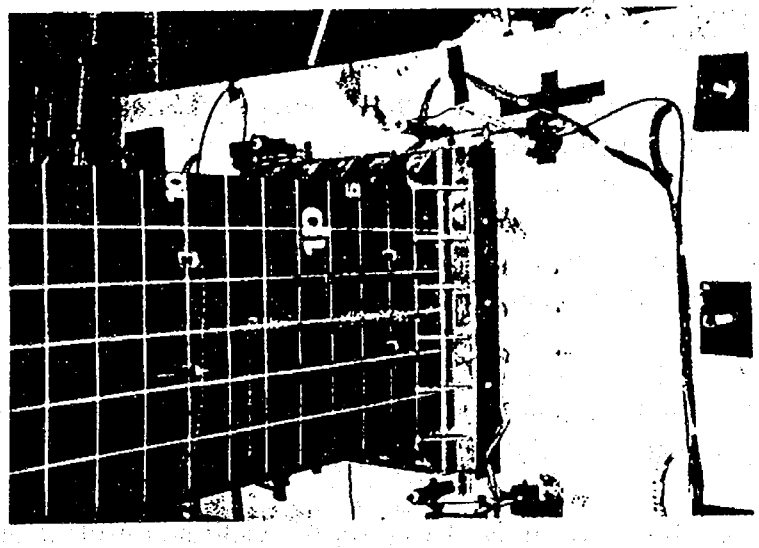


Photo 2 Steel Jacket and Anchor

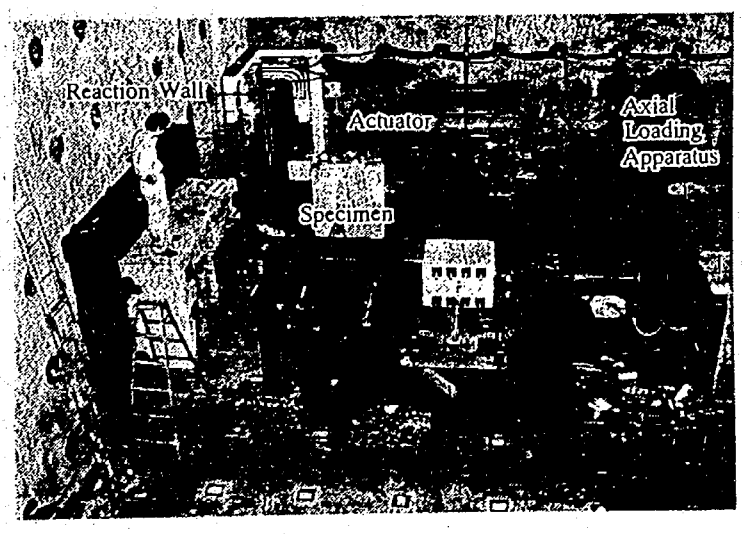


Photo 3 Set-up of Cyclic Loading Test

Loading Procedure

Photo 3 shows the way in which each specimen was loaded. While an axial force equivalent to a dead-load reaction was applied to each specimen laid down, a level load was applied to it by an actuator installed on a reaction wall. An axial force of 55 tf was used in this test. This is equivalent to a compressive stress of 15.3 kgf/cm ^{2}.

The yield displacement at the loading point was determined here when the longitudinal reinforcement of the base of the as-built specimen yielded, or the anchor bars of each retrofitted specimen yielded. Alternative displacements were given to the specimens by the displacement control. The loading displacement was made by a sine wave; the loading speed 3 cm/sec; and the number of loading cycles per loading step was to be three. The ultimate displacement during the test was defined here as the displacement when the strength was deteriorated to the yield strength.

RETROFITTING EFFECT OF STEEL JACKET WITH ANCHOR BARS

Hysteresis loop and aggravation of damage

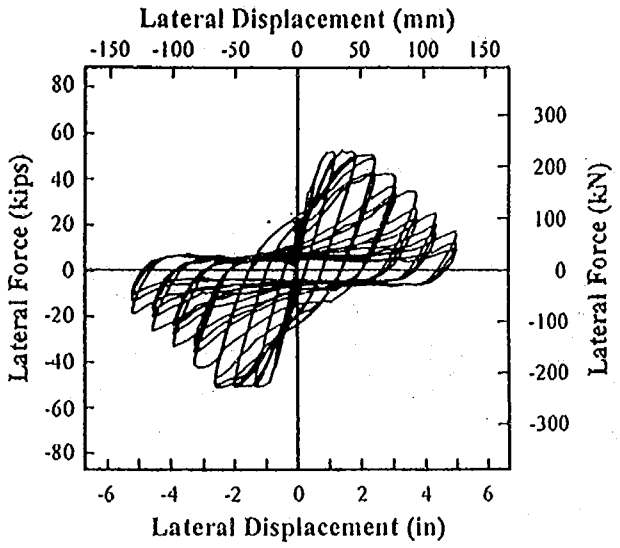
Figure 3 shows the hysteresis loops of the relationships between lateral load and the displacement at the loading points of all the specimens. Figure 4 illustrates the damage to specimens P-1 and P-2 was aggravated.

In the case of P-1, the as-built specimen, based on the value for the longitudinal reinforcement strain at the base, the yield displacement was measured to be 16.0 mm. Its peak strength was 23.1 tf. This was maintained until 4 δ y was loaded, when its cover concrete started to spall off. In the stage of 5 δ y loading, the core concrete started to suffer damage, and the hysteresis loop began to become unstable. When even greater loads continued to be applied, damage to the core concrete was aggravated, with the level strength gradually reduced.

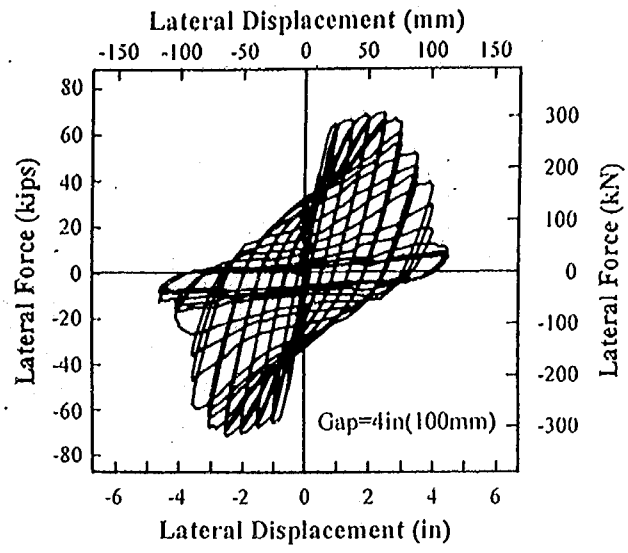
In the case of P-2, a retrofitted specimen, based on the yield strain of its anchor bars, the yield displacement was measured at 12.7 mm. In comparison with P-1, its yield displacement was smaller, because the flexural stiffness was increased by the steel jacket. Its peak strength was 31.8 tf. This was maintained until 6 δ y was loaded. Its anchor bars started to buckle under the load of 4 δ y. In the stage of the 6 δ y loading, seven anchor bars were broken. At the same time, the external edge of the concrete pier, in the 10cm vertical gap provided at the base, began to fail due to the cyclic pressure, with the lateral strength reduced. Under the 7 δ y loading, a total of ten anchor bars broke, and two longitudinal reinforcements of the pier were also broken, with the lateral strength reduced below the yield strength. Even under the final 8 δ y loading, the steel jacket did not suffer from deformations such as buckling or swelling out.

Strength and ductility

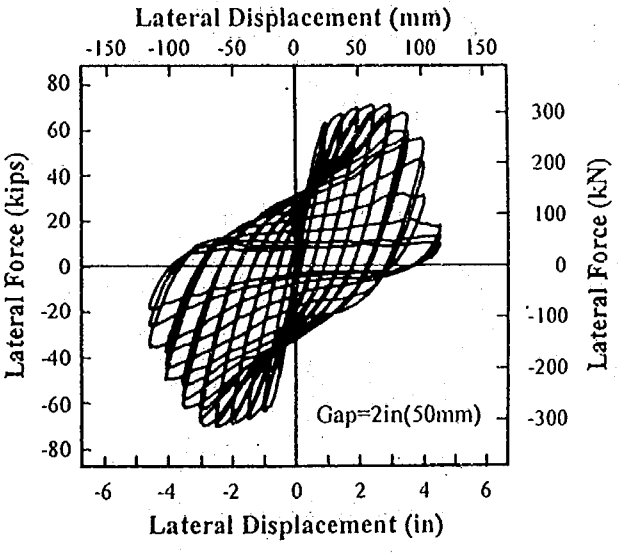
Figure 5 compares the envelope curves of the hysteresis loops in the four specimens. Table 1 compares their strength and ductility. The comparison between P-1 and P-2 shows that the peak



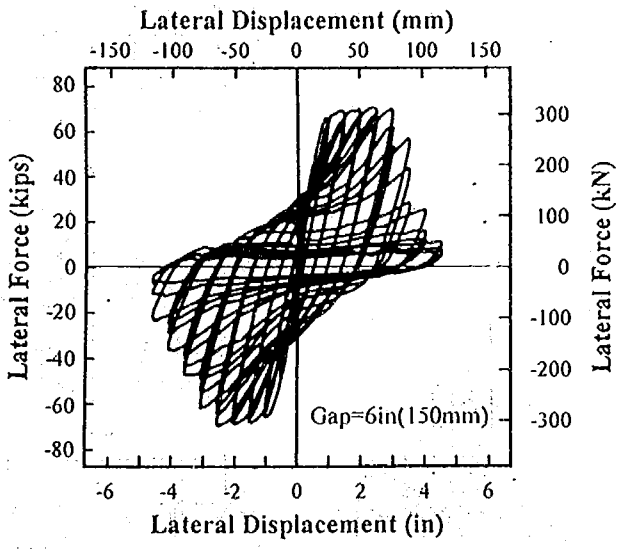
(a) P-1 Specimen



(b) P-2 Specimen

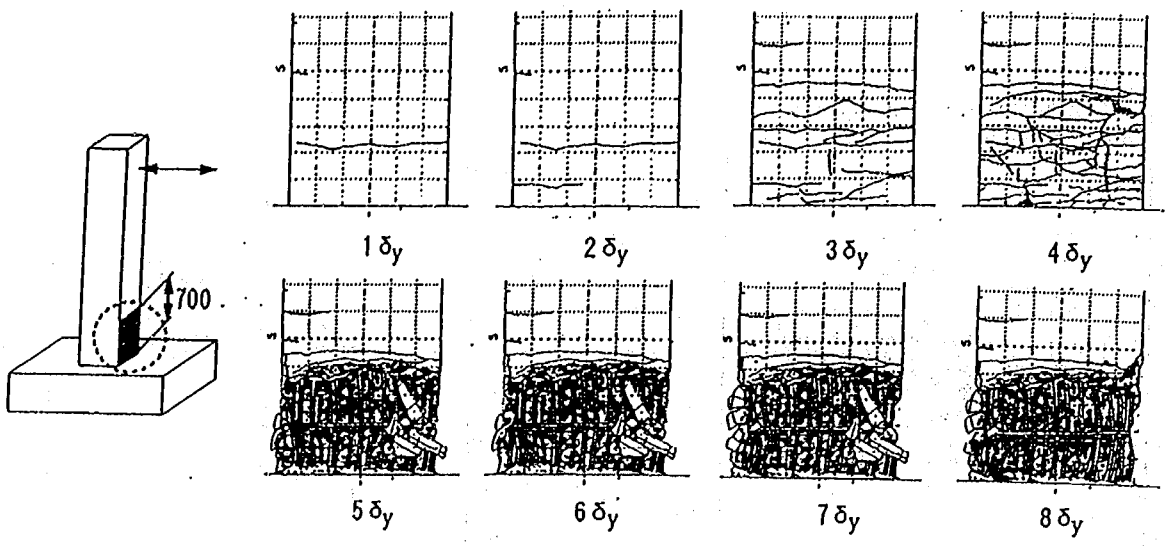


(c) P-1 Specimen

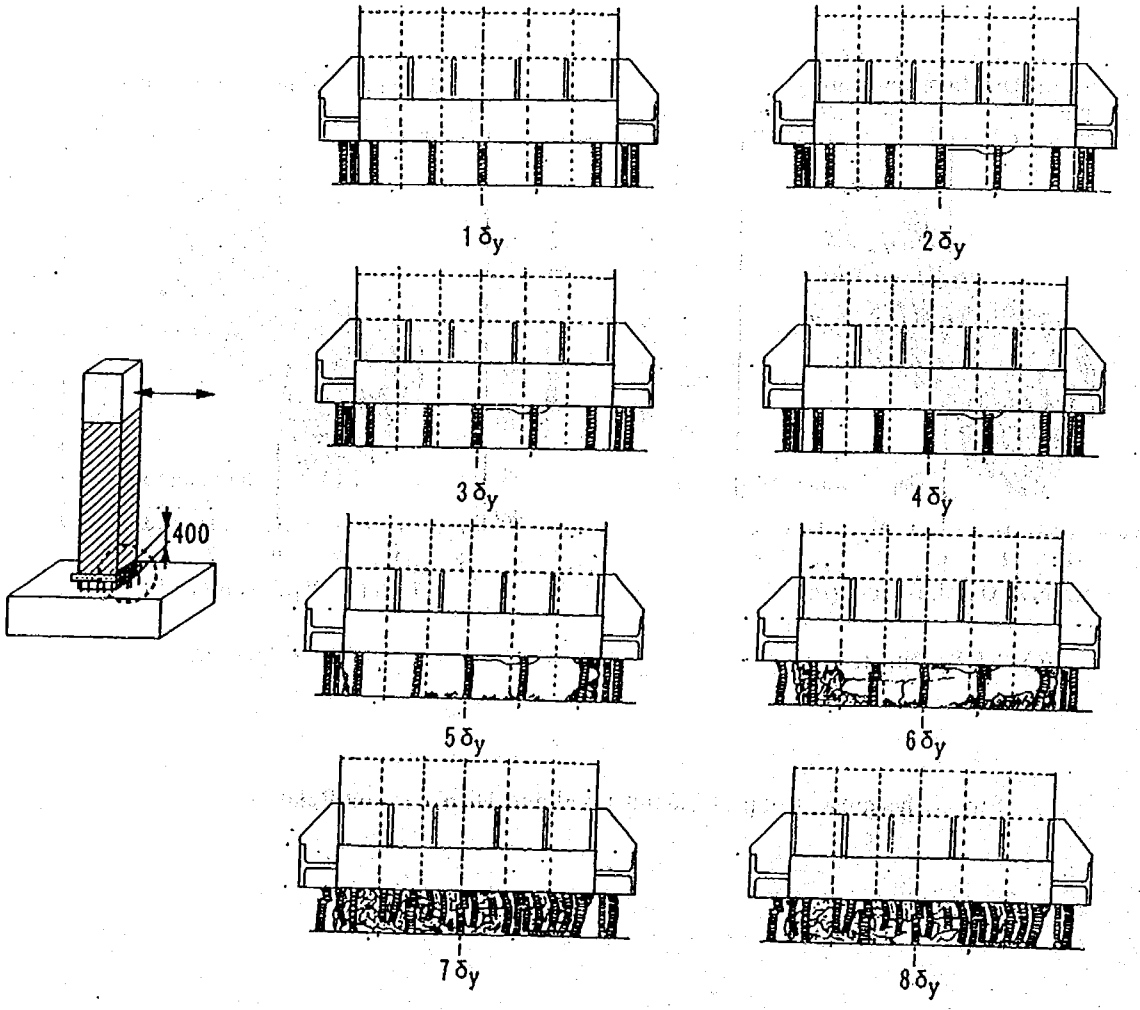


(d) P-2 Specimen

Fig. 3 Hysteresis Roop of Lateral Load and Displacement Relation



(a) P-1 Specimen



(b) P-2 Specimen

Fig.4 Damage Process Observed in Specimens

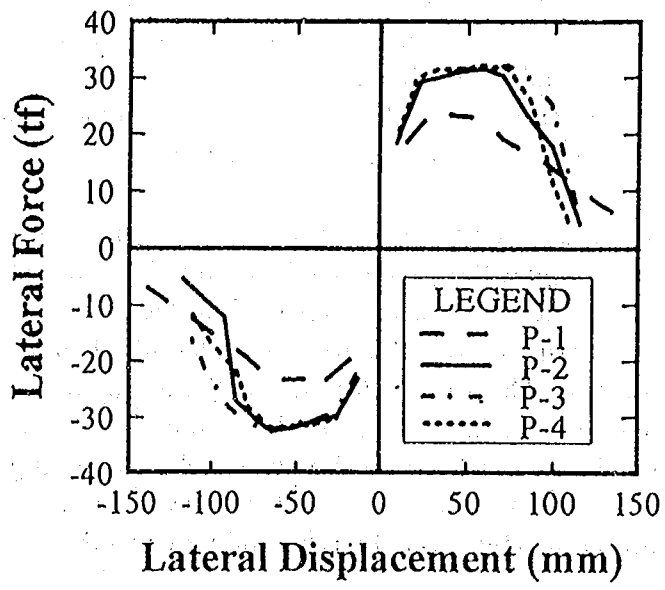


Fig. 5 Comparison of Envelope of Hysteresis Roop

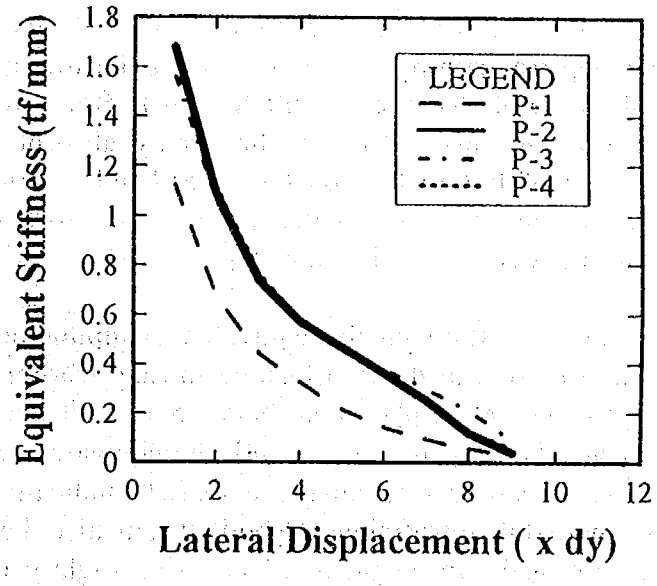


Fig. 6 Effect of Retrofit on Equivalent Stiffness

Table 1 Observed Strength and Ductility

Specimen		P-1	P-2	P-3	P-4
Strength	Yield Strength (tf)	18.8	21.3	20.2	21.5
	Peak Strength (tf)	23.1	31.8	31.7	31.9
	P_M/P_y	1.23	1.49	1.57	1.48
Ductility	Yield Displacement (mm)	16.0	12.7	12.7	12.7
	Ultimate Displacement (mm)	87.0	96.5	110.9	96.0
	Ductility Factor	5.4	7.6	8.7	7.6

strength and the ductility factor of the pier were enhanced by the steel jacket, with a controlled increase in flexural strength. Also, while the effect of the vertical gap length on the peak strength was only slight, the smaller the length, the larger was the ductility ratio. Based on the result of this test, it is recommended to make the vertical gap length small, at least about 5 cm, in the case of piers with dimensions similar to these specimens.

Figure 6 shows the relationship between equivalent stiffness and lateral displacement. Equivalent stiffness was defined here as being the gradient of the straight line connecting the points of the maximum and minimum displacements in the first loading loop in each loading step. The figure shows that the equivalent stiffnesses of P-2 to P-4 under the 1 δ y loading were about 1.5 times greater than that of P-1. The reason for this will be that the flexural stiffnesses of the retrofitted specimens were greater than that of the as-built one, because of their increased stiffness due to the anchor bars, and because the steel jackets covering the whole height of the piers also functioned as a longitudinal reinforcement. However, the effect of the difference in the vertical gap length was not noticeable over the range of 5 to 15 cm.

Energy absorption

Figure 7 compares the specimens with regard to accumulated energy absorption. Energy absorption in each loading step was computed here by integrating the hysteresis loop concerned. The figure shows that in the case of P-1, the as-built specimen, from around the time of 5 δ y, when the core concrete started to suffer damage, the energy absorption in each loading step began to decrease. In the case of P-2 to P-4, on the other hand, energy absorption was stable even after 5 δ y. It was also found that the smaller the vertical gap length, the greater was the energy absorption under loads above 7 δ y loading step.

Figure 8 shows effect of the retrofitting on the equivalent damping ratio. The ratio computed was based here on the hysteresis loop in the first loading in each loading step. While the ratio of P-1 was greater in the range of lateral displacement below 5 δ y, it began to decrease when the displacement increased beyond that. On the other hand, the equivalent damping ratios of P-2 to P-4 rose constantly as the lateral displacement increased, indicating that stable damping performance was obtained with the retrofitting method. It can also be seen that the damping performance of P-4, with a vertical gap length of 15 cm, was slightly poorer than those of P-2 and P-3 after 7 δ y loading step.

Strain Performance

Figure 9 compares the reinforcement and the steel jacket of P-2 with regard to the peak axial strain on the tensile side of the section at a height of 20 cm from the base at each loading step. Under the load for 1 δ y, the axial strain of the jacket was 0.0838%, and it had not yet yielded. Since the design had foreseen that five anchor bars on the tensile side would yield under this load, it is estimated from the yield strength (observed value: 3,916 kgf/cm ^{2}) and section area of the anchor bars that an axial strength, Na, of the value obtained by the following formula was at work:

$$N_a = 3{,}916 \times (0.843 \times 5) = 1.65 \times 10^4 \text{ kgf} \qquad (1)$$

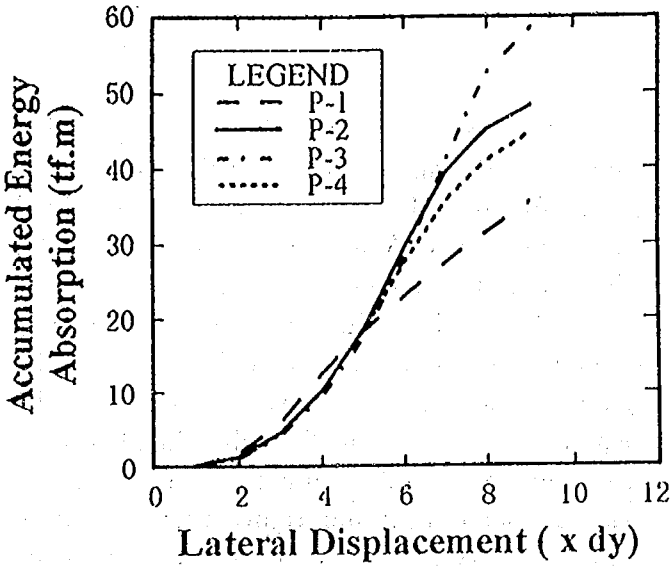


Fig. 7 Effect of Retrofit on Accumulated Energy Absorption

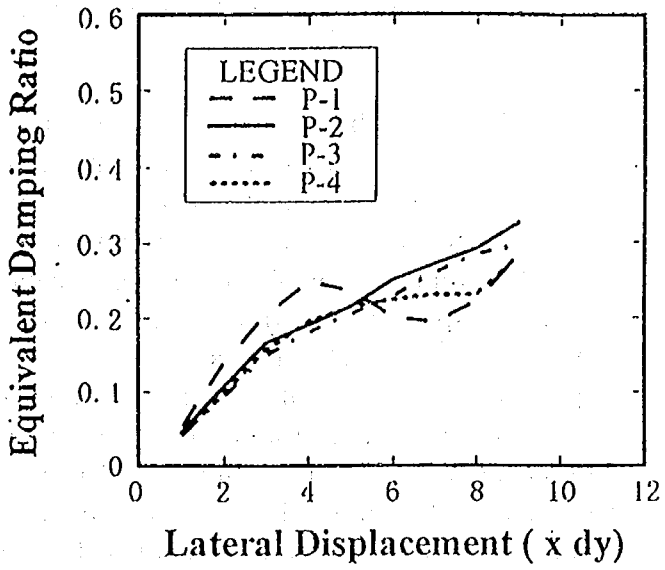


Fig. 8 Effect of Retrofit on Equivalent Damping Ratio

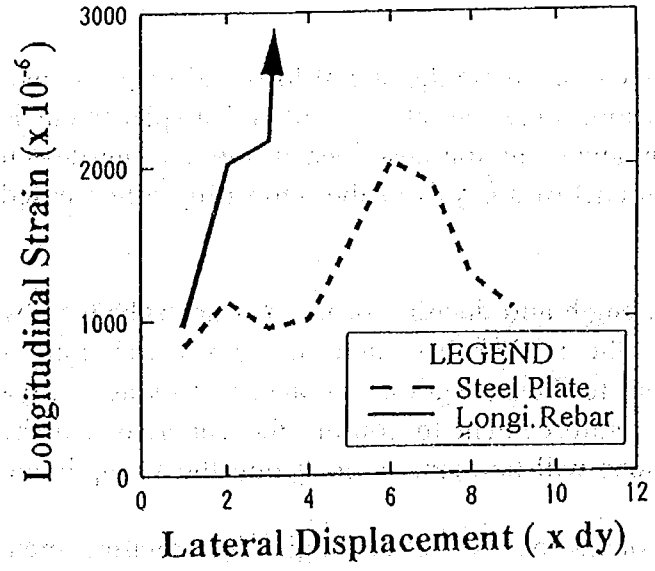


Fig. 9 Axial Strain of Longitudinal Reinforcement and Steel Plate in Specime P-2

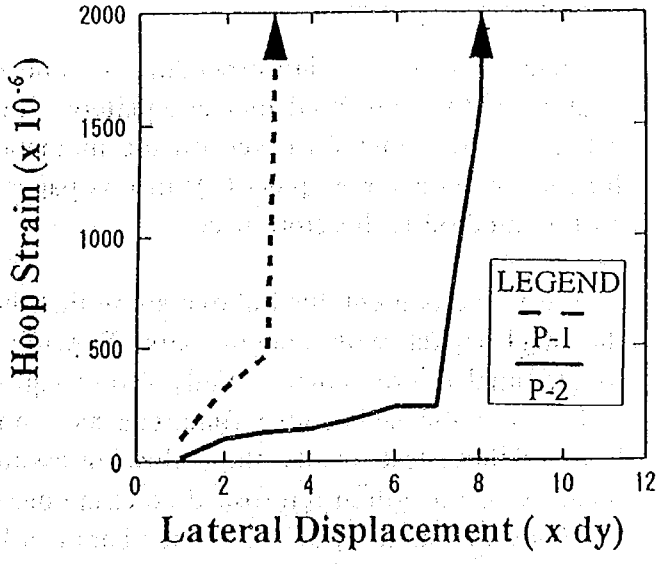


Fig. 10 Comparison of Strain of Hoop

Assuming this axial strength to be the tensile strength propagated to the tensile side of the steel jacket, the strain produced in the jacket is computed as follows:

$$\varepsilon_j = 1.65 \times 10^{4} / (0.16 \times 60) \times 2.1 \times 10^{6}$$
$$= 818 \times 10^{-6} \qquad (2)$$

As can be seen, the strain on the jacket thus obtained agrees well with the observed value mentioned above. Consequently, judging from the strains on the anchor bars and the steel jacket under the elastic loading, it can be said that the jacket functioned effectively as a longitudinal reinforcement of a strength equivalent to that of the anchor bars. Also, because the jacket did not suffer from any visible plastic deformation, such as swelling out under the loads for 1 δ y or more displacements, it can be expected that the jacket will produce the proper effect of confining the concrete. The axial strain on the jacket peaked under the load for 6 δ y. The displacement was equivalent to the one immediately before the anchor bars were broken, and the strength began to decrease after remaining stable near its maximum. On the other hand, Figure 10 compares P-1 and P-2 with regard to the strain of the hoop reinforcement positioned at the section at a height of 40 cm from the base. It can be seen from the figure that the strain produced in the hoop reinforcement of P-2 was smaller at every loading step, indicating that the jacket functioned effectively as a hoop reinforcement confining the lateral deformation of the concrete pier.

ANALYSIS OF STRENGTH AND DUCTILITY OF REINFORCED CONCRETE PIERS RETROFITTED BY STEEL JACKET WITH ANCHOR BARS

Analysis Procedure

To make a seismic design procedure, it is necessary to estimate the lateral load and displacement relation of the retrofitted pier adequately. The relation between lateral load and displacement is calculated by a method based on the moment-curvature relation described in the seismic design for reinforced concrete piers (5). In this paper, a model of analysis of the retrofitting effect based on this method is therefore used.

The test results mentioned above show that the strength and ductility of the pier are enhanced by the steel jacket with anchor bars. Specifically, the anchor bars and the jacket function as longitudinal reinforcements. Only forces equivalent to the strength of the anchor bars act on the jacket, and the jacket also functions as a hoop reinforcement to confine the concrete. On the basis of these test results, the following assumptions will be made in analyzing the strength and ductility of retrofitted reinforced concrete piers.

(1) Only the strength of the anchor bars can be counted as a effective longitudinal reinforcement by the steel jacket. Reinforcement bars are assumed to be positioned at the external edge of the concrete, as shown in Figure 11.
(2) The whole sectional area of the jacket works as a hoop reinforcement. This effect, combined with that of the existing hoop reinforcement, can be taken into account the stress-strain curve.
(3) The vertical gap length is understood to be better as small as possible, and the steel jacket and the footing will not expected to come into contact if the pier becomes deformed, the

confining strength of the jacket can be considered to be propagated into the concrete in this section. The confining effect on the gap section should be the same as that on the section covered by the jacket.

With regard to the modeling of the position of the anchor bars, there are two potential approaches. One is to assume that the anchor bars are positioned where they are actually anchored in the base (55.6 mm outside the external edge of the concrete pier, in the case of P-2); and the other is to assume that they are positioned on the external edge of the concrete pier, where the steel jacket is placed. In the former case, while the conditions in the actual structure and the analysis model correspond to one other in relation to the vertical gap section with a length from the pier base of 5 to 15 cm, in the section covered by the jacket the flexural stiffness tends to be overestimated, because the effective height of the anchor bars is greater than it actually is. It was therefore decided that, in the design model, the anchor bars should be arranged on the external edge of the concrete pier.

In this analysis, the model of the stress-strain curve in concrete proposed by Hoshikuma et al. (6) was used, since it allows the confining effect of the hoop reinforcement to be taken into consideration. However, the strain produced when compressive stress is reduced to 80% of its peak is considered as the ultimate strain (2). This is equivalent to the strain produced when the concrete starts to spall off due to the compression.

Analyzing retrofitting effect upon specimens

To verify the method of analysis, the strength and ductility of P-2 were analyzed, and a comparison between these results and the test results is carried out. Values obtained from a materials test were used in the analysis.

The volumetric ratio of lateral reinforcement of the reinforced concrete pier, ρ_s, was computed by the following equation, converting the steel jacket into hoop reinforcement:

$$\rho_s = \frac{4A_h}{s \cdot d_h} + \frac{4t}{d_j} \cdot \frac{f_{yj}}{f_{yh}} \qquad (3)$$

where:

A_h: section area of a hoop reinforcement (cm^2)
s: spacing between hoop reinforcements (cm)
d_h: effective length of hoop reinforcement (2) (cm)
d_j: effective length of steel jacket (cm)
t: thickness of steel jacket (cm)
f_{yh}: yield strength of hoop reinforcement (kgf/cm^2)
f_{yj}: yield strength of steel jacket (kgf/cm^2)

In Eq. (3), the first term is the volumetric ratio of the lateral reinforcement of the pier, while the second term gives the volumetric ratio of the steel jacket as converted into hoop reinforcement. The effective length of the jacket, dj, can be assumed here as the side length of the section of the concrete pier, in the case of structures like this, in which steel plates are placed like a jacket. Consequently, in the case of the specimens for this test, the effective length of the jacket, d_j, was

60 cm. Hence, the volumetric ratio of lateral reinforcement of P-1, ρ_s, was computed to be 0.00253. The ratio of P-2, ρ_s, was 0.0115. Figure 12 shows the stress-strain curve for the concrete pier obtained by using these values.
Using this stress-strain curve for the concrete, an analysis was made of the moment-curvature relation of the section, and the lateral load and displacement relation at the loading point was computed. Figure 13 compares the analysis results and the envelope curve of the loading hysteresis loop for P-1 and P-2. In the analysis, the peak strengths of P-1 and P-2 were computed to be 24.1 tf and 31.1 tf, respectively. These figures both agreed well with the test results. It was concluded, therefore, that the method of analysis was able to estimate the strength of the retrofitted piers with sufficient precision.

On the other hand, the ductility factors of P-1 and P-2 calculated in this analysis were 3.0 and 5.3, respectively. The corresponding test results were both higher than these analysis values. This is due to a difference in definition of ultimate stage. In the loading test, on the one hand, ultimate displacement was defined as the lateral displacement recorded when the strength was reduced to the yield strength. In the analysis, on the other hand, ultimate displacement was defined as the lateral displacement recorded when the strain of the most external edge of the concrete pier reached its ultimate strain. The ultimate displacement of P-2 obtained by the analysis method was 82.5 mm. To compare this with the damage caused in the test when a lateral displacement of this extent was effected, the anchor bars began to buckle, reaching the stage of damage immediately before breaking, and the concrete started to spall off, with the peak strength starting to fall after having remained stable. This damage degree corresponds to the state defined as "ultimate" in the analysis. On the other hand, when P-2 was so deformed that its strength had been reduced to yield strength, the anchor bars had already broken, and the longitudinal reinforcement was also about to break. Based on these considerations, the ultimate displacement obtained by the method had a value suitable for the design, from the points of view of residual strength, degree of difficulty of restoration, etc. It should be noted that the plastic hinge length would be different between P-1 and P-2, as shown in Figure 4. In above analysis, the ductility is calculated without taking account of the effect of the plastic hinge length, which may cause the under- or overestimate of the ultimate displacement.

CONCLUSIONS

We have proposed here a method of designing a steel jacket with anchor bars as a method of enhancing the ductility of reinforced concrete piers while controlling the increase in its strength. We carried out a lateral loading test using large models, including models retrofitted with this method. We also examined a way of analyzing the retrofitting effect, i.e., the effect of enhancing the strength and ductility with this method. The following is the summary of results of the study:

(1) The test clearly showed that the ductility of a pier can be enhanced while controlling the increase in its strength using a steel jacket with anchor bars. The pier's energy absorption and damping performance were also enhanced.
(2) It was confirmed that the jacket and hoop reinforcement were strained in such a way that the steel jacket functions effectively as a longitudinal and hoop reinforcement, with a strength equivalent to that of the anchor bars.
(3) A comparison of the three cases with a vertical gap between the lower end of jacket and the

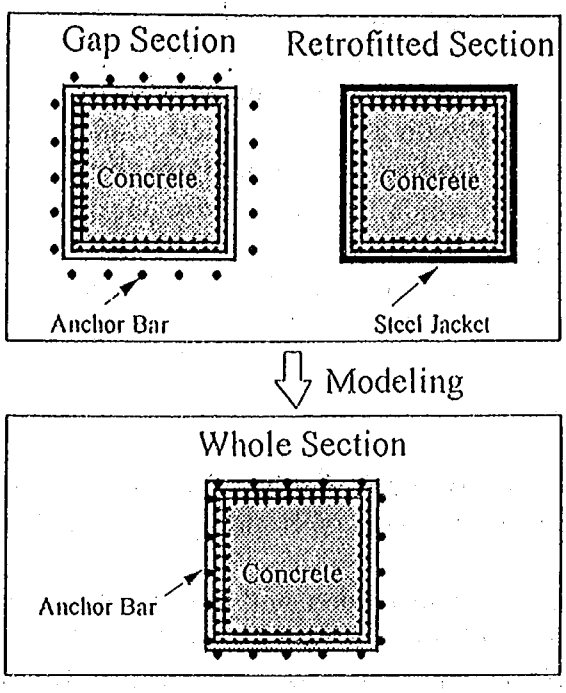


Fig. 11 Analyzing Model of Steel Jacketing with Anchor Bars

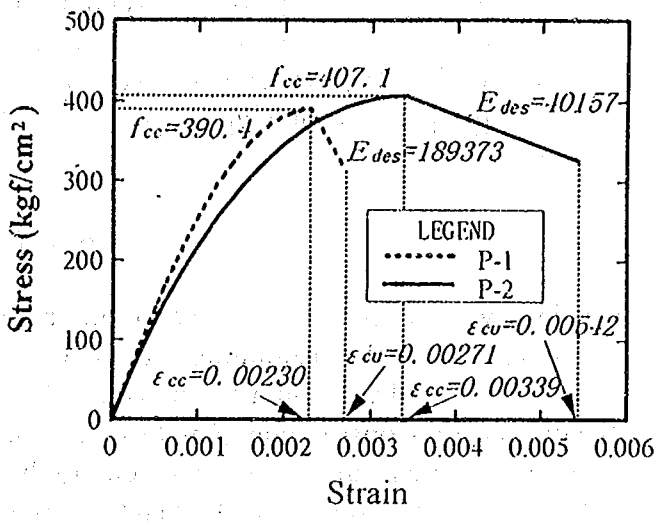
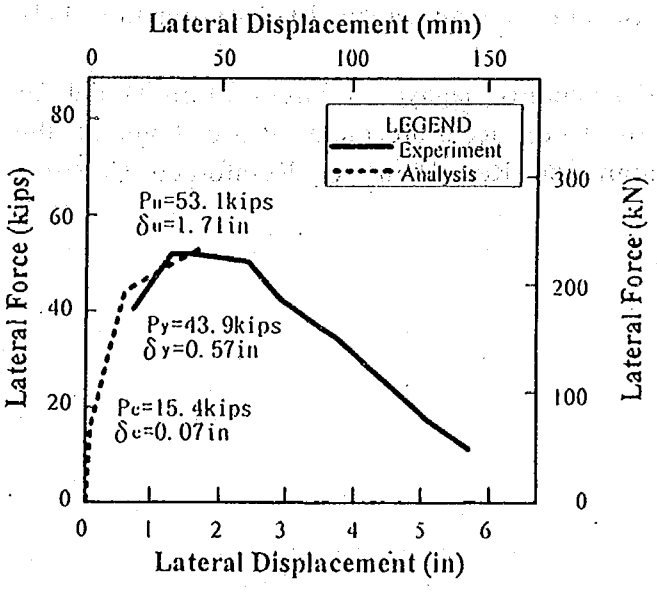
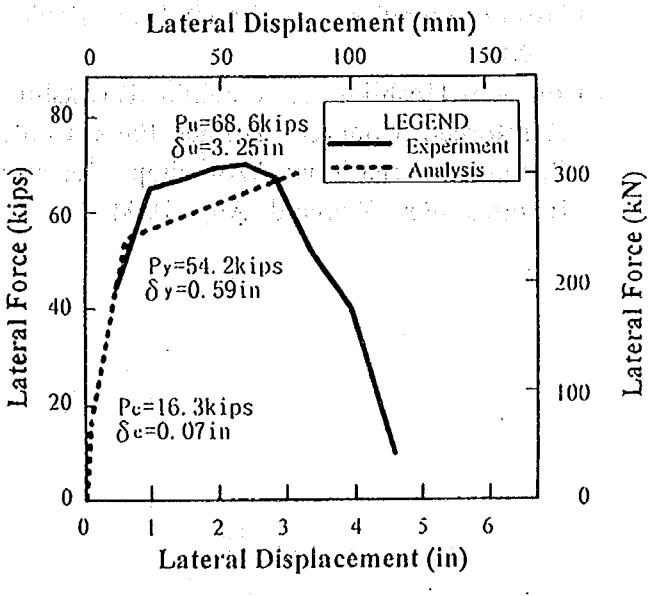


Fig. 12 Stress-strain Curve Used in Analysis



(a) P-1 Specimen



(b) P-2 Specimen

Fig. 13 Comparison of Lateral Load and Displacemetn Relation

top of the base -5cm, 10cm and 15cm- showed that, while the peak strengths were all equal, the smaller the vertical gap length, the larger the ductility factor.

(4) A method of analyzing the retrofitting effect of this type of steel jacket with a controlled increase in flexural strength was described. It was confirmed that the strength calculated according to this method of analysis corresponded well with the observed test results. On the basis of the results of the test (number of cycles of loading: 3), the ultimate displacement obtained by this analysis is equivalent to the stage in which the anchor bars buckle, having reached the stage of damage that immediately precedes breaking. At this stage, concrete starts to spall off, and the peak strength begins to deteriorate after having remained stable for a time.

REFERENCES

1) Ministry of Construction: Report on the Damage of Highway Bridges by the Hyogo-ken Nanbu Earthquake, Committee for Investigation on the Damage of Highway Bridges Caused by the Hyogo-ken Nanbu Earthquake, 1995
2) Ministry of Construction: Guide Specifications for Reconstruction and Repair of Highway Bridges Which Suffered Damage due to the Hyogo-ken Nambu Earthquake, Feb. 1995
3) Kazuhiko Kawashima, G.A. MacRae, Jun-ichi Hoshikuma and Kazuhiro Nagaya: Residual Displacement Response Spectrum and its Application to Evaluate Residual Displacement Developed in Reinforced Concrete Bridge Columns, 28th Joint Meeting of U.S.-Japan Panel on Wind and Seismic Effects, UJNR, May 1996
4) Kazuhiko Kawashima, Shigeki Unjo and Hiroyuki Iida: Seismic Inspection and Seismic Strengthening of Reinforced Concrete Piers at Mid-height Where Main Reinforcement is Terminated, First U.S.-Japan Workshop on Seismic Retrofit of Bridges, UJNR, Tsukuba, Dec. 1990
5) Design Specifications for Highway Bridges, V Seismic Design, Japan Road Association, Feb. 1990
6) Jun-ichi Hoshikuma, Kazuhiko Kawashima and Kazuhiro Nagaya: A Stress-Strain Model for Reinforced Concrete Bridge Piers Confined by Hoop Reinforcement, Proceedings of the Second International Workshop, Seismic Design and Retrofitting of Reinforced Concrete Bridges, New Zealand, Aug. 1994

AN EXPERIMENTAL STUDY ON SEISMIC RETROFIT OF REINFORCED CONCRETE BRIDGE PIERS

Hiroyuki IKEDA*[1], Norifumi WADA*[2], Koji OSADA*[3],
Yoshinori IGASE*[4] and Yoji TAMURA*[5]

*1) Deputy Section Head, Structural Engineering Division, Japan Highway Public Corporation
*2) Deputy Section Head, Structural Engineering Division, Tokyo 1st Construction Bureau, Japan Highway Public Corporation
*3) Engineer, 2nd Maintenance Section, Tokyo 1st Operation Bureau, Japan Highway Public Corporation
*4) Deputy Head of Bridge Section, Research Institute, Japan Highway Public Corporation
*5) Engineer, Bridge Section, Research Institute, Japan Highway Public Corporation

ABSTRACT

Aiming at improving the ductility of the existing reinforced concrete bridge piers, the authors studied the effectiveness of seismic retrofit methods, such as covering wall-type piers with reinforced concrete, steel plates or carbon fibers and covering column-type piers with carbon fibers. Then, seismic performances of retrofitted piers were examined by carrying out alternating repeated load tests on scale-models. The results showed that the deformability of piers with a square cross section whose aspect ratio was up to 1:3 was improved by reinforced concrete, steel plates, or carbon fibers covering methods. Partial retrofit around the base perimeter was also found to be extremely effective in improving the ductility. As for the wall-type piers whose aspect ratio was 1:5, the most effective retrofit method was to restrain the base region with tension members.

INTRODUCTION

The Hanshin-Awaji earthquake of 17th January 1995 caused devastating damages on various infrastructures, including highways operated by JH (Japan Highway Public Corporation), such as Meishin Expressway, Chugoku Expressway and Dai-Ni Shinmei Route. Hitherto unexperienced seismic motion is considered to have occurred on the existing structures, resulting in the extensive damages on bridge piers which were designed based on the old Seismic Performance Criteria before the amendments were adopted to the shear force calculation method and the steel ratio reduction sections.

Particularly, some of the bridge piers that had been designed before the 1980 amendments to the Specifications for Highway Bridges had inadequate anchorage length of the longitudinal reinforcement or insufficient amount of hoop ties. Consequently, retrofit works employing the Reinforced Concrete Covering Method or Steel Plate Covering Method have been carried out on old bridge piers to improve their ultimate strength. However, in order to withstand an extreme earthquake like the Hanshin-Awaji, a retrofit method should improve not only the strength but also the deformability which leads to the ductility improvement so that the piers will become structurally persistent. Therefore, it is important to employ a retrofit method which improves both the ductility and energy absorption.

As far as piers with a circular cross section or a square cross section of a small aspect ratio are

concerned, the Reinforced Concrete Covering Method and Steel Plate Covering Method have proved to improve the ductility by helping to restrain the concrete and prevent the buckling of the longitudinal reinforcement[1]. Nevertheless, these methods might not be effective for piers with a large aspect ratio such as wall-type piers, because the restraining effect would be limited for such piers. To retrofit the wall-type piers effectively, JH has been doing researches on such methods as drilling a pier's structural frame horizontally to add intermediate restraining bars and covering the base circularly to enhance the restraining effect.

In addition to the conventional methods, another way of retrofitting which is effective as well as offering good workability should be developed. Carbon fibers are highly flexible and have a high rupture strength in practice. If their restraining effect as hoop ties is verified, they can help to develop an extremely effective seismic retrofit method. Therefore, it is necessary to develop a suitable design system and practical application of them.

All the above things considered, JH carried out the following three tests:
(1) Seismic retrofit performance tests for the wall-type piers with the aspect ratio of 1:3
(2) Seismic retrofit performance tests for the wall-type piers with the aspect ratio of 1:5
(3) Seismic retrofit performance tests on the Carbon Fiber Covering Method

In this paper, we report on the test results and the feasibility of the seismic retrofit methods.

SEISMIC RETROFIT PERFORMANCE TESTS FOR WALL-TYPE PIERS WITH THE ASPECT RATIO OF 1:3 (TEST 1)

One of the seismic retrofit methods for the wall-type piers is to drill their structural frame horizontally and add intermediate restraining bars, which however, requires laborious, time-consuming operations. Assuming that the wall-type piers can be effectively strengthened without adding intermediate restraining bars when their aspect ratio is about 1:3, we carried out scale model tests to examine the improvement in ductility when adding reinforced concrete and steel plates to the pier perimeter. Also examined in the tests were the piers whose bases were elliptically covered with steel plates.

OUTLINE OF THE TESTS (TEST 1)

(1) Test specimens

The standard specimen was a one-fifth scale model of a wall-type pier (with the aspect ratio of 1:3) usually employed in the bridge design of JH. The specimens were designed so that the tension reinforcement ratio and the hoop tie ratio represented those of the real pier, and there were no sections where the reinforcement was reduced. Table 1 shows the dimension, and Table 2 and Figure 1 give the type, size, shape and bar arrangement of each specimen.

Table 1: Dimensions of the specimens

	Dimension (mm)			Tension reinforcement ratio (%)	Hoop tie ratio (%)
	Long side: B	Short side: D	Height: H		
Real piers	6,000	2,500	12,500	0.43	0.06
Specimens	1,500	500	2,500	0.50	0.04

Table 2: List of the specimens

Specimen symbol	Type of retrofit	Range of retrofit (h)	Retrofit thickness (t)	Notes
No. 1-1	Standard (no retrofit)	—	—	D16 @ 87.5 for the main longitudinal reinforcement, and D6 @ 100 for the hoop ties
No. 1-2	Reinforced concrete covering	Throughout the height	5 cm	D16 @ 200 for the main longitudinal reinforcement, and D10 @ 100 for the hoop ties
No. 1-3	Steel plate covering	Throughout the height	2.3 mm	Filler: epoxy resin, 3 mm
No. 1-4	Steel plate covering	1D from the base	2.3 mm	Filler: epoxy resin, 3 mm
No. 1-5	Steel plate covering	Throughout the height	2.3 mm	Filler: shrinkage-compensating mortar, 10 mm
No. 1-6	Steel plate covering	1D from the base	2.3 mm	Elliptical retrofit

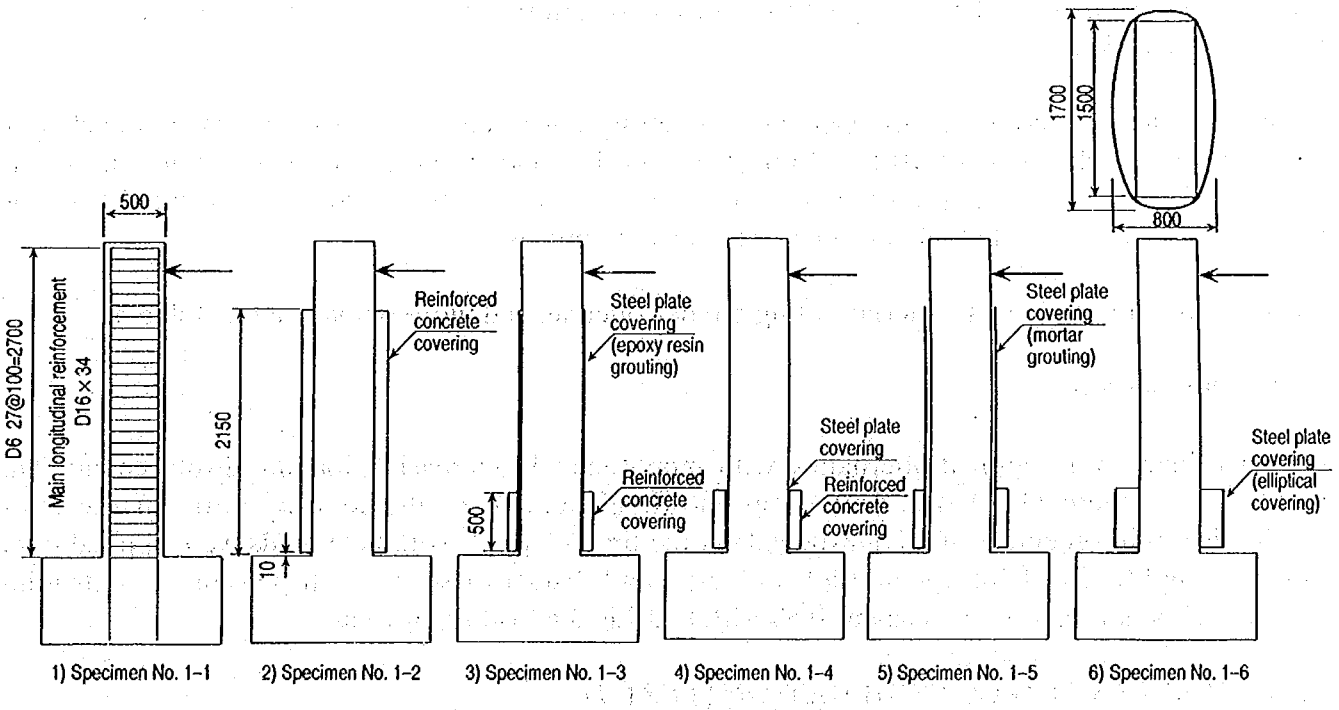


Figure 1: Shape of the specimens

The specimen *No. 1-1* is the standard specimen without retrofit. The specimen *No. 1-2* was covered with reinforced concrete throughout, while steel plates were attached to the specimen *No. 1-3* throughout. For the specimen *No. 1-4*, steel plates were attached only to a section between the base and 1D (the short side length of the standard specimen) to examine an economical retrofit method. For the specimen *No. 1-5*, shrinkage-compensating mortar instead of epoxy resin was grouted to the space between the original structure and cover plates with regard to workability on site. To examine a more effective retrofit method, the retrofitted cross section of the specimen *No. 1-6* was designed to be an elliptical shape, the outer surface of which was covered with steel plates. When arranging the reinforcing bars in each retrofit method, the hoop ties volume ratio of the real piers was given to the specimens. In the calculation, the total areas of the steel plates were converted into the hoop ties.

Table 3: Results of material testing on concrete

Specimen symbol	Compressive strength (MPa)	Elastic modulus (GPa)	Poisson's ratio
1-1 to *1-6*	31	28	0.21

Table 4: Results of material testing on reinforcing bars

Specimen symbol	Yielding point (MPa)	Tensile strength (MPa)	Elastic modulus (GPa)
1-1 to *1-6*	357	513	192

Apart from *No. 1-6*, the specimens with steel cover plates had protect concrete in a section between the base and 1*D*. The bar arrangement of the protect concrete was same as that of the retrofitted part of *No. 1-2*.

The shape and size of the cross section of *No. 1-6* were determined according to the Elliptical Steel Jacket Method[2] that has been adopted by Caltrans (California Department of Transport) since the Loma Prieta quake.

Because the test objective was to examine the ductility improvement, the footing was not anchored, and there was a clearance of 10 to 20 mm between the footing and each retrofit material, i.e. the reinforced concrete, steel plates or protect concrete, so that the vertical force would not be transmitted to the retrofitted sections during the loading process.

Table 3 shows the results of material testing on the concrete, and those on bars are in Table 4.

(2) Loading method

Repeated loads were applied alternately with monotonically increasing loading displacement. The yield displacement (1δy) was defined as the displacement of the loading point of the main longitudinal reinforcement in the tensile side at the time of yield. Alternate loads were applied three times at amplitudes of integer multiples of the yield displacement by a displacement controlling system. The axial force was constant (0.59 MPa) during the loading process.

TEST RESULTS AND CONSIDERATION (TEST 1)

(1) Hysteresis curve and progress in damages

Table 5 shows the yielding displacement, yielding load, maximum load, ductility factor and energy absorbing capacity, and Figure 2 gives the load-displacement curve of each specimen. The ductility factor was calculated based on the "Rehabilitation Specifications"[3]. Here, the "ultimate state" was defined as the state where the load in each cycle became smaller than 80% of the maximum load and would not recover even after the loading displacement amplitude was made larger.

The specimen *No. 1-1* reached the ultimate state in the second cycle of 5δy, with the main longitudinal reinforcement buckling on the D-surface.

Table 5: List of test results

Specimen symbol	Yielding displacement (mm)	Yielding load (kN)	Maximum load (displacement amplitude) (kN)	Ductility factor	
				Test results	Calculation values
No. 1-1	13	276.5	292.2 (–3δy)	5	2.0
No. 1-2	10	277.5	301.1 (–6δy)	9	1.9
No. 1-3	8	280.5	294.2 (–4δy)	11	3.2
No. 1-4	12	278.5	301.1 (+5δy)	8	2.7
No. 1-5	10	279.5	299.1 (–5δy)	10	3.0
No. 1-6	12	261.8	295.2 (+5δy)	9	2.4

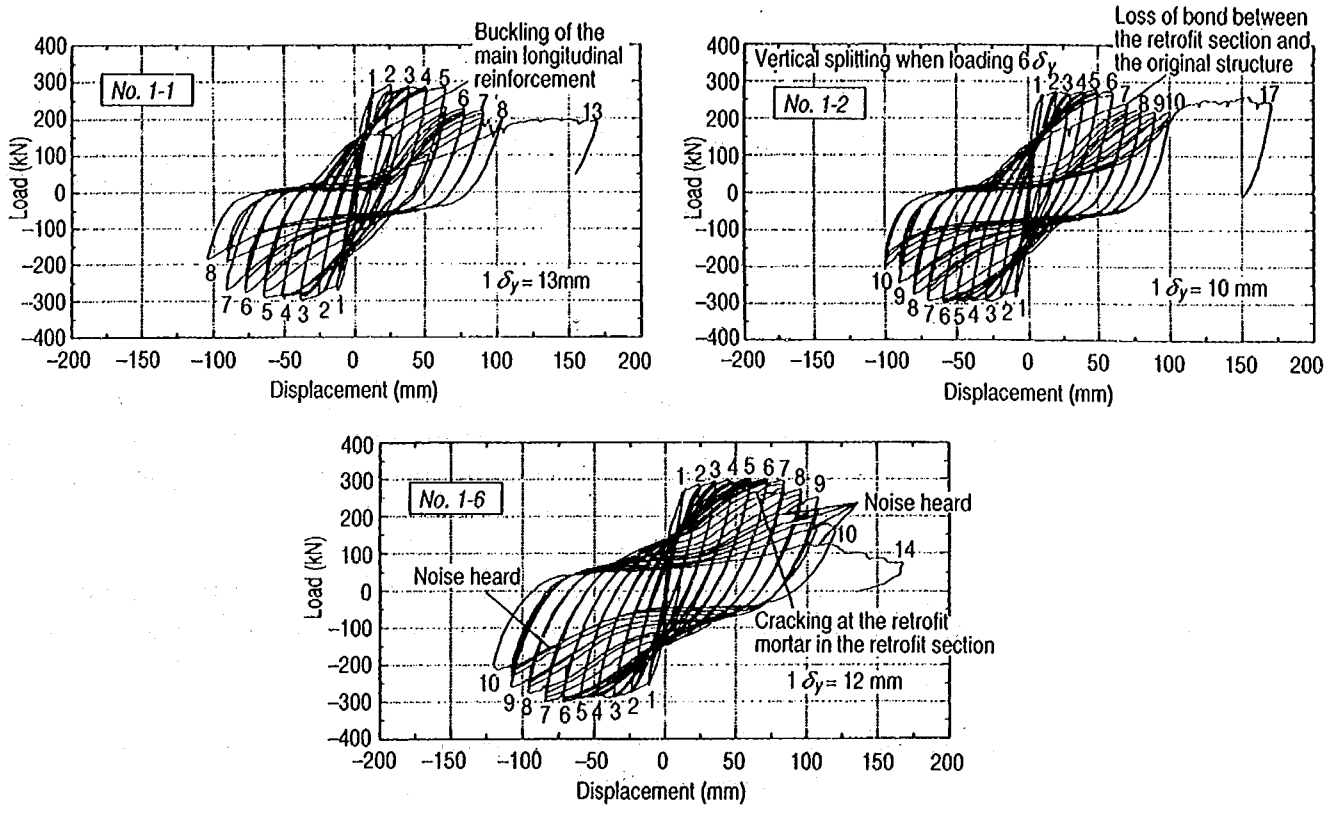


Figure 2: Load-displacement curves

Vertical cracking along the original structure side occurred on the A- and C- surfaces of the specimen *No. 1-2* under 6δy. The D-surface, to which the load was applied first, lost bond under 7δy, and so did the B-surface under 9δy, and finally the specimen reached the ultimate state. The load decreased rapidly after the bind was lost in the first cycle of 7δy, but it was less severe than in the case of *No. 1-1*.

The strength of the specimen *No. 1-3* was almost as same as that of the specimens *No. 1-1* and *No. 1-2*, but the yielding displacement was smaller than those of the other two. Vertical cracking occurred under 6δy on the short side of the protect concrete, causing a gradual reduction in load. The protect concrete at the corners gradually lost bond after the loading of 8δy, but the reduction rate after the

maximum load was small. The specimen reached the ultimate state in the first cycle of $12\delta y$ accompanied by the breakage of the reinforcing bars. However, the steel plates never lost bond.

Having a retrofit only up to $1D$, the specimen *No. 1-4* showed the same yielding displacement as *No. 1-1*. While loading $5\delta y$, the bond between the cover plates and the protect concrete was lost as vertical cracking occurred, and the load started to decrease. The load reduction rate was small as it was for *No. 1-3*. The reinforcing bars broke under $7\delta y$ and the specimen reached the ultimate state under $8\delta y$ with the cover plates losing bond with the original structure.

The specimen *No. 1-5* was retrofitted in the same way as *No. 1-3*, but had shrinkage-compensating mortar as the filler instead of epoxy resin. As the bond was lost at an early stage, the yielding displacement was almost the same as that of *No. 1-2*. The loss of bond between the cover plates and protect concrete caused vertical cracking under $6\delta y$, resulting in a load reduction. Under $8\delta y$ the corner concrete lost bond, and the main longitudinal reinforcement broke after the third cycle of $9\delta y$. The load reduction was small, and the ultimate state came just after the loading of $10\delta y$.

The specimen *No. 1-6* was retrofitted up to $1D$ in an elliptical shape. As had been expected, the yielding displacement was same as that of *No. 1-4* whose retrofitted section was the same. There was a small load reduction after the maximum load under $5\delta y$, which became greater in the 2nd cycle of $7\delta y$ after cracking occurred in the mortar between the cover plates and structural frame. The specimen reached the ultimate state under $9\delta y$ when the reinforcing bars broke.

(2) The maximum load and the effect

Figure 2 shows the load-displacement curve of the specimens *No. 1-1*, *-2* and *-3*. There is little difference in their maximum loads. However, just after the loading displacement exceeded 60 mm, the specimens *No. 1-1* and *No. 1-2* showed a rapid load reduction. The ductility of *No. 1-1* was smaller than that of *No. 1-2* in that *No. 1-1* had a larger yielding displacement and showed a rapid load reduction when the displacement amplitude was still small.

All the specimens with cover plates showed a gradual load reduction. In particular, the specimen *No. 1-6* showed a remarkable performance, keeping the maximum load until the loading displacement exceeded 80 mm.

Figure 3 gives the energy absorption of each specimen. The specimen *No. 1-6* showed a remarkable performance, especially when the displacement amplitude became larger.

SUMMARY OF THE RESULTS (TEST 1)

We have seen the result of the alternating horizontal loading tests on scale models of the wall-type pier, to study the improvement in deformability brought about by reinforced concrete and steel plate coverings, base covering with steel plates, and elliptical retrofit. The results can be summarized as follows:

1) Because the long side of a wall-type pier has a little restraining effect, it is considered to be difficult to improve the ductility by retrofitting the outer surfaces only. However, the load reduction caused by the loss of bond of concrete cover can be restricted to a certain extent by covering with reinforced concrete or steel plates.

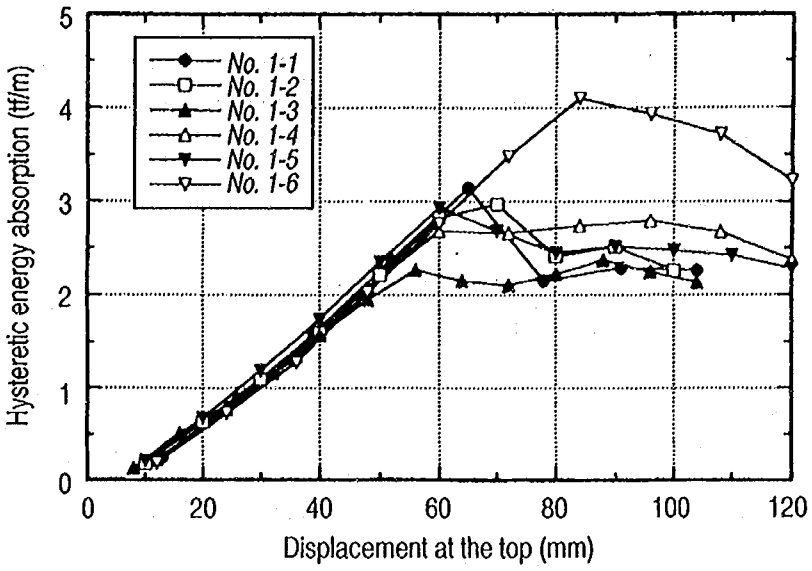


Figure 3: Hysteretic energy absorption curves

2) There is no problem in using shrinkage-compensating mortar as the filler for the steel cover plates to improve the ductility around the base.
3) Partial retrofit around the base perimeter is similarly effective. In particular, retrofitting up to 1*D* is enough to obtain satisfactory performance when employing a method with a high restraining effect such as the elliptical retrofit, and the ductility can be sufficiently improved without drilling piers and inserting steel.

As the elliptical retrofit method showed good results, the authors are planning to carry out further tests on it with various degrees of retrofit for the practical application in the near future.

SEISMIC RETROFIT PERFORMANCE TESTS FOR WALL-TYPE PIERS WITH THE ASPECT RATIO OF 1:5 (TEST 2)

As described in the previous chapter, reinforced concrete or steel plates covering proved to be effective. However, separate examination is necessary for the wall-type piers with an aspect ratio of more than 1:3. We consequently carried out scale model tests on wall-type piers with the aspect ratio of 1:5 that were retrofitted with steel cover plates to study the ductility improvement by restraining the concrete as well as finding an effective way of enhancing the restraining effect.

OUTLINE OF THE TESTS (TEST 2)

(1) Test specimens

The standard specimen was about one-third scale model of a real bridge pier. The tension reinforcement ratio and the hoop tie ratio of the specimen were the representation of those of the real pier, and there was no steel ratio reduction. Table 6 shows the dimension, and Table 7 and Figure 4 give the type, size, shape and bar arrangement of the specimens.

The standard specimen *No. 2-1* was not retrofitted. The specimen *No. 2-2* was covered with steel plates throughout and had protect concrete (depth: 10 cm, restraining rebars D6 × 5) up to 1*D* (the

Table 6: Dimensions of the specimens

	Dimensions (mm)			Tension reinforcement ratio (%)	Hoop tie ratio (%)
	Long side: B	Short side: D	Height: H		
Real pier	6,000	1,200	4,720	0.98	0.00
Specimens	2,500	500	2,000	0.50	0.02

Table 7: List of the specimens

Specimen symbol	Type of retrofit	Aramid rods retrofit range (h)	Retrofit thickness (t)	Notes
No. 2-1	Standard (without retrofit)	—	—	D13 @ 62.5 for the main longitudinal reinforcement, and D6 @ 125 for the hoop ties
No. 2-2	Steel plate covering	—	2.3 mm	Filler: epoxy resin, 3 mm
No. 2-3	Steel plate covering	Throughout the height (ϕ6, horizontal pitch @ 500, vertical pitch @ 250)	2.3 mm	Filler: epoxy resin, 3 mm
No. 2-4	Steel plate covering	1D from the base	2.3 mm	Filler: epoxy resin, 3 mm
No. 2-5	Steel plate covering	Throughout the height	2.3 mm	Filler: shrinkage-compensating mortar, 20 mm

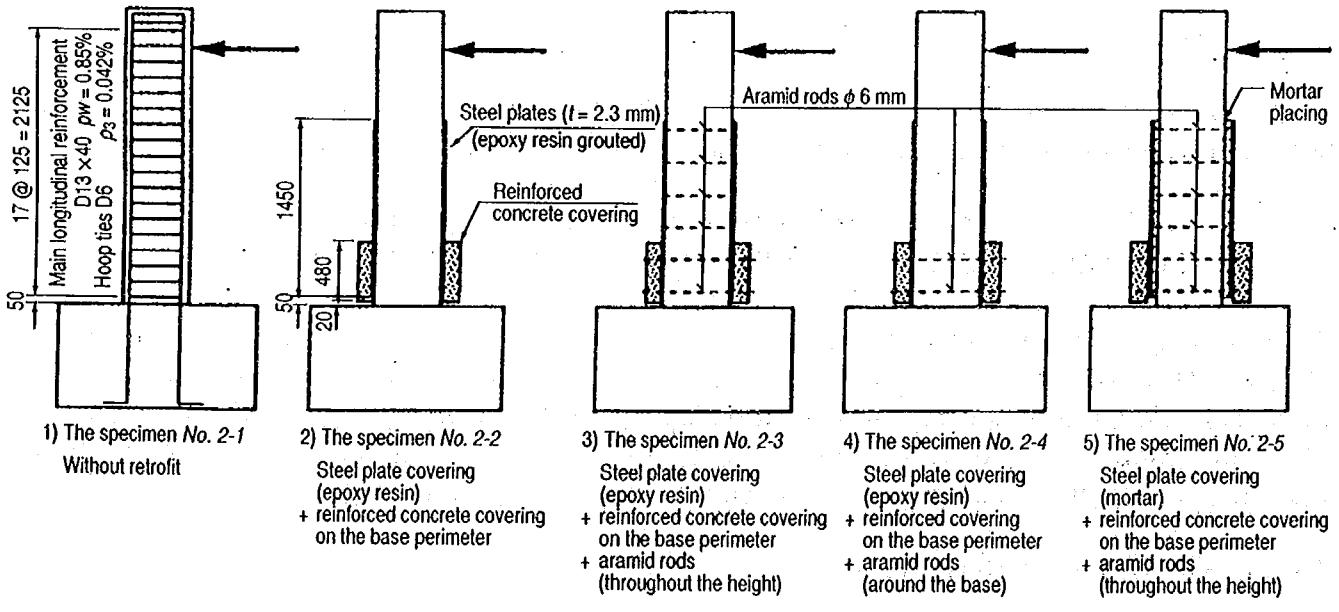


Figure 4: Shape of the specimens

length of the short side of the standard specimen) from the base. In addition to the same retrofit as *No. 2-2*, the specimen *No. 2-3* had aramid rods (ϕ6 mm) throughout the height to fix the cover plates and enhance the restraining effect of the concrete inside. The specimen *No. 2-4* was almost the same as *No. 2-3*, but had aramid rods only up to 1D from the base. The specimen *No 2-5* was also almost the same as *No. 2-3*, but had shrinkage-compensating mortar instead of epoxy resin grouted to the space between the original structure and the cover plates in view of workability on site.

Table 8: The results of material testing on concrete of the original structure

Specimen symbol	Compressive strength (MPa)	Elastic modulus (GPa)
2-1 to *2-5*	33.0	24

Table 9: Results of material testing on reinforcing bars

Specimen symbol	Yielding point (MPa)	Tensile strength (MPa)	Elastic modulus (GPa)
2-1 to *2-5*	360	497	181

Table 10: List of test results

Specimen symbol	Yielding displacement (mm)	Yielding load (kN)	Maximum load (displacement amplitude) (kN)	Ductility factor	
				Test results	Calculation values
No. 2-1	9.8	554.1	610.0 ($-5\delta y$)	5	1.9
No. 2-2	5.8	575.7	616.8 ($-7\delta y$)	8	2.8
No. 2-3	5.4	511.9	677.6 ($-12\delta y$)	12	4.3
No. 2-4	6.0	545.2	702.2 ($-11\delta y$)	12	4.3
No. 2-5	5.3	554.1	681.6 ($-11\delta y$)	12	4.3

Table 8 gives the results of material testing on the concrete of the original structure, and Table 9 shows those on reinforcing bars.

(2) Loading method

Repeated loads were applied alternately with monotonically increasing loading displacement. The yield displacement ($1\delta y$) was defined as the displacement of the loading point of the main longitudinal reinforcement in the tensile side at the time of yield. Alternate loads were applied three times at amplitudes of integer multiples of the yield displacement by a displacement controlling system. The axial force was constant (0.98 MPa) during the loading process.

TEST RESULTS AND CONSIDERATION (TEST 2)

(1) Hysteresis curve and progress in damages

Table 10 shows the yielding displacement, yielding load, maximum load, ductility factor and energy absorbing capacity. The ductility factor was calculated, based on the "Rehabilitation Specifications"[3]. As in the previous tests described in the Section 2.2, the "ultimate state" was defined as the state where the load in each cycle became smaller than 80% of the maximum load and would not recover even after the loading displacement amplitude was made larger.

The specimen *No. 2-1* experienced the loss of bond of cover concrete and the buckling of reinforcing bars around up to $1D$ (50 cm) from the base under $6\delta y$, losing the strength rapidly. At that time, the hoop ties hardly helped to prevent the buckling of the main longitudinal reinforcement which never broke.

As for the specimen *No. 2-2*, opening between the protect concrete and cover plates started to appear during the loading of $7\delta y$. The cover plates and protect concrete near the base started to bulge under $8\delta y$, followed by the gradual reduction in strength. The amount of the bulge was about 30 mm. When the cover plates and protect concrete were taken off, it was found that while the main longitudinal reinforcement at the ends broke at the base due to the restraint by the cover plates and hoop ties, they buckled at the center as those of *No. 2-1* did.

The reinforcing bars of the specimen *No. 2-3* started to break under $12\delta y$, and broke successively during the loading of $13\delta y$ causing a reduction in strength. There was no damaging cracking or bulging observed in the protect concrete at the ultimate state. Furthermore, when the protect concrete and cover plates were taken off, the surface of the concrete was found intact; the displacement concentrated on the base part only. The main longitudinal reinforcement broke at the base because of active restraint of the aramid rods as was the case for the ends of *No. 2-2*. Because the stress of the main longitudinal reinforcement in the section between the base and $0.5D$ (25 cm) was within the elastic range, it is clear that the displacement concentrated on the base region owing to the active restraint.

While *No. 2-3* had the aramid rods throughout its height, the specimen *No. 2-4* had them only up to $1D$. Thus, the yielding displacement was almost the same as that of *No. 2-2*. The reinforcing bars started to break under $12\delta y$, resulting in the decrease in strength. The breaking behavior was same as that of *No. 2-3*.

The specimen *No. 2-5* had the same retrofit as *No. 2-3* but mortar was used as the filler instead of epoxy resin. Both the yielding displacement and breaking behavior were almost identical to those of *No. 2-3*.

(2) The maximum load and seismic retrofit performance

Figure 5 gives load-displacement curve of *No. 2-1*, *-2* and *-4*. The maximum load and the maximum displacement of the specimens *No. 2-3*, *-4* and *-5*, all of which had aramid rods, were a little larger than those of the specimens *No. 2-1* and *-2*.

When compared with *No. 2-1*, the specimen *No. 2-2* showed an improved ductility but had almost the same absolute displacement at the top. It is because the apparent rigidity of *No. 2-2* increased owing to the reinforcement by the cover plates, which reduced the yielding displacement.

Figure 6 shows the energy absorption of each specimen. The energy absorption of those with the aramid rods showed a remarkable performance, leading to a conclusion that the active restraint by prestressing is an effective means of strengthening the wall-type pier.

Though covered with the steel plates, the energy absorption of *No. 2-2* was not so different from that of *No. 2-1*. It means that steel cover plates alone cannot promise sufficient performance for the wall-type piers of a large aspect ratio.

The specimens *No. 2-4* and *-5* had a similar performance to that of *No. 2-3*, which proved that retrofitting only up to $1D$ is enough to obtain satisfactory results, and that using a different kind of filler makes no difference in the seismic retrofit performance.

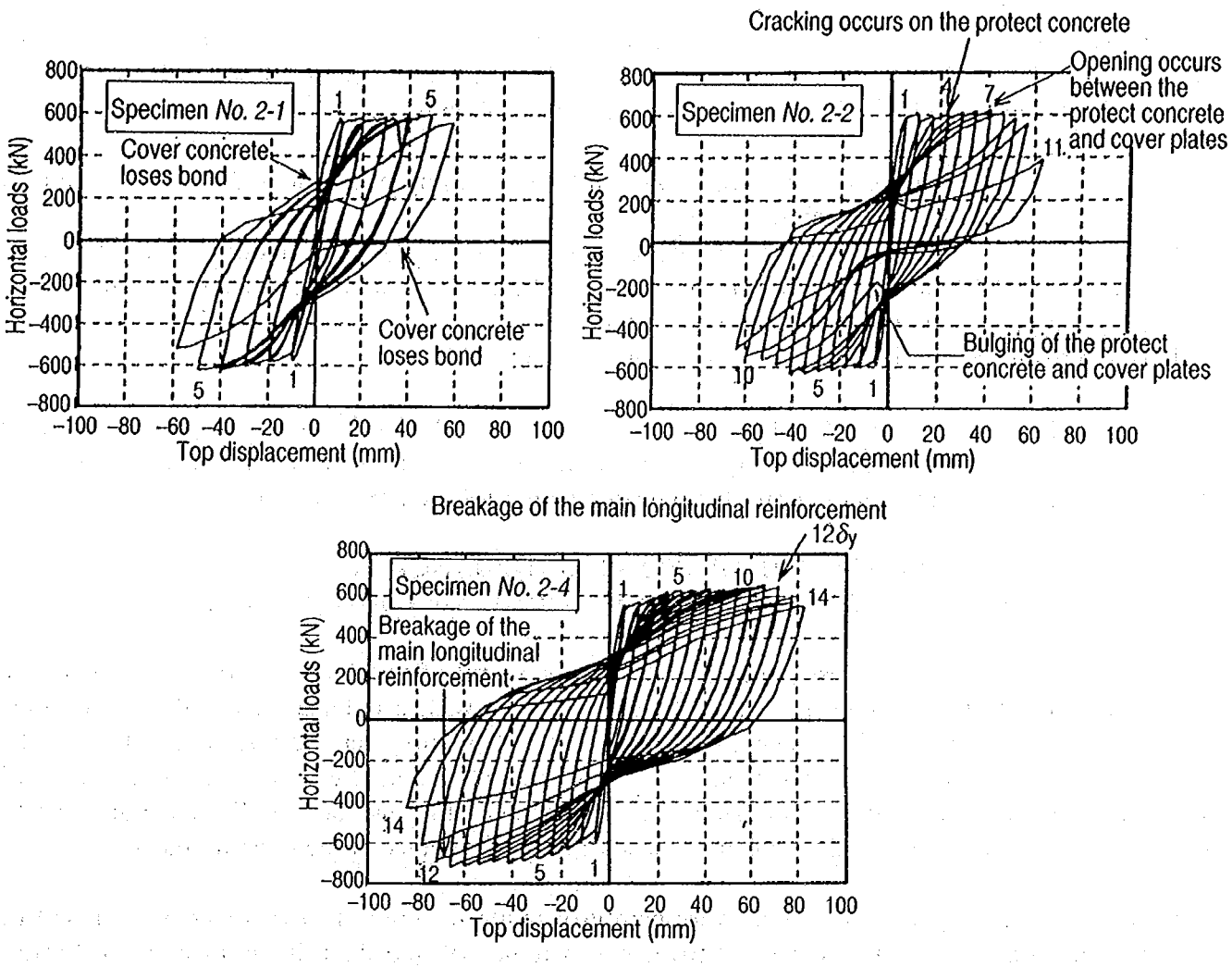


Figure 5: Load-displacement curves

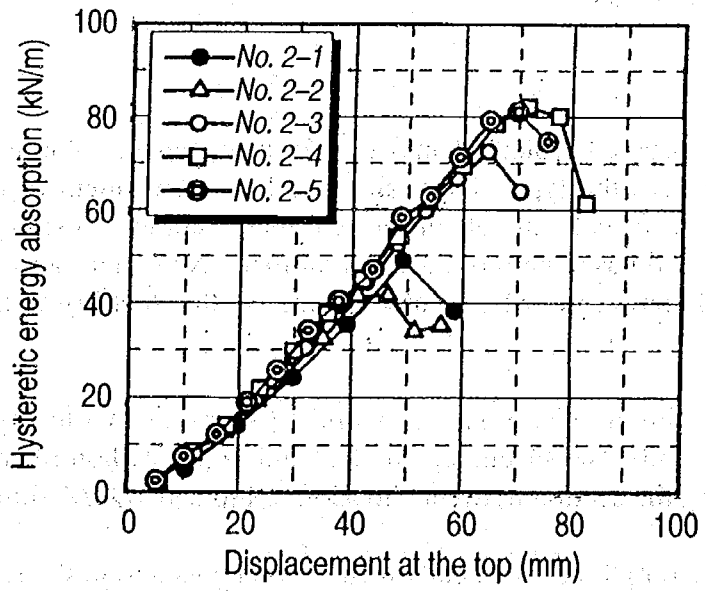


Figure 6: Hysteretic energy absorption curves

SUMMARY OF THE RESULTS (TEST 2)

We have seen the test results of alternate horizontal loading on scale models of the real piers with the aspect ratio of 1:5, and examined the improvement in deformability when restraining the steel cover plates with aramid rods. The results can be summarized as follows:

1) Because the long side of a bridge pier has a little restraining effect, it is difficult to improve ductility by covering with steel plates only.
2) Enhancing the restraining effect of the inner concrete improves the deformability of the structure.
3) There is no problem in using shrinkage-compensating mortar as the filler for the steel cover plates to improve the ductility in the base region.
4) Partial retrofit around the base perimeter is similarly effective.

The tests verified the seismic retrofit performance of aramid rods, but it became important to clarify to what extent a degree of prestressing influences the ductility improvement. Further studies on specimens without prestresses to clarify the impact are kept for the next occasion.

SEISMIC RETROFIT PERFORMANCE TESTS ON THE CARBON FIBER COVERING METHOD (TEST 3)

There have been a number of researches[4)-7)] on the seismic retrofit performance of the Carbon Fiber Method in shear reinforcement as well as for the sections with a reduced steel ratio of the main longitudinal reinforcement. The feasibility of the method has thus been well verified. On the other hand, studies on the ductility improvement by carbon fibers' restraint effects are still in progress. It is therefore necessary to clarify to what extent the carbon fibers improve the ductility by regulating the deformability and in what way they enhance the seismic performance of the existing piers.

Consequently, using specimens which were carefully made to represent real piers, we carried out scale model tests to study the seismic retrofit performance of and ductility improvement brought about by the Carbon Fiber Method.

OUTLINE OF THE TESTS (TEST 3)

(1) Test specimens

In designing specimens, we adopted typical shapes of two-independent-column-type and the wall-type. Table 11 and Figure 7 give the type, shape, size and bar arrangement of the specimens. The specimens were about one-fourth scale models of the real piers, and the tension reinforcement ratio and hoop tie ratio were designed based on those of the real piers. Note that there was no reduction in reinforcement in the axial direction in order to concentrate on the ductility improvement effect of carbon fibers.

The aspect ratio of the specimens *No. 3-1*, *-2*, *-3* and *-4* was 1.5, while that of the wall-type specimens *No. 3-5* and *-6* was 3.0. The specimens *No. 3-4* and *-6* had carbon fibers in the direction of the hoop ties concentrating on the section between the footing top and 1*D* (*D*: short side length).

With respect to the bonding strength between carbon fibers and concrete in the real pier, the bonding area of carbon fibers in the specimen *No. 3-4* was reduced to 1/4. It was because one layer of carbon

Table 11: List of the specimens

Specimen symbol	Cross section size	Hoop ties	Carbon fibers in the direction of the hoop ties	Main longitudinal reinforcement	Carbon fibers in the direction of the main longitudinal reinforcement	Retrofitting range of carbon fibers in the direction of the hoop ties
NO. 3-1	450 × 300	D6 @ 250 (0.056%)	— (0%)	22-D13 6-D10 (2.38%)	—	—
NO. 3-2			One layer (0.05%)		1/4 of a layer	Between the footing top and 3*D*
NO. 3-3			Two layers (0.1%)			Between the footing top and 3*D*
NO. 3-4			Two layers (0.1%)			0.1% between the footing top and 1*D* 0.05% between 1*D* and 3*D*
NO. 3-5	900 × 300	D6 @ 250 (0.028%)	— (0%)	34-D13 6-D10 (1.76%)	—	—
NO. 3-6			Four layers (0.1%)		1/4 of a layer	0.1% between the footing top and 1*D* 0.03% between 1*D* and 3*D*

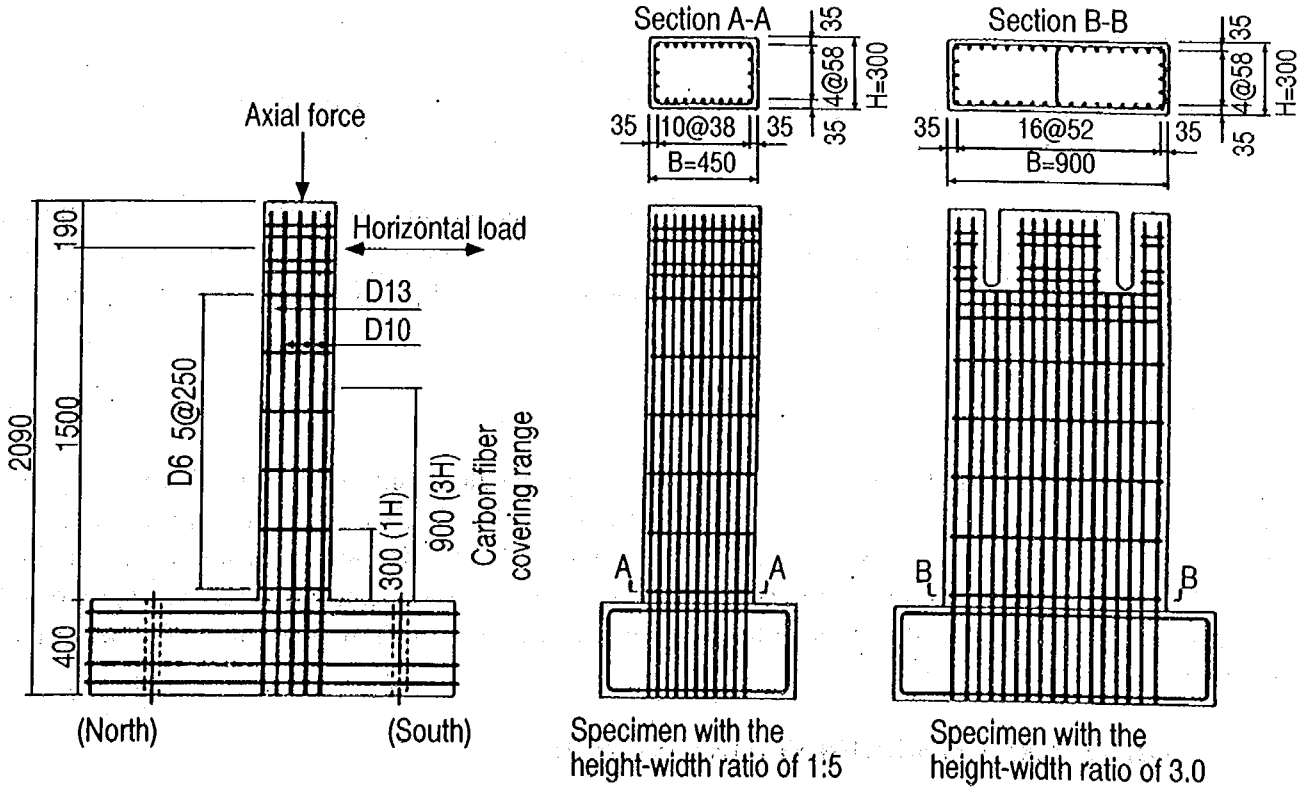


Figure 7: Shape of the specimens

fibers in a specimen was equivalent to four layers in a real pier.

The bonding procedure of the carbon fibers was the following: the surfaces were prepared, primer was applied, carbon fibers were applied in the direction of the main longitudinal reinforcement,

Table 12: Physical properties of carbon fibers

Specimen symbol	Design thickness (mm)	Fiber area weight (g/m^2)	Tensile strength (MPa)	Elastic modulus (GPa)
3-1 to *3-3*	0.110	200	4220	243
3-4 to *3-6*	0.110	201	4047	252

Table 13: Results on material testing on concrete

Specimen symbol	Compressive strength (MPa)	Elastic modulus (GPa)	Poisson's ratio
3-1 to *3-6*	30	18	0.20

Table 14: Results on material testing on reinforcing bars

Specimen symbol	Yielding point (MPa)	Tensile strength (MPa)	Elastic modulus (GPa)
3-1 to *3-6*	363	542	174

epoxy resin was impregnated, carbon fibers were applied in the direction of the hoop ties, and epoxy resin was again impregnated. The lapping length of the carbon fibers was 100 mm, and the corners of the specimens' cross section were edged with a radius of 30 mm.

Table 12 gives the physical properties of carbon fibers. The tensile strength of the fiber itself after the hardening was about 45 MPa. Table 13 gives the results of loading tests on a concrete column sample that was cured at the same time as the specimens, and the physical properties of the reinforcing bars used for the specimens are shown in Table 14.

(2) Loading method

The mean value of displacements obtained when loading the calculated yielding load was designated as $1\delta y$. Then, the alternate loads were applied, increasing by $1\delta y$ once at each displacement stage until the end of the loading process. The axial stress was 0.59 MPa for all the specimens, calculated from the weight of the upper structure. Whichever the aspect ratio, the loading process started with the specimen without retrofit, whose yielding displacement was then designated as that of the retrofitted specimens.

TEST RESULTS AND CONSIDERATIONS (TEST 3)

(1) Maximum load and residual strength

The yielding displacement (δy) of the specimen *No. 3-1* was 13.9 mm, and that of the specimen *No. 3-5* was 12.2 mm. Because of the restriction on strokes of the actuator, the maximum displacement of each specimen was 7–8 times larger than the yielding displacement.

Table 15 gives the maximum load, displacement amplitude under the final loading, residual strength

Table 15: Test results

Specimen symbol	Maximum load (kN)	Final loading	Residual strength (kN)	Ductility factor
No.3-1	111	$\pm 7\delta y$	16 (14%)	5
No.3-2	118	$\pm 7\delta y$	82 (70%)	9
No.3-3	118	$\pm 7\delta y$ five times	106 (92%)	11
No.3-4	121	$\pm 6.9\delta y$ five times	112 (93%)	8
No.3-5	179	$\pm 7\delta y$	92 (51%)	10
No.3-6	185	$\pm 7.8\delta y$	157 (85%)	9

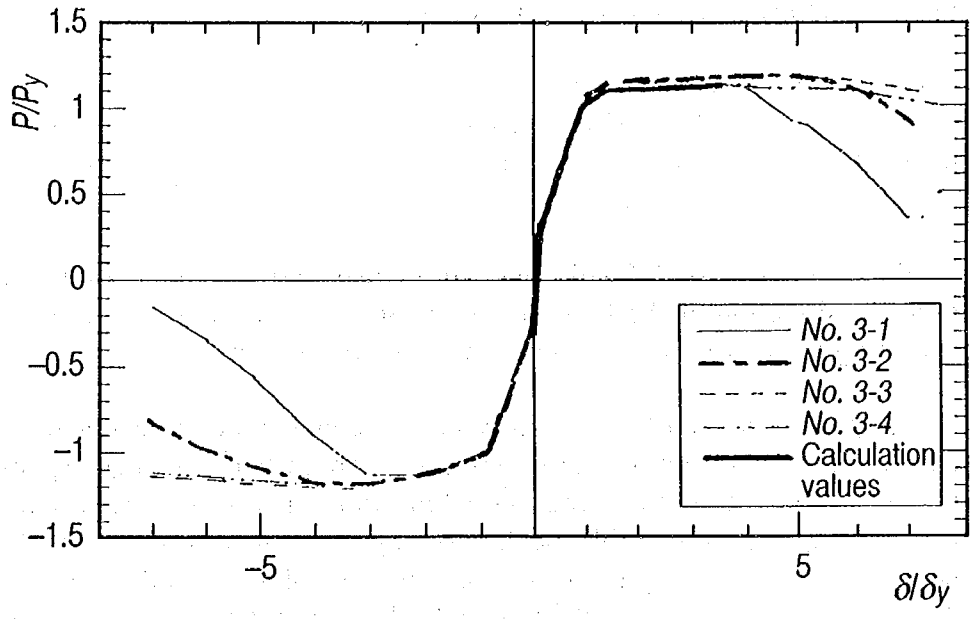


Figure 8: Load-displacement envelope (1:1.5)

and ductility factor. The ultimate displacement of each specimen was defined as the maximum displacement which would not be below the calculated yielding load on the load-displacement curve. It was then divided by δy to be designated as the ductility factor of each specimen.

(2) Seismic retrofit performance for piers with the aspect ratio of 1:1.5

Figure 8 shows the load-displacement envelope drawn from the test results and calculated values of the specimens *No. 3-1, -2, -3* and *-4*. As seen in the diagram, the test results agreed with the calculation values well.

In the specimen *No. 3-1*, diagonal cracks remarkably grew around $4\delta y$, followed by the buckling of the main longitudinal reinforcement, the loss of bond of the cover concrete, and a reduction in strength. The residual strength under $-7\delta y$ was 16 kN, and there was little horizontal strength left. The rupture extended to a large area, and big vertical cracks were observed in a section between the footing top and about $3D$ alongside the main longitudinal reinforcement. Even the concrete inside the hoop ties ruptured around the height $1D$.

The specimen *No. 3-2* with one carbon fiber layer in the direction of the hoop ties started to have carbon fibers' bulging on the compressive side in the section between the footing top and 1*D* while loading $-5\delta y$, causing a decrease in strength. The buckling of the main longitudinal reinforcement should have started around that time. Under $-6\delta y$, the bulging carbon fibers in the direction of hoop ties ruptured from the corner with a massive crash. At the same time, the carbon fibers in the direction of the main longitudinal reinforcement also ruptured.

Because the specimen *No. 3-3* with two layers of carbon fibers showed no noticeable decrease in strength up to $-7\delta y$, five cycles of alternate $7\delta y$ loads were applied to finish the test. The residual strength during the first cycle was 93% of the maximum strength, which was still 70% in the fifth cycle. The damages concentrated on the section between the footing top and 1*D* as was the case for *No. 3-2*. Carbon fibers started to bulge a little under $-5\delta y$. Bond of the lapping section of the carbon fibers was lost under the first cycle of $-7\delta y$, and the carbon fibers in the direction of the main longitudinal reinforcement ruptured in the fifth cycle of $7\delta y$ with more damages at the lapping part. It was felt that the lapping length should have been a little longer.

When the aspect ratio was 1.5, the retrofitted specimens experienced the buckling of the main longitudinal reinforcement under a load which was $1\delta y$ larger than that in the specimen without retrofit. It was confirmed that the retrofitting amount of 0.1% in surface ratio can prevent a rapid reduction in strength even while loading $7\delta y$.

The deformability of the specimen *No. 3-4* which had an intensive retrofit in the section between the footing top and 1*D* in the direction of the hoop ties was same as that of *No. 3-3*, proving that the section between the footing top and 1*D* is the crucial part to be retrofitted.

The specimen *No. 3-3* and the specimen *No. 3-4* where concrete and carbon fibers were bonded in an area of 1/4 showed a difference of 3% in the maximum strength because these specimens took different values in the yielding strength of the main longitudinal reinforcement. Otherwise, the shapes of the two envelopes were almost identical, showing that changes in the bonding strength between carbon fibers and concrete hardly influence the behaviors of a pier under a load. As we have seen in the tests, the ductility of a real pier should equally be improved by installing carbon fibers. While experiencing a large displacement, the carbon fibers eventually lost bond with each other at the lapping section of the specimen *No. 3-3*, and the carbon fibers in the direction of the hoop ties ruptured in several parts in the specimen *No. 3-4*.

(3) Seismic retrofit performance for piers with the aspect ratio of 1:3

Figure 9 shows the load-displacement curve for the aspect ratio of 3.0. When the aspect ratio took a large value of 3.0, the calculated yielding load became about 10% smaller than the yielding load on the positive side of the envelope, almost corresponding to the test results on the negative side.

The difference caused by the presence of retrofit was 7% at maximum, and a slight improvement in the flexural strength by carbon fibers in the main longitudinal direction was observed.

The specimen *No. 3-5*, which had the aspect ratio of 3.0 and was without retrofit, developed diagonal cracks rapidly under $4\delta y$. Under $-5\delta y$, all the main longitudinal reinforcement on the compressive side buckled, and the concrete across the width up to 1.5*D* exfoliated, reducing the strength to 84% of the maximum. The residual strength under $7\delta y$ was 50% of the maximum.

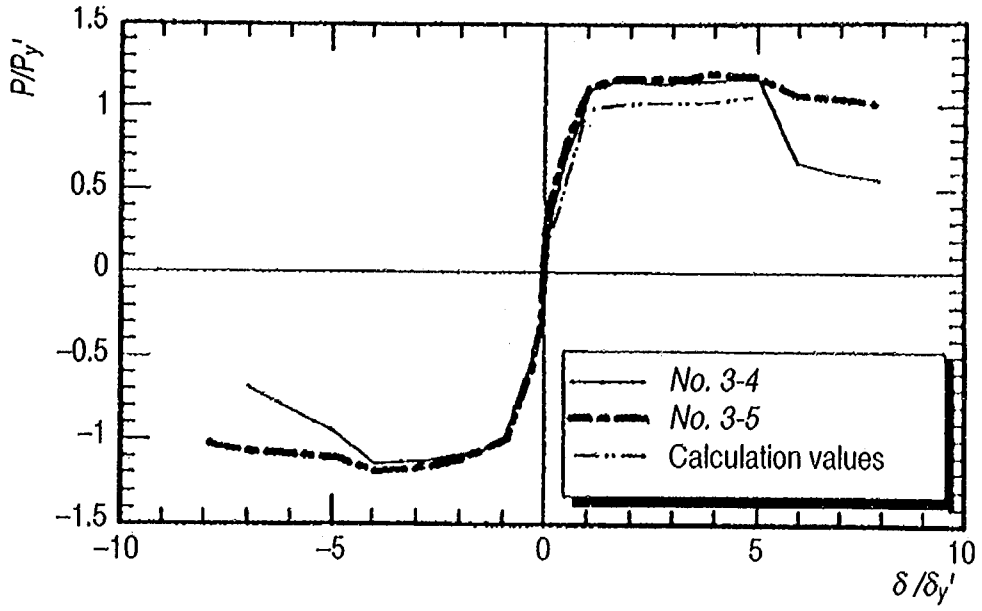


Figure 9: Load-displacement envelope (1:3.0)

The buckling of the main longitudinal reinforcement of the specimen *No. 3-6* did not follow the same process observed in the tests on the aspect ratio of 1.5. It occurred while loading $-5\delta y$ accompanied by the bulging of carbon fibers with a massive noise. However, the decrease in strength was small, still keeping 95% of the maximum. The amount of carbon fibers was 0.1%, concentrating on the region between $1D$ and the footing top. The carbon fibers did not rupture even under $7\delta y$, keeping 87% of the maximum.

SUMMARY OF THE RESULTS AND CONCLUSION (TEST 3)

The results obtained from this study can be summarized as follows:

1) It was confirmed that covering with carbon fibers improves the ductility of an existing bridge pier by regulating its deformability.
2) A ductility of more than 7 is obtained for an existing bridge pier when the amount of carbon fibers is 0.1% in the surface ratio.
3) It was proved that when aiming at the improvement in deformability, the region between the footing top and $1D$ is crucial in retrofitting.
4) Covering with carbon fibers improves the ductility of the wall-type piers with the aspect ratio of 3.0, but the seismic retrofit performance was less good than that of the specimens with the aspect ratio of 1.5.
5) Reducing the area where carbon fibers are bonded to concrete in the direction of the hoop ties to 1/4 resulted in almost the same behavior under a load, showing that the bonding factor has a little impact on the ductility. In that case however, the carbon fibers in the direction of the hoop ties ruptured on reaching the ultimate state.
6) Covering with carbon fibers reduced both the number of damaged regions and their areas compared with a pier without retrofit.

In this paper, only static loading tests have been reported to show the seismic retrofit performance of the Carbon Fiber Method in terms of ductility. However, quasi-dynamic loading tests have also been

carried out, and the seismic performance of retrofitted bridges has been confirmed in other studies[8]. The further researches to be carried out in the near future include the seismic retrofit performance of bridge piers that have hollow cross sections with several steel ratio reduction sections.

CONCLUSIONS

Three different tests were described in this paper, confirming the behavior of retrofitted wall-type piers and the seismic retrofit performance of the Carbon Fiber Method.

Aiming at retrofitting 7100 reinforced concrete bridge piers by fiscal 1997, JH (Japan Highway Public Corporation) has been carrying out retrofit projects since fiscal 1995, taking the results obtained in this study into consideration.

REFERENCES

1) Kawashima, K., Unjoh, S. and Iida, H., "Seismic Inspection and Seismic Strengthening Methods of Reinforced Concrete Bridge Piers at Mid-Height where Main Reinforcements are Terminated with Inadequate Anchorage Length" (in Japanese), *Report of Public Work Research Institute*, the Ministry of Construction, Vol. 189, Sep. 1993.
2) Department of State Highway, Department of Transportation of United States of America, *Seismic Retrofitting Manual for Highway Bridges*, May 1995.
3) Japan Road Association, *Reference for Applying the Guide Specifications for Reconstruction and Repair of Highway Bridges Which Suffered Damage due to the Hyogo-ken Nanbu Earthquake*, (in Japanese), 1995.
4) Uji, K., "Improvement of Shear Capacity of Existing Reinforced Concrete Members with Sheet Type Carbon Fibre Reinforcement" (in Japanese), *Concrete Research and Technology*, Vol. 3, No. 2, July 1992, pp.37-47.
5) Okajima, T., Katsumata, H., Ishida, H. and Higashida, N., "Seismic Retrofit of Existing Reinforced Concrete Bridge Piers Using Carbon Fibers: Phase 2 Loading Tests" (in Japanese), *Proceedings of the 45th annual lecture meeting of the Japan Society of Civil Engineers*, Part Five, Sep. 1990, pp. 824-825.
6) Fujiwara, H., Higashida, N., Ohno, R. and Odajima, T., "Seismic Retrofit Effects by Carbon Fibers for Reinforced Concrete Bridge Piers: Phase 1 Loading Test" (in Japanese), *Proceedings of the 46th annual lecture meeting of the Japan Society of Civil Engineers, Part Five*, Sep 1991, pp.770-771.
7) Yamaguchi, T., Takemura, H., Yanai, S. and Ikeda, S., "Seismic Properties and Dynamic Response Behavior of Reinforced Concrete Columns" (in Japanese), *Proceedings of the Japan Concrete Institute*, Vol. 16, No. 2, 1994, pp. 1265-1270.
8) Osada, K., Ohno, S., Yamaguchi, T. and Ikeda, S., "Seismic Strengthening of Reinforced Concrete Piers with Carbon Fiber Sheets" (in Japanese), *Proceedings of the Japan Concrete Institute*, Vol. 18, No. 2, 1996, pp. 83-88.

RETROFITS OF REINFORCED CONCRETE BRIDGE COLUMNS WITH PRESTRESSING STEEL TIES

Tamio YOSHIOKA*
*Director of research Laboratory, Oriental Construction Co.,Ltd.,Tokyo

ABSTRACT

Seventeen circular and three rectangular (square) specimens were tested to investigate strength, ductility, hysteretic characteristics, energy absorption, damping and residual displacement of retrofitted reinforced concrete bridge columns by means of concrete jacketing, prestressing steel ties and planned plastic hinge induced by a thin slit at the column foot. Results show that the thin slit surely forms the plastic hinge at the planned position and hardly influences degradation. Post-tensioned strand ties of circular columns improve shear crack behavior, but hardly improve strength, ductility, energy absorption etc.

INTRODUCTION

Reinforced concrete (RC) bridge columns, which were designed in accordance with Japanese codes prior to 1980, have been damaged in destructive earthquakes such as the 1995 KOBE earthquake because of inadequate reinforcements at the middle of columns, where longitudinal rebars are terminated, and/or insufficient ductility and shear strength.

These bridge columns are now under retrofitting mainly by means of concrete/steel jacketing and carbon fiber strengthening in Japan[1),2),3)].

Basic concepts of retrofitting RC bridge columns are: (1) strengthening at the middle of columns, where longitudinal rebars are terminated, to prevent shear failure there, (2) flexural rupture within columns without collapse in foundations, because columns could be easily repaired after the earthquake.

In order to improve ductility and shear strength ties should be increased and they have to be adequately anchored in the concrete to confine the core concrete. Hook anchorage, however, seems difficult to be executed in very thin concrete jacketing around existing RC column. Welding ties at the construction site, which is recommended in the latest Japanese code, could not be surely inspected.

Prestressing steel ties in lieu of rebars could make it possible, (1) to anchor and couple ties with anchorage and coupling devices of prestressing tendons, (2) to improve ductility and shear strength thanks to greater yield strength of prestressing steel than conventional rebar and (3) to integrate existing and newly executed concrete without deep chipping of existing concrete as well as to improve shear crack behavior when they are post-tensioned.

Table 1 Specimens

(unit:cm)

specimen No.	shape of section	slit width	unbonding length	kind of tie	material of tie	post-tensioning	spacing of tie	longitudinal reinforcement
C-0(existing)	circular	----	----	tie	rebar	non	30.0	----
C-1	circular	2.5	5.0	tie	rebar	non	10.0	rebar
C-2	circular	2.5	0.0	tie	P. bar	non	10.0	rebar
C-3	circular	2.5	5.0	tie	P. bar	non	10.0	rebar
C-4	circular	2.5	5.0	tie	P. bar	non	15.0	rebar
C-5	circular	2.5	10.0	tie	P. bar	non	10.0	rebar
C-6	circular	2.5	-5.0	tie	P. bar	non	10.0	rebar
C-7	circular	2.5	10.0	tie	strand	tensioning	10.0	rebar
C-8	circular	2.5	10.0	tie	strand	tensioning	12.0	rebar
C-9	circular	2.5	10.0	tie	strand	tensioning	18.0	rebar
C-10	circular	----	0.0	tie	strand	tensioning	5.0	non
C-11	circular	----	0.0	tie	strand	tensioning	10.0	non
C-12	circular	----	0.0	spiral	strand	non	10.0	non
C-13	circular	----	0.0	spiral	strand	non	5.0	non
C-14	circular	2.5	10.0	spiral	strand	non	10.0	rebar
C-RC	circular	0.0	0.0	tie	rebar	non	10.0	rebar
C-JC	circular	0.0	0.0	steel	steel	----	----	----
R-0	rectangular	2.5	10.0	tie	P. bar	non	10.0	rebar
R-1	rectangular	2.5	10.0	tie	P. bar	non	10.0	rebar+P. bar
R-2	rectangular	2.5	10.0	tie	P. bar	non	10.0+3.4	rebar

A thin slit located at the column foot could form a plastic hinge at the planned position, namely the column foot. Unbonding between concrete of the footing and newly anchored longitudinal rebars at the upper region of the footing could lead to greater deflection of the column and prevent spalling of concrete from the footing due to pull-out of rebars.

Seventeen circular and three rectangular (square) specimens were tested to investigate retrofits of RC bridge columns by means of prestressing steel ties and the planned plastic hinge at the column foot. In this paper, results and discussions are presented.

OUTLINE OF THE TEST

SPECIMENS

Table 1 presents a summary of the specimen properties. Parameters of specimens are the shape of the section, the slit width (refer to Fig.2), unbonding length of longitudinal rebars at the upper region of the footing, kind of transverse reinforcement (tie or spiral), material of tie, transverse post-tensioning, spacing of tie and longitudinal reinforcement. The first alphabet C of specimen's No. means the circular section and R the rectangular section. Specimen C-0 corresponds to an existing RC column, in which longitudinal rebars are terminated at the middle of the column. In specimen C-0 shear/flexural failure is expected at the middle of the column because of insufficient development length of longitudinal rebars. All specimens but C-0 are strengthened by concrete jacketing or direct winding of prestressing strands around the

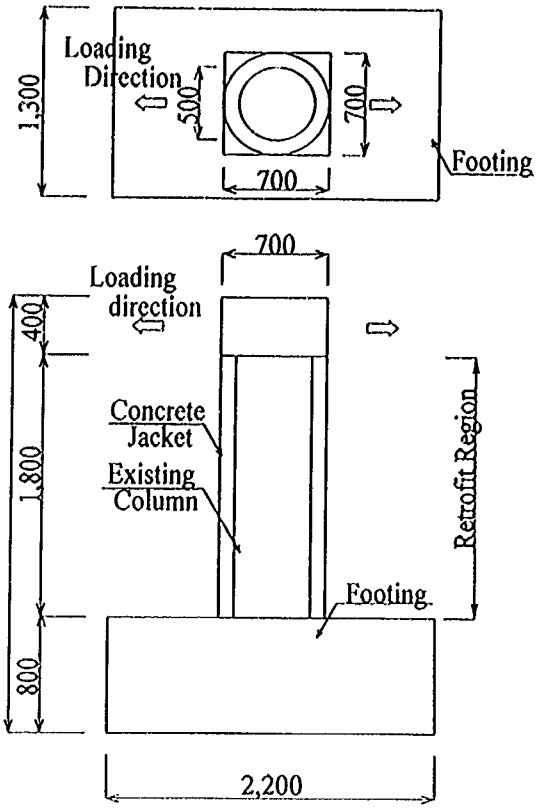


Fig.1 Dimensions of the specimen

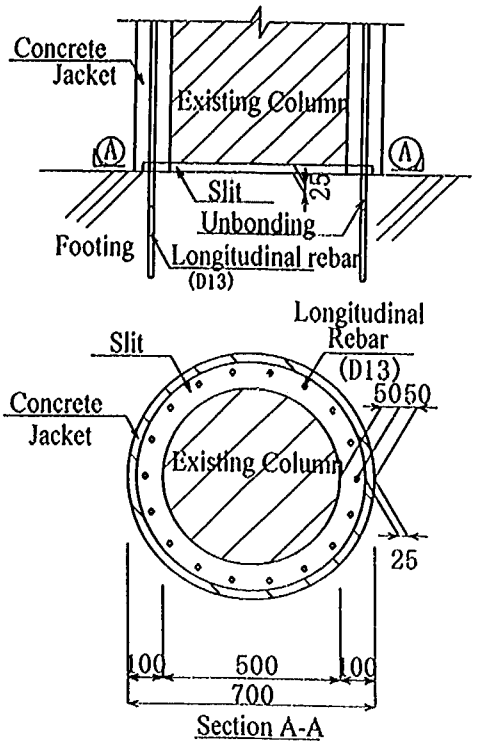


Fig.2 Detail of the column foot

existing column model C-0. Specimens C-1 through C-6 are planned to investigate the effects of the unbonding length of longitudinal rebars on ductility and strength. Specimens C-7,C-8 and C-9 are transversely post-tensioned with prestressing steel ties (strands), which are stressed to the half of the yield strength of the strand. Specimens C-10 through C-13 are not concrete-jacketed in order not to enhance flexural strength. Specimens C-10 and C-11 are post-tensioned with prestressing steel ties and specimens C-12 and C-13 are spirally wound with non-tensioned strands by manpower. Specimen C-14 is reinforced longitudinally with conventional rebars and transversely reinforced with non-stressed strand around longitudinal rebars by manpower and concrete-jacketed.

Specimen C-RC corresponds to the so-called concrete jacketing, without slit and unbonding of longitudinal rebars. Specimen C-JC is a specimen for the steel-jacketing. C-RC and C-JC are specimens for comparison.

Specimens R-0,R-1 and R-2 of the rectangular section are concrete-jacketed with 10cm concrete around 50x50cm existing columns. Existing column model of 50x50cm rectangular section has slightly greater shear and flexural strength than specimen C-0 of the circular section of 50cm diameter. Specimen R-1 is longitudinally post-tensioned with prestressing bars, which are embedded and anchored in the concrete jacket (not placed through the footing). Longitudinal prestress of specimen R-1 is approximately 1.0MPa. Specimen R-2 is very richly reinforced with prestressing steel ties in the plastic hinge region in order to try to improve the ductility of the plastic hinge, because rectangular ties less confine the core concrete than circular ones. The lowest tie of all specimens but specimen R-2 are located at the same

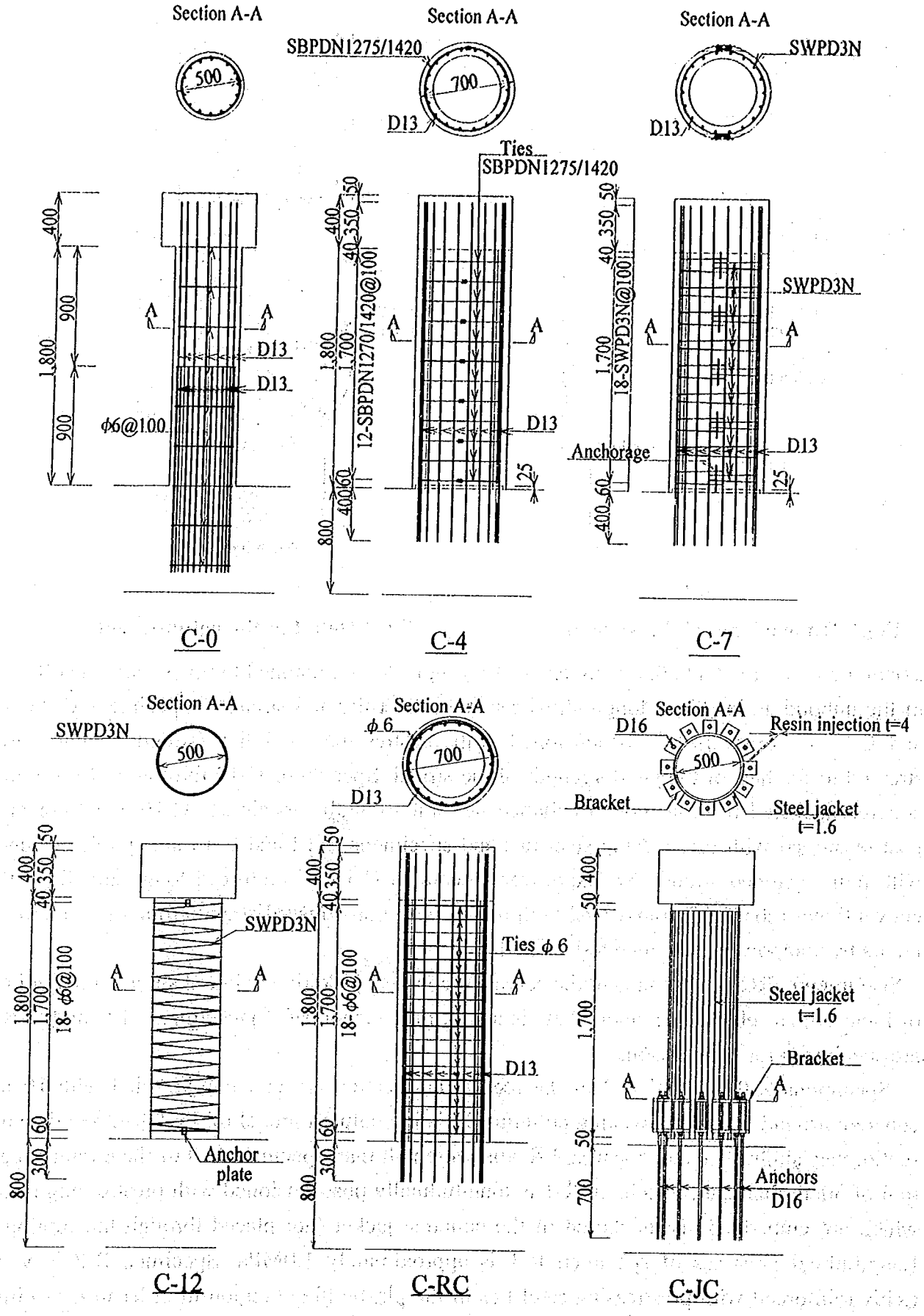


Fig.3 Rebar placing of typical specimens

Table 2 Design Values

item	symbol	unit	C-0	C-1	C-2,3,5,6	C-4	C-7	C-8	C-9
cracking load	Pc	kN	28.8	34.6	34.6	34.6	34.6	34.6	34.6
yielding load	Py	kN	88.5	136.7	136.7	136.7	136.7	136.7	136.7
ultimate bending strength	Pu	kN	123.6	194.3	194.3	194.3	194.3	194.3	194.3
ultimate shear strength	Ps	kN	115.9	269.9	532.1	421.2	364.2	336.7	290.9
Ps/Pu			0.9	1.4	2.7	2.2	1.9	1.7	1.5
cracking disp.	δ c	cm	0.08	0.03	0.03	0.03	0.03	0.03	0.03
yieling disp.	δ y	cm	0.62	0.28	0.29	0.28	0.28	0.28	0.28
ultimate disp.	δ u	cm	1.76	0.70	1.01	0.87	0.81	0.78	0.73
failure mode			shear	flexure	flexure	flexure	flexure	flexure	flexure
item	symbol	unit	C-10,12	C-11	C-13	C-14	R-0	R-1	R-2
cracking load	Pc	kN	28.8	28.8	28.8	34.6	53.6	53.6	53.6
yielding load	Py	kN	87.0	86.4	87.0	136.7	164.1	164.1	164.1
ultimate bending strength	Pu	kN	128.6	131.1	128.7	194.3	218.3	218.3	218.3
ultimate shear strength	Ps	kN	244.2	372.1	245.4	364.2	267.6	527.7	417.7
Ps/Pu			1.9	2.8	1.9	1.9	1.2	2.4	1.9
cracking disp.	δ c	cm	0.08	0.08	0.08	0.03	0.03	0.03	0.03
yieling disp.	δ y	cm	0.62	0.63	0.62	0.28	0.18	0.19	0.18
ultimate disp.	δ u	cm	3.88	6.67	3.91	0.81	0.54	0.65	0.60
failure mode			flexure	flexure	flexure	flexure	flexure	flexure	flexure

height of 6cm from the top of the footing. The spacing of ties is considered as a parameter, but other parameters, such as constant products of multiplying reinforcement ratio of ties by the yield strength of reinforcement, are not taken into consideration. The ratio of sectional area of similarly spaced ties is rebar(diameter=6mm):strand(diameter=2.9mm):prestressing bar(diameter=7.1mm)=1.0:0.70:1.41.

In the column of "kind of tie" in Table 1 "tie" means independent closed ties and "spiral" continuously wound prestressing strands. Ties of indented prestressing bars are coupled with couplers. Newly developed anchorage system is used for strand ties, which can keep the tie closed after the rupture of concrete around the anchorage.

In the column of "material of tie" in Table 1 "rebar" means round bar of 6mm diameter (yield strength = 235MPa), "P.bar" indented prestressing bar of 7.1mm diameter (yield strength =1,275MPa, tensile strength =1,420MPa), "strand" 7-wire unbonded prestressing strand of 2.9mm diameter (yield strength =1,715MPa, tensile strength = 1,910MPa).

In the column of "longitudinal reinforcement" of Table 1 "rebar" means concrete jacketing with longitudinal rebars and "non" direct winding of prestressing strands without jacketing in order to improve both ductility and shear strength without enhancement of flexural strength.

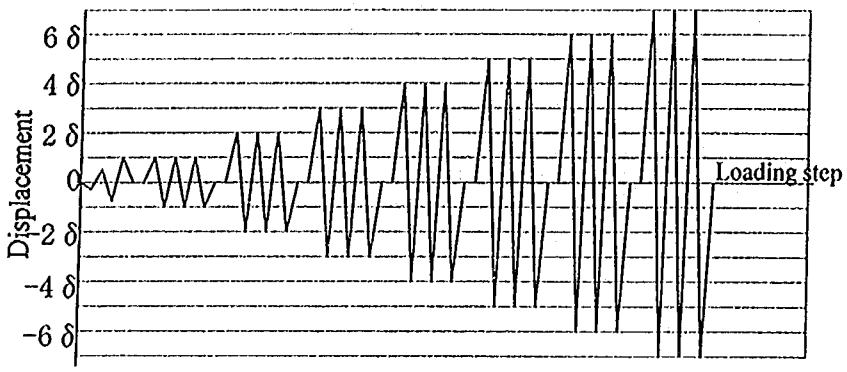


Fig.4 Loading

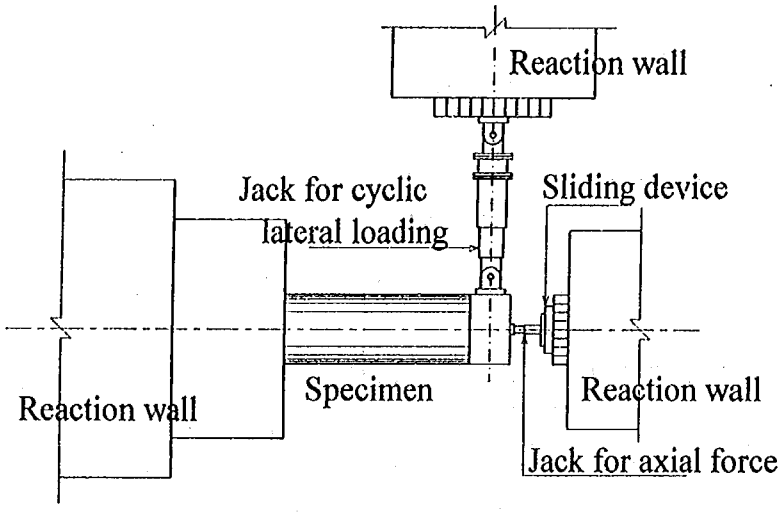


Fig.5 Loading system

Conventional concrete of the compressive strength of 25.5MPa is used for existing columns and footings, self compacting high performance concrete of the compressive strength of 40.0MPa is chosen for the concrete-jacketing to assure concreting into very thin jackets.

Fig.1 shows main dimensions of the specimen and Fig.2 presents the detail of the slit at the column foot and unbonding of longitudinal rebars at the upper region of the footing. Fig.3 shows rebar placing of typical specimens of C-0, C-4,C-7,C-12,C-RC and C-JC.

In Table 2 computed design values are summed up in accordance with "Design Specifications for Highway Bridges"[4]. As shown in the table the ratio of shear strength to flexural strength of strengthened specimens (Pu/Ps) varies from 1.2 to 2.8. In seven specimens the ratio exceeds 2.0. Only two specimens are classified with the ratio of less than 1.5. This means that specimens tend to be slightly over-strengthened in shear.

LOADING

Cyclic lateral loading tests were performed. At first axial compressive force corresponding to 1.0MPa in the existing column was applied. Lateral loading was carried out until the first yielding of the longitudinal rebars. Prior to the cyclic bending test a direct tension test of rebars was performed to know yielding strain of rebars and the judgment of rebar yielding in the cyclic bending test was that the rebar yields when the measured strain of a longitudinal

Table 3 Results of measurements

specimen No.	Comp. strength(MPa) existing	jacket	yielding Disp. (mm)	yielding load (kN)	Max. load (kN)	ultimate load (kN)	ultimate Disp. (mm)	ductility factor	δ at buckling
C-0	19.9	-	14.2	123	154	131	42.2	3.0	3
C-1	21.9	35.8	6.4	189	288	215	67.5	10.5	9
C-2	20.6	39.9	5.1	151	274	185	69.7	13.7	13
C-3	22.8	30.7	6.6	196	293	240	67.5	10.2	10
C-4	21.3	35.6	7.3	177	275	181	109.7	15.0	9
C-5	24.3	33.5	9.2	235	302	240	78.8	8.6	5
C-6	23.5	35.1	8.8	216	288	221	55.3	6.3	7
C-7	22.8	34.2	9.3	210	316	241	75.9	8.2	7
C-8	23.4	33.9	7.6	192	296	213	81.6	10.7	7
C-9	25.4	35.9	6.8	196	305	204	74.5	10.9	8
C-10	24.2	-	14.7	128	156	147	91.8	6.2	6
C-11	24.2	-	13.4	118	156	126	79.8	6.0	5
C-12	25.5	-	15.5	123	147	130	79.8	5.1	5
C-13	26	-	14.8	115	149	133	78.5	5.3	6
C-14	21.7	30.5	7.7	186	276	213	81.5	10.6	9
C-RC	22.8	30.7	5.3	175	309	192	97.5	18.4	15
C-JC	25.3	-	13.4	175	250	197	128.5	9.6	9
R-0	22.7	27.2	5.0	196	282	207	54.4	9.1	8
R-1	22.1	28.2	3.7	175	275	193	47.7	9.0	9
R-2	22.2	28.6	5.2	205	283	224	59.0	10.7	10

rebar in the cyclic bending test reaches this yielding strain. Loading was further carried out with displacement on the basis of the yield displacement $\delta_y, 2\delta_y, 3\delta_y \cdots\cdots$. The loading was carried out three times at the same displacement until the section failure (generally rupture of the longitudinal rebars). Fig.4 shows the loading pattern used.

LOADING SYSTEM

Specimens were horizontally placed. Longitudinal axial and lateral cyclic loading was carried out using reaction walls. To keep the longitudinal loading stable, a sliding device was used not to produce eccentricity and/or lateral reaction. Fig.5 shows the loading system used.

MEASUREMENTS

Steel strains were measured with strain gauges on longitudinal rebars and ties. Strains of ties were not measured when unbonded prestressing steel ties were post-tensioned. Lateral displacements were measured with transducers at the loading point, the middle of the column and the column foot. Longitudinal displacement at the column foot was also measured to know pull-out of longitudinal rebars from the footing.

RESULTS AND DISCUSSIONS

FAILURE MODE

Table 3 and 4 present results of measurements and brief descriptions of the failure mode of each specimen, respectively. Here the yield displacement means the displacement that the

Table 4 Brief description of failure

S.No.	brief description of failure
C-0	flexural-shear failure at the rebar termination, buckling of longitudinal rebars at the rebar termination without rupture
C-1	flexural failure at the column foot, rupture of the lowest tie, buckling of longitudinal rebars between the first and second ties from the column foot
C-2	flexural failure at the column foot, disconnection of the lowest tie at coupler due to misconnecting, buckling and rupture of longitudinal rebars below the second tie, damage of the top surface of the footing
C-3	flexural failure at column foot, disconnection of the lowest tie due to misconnecting, buckling of longitudinal rebars below the second tie
C-4	flexural failure at the column foot, buckling and rupture of longitudinal rebars below the lowest and between the lowest and the second ties
C-5	flexural failure at the column foot, disconnection of the lowest tie due to misconecting, buckling and rupture of longitudinal rebars below the lowest and between the lowest and the second ties
C-6	flexural failure at the column foot, disconnection of the lowest tie due to misconecting, buckling and rupture of longitudinal rebars below the second tie ,damage at the top surface of the footing
C-7	flexural failure at the column foot, buckling and rupture of longitudinal rebars below the lowest and between the lowest and the second ties
C-8	ditto
C-9	ditto
C-10	flexural failure at the rebar termination, buckling and rupture of longitudinal rebars at the rebar termination
C-11	flexural failure at the rebar termination, buckling of longitudinal rebars at the rebar termination
C-12	ditto
C-13	flexural failure at the rebar termination, buckling and rupture of longitudinal rebars at the rebar termination
C-14	flexural failure at the column foot, buckling and rupture of longitudinal rebars below the lowest and between the lowest and the second ties
C-RC	flexural failure at the column foot, rupture of the lowest tie, buckling and rupture of longitudinal rebars between the lowest and second ties,large cracks and spalling of concrete at the top surface of the footing
C-JC	yielding of longitudinal rebars in existing column prior to anchors' yielding, swelling of steel above brackets, buckling and rupture of longitudinal rebars without buckling of anchors
R-0	flexural failure at the column foot, buckling and rupture of longitudinal rebars below the lowest and between the lowest and the second ties
R-1	flexural failure at the column foot, buckling and rupture of longitudinal rebars below the lowest tie
R-2	ditto

outermost longitudinal rebar is likely to yield, the yielding load is the load at the yield displacement, the ultimate displacement corresponds to the displacement at the yielding load after the maximum loading and the ultimate load means the load at the ultimate displacement.

Fig.6 shows crack patterns and failure modes of several specimens after unloading at the final stage. In specimen C-0 typical X-shape spalling of concrete is observed at the position of the longitudinal rebar termination. This fact indicates that the effect of shear is remarkable. All concrete-jacketed specimens show flexural failure at the column foot without obvious shear cracks at the longitudinal rebar termination.

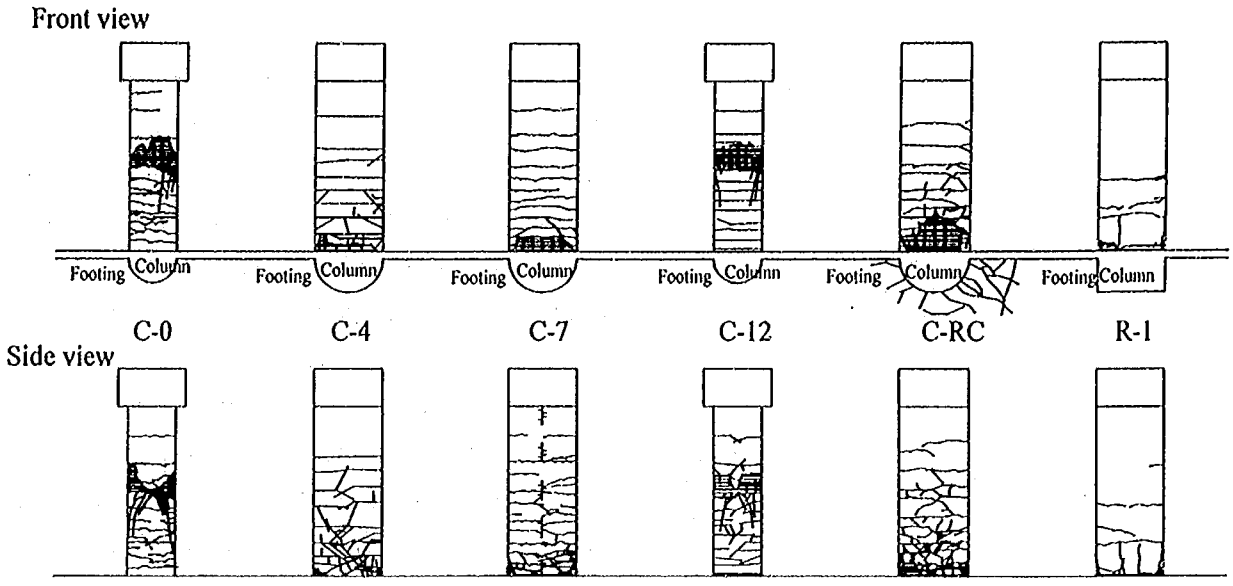


Fig.6 Crack patterns of typical specimens

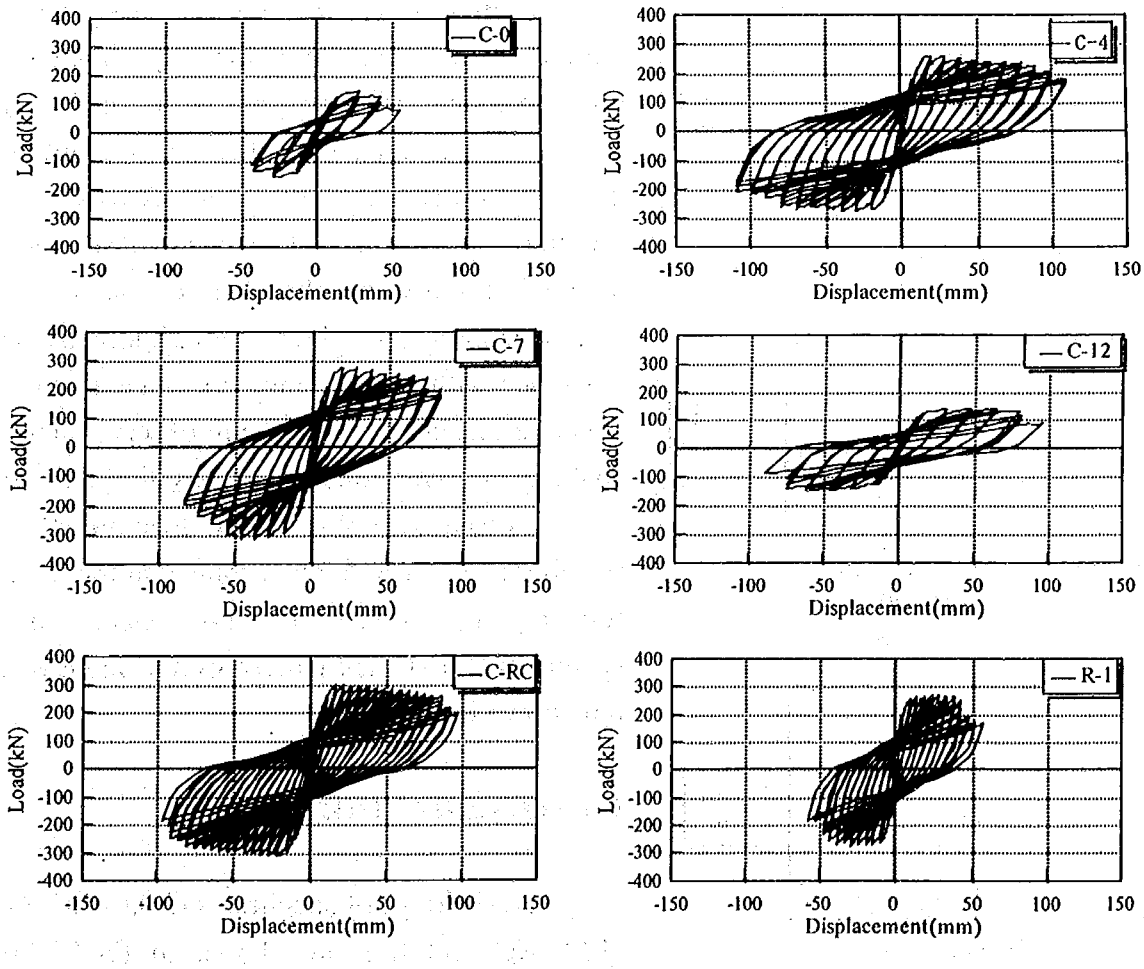


Fig.7 Hysteresis loops

In specimens C-4,C-7 and R-1 with the slit at the column foot and unbonding of longitudinal rebars at the upper region of the footing the plastic hinge is firmly formed at the column

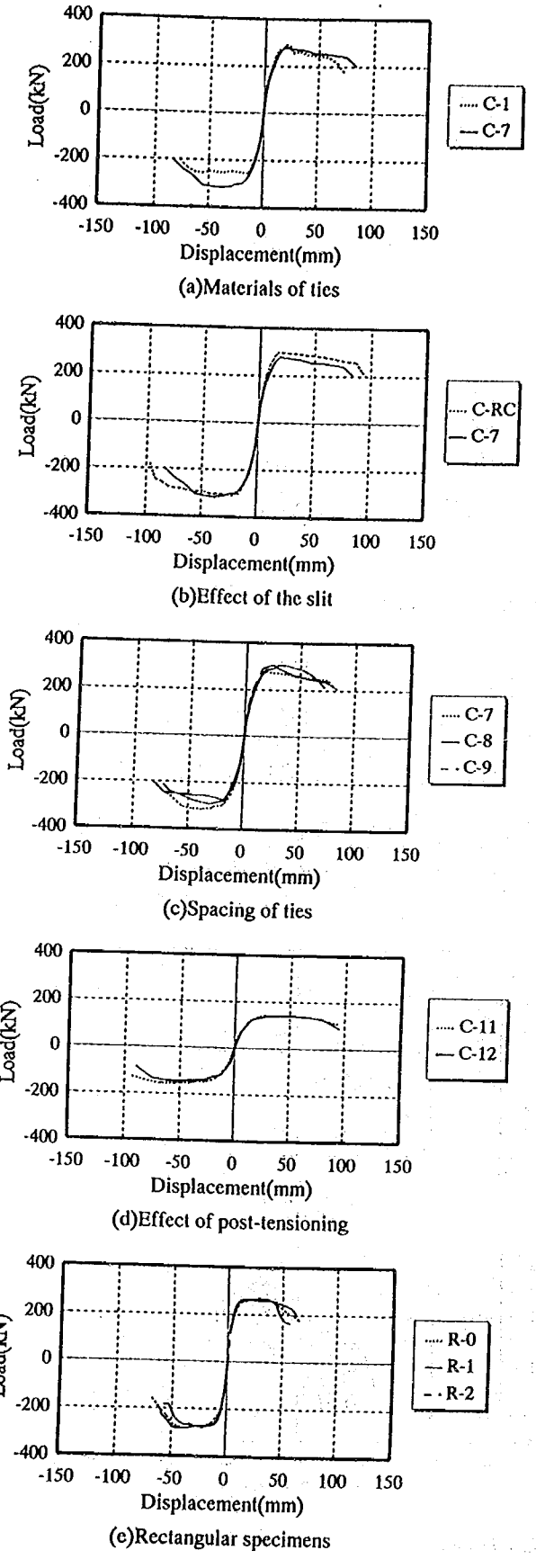


Fig.8 Load-displacement relation

foot, while the top surface of the footing is seriously damaged in specimen C-RC without the slit and unbonding of longitudinal rebars.

In Fig.6 there is obvious difference of damages at the column foot between specimen C-7 with both the slit and unbonding of longitudinal rebars and specimen C-RC without both the slit and unbonding. In specimen C-7 the lowest tie (strand) is not likely to yield.

Specimen C-12, which is directly wound around the existing column model C-0 by strands, shows flexural failure at the rebar termination. Being different from specimen C-0, which showed shear failure at the rebar termination, little effect of shear is observed. That means the ultimate shear strength is improved by winding strands directly around the concrete column without tensioning. Comparing specimen C-10 post-tensioned transversely with prestressing steel ties with specimen C-12, which is not post-tensioned transversely, some differences are observed on shear cracks. Transverse post-tensioning could improve the shear crack behavior.

In specimen R-1, which is longitudinally post-tensioned with prestressing bars embedded in the concrete jacket, less cracks are observed and the spalling of cover concrete is very limited within narrow area at the column foot. Specimen R-2, in which ties are very richly arranged at the column foot region, showed the same phenomena as specimen R-1 (Crack pattern of specimen R-2 is not shown in Fig.6).

HYSTERESIS LOOPS

Hysteresis loops of specimens C-0,C-4,C-7,C-12,C-RC and R-1 are shown in Fig.7. From these figures it is indicated that the strength and ductility of strengthened specimens are improved, comparing with specimen C-0. In

specimen C-12, which is directly wound around existing column model C-0 with strands by manpower without post-tensioning, the ductility is distinguishedly improved without enhancement of flexural strength, comparing with specimen C-0.

Hysteresis loops are slightly different in (+) and (-) region. When (+) region is only considered, followings can be observed. After yielding of longitudinal rebars, the rigidity starts to decrease. At $2 \sim 3\delta_y$(δ_y:the yield displacement) the ultimate strength is reached. After that the load decreases gradually. At $7 \sim 8\delta_y$, when spalling of cover concrete and/or buckling of longitudinal rebars start, sustained load decreases rapidly. Every hysteresis loop shows typical spindleshape. No significant difference can be observed between specimen C-7, in which strand ties are post-tensioned, and other specimens with non-prestressed ties.

LOAD-DISPLACEMENT RELATION

Fig.8 shows several load-displacement relations. In Fig.8(a) it is aimed at to compare the effect of different tie materials between specimen C-1 with rebar ties and specimen C-7 with strand ties. The figure shows that specimen C-7 has slightly better ductility and strength than specimen C-1. In specimen C-1 the lowest tie ruptured and the second tie from the column foot supposedly yielded, while all ties were still in elasticity in specimen C-7. However no significant difference is observed in the load-displacement relation between specimens C-1 and C-7. This could be because yielding of ties and buckling of longitudinal rebars occur almost at the same time.

Fig.8(b) is a figure to observe the effect of the slit (a weak point) at the column foot. Although the slit makes the section decrease at the column foot, the slit hardly influences both ductility and strength. Fig.8(c) shows the effect of tie spacings (10,12 and 18cm). Within this figure tie spacing hardly influences load-displacement relation. This could be caused by oversupplied ductility resulting from too thick concrete jacketing. This also means that the structure ductility depends on the plastic rotational capacity of the plastic hinge formed at the column foot, if RC column is adequately strengthened in shear and flexural failure happens prior to shear failure. Significant difference of tie spacing in load-displacement relation is not observed, because each lowest tie, with which the plastic rotational capacity of the plastic hinge could be largely influenced, has the same conditions. Fig.8(d) is aimed at to know the effect of the transverse post-tensioning of strand ties. No significant difference is observed. This fact means that the transverse post-tensioning of strand ties hardly influences both strength and ductility. Fig.8(e) shows the comparison of load-displacement relation between rectangular cross-section specimens R-0, R-1 and R-2. In specimen R-1 rapid decrease of the strength starts earlier than specimens R-0 and R-2. This could be due to early rupture of longitudinal rebars. Since the spalling of the cover concrete is very narrowly limited in specimen R-1 (refer to Fig.6), yielding of ties and buckling of longitudinal rebars could not be well observed. The reason of the early rupture of longitudinal rebars is now under investigation. Although tie spacing of specimens R-0 and R-2 is different, no significant difference is observed

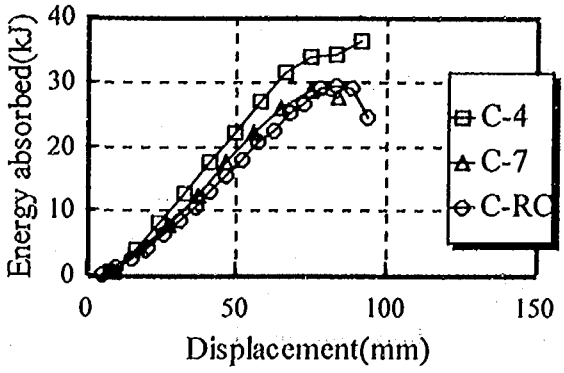
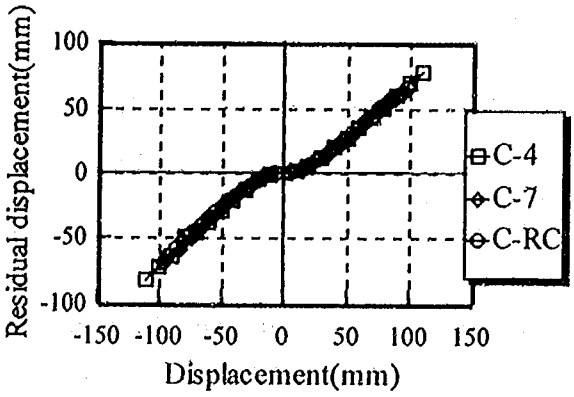


Fig.9 Energy absorption



(a) Circular specimens

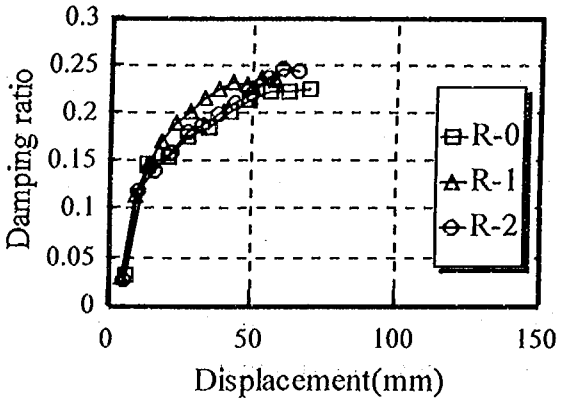
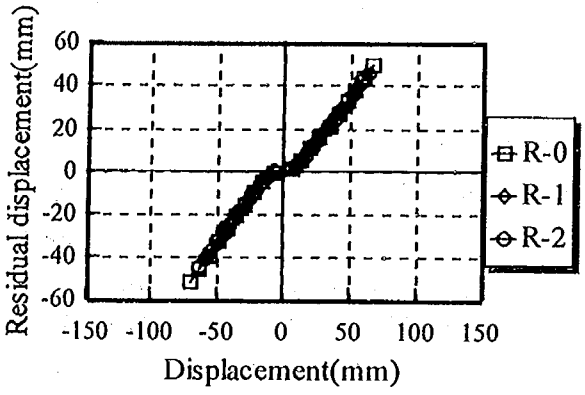


Fig.10 Equivalent damping ratio



(b) Rectangular specimens

Fig.11 Residual displacement at each hysteresis loop

in load-displacement relation. This is because the lowest tie, which influences the plastic rotational capacity of the plastic hinge, neither yield nor rupture and the structure ductility is governed by the plastic rotational capacity of the plastic hinge.

ENERGY ABSORPTION CAPACITY

Fig.9 shows the amount of energy absorbed during one loading cycle in specimens C-4,C-7 and C-RC, which are calculated from the area of the hysteresis loop[5]. This figure shows that the amount of energy absorbed of specimens C-7 and C-RC is similar, although the damage patterns are different at the column foot (in the spalling region of cover concrete). It is considered that the slit and/or post-tensioning strand-ties with high yield strength has little influence upon the amount of energy absorption.

Fig.10 shows the effective damping ratio. The effective damping ratio is obtained from the following equation[5];

$$h_e = \frac{1}{2\pi}\frac{\Delta W}{W}$$

where ΔW and W are the amount of elastic input energy and the amount of energy absorbed, respectively. Damages in specimens R-1 and R-2 are very limited at the column foot,

comparing with specimen R-0. No significant difference, however, of the effective damping ratio is observed in Fig.10. Post-tensioning longitudinal prestressing bars in the concrete jacket and very richly placed ties at the column foot region cause no problem on both the amount of energy absorption and the effective damping ratio.

RESIDUAL DISPLACEMENT

Fig.11 shows residual displacements at each loading cycle. Fig.11(a) is for some of circular specimens and Fig.11(b) for some rectangular specimens. From Fig.11(a) there is almost no effects of both tie materials and providing the slit at the column foot on the residual displacement . Longitudinal post-tensioning in the concrete jacket and rich ties at the column foot region are not useful for improving the residual displacement.

CONCLUSIONS

Cyclic loading tests were carried out to investigate the effect of retrofitting RC bridge columns, which have longitudinal rebars terminated at the middle of the column and are strengthened with concrete jacketing and/or prestressing steel ties. Consequently following conclusions are drawn:

(1) The structural ductility of RC bridge column depends on the plastic rotational capacity of the plastic hinge, when flexural failure occurs prior to shear failure.

(2) Since the plastic rotational capacity of the plastic hinge depends on the strength and spacing of transverse reinforcements, it is expected useful to use prestressing tendons with high yield strength as transverse reinforcements.

(3) Planned plastic hinge by providing a thin slit at the column foot hardly influences strength, ductility, amount of energy absorbed and residual displacement, though the section is decreased at the column foot.

(4) In case of providing the slit at the column foot and unbonding of longitudinal rebars at the upper region of the footing, the plastic hinge is surely formed at the column foot and it is possible to control the plastic rotational capacity of the plastic hinge.

(5) Post-tensioned strand-ties of the circular column improve shear crack behavior but hardly influence strength, ductility, energy absorption and residual displacement.

(6) Both post-tensioned prestressing bars, which are placed longitudinally in the concrete jacket and are not placed through the footing, and very richly placed ties in the plastic hinge region cause no degradation of energy absorption but hardly reduce residual displacement.

REFERENCES

1)Japan Road Association:Reference for Applying the Guide Specifications for Reconstruction and Repair of Highway Bridges which suffered Damage due to Hyogo-ken Nanbu Earthquake 1995, June 1995

2)Metropolitan Expressway Public Corporation:Seismic Retrofitting Design Manual for Existing RC Columns (Draft), November,1995

3)Kawashima,Unjyo,Iida:Seismic Inspection and Seismic Strengthening Methods of Reinforced Concrete Bridge Piers at Mid-Height where Main Reinforcements are Terminated with Inadequate Anchorage Length,Report of PWRI,Vol.189.Sep.1993

4)Japan Road Association:Design Specification of Highway Bridges,"Part IV Concrete Bridges",Feb.1990

5)Kawashima,Hasegawa,Nagashima,Oyama,Yoshida:Seismic Design Method of Reinforced Concrete Bridge Piers based on Dynamic Strength and Ductility,Report of PWRI,Vol.190,Sept.1993

Session 5

Retrofit Methods for RC Columns 2

(Co-Chairs: Y. Adachi, P. Clark)

"Development of Base Isolation System of Existing Bridges"
by Y. Hishiki, T. Takeda, H. Nagumo, T. Ichinomiya, Y. Okimi
Presented by: Hiroyuki Nagumo

"An Experimental Study on Ductility of RC Pier Models Winded with FRP Tape"
by H. Mikami, M. Sato, H. Konno, N. Kishi
Presented by: Hiroshi Mikami

"Seismic Retrofit of Bridge Columns using Prefabricated Composite Jackets"
by Y. Xiao
Presented by: Yan Xiao

"Seismic Retrofit of Reinforced Concrete Bridge Piers by Carbon Fiber Sheet"
by M. Hosotani, K. Kawashima, J. Hoshikuma
Presented by: Manabu Hosotani

"Experimental Study Concerning Retrofit of RC Column by CFRP Sheet"
by F. Hakamada, J. Maekawa, J. Hoshikuma
Presented by: Fumio Hakamada

Development of Base Isolation System for Existing Bridges

Yoshihiro Hishiki, Tetsuo Takeda,
Hiroyuki Nagumo, Toshimichi Ichinomiya,
Yoshihide Okimi

ABSTRACT

Base isolation is one of the effective systems for providing earthquake resistance to structures, since it can reduce to a great extent a structural response to earthquakes. However, base isolation systems applied to existing road bridges cannot exhibit their full capabilities during an earthquake because the narrow space between girders of the bridge limits the movement of girders along longitudinal direction. Replacing bridge bearings is thought to be difficult since it requires extensive chipping of piers and girders, and causes lengthy traffic jams on the bridge. A recently developed base isolation system solves all these problems.

The system is verified through performing three-dimensional shaking table test. The experimental results demonstrate that the acceleration of girder could be reduced to one third compared with the case without base-isolation. It is also confirmed that the relative displacement between pier and girder in a miner earthquake was 5mm. Analysis can simulate the experimental results by modeling the system into a bilinear spring. Furthermore it is showed with non-linear dynamic analysis that the model bridge, which was damaged due to Hyogo-Ken Nanbu Earthquake, can secure the aseismic safety for the earthquake by applying the system.

Installation method for this system is described at the last part.

INTRODUCTION

Applications of seismic retrofitting are now undertaken in Japan after the Hyogo-Ken Nanbu Earthquake. One method is reinforced concrete cover , and the other method is steel jacketing. However, if piers are located in a river, or under the bridge used for commercial purposes, these methods are complicated. Because higher obstruction ratio of the river is caused and business establishments must be closed by the works. In such cases, installation of a base isolation system is recommendable, because without touching the piers, a base isolation system can reduce the seismic responses.

However, applying conventional base isolation systems to existing road bridges is expected to be difficult. The narrow space between bridge girders prevents the base isolation system from producing sufficient effect, since it can lead to the breakage of expansion devices or collision with girders. Moreover, replacing existing bearings with base isolation bearings is itself a very tough work to execute since it involves extensive chipping of the top of piers and the lower slabs of main girders, and requires a special attention to the traffic jams on the bridge during replacement work. A new base isolation system is herein developed which can eliminate these problems.

This paper outlines the new system and its abilities, as well as installation method for this system when applied to existing bridges.

OUTLINE OF NEW BASE ISOLATION SYSTEM

In this section, the outlines of the system is described.

Structural Features

The base isolation devices used in this system are sliding bearings and horizontal force dampers (see Fig.1). The new system differs from conventional base isolation systems which use rubber base isolation bearings. It remarkably reduces the seismic forces and girder displacement through dual damping effects: frictional damping by sliding bearings, and hysteresis damping by horizontal force dampers.

The sliding bearings are produced by improving the existing bearings (of steel or rubber) such that they can bear the weight of bridge girders and at the same time to accommodate displacement(of longitudinal or transverse, or two directions) due to base isolation in an earthquake.

A horizontal force damper is made of high damping rubber or laminated rubber containing lead plugs, which are known to be effective materials for base isolation bearings. The damper bears no weight of the bridge girders and thus is not regarded as a simple bearing. This frees the damper from the possibility of buckling, overturning due to vertical force when the girders undergo large displacement. Therefore it allows greater design freedom than conventional base isolation bearing. Also, the potential for decreasing the number of lamination layers in the damper offers the prospect of cost reduction.

The bridges equipped with a conventional base-isolation bearing would move with large displacement, so that there is a danger of breakage of expansion devices and collision with girders even in a minor earthquake that may occur several times in their lifetimes. At restoration work of highway bridge damaged by Hyogo-Ken Nanbu Earthquake, the end of bridge girder which was applied the conventional base isolation bearings was cut off in order to secure the longitudinal space of girders. Its space is 0.15m which was designed by the seismic coefficient method[1)] corresponded to a minor earthquake.

In contrast, the new system restricts displacement in the earthquake to a narrow range. For example, the relative displacement between girder and pier, of a RC bridge with span of 20m and width of 10m, is 5mm. It eliminates the potential breakage of expansion devices and collision with the next girder, and allows base-isolationing the bridges even to the transverse direction.

Installation Features

The modification of existing bearings into sliding ones hardly requires chipping work on piers and girders due to replace anchor bolts or for other purposes. The use of brackets fixed to pier to support the horizontal force dampers permits their easy installation without any restrictions of workability. These features eliminate the need to jack up the girders and also eliminate almost all need to stop traffic on the bridge. Detail is described in the part of "INSTALLATION"

BASIC CHARACTERISTICS OF NEW SYSTEM

To know the basic characteristics of the present system, a shaking table test was conducted by using actual seismic waves as input motion.

The Model

Relation between Model and Real Bridge; The model used in the test is a scaled model of a typical elevated road bridge, as shown in Fig. 2. Table 1 shows the dimensions of the model bridge, and Fig. 3 shows the detailed dimensions of the model.

Table-1 Outline of the model bridge

Width	11m(2 lanes)
Span	20m(1 span in simple supported bridge)
Load on 1 bearing	1000kN(4bearings per bridge pier)
Ground	$0.2 \leqq TG \leqq 0.6$ (seconds) TG: natural period of ground
Natural Period	0.4 seconds(without base isolation)

The explanations of the components of specimen are described below.

a. Bridge girder : The painted part in gray in Fig.3 represents it. It weighs 245kN and is borne by 4 sliding bearings.
b. Sliding bearing : It consists of plates of Teflon and stainless steel and bears the same stress for real bridge's bearing.
c. Horizontal force damper : It makes of high damping rubber. The specimen has two horizontal force dampers. According to Base-Isolation Design Manual for Highway Bridges[2], it is designed to have natural period of 0.7 seconds at level 1 earthquake and 1.0~1.2 seconds at level 2 earthquake without friction of bearing. Herein, level 1 earthquake is a miner one that may occur several times in their lifetime and corresponds to the seismic coefficient method specified in the Specification for Highway Bridges(part V : seismic design)[1]. Level 2 earthquake is a disastrous one that may occur one time or may not occur in their lifetime and corresponds to the method of ultimate horizontal strength during an earthquake specified in the Specification[1] described above.
d. Pier : The laminated rubber pad and upper beam in Fig.3 represent it. The rigidity of the pad is determined to have a natural period of 0.4 seconds when the specimen is not base-isolated.

Similarity Law; The shaking table has a ability for simultaneous vibration at three-dimension (horizontal two directions :19.6m/s^2, vertical direction:9.8m/s^2) if a specimen weighs within 300kN. Since assumed real elevated road bridge weighs about 4000kN, a scaled model must be used in the test. However, if the specimen can be assumed to have been divided the real bridge (including bearings and base isolation devices and pier) into equal portions so that each section can reach about 300kN, which is the maximum weight that the shaking table can support, and to take one part as the specimen, the acceleration and displacement observed at the equally-divided bridge can be regarded as having been observed in a real bridge and the experimental results will be evaluated without the similarity low. Therefore, the specimen was determined to weigh 245 kN, which is 1/16 the weight of the real bridge.

Outline of the Test

Test Cases; Prior to the test of the new system, a preparatory test

was conducted to understand the dynamic characteristics of a specimen without base isolation for the purpose of comparison. In the test of the model without base isolation, the frames were braced such that there would be no relative displacement between the mass and the pier of the specimen.

In the test of the base isolated specimen it was possible to reduce the number of steel plates in the rubber pads comprising the horizontal force damper because no vertical force would act on the damper. Therefore, the model was tested with each of two different dampers. One had 7 layers of rubber lamination, the same type as a conventional base isolation device in Japan, and the other had 3 layers of rubber lamination.

Input Waves; The input waves for each case of the test are presented in Table 2. The level 1 wave was calculated by the seismic coefficient method [1]. It is a seismic wave obtained by adjusting the acceleration of an original wave such that the response acceleration of a specimen which has a natural period of 0.4 seconds becomes about 2.0m/s^2 to 3.0m/s^2 in the acceleration response spectrum for a damping factor of 5%. The maximum acceleration of the input seismic wave was 1.0m/s^2.

The level 2 wave in the table was calculated by the method of ultimate horizontal strength during an earthquake[1]. It is a seismic wave obtained by adjusting the acceleration of an original wave such that the response acceleration of a specimen which has a natural period of 0.4 seconds becomes about 10.0m/s^2 in the acceleration response spectrum for a damping factor of 5%. The maximum acceleration of the input seismic wave was 4.0m/s^2.

Table-2 Input waves in the tests

	without base isolation	with this system
Level 1	Kushiro Kobe	Kushiro Kobe
Level 2	Kushiro Kobe	Kushiro Kobe
Original	– –	Kushiro Kobe*

Kushiro: Seismic wave recorded at JMA Kushiro Station at Kushiro oki Earthquake in 1993

Kobe: Seismic wave recorded at JMA Kobe Station at Hyogo-ken nanbu Earthquake in 1995

*) Note: Before being input, the seismic waves were adjusted such that maximum acceleration would be 7.0m/s^2.

Test Results

Comparison of Time History Response; Fig. 4 and 5 show comparisons of time history responses of mass acceleration for the model without base isolation and the model with base isolation. Since no difference in dynamic characteristic was observed between the specimens with different laminations, only test results for the 3 layer case are shown.

For both cases of input level 1 and 2, girder acceleration and pier displacement were reduced by base isolation. The degree of reduction was greater for level 2 input. This demonstrates the effectiveness of hysteresis damping by the horizontal force dampers.

Effect of Base Isolation; The maximum acceleration responses of the mass (girder) and the maximum response displacements of laminated rubber pad (pier) are shown in Tables 3 and 4 respectively. The ratios shown in tables indicate that this system reduces acceleration and displacement to one-half or one-third as compared with the case without base isolation.

Table-3 Maximum acceleration of girder

Input waves		A: without base isolation	B: with this system	B/A
Level 1	Kushiro	4.7	2.0	0.43
	Kobe	3.9	1.8	0.46
Level 2	Kushiro	14.0	3.7	0.26
	Kobe	12.6	4.8	0.38
Original	Kushiro	29.0	5.3	0.18
	Kobe	18.7	10.3	0.55

unit: m/s^2

Table-4 Maximum deformation of pier

Input waves		A: without base isolation	B: with this system	B/A
Level 1	Kushiro	19	7	0.36
	Kobe	16	7	0.41
Level 2	Kushiro	63	13	0.20
	Kobe	57	16	0.28

unit: mm

Table 5 shows the displacement of the horizontal force damper (displacement of the girder relative to the pier). Displacement caused by level 1 input waves was less than 5 mm. This small displacement clearly indicates the effect of reducing displacement, which is an excellent feature of this new system.

Table-5 Displacement of horizontal force damper

Input waves		Displacement
Level 1	Kushiro	5
	Kobe	4
Level 2	Kushiro	35
	Kobe	57
Original	Kushiro	91
	Kobe	184

unit: mm

Simulation Analysis

Analytical Model; The non-linear time history response analysis is done to simulate the results of the shaking table test. The analytical model employed is illustrated in Fig.6.This model is two mass points system with two degrees of freedom. Mass point 1 represents the mass of the part of the specimen above the sliding bearing, and mass point 2 corresponds to the mass of the specimen below the sliding bearing.

The horizontal force damper is modeled by a non-linear spring that has a bilinear hysteresis characteristic (see Fig. 7).The hysteresis characteristic of the horizontal force damper made with high damping rubber was determined according to Base-Isolation Design Manual for Highway Bridge[2]. The shearing displacement of the rubber must be known in order to calculate the hysteresis characteristic of the high damping rubber. This analysis used the maximum shearing displacement obtained in the shaking table test. The sliding bearing was assumed to have a friction coefficient of 0.15 and is represented by a rigid plasticity model with a rectangular displacement-load relation (see Fig.8).

In the dynamic characteristic test of the model without base isolation, it was acquired that the natural period of the laminated rubber pad representing the pier was 0.4 seconds and its damping factor was 0.03. Therefore the pier is modeled by a linear spring causing a natural period of 0.4 seconds and a dashpot with a damping ratio of 0.03. The reason for using a linear spring and a dashpot to represent the laminated rubber pad is that the rubber pad, made of natural rubber, is thought to have almost no amplitude dependency.

Analysis cases are the same as for the test ones previously described.

Results of Analysis; Fig.9 shows the response acceleration of mass point 1 (girder) obtained by the non-linear response analysis together with the data from the shaking table test. Since the response values are almost similar for both test cases, only results using Kobe as input waves are shown. This confirms that a model formulated in the manner described above can well simulate the functions of the sliding bearing and the horizontal force damper with sufficient accuracy.

Comparison between New and Conventional Systems; This new base isolation system was compared by analysis with a conventional system in which base isolation rubber bearings are used. The result is shown in Table 6. The analytical model of the conventional system used for this comparison was obtained by removing the non-linear spring representing the sliding bearing from the analytic model of the new system depicted in Fig.6. The level 1 seismic wave obtained by JMA Kushiro station and JMA Kobe station were used as input waves.

Table-6 Comparison between This System and Conventional System

	This System		Conventional System	
Input waves	Kushiro	Kobe	Kushiro	Kobe
Deformation of Pier	9.5mm	9.8mm	8.6mm	8.5mm
Acceleration of Girder	2.4 m/s^2	2.3 m/s^2	2.3 m/s^2	2.2 m/s^2
Displacement of Sliding Bearing	3.8mm	3.0mm	16.6mm	14.2mm

The new system gives a little larger displacement of pier than the conventional system. However, the acceleration values of mass point 1 (girder) were almost identical. This suggests that effects of these two base isolation systems are almost equal. On the other hand, the relative displacement between pier and girder with the new system was as small as 20% of the case with a conventional system. This indicates that the new system reduces the both of the seismic forces and girder displacement in level 1 earthquake. Specially, the friction damping by the sliding bearing is effective in reducing the displacement of girder in level 1 earthquake.

SAFETY VERIFICATION OF BRIDGE WITH THE NEW SYSTEM

To verify the aseismic safety of bridge in which the new system is installed, a model bridge is assumed. It is the same bridge which was damaged by the Hyogo-Ken Nanbu Earthquake. It is analyzed by the non-linear time-history analysis.

Analysis Condition

A general view of the model bridge is shown in Fig.10. It consists of RC hollow girder and RC piers. The horizontal force dampers were designed according to the Base Isolation Design Manual for Highway Bridge[2] and were installed on piers P3 and P4 which formerly had fixed bearings. Each of the piers was provided with four single-layer high damping rubber pads of 41 cm x 80 cm x 6 cm. The friction coefficient of the bearing plate was set at 0.15. The analytical model is shown in Fig.11. The seismic wave recorded at the JMA Kobe station(the maximum acceleration:8.18m/s2) was used as input.

Analysis Results

The bending moment-curvature curve at the bottom section of pier P3 in bridge without base isolation is shown in Fig.12, and that for the base-isolated bridge is shown in Fig. 13.

The analysis revealed that though seismic response exceeded the ultimate strength of the bottom section of pier P3 without base isolation, the response was below the yield strength when the bridge was base-isolated. Moreover, the maximum displacement of the main girder relative to the pier was 10 cm. It was within the allowable move displacement of sliding bearing. This proved that the new system could adequately secure the aseismic safety of the model bridge.

INSTALLATION

Installation Procedure

The installation procedures are described below.

a. Scaffolding : Frameworks or a staging vehicles as scaffolds are used for installation of this system.
b. Modification of existing bearings into sliding bearings : The examples of bearing modification are shown in below part.
c. Installation of horizontal force dampers : Installation of horizontal force dampers at the bottom of girder is used for the resin anchors , etc. See Fig. 14.
d. Installation of brackets : Installation of brackets on pier is used for the PC steel bars, resin anchors, etc. See Fig. 14.

Examples of Modification of Bearing

The examples of bearing modification are shown in Fig.15.

a. B.P bearing : It is only necessary to cut away the bearing's side blocks. See Fig.15.
b. Roller bearing : At first the girder is jacked up and temporary supports are provided, the roller bearing is replaced with the sliding bearing and the sliding bearing is welded in place. See Fig.15.

Examples of Installation of Horizontal Force damper

The installation examples of horizontal force damper are shown in Fig.16.

a. Steel Girder : Welding can be used for installation of horizontal force dampers to girder. See Fig.16.
b. Concrete Girder : Horizontal force dampers are installed by widening at the ends of girder cross beams. See Fig.16.

CONCLUSION

The base isolation system is one of the attractive choices for aseismic reinforcement for piers. However , in order to actually implement the base isolation scheme to existing bridges, we have to overcome some technical problems.

A new base isolation system that can be applied to existing bridges introduced in the present investigation. After conducting tests and analysis, it is proved that the present system is a useful tool to reduce the dynamic response during Earthquakes.

The results are described below.

a. In the test ,the acceleration of bridge girder which is modeled from the RC bridge(the span of 20m and the width of 10m) and applied the new system is reduced to one half or one third as compared with the case without-base-isolation.
b. The relative displacement of pier and girder is about 5mm in a miner earthquake. Its magnitude of displacement hardly has a danger of breakage of expansion devices and collision with the next girders.
c. Analytically compared with the conventional system, the relative displacement of pier and girder in a miner earthquake at the new system is one fifth as large as the conventional system's because of hysteresis damping by the horizontal force damper and the frictional damping by sliding bearing.
d. Modeling the hysteresis characteristics of the horizontal force damper and the sliding bearing into respectively the bilinear springs can simulate the experimental results.
e. It is confirmed that the assumed bridge, which was damaged in Hyogo-ken Nanbu Earthquake, has the aseismic safety for the earthquake by applying the new system.

In the future, this system will be actually installed in bridges in Japan, and useful site data will be obtained to improve the present system further.

This development has been carried out through a joint research with Oiles Co. Ltd. and Bridgestone corporation.

REFERECES

1) Japan Road Association: Specification for Highway Bridges (Part V: Seismic Design), February, 1990.

2) Public Works Research Institute, Ministry of Construction: Base-Isolation Design Manual for Highway Bridges (draft), March, 1992.

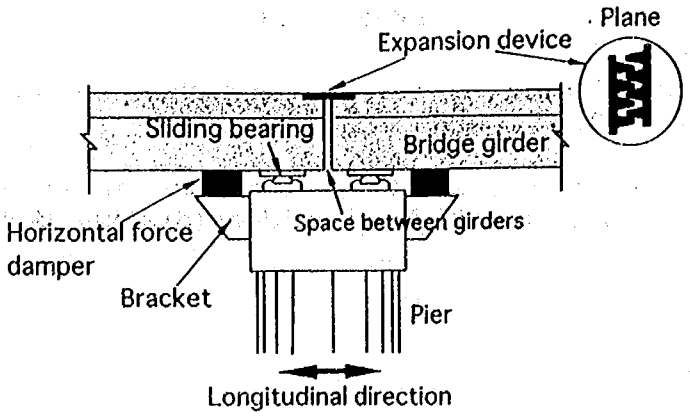


Fig.1 Outline of the new system

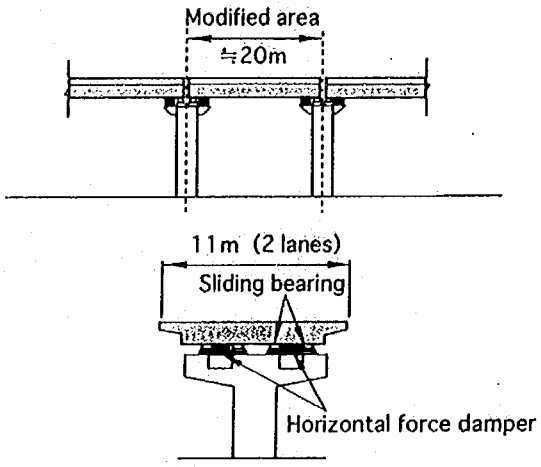


Fig.2 Assumed real elevated road bridge

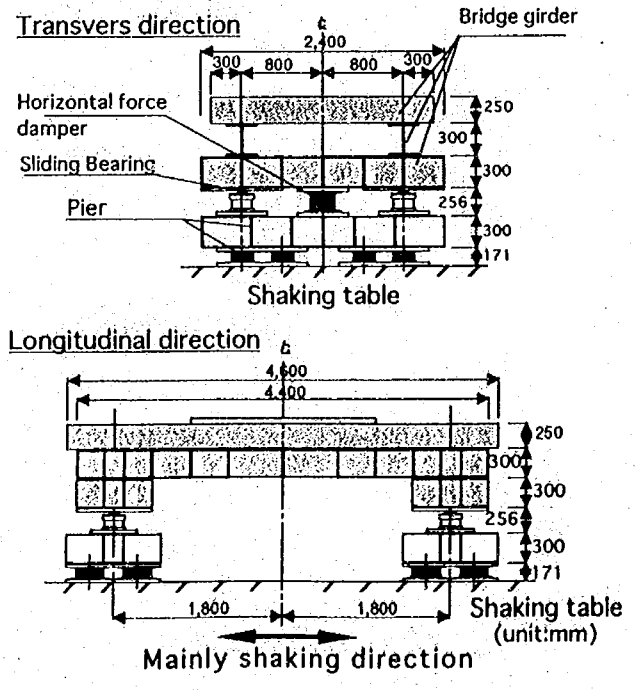
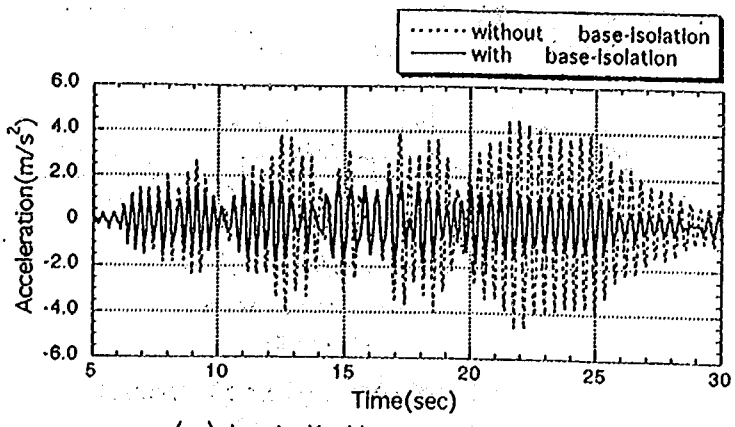
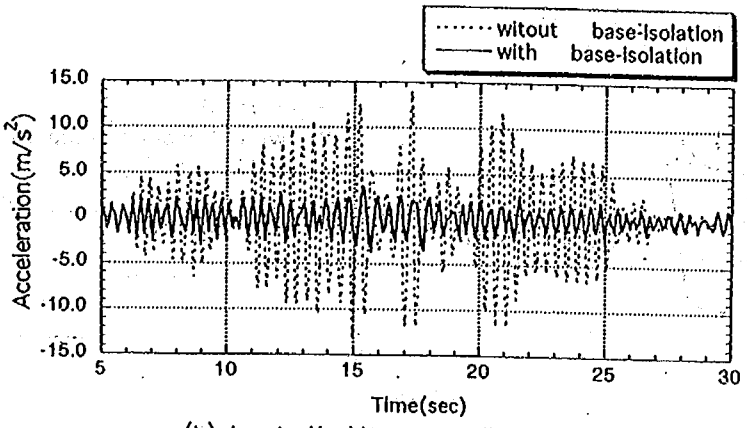


Fig.3 General view of the specimen

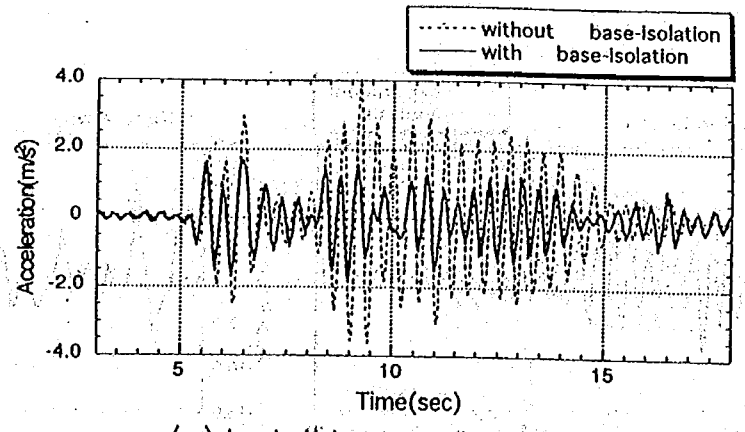


(a) Input : Kushiro wave adjusted to level 1

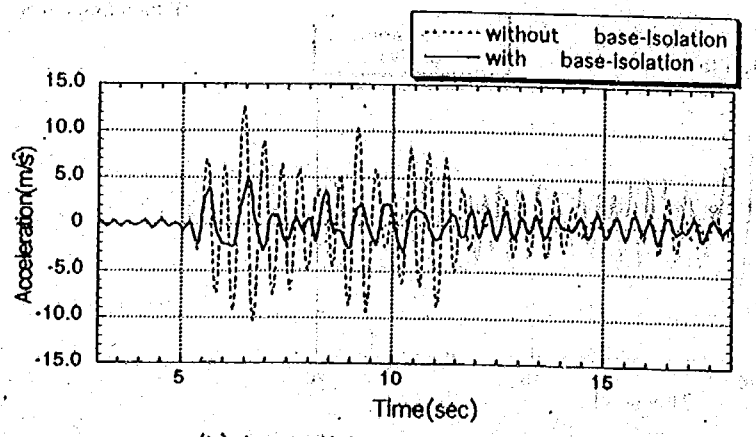


(b) Input : Kushiro wave adjusted to level2

Fig.4 Girder acceleration(input:Kushiro wave)



(a) Input : Kobe wave adjusted to level 1



(b) Input : Kobe wave adjusted to level 2

Fig.5 Girder acceleration(input:Kobe wave)

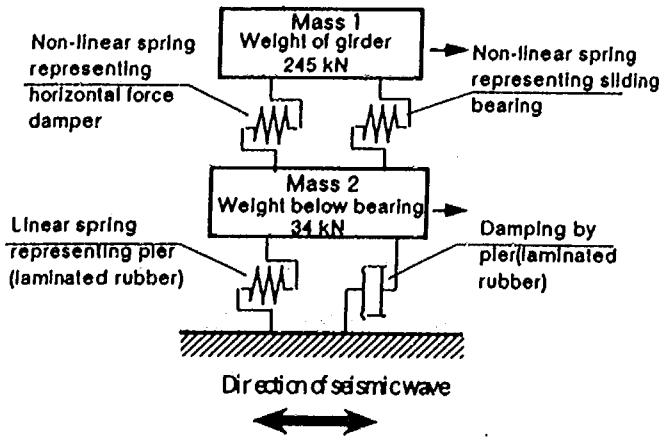


Fig.6 Analytical model

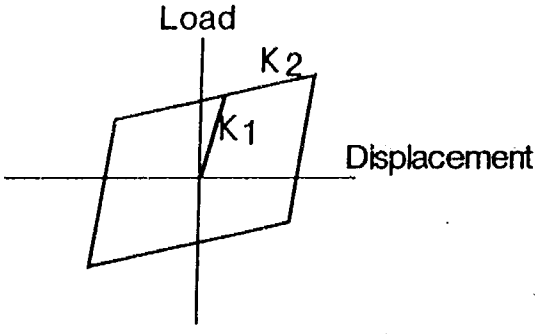


Fig.7 Characteristics of horizontal force damper in analysis

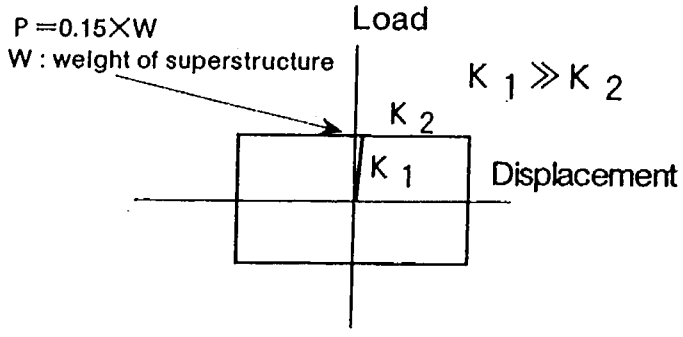
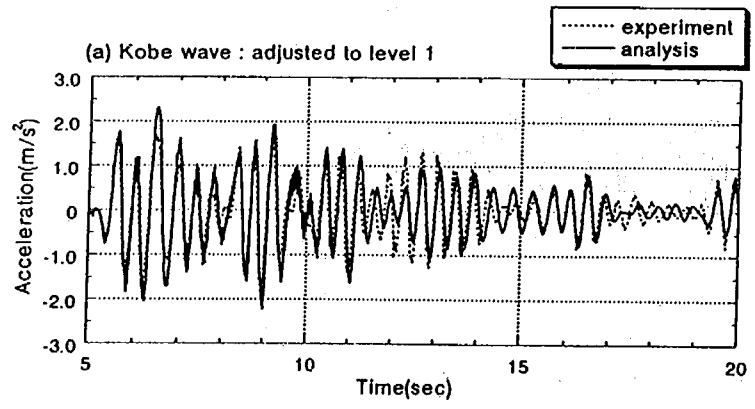
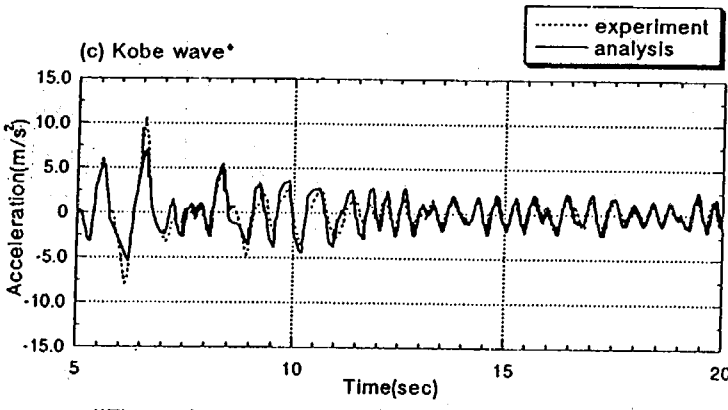


Fig.8 Load-Displacement relation of sliding bearing in analysis





*)The maximum acceleration in input wave is adjusted to 7.0m/s²

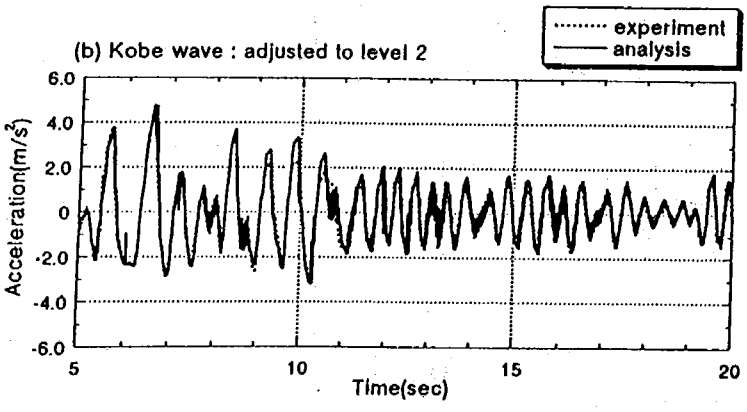


Fig.9 Comparison between girder acceleration of analysis and experiments

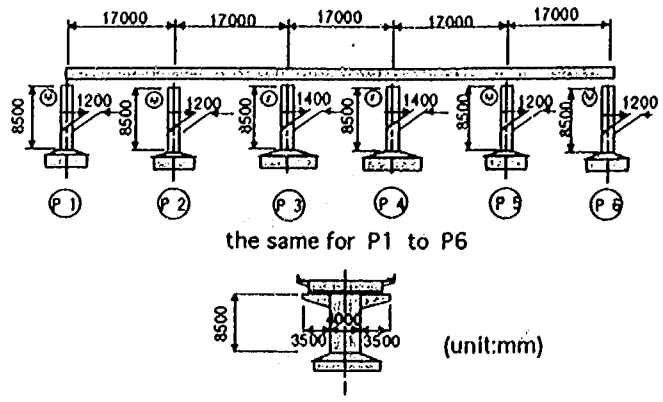


Fig.10 General view of the model bridge

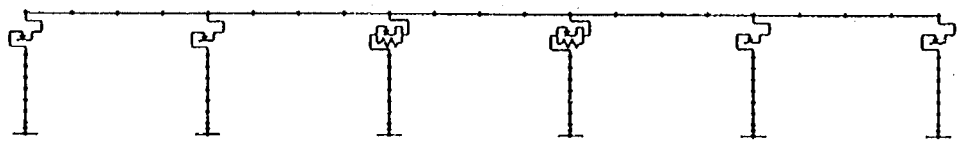


Fig.11 Analytical model of the model bridge

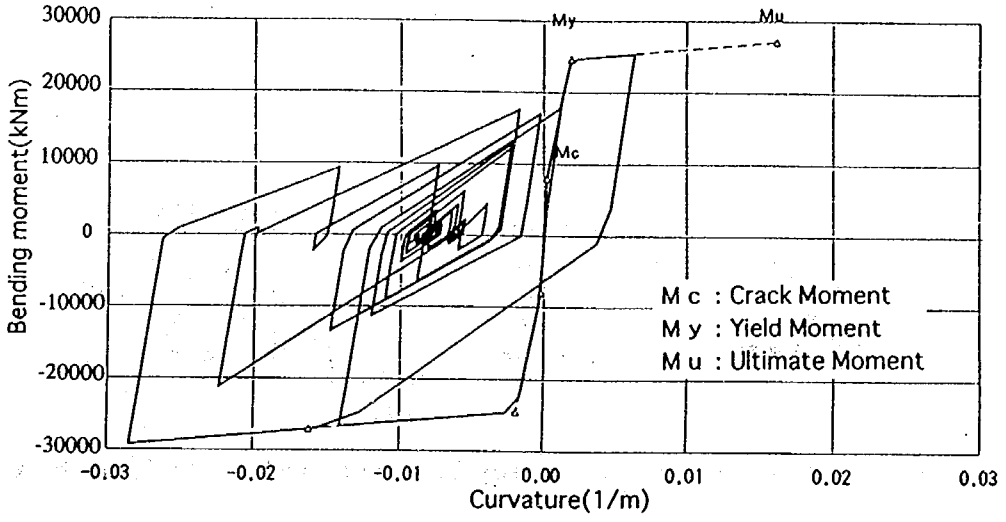


Fig.12 M-ϕ curve for bottom of pier P3 without base-isolation

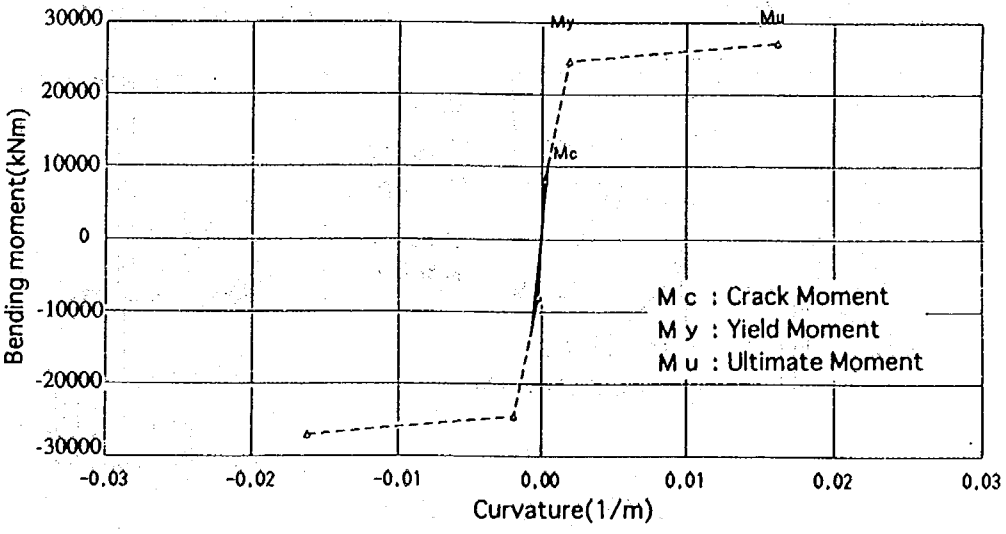


Fig.13 M-ϕ curve for bottom of pier P3 with base-isolation

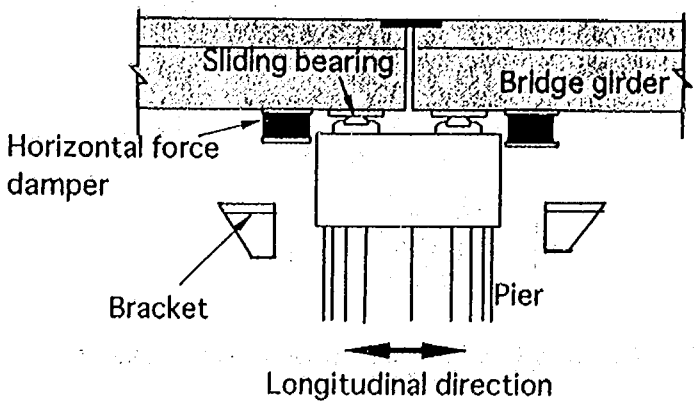


Fig.14 Outline of the installation

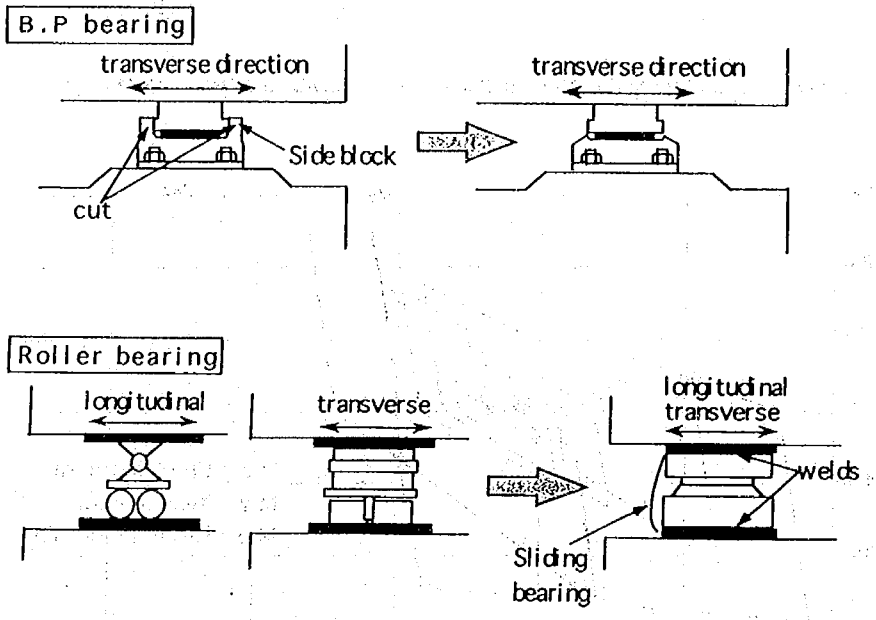


Fig.15 Modification of existing bearing into sliding bearing

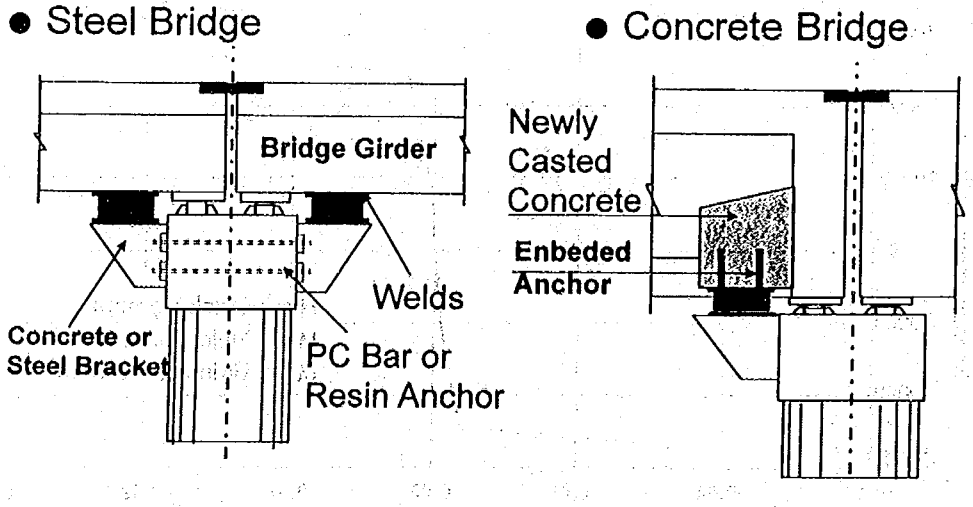


Fig.16 Examples of installation of horizontal force damper

An Experimental Study on Ductility of RC Pier Models Winded with FRP Tape

Hiroshi MIKAMI	Mitsui Construction Co., Ltd.
Masashi SATO	Hokkaido Development Bureau
Hisashi KONNO	Hokkaido Development Bureau
Norimitsu KISHI	Muroran Institute of Technology

ABSTRACT

In this paper, FRP (Fiber Reinforced Plastic) tape winding method was proposed as one of seismic retrofit methods for RC piers. Ductility improvement of RC piers retrofitted with FRP tape winding was experimentally discussed comparing with the results obtained from the cases of both AFRP (Aramid FRP) and CFRP (Carbon FRP) tape winding and case of no winding.

Lateral alternative loading test was conducted by using 1/3rd to 1/5th scales RC pier models, of which rebar arrangement was stepped and a 20 tf weight lead block was set on to mock the weight of superstructure.

From this study, following results were obtained;

1) Ductility near the rebar arrangement stepped was extremely improved by retrofitting with AFRP and/or CFRP tape winding.
2) RC piers retrofitted with AFRP and CFRP tape winding tend to collapse due to rebar buckling and tape rupture at the corners, respectively.

INTRODUCTION

The Hanshin-Awaji great earthquake, occurred in January 1995, destroyed many RC piers accompanying with a brittle failure mode. Since FRP tape and sheet made from Carbon and/or Aramid fiber have high tensile strength and good workability, it may be possible to apply them as one of retrofitting materials for structural members. Particularly, a brittle failure mode of RC pier mentioned above may be prevented by retrofitting them with a winding tape method.

In this paper, an applicability of FRP tape as winding material for retrofitting RC piers was experimentally discussed focusing on the ductility. RC pier models were tested with a lateral alternative loading. Taking the parameters of stepped rebar arrangement, tape winding and tape material, the ductility of RC piers was evaluated

by using characteristics of hysteresis loop between load and displacement, displacement distribution, residual displacement ratio, ultimate plasticity coefficient, equivalent stiffness and equivalent damping coefficient.

EXPERIMENTAL OVERVIEW

Test specimens

Test specimens used in this study are listed in Table 1. In this table, nominal name of RC pier models refers to : 1) the first letter means winding tape material in which N, A and C are for no winding, Aramid and Carbon tape winding, respectively, 2) the second letter means the condition of rebar arrangement, in which -0 and -1/3 stand for fully and stepped arrangement, respectively. In case of -1/3 test specimens, rebar ratio was reduced from 1.9 % to 0.95 % at the 1/3rd of pier height from the basement, in which D13 steel rebars were used. The stirrups were arranged using D10 steel rebar with 10 mm spacing.

Dimensions and rebar arrangement of test specimens are shown in Fig. 1. A 20 tf weight lead block was set onto the top of pier model to mock the weight of superstructure. A footing of pier model was anchored to rigid concrete foundation by using 8 PC steel strands.

Figure 2 shows a set up of FRP tape winding. FRP tapes with 37.5 mm width were winded in 9 steps with an interval of 37.5 mm. The covered area extends from $-B/2$ to $+B$ (B : width of pier model), measured from the point of rebar arrangement stepped.

Table 1. Lists of test specimens.

Specimen	Type of winding	Location of rebar stepping
N-0	Non	Full
N-1/3	Non	$h = H \times 1/3 = 50$ cm
A-1/3	Aramid tape	$h = H \times 1/3 = 50$ cm
C-1/3	Carbon tape	$h = H \times 1/3 = 50$ cm

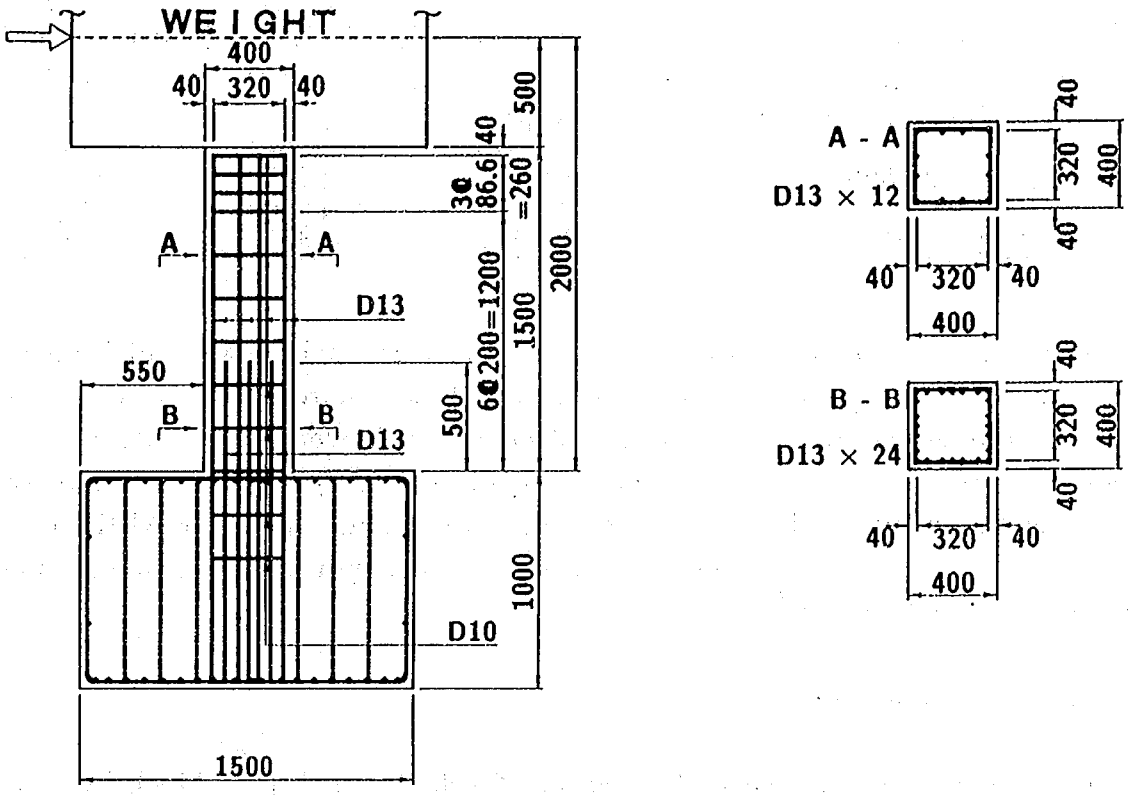


Figure 1. Dimensions of a test specimen and rebar arrangement.

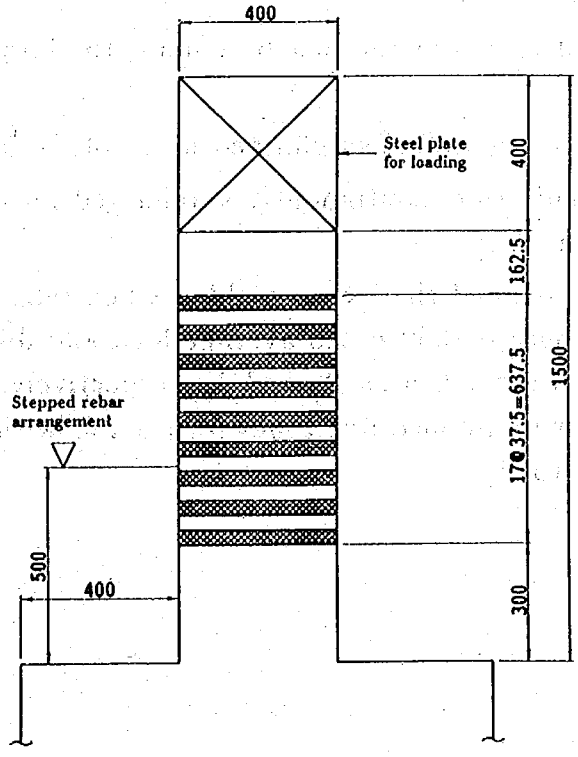


Figure 2. Tape winding set up.

Table 2. Material properties of FRP tape.

FRP tape (37.5 mm in width)	Young's modulus (kgf/mm^2)	Tensile strength (kgf/cm^2)	One layer thickness (mm)	No. of layers	E × A (tf)	Ultimate tensile capacity (tf)
Carbon tape	23,500	50,000	0.165	4	581.6	12.4
Aramid tape	11,100	29,000	0.306	2	254.7	6.7

The interval winding method was applied for the easy maintenance of bridge pier. AFRP and CFRP tapes were winded in 2 and 4 layers, respectively, to be nearly equal of retrofitting volume ratio (0.16 to 0.17 %). However, both of tensile stiffness (Young's modulus, E by cross sectional area of tape, A) and the ultimate tensile capacity for this winded CFRP tapes are bigger than twice those for AFRP tapes as listed in Table 2. An average concrete compressive strength at the commencement of experiment was 260 kgf/cm^2.

Lateral alternative loading

The lateral loads were applied at the center of 100 cm thick lead block by using an alternative pull and push hydraulic jack. In this study, push and pull loadings were named as positive and negative one, respectively. The upper area of pier model was stiffened by steel plate to effectively transfer the load downward. Loading force and displacements at the locations of the loading point and 20, 50, 100 cm high from the pier basement were measured.

In the elastic region of rebars at the pier basement, the lateral alternative loads were surcharged as follows;

1) positive and negative loads were surcharged up to 500 μ of tensile rebar strain.
2) those alternative loads were continuously surcharged for each 1000, 1300 and 1500 μ of the rebar strain.

In this study, it was assumed that rebar yielded when rebar strains at the both sides of pier basement reached to 1500 μ. An average load and displacement in the positive and negative loading were taken as P_y and δ_y, respectively. After the rebar yielding, the alternative loads were applied five times for each δ_y with an increment of δ_y up to the load not reaching to P_y.

EXPERIMENTAL RESULTS AND DISCUSSIONS

Relationships between load and displacement

Figure 3 through 6 show hysteresis loops between lateral load and the displacement at loading point for all test specimens. The result for test specimen N-0 (Fig. 3) shows that the maximum load was 1.3 P_y at 2 δ_y stage. At the 3rd positive loading in 4 δ_y stage, the maximum load was smaller than the value of P_y due to compression failure of concrete at the pier basement.

As for the result of test specimen N-1/3 (Fig. 4), both values of P_y and δ_y were almost the same with results for test specimen N-0. The rebars both at the arrangement stepped and the pier basement yielded at the same loading level. At the 4th

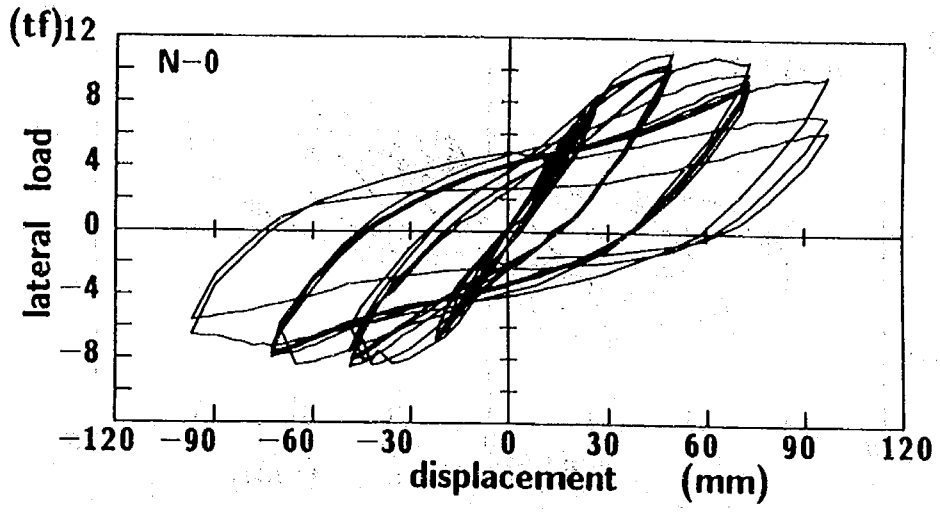


Figure 3. Load-displacement curve for N-0 specimen.

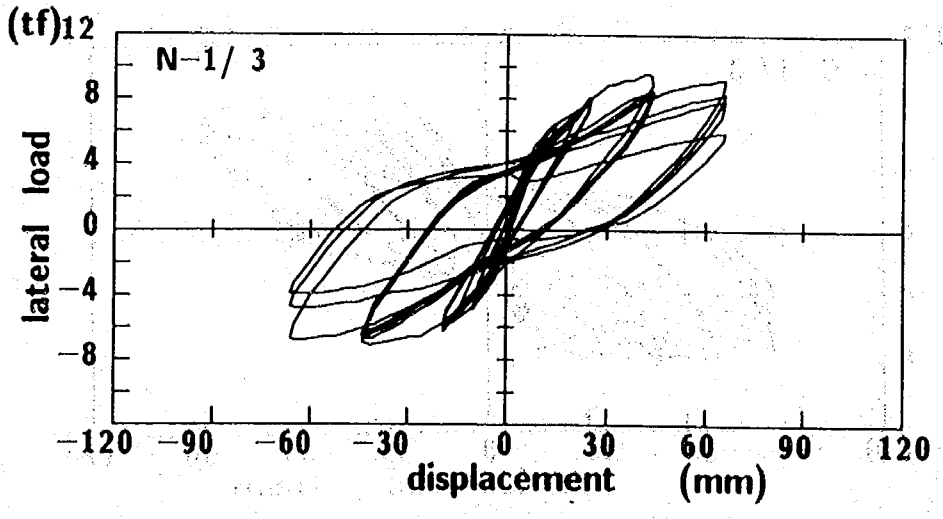


Figure 4. Load-displacement curve for N-1/3 specimen.

positive loading in 3 δ_y stage, the concrete peeled off and rebars buckled at the arrangement stepped. And the load did not reach up to the value of P_y. Since the values of P_u and δ_u for test specimen N-1/3 were smaller than those for test specimen N-0, the energy absorption ability is remarkably decreased by stepped rebar arrangement.

Figure 5 shows that hysteresis loop for test specimen A-1/3 which is stiffened with AFRP tapes winding. In this case, the values of P_y and δ_y were 10 % greater and 15 % smaller than those of test specimen N-1/3, respectively. The final loading was at the 4th positive ones in 5 δ_y stage, of when the exposed concrete between winding tapes was peeled off and the rebars buckled near the arrangement stepped. However, the winded AFRP tapes did not damage at all.

The hysteresis loop for test specimen C-1/3 is shown in Fig. 6. The value of P_y and

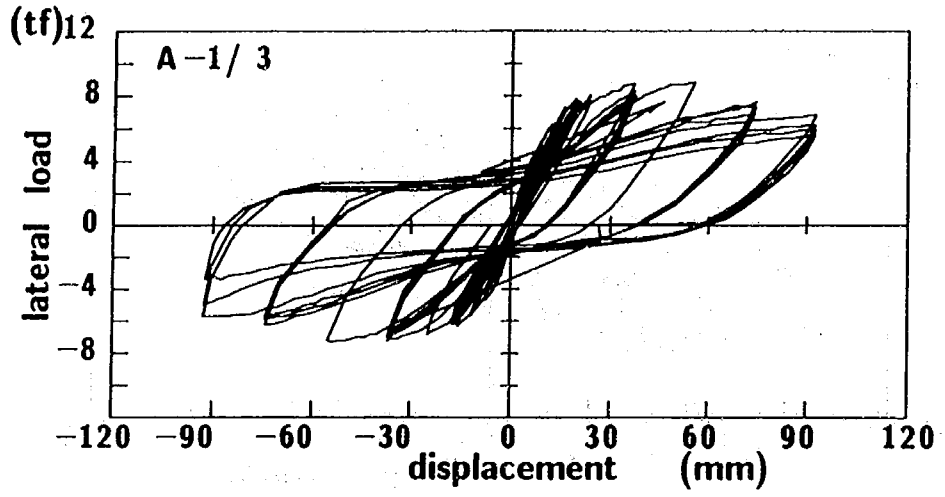


Figure 5. Load-displacement curve for A-1/3 specimens.

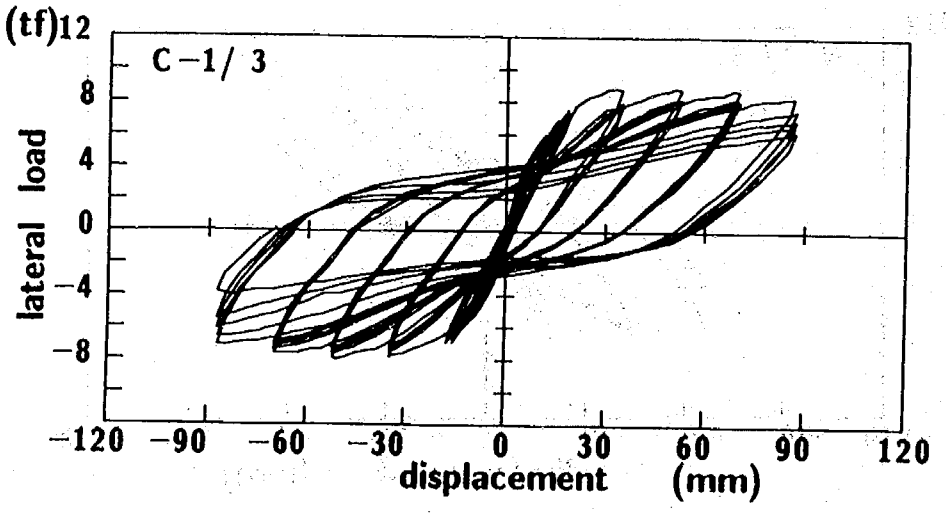


Figure 6. Load-displacement curve for C-1/3 specimens.

δ_y were almost the same with the results for test specimen A-1/3. Although the displacement amplitude was increased, the maximum load for each loading step did not decrease. But, at the final loading stage, pier model was suddenly collapsed with the winding CFRP tapes ruptured at the corners of pier model near the rebar arrangement stepped. Then, these results imply that; 1) since P_u and δ_u of the pier model were reduced by stepping rebar arrangement, the energy absorption ability of pier model with stepped rebar arrangement has smaller than that for fully rebar arrangement one, 2) bending capacity of pier model near the rebar arrangement stepped can not be increased by stiffening the pier with FRP tape winding, 3) but, deformation capacity can be extremely improved, 4) comparing the results of the case using AFRP with the case using Carbon tape winding, loading capacity did not differ so much, 5) in spite of that total tensile stiffness and tensile capacity of winding CFRP tapes are two times bigger than those of AFRP ones, the case of CFRP tape winding collapsed due to tape rupture near the corners.

Figure 7 shows the envelops of the hysteresis loops for -1/3 pier models along with the analytical result for N-1/3 pier model, which is obtained by means of multi-section method. Since the experimental envelop for N-1/3 pier model is distributed in the smallest area in displacement among 3 pier models, N-1/3 pier model must possess the smallest ductility capacity among them. The envelops for both A and C-1/3 pier models are similar and they may possess almost the same ductility. The analytical results on P_y and P_u are similar with the experimental ones. However, the value of δ_u is about 1/5 of test results. This difference may cause from the rebar slipping effect at pier basement, in which 70 % of the value δ_u is generated due to this effect and it was not included in the analysis.

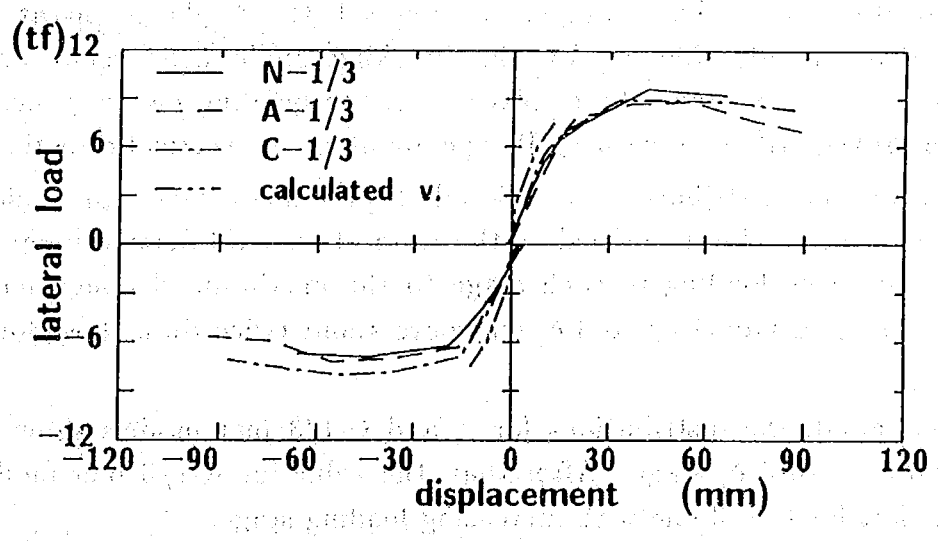


Figure 7. Envelop of load-displacement relationship and theoretical value.

Table 3. List of experimental results.

Specimen	Displacement (mm)		Lateral load (tf)						Ultimate plasticity coefficient, μ_u (δ_u/δ_y)
			P_y			P_u			
	δ_y	δ_u	+ve	−ve	Average	+ve	−ve	Average	
N-0	24.2	96.8	8.2	6.8	7.5	11.0	8.5	9.8	4.0
N-1/3	21.9	65.7	8.0	6.0	7.0	9.2	7.0	8.1	3.0
A-1/3	18.5	90.0	8.9	6.2	7.6	8.8	7.2	8.0	4.9
C-1/3	17.4	90.0	7.5	7.0	7.3	9.0	8.0	8.5	5.2

Ductility capacity

General experimental results are listed in Table 3. In this study, an ultimate plasticity capacity coefficient μ_u was defined as δ_u/δ_y. The table shows that the coefficient μ_u for N-1/3 pier model is the smallest one among all pier models experimented here and the values for retrofitted pier models of A, C-1/3 are bigger than that for N-0 pier model which is reinforced with full rebar arrangement. From these results, it can be shown that the ductility of RC pier with stepped rebar arrangement must be improved by retrofitting winding FRP tapes similarly to its level of RC pier with full rebar arrangement.

Deformation along pier height for -1/3 pier models are shown in Fig. 8, in which the results at the 1st positive loading in each stage were used. The deformation for N-1/3 pier model shows a smooth distribution. Since A and C-1/3 pier models rotated about the location near rebar arrangement stepped, the displacement at top of pier model might be mainly affected by the breaking angle near rebar arrangement stepped. In order to improve the displacement, the bending capacity near the area should be improved stiffening with FRP tape gluing in the vertical direction, etc.

Figure 9 shows the distribution of residual displacement ratio for each -1/3 pier model, in which this value is defined as the ratio of residual displacement at unloading after 1st positive loading in each stage to the maximum displacement δ_u. The values for N-1/3 pier model up to 3 δ_y stage are about twice than those for other pier models.

On the other hand, the distributions for A and C-1/3 pier models show almost the same tendency up to 3 δ_y stage. After that, the value for A-1/3 pier model is found bigger than that for C-1/3 one with increasing loading stage.

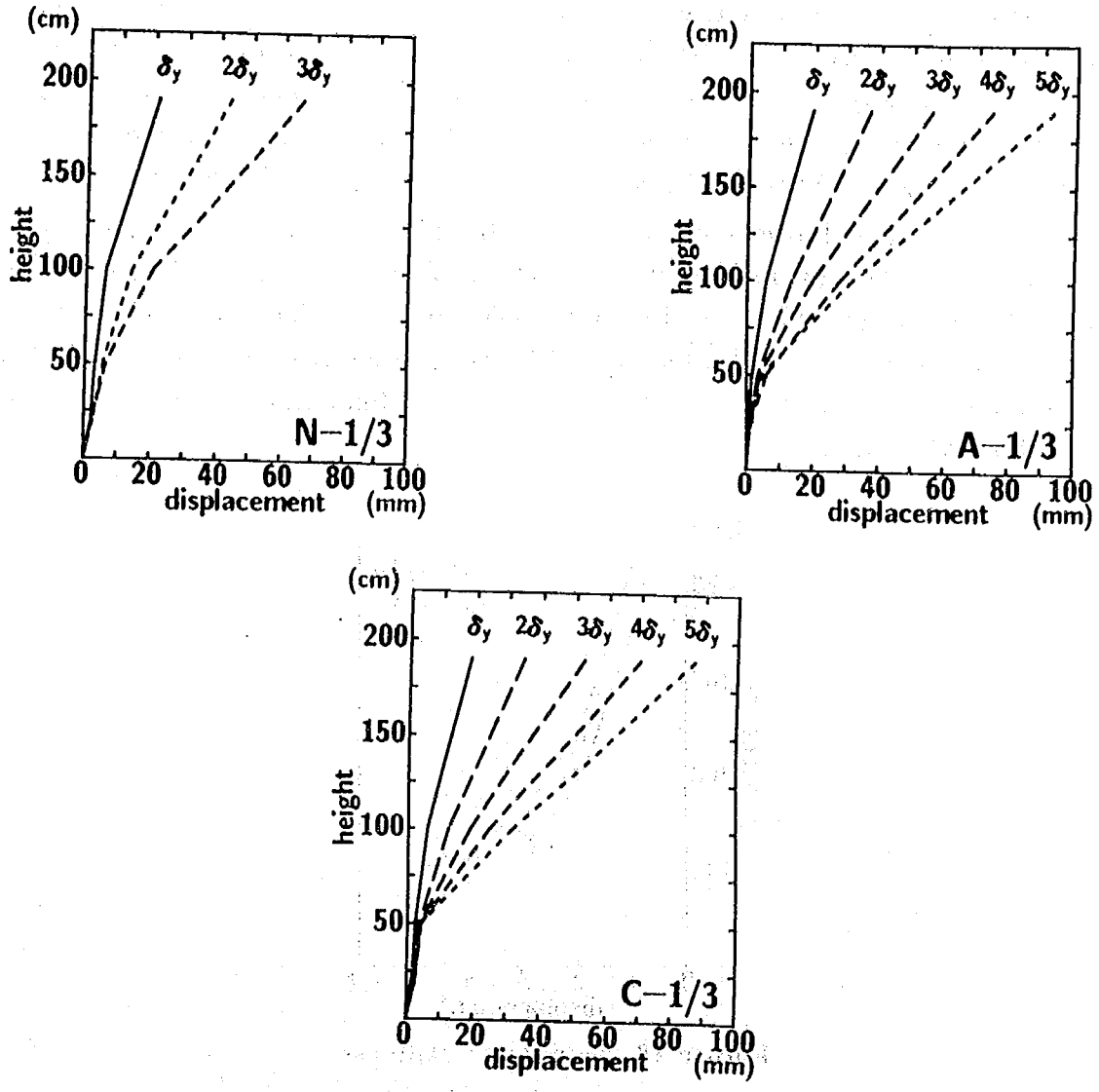


Figure 8. Distribution of pier deformation.

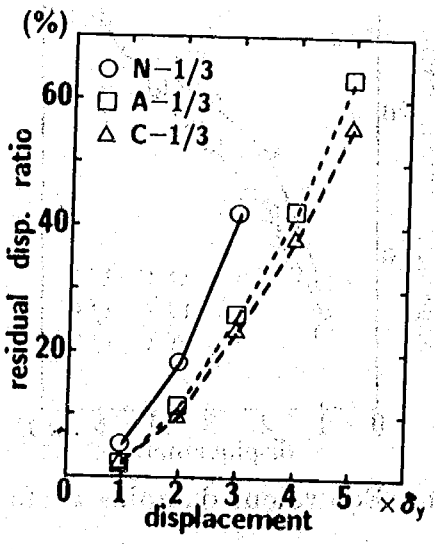


Figure 9. Residual displacement ratio.

Figure 10 shows the distribution of equivalent stiffness for each pier model obtained by using relationship between load and displacement at the 1st positive and negative loadings in each stage[1]. The distributions for all pier models decrease exponentially with increasing loading stage. The values for N-1/3 pier model decrease from 350 tf/m at δ_y stage to 1/3 of this value at the final stage. For A-1/3 pier model, the stiffness at δ_y stage is about 400 tf/m and decreases to 1/6 of this value.

Figure 11 shows distributions of equivalent damping coefficient obtained by using hysteresis loops at the 1st loading in each stage. The gradients for these pier models changed at 2 δ_y stage and after that, remained constant. The coefficients for N, A and C-1/3 pier models are 8 %, 6.5 %, 5.7 % at δ_y stage and 20 %, 26 %, 26.5 % at the final stage, respectively. Then, the coefficients at final stage increase up to $3 \sim 5$ times of those at δ_y stage.

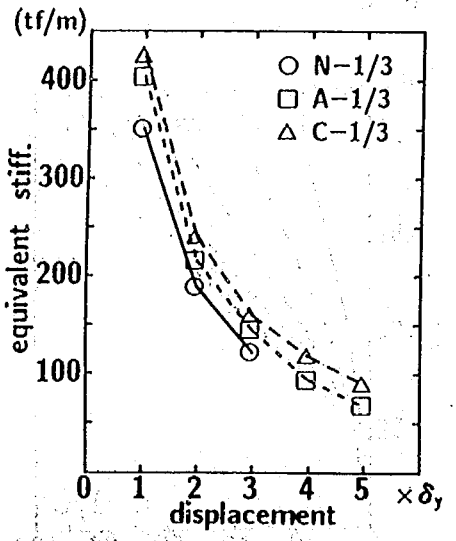


Figure 10. Equivalent stiffness.

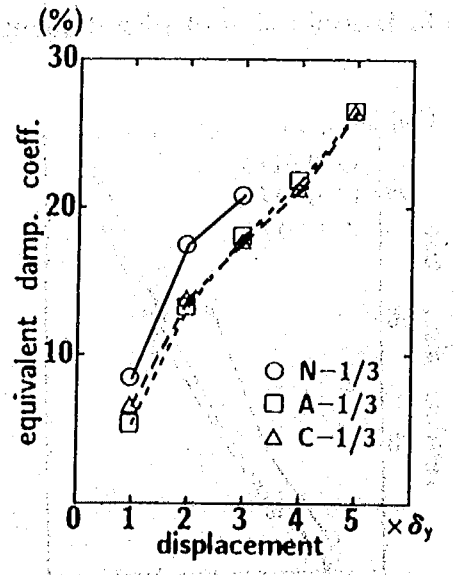


Figure 11. Equivalent damping coefficient.

CONCLUSION

In this paper, proposing FRP (Fiber Reinforced Plastic) tape winding method as one of seismic retrofit methods for RC piers, ductility improvement of RC piers winded with FRP tapes was considered by lateral alternative loading against 1/3rd to 1/5th scale RC pier models. The results obtained from this study are summarized as follows;

1) Since ductility of RC pier is extremely decreased by stepping rebar arrangement, more attention should be paid during design.
2) By retrofitting near the rebar arrangement stepped with FRP tape winding, deformation capacity can be increased and ductility can be remarkably improved.
3) Aramid FRP tape has a good durability. But Carbon FRP tape tend to rapture with brittle failure mode at the corners of RC pier.

Reference

[1] M.Oota: An experimental study on behavior of RC bridge pier subjected to alternative loading, Proc. of JSCE, No. 292, pp. 65 $\sim$ 74, 1979.

1996 U.S.-Japan Workshops on Seismic Retrofitting and
Earthquake Protective Systems for Bridges

SEISMIC RETROFIT OF BRIDGE COLUMNS USING PREFABRICATED COMPOSITE JACKETS

Yan Xiao, Ph.D., PE.
Assistant Professor of Civil Engineering
University of Southern California
Los Angeles, CA 90089-2531

ABSTRACT

This paper describes an on-going multi-phase research program to develop methods for seismic analysis and retrofit design of bridge columns using prefabricated composite jackets. Three 1:2 scale circular columns have been tested and the results established the effectiveness of the prefabricated composite jacketing systems for flexural retrofit of columns with lap-spliced reinforcement. Recent progress of experimental studies on flexural and shear retrofit using prefabricated composite jackets is also briefly introduced.

INTRODUCTION

Several recent destructive earthquakes have indicated that bridges designed and constructed based on older seismic design provisions are vulnerable to catastrophic collapse resulted from the failure of reinforced concrete columns [Priestley, et.al., 1987; EERI, 1990, 1995]. Due to the practice using elastic analyses along with much smaller earthquake forces compared to current design standards, columns in many existing bridges typically have the following potential problems:

i. Undependable flexural capacity due to poor details in longitudinal lap-splices.
ii. Insufficient ductility due to improper transverse confinement.
iii. Insufficient shear strength.
iv. Improper details and insufficient strength in the column/footing and column/superstructure joints.

There is an urgent need to upgrade existing older bridges to current seismic design standards in regions with high seismicity. Steel jacketing has been proved to be an effective measure to retrofit bridge columns for increased strength and ductility [Chai, Priestley and Seible 1991; Priestley, et.al., 1994; Xiao, Priestley and Seible 1996]. Although steel jacketing has been widely used in practices in California and elsewhere, the society is also looking for other alternatives to improve the retrofitting process for the vast number of existing, structurally deficient bridges both in the U.S. and throughout the world. One of the key areas is to ease construction.

Advanced composite materials have been recently recognized and applied to bridge retrofit. The general expectations from composite retrofit systems include light weight, high stiffness or

strength to weight ratios, etc. Several composite jacketing systems have been developed and validated in laboratory or field conditions. Matsuda et.al. [1990] tested a system for bridge pier retrofit using unidirectional carbon fiber sheets wrapped longitudinally and transversely in the potential plastic hinge region or in the region of main bar cut-off. The carbon fiber sheets were bonded to the concrete surface using epoxy resin. Another composite wrapping system using E-glass fiber, which is much more economic than carbon fiber, has been developed by Priestley and Seible [1991, 1993]. Priestley et.al.'s test results on 40% scale bridge piers wrapped with the glass fiber composite jacketing demonstrated significant improvement of seismic performance with increased strength and ductility. Priestley and Seible also developed a full design package for seismic retrofit of existing columns using different retrofit jacketing systems. Saadatmanesh, et.al. [1994] have proposed a wrapping technique using glass fiber composite straps for column retrofit. Most recently, Seible et.al.[1995] have experimentally validated a carbon fiber retrofit system, which utilizes an automated machine to wrap carbon bundles to form a continuous jacket. Successful field construction demonstration is also reported by Seible et.al. [1995].

These composite retrofit measures can be categorized as in-situ fabricated jacketing which involves hand or automated machine placement of epoxy saturated glass or carbon fabrics on the surface of existing concrete. An in-situ fabricated jacket can match the shape of the existing column. However, due to the fact of in-situ fabrication, these systems may need special attention to the job-site quality control and curing of the composite jackets.

Prefabricated composite jacketing systems for retrofitting reinforced concrete columns have been recently investigated at the University of Southern California. These retrofit systems utilizes multi-layer prefabricated E-glass fiber reinforced composite cylindrical shells. The shells are made either continuously like coils or cut into individual single-layer shells with slits. When a column is retrofitted, the shells are opened and clamped around the column. Adhesive is applied to bond the shells to each other and to the column to form a continuous jacket. The slits of the single-layer shells are staggered but not butt-bonded and the continuity relies on the subsequent layer. The prefabricated jacketing system is expected to have superior constructability in terms of the quality control and the speed of installation.

EXPERIMENTAL PROGRAM

Model Column Design

Three model columns have been constructed and tested. The model columns were designed based on a 1:2 scale of typical 1.2m (4ft.) diameter prototype columns. As shown in Fig.1, the 2.44m (8ft.) tall and 0.61m (2ft.) diameter model columns were reinforced with 20 deformed #6 (nominal diameter= 6/8in.=19.1mm) bars which constituted a longitudinal steel ratio of 2% of the gross area of column section. The longitudinal steel bars were lap-spliced for a length of 381mm (15in.) near the bottom of the column. Round #2 (diameter=1/4in.=6.4mm) hoops spaced at 127mm (5in.) were used as transverse reinforcement.

Due to the difficulties in obtaining Grade 40 (nominal strength =40ksi=276MPa) steel as specified in the prototype bridge construction, Grade 60 (nominal strength =60ksi=414MPa) steel was used. Actual yield strength of the Grade 60 steel was 462MPa (67ksi) based on tensile test

results. Compared to columns reinforced with Grade 40 steel with the same longitudinal steel ratio, a column reinforced with Grade 60 steel subjects higher demand for shear and bond in the lap-splice region. This implies that the test condition in this program was even more severe than the condition of most existing columns, where Grade 40 steel is common. In addition, the test can also provide an important experimental background for retrofitting older bridges where the designed Grade 40 steel may actually have substantial over-strength. Ready mixed concrete was used throughout. Concrete 28-day cylinder strength was 44.8MPa (6.5ksi).

The main experimental parameter was the retrofitting scheme. One model column was tested under the condition of "as built" while the other two columns were tested after being retrofitted with jacketing. The failed "as built" column was repaired by first replacing the loosened concrete with quick-set cement, and then installing a 4-layer jacket in the lower half region. The repaired column was then tested to failure. Retrofit and repair details are shown in Fig.2(a) to (c), respectively.

Retrofit Procedure

Each layer of the jackets was prefabricated with unidirectional glass fiber sheets and 2-part epoxy. The layer thickness is approximately 3.2mm (1/8in.). The fiber reinforcement is arranged in such way that 90% of the fibers are oriented in the circumferential direction and 10% in the longitudinal direction. The elastic modulus and ultimate strength in the circumferential direction are 48,300MPa (7,000ksi) and 552MPa (80ksi), respectively, based on the tension tests on flat coupons of the composite jackets. Urethane based high strength adhesive was used to bond the prefabricated jackets to form a continuous jacket. Prior to applying the first layer of the composite shells, the column surface was cleaned with high pressure air gun. Fig.3 shows the main retrofit procedures for one of the retrofitted test specimens.

Test Method

The test setup was designed to subject the model columns to constant axial load and cyclic horizontal forces in a single curvature condition, as illustrated in Fig.4. The horizontal force was applied by a ±152mm (±6in.) stroke actuator with the capacity of 1023kN (230kips) in compression and 832kN (187kips) in tension. An axial load of 712kN (160kips) was applied to the column by post-tensioning two 51mm (2in.) diameter high-strength rods with a hydraulic jack at the top of the column. The ratio of the applied axial load to the column axial load capacity was about 5%, which is among the range of typical axial load ratios of columns in multi-column bent bridges in California. The footing was post-tensioned to a reaction beam using eight high strength rods. Instrumentation included all the applied forces and horizontal displacement. Strain gauges were applied to measure the strains of reinforcing steel and composite jacket.

All specimens were subjected to a number of lateral cyclic loading while the axial load was maintained constant. The lateral loading sequence was controlled by displacement increment. The initial loading cycles were applied corresponding to a peak displacement increment of 2.5mm (0.1in.), until the column developed the calculated capacity corresponding to the first yield of longitudinal steel, H_y. Then the yield displacement, Δ_y was determined using the following equation:

$$\Delta_y = \frac{H_{if}}{H_y}\Delta_1 \qquad (1)$$

where Δ_1, is the average of the measured displacements corresponding to the first yield capacity, H_y, in the push and pull directions; H_{if}, is calculated ideal flexural capacity based on an extreme concrete compressive strain of 0.005 and stress-strain model for confined concrete recommended by Mander, Priestley and Park [1988]. After the column developed the first yield capacity, three complete loading cycles were performed corresponding to peak displacement ductility factors, μ_Δ=1, 1.5, 2, 3, 4, 6, and 8. The displacement ductility factor μ_Δ was defined as the ratio of displacement Δ to yield displacement Δ_y. Note that actual loading procedures for different specimens were somewhat deviated from the standard loading procedure due to the difficulties in displacement control system used in the tests.

EXPERIMENTAL RESULTS

Observations

The "as built" model column, C1-A, developed an unstable response due to premature lap-splice failure between the longitudinal reinforcement and starter bars. At a displacement of 5mm (0.2in.), the first flexural crack was observed at the bottom end of the column. As the displacement increased to 13mm (0.5in.), flexural cracks extended into the whole lap-splice region and then propagated upward. The first vertical crack appeared in the lap-splice region at a displacement of 28mm (1.1in.), indicating the initiation of bond slip. After one cycle at a peak displacement of 41mm (1.6in.), vertical cracks were fully spreaded within the lap splice region, indicating the bond slip failure of lap-splices, as shown in Fig.5(a). The test was terminated when the lateral force capacity dropped to 50% of the maximum capacity at a displacement of 61mm (2.4in.).

The retrofitted columns performed in a consistently stable fashion throughout testing. Flexural cracks were observed at the column base where a gap of about 19mm (o.75in.) was intentionally provided to prevent the footing from over-loading. At the final stages of loading corresponding to a displacement ductility factor of 8.0, fine horizontal cracks were observed on the surface of the prefabricated composite jacket, as shown in Fig.5(b). This was expected because of the smaller fiber content in the longitudinal direction. The repaired column C4-RP4 also exhibited improved performance comparing to the "as built" column. The maximum circumferential strain of jackets recorded for all retrofitted columns was approximately 0.001 to 0.0015 at the bottom of the jacket, similar to the effective strain of 0.001 suggested by Priestley and Seible for composite retrofit [1991]. No delamination or rupture across the circumferential fibers of the jackets was observed in any testing of the retrofitted or repaired columns.

At large displacements, deterioration of the bond in the lap-splices was observed for all the retrofitted and repaired columns as evidenced by the pull-out of the starter bars during the opening of the cracks at the base of the columns. This indicated that performance of the retrofitted or repaired columns at large displacements was also influenced by bond deterioration of the lap-spliced longitudinal bars.

Horizontal Force - Displacement Responses

Plots of horizontal force versus displacement obtained from all four tests are shown in Fig.6(a) to Fig.6(d). Calculated capacities corresponding to the first yield of longitudinal steel, H_y, and ideal flexural capacity, H_{if}, are also shown in these diagrams by dashed lines.

"As Built" Model Column: Fig.6(a) shows that the "as built" model column C1-A developed unstable hysteresis hoops and had rapid degradation in load carrying capacity due to the lap-splice failure. The predicted ultimate flexural strength was not achieved. A maximum horizontal force of 231kN (52kips), slightly larger than the calculated first yield capacity, was noted in the pull direction corresponding to a displacement of 13mm (0.5in.). After the column suffered lap-splice failure, its load carrying capacity stabilized at about 112kN (25kips), which was essentially the restoring force due the applied axial load as the column started rocking about its base.

Retrofitted Model Columns: Compared to "as built" column C1-A, the two retrofitted columns, C2-RT4 and C3-RT5 exhibited significantly improved seismic performance and demonstrated the effectiveness of the retrofit, as shown in Fig.6(b) and (c), respectively. The retrofitted column with 4-layer jacketing developed stable hysteretic response up to the first cycle corresponding to a displacement ductility factor of about 6.0. The retrofitted column with 5-layer wrapping developed even higher load carrying capacity and a larger ductility factor. Although the load carrying capacities of the retrofitted columns degraded gradually at ductility factor of 6.0, the columns could develop 70% to 80% of the ideal flexural strength even at a displacement ductility factor as large as 8.0. The gradual degradation of the capacity at large ductility levels was considered due to the bond slip in the lap-spliced longitudinal bars. Such bond slip mechanism can be considered acceptable for seismic retrofit as long as the retrofitted column develops the required load carrying capacity and ductility. A gradual bond slip failure mechanism of the lap-spliced longitudinal bars may be even beneficial since the total failure mode of a column due to the rupture of longitudinal bars can be avoided.

Repaired Model Column: The repaired column C4-RP5 developed a maximum load carrying capacity approximately equal to the first yield strength calculated on the basis of the virgin section condition, as described in Fig.6(d). The ductility factors shown in Fig.6(d) are based on the yield displacement defined for "as built" column C1-A. By comparing the hysteretic responses shown in Fig.6(a) and (d), it can be seen that the repaired column developed improved behavior than the original "as built" column. However, the hysteresis loops of the repaired column are significantly pinched.

ANALYTICAL APPROACH

Analytical Model

Experimental results indicated the necessity to consider bond deterioration in a rational assessment or retrofit design of bridge columns with lap-spliced longitudinal bars. In an early study, Xiao et al. [1987] have developed a simple analytical model for analyzing the lateral force and displacement performance of short reinforced concrete columns considering both flexural deformation and bond slips in longitudinal bars. A similar model is developed for analyzing the performance of columns with lap-splices, as shown in Fig.7. The analysis is essentially based on

the moment curvature analysis with taking into consideration the bond slips of the lap-spliced longitudinal bars.

A hinge is assumed at the bottom of the column, and the upper portion of the column is considered as an elastic beam column. Within the hinge, the curvature is assumed uniform, while a linearly distributed curvature is assumed for the upper portion, as shown in Fig.7(b). Bond links are assumed for all the lap-splices above the hinge length, as shown in Fig.8(c).

Hinge Length: Priestley et.al. have suggested the following fixed length of plastic hinges for analyzing inelastic flexural behaviors of reinforced concrete columns with or without jacketing [Priestley and Seible, 1991]:

for "as built" columns: $$L_p = 0.08h + 0.022 d_{lb} f_y \quad (2a)$$

for retrofitted columns: $$L_p = g + 0.044 d_{lb} f_y \quad (2b)$$

where, L_p is the plastic hinge length; h is the height of the column; d_{lb} is diameter of a typical lap-spliced longitudinal bar; f_y is the yield strength of the longitudinal reinforcement; and g is the gap provided at the bottom of the jacket.

In the proposed approach, the hinge length, L_h, is assumed variable corresponding to the steel stress of the extreme critical tensile bar, f_s. The expression takes the same format of equation (2) but uses a variable steel stress, f_s, instead of the yield strength, f_y.

for "as built" columns: $$L_h = 0.08h + 0.022 d_{lb} f_s \quad (3a)$$

for retrofitted columns: $$L_h = g + 0.044 d_{lb} f_s \quad (3b)$$

Confined Concrete: Mander, Priestley and Park's stress strain model [1988] is assumed as the constitutive law of the confined concrete. An effective confinement stress provided by the prefabricated jacket is calculated using the following equation.

$$f_l = \frac{2t_j}{D_j - 2t_j} E_j \varepsilon_j \quad (4)$$

where, f_l is the effective confinement stress; D_j and t_j are the diameter and the effective thickness of the jacket; E_j is elastic modulus of the composite in the circumferential direction; and ε_j is the effective strain in the jacket. The effective strain of ε_j=0.001 suggested by Priestley and Seible [1991] is used in the analysis.

Bond Links: It is assumed that in the lap-splice region, the stresses in the starter bars are transferred to the longitudinal column bars through a series of bond links, which are distributed throughout a length of, L_b given by the following equation.

$$L_b = L_s - 0.022 d_{lb} f_s \quad (5)$$

where, L_s is the length of the lap-splices; d_{lb} is the diameter of a typical lap-spliced longitudinal bar; and f_s is the stress of a longitudinal bar. It should be noted that the length of the bond links

defined by equation (5) is different for rebars at different location in a column section. However, for simplicity, L_b, is calculated based on the stress of the extreme tensile bar in the column section. The bond stresses are actually distributed throughout the lap-splice length, L_s, with the peak bond stress occurs within L_s and zero bond stresses at its ends. In this study however, a constant bond stress is essentially used for simplicity. The second term in equation (5) is provided to minimize the influence due to ignoring the nonlinear distribution of bond stresses within L_s. In future studies, more detailed analysis and calibration of the bond transfer mechanism should be addressed.

The constitutive law for the bond links is expressed by bond stress, τ_b - slip, S_b, relationship, given by the following equation based on a form of Popovic's equation [1973].

$$\tau_b = \frac{\tau_{bc}' \, r(S_b / S_{bc})}{r - 1 + (S_b / S_{bc})^r} \tag{6}$$

where, τ_{bc}' is the peak bond stress between the rebar and confined concrete; S_{bc}, is the bond slip corresponding to τ_{bc}'; and r is the parameter which defines the shape of the curve expressed by equation (6), for different transverse confinement. Peak bond stress, τ_{bc}', can be expressed by the following equation,

$$\tau_{bc}' = \tau_{b0}' + 1.4 f_l \tag{7}$$

In the above equation, the first term, τ_{b0}', expresses the bond strength for steel bars in plain concrete; and the second term expresses the bond strength increment as a consequence of confinement, where, f_l is the effective confinement stress calculated using equation (4) and the coefficient 1.4 is determined based on the shear friction coefficient recommended by ACI318-89 [ACI318, 1989]. On the other hand, following ACI408 Committee report[ACI408, 1992], the first term of equation(7) is given by,

$$\tau_{b0}' = 20\sqrt{f_c'} / d_{lb} \le 5.52\,\text{MPa} \tag{8}$$

It should be pointed out that based on trial analyses the upper limit in equation (8) was ignored. Parameters, S_{bc}, and r in equation (6) are determined using the following empirical equations which were developed for this study using results of pull-out tests on deformed reinforcing bars with different confinement conditions conducted by Giuriani, et.al. [1991].

$$S_{bc} = S_{b0}\left(1 + \alpha \frac{f_l}{f'_c}\right) \tag{9}$$

where, S_{b0}=0.25mm (0.01in.); and α=75.0.

$$r = r_0 - k_r \frac{f_l}{f'_c} \tag{10}$$

where, r_0=2.0; k_r=13.0. The maximum value for r should be limited to less than 1.0.

Analytical Procedure: The analytical procedure involves trial and error loops for searching the correct values of the compression zone depth and the bond slip of each individual bar in the critical section, corresponding to each drift displacement increment. The equilibrium condition between bond and tensile force is used as the criteria in finding the bond slip of a lap-spliced bar. The equilibrium condition of the calculated internal axial force and the applied axial load is used as the governing criterion to determine the calculation step of correct neutral axis position in the critical section.

Analytical Results

Analyses have been conducted to simulate the horizontal force - displacement responses of the model columns tested in this study. Fig.8(a) and (b) show the comparisons of the analytical and the current test results of the "as built" column C1-A and the retrofitted model column, C2-RT4, respectively. Solid lines in Fig.8 describe the analytical results predicted using the proposed model, with taking into consideration the bond slip of the lap-spliced longitudinal reinforcement. Dashed lines in Fig.8 show the results of the upper bound analysis in which bond slips of the lap-splices are ignored.

As shown in Fig.8, the analysis based on the proposed model for lap-spliced column agrees well with the test results and shows reasonable conservatism for both the "as built" and the retrofitted conditions. It should be pointed out that the analytical results, which take into consideration the bond-slip for the retrofitted column models, indicate a slightly more rapid degradation after exceeding the peak horizontal load carrying capacity. This is probably due to the conservative nature of the proposed simplified bond-slip law. However, if the ultimate displacement is defined as the lateral displacement corresponding to the point where the horizontal load carrying capacity drops to 85% of the peak capacity, the ductility predicted by the analysis is close to the actual ductility achieved by the test specimens, as shown in Fig.8(b).

RETROFIT DESIGN RECOMMENDATIONS AND EXAMPLES

The proposed analytical methods can be used as a tool for seismic assessment and retrofit design of existing reinforced concrete bridge columns with lap-spliced longitudinal reinforcement. The procedure involves trial designs of the layer numbers of the prefabricated jackets and prediction of ultimate ductility. If the calculated ductility is less than what is required for retrofit, then the number of jacket layers should be increased and the corresponding ductility factor recalculated until the predicted ductility factor exceeds the required value.

The procedure is demonstrated using a column example shown in Fig.9(a). The analysis using the proposed model for the existing column indicates that the column is not able to develop its ideal flexural capacity or any ductility, thus retrofit is necessary. A 3-layer wrapping is first assumed for retrofitting the example column. The ductility factor for the 3-layer retrofit is calculated as 5.0, corresponding to the 85% reduction of the load carrying capacity. By doubling the layers to a 6-layer retrofit, a ductility factor of 6.5 is obtained and the design requirement can be satisfied. The number of layers can be further increased to give further design safety. For example, if 9 layers of composite jacketing is used, a ductility factor as high as 8.5 can be expected. Horizontal force - displacement responses for all the calculated cases are summarized in Fig.9(b).

CONCLUSIONS

A prefabricated glass fiber composite jacketing system for seismic retrofit of bridge columns with lap-spliced rebars has been experimentally and theoretically studied. Test results of an "as built" model column indicate that columns with poor lap-splice details are vulnerable to premature brittle failure due to the bond deterioration of the lap-spliced rebars. Such failure pattern can be delayed using the prefabricated composite jacketing, as demonstrated by significantly improved hysteretic responses and increased ductility of the retrofitted model specimens.

Bond slip in lap-spliced rebars can cause a gradual degradation of load carrying capacity of a retrofitted column after the required ductility is developed. Such mechanism may be considered beneficial for retrofit, since a column can be retrofitted with lesser jacket thickness and the total failure mode of the column due to the rupture of longitudinal bars can be avoided.

An analytical approach that takes into consideration the deformation due to the bond slip in lap-spliced longitudinal reinforcement has been developed. Comparison of analytical and test results indicates that the analysis provides a rational explanation and prediction to the behavior of columns with lap-spliced longitudinal reinforcement. The proposed method can be used as a useful tool for seismic assessment and retrofit design of columns with lap-spliced rebars as demonstrated by a design example.

PROGRESS OF STUDIES ON SHEAR RETROFIT

Three one half scale bridge model columns have been recently tested to investigate the effectiveness of shear retrofit using prefabricated composite jacketing. The columns have a circular cross section with a diameter of 610mm and reinforced with 20 #6 Grade 40 reinforcing bars. The shear aspect ratio was 1.5 (column height to diameter ratio of 3). The columns were subjected to constant axial load and cyclic shear under a double bending condition using the test setup shown in Fig.10. One column was tested in an "as built" condition, while the other two columns were tested after retrofit using multi-layer individual or continuous prefabricated composite cylindrical shells. Fig.11 compares the hysteresis loops for the "as built" column and a retrofitted column. The "as built" column suffered a sudden shear failure during the loading cycle corresponding to a limited ductility factor of 3.0. The retrofitted columns developed significantly improved seismic performance characterized by large energy absorption capacities and stable hysteretic responses up to displacement ductility factors of 12 to 14.

ACKNOWLEDGMENTS

The research described in this paper was funded by C.M.I., Inc. The prefabricated composite jackets used in the project were manufactured by a joint venture of C.M.I. Inc. and NCF Industries, Inc. Special thanks are due to Mr. B. Olson, project engineer of C.M.I., Inc. The author wish to thank Prof. G.R. Martin of USC for his cooperation. Valuable contributions from graduate research assistants R. Ma, H. Wu, and C. Garcia are gratefully appreciated. Thanks are also due to Mr. M. Sultan, Mr. L.H. Sheng, engineers of California Department of Transportation

(Caltrans) for their valuable technical inputs. The comments and conclusions described in this paper are solely those of the author's, and do not necessarily reflect the views of the funding agency.

REFERENCES

ACI Committee 318, (1989), "Building Code Requirements for Reinforced Concrete and Commentary (ACI318-89/ACI418R-89)," American Concrete Institute, Detroit, 1989.

ACI 408 Committee, (1992), "State-of-the-Art Report on Bond Under Cyclic Loads," American Concrete Institute, Report ACI 408.2R-92, 32p.

Chai, Y.H.; Priestley, M.J.N.; and Seible, F., (1991), "Seismic Retrofit of Circular Bridge Columns for Enhancing Flexural Performance," *ACI Structural Journal*, Vol.88, No.5, Issue, pp.572-584.

EERI, (1990), "Loma Prieta Earthquake Reconnaissance Report," *Earthquake Spectra*, Earthquake Engineering Research Institute, May.

EERI, (1995), "Preliminary Reconnaissance Report on The Hyogo-Ken Nanbu Earthquake of January 17, 1995," Earthquake Engineering Research Institute, 95-04, February, p 112.

Giuriani, E.; Plizzari, G.; and Schumm, C., (1991), "Role of Stirrups and Residual Tensile Strength of Cracked Concrete on Bond," *ASCE Journal of Structural Engineering*, Vol.117, No.1, January, pp.1-18.

Mander, J.B.; Priestley, M.J.N.; and Park, R., (1988), "Theoretical Stress-Strain Model for Confined Concrete," ," *ASCE Journal of Structural Engineering*, Vol. 114, No.8, August, pp.1827-1849.

Matsuda, T.; Sato, H.; Fujiwara, H.; and Higashira, N., (1990), "Effect of Carbon Fiber Reinforcement as a Strengthening Measure for Reinforced Concrete Bridge Piers," *Proceedings of the First U.S.-Japan Workshop on Seismic Retrofit of Bridges*, Public Works Research Institute, Ministry of Construction, Tsukuba Science City, Japan, December 17-18.

Popovics, S. (1973), "A Numerical Approach to the Complete Stress-Strain curves for Concrete," *Cement and Concrete Research*, 3(5), 583-599.

Priestley, M.J.N., (1987), "Damage of the I-5/I605 Separator in the Whittier Earthquake of October 1987," *Earthquake Spectra*, Vol.4, No.2, pp.389-405.

Priestley, M.J.N.; and Seible, F., (1991), "Seismic Assessment and Retrofit of Bridges," Edited by M.J.N. Priestley and F. Seible, University of California at San Diego, *Structural Systems Research Project*, Report No. SSRP-91/03, July, 418p.

Priestley, M.J.N.; Seible, F.; Xiao, Y.; and Verma, R. (1994), "Steel Jacket Retrofit of Squat RC Bridge Columns for Enhanced Shear Strength - Part 1 - Theoretical Considerations and Test Design; and Part 2 - Experimental Results," *ACI Structural Journal*, American Concrete Institute, Vol.91, No.4, July-August, pp.394-405; and Vol.91, No.5, September-October, pp.537-551.

Saadatmanesh, H.; Ehsani, M.R.; and Li, M.W. (1994), "Strength and Ductility of Concrete Columns Externally Reinforced with Fiber Composite Straps," *ACI Structural Journal*, July-August Issue, pp.434.

Seible, F. and Priestley, M.J.N., (1993), "Retrofit of Rectangular Flexural Columns with Composite Fiber Jackets," California Department of Transportation, *Proceedings of the Second Annual Seismic Research Workshop*, Sacramento, March 16-18.

Seible, F.; Hegemier, G.A.; and Innamorato, D., (1995), "Developments in Bridge Column Jacketing Using Advance Composites," *Proceedings of the National Seismic Conference on Bridges and Highways*, Federal Highway Administration and California Department of Transportation, San Diego, California, December 10-13.

Xiao, Y.; Sakino, K; and Tomii, M., (1987), "Ultimate Moment and Mechanical Behavior of Reinforced Concrete Short Circular Columns Confined in Steel Tube," *Transactions of Japan Concrete Institute*, Tokyo, Japan, Vol.9, pp.389-396.

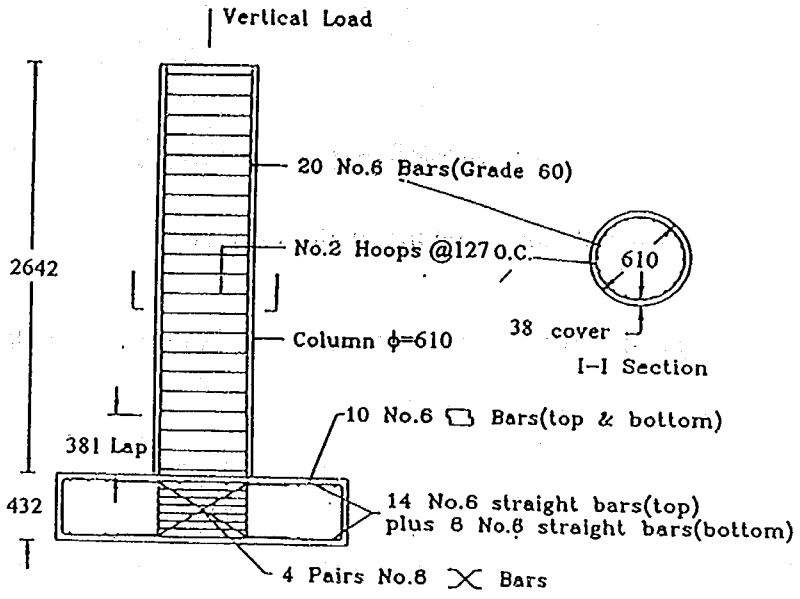
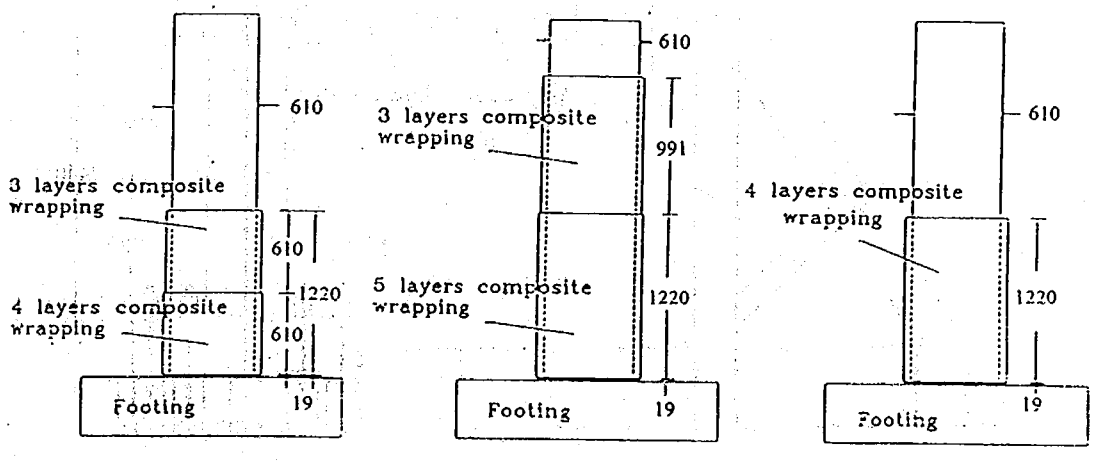


Fig.1 Model Column Details



(a) Retrofit: C2-RT4 **(b) Retrofit: C3-RT5** **(c) Repair: C4-RP4**

Fig.2 Retrofit and Repair Details



(a) Applying Adhesive to Column Surface (b) Installation of Jackets (c) Curing of Adhesive

Fig.3 Installation of Prefabricated Composite Jackets

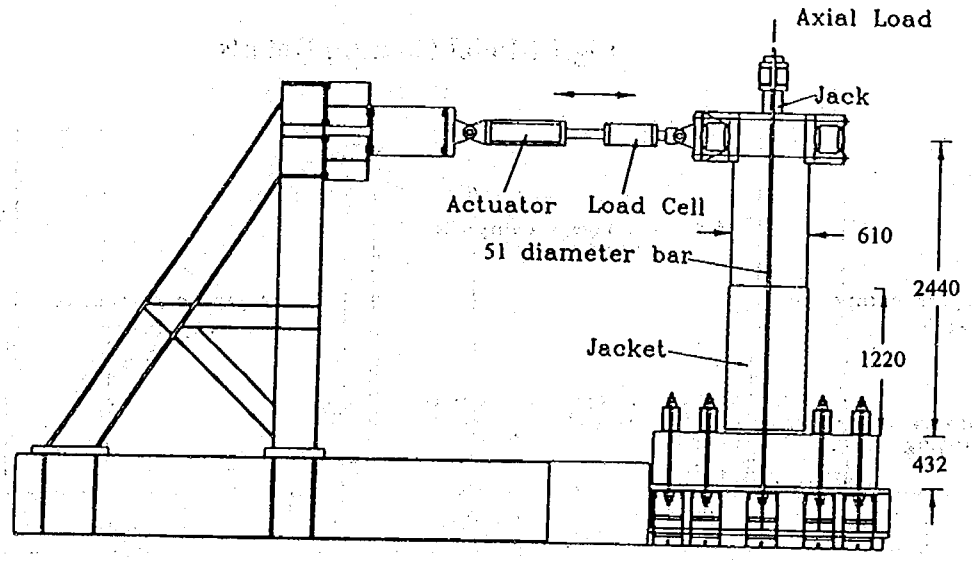
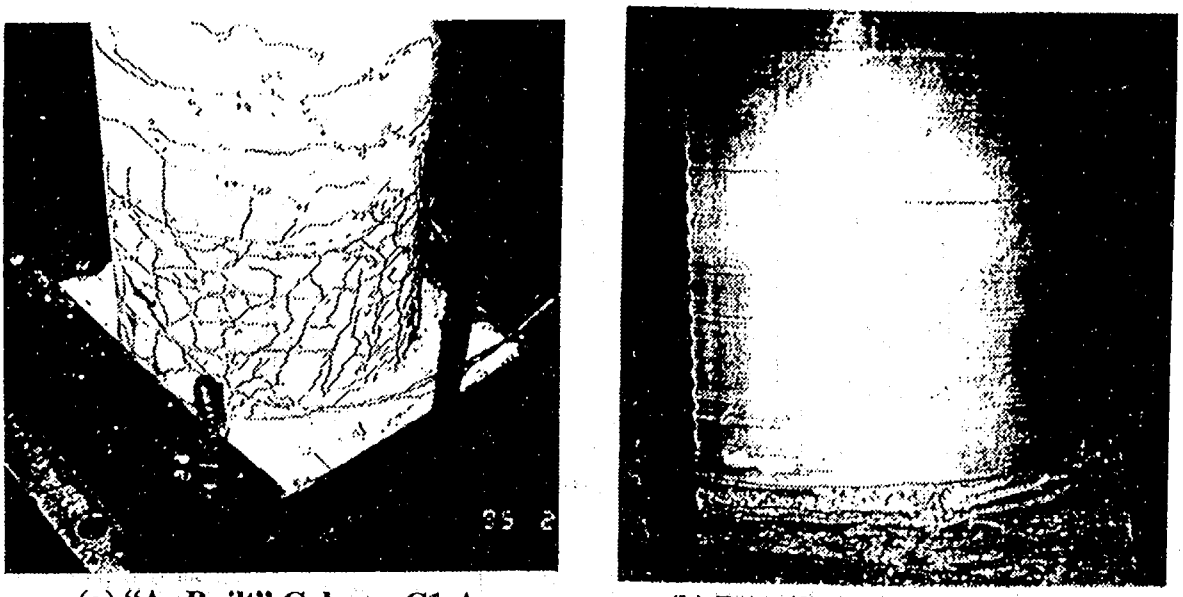
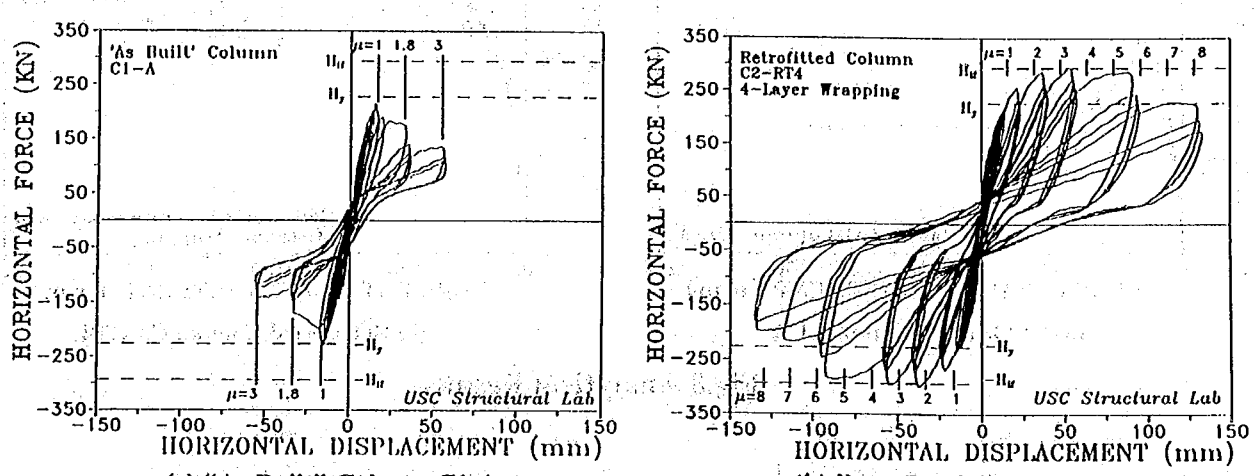


Fig.4 Test Setup

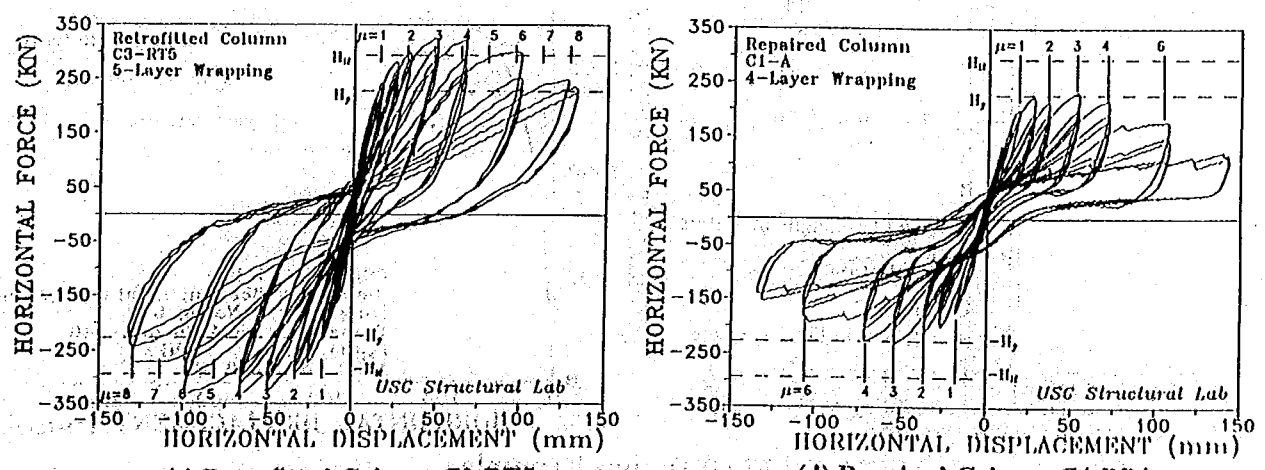


(a) "As Built" Column C1-A (b) Retrofitted Column C2-RT4

Fig.5 Crack Patterns



(a) "As Built" Column C1-A (b) Retrofitted Column C2-RT4



(c) Retrofitted Column C3-RT5 (d) Repaired Column C4-RP4

Fig.6 Horizontal Force - Displacement Responses of Model Columns with Lap-Splices

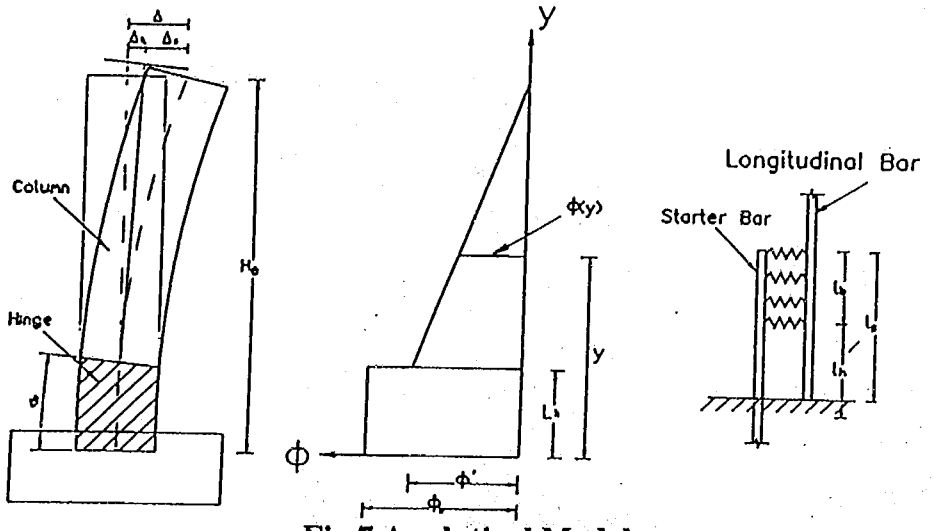
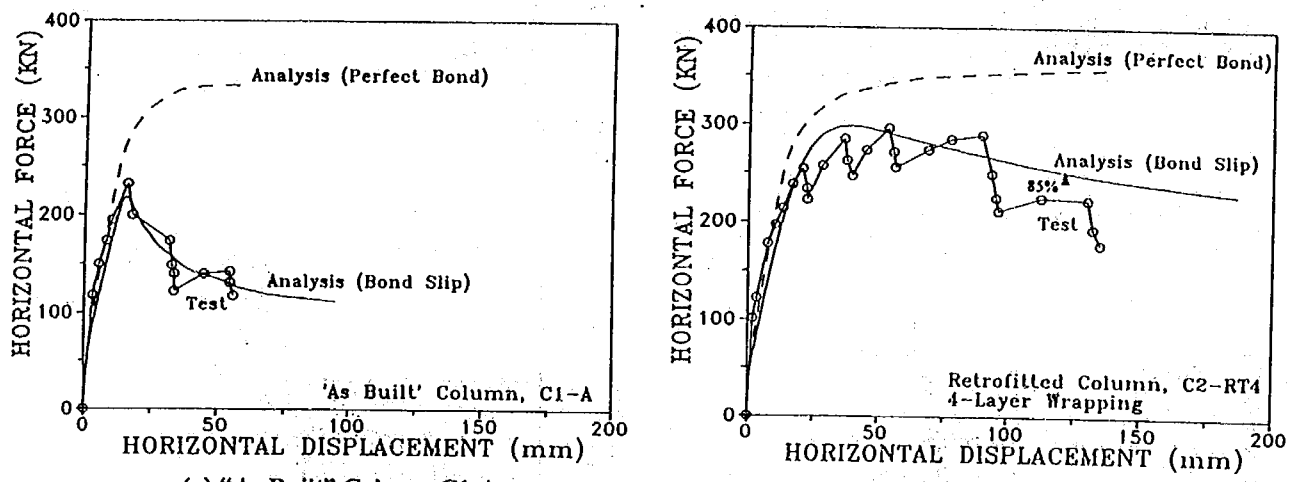


Fig.7 Analytical Model



(a) "As Built" Column C1-A

(b) Retrofitted Column C2-RT4

Fig.8 Analytical Results

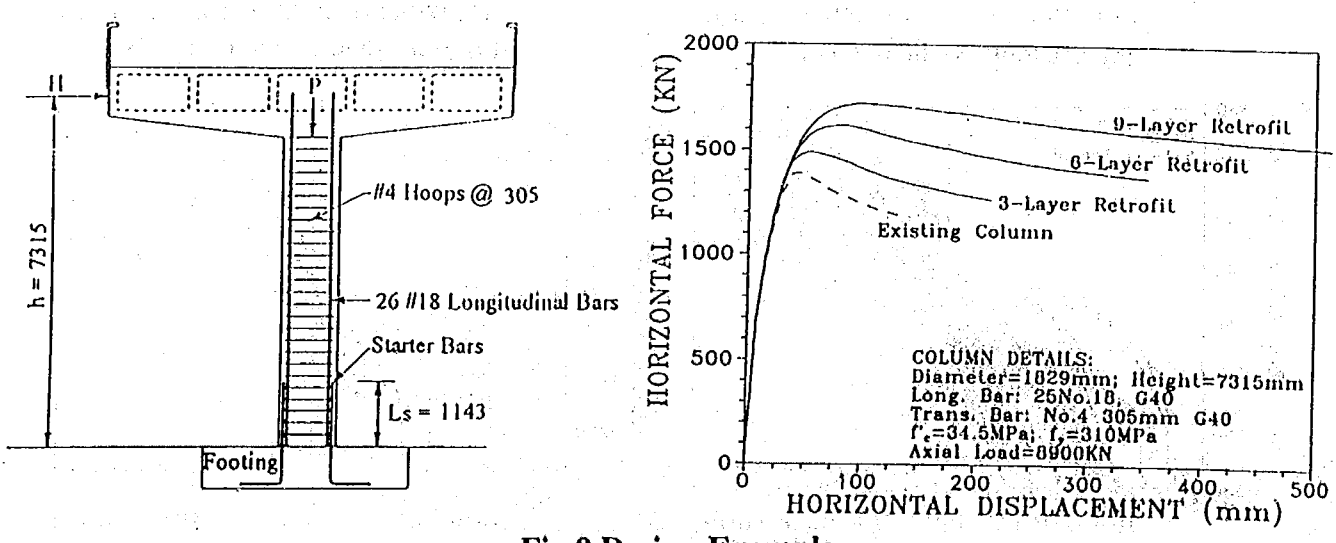


Fig.9 Design Example

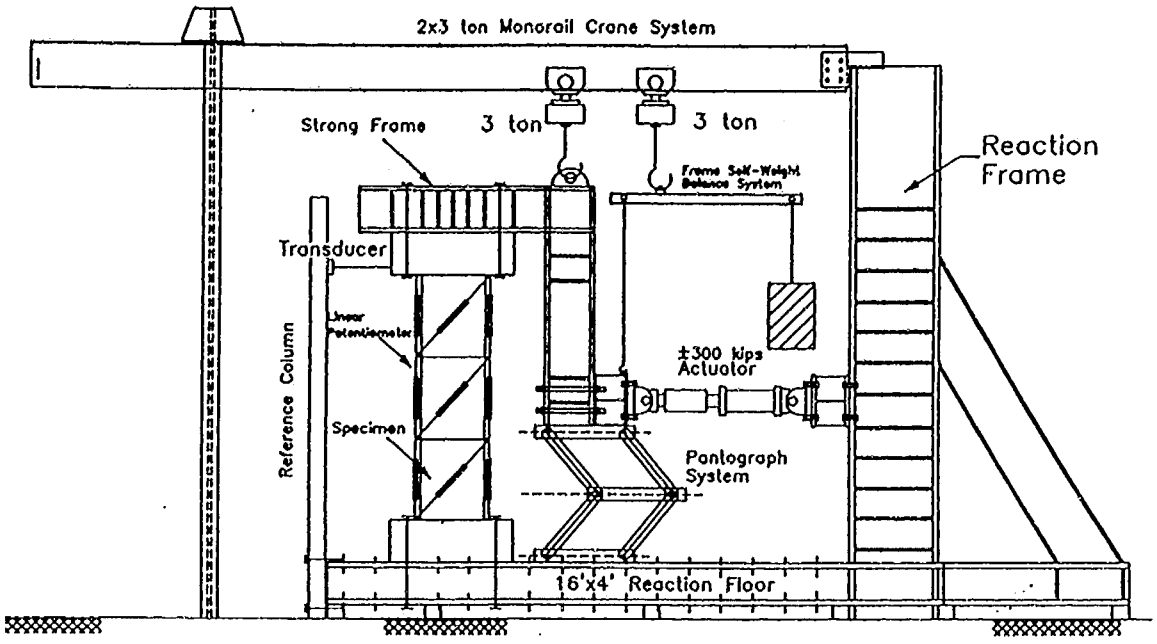
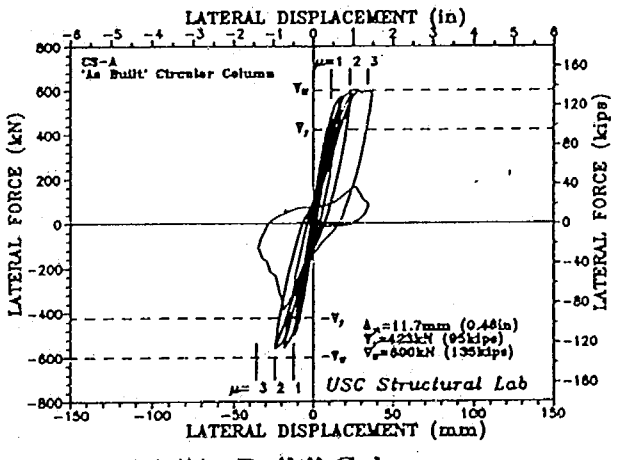
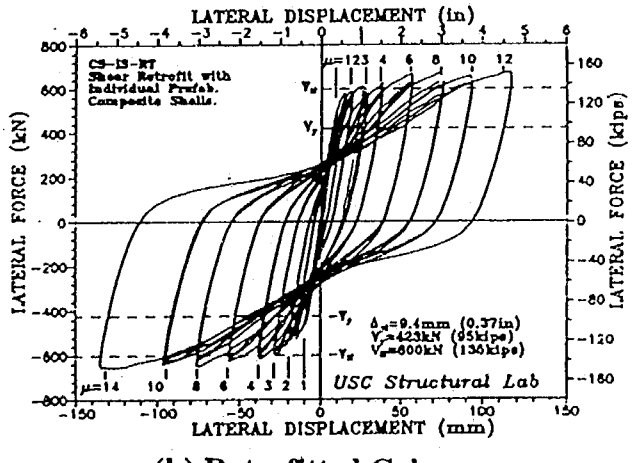


Fig.10 Shear Test Setup

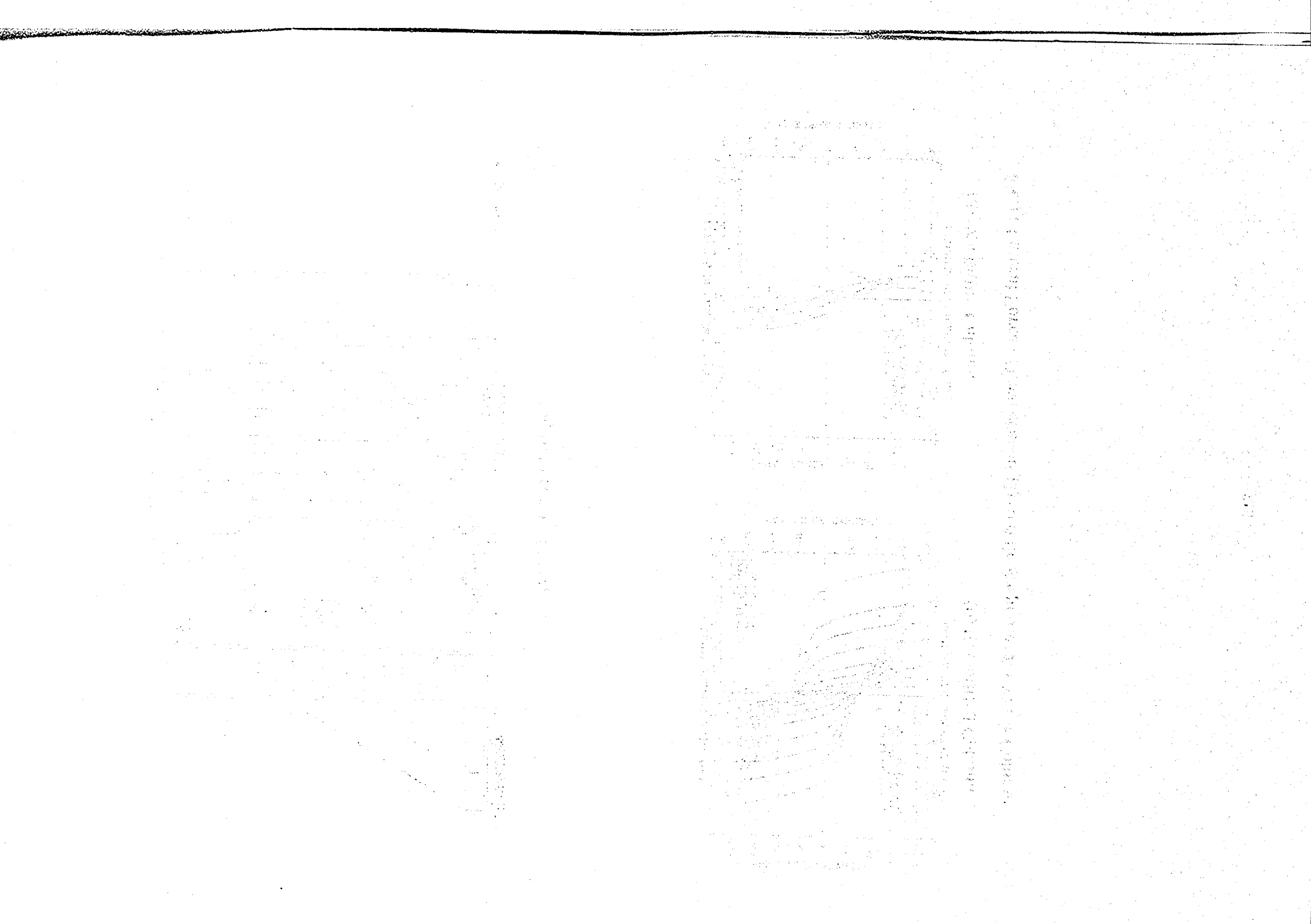


(a) "As Built" Column



(b) Retrofitted Column

Fig.11 Lateral Force - Displacement Hysteretic Responses for Shear Columns



SEISMIC RETROFIT OF REINFORCED CONCRETE BRIDGE PIERS BY CARBON FIBER SHEETS

Hosotani, M.[1]; Kawashima, K.[2] and Hoshikuma, J.[3]

1) Research Student, Tokyo Institute of Technology (Taisei Corporation), O-okayama, Meguro-ku, Tokyo, 152, Japan

2) Professor, Department of Civil Engineering, Tokyo Institute of Technology, O-okayama, Meguro-ku, Tokyo, 152, Japan

3) Research Engineer, Earthquake Engineering Division, Public Works research Institute, Ministry of Construction, Tsukuba Science City, 305, Japan

ABSTRACT

Most of reinforced concrete bridge piers which suffered damage by the 1995 Hyogoken-Nanbu Earthquake were designed with seismic standards in 1960s which didn't take account of importance of ductility. Therefore, existing reinforced concrete columns which were designed with seismic standards in 1960s must be strengthened urgently. As one of seismic strengthening methods of reinforced concrete columns, carbon fiber sheets jacketing is attracted attention because of its good workability. To reflect confinement by carbon fiber sheets in seismic strengthening of reinforced concrete columns, a series of compressive loading tests of concrete cylinders were conducted and a stress-strain relation was obtained. Further, a stress-strain model of confined concrete by carbon fiber sheets is proposed.

INTRODUCTION

Hyogo-ken Nanbu earthquake of January 17, 1995 caused destructive damage to various structures. The bridges also suffered extensive damage, in particular at their piers. It has been pointed out that the piers which suffered damage were designed and constructed by the Design Specifications issued in 1960s[1]. At those days, the importance of confinement of core-concrete by tie reinforcements was not recognized at all. Because there are a number of bridges which were designed based on the similar design concept, it is obvious that seismic retrofit is required for those bridges which are vulnerable to the extreme earthquakes such as the Hyogo-ken Nanbu earthquake.

Seismic retrofit has been extensively conducted throughout the country for reinforced

concrete piers which were designed by the pre-1980 Design Specifications. The steel jacketing with a controlled increase of flexural strength has been widely adopted for seismic retrofit of reinforced concrete pier[2)3)4)]. Although the steel jacketing is effective from various points such as the effective confinement, an increase of shear capacity as well as flexural strength and cost, it is unable to adopt at the sites where enough space to handle the steel jacket is not available and where restriction of traffic is significant.

Various new technical developments with use of advanced and high performance materials have been made to provide an adequate solution for the limitation of the steel jacketing method. One of the most interesting materials may be the carbon fiber sheet. It is light, easy to handle, strong in tension and is good in workability. For example, the carbon fiber sheet has a tensile strength of 3.0 kN/mm^2 which is about ten times higher than steel. The weight is only 18 kN/m^3, and it is only 1/5 of steel. It takes only 30 minutes to place a sheet on surface of a reinforced concrete pier. Thus, it has been considered effective to use the carbon fiber sheets to confine the concrete of a pier. It has been found that the carbon fiber jacketing is effective to improve the shear capacity of a reinforced concrete pier at a termination point of longitudinal reinforcements with inadequate anchoring length[5)]. It has been also recognized that the carbon fiber sheet is effective to increase the flexural capacity of a reinforced concrete pier at the plastic hinge zone. Although cyclic loading tests have been conducted at various organizations, few information is available on how much increase of strength and strain can be obtained by providing the confinement by the carbon fiber sheet.

To develop on appropriate stress vs. strain relation of concrete confined by the carbon fiber sheets, a series of compressive loading tests of concrete cylinders was conducted. This papers presents the test results, and a model of stress vs. strain relation under the confinement by the carbon fiber sheets.

TEST SPECIMENS AND TEST PROCEDURE

Table 1 shows the size and reinforcements of specimens. The parameters considered in the test are shape (circular and square), and volume and elastic modulus of carbon fiber sheet. The specimens were 600 mm in height, 200 mm in either width or diameter. The design strength of concrete was set to be 30N/mm^2. Deformed reinforcements of 6 mm with a yield strength of 295 N/mm^2 (SD295, D6) were provided in the longitudinal direction, while no hoop reinforcements were provided in the specimens. This is because to isolate the effect of carbon fiber sheet. Axial reinforcement ratio was 1 %.

There were three series of specimens; the first was the specimens without confinement by the carbon fiber sheet. They are called as N-series. The second was the specimens confined by the carbon fiber sheet with a normal elastic modulus of 2.30×10^5 N/mm^2, while the third was the specimens confined by the carbon fiber sheet with a high elastic modulus of 3.92×10^5 N/mm^2. Table 2 compares the mechanical properties of the two types of carbon fiber sheet. Tensile strength is essentially the same between the normal-modulus and high-modulus type carbon fiber. It should be noted however that the rupture strain is smaller in the high-modulus type (1.0%) than in the normal-modulus type (1.5%).

A carbon fiber ratio (volumetric ratio of carbon fiber sheet) was defined as

$$\rho_{CF} = 4 \times n \times t_{CF} / d \qquad (1)$$

where t_{CF} = thickness of a layer (mm), n = number of layers of carbon fiber sheets, d = diameter or the length of a concrete specimen.

Taking account of application to a pier, the carbon fiber ratio ρ_{CF} was set in S series in the range of 0.05~0.15%. This corresponds to put 2~6 layers of carbon fiber sheet in a reinforced concrete column with a diameter of 3m. ρ_{CF} in S-4 ,S-12 and H series is in the range of about 0.15~1.5%. The reason for this is that larger confinement effect can be obtained by given larger ρ_{CF} .

Fig.1 shows the adhesion of carbon fiber sheet. Carbon fiber sheet was wrapped in circumferential direction. The length of lap splice was 10cm. Corners of the square specimens were rounded to prevent rupture of carbon fiber sheets due to stress concentration The radius of the corner was 30mm. The characteristic of carbon fiber sheets is shown in Table 2. The specimens were subjected to an uniaxial compressive loading under the displacement control with the loading rate of 0.2mm/min. Deformation of the specimens between the top and the bottom was measured by four displacement sensors to determine the longitudinal strain by dividing the displacement by the height of the specimens.

STRESS VS. STRAIN RELATION OF UNCONFINED CONCRETE CYLINDERS

Fig.2 shows the stress-strain relation of unconfined concrete cylinders. The initial stiffness was almost the same in the specimens, and was about 2.0×10^5N/mm^2 with the strain corresponding to the peak stress being about 3,000~3,500 μ. The concrete cylinders failed at the strain of carbon fiber sheet of about 4,000 μ after the peak stress.

Fig.3 shows the relation between the stress of concrete and the circumferential strain of carbon fiber sheets. At the initial loading stage, the circumferential strain of carbon fiber sheet increases as the stress of concrete cylinder increases.

The circumferential strain begins to increase sharply after it reached at about 500 μ, and becomes almost stable at a strain of 1,500 μ. That is to say, concrete cylinder begins to expand sharply at the circumferential strain of about 500 μ and failed at the circumferential strain of about 1500 μ. If the circumferential strain of concrete cylinder at its failure is defined as ε_{pf}, then ε_{pf} is in the range of about 1,200~1,700 μ.

EFFECT OF CARBON FIBER RATIO ρ_{CF}

Fig.4 shows the stress-strain relation of confined concrete by the carbon fiber sheet. Allows in Fig.4 shows where the carbon fiber sheet ruptured. As soon as the rupture of the carbon fiber sheet, the concrete cylinders also failed.

When ρ_{CF} is in the range of 0.05~0.15%, the peak stress of concrete f_{cc} is about 37~41N/mm^2 and the strain corresponding to the peak stress ε_{cc} is about 2,500~3,000 μ regardless of the carbon fiber ratio ρ_{CF} and the cross sectional shape of concrete cylinder. However, the deteriorating rate of the stress after the peak stress decreases and the strain of concrete at the rupture of the carbon fiber sheet increases as the carbon fiber ratio ρ_{CF} increases.

When ρ_{CF} is larger than a certain value, the stress of concrete keeps increasing without the deterioration of the stress until the rupture of the carbon fiber sheet. However, when the strain of concrete cylinder reaches 3,000~3,500 μ, the increasing rate of the stress in a stress-strain relation becomes smaller. This gradient is defined as the second gradient E_g. The second gradient is larger in circular cylinder than in square cylinder.

Fig.5 shows the relation between the stress of concrete and the circumferential strain of carbon fiber sheets. In the range of the carbon fiber ratio from 0.05 to 0.15%, after the stress of concrete takes its peak value at a certain strain of the carbon fiber sheet, the stress of concrete decreases at further increase of the strain of carbon fiber sheet. Defining the strain of the carbon fiber sheet at the peak stress of concrete as ε_{CFc}, the ε_{CFc} is about 1,100~2,500 μ. It means that the stress induced in the carbon fiber sheet is 250~550N/mm^2 at the strain of 1,100~2,500 μ, because the elastic modulus of the carbon fiber sheet is 2.43×10^5N/mm^2.

Because the rupture strength of the carbon fiber sheet is about 3,500N/mm^2, it is only 1/10 of the rupture strength.

On the other hand, when the carbon fiber ratio ρ_{CF} is 1.336% (S-4 and S-12), the stress of concrete keeps increasing as the strain of carbon fiber sheets increases, although the gradient in the stress-strain relation becomes smaller over a certain strain of the carbon fiber sheet. Defining the strain of the carbon fiber sheet where the gradient changes from the initial value to the second gradient as ε_{CFt}, the ε_{CFt} is about 1,800~1,900 μ. Because the strain corressponding to the peak stress ε_{CFc} is about 1,100~2,500 μ, it seems safety to think that the range of ε_{CFt} is almost equal to that of ε_{CFc}. Considering that the circumferential strain at the failure of concrete cylinder ε_{pf} is about 1,200~1,700 μ, over the strain of 1,100~2,500 μ induced in the carbon fiber sheet regardless of the carbon fiber sheet ρ_{CF}, the concrete cylinder started to fail and the axial stress of concrete decreased sharply.

EFFECT OF HIGH ELASTIC MODULUS CARBON FIBER SHEET

Fig.6 compares the stress-strain relation of concrete cylinders confined by the normal-modulus type and high-modulus type carbon fiber sheets. The test data for concrete cylinders with the carbon fiber ratio ρ_{CF} is almost the same carbon fiber ratio are presented here. The axial stress f_t and the second gradient E_g is larger in the normal-modulus type than the high-modulus type in both circular and square specimens.

Fig.7 compares the circumferential strain vs. the axial stress relation between the normal-modulus type and the high-modulus type carbon fiber sheets. When the circumferential strain of carbon fiber sheets in all specimens reaches 1,600~2,500 μ, the initial gradient in stress-strain relation change largely from initial gradient to the second gradient.

MODELING OF THE STRESS-STRAIN RELATION

As has been noted, when the circumferential strain of concrete cylinder reaches 1,100~2,500 μ, the increasing rate of the axial stress of concrte cylinder changes from the initial gradient E_c to the second gradient E_g regardless the carbon fiber ratio ρ_{CF} and the elastic modulus of carbon fiber sheet E_{CF}. Over the circumferential strain of concrete cylinder of 1,100~2,500 μ, if ρ_{CF} is in the range of 0.05~0.15%, the axial stress of concrete cylinder decreases sharply, and if ρ_{CF} is in the range of more than about 1.0%, the axial stress of concrete cylinder increases linearly. Accordingly, the stress-strain relation can be divided the first region and the

second region as shown in Fig.8. The first region can be modeled by a second order parabola and the second region is modeled by a straight line. In this model, factors for controlling the stress-strain relation of confined concrete by carbon fiber sheet are f_t, ε_t, E_g and ε_{cu}.

If E_g <0, a stress-strain model is given as

1) the first region ($0 \leqq \varepsilon_c \leqq \varepsilon_t$)

$$f_c = E_c \varepsilon_c \left\{ 1 - \frac{1}{n} \left(\frac{\varepsilon_c}{\varepsilon_t} \right)^{n-1} \right\} \tag{2}$$

$$n = \frac{E_c \varepsilon_t}{E_c \varepsilon_t - f_t}$$

2) the second region ($\varepsilon_t \leqq \varepsilon_c \leqq \varepsilon_{cu}$)

$$f_c = f_t + E_g (\varepsilon_c - \varepsilon_t) \tag{3}$$

where E_c = initial stiffness(MPa).

Eq.(2) is considered the following four boundary conditions.

1)initial condition: ε_c=0 at f_c=0

2)initial stiffness condition: ε_c=0 at $\partial f_c / \partial \varepsilon_c = E_c$ (4)

3)final condition1): $\varepsilon_c = \varepsilon_t$ at $f_c = f_t$

4)final condition2): $\varepsilon_c = \varepsilon_t$ at $\partial f_c / \partial \varepsilon_c$=0

If $E_g \geqq 0$, the final condition2) in four conditions of Eq.(4) is assumed as

1)initial condition: ε_c=0 at f_c=0

2)initial stiffness condition: ε_c=0 at $\partial f_c / \partial \varepsilon_c = E_c$ (5)

3)final condition1): $\varepsilon_c = \varepsilon_t$ at $f_c = f_t$

4)final condition2): $\varepsilon_c = \varepsilon_t$ at $\partial f_c / \partial \varepsilon_c = E_g$

because the axial stress of confined concrete transfer smoothly from the first region to the second region. In this case, a stress-strain relation in the second region is expressed as Eq.(3). However, Eq.(2) must be rewrite as

$$f_c = E_c \varepsilon_c \left\{ 1 - \frac{1}{n} \left(1 - \frac{E_g}{E_c} \right) \left(\frac{\varepsilon_c}{\varepsilon_t} \right)^{n-1} \right\} \tag{6}$$

$$n = \frac{(E_c - E_g)\varepsilon_t}{E_c \varepsilon_t - f_t}$$

A broken line of Eq.(6) in Fig.8 shows that the axial stress of confined concrete transfers smoothly from the first region to the second region in the stress-strain relation.

THE STRESS AT THE TRANSFERRING POINT FROM THE FIRST PART TO THE SECOND PART f_t

If $E_s \leqq 0$, then $f_t = f_{cc}$. On the other hand, if $E_s > 0$, when the axial strain of concrete cylinder increases sharply as the axial stress of concrete cylinder increases, the stress induced in concrete cylinder is defined as f_t.

Fig.9 shows the confinement effect vs. the axial stress f_t relation. When the axial stress reaches f_t, the tension induced in carbon fiber sheets is expressed as $\varepsilon_{CFt} \times E_{CF}$ (E_{CF} = elastic modulus of carbon fiber sheet). Therefore, confinement effect by carbon fiber sheet is expressed as $\varepsilon_{CFt} E_{CF} \times \rho_{CF}$. When the axial stress reaches the f_t, the circumferential strain of carbon fiber sheet ε_{CFt} is assumed as 1,500 μ. This reason for this is that the ε_{CFc} is about 1,100~2,500 μ when ρ_{CF} is in the range of 0.05~0.15% and the ε_{CFt} is about 1,800~2,500 μ when ρ_{CF} is large. By regressing the test data, the following relation is obtained as

$$\frac{f_t}{f_{co}} = 1.0 + 1.93\frac{\rho_{CF}\varepsilon_{CFt}E_{CF}}{f_{co}} \quad : \text{for circular confinement} \tag{7}$$

$$\frac{f_t}{f_{co}} = 1.0 + 1.53\frac{\rho_{CF}\varepsilon_{CFt}E_{CF}}{f_{co}} \quad : \text{for square confinement} \tag{8}$$

where f_{co} = the strength of unconfined concrete(N/mm^2).

Eq.(7) and Eq.(8) can reproduce the experiment results rather exactly in Fig.9.

THE STRAIN AT THE TRANSFERRING POINT FROM THE FIRST PART TO THE SECOND PART ε_t

In the same way, expressing confinement effect by carbon fiber sheet as $\varepsilon_{CFt} E_{CF} \times \rho_{CF}$, the axial strain of concrete cylinder ε_t vs. $\rho_{CF}\varepsilon_{CFt}E_{CF}/f_{co}$ relation is shown in Fig.10. By regressing the test data, the following relation is obtained as

$$\varepsilon_t = 0.00343 + 0.0939\frac{\rho_{CF}\varepsilon_{CFt}E_{CF}}{f_{co}} \quad : \text{for circular confinement} \tag{9}$$

$$\varepsilon_t = 0.00330 + 0.0995\frac{\rho_{CF}\varepsilon_{CFt}E_{CF}}{f_{co}} \quad : \text{for square confinement} \tag{10}$$

Eq.(9) and Eq.(10) can reproduce the experiment results rather exactly as shown in Fig.11.

THE SECOND GRADIENT E_g

Confining concrete cylinder with hoop reinforcement, because the tension induced in hoop reinforcement reaches yield strength at the second region, a certain fixed confining pressure keeps acting to concrete cylinder until the failure of concrete cylinder. On the other hand, confining concrete cylinder with carbon fiber sheet, because carbon fiber sheet keeps being in elastic range at the second region, the confining pressure acting to concrete cylinder keeps increasing until the failure of concrete cylinder.

It is known that the second gradient E_g is proportion to $f_{co}^2/\rho_s f_{yh}$ (ρ_s = the volumetric ratio of hoop reinforcement, f_{yh} = yield strength of hoop reinforcement) in confined concrete by hoop reinforcement[6]. However, in confined concrete by carbon fiber sheet, the increasing of the confining pressure at the second region must be considered. From Fig.4 and Fig.6, it is cleared that the second gradient E_g becomes larger as the ρ_{CF} or E_{CF} increases. Therefore, by expressing the effect of the increasing confining pressure as $\sqrt{\rho_{CF}}E_{CF}$, the second gradient is given as

$$E_g = \alpha\frac{f_{co}^{\ 2}}{\rho_{CF} f_{CF}} + \beta\sqrt{\rho_{CF}}E_{CF} \tag{11}$$

where α and β is calculated from test results.

Eq.(12) and Eq.(13) shows the result of α and β calculated with a regression analysis.

$$E_g = -7.427\frac{f_{co}^{\ 2}}{\rho_{CF} f_{CF}} + 0.086\sqrt{\rho_{CF}}E_{CF} \text{ : for circular confinement} \tag{12}$$

$$E_g = -13.726\frac{f_{co}^{\ 2}}{\rho_{CF} f_{CF}} + 0.023\sqrt{\rho_{CF}}E_{CF} \text{ : for square confinement} \tag{13}$$

When $E_g<0$, the second gradient E_g is defined as average of modulus from the strain corresponding to the peak stress ε_{cc} to the ultimate strain ε_{cu} as shown in Fig.11(a). When $E_g \geqq 0$, the second gradient E_g is defined as average of modulus from the axial strain ε_t to the ultimate stain ε_{cu} as shown in Fig.11(b).

THE ULTIMATE STRAIN ε_{cu}

Fig.4 shows that the ultimate strain ε_{cu} of confined concrete by the carbon fiber sheet increases as ρ_{CF} increases. Fig.6 shows that the ultimate strain ε_{cu} becomes larger in confined concrete by normal-modulus type than by high-modulus type, because the rupture strain ε_{CFu} of normal-modulus type is larger than that of high-modulus type. Therefore, ρ_{CF} and ε_{CFu} is

considered as parameters influencing to the ultimate strain ε_{cu}.

Fig.12 shows the relation between ε_{cu} and $\rho_{CF} f_{CF} / E_{CF}$.

From a regression analysis, the following relation is obtained as

$$\varepsilon_{cu} = 1.384\sqrt{\rho_{CF}\left(\frac{f_{CF}}{E_{CF}}\right)} \text{ : for circular confinement} \quad (14)$$

$$\varepsilon_{cu} = 1.212\sqrt{\rho_{CF}\left(\frac{f_{CF}}{E_{CF}}\right)} \text{ : for square confinement} \quad (15)$$

COMPARISON WITH TEST RESULTS

To show the effectiveness of the proposed model, the stress-strain relation calculated by proposed model was compared with the test results as shown in Fig. 13.

From this comparison, it is observed that the proposed model provides good agreement with test results.

Fig.14 shows that the stress-strain relation calculated by the volumetric ratio of hoop reinforcement ρ_s equivalent to carbon fiber ratio ρ_{CF}, based on "Guide Specifications for Reconstruction and Repair of Highway Bridges Which Suffered Damage due to the Hyogo-ken Nanbu Earthquake".

Both the axial stress and the ultimate strain Calculated based on Guide Specifications is evaluated more excessively than the test results.

CONCLUSION

To propose a stress-strain model of confined concrete with carbon fiber sheets, a series of loading tests were conducted for twenty-two confined concrete specimens. The conclusion from the study presented herein may be deduced as;

1) When ρ_{CF} is in the range of 0.05~0.15%, the peak stress of concrete f_{cc} is about 37~41N/mm^2 and the strain corresponding to the peak stress ε_{cc} is about 2,500~3,000 μ regardless of the carbon fiber ratio ρ_{CF} and the cross sectional shape of concrete cylinder. However, the deteriorating rate of the stress after the peak stress decreases and the strain of concrete at the rupture of the carbon fiber sheet increases as the carbon fiber ratio ρ_{CF} increases.

2) When ρ_{CF} is larger than a certain value, the stress of concrete keeps increasing without the deterioration of the stress until the rupture of the carbon fiber sheet. However, when the strain of concrete cylinder reaches 3,000~3,500 μ, the increasing rate of the stress in a stress-strain relation becomes smaller.

3)Defining the strain of the carbon fiber sheet at the peak stress of concrete as ε_{CFc} in the range of the carbon fiber ratio from 0.05 to 0.15%, the is about 1,100~2,500 μ. Defining the strain of the carbon fiber sheet where the gradient changes from the initial value to the second gradient as ε_{CFt} in the carbon fiber ratio of 1.336%, the ε_{CFt} is about 1,800~1,900 μ. The value of ε_{CFc} is almost the same as the value of ε_{CFt}. Therefore, over the strain 1,100~2,500 μ induced in the carbon fiber sheet, the concrete cylinder started to fail and the axial stress of concrete decreased sharply.

4)Considering four factors for controlling the stress-strain relation of confined concrete f_l, ε_l, E_s and ε_{cu}, a model of stress vs. strain of confined concrete by the carbon fiber sheet is proposed as Eq.(2),Eq.(3) and Eq.(6).

5)The proposed model seems to provide good agreement with the test results of confined concrete by the carbon fiber sheet.

REFERENCES

1) Ministry of Construction: Report on the Damage of Highway Bridges by the Hyogo-ken Nanbu Earthquake, Committee for Investigation on the Damage of Highway Bridges Caused by the Hyogo-ken Nanbu Earthquake, 1995

2) Japan Road Association: Guide Specifications for Earthquake Hazard Mitigation for Road Transportation Facilities, Pre Earthquake Countermeasures, 1987

3) Kawashima, K., Nishikawa, K., Nakano, M., Unjoh, S., Kimura, Y. and Hoshikuma, J.: Guide Specifications for Reconstruction and Repair of Highway Bridges which suffered damage due to the Hyogo-ken Nanbu Earthquake, Proc. 28th Joint Meeting of the UJNR Panel on Wind and Seismic Effects, NIST Special Publication SP 904, pp. 159-174, 1996

4) Kawashima, K.: Impact of Hanshin/Awaji Earthquake on Seismic Design and Seismic Strengthening of Highway Bridges, Report No. TIT/EERG 95-2, Department of Civil Engineering, Tokyo Institute of Technology, 1996

5) Uji, K., Yokota, K. and Ikeda, S.: Property of RC Structure Reinforced with Sheet Type Carbon Fiber, Proceedings, Japan Concrete Institute, Vol.148, No.2, pp695-700, 1992

6) Hoshikuma, J., Kawashima, K. and Nagaya, K.: A Stress-Strain Model for Reinforced Concrete Columns Confined by Lateral Reinforcement, Journal of Materials, Concrete Structures and Pavements, Japan Society of Civil Engineers, No.520, V-28, pp.1-11, 1995.8

Table 1 Test Specimens

Series		Section	Size	Strength of Concrete (N/mm^2)	Carbon Fiber Sheet		
					Nominal Elastic Modulus (N/mm^2)	Weight of Carbon per Unit Area (g/m^2)	ρ_{CF} (%)
N	N-1	Circular	ϕ200mm ×h 600mm	30	–	–	–
	N-2						
	N-3						
	N-6	Square	□200mm ×h 600mm				
	N-7						
	N-8						
S	S-1	Circular	ϕ200mm ×h 600mm	30	2.30×10^5	200	0.056
	S-2						0.111
	S-3						0.167
	S-4					300	1.336
	S-9	Square	□200mm ×h 600mm			200	0.056
	S-10						0.111
	S-11						0.167
	S-12					300	1.336
H	H-1	Circular	ϕ200mm ×h 600mm	30	3.92×10^5	300	0.169
	H-2						0.338
	H-3						0.676
	H-4						1.352
	H-5	Square	□200mm ×h 600mm				0.169
	H-6						0.338
	H-7						0.676
	H-8						1.352

Table 2 Mechanical Properties of Carbon Fiber Sheet

		Normal Elastic Modulus Type		High Elastic Modulus Type
Design Value	Weight of Carbon per Unit Area (g/m^2)	200	300	300
	Thickness (mm)	0.111	0.167	0.163
	Tensile Strength (N/mm^2)	3,481		2,942
	Elastic Modulus (N/mm^2)	2.30×10^5		3.92×10^5
	Rupture Strain (%)	1.5	1.5	1.0
Measured	Weight of Carbon per Unit Area (g/m^2)	200	300	309.5
	Thickness (mm)	0.110	0.167	0.169
	Tensile Strength (N/mm^2)	4,227	4,433	3,972
	Elastic Modulus (N/mm^2)	2.43×10^5	2.52×10^5	4.39×10^5
	Rupture Strain (%)	1.74	1.76	0.90

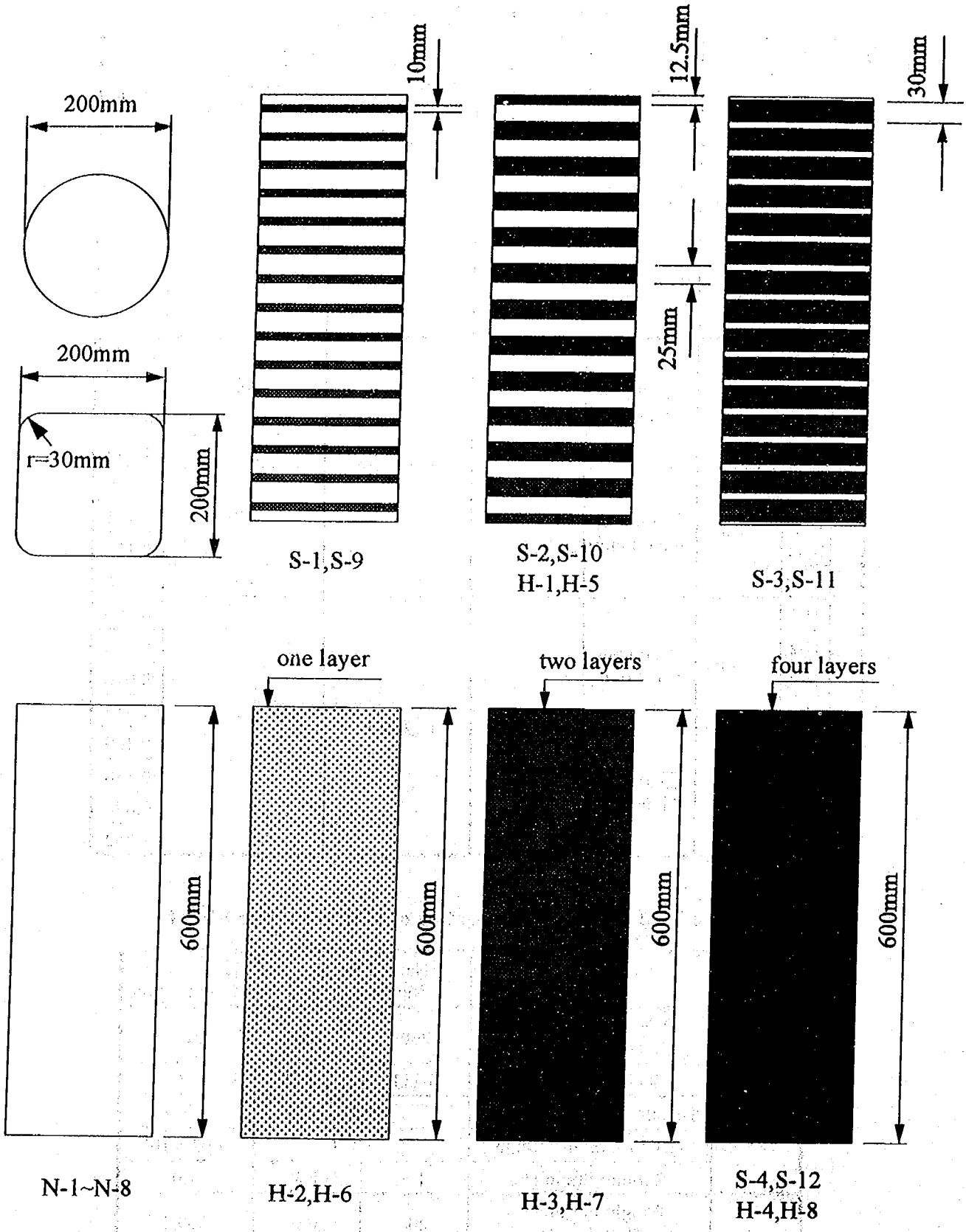


Fig.1 Adhesion of Carbon Fiber Sheet

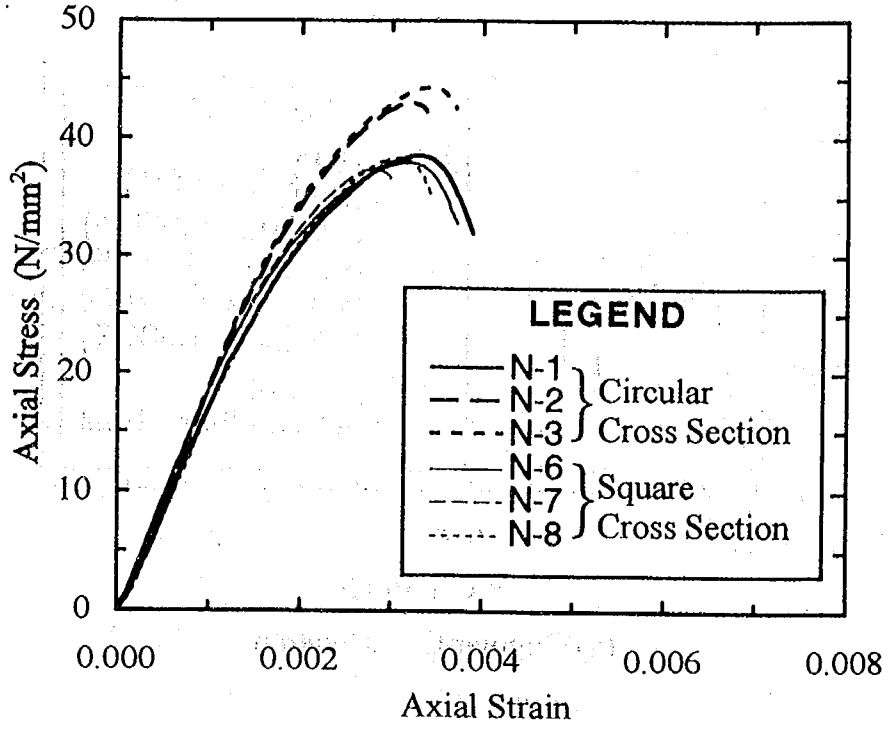


Fig.2 Stress vs.Strain Relation of Unconfined Concrete Cylinders

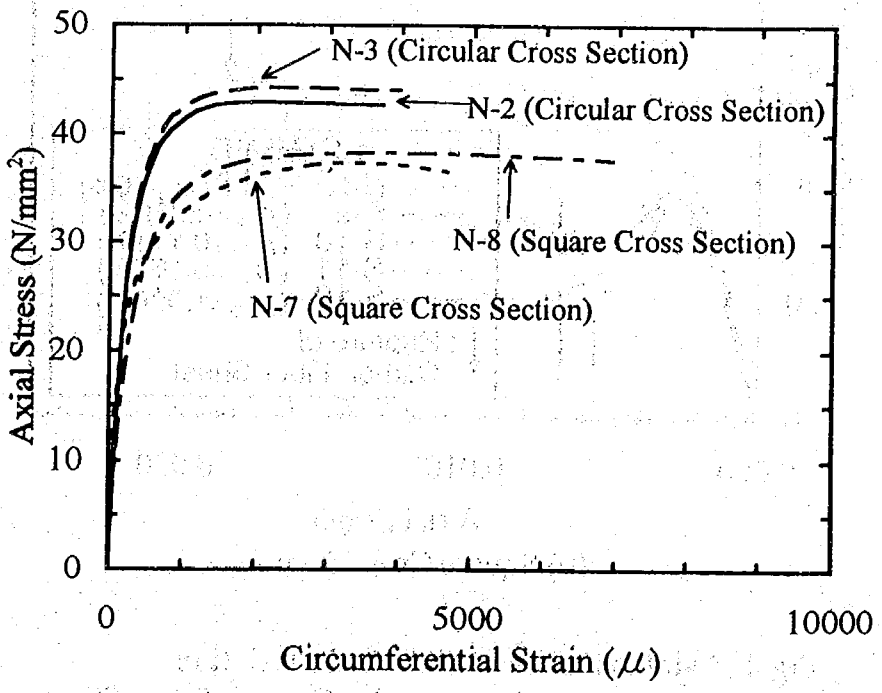
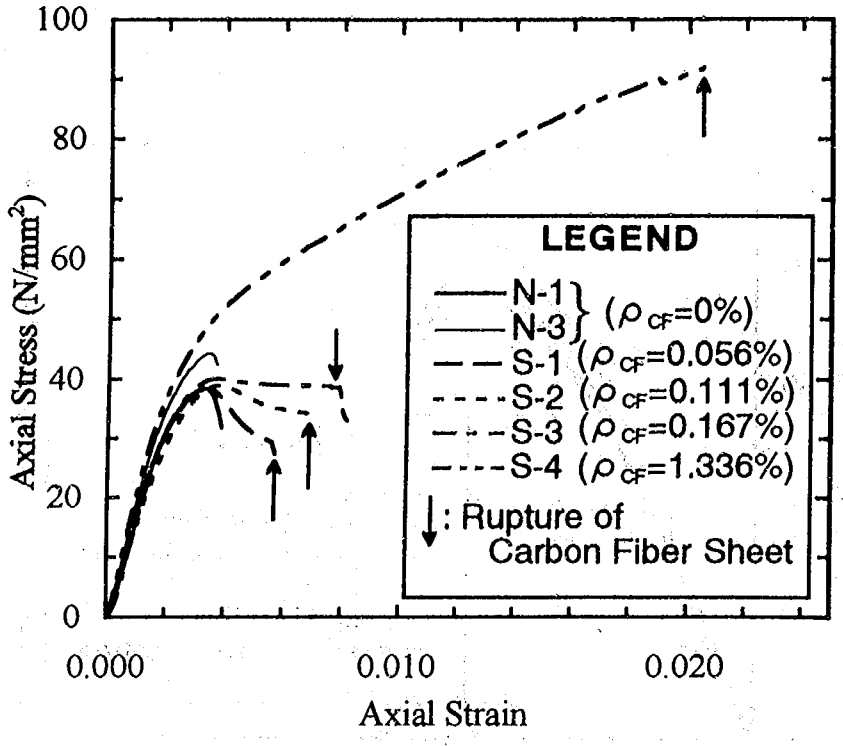
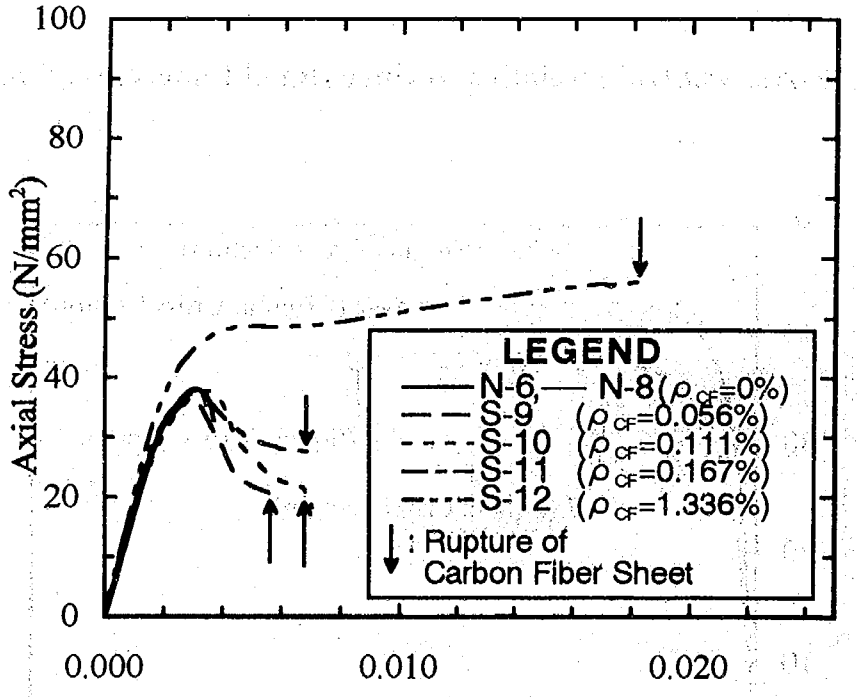


Fig.3 Axial Stress vs. Circumferential Strain of Unconfined Concrete Cylinders

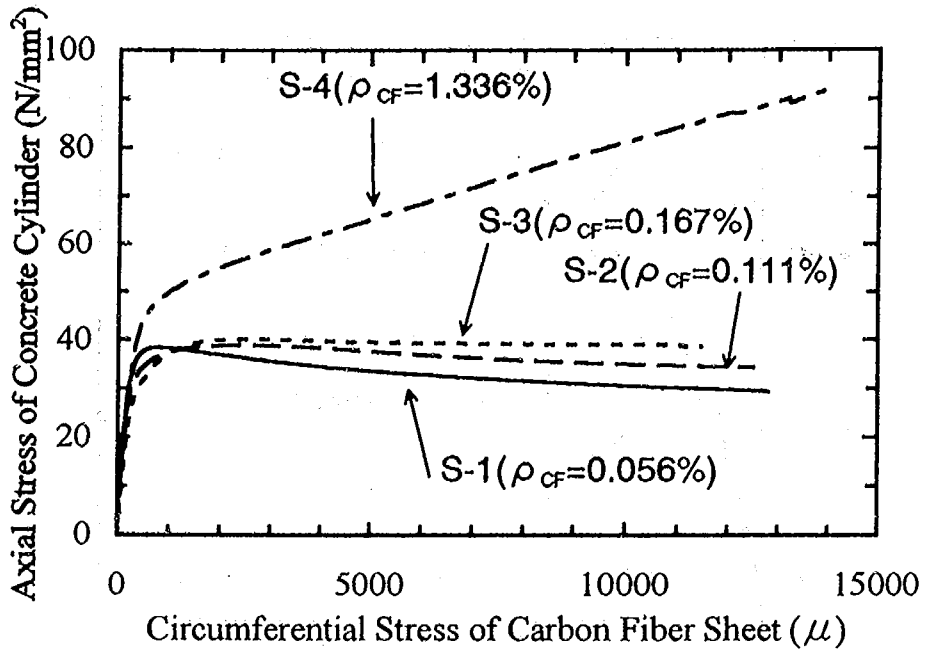


(a) Circular Cross Section

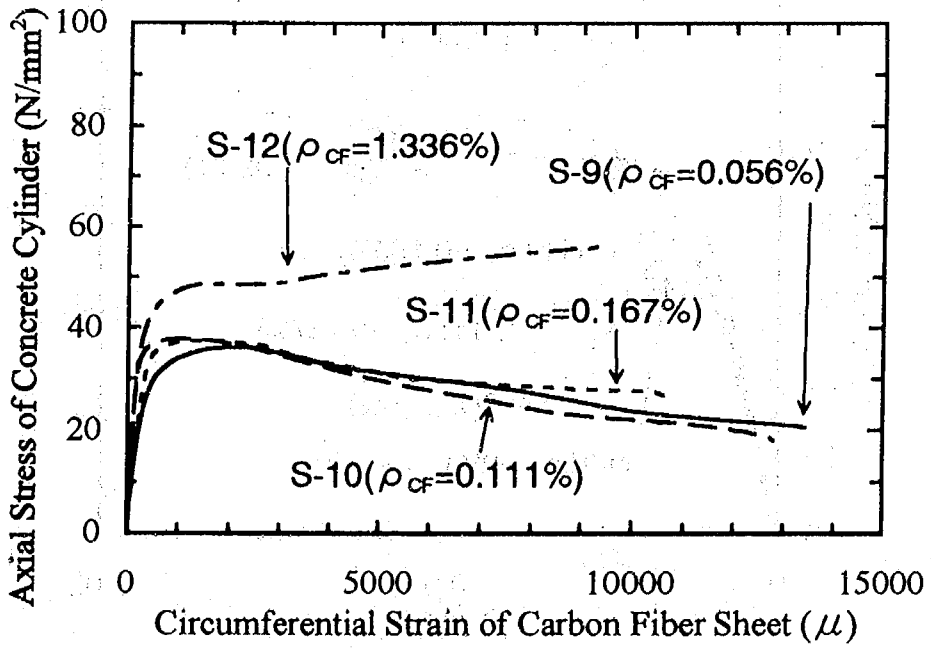


(b) Square Cross Section

Fig.4 Axial Stress vs. Axial Strain Relation of Confined Concrete by Carbon Fiber Sheet

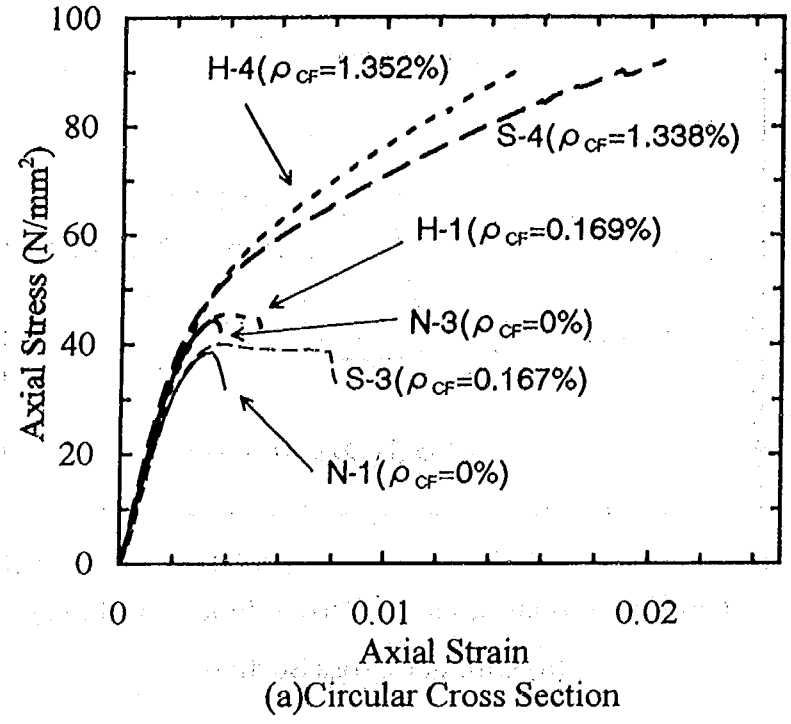


(a) Circular Cross Section

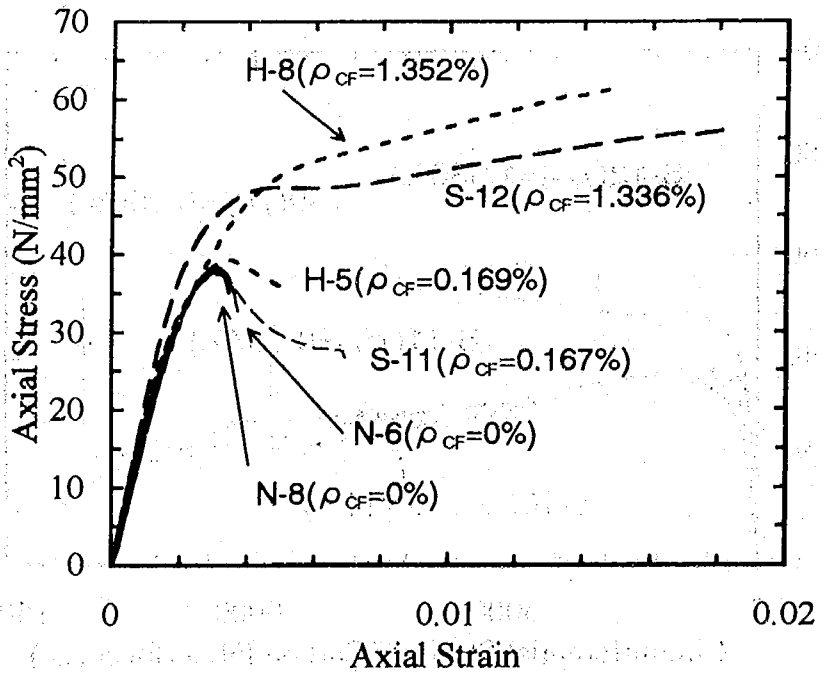


(b) Square Cross Section

Fig.5 Relation between Axial Stress of Concrete and Circumferential Strain of Cabon Fiber

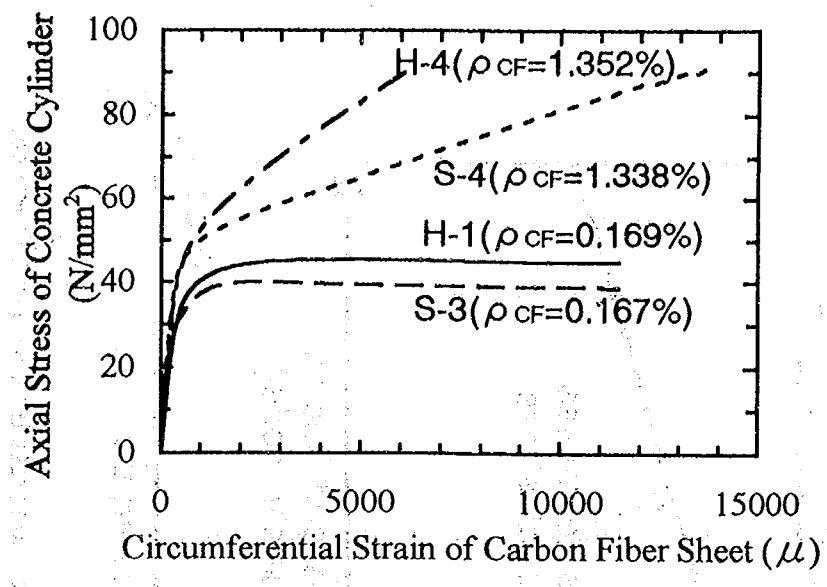


(a)Circular Cross Section

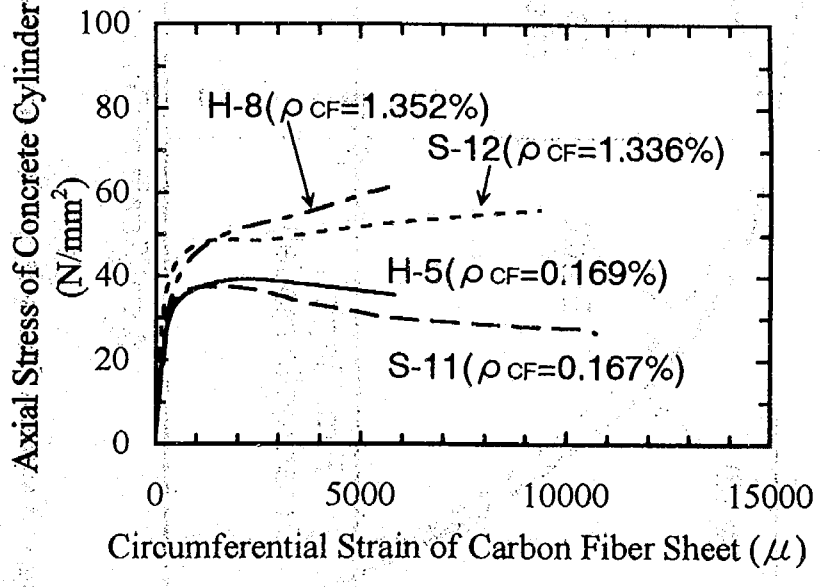


(b) Square Cross Section

Fig.6 Comparison the Stress-Strain Curve of Confined Concrete by the Normal-Modulus Type Carbon Fiber Sheet with by the High-Modulus Type in Same ρ_{CF}-value



(a) Circular Cross Section



(b) Square Cross Section

Fig.7 Comparison Relation Axial Stress of Concrete and Circumferential Strain of Carbon Fiber Sheet by Normal-Modulus Type Carbon Fiber Sheet with by High-Modulus Type Carbon Fiber Sheet in Same ρ_{CF}-Value

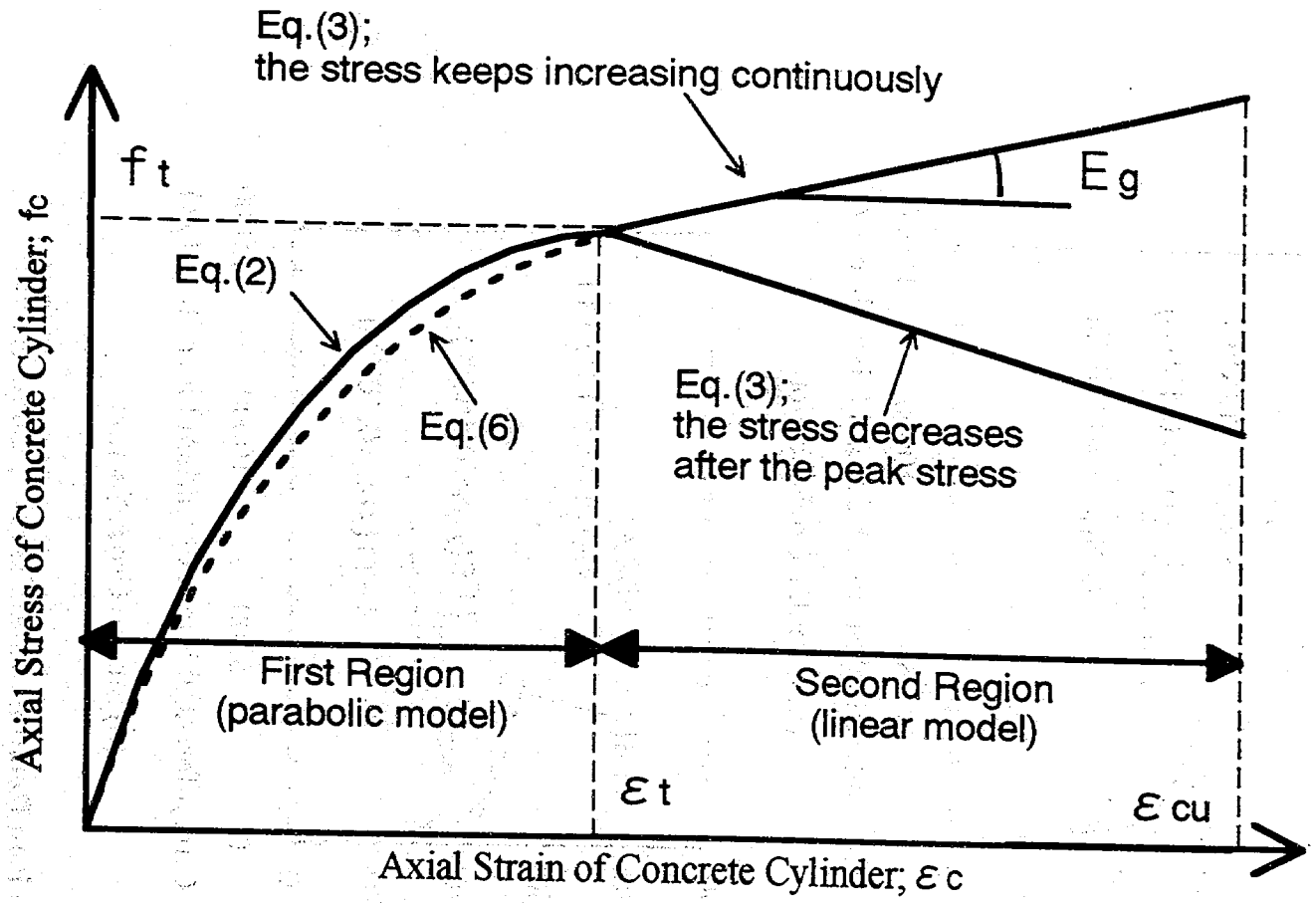
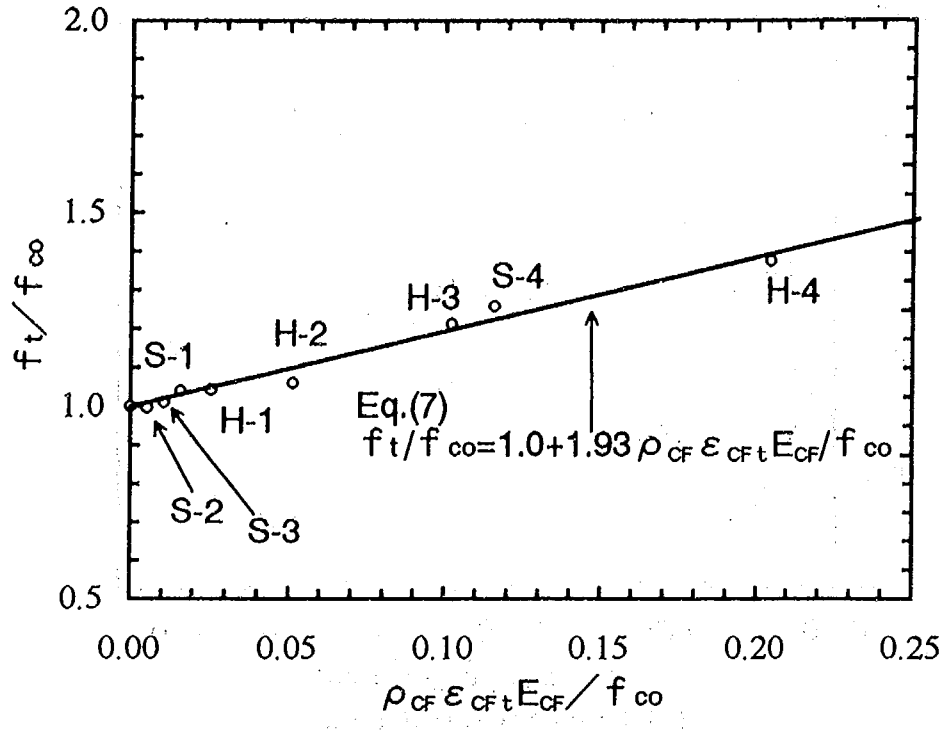
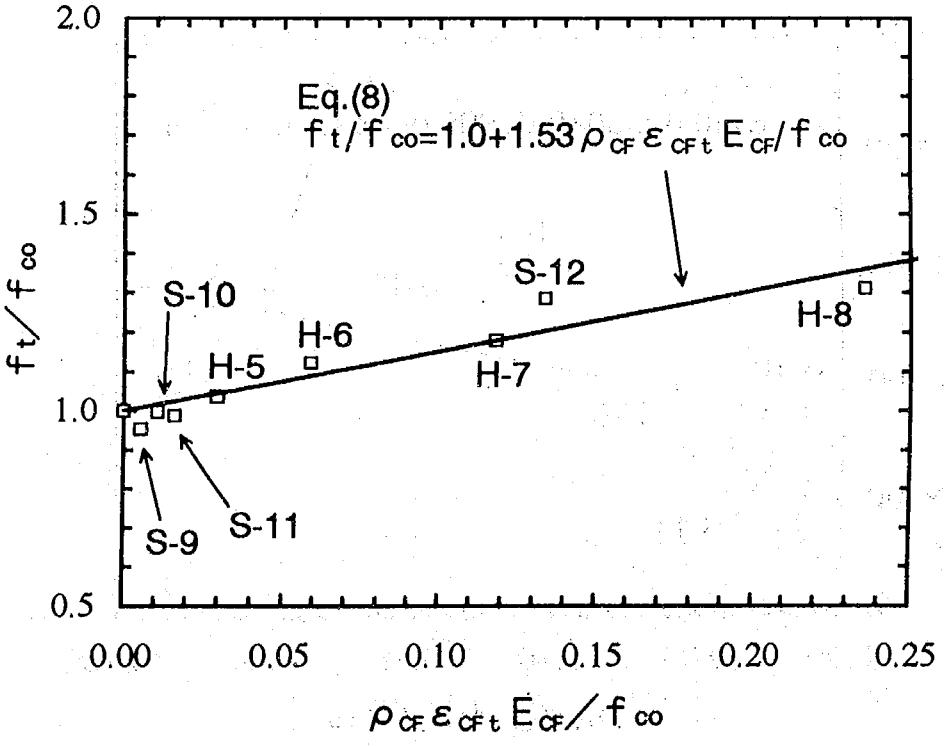


Fig.8 Proposed Stress-Strain Relation of Confined Concrete by Carbon Fiber Sheet

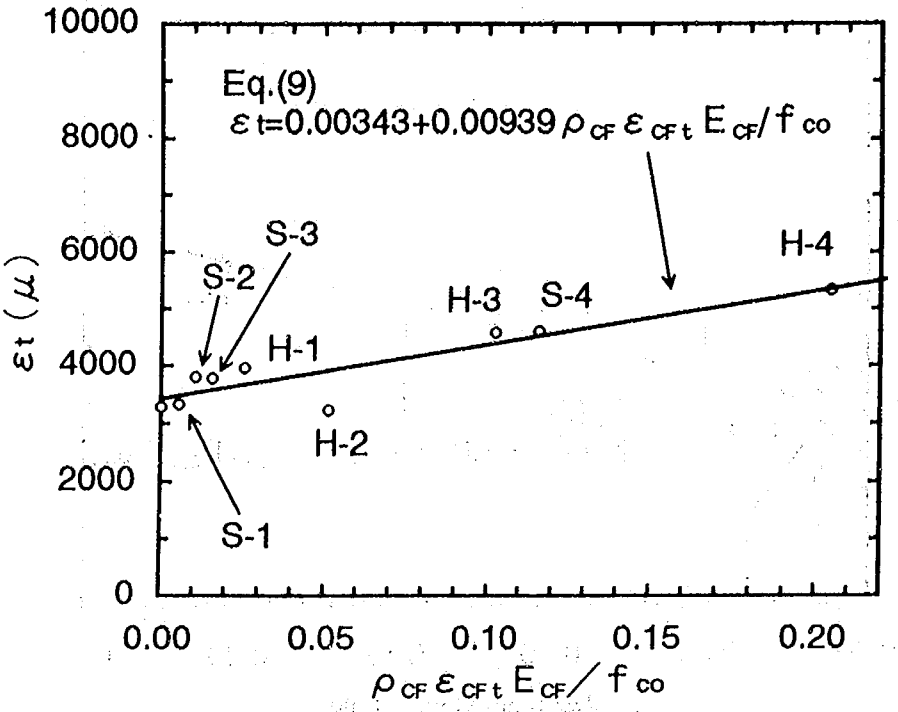


(a) Circular Cross Section

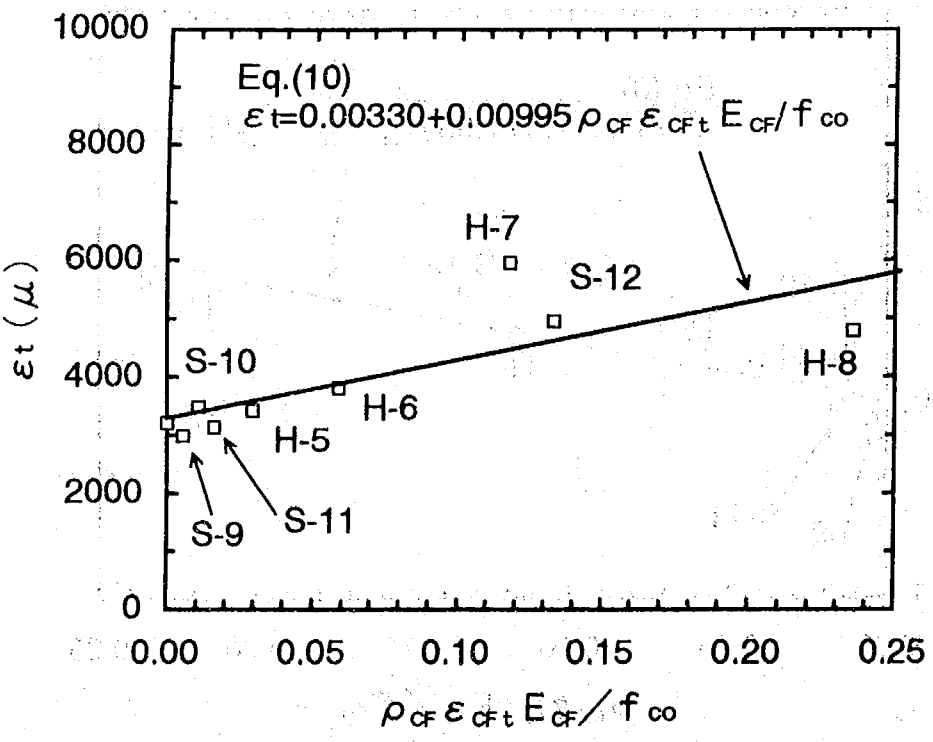


(b) Square Cross Section

Fig.9 Relation between Confinement Effectiveness and the Axial Stress; ft

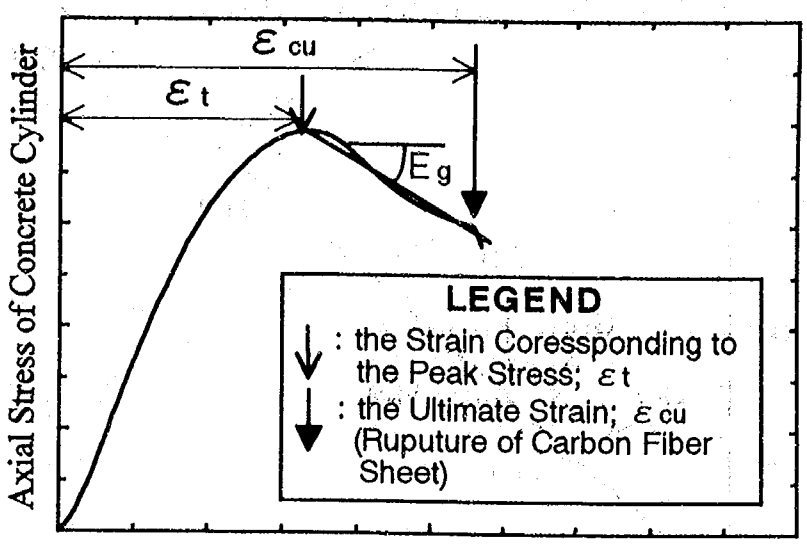


(a) Circular Cross Section

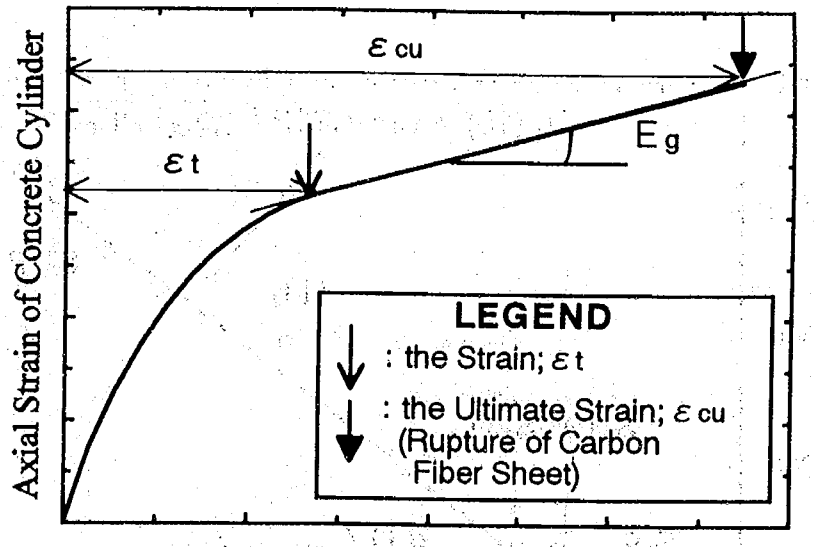


(b) Square Cross Section

Fig.10 Relation between Confinement Effectiveness and the Axial Strain; ε_t

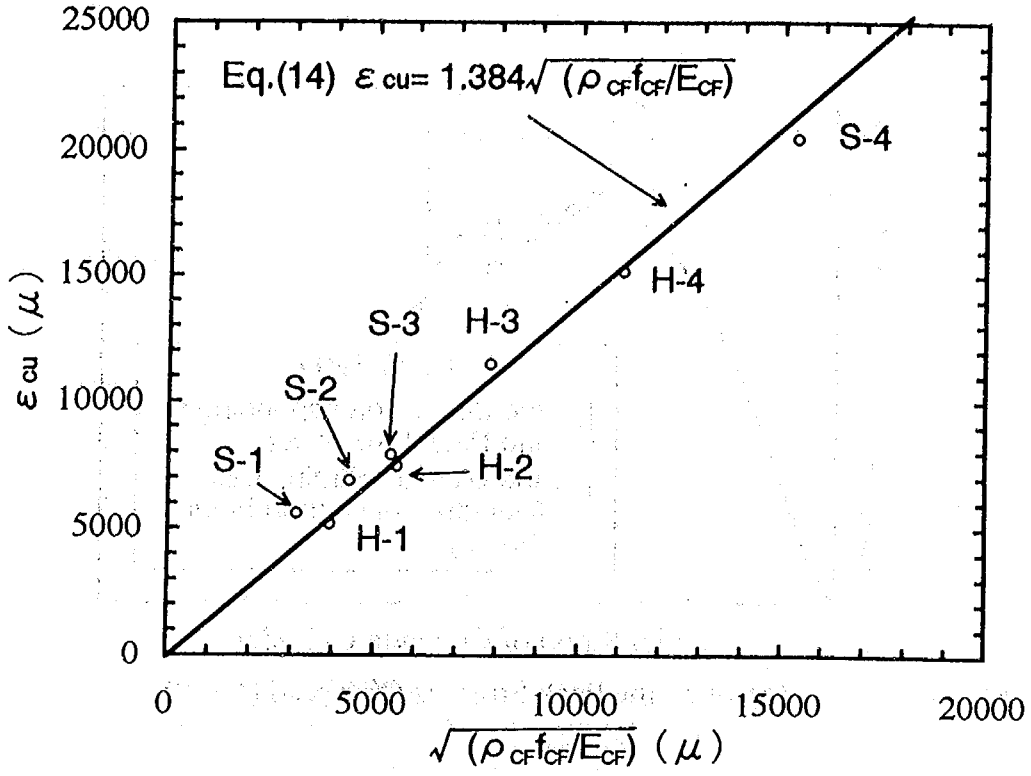


(a) when the Peak Stress is Observed ($E_g<0$)

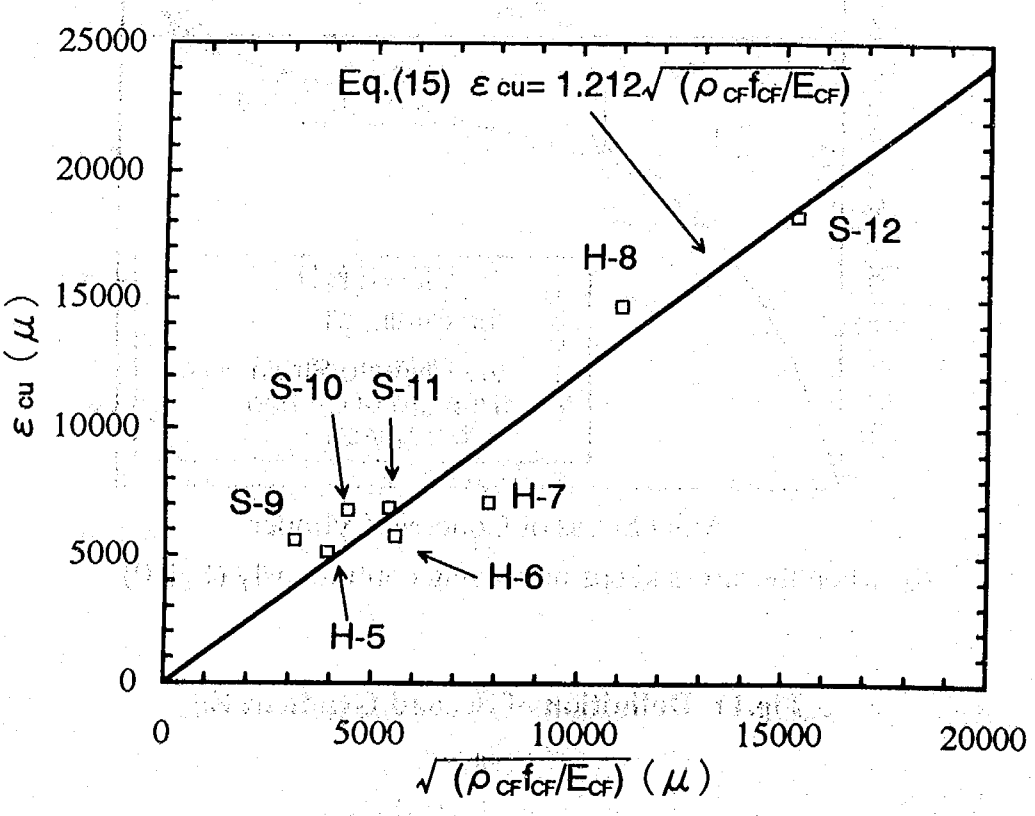


(b) when the stress keeps increasing continuously ($E_g \geqq 0$)

Fig.11 Definition of Second Gradient E_g

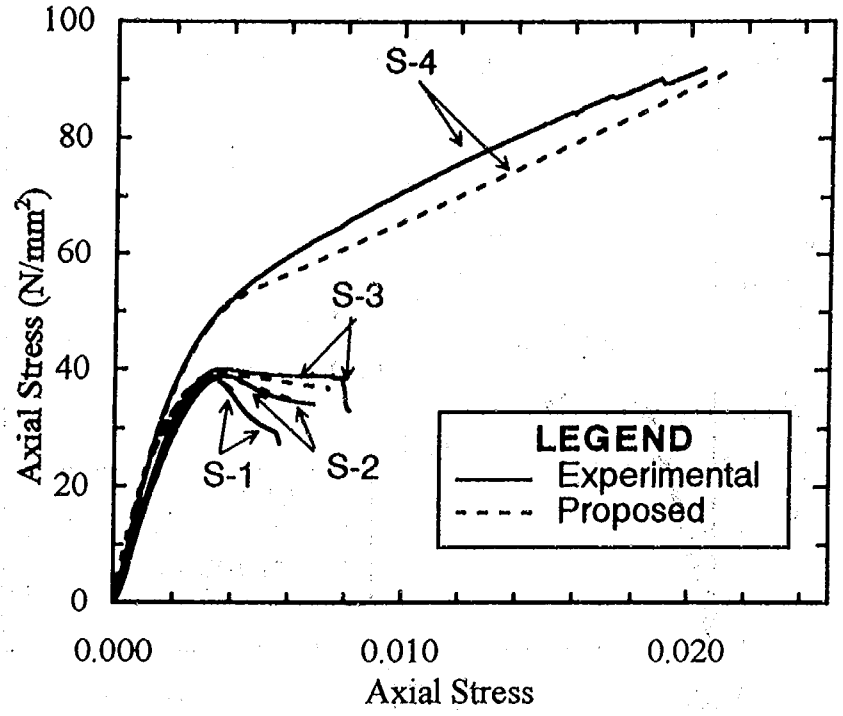


(a) Circular Cross Section

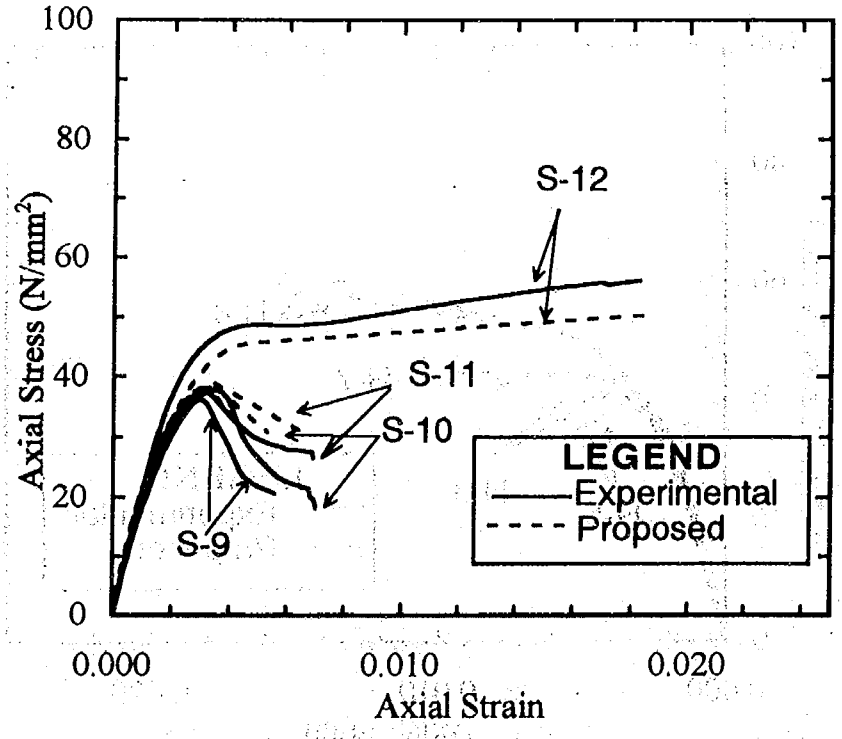


(b) Square Cross Section

Fig.12 Relation between Confinement Effectiveness and Ultimate Strain ε_{cu}

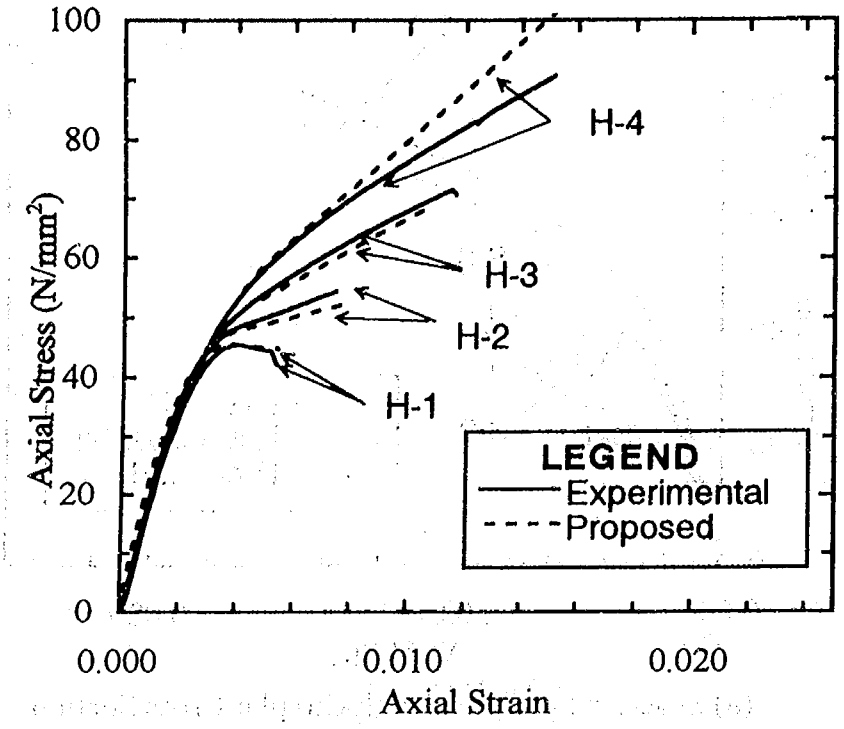


(a) S-Series Specimens with Circular Cross Section

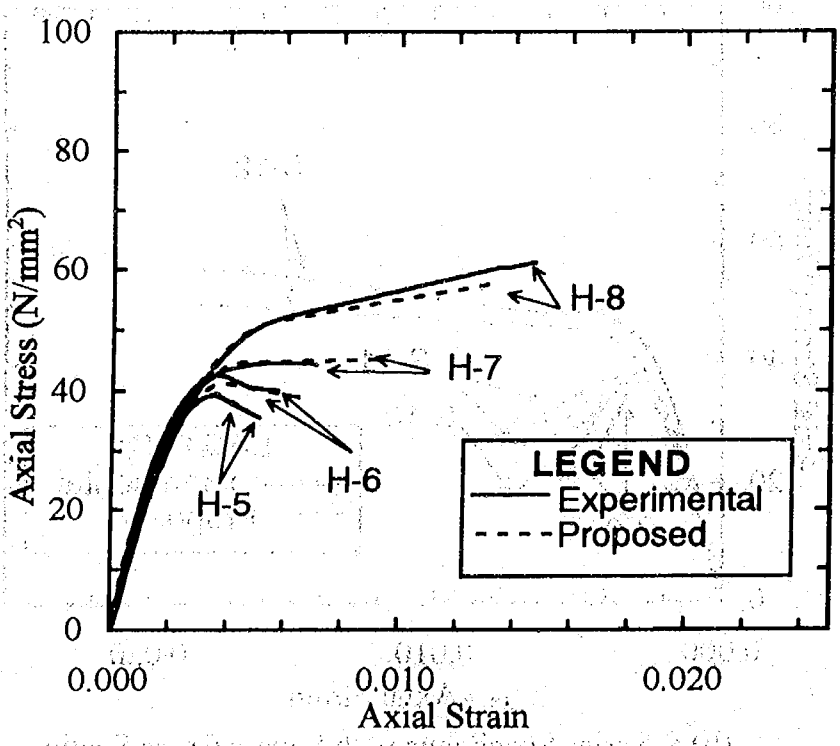


(b) S-Series Specimens with Square Cross Section

Fig.13 Comparison with Stress-Strain Curve between Test Results and Proposed Model

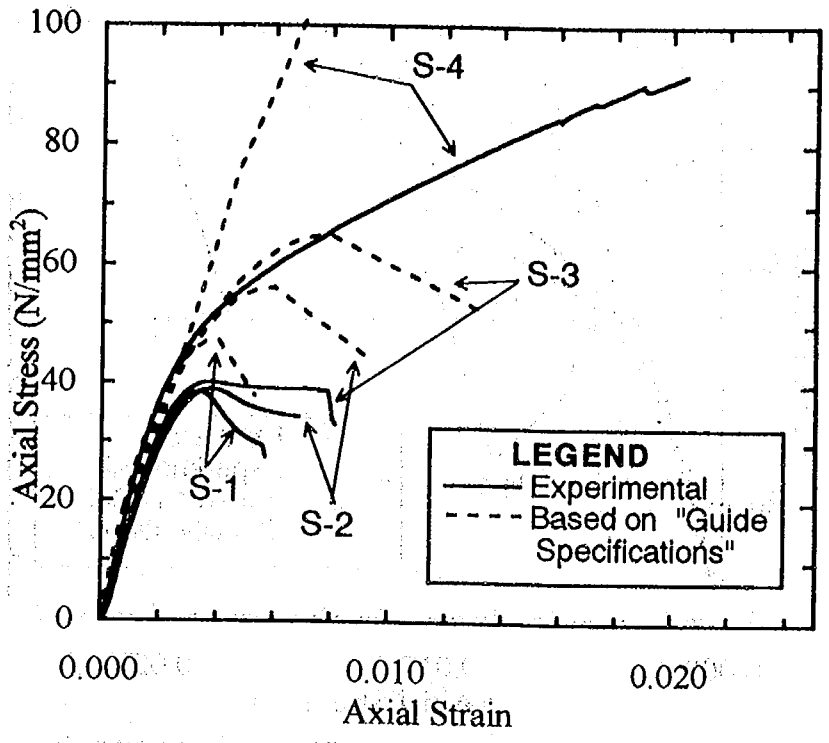


(c) H-Series Specimens with Circular Cross Section

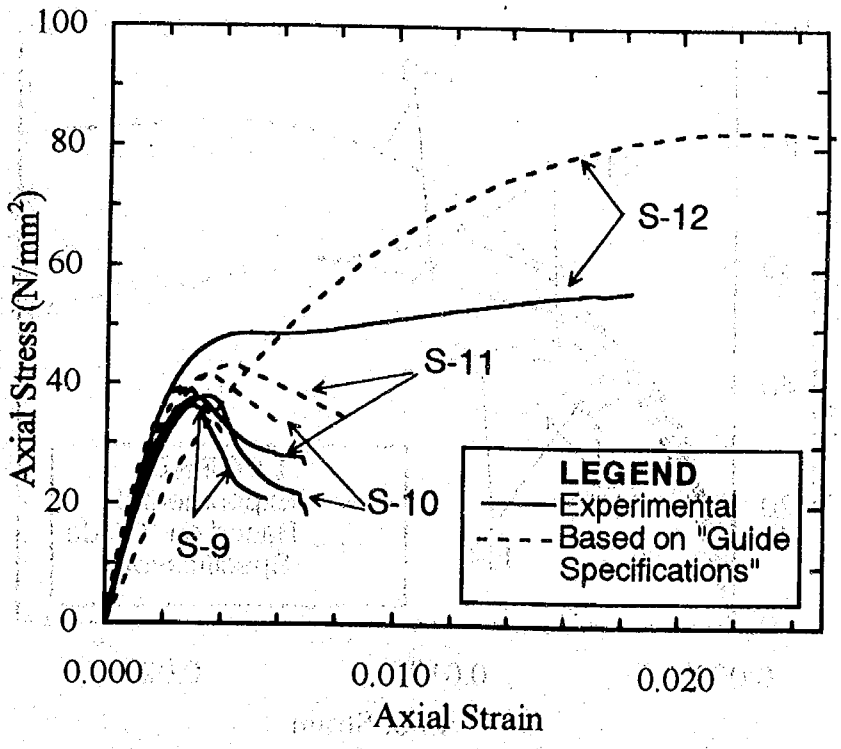


(d) H-Series Specimens with Square Cross Section

Fig.13 continued

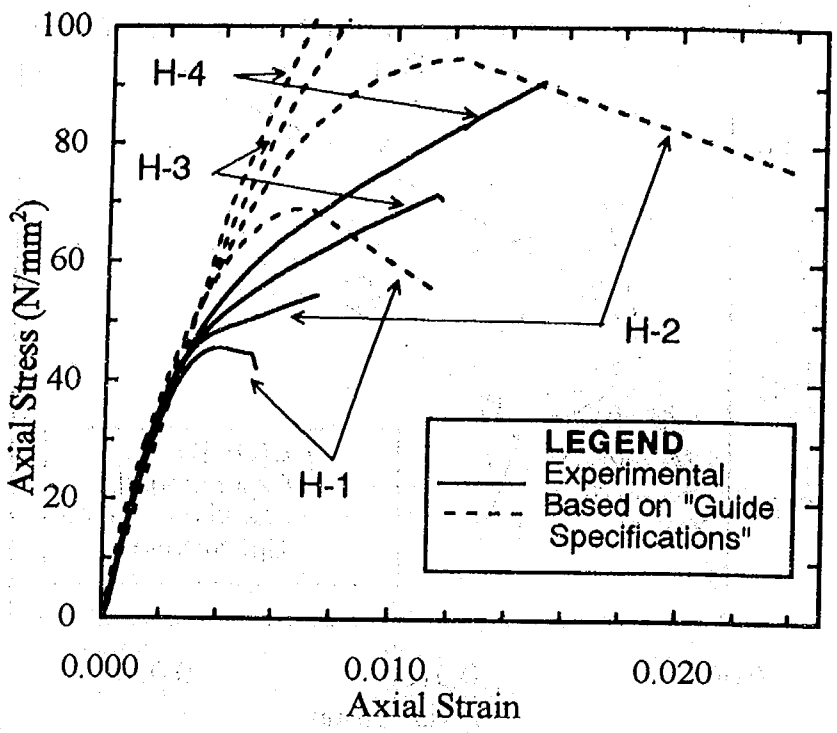


(a) S-Series Specimens with Circular Cross Section

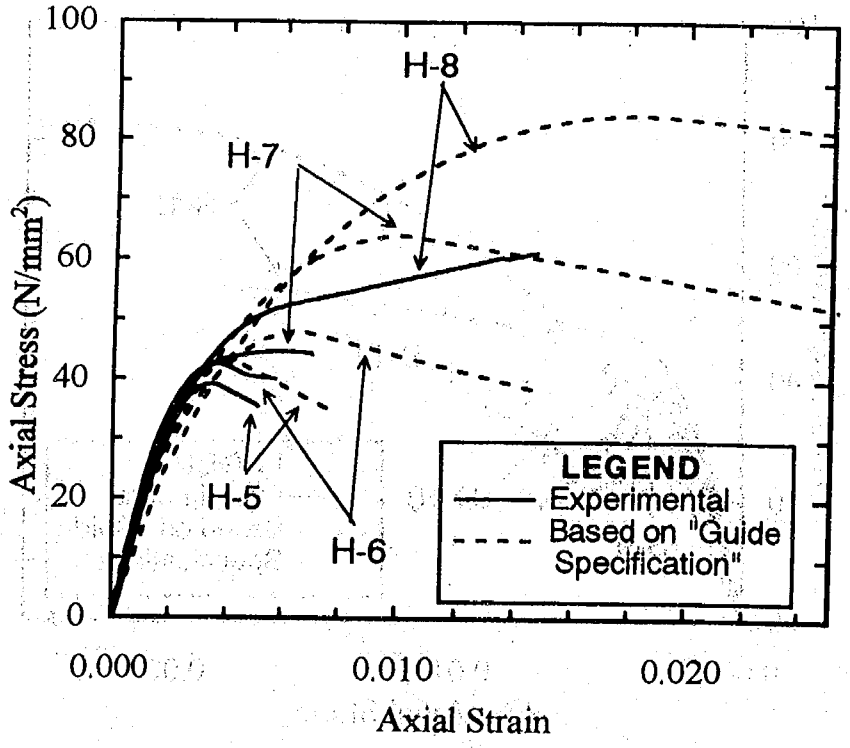


(b) S-Series Specimens with Square Cross Section

Fig.14 Comparison Stress-Strain Curve Calculated Based on "Guide Specifications" with Test Results



(c) H-Series Specimens with Circular Cross Section



(d) H-Series Specimens with Square Cross Section

Fig.14 continued

The 3rd US-Japan WS on Seismic Retrofit of Bridges
Osaka City, Japan, December 10-11, 1996

Experimental Study Concerning Retrofit of RC Column by CFRP Sheet

Fumio Hakamada [1], Yorimichi Maekawa [1] and Jun-ichi Hoshikuma [2]

1).Structural Engineer, Maintenance Division, Hanshin Expressway Public Corporation
2).Research Engineer, Earthquake Engineering Division, Public Works Research Institute, Tsukuba Science City, Japan

ABSTRACT

A set of experiment was implemented for RC cantilever column retrofitted by Carbon Fiber Reinforced Plastic(CFRP) sheet. The objective of the retrofit is ductility enhancement or bending capacity strengthening at column base for columns of round as well as rectangular cross section. An additional experiment on rectangular section is also shown and discussed. An analysis is made before each experiment based on a crude estimate of the structural behavior so that it could explain the phenomena of the experiment. Then design method is briefly discussed. Review of the experiment is shown and inherent problems are to be pointed out for further study.

1. INTRODUCTION

Recent earthquake hit Kobe 1995 revealed that some of the reinforced concrete column exhibits brittle shear failure when the structure is built before 1970. Besides, current earthquake design code, called Tentative design code for repair of damaged Kobe line ordered by Ministry of Construction enacted Feb.9 1995[1](hereafter called Tentative Code), and subsequent requirements specify each bridge column abide by the revised one. So overall strengthening program of existing columns has got started. As for the columns in urban area, ones for urban highway, because of limited land use, retrofit by steel plate jacket is preferred to RC jacket in general. But when the space is further so limited that heavy machinery is not free to introduce, or no further thickness is allowed at all, sometimes the general method can not be applied. Retrofit by CFRP sheet is yet common as a tool of seismic retrofit at column base, but could be advantageous in this situation in various respects. In order to clarify structural uncertainty and to be utilized for design purpose, an experimental study was made through 6 specimens of 7 tests.

2. RC RETROFIT IN GENERAL

In general RC column retrofit can be classified as Table 1 from a view point of materials used. On the other hand from a view point of objectives, RC retrofit can be divided as shown in Table 2

Retrofit for strengthening of premature termination is well established, so no discussion is made here.

Though it is still not certain of the structural behavior of CFRP retrofitted column during earthquake, it is widely presumed one of the effective methods of retrofit design. Several experiments are conducted to investigate the structural behavior of retrofitted column in

comparison with base model, and several observations are revealed so that they will be utilized for the practical application.

Table 1 Material Classification
1. RC jacket
2. Steel plate jacket
3. CFRP jacket
4. PC tendon

Table 2 Objective Classification
1. Shear capacity strengthening
2. Ductility enhancement
3. Moment capacity strengthening
4. Strengthening of premature termination

In the following paper the following nomenclature was used with the definitions below.

BASE SPECIMEN: "base" identical model for which any retrofit is made.

SHEAR CAPACITY STRENGTHENING: One of the objectives of retrofit where transverse strengthening is made so that column would not exhibit shear failure.

DUCTILITY ENHANCEMENT: One of the objectives of retrofit where transverse strengthening is made so that column exhibits larger ductility, with virtually no strength increase.

MOMENT CAPACITY STRENGTHENING: One of the objectives of retrofit where longitudinal reinforcement is added so that bending moment increase is achieved. Ductility enhancement is accompanied.

Figure 1 shows the illustrative concepts of each.

SHEAR FAILURE: One of failure modes when shear strength is less than yield strength of the section, column fails before it reaches yield strength.

BENDING SHEAR FAILURE: One of failure modes when shear strength is greater than yield strength but less than ultimate bending strength, column fails between its yield and ultimate.

BENDING FAILURE: One of failure modes when shear strength is greater than ultimate bending strength, and column sustains its full ultimate capacity to fail by bending.

Figure 2 shows each failure point in load deflection curve.

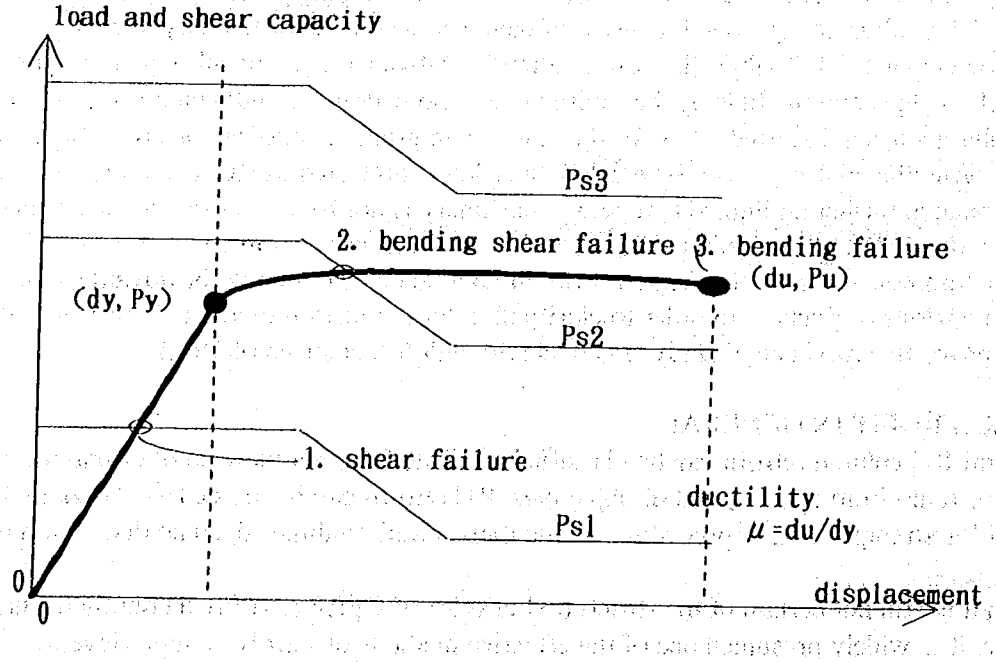
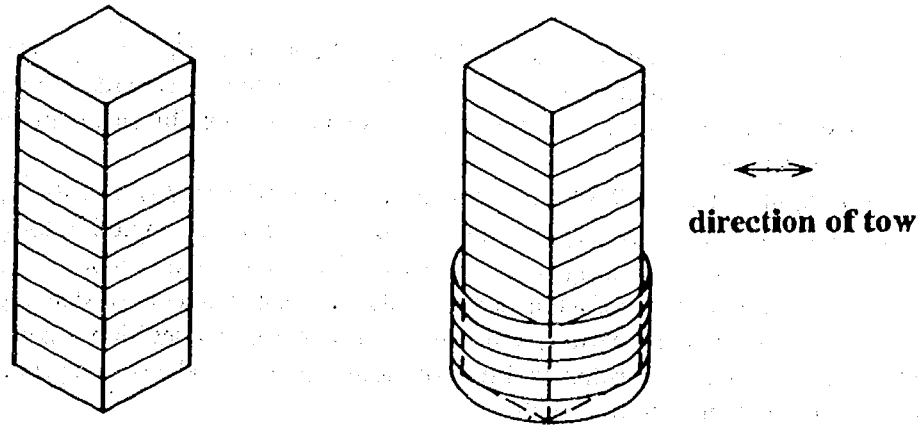
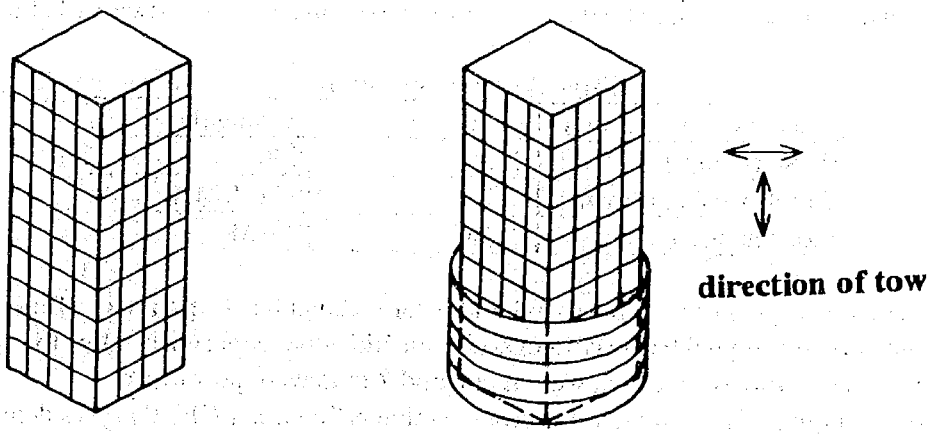


Figure 2 Load deflection curve and failure modes



(1)Shear capacity strengthening and Ductility enhancement



(2)Moment capacity strengthening

Figure 1 Illustrative view of CFRP retrofit

YIELD POINT: State is called when one of the strain gauges of tension rebar exhibits yield strain at the column base.

ULTIMATE STATE: State is called when an envelop of hysteresis so deteriorates after peak that reaction is less than 80% of the maximum.

CFRP: Carbon Fiber Reinforced Plastic, Carbon Fiber impregnated by epoxy.

Generally speaking because of the insufficiency of confinement, rectangular section reveals less ductility compared with round column. This effect is taken into consideration in Tentative Code. This is caused by the fact that the rectangular section cannot exhibit full confinement but only at corners of the section.

As for an application of CFRP, it is shown that Japan Highway Authority [2] performs for aseismic retrofit at premature termination, where CFRP sheet is adopted in longitudinal direction at mid section so that plastic hinge location is transformed to column base. It may be stated it is not so common to introduce CFRP as a tool of ductility enhancement or bending moment strengthening. There exist various concerns, such as working condition, maintenance, durability, scale factor, economics or aesthetics, but structural behavior analysis and proposal of design method are the first steps to deal with.

3. EXPERIMENT

3.1 SPECIMEN AND LOAD CONDITION

A prototype of existing column was chosen to be modeled in the experiment, for round and circular shape as well. The scale was chosen so that the specimen is within the capacity of the laboratory in Public Research Work Institute.

Two representative column shapes were chosen. Both are RC single column with round and rectangular cross section. And taking into account of the capacity of the research laboratory, 1/5 model was chosen. The identical number of the experiment is as shown in Table 3.

Table 3 List of specimen

objective/cross section	round	rectangular
(base column)	C00	S00
ductility enhancement	C21	S41, S21K
moment strengthening	C21M	S21M

There are 6 specimens, 3 for round and 3 for rectangular. Experiment of one of the rectangular column was interrupted halfway to exercise an additional experiment after the specimen is repaired. Therefore 6 specimen were made and 7 tests were performed.

For example, S41 shows that the cross section is Square, 4 CFRP layers delivered at base and 1 the rest. Figure 3 (1)~(7) show each specimen. All retrofit is made to base model so that the effect of CFRP becomes apparent. Numbers of the sheet was selected so that it will exercise structural behavior in a model as expected. It can be stated all experiment was executed to consolidate the assumed analysis method shown later.

C21 and S41 are models of shear capacity strengthening. After shear failure is prevented ductility enhancement is also intended. All reinforcement is made by CFRP in circumferential direction at base model. For rectangular section the corner is rounded with radius of 50mm so that CFRP will not rupture by sharp edge. The lap length in the fiber direction is 20cm, and 0 in transverse direction. These values are absolute, not to be scaled down.

In a Tentative Code ordered by MOC, there appear many cases that moment strengthening is required. Though it is not appropriate to apply CFRP material to this objective, as long as where

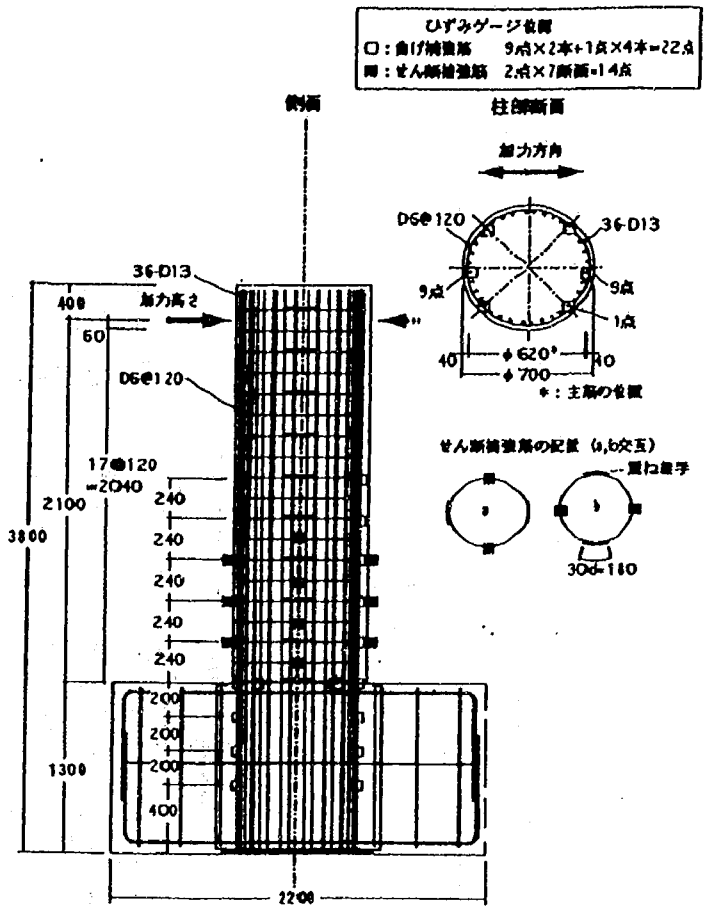


Figure 3(1) Specimen (C00)

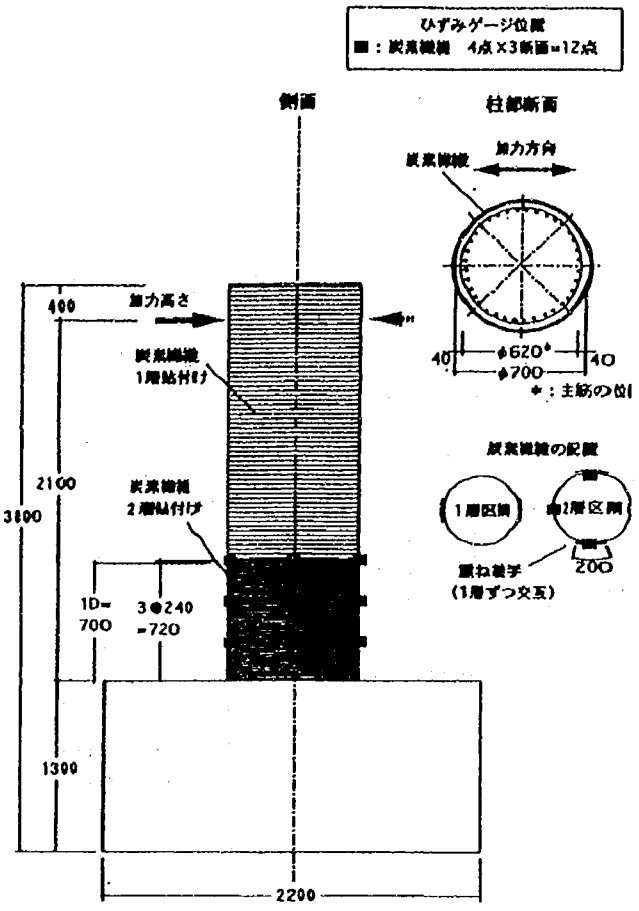


Figure 3(2) Specimen (C21)

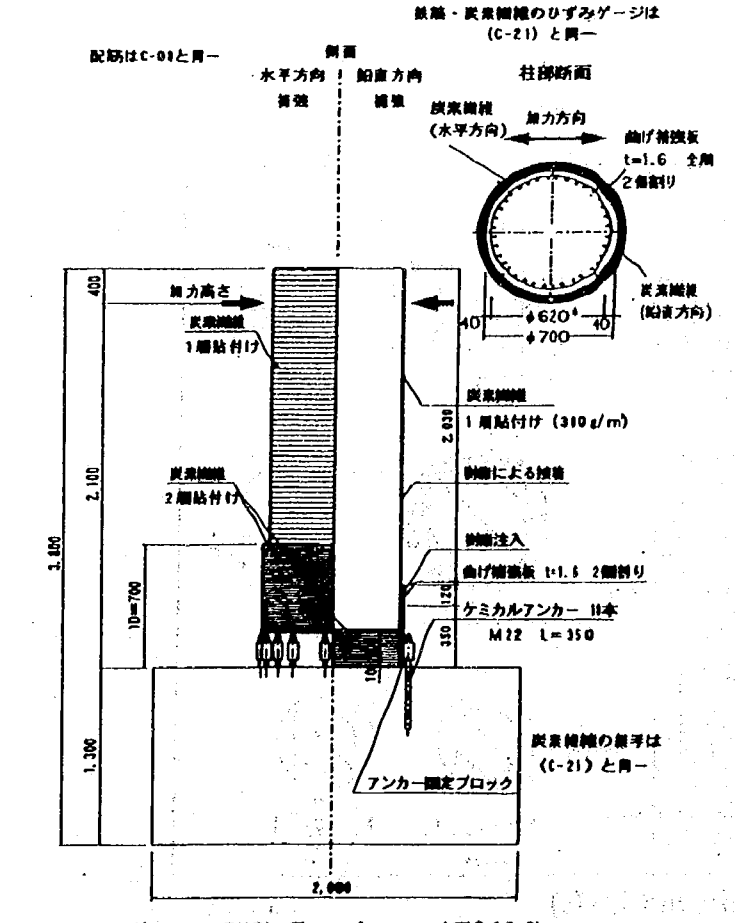


Figure 3(3) Specimen (C21M)

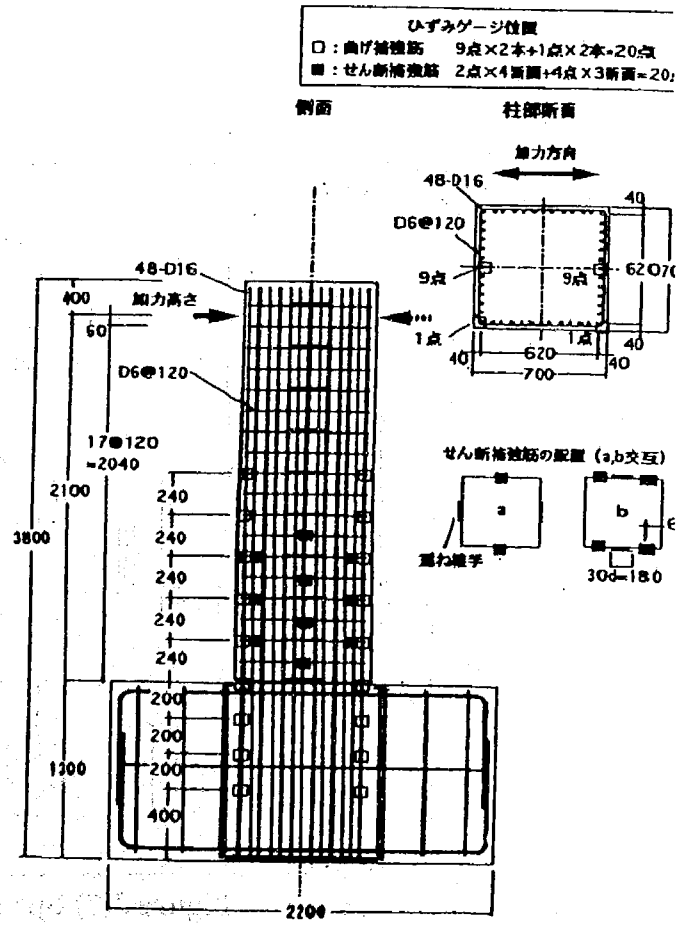


Figure 3(4) Specimen (S00)

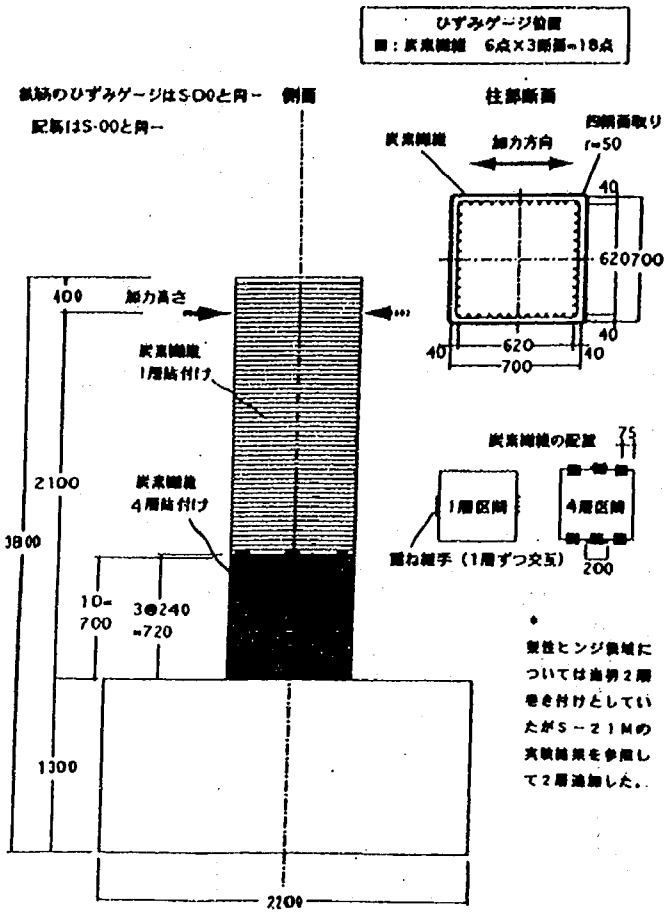


Figure 3(5) Specimen (S41)

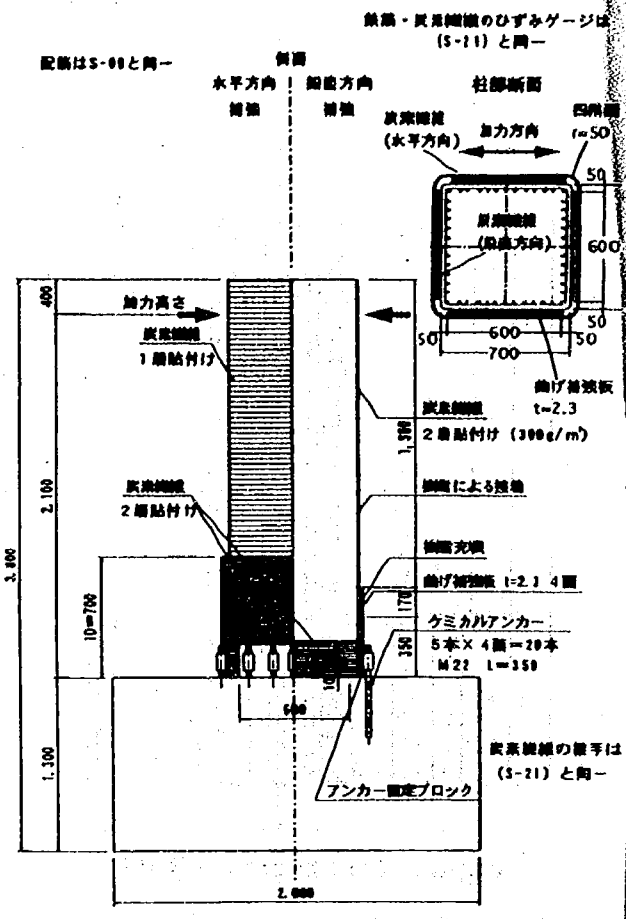


Figure 3(6) Specimen (S21M)

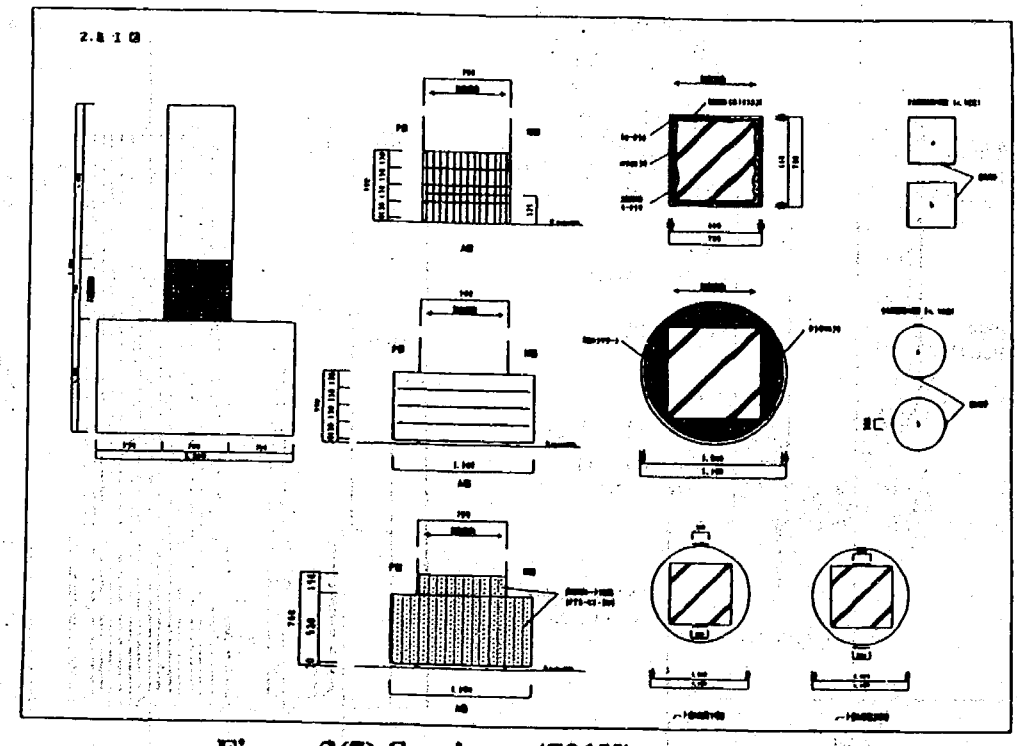


Figure 3(7) Specimen (S21K)

the conventional method is no longer applicable by site constraints, alternative device has to be introduced. C21M and S21M are models for moment capacity strengthening. Because CFRP per se does not have any ductility, in order that the column exhibits any ductility, which is essential for practical aseismic retrofit, a ductile element such as steel plate has to be introduced at plastic hinge zone.

Also because it was assumed the application would be limited to when conventional method is hardly applicable, the steel plate must be as small as possible. It was assumed that 0.5*D, where D is the depth of the section, would be a minimum plastic hinge zone and free length of the steel plate was so decided. Steel plates are not necessarily connected in circumferential direction, or may be divided vertically into a strip of plate. Steel plate and CFRP, CFRP designed strong enough to surpass steel plate, were glued by epoxy in vertical direction.

To exemplify loose structural behavior whatsoever it may be, tie bar was lap spliced in cover concrete for all specimen.

Figure 4 shows the load condition. After the yield point δ y is detected, experiment started for required displacement δ y multiplied by 1,2,3... . AT each step 3 sinusoidal input waves are programmed to apply at speed 3cm/second. Vertical load is kept intact in magnitude and direction. 23kg/cm2 for round column, 17kg/cm2 for rectangular column, which reflects practice.

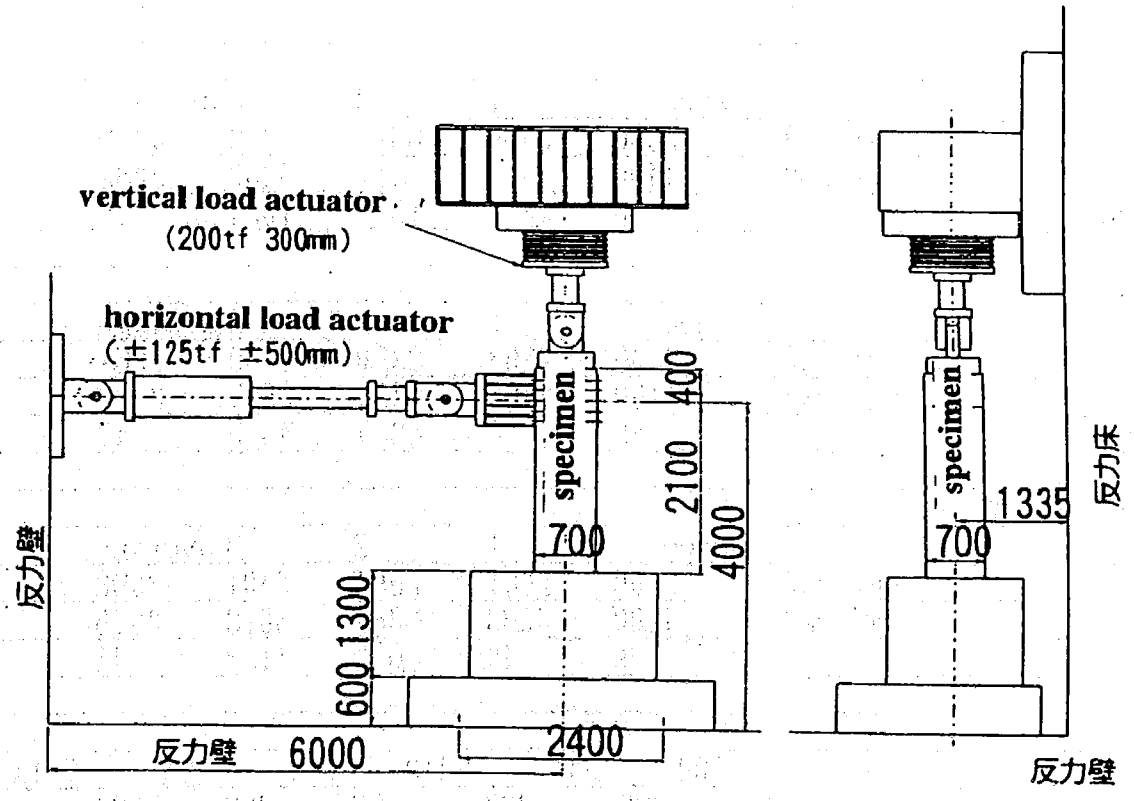


Figure 4 Load condition

3.2 MATERIAL

Material test results are listed in Table 4. Test result of CFRP cohesion is shown in Figure 5. In practice, steel plate surface on cohesion is painted with wash primer not to cause rust. So

Table 4 Material test

1)rebar

D16

		spec	1	2	3	average
yield	kgf/cm2	3000	3701	3701	3701	3701
ultimate	kgf/cm2	4490	5446	5498	5498	5481
elongation	%	16	20.1	20.2	20.3	20

D13

		spec	1	2	3	average
yield	kgf/cm2	3000	3788	3749	3702	3746
ultimate	kgf/cm2	4490	5193	5193	5233	5206
elongation	%	16	19.3	19.9	19.8	20

D6

		spec	1	2	3	average
yield	kgf/cm2	3000	3539	3379	3218	3379
ultimate	kgf/cm2	4490	5312	5312	5230	5285
elongation	%	16	18.4	18.8	18.4	19

steel plate t=2.3

		spec	1	2	3	average
yield	kgf/cm2	2500	2263	2260	2259	2261
ultimate	kgf/cm2	4100	3466	3437	3507	3470
elongation	%	29	46	48.7	46.3	47

steel plate t=1.6

		spec	1	2	3	average
yield	kgf/cm2	2500	2601	2591	2601	2598
ultimate	kgf/cm2	4100	3668	3681	3678	3676
elongation	%	29	40	40.9	41.3	41

concrete

		S00	S41	S21M	C00	C21	C21M
compressive strength	kgf/cm2	295	268	266	336	294	324
Elastic Modules	*e5 kgf/cm	2.39	2.37	2.31	2.55	2.39	2.52
tensile strength	kgf/cm2	24.4	25.6	24.3	30.5	25.8	26.9
days passed	days	51	59	21	49	57	27

the effect of the paintings on the cohesion strength is tested. Cohesion test sampled from model is also executed. Note that cohesion strength at unit length decreases as the total length increases. This scale effect has to be taken into consideration in a practical design.

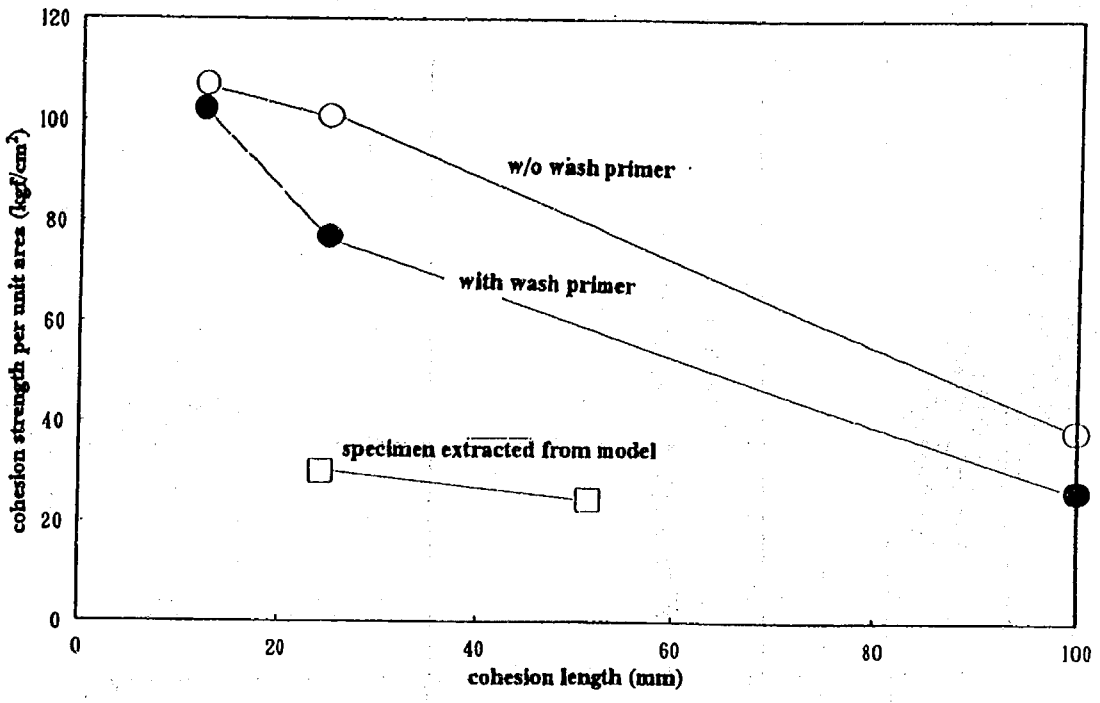


Figure 5 Cohesion between steel plate and CFRP

3.3 EXPERIMENT

The results of experiment are shown next. Hysteresis record is shown in Figure 6 (1)～(7) with calculated points of yield and ultimate. Calculated values are given by converting CFRP to equivalent tie rebar on yield strength ratio. For each cross section, observations are as follows;

ROUND COLUMN: Though it was assumed that the column C00 would exhibits shear failure, it failed by bending showing good ductility. C21 exhibited remarkable and stable ductility until CFRP and vertical rebar were ruptured and load reaction dropped significantly. C21M showed more than C21 owing that CFRP rupture did not take place. No strength increase was achieved in C21M because the cohesion between steel plate and CFRP was apparently not sufficient. After the test CFRP and steel plate were removed to find that the surface concrete is apparently complete, only bending cracks found. It should be noted CFRP ruptured in C21, not in C21M.

RECTANGULAR COLUMN: Again it was assumed that it would fail by shear, it failed by bending shear. At a final stage shear failure mode was apparent, quite contrary to that of C00. S41 showed bump in a opposite plane to load applied. It was assumed that bending failure started and experiment was interrupted though it could be expected that it would sustain a load to some extent. S21M model failed at an early stage. Moment strength increase was not again complete. It was considered that the cohesion was not enough and that the edge of the steel plate caused rupture of the sheet at an early stage.

Outer debris of S41 specimen was removed and covered by tube concrete, then CFRP was rounded by 2 layers. No epoxy was injected into damaged column because it was assumed that cracks were caused by bending moment, no shear dislocation seemed to exist. The experiment was repeated and load deflection curve was shown in Figure 6(7). It seemed no crush of concrete was discerned. It was reaffirmed afterward when tube concrete was removed and found that no crush of concrete was found except for gap zone at the base. CFRP ruptured at the bottom of the tube, at

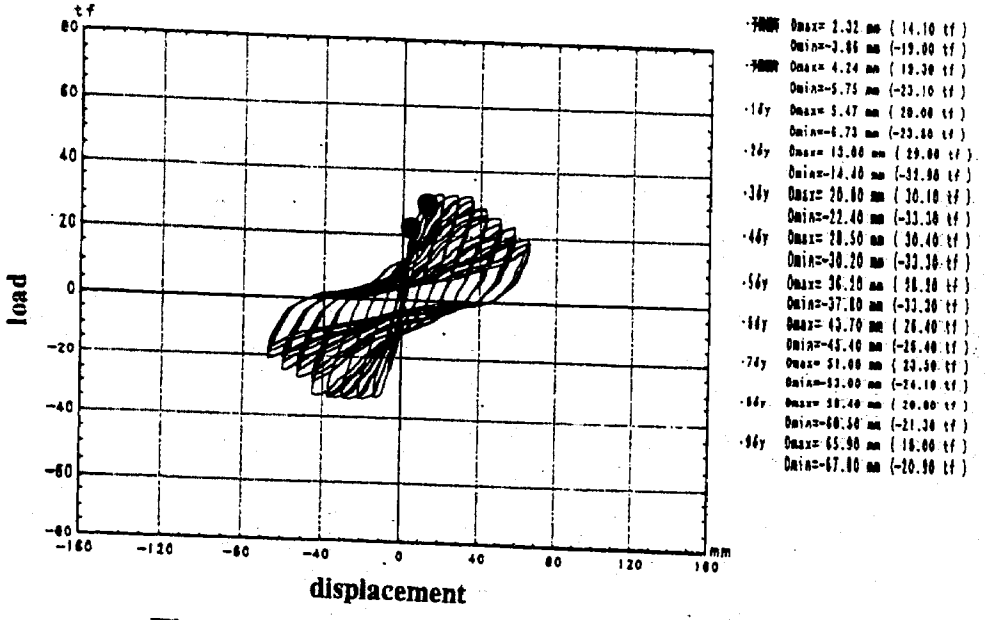


Figure 6(1) Hysteresis (C00)

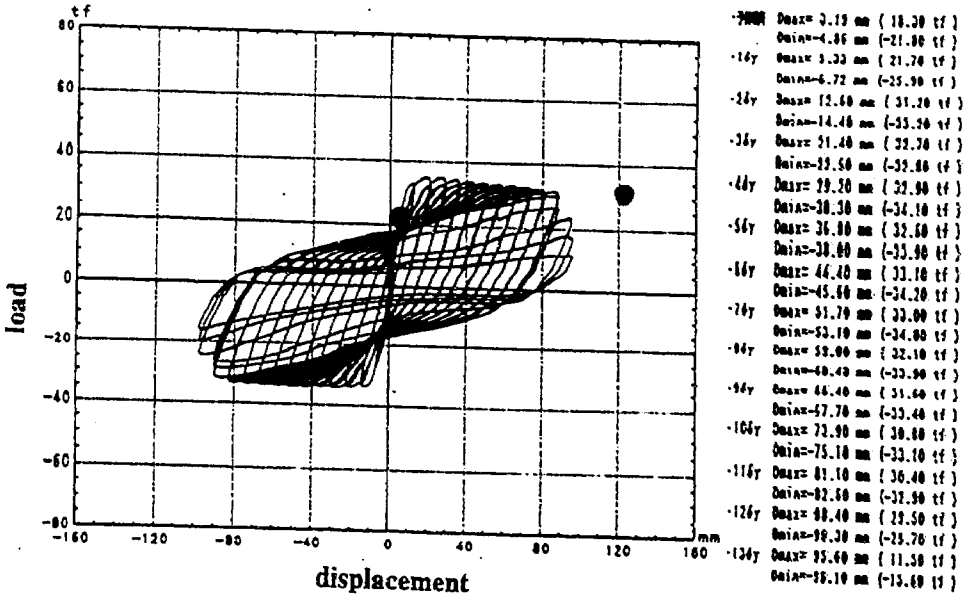


Figure 6(2) Hysteresis (C21)

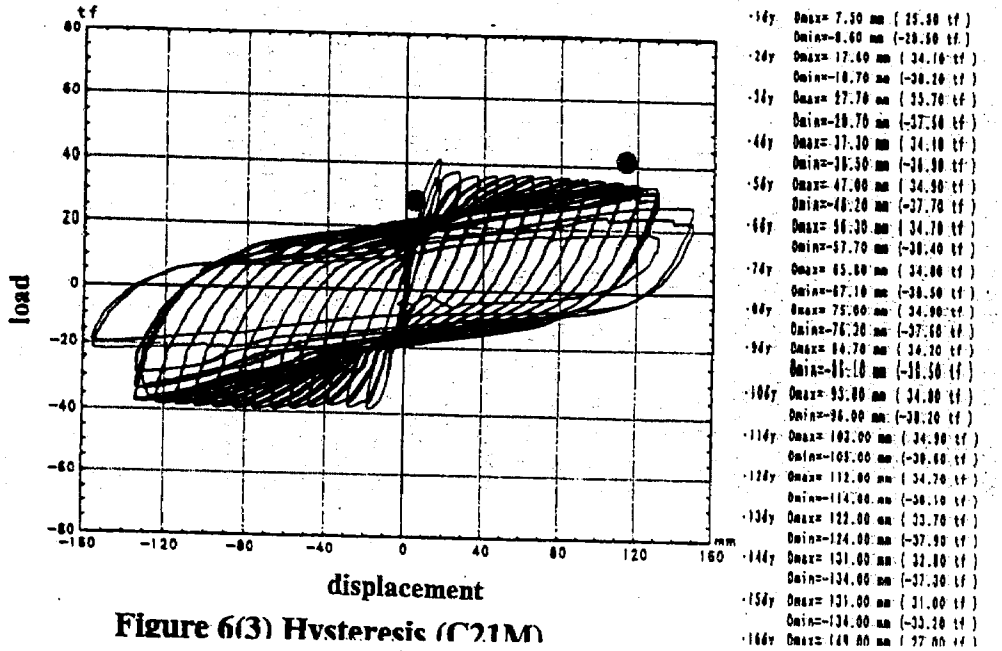


Figure 6(3) Hysteresis (C21M)

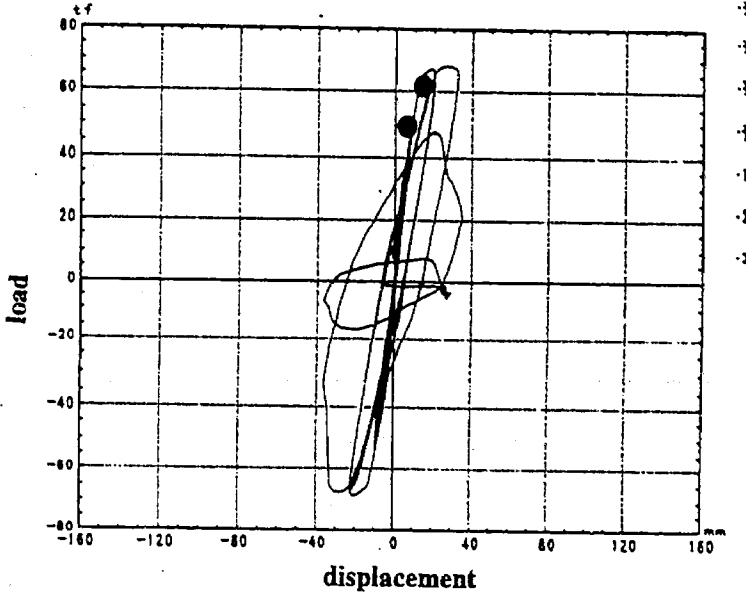


Figure 6(4) Hysteresis (S00)

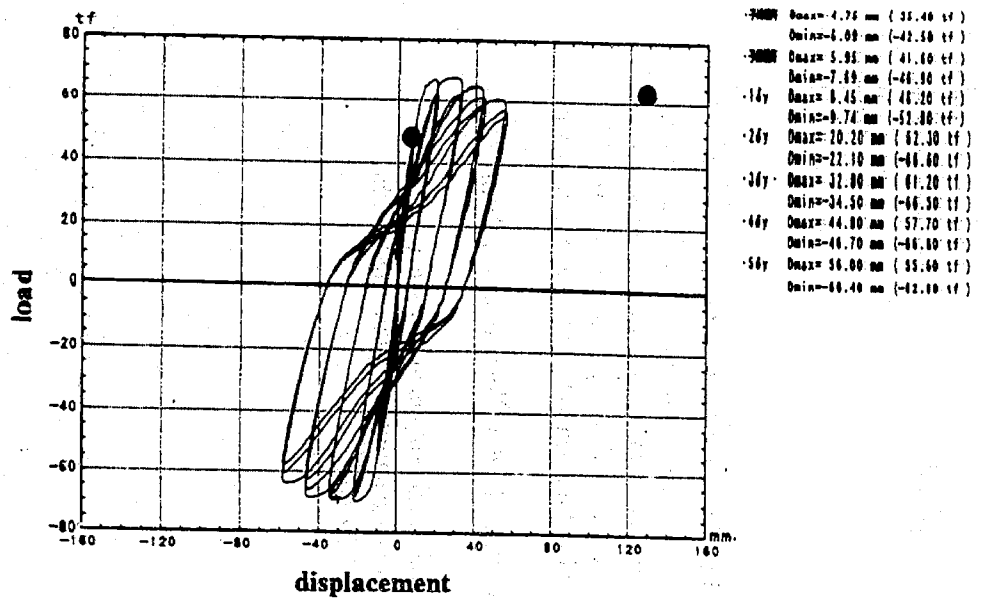


Figure 6(5) Hysteresis (S41)

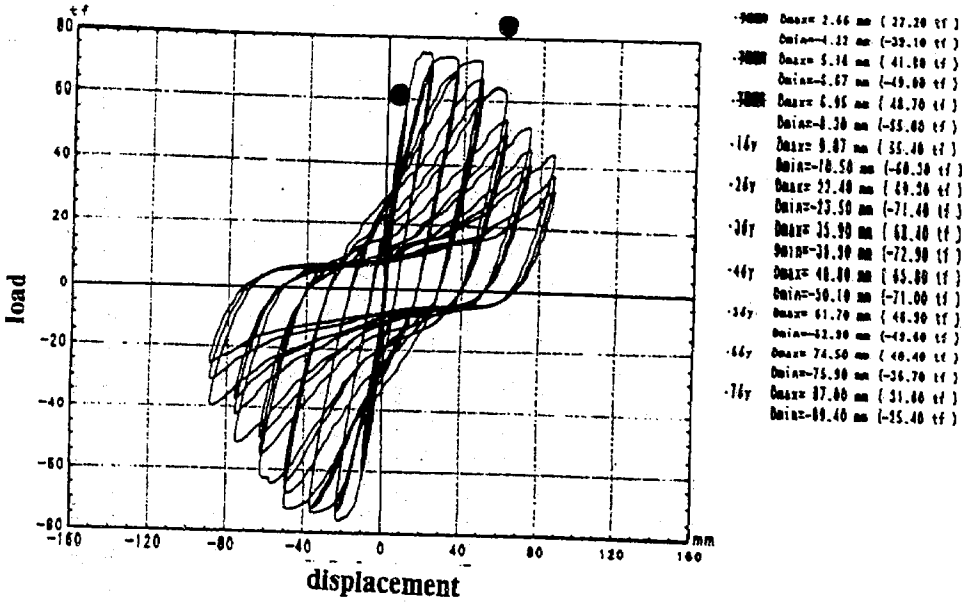


Figure 6(6) Hysteresis (S21M)

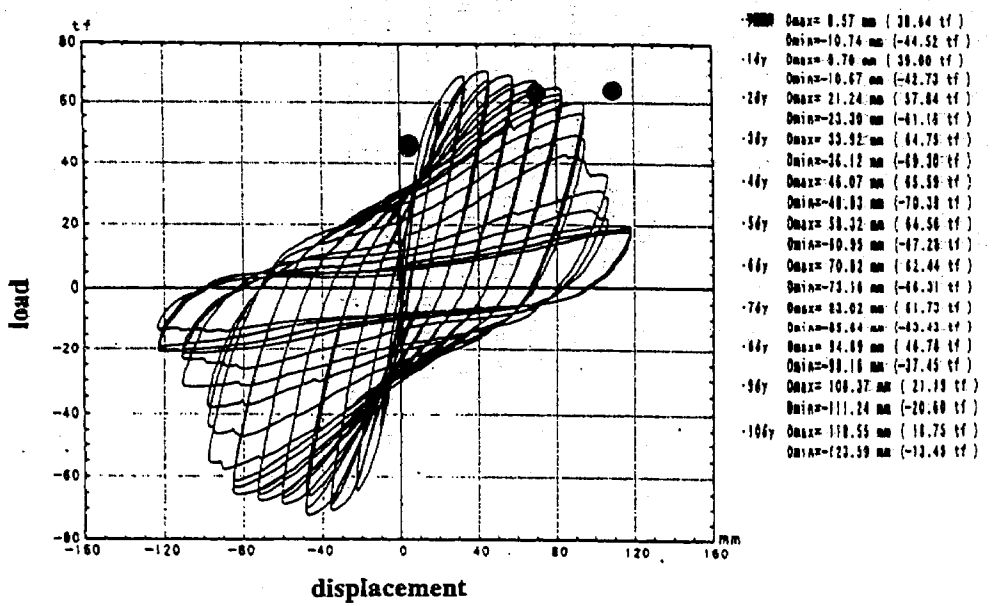


Figure 6(7) Hysteresis (S21K)

around the rectangular corner.

3.4 STRAIN DISTRIBUTION

An example strain distribution of rebar in vertical direction is shown in Figure 7. The distribution does not change so much between each specimen in spite of the discrepancy of each final failure mode. Considering that the crack did not develop after 2-3 δ y, most of the deformation is attributable to inelastic region shown in the Figure. From observation it may be stated that the length of plastic hinge zone is more than just a conventional assumption of deflection calculation.

Strain distribution of CFRP in circumferential direction is shown in Figure 8. Unfortunately strain gage was not installed where CF ruptured. Strain distribution consists of the confinement oriented strain and shear oriented strain, respectively. The two modes are independent each other. Confinement oriented strain converges rapidly with respect to height, while shear oriented one is deemed as constant as long as it concerns with plastic hinge zone. Though it is a speculation, it was estimated that at C21, the confinement strain would have reached at its maximum of 15,000 μ and ruptured. While at C21M because the CFRP was detached from concrete, the tensile strain was redistributed would not have reached at its maximum anywhere. In the case of S21K, it is not easy to conclude, but understood that at one of the corner of rectangular section, the greatest tension was introduced to CFRP, which leads to rupture of CFRP at the bottom.

4 ANALYSIS

The Tentative Code is used for analysis, except that the allowable stresses are replaced with required values of material and CFRP is replaced with an equivalent tie bar on yield strength base as shown below.

volumetric tie bar ratio: pw = 4*Ah/(s*bf)
CFRP contribution to above is;
Ah += n*(s*t)*(bf/B)*(fcf/fyh)
In case of tube stiffening;
Ah += n*(s*t)*(bf/Dtube)*(fcf/fyh)

Shear capacity is also calculated on an equivalent yield strength as,

CFRP contribution to shear can be calculated as follows,
nAh += 2*n* s*t*(fcf/fyh)*(D/dw)
In case of tube stiffening;
Sc = tau* π *$Dtube^2$/4
nAh += 2*n* s*t*(fcf/fyh)*(Dtube/dw)

where notations are pw: volumetric tie bar ratio defined in Tentative Code, Ah: cross sectional area of tie bar; B: width, bf: distance between centroids of outer longitudinal reinforcement along B, D: depth, dw: distance between centroids of outer longitudinal reinforcement along D, s: space of tie bar, t: thickness of CFRP, n: number of layers of CFRP, fyh: allowable yield strength, fcf: allowable carbon fiber yield strength, Dtube: diameter of tube, tau: concrete shear strength, nAh: area of equivalent tie bar against shear.

This model will be called "model 1". On the other hand, Priestly et al [3] proposes on shear strength, the results will be referred as "model 2".

As for ductility calculation, maximum concrete strain and rebar tension strain were assumed, and internal moment capacity, curvature and deflection were calculated simultaneously. The results of the experiment and two models are summarized in Table 5.

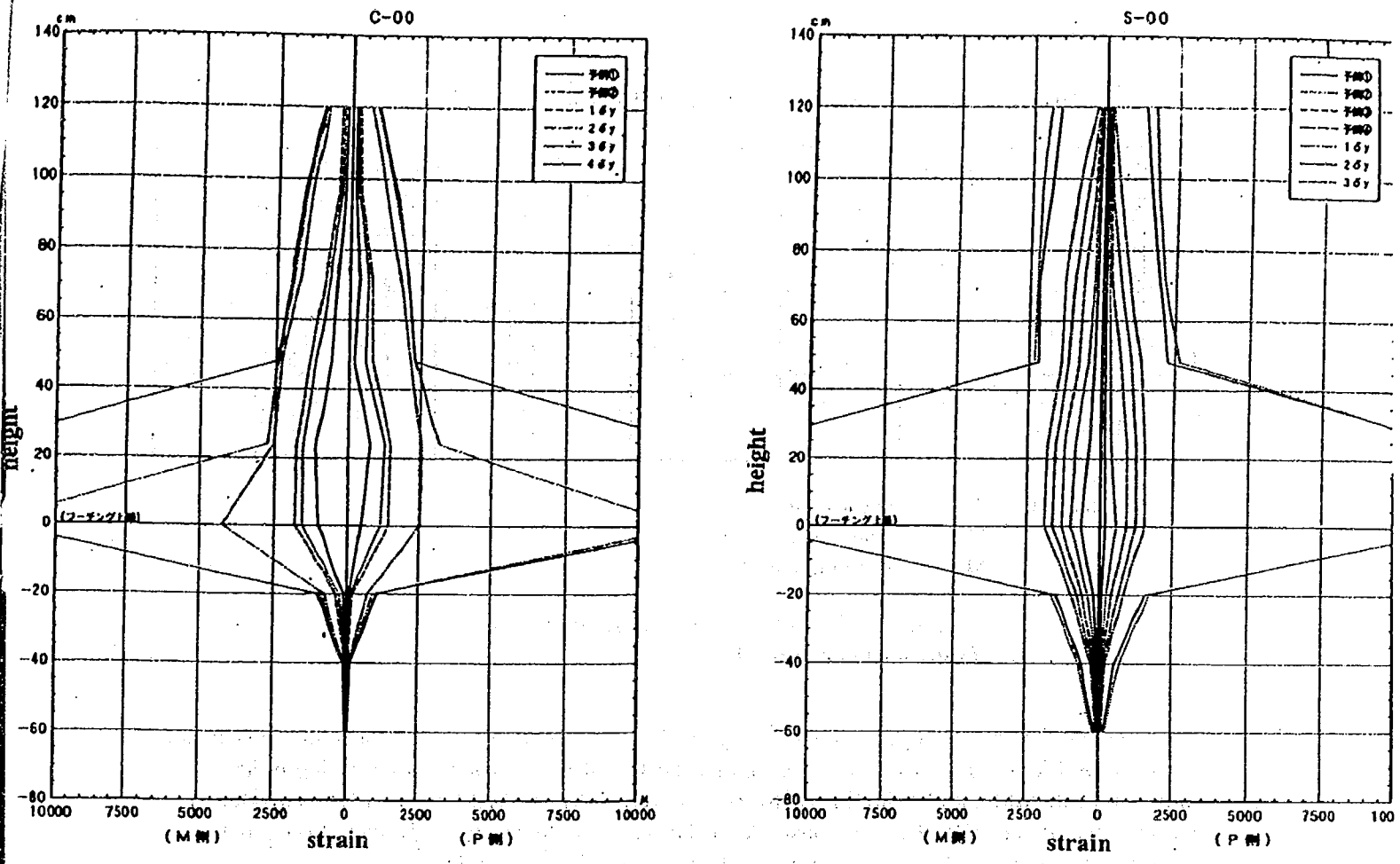


Figure 7 Strain distribution of vertical reinforcement

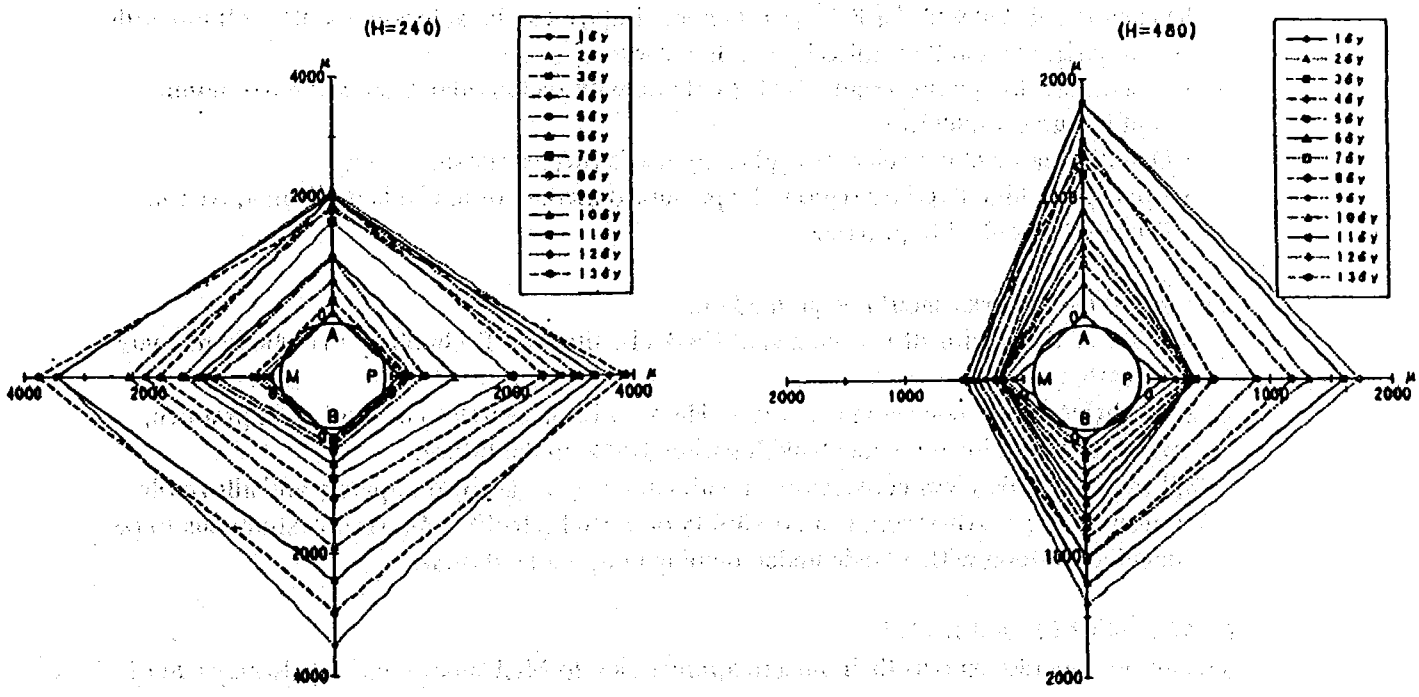


Figure 8 Strain distribution of CFRP in horizontal direction

Table 5 Comparison of experiments and model

i.d.	shape	objective			failure mode			ductility		
		shear	ductility	moment	exp.	model 1	model 2	exp.	model 1	model 2
C00	round				M	S	M	5.0	(2.6)	4.0
C21	round		○		M	M	M	12.0	19.8	19.8
C21M	round		○	○	M	M	M	15.0	17.7	19.3
S00	rectangular				MS	S	MS	2.0	(2.77)	(4.44)
S41	rectangular	○	○		M?	M	M	>5.0	19.1	19.1
S21M	rectangular	○	○	○	MS	M	M	4.0	9.4	10.9
S21K	tube	○	○		M	M	M	7.0	18.9	19.4

legend S shear failure
MS bending shear failure
M bending failure

() denotes final ductility though interrupted by shear
? experiment interrupted

It is concluded that strength estimate is agreeable. To predict displacement or ductility is not so easy a problem. But when considering that the Tentative Code assumes a ceiling in its appraisal of ductility, and reduction factor of 2/3 is considered when the ductility is introduced into practice, it is practically of no obstacle of the diversity shown in the Table. So from a practical view point, authors assume the analysis would give agreeable results.

5. CONCLUSIONS

The results of the experiment lead to the following conclusions;

1. RC column retrofit through CFRP sheets exhibits great structural improvement for round as well as rectangular cross section.
2. Ductility improvement of round column by CFRP sheet is significant.
3. When retrofitted with CFRP sheet, bending failure can be achieved for RC column with rectangular section that failed by bending shear.
4. When retrofitted with round tube for column with rectangular cross section, column exhibits further ductility.
5. Detail of moment capacity strengthening needs further consideration.
6. Apart from high ductility region, the presumed method of analysis gives an agreeable result to be applied to practice.

The following remarks should be pointed out;

1. Additional experiment is executed at Osaka Institute of Technology to embody moment strength increase.
2. Tentative design code is under way in Hanshin Expressway to be applied in practice, which will require adjustments with national code in the future.
3. Tentative Code gives conservative results in view of the shear capacity and allowable stress design. Also there is a possibility of partial retrofit. So further study has to be developed along with a basic understanding of aseismic design.

6. ACKNOWLEDGMENTS

The authors would express their sincere appreciation to Mr.Uemura and Mr. Kobayashi of

Tonen Corporation for their assistance of the understanding of CFRP characteristics and the material offered, Dr.Ohuchi of Technical Research Institute of Obayashi Corporation for his advice on the experimental planning, and Professor Kawashima of Tokyo Institute of Technology and Professor Kobayashi of Osaka Institute of Technology for their leadership in each of the engineering study committees.

REFERENCES

1.Tentative design code for repair of damaged Kobe line, Ministry of Construction, Feb.9 1995(in Japanese)

2.Tentative design manual for CFRP retrofit of RC column, Bridge Research Laboratory, Japan Highway Authority, Feb.1995(in Japanese)

3.M.J.N.Priestley, F.Seible, Y.H.Chai; Design Guidelines for Assessment Retrofit and Repair of Bridges for Seismic Performance, University of California San Diego, August 1992

Session 6

Retrofit Methods for Steel Columns, Superstructure and Restrainers

(Co-Chairs: K. Tamura, Y. Xiao)

"Cyclic Behavior of Shear Links in Retrofitted Richmond-San Rafael Bridge Towers"
by A. Itani
Presented by: Ahmad Itani

"An Experimental Study on Seismic Retrofit of Steel Bridge Piers"
by K. Nishikawa, J. Murakoshi, Y. Josen, M. Takahashi
Presented by: Jun Murakoshi

"Intermediate Hinge Restrainers for Bridges: Performance, Design and Retrofit"
by R. DesRoches, G. Fenves
Presented by: Gregory Fenves

"Seismic Vulnerability Analysis of Steel Bridge Bearings"
by J. Mander, D-K Kim, I. Buckle
Presented by: John Mander

CYCLIC BEHAVIOR OF SHEAR LINKS IN RETROFITTED RICHMOND-SAN RAFAEL BRIDGE TOWERS

Ahmad M. Itani, Ph.D., P.E.
Department of Civil Engineering
University of Nevada, Reno

ABSTRACT

This paper discusses the proposed seismic retrofit of the Richmond-San Rafael bridge towers and the testing program that is underway for the proposed shear links. The basic concept behind this retrofit is to install new eccentric braced towers between the existing towers. The geometrical properties of the proposed shear links, that are located between the eccentric braces, in the retrofitted towers exceed the previously tested shear links for steel building. Full scale testing of the upper and lower bounds of the proposed shear links is being conducted to verify their cyclic behavior, ductility, and rotational capacity that were assumed during the retrofit design.

INTRODUCTION

The Richmond-San Rafael Bridge (RSRB) is one of the longest steel bridges in the State of California. It stretches more than 6401 m (21,000 ft) between San Quentin in Marin and Richmond in Contra Costa County. The truss structure includes two, double deck, 1070 ft cantilever trusses spanning the east and the west shipping channel. Double deck trusses with spans of 88.1 m (289 ft) connect the cantilever trusses to each others and to the approach spans. Similar to the San Francisco-Oakland bridge, the bridge truss members are riveted built-up sections made of angles, plates that interconnected to each others by lacing members. Figure 1 show an intermediate chevron braced tower and its connection to the double deck superstructure.

The specified performance level for the bridge is established by Caltrans is to prevent any collapse during Safety Evaluation Earthquake [1]. Under this criteria the structure will have limited service level after a maximum credible earthquake and will suffer significant damage.

The proposed retrofit strategy for the towers that was developed by Caltrans consulting engineers [1] and approved by Caltrans and its Peer Review Panel is to remove the chevron braces from the existing towers and to install new eccentric braced towers between the existing towers. Figures 2 and 3 show the proposed eccentric braced towers for intermediate towers that can carry lateral forces while Figure 4 shows a tower that can carry lateral and longitudinal forces. By utilizing this strategy, the inelastic activity will be limited to the eccentric braced towers. The shear links inside the eccentric towers will

yield at a pre-determinate level and limit the inertia forces to their ultimate capacity. By limiting the seismic forces on the bridge, non ductile truss members will not experience yielding and buckling.

The retrofitted towers of Richmond-San Rafael Bridge (RSRB) play a significant role in the overall seismic behavior and performance of the bridge. These towers are responsible of transferring the inertia forces that are generated, during an earthquake, in the superstructure to the foundation. Therefore, the components of these towers lie in the direct seismic load path and thus any premature failure in these members will interrupt the load path and might cause inadequate seismic behavior.

In order to ensure a satisfactory performance, the tower components should be able to withstand severe deformation without early fracture. The uncertainties that are generally associated with seismological and geotechical studies make it very difficult to determine the magnitude of forces that should be resisted by tower members. Therefore, limit state procedure is emerging as a reliable method that could be used in the seismic evaluation of structures. This procedure relates the ultimate capacity of the system to the ultimate deformation capacity of the individual members. Based on this, the rotational capacities of the tower component should be known in order to determine the overall seismic response of the towers. This paper discusses the evaluation of the deformation capacities for various tower components of the bridge in order to assess their seismic behavior and performance during severe ground motion.

PROOF TESTING OF PROPOSED SHEAR LINKS

The proposed retrofit strategy for the seismic upgrading of the Richmond-San Rafael Bridge includes the installation of eccentric braced frames at the majority of the existing steel tower bents to prevent instability resulting from a non-ductile failure of the existing brace members. These new towers, Figures 2, 3, and 4 will resist the lateral seismic and wind forces, while the existing towers continue carry the gravity load of the superstructure. During severe ground motion, the horizontal beam between the eccentric braces will be activated and will dissipate the input energy by yielding of the web and ends of the shear link. The survival of the bridge will rely on the satisfactory performance of the new 72 eccentric braced frames and approximately 260 shear links.

The viability of eccentric braced systems for seismic resistant construction is based largely on the system's stable and predictable inelastic behavior under lateral cyclic load. In a well designed eccentric braced frame, the inelastic activity will be limited primarily to the link beams, located between the eccentric braces, that are designed and detailed to withstand severe cyclic deformation. During severe earthquakes, these shear links will act as a ductile fuse that will dissipate the energy through hysteretic behavior by yielding of the web and ends of the beam. Thus, the web and ends of shear links will be subjected to relatively high strains, which in some cases may cause premature fracture such as was observed during Northridge earthquake in steel moment resisting frames.

The dimensions of the shear links that are proposed for the seismic retrofit of RSRB have a common web thickness (t_w) equal to 9.15 mm (3/8") and a depth (d) that varies between 762 mm (30") to 407 mm (16") as an upper and a lower bound [16]. This makes the shear link web compactness ratio (D/t_w) varies between 72 and 35. This range of compactness ratio have never before been built or tested before [2, 3, 4, 5, 6]. Most of the available information on shear links that were tested by Prof. Popov et al. does not fit in this range. This means that the design equations and plastic hinge rotational capacity that were used in the design process should be validated by proof testing at least the upper and lower bound of the web compactness ratio. These tests will provide information on the actual strength, ductility, energy dissipation capacity, and rotational capacity of the proposed built-up shear links under cyclic deformation.

According to the proposed retrofit strategy, the existing towers are still required to carry the gravity load transmitted through the superstructure. During severe ground motion, the tower legs will be subjected to lateral displacement in addition to the gravity load causing the formation of plastic hinges at the tower base. Recent investigation by Caltrans consulting engineers exposed several deficiencies in the existing tower legs such as local plate buckling in the expected region of the plastic hinge, high strain values at the base of the column which might cause fracture in the steel, and the possibility of shifting the plastic hinge from the base of the column to another location. These deficiencies have caused some concern that the existing tower legs might suffer premature failure and thus interrupt the gravity load path. This leads to an inadequate overall seismic performance. To prevent these deficiencies, Caltrans consulting engineers have suggested several retrofit items at the lower legs. These items include filling the tower legs with concrete at the base and adding continuous cover plates that will be bolted to the longitudinal faces of the column.

OBJECTIVES AND SCOPE OF THE PROOF TESTING

The main objectives of the proposed tests are:

1. To conduct cyclic tests of two shear link specimens that have the upper and lower bounds of the web compactness ratio (D/t_w) which is equal to 72 and 35 respectively.
2. To use the results of the proposed cyclic tests to verify the ± 0.09 rad end rotation at the end of the link beam that is used in the design process.
3. Modify and refine, if necessary, the design detail of the shear link to achieve the ± 0.09 rad rotational capacity.

In order to achieve these objectives, two cyclic full scale tests will be conducted on shear links to understand their behavior and to verify that the assumed rotational capacity can be developed. After discussions with Caltrans and its consulting engineers a

decision was made to test the upper bound and the lower bound of these links. If the test results showed the ability of these specimens to achieve ±0.09 rad rotation, then the design assumption will be verified and no further action would be needed. However, if the ±0.09 rad rotation is not achieved, these tests will provide additional information to modify and refine the details of the shear link to achieve the required rotational capacity.

The proposed test set-up is shown in Figure 5. One-half length of an actual shear link in the eccentric braced towers will be subjected to cyclic forces at the moment inflection point by means of two hydraulic actuators. The total capacity of the two actuators is ± 3114 KN (700 kips) in pull and push with a stroke of ± 254 mm (10").

Various instrumentation will be used to monitor the behavior of the specimen such as load cells for force-displacement, linear variable displacement transducers (LVDT) for plastic rotations at the intersection with diagonal brace, and strain gages and rosettes to measure strains and shear strains inside the shear link segment. A total of 90 channels will used in this test to monitor the strains at strategic locations inside the web of the link beam and its inelastic rotation.

ACKNOWLEDGMENTS

The development of the information provided in this paper was funded by Caltrans. Acknowledgments are due to Caltrans CCMB engineers and Ben C. Gerwick, Inc design team for their prompt response in providing details and assistance for the EBF tests. Professor Egor P. Popov serves as a technical consultant for the EBF tests. His comments and assistance during the design of the test set-up is sincerely appreciated.

REFERENCES

1. Seismic Retrofit Project No. 612, Richmond-San Rafael Bridge, Structural Drawings by Gerwick/Sverdrup/DMJM, Joint Venture, drawing date 6/7/96

2. Popov, E.P. and Malley, J. O., 1983, "Design of Links and Beam-to-Column Connections for Eccentrically Braced Frames," UCB/EERC-83/02

3. Malley, J.O. and Popov, E.P., 1983, "Design Consideration for Shear Links in Eccentrically Braced Frames," UCB/EERC-83/24

4. Hjelmstad, K.D. and Popov, E. P., 1983, "Seismic Behavior of Active Beam Links in Eccentrically Braced Frames," UCB/EERC-83/15

5. Kasai, K. and Popov, E. P., 1986, "A Study of Seismically Resistant Eccentric Braced Steel Frames Systems," UCB/EERC-86/01

6. Engelhart, M.D. and Popov, E.P., 1989, "Behavior of Long links in Eccentrically Braced Frames," UCB/EERC-89/01

Table 1: Comparison between previous test ranges and proposed shear links

Previous Tests	Test 1: BU30	Test 2: BU16
$\alpha = a/D = 0.42\text{-}2.4$	0.194	0.615
$\beta = D/t_w = 40.1\text{-}57$	72	34.67
$b/2t_f = 5.4\text{-}9.6$	4.66	4.66
$a/t_w = 21\text{-}57$	14	21.33

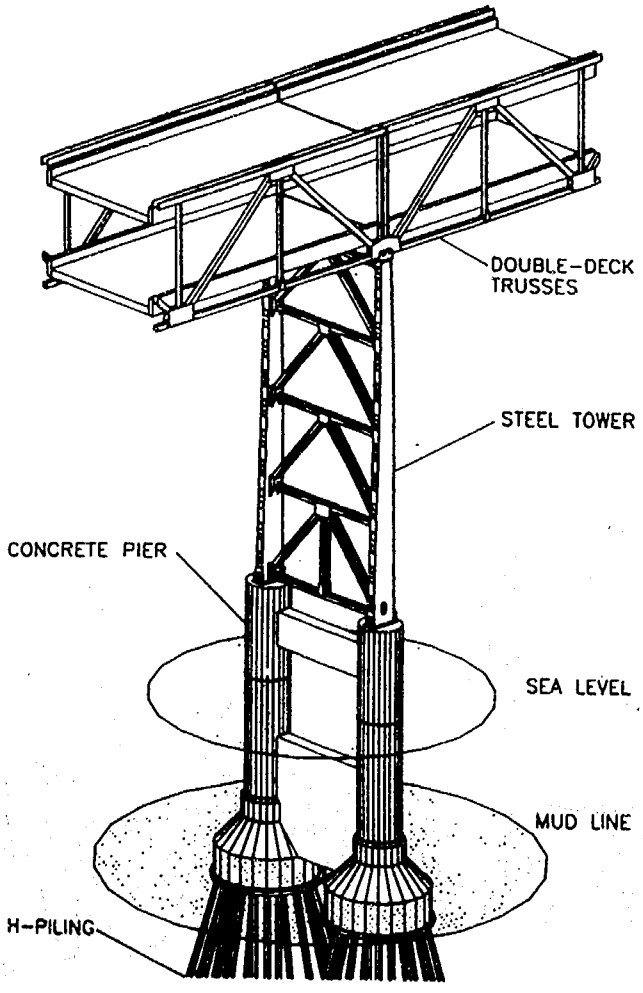


Figure 1: Existing intermediate towers of RSRB

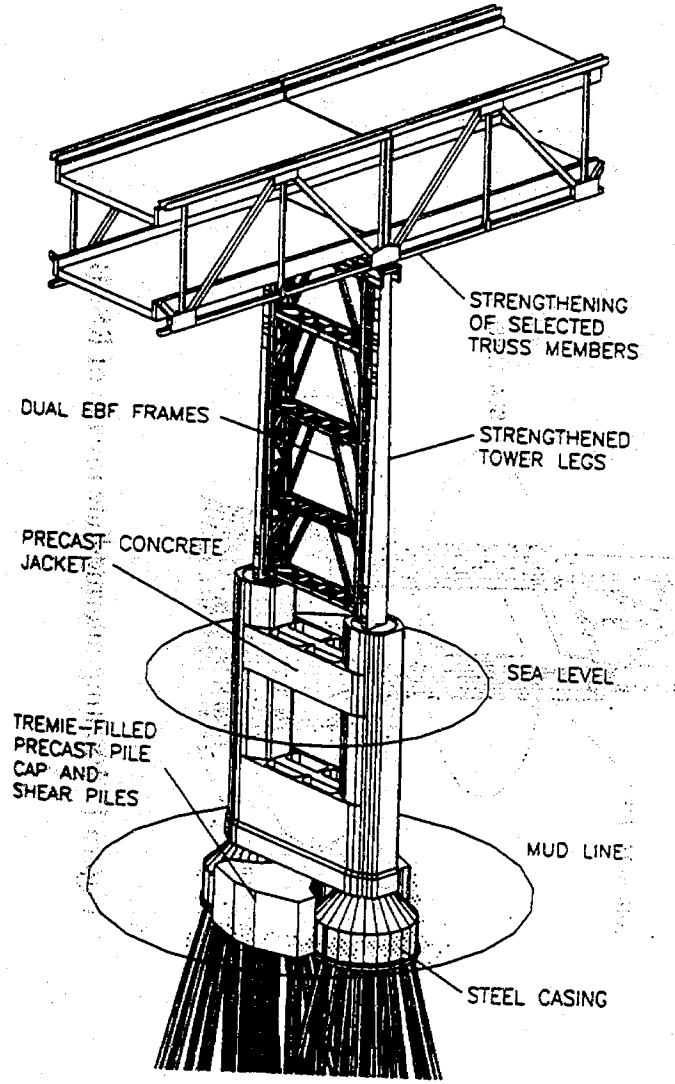


Figure 2: Proposed EBF for intermediate towers

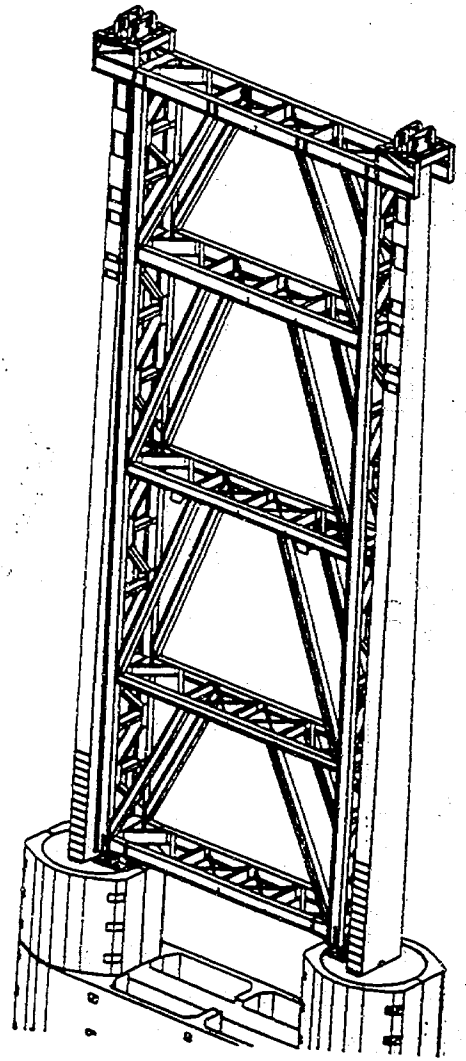


Figure 3: Details of proposed EBF

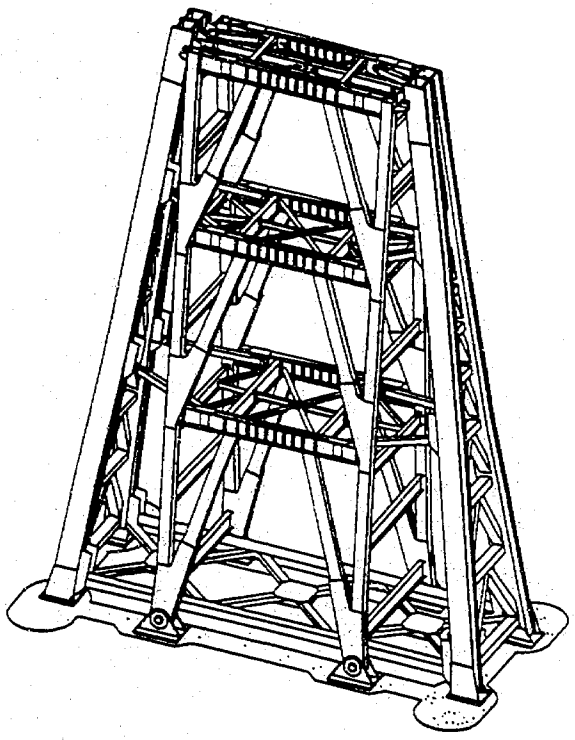


Figure 4: Details of proposed EBF cantilever towers

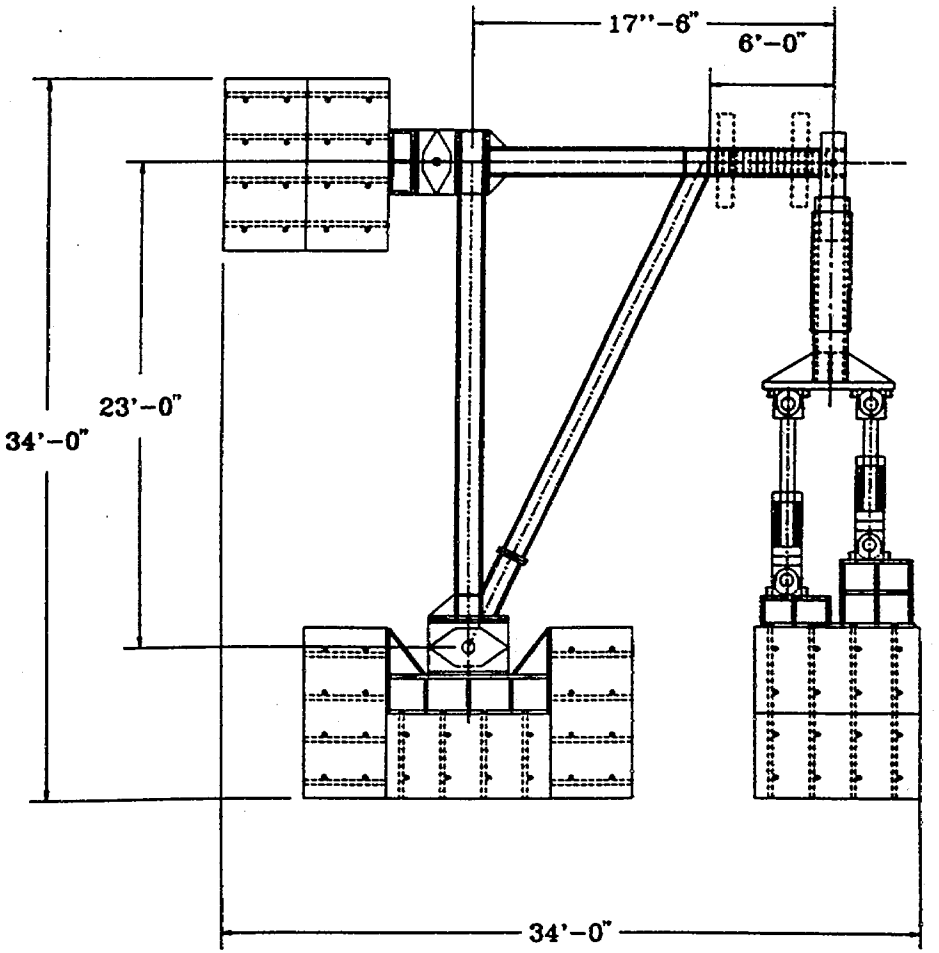


Figure 5: Test set-up for shear links



AN EXPERIMENTAL STUDY ON SEISMIC RETROFIT OF STEEL BRIDGE PIERS

Kazuhiro Nishikawa
Head, Bridge Division, Public Works Research Institute, Ministry of Construction
Jun Murakoshi
Senior Research Engineer, Ditto
Yasushi Josen
Research Engineer, Ditto
Minoru Takahashi
Assistant Research Engineer, Ditto

ABSTRACT

This paper deals with several methods of seismic retrofit for existing steel bridge piers. Based on the investigation of damaged steel piers, authors identify the failure modes which should be avoided to prevent piers from failure, and propose retrofit methods of steel bridge piers. In order to investigate the effectiveness of proposed retrofit methods, cyclic lateral loading tests were carried out with eighteen specimens including eleven with rectangular sections and seven with circular sections. Test results indicates the effectiveness for rectangular piers to strengthen corners by corner plates and for circular piers to build outer pipe around the existing piers with a small clearance.

INTRODUCTION

Steel piers of elevated highway bridges in Japan suffered heavy damage due to the Hyogo-ken Nanbu earthquake for the first time. The damage includes of collapse of two steel piers. After the earthquake, the "Guide Specifications for Reconstruction and Repair of Highway Bridges Which Suffered Damage due to the Hyogo-ken Nanbu Earthquake" was issued by the Ministry of Construction on February 27, 1995[1]. In this guide specifications, it was specified that dynamic strength and ductility shall be assured not only for concrete piers but also for steel piers and it was decided to tentatively use steel piers with infilled concrete for reconstruction and repair. This approach is certainly one of the most effective and easiest methods to improve the ductility of steel piers, however, one of the demerits is that it also increase the load bearing capacity greatly and weight of piers, which will be imposed on anchors. Most of steel piers are used for elevated highway in urban areas, which means that retrofit work including anchors seems difficult from the point of view of constructibility and economy.

Considering these restriction, PWRI started a joint research with Metropolitan Expressway Public Corporation, Hanshin Expressway Public Corporation, Japan Association of Steel Bridge Construction and The Kozai(steel material) Club in order to establish methods to strengthen both existing and newly constructed rectangular and circular steel bridge piers. In this research, more than 60 large scale specimens, which are about one-third scale models of actual bridge piers, have been tested under a constant compressive axial load and cyclic horizontal load during 1995 and 1996. This paper deals with a part of this research mainly conducted by PWRI for developing seismic retrofit methods of existing steel bridge piers. Authors briefly introduce the damage of

steel piers by the Hyogo-ken Nanbu Earthquake, identifies failure modes which should be avoided to prevent piers from failure according to the features of the damages, propose retrofit methods of steel bridge piers and report the effectiveness of proposed methods by loading tests with eighteen specimens including eleven with rectangular sections and seven with circular sections.

DAMAGE OF STEEL PIERS AND ULTIMATE LIMIT STATES

Outline of the Damage of Steel Piers

The earthquake caused damage to elevated highway bridges on National Highway Route(NHR) 2, 43 and 171, the Meishin Expressway(JHM), Chugoku Expressway(JHC), and the Route 3 Kobe Highway and Route 5 Harbor Highway of the Hanshin Expressway(HER3 and HER5). Among these bridges, the number of steel piers inspected was 355. Damage were classified into 5 classes from As to class D for steel bridge. Table 1 shows the damage definition of steel piers. Class A is categorized for falling off or collapse, A is major damage , B is moderate damage, C is minor damage and D is very slight or no damage. Table 2 shows the number and the percentage of damaged piers by class. Among them, the percentage of the steel piers judged to be class B or higher are about 14%. Two rectangular piers were crushed in compression due to the rupture of the welding at the corners.

Fig. 1(a) shows an example of local buckling in the bottom of a rectangular pier. Many stiffened plates in piers with rectangular section buckled and out-of-plane deformation occurred in the bottom or the mid height of the piers. Fig. 1(b) shows the collapse of the rectangular pier of HER3. This pier have T-shaped steel frame supported by two reinforced concrete piers. It was estimated four stiffened plates composing rectangular section of the pier failured from the corner along the weld lines after the local buckling of the stiffened plates at the bottom of the piers. In case of circular piers, Fig. 1(c) shows a typical elephant foot buckling. Fig. 1(d) shows the cracking along the circumference after progress of deformation. Fig. 1(e) is another damage of circular piers in HER3. The residual displacement is remarkable in this pier.

Failure Modes and Concepts of Seismic Retrofit of Steel Piers

As a result of detail survey of the damaged steel piers, it was clear that occurrence of local buckling, which was supposed as an ultimate state of steel piers in the previous Japanese design code, is not always an actual ultimate limit state and that it is essential to avoid the failure mode which causes sudden decrease of bearing capacity or unstable state and to increase the ductility of piers after the local buckling. From the deformation and fracture patterns of steel bridge piers damaged in the earthquake, the failure modes which should be avoided, were assumed as follows (see Fig. 2) :

(1) Rectangular piers

For rectangular section, it was proposed that breaking of corners or buckling of corners should be failure modes. Such failure mode was observed in the two piers that completely collapsed in the earthquake. Actually, it is known that the corners have a higher buckling strength than other parts. If the breaking of corners occurs, it can cause sudden decrease of bearing capacity in lateral direction after the peak strength, and ductility can't be expected. Fig. 3 shows an example of breaking of corners of a specimen obtained from the cyclic loading

test. Since the specimen was filled with concrete at a certain height, breaking of corners are likely to occur. It was observed that the specimen rapidly lost bearing capacity and increased in deformation as soon as the corners started to partially break with the progress of the local buckling of stiffened plates. This failure mode seems shear failure of concrete piers, therefore it is important to avoid this kind of failure mode.

(2) Circular piers

As to the characteristic of buckling of circular piers, buckling occurred at the limited portion of the pipe for the vertical direction, therefore progress of deformation resulted in the large residual displacement, or cracking along the circumference, which are considered unstable state for supporting superstructure. Such large residual displacement and/or cracking due to buckling should be considered as a failure mode.

Above identification of failure modes focuses on the deformation and accompanying fracture patterns of steel bridge piers. The breaking and cracking of steel members, probably due to brittle fracture or low-cycle fatigue, were reported as other types of damage to steel bridge piers in the Earthquake. How to evaluate such damage patterns and how to cope with them are also important, however, this paper does not discuss such failure because they are considered exceptional cases.

Basic Concepts about Seismic Retrofit

The general countermeasures presented in the previous studies[4],[5] for improving the seismic performance of steel bridge piers are as follows:

1) Improve structural parameters related to buckling strength
   (Decrease the width/thickness ratio of stiffened plates or the diameter/wall thickness ratio of steel pipes, increase the stiffness of stiffeners, or reduce the diaphragm spacing.)
2) Fill the steel column with concrete, or combine the steel pier with concrete into a composite structure.

These methods aim at preventing the local buckling of steel bridge piers and improving the ductility, and consequently increase the maximum load bearing capacity and stiffness of steel bridge piers at the same time. However, considering features of the damage as mentioned above, there is no need to stick to these conventional countermeasures, and other ideas can be proposed. The concrete filling method is one of the most effective and easiest methods to enhance both strength and ductility from the previous studies and our experiments. This approach has been used on many steel bridge piers in Kobe for reconstruction and repair of damaged highway bridges by the earthquake. However, in the case of existing piers, most of which are located in urban area, larger seismic force will be imposed on the anchors. This method is not advisable if the retrofit of the anchors are also necessary. Fig. 4 illustrates image of relationship between load bearing capacity and ductility before and after the retrofit. If the ductility is increased without greatly increasing the initial stiffness or maximum load bearing capacity, their seismic performance can be ensured without retrofitting the anchors. The following requirements were considered for proposing retrofit methods.

- Avoid failure modes
- Improve ductility
- Less increase in strength (Less increase in seismic force to anchors)
- Easy retrofit work on site

Fig. 5 illustrates the image of the seismic retrofit methods we proposed. Fig. 6 shows the behavior after the local buckling. As to rectangular piers, four corners are strengthened with flat plates or angle plates to prevent cracking at corners after local buckling. The concept is that even after the local buckling of the stiffened plates near the maximum load, the pier can maintain its bearing capacity as a kind of rigid frame structure composed of the four corners acting as columns and stiffened panels acting as bracings. As to circular section, another steel pipe is set around the bottom part of the pier with a small space between the existing pipe and the outer pipe. This outer pipe and the small space are important to control out-of-plane deformation after the local buckling. This outer pipe controls the deformation of the pier accompanying local buckling near the maximum load to prevent the large deformation of the pier and help the pier to keep the bearing capacity and improve ductility.

LOADING TESTS ON EFFECTIVENESS OF PROPOSED RETROFIT METHODS

Outline of Test Specimens

Typical test specimens are described in Table 3. They consists of eleven rectangular specimens and seven circular specimens. "As-built"(Original) types mean non-retrofit specimens, which have the section of typical existing piers, and the other types are retrofit ones. Yield stress of each specimen was obtained from the tension test of each material, and structural parameters for buckling are given with the yield stress of each specimen. Shape and size of each specimen are given in Fig. 7. Specimens are around one-third scale models of existing piers. Dimensions of the cross section are determined to be large enough to simulate the effect of corner plates and size of welding. The height of retrofitting is 1,800mm from the base of the column for rectangular specimens. The outer pipe of circular specimens was installed to the height of 600mm to cover the base region where the pier is expected to be buckled.

The values of structural parameters of stiffened panels were determined by referring to those for existing steel bridge piers designed by the past design codes. R_f and γ/γ^* of No.20 were set at approximately 0.55 and 0.9 respectively, where γ^* is the minimum necessary stiffness ratio of stiffeners obtained from elastic buckling theory. The stiffened plates of Specimen M8 have a larger width/thickness ratio than that of No.20. R_f of M8 is 0.85, close to maximum value in actual piers.

Retrofit for Rectangular Specimens

Retrofit methods for rectangular specimens are classified into three types by the types of reinforcement members and the connecting methods. Specimen No.11 is relatively stiff strengthening, in which flat plates (corner plates) are connected with high-strength bolts of the torque shear type between the vertical stiffeners at the inside of each corner. A triangle closed section of each corner is considered to have relatively high flexural stiffness and torsional stiffness as a column. Specimen K3 has smaller size of corner plates than that of Specimen No.11. Specimen No.5 is relatively flexible strengthening. Flat plates were placed between the angle plate and stiffened panels to avoid inside corner fillet weld. Specimen No.12 has smaller size of angle plates than that of No.5. Specimen No.22 is intended to apply to newly constructed piers. Corner plates are connected at corners by welding. Specimen No.18, No.33 and No.23 is for

investigating effect of axial force ratio.

Retrofit for Circular Specimens

Specimen No.6 and No.8 are different in diameter/thickness ratio. Outer pipe of retrofit specimens is placed over the as built pipe with small spacing to control the deformation after the buckling. The outer pipe is completely separated from as built pipe. The outer pipe does not contribute to increase the stiffness and the load bearing capacity of the as built pipe. When the pier locally buckles and deforms to a certain degree, the outer pipe restrains the further deformation at initial buckling section. The spacing between the two pipes was set at 10mm for both specimens No.7 and No.9. In case of Specimen No.15, the gap was set at 5mm.

In case of actual retrofit work, the outer pipe is divided into several arc members at the shop and welded on site. The gap should be filled with soft sealant or elastic material in order to prevent the corrosion.

Loading Method

All test specimen were loaded with two hydraulic jacks installed in the horizontal and vertical direction respectively in a fully rigid frame as shown in Fig. 8. Fig. 9 shows the experimental setup. With the axial force kept constant by the vertical jack, the cyclic lateral load was applied by the horizontal jack at the loading point of the head of specimen. The axial force was basically set at 15% of the full-section yield load calculated from the nominal yield stress, which is generally taken as average value of axial force in existing steel bridge piers. The horizontal loading program is shown in Fig. 10, where δ_{yo} is the displacement of the loading point when the specimen yields at the lower end. The specimen was first alternately loaded up to δ_{yo} and then alternately loaded by gradually increasing the amplitude as integral multiples of the displacement δ_{yo} like $\pm 2\,\delta_{yo}$, $\pm 3\,\delta_{yo}$, until the horizontal load dropped fully below the yield horizontal load. One cycle number was applied at each level of $n\,\delta_{yo}$. This loading pattern was adopted by considering the characteristics of ground motion of Hyogo-ken Nanbu Earthquake that the seismic force is very large but duration time is so short that the number of cyclic of seismic response is relatively small. The basic displacement δ_{yo} under cyclic loading is calculated by

$$\delta_{yo} = \frac{H_y h}{3EI} \qquad \cdots\cdots(1)$$

$$H_y = \left(\sigma_y - \frac{P}{A}\right)\frac{z}{h} \qquad \cdots\cdots(2)$$

where σ_y is the yield stress of the steel, z is the section modulus of the specimen.

Experimental Results

Failure Processes

Fig. 11 shows the process of failure for as-built rectangular and circular section respectively. As to the rectangular specimen, the deformation of stiffened panels gradually increased beyond the peak load. As to the circular specimen, convex local buckling in the

column base on the compression side occurred just before the peak horizontal load. Subsequent cyclic loading gradually increased the buckling deformation and extended it into the circumferential direction. Finally, this buckling deformation met with similar buckling deformation progressing from the opposite side, resulting into the elephant foot buckling mode.

Fig. 12 shows the difference of appearance after the peak load between as-built section and retrofit specimen for rectangular sections. With the increase of deformation, corners of as built specimen No.20 gradually lost straightness and twisted. On the other hand, retrofit specimen No.11 kept straightness of each corner even after the peak load for a while.

Fig. 13 shows the downward view of inside of retrofit specimen No.15 from the upper side after the test. Because of restriction of out-of-plane deformation by outer pipe, deformed areas of the pipe dispersed to upper side. After the contact of the existing pipe with the outer pipe, the deformation of the first mode was prevented, and next buckling occurred as the second deformation mode.

Horizontal Load - Horizontal Displacement Relations

Table 4 shows the test results. δ_u is defined as displacement at which the horizontal load hardly falls down below the maximum level (97% of the maximum level). The horizontal load-horizontal displacement relationship(hysteresis loops) of main specimens are shown in Fig. 14 and Fig. 15. The load-displacement envelopes of as built sections are also shown by dotted lines in the figures. The maximum displacement at which the corners can be kept straight are indicated by the inverted triangle symbol ($\triangledown$) in the hysteresis loops of Fig. 14. Encircled figures on the hysteresis loop indicate multiples of δ_y. The envelopes of the horizontal load-horizontal displacement relations are separately shown for the specimens of the same basic section in Fig. 16 and Fig. 17.

Deterioration of Specimen No.20 and M8 after the peak load is considerable. Compared to this, retrofit specimens are expected to have more ductility. Especially, Specimen No.5 and No.22 maintained the straightness of the corners until the displacement reached about -6 δ_{y0}. In this way, strengthening of corners by corner plates is considered to change the original structure into a stable rigid frame structure composed of four corner columns and web panel bracings as shown in Fig. 6 after the local buckling of the stiffened panels and to delay the deterioration of load bearing capacity. Fig. 18 shows the effect of corner plates bolted at corners on ductility. δ_u / δ_y is ductility factor. $I_{retrofit} / I_{as\text{-}built}$ is ratio of moment of inertia of retrofit section to that of as built section. With increase of ratio of inertia of moment up to 1.2, the ductility factor increase from 2.5 to around 6. It is not so difficult to increase the ratio up to 1.2 in practical retrofit design.

As to circular sections, the ductilities of specimens with outer pipe are improved after the maximum loading point. Deterioration slope in envelope of Specimen No.7 and No.15 after the peak are gentle compared to Specimen No.6 and No.8 respectively. As to Specimen No.7 and No.15, the deformed portion of the column body was considered to have contacted the outer pipe around the peak load. However, in Specimen No.9, before the horizontal load fell down below the maximum load, the outer pipe did not function effectively. The reason is that the gap in specimen No.9 was relatively large when considering the ratio of gap to the thickness of the existing pipe.

CONCLUSIONS

Concepts of seismic retrofit of steel bridge piers and proposed retrofit methods were described in the paper. Loading tests were carried out with eleven rectangular specimens and seven circular specimens to clarify the effectiveness of proposed retrofit methods. From the behavior of specimens after the local buckling, it is confirmed that the proposed methods are effective to improve ductility without much increase of strength of the steel bridge piers. The results from the loading tests are concluded as follows:

1) For rectangular steel columns, strengthening of the corners by corner plates is effective to maintain the bearing capacity and improve the ductility as well as prevent cracking at corners after local buckling of stiffened panels. Even after the local buckling of the stiffened plates after the maximum load, corner parts of the retrofit specimens can keep the straightness of the corners for a while as a kind of rigid frame structure composed of the four corners acting as columns and stiffened panels as bracings.
2) For circular steel columns, installation of an additional outer pipe around the bottom of the pier with a certain gap is effective to improve the ductility without changing the initial stiffness and the maximum bearing carrying capacity. This outer pipe and the gap can restrain the progress of the first buckling mode, control the amount of out-of-plane deformation after local buckling, and help the pier to improve the ductility.

REFERENCES

[1] Ministry of Construction : Guide Specifications for Reconstruction and Repair of Highway Bridges Suffered Damage due to the Hyogo-ken Nanbu Earthquake, 1995.2.

[2] Committee for Investigation on the Damage of Highway Bridges Caused by the Hyogo-ken Nanbu Earthquake : Final Report on the Damage of Highway Bridges by the Hyogo-ken Nanbu Earthquake, 1995.12.

[3] Japan Road Association : Reference for Applying the "Guide Specifications for Reconstruction and Repair of Highway Bridges which Suffered Damage due to the Hyogo-ken Nanbu Earthquake", 1995.6.

[4] Japan Society of Civil Engineers, Committee of Steel Structures, Sub-Committee on Inelastic Behavior of Steel Structures : Inelastic Behavior of Steel Structures and Earthquake Resistant Design Methods, Journal of Structural Mechanics and Earthquake Engineering, No.489/I-27, 1994.4.

[5] Japan Society of Civil Engineers, Committee of New Technologies in Steel Structures : The Report of New Technologies for Steel Structures, 1993.3.

[6] Japan Road Association : Design Specifications of Highway Bridges - Part V Seismic Design, 1990.2.

Table 1 Definition of Damage Degree of Steel Piers

Damage Degree	Definition
As	Collapsed. Extremely serious damage or deformation.
A	Cracking, buckling or serious deformation.
B	Partial buckling or deformation of members.
C	Localized light buckling or deformation.
D	No damage, or if there is, extremely minor damage that will not effect the load bearing capacity.

Table 2 Damage Degree of Steel Piers (number)

Damage Degree					Total
As	A	B	C	D	
4 (1%)	11 (3%)	36 (10%)	138 (39%)	166 (47%)	355 (100%)

Table 3 Test Specimens

(a) Rectangular Section

Specimen	Type	Dimension of Corner or Angle Plates	Steel Grade	σ_y (kgf/cm²)	$\frac{N}{Ny}$	R_R	R_F	$\bar{\lambda}$
No.20	As-Built		SM490	4,160	0.125	0.585	0.611	0.272
No.18	As-Built		SM490	3,900	0.197	0.567	0.591	0.264
No.11	Corner Plates (Bolted)	4-PL 295X6	SM490	3,770	0.128	0.557	0.581	0.259
No.33	Corner Plates (Bolted)	4-PL 295X6	SM490	3,750	0.154	0.556	0.580	0.258
K3	Corner Plates (Bolted)	4-PL 220X4.5 (S)	SM490	3,940	0.122	0.570	0.594	0.265
No.22	Corner Plates (Welded)	4-PL 170X9	SM490	3,900	0.106	0.567	0.591	0.261
No.23	Corner Plates (Welded)	4-PL 170X9	SM490	3,910	0.169	0.567	0.592	0.261
No.5	Angle Plates (Bolted)	4-L 90X90X9, 8-Fill 90X9	SM490	3,770	0.128	0.557	0.581	0.258
No.12	Angle Plates (Bolted)	4-L 75X75X6, 8-Fill 75X4.5 (S)	SM490	3,770	0.128	0.557	0.581	0.259
M8	As-Built		SM490	3,590	0.134	0.652	0.847	0.251
No.28	Corner Plates (Bolted)	4-PL 295X6	SM490	3,780	0.134	0.669	0.869	0.257

(b) Circular Section

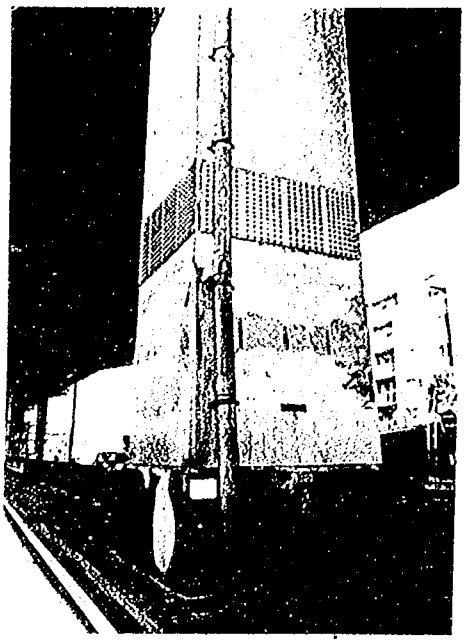
Specimen	Type	Steel Grade	σ_y (kgf/cm²)	$\frac{N}{Ny}$	R_t	$\bar{\lambda}$
No.6	As-Built	SM490	3,510	0.137	0.0763	0.283
No.7	Outer Pipe (Gap=10mm)	SM490	3,540	0.136	0.0769	0.285
No.8	As-Built	SS400	2,960	0.122	0.115	0.258
No.29	As-Built	SS400	3,150	0.199	0.123	0.268
No.9	Outer Pipe (Gap=10mm)	SS400	2,850	0.126	0.111	0.253
No.15	Outer Pipe (Gap= 5mm)	SS400	3,130	0.115	0.122	0.267
No.31	Outer Pipe (Gap= 5mm)	SS400	3,150	0.199	0.123	0.268

Note : σ_y = Yield Stress, N/N_y = Axial Force Ratio, $\bar{\lambda}$ = Slenderness Ratio $(=1/\pi\sqrt{(\sigma_y/E)}\cdot(l/r))$
R_R = Width/Thickness Ratio of Flange Panel $(= b/t\cdot\sqrt{(\sigma_y/E)\cdot 12(1-\nu^2)/\pi^2 k_R})$
R_F = Width/Thickness Ratio between Longitudinal Ribs $(= b/t\cdot\sqrt{(\sigma_y/E)\cdot 12(1-\nu^2)/\pi^2 k_F})$
R_t = Radius/Thickness Ratio $(= (R/t)\cdot(\sigma y/E)\cdot\sqrt{3(1-\nu^2)})$

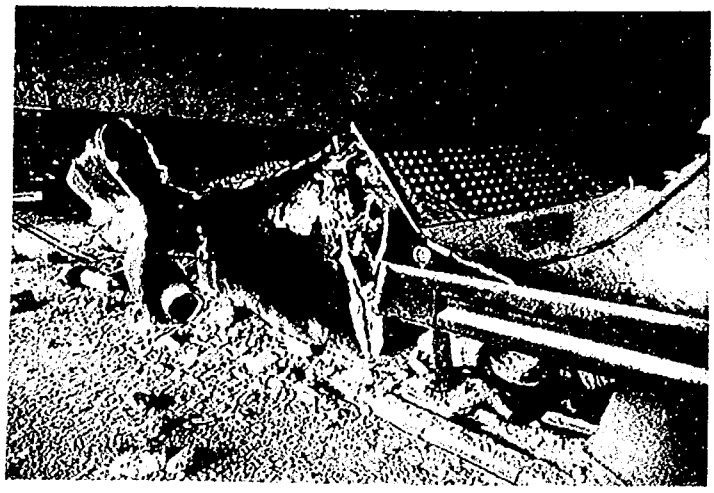
Table 4 Test Results

Specimen			$\frac{N}{Ny}$	P_y (tf)	P_u (tf)	$\frac{P_u}{P_y}$	δ_y (mm)	δ_m (mm)	δ_u (mm)	$\frac{\delta_m}{\delta_y}$	$\frac{\delta_u}{\delta_y}$
Rectangular Section	No.20	As-Built	0.125	114	140	1.23	14.7	38	42	2.6	2.9
	No.18	As-Built	0.197	98	130	1.33	14.0	28	36	2.0	2.6
	No.11	Corner Plates (Bolted)	0.128	103	153	1.49	12.4	60	72	4.8	5.8
	No.33	Corner Plates (Bolted)	0.154	99	148	1.49	14.4	54	65	3.8	4.5
	K3	Small Corner Plates (Bolted)	0.122	108	151	1.40	14.3	47	56	3.3	3.9
	No.22	Corner Plates (Welded)	0.106	129	173	1.34	16.0	58	78	3.6	4.9
	No.23	Corner Plates (Welded)	0.169	120	162	1.35	16.4	44	57	2.7	3.5
	No.5	Angle Plates (Bolted)	0.128	103	175	1.70	11.6	49	62	4.2	5.4
	No.12	Small Angled Plates (Bolted)	0.128	103	150	1.46	12.4	43	53	3.5	4.3
	M8	As-Built	0.134	101	111	1.10	18.4	34	36	1.9	2.0
	No.28	Corner Plates (Bolted)	0.134	106	153	1.44	14.8	44	55	3.0	3.7
Circular Section	No.6	As-Built	0.137	86	157	1.83	12.6	51	78	4.1	6.2
	No.7	Outer Pipe (Gap=10mm)	0.136	87	161	1.86	13.3	59	98	4.4	7.4
	No.8	As-Built	0.122	42	61	1.43	9.4	26	35	2.8	3.7
	No.29	As-Built	0.199	41	54	1.31	9.1	24	29	2.6	3.2
	No.9	Outer Pipe (Gap=10mm)	0.126	41	61	1.51	9.8	26	35	2.6	3.6
	No.15	Outer Pipe (Gap=5mm)	0.115	45	66	1.47	10.3	36	48	3.5	4.7
	No.31	Outer Pipe (Gap=5mm)	0.199	41	55	1.35	9.1	34	40	3.7	4.4

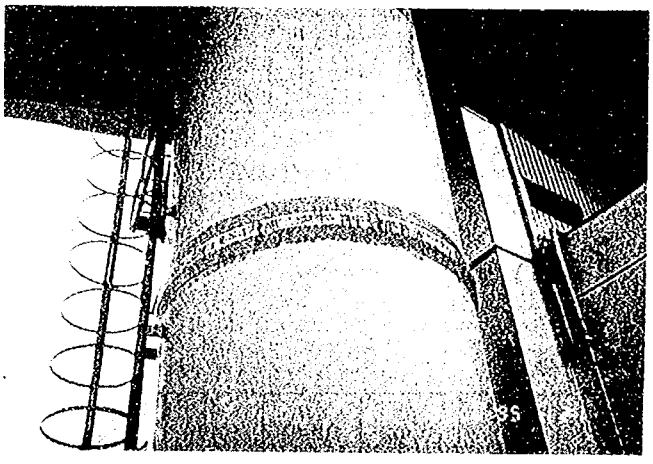
Note : N/N_y = Axial Force Ratio, P_y = Horizontal Yield Load, P_u = Maximum Horizontal Load
δ_y = Yield Horizontal Displacement, δ_m = Horizontal Displacement at P_u, δ_u = Displacement at 97% of P_u



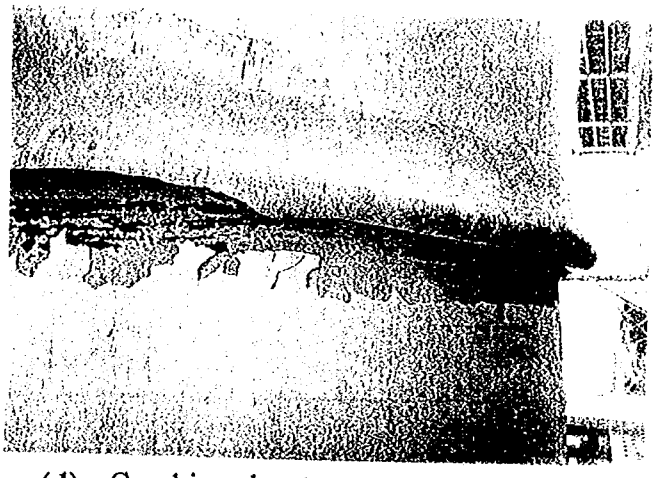
(a) Local buckling
at the bottom part



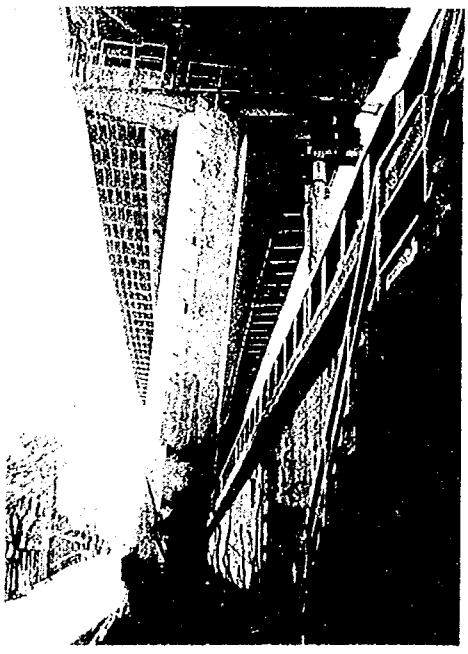
(b) Collapsed pier
(Breaking of corners)



(c) Elephant foot buckling
at the changing part of sections

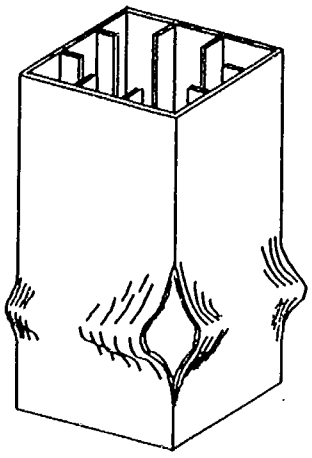


(d) Cracking due to progress
of local bucklong

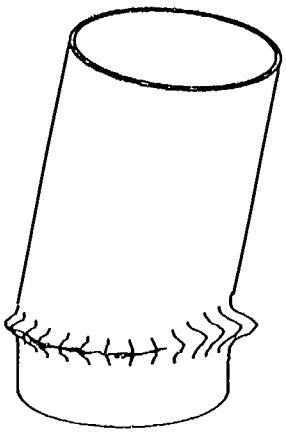


(e) Residual Displacement
Due to Local Buckling

Fig. 1 Damage of Steel Piers

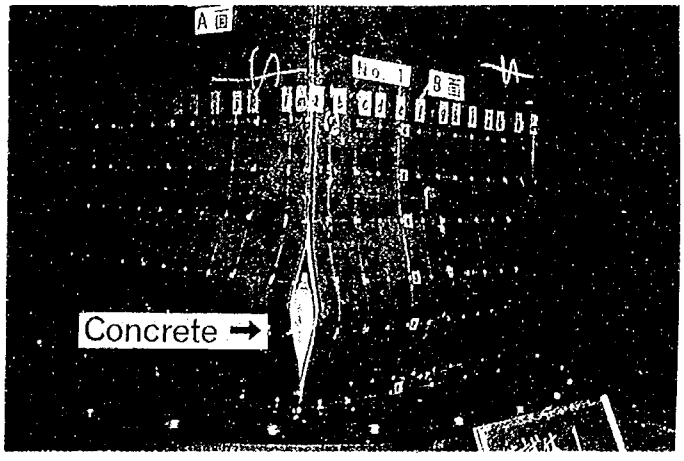


(a) Breaking of Corners



(b) Progress of Local Deformation, Large Residual Displacement, Cracking at Deformed Point

Fig. 2 Failure Mode



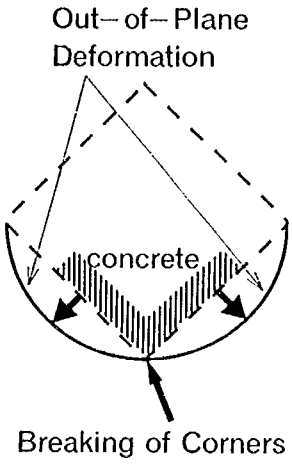


Fig. 3 Breaking of Corners of a Specimen under Cyclic Loading Test

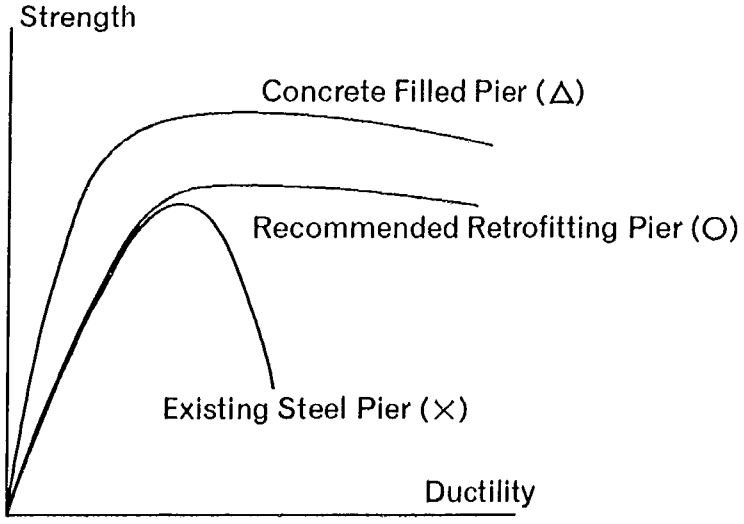
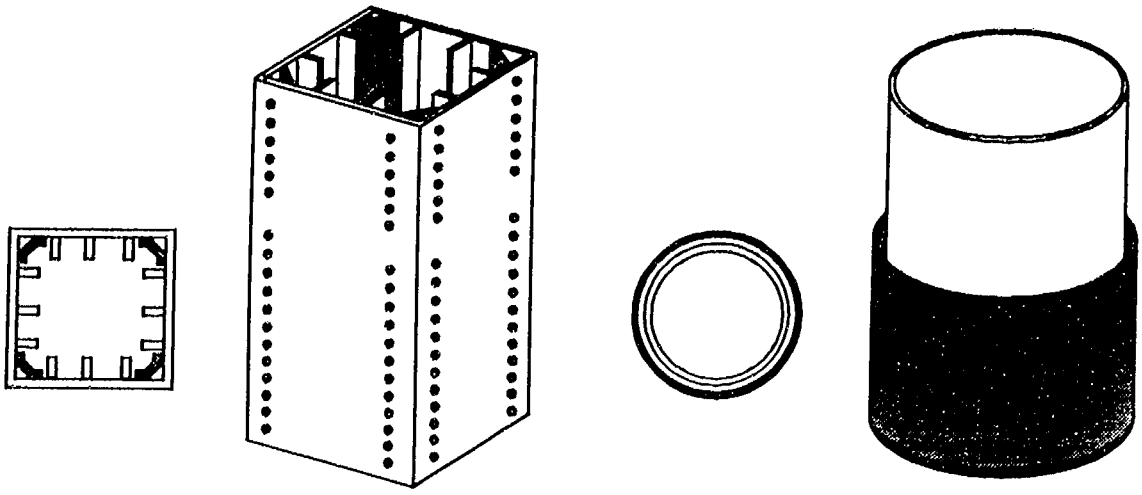
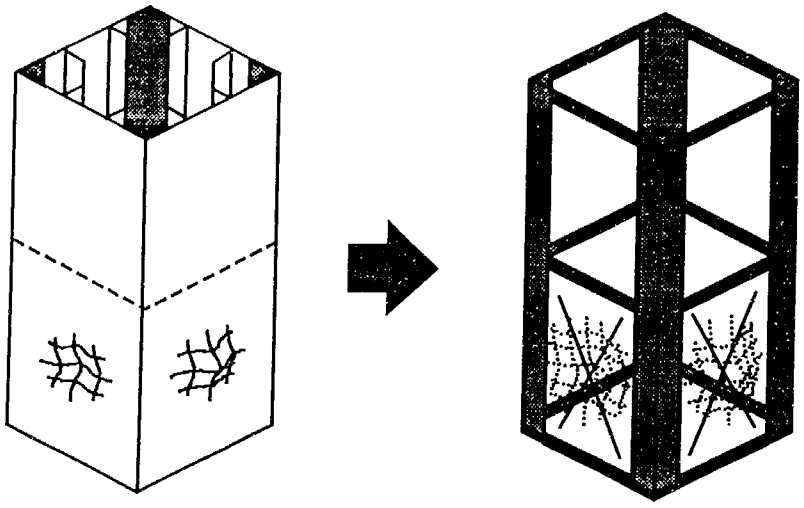


Fig. 4 Effect of Retrofit of Steel Piers

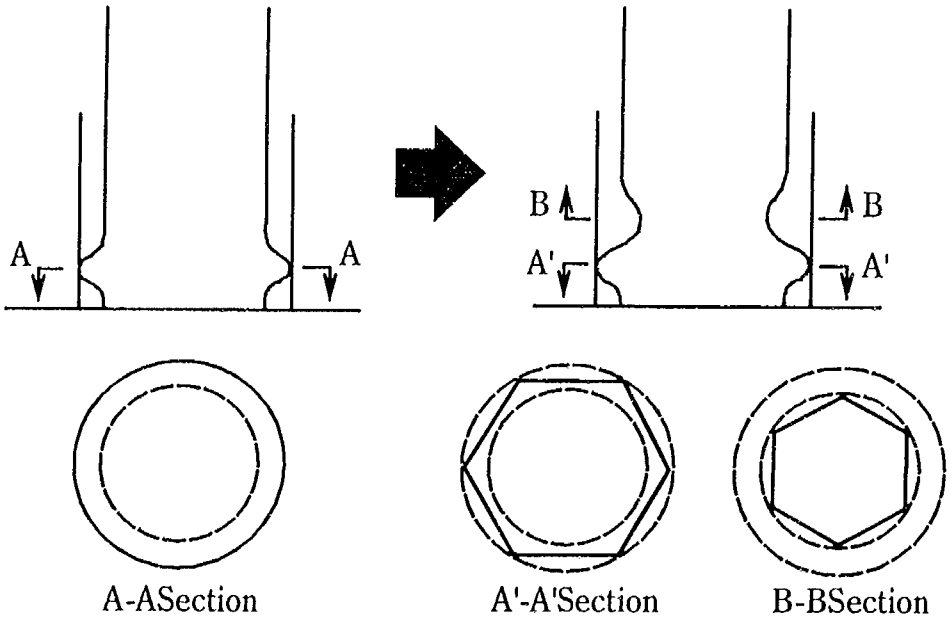


(a) Rectangular Piers (b) Circular Piers

Fig. 5 Image of Proposed Seismic Retrofit of Steel Piers



(a) Rectangular Piers



(b) Circular Piers

Fig. 6 Behaviors After Local Buckling

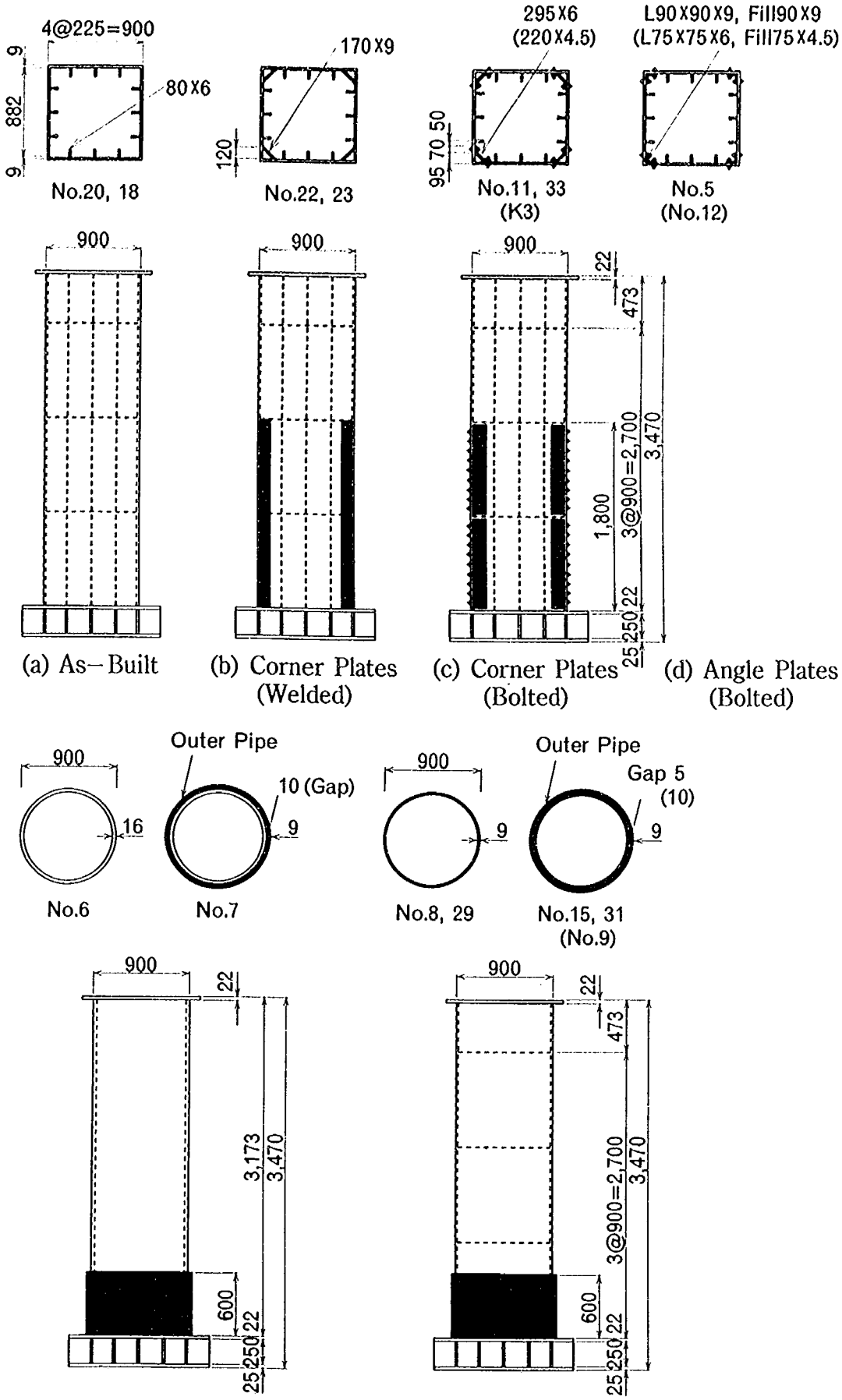


Fig. 7 Shape and Size of Specimens

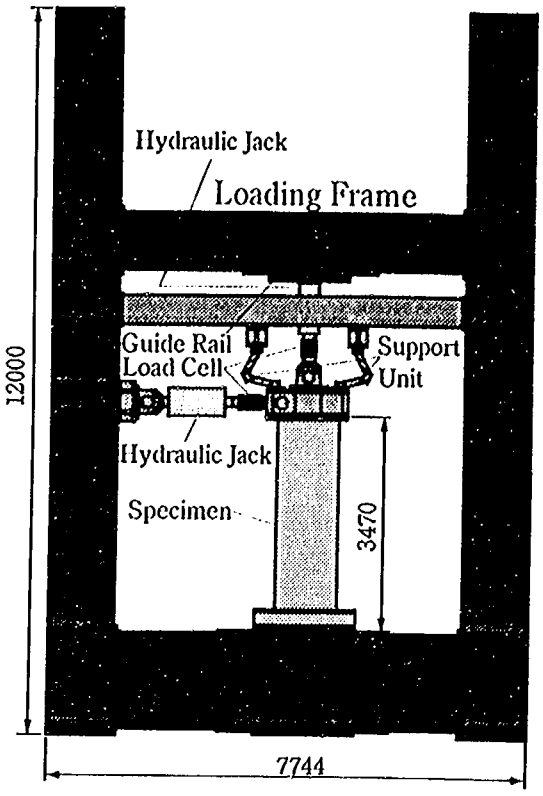


Fig. 8 Test Specimen and Detail of Load Application

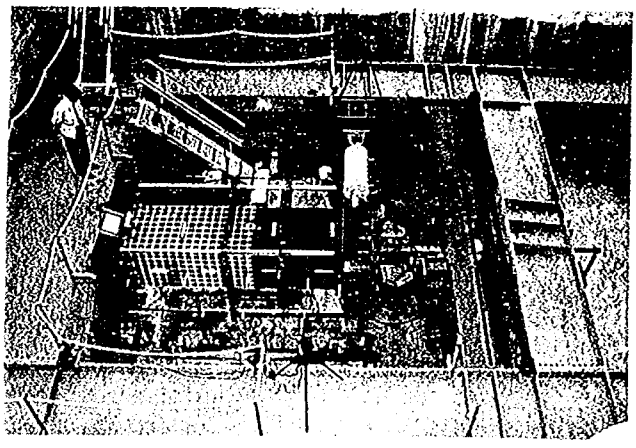


Fig. 9 Test Setup

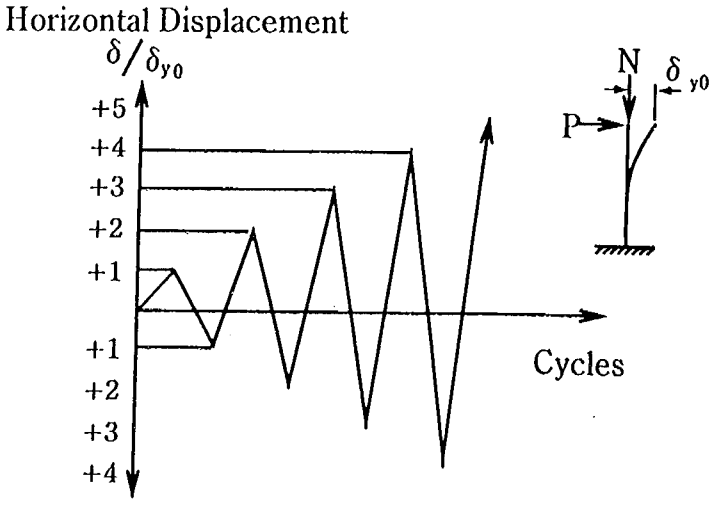
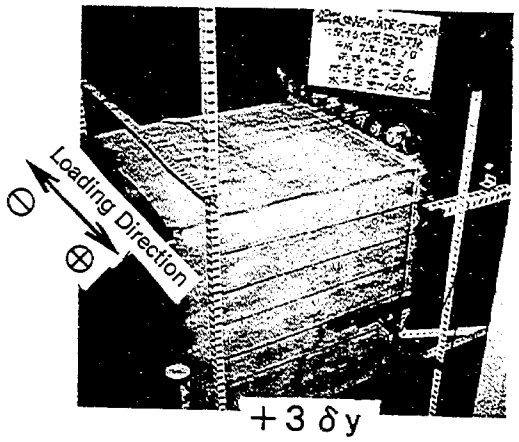
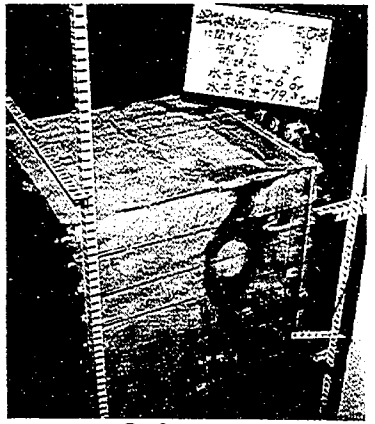


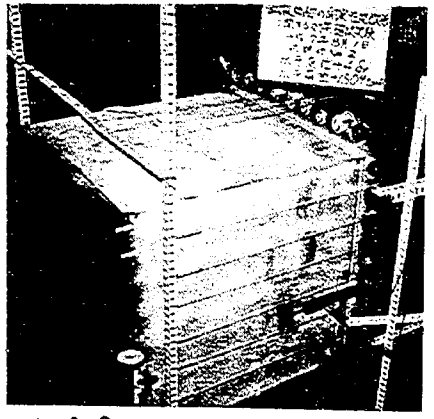
Fig. 10 Type of Horizontal Loading



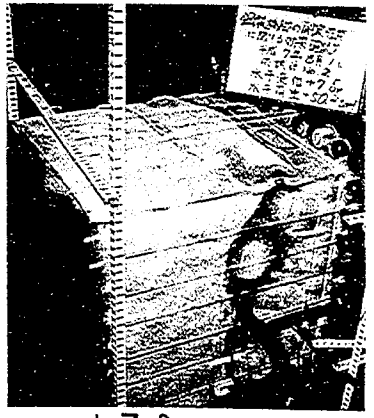
+3 δy



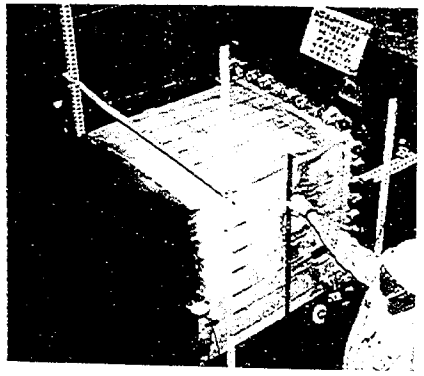
+6 δy



+4 δy Around Peak Load

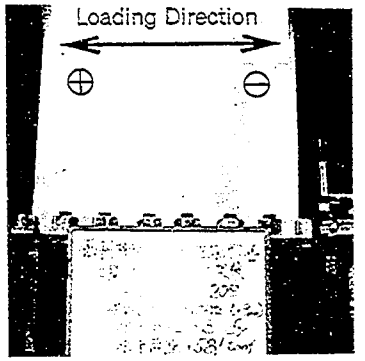


+7 δy

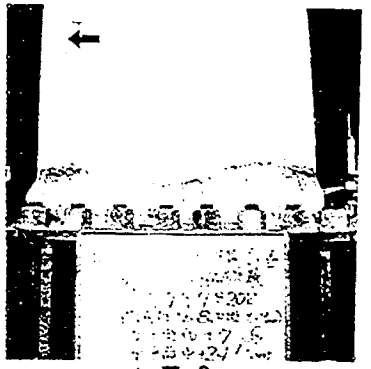


+5 δy Just before the Loss of Straightness of Corners

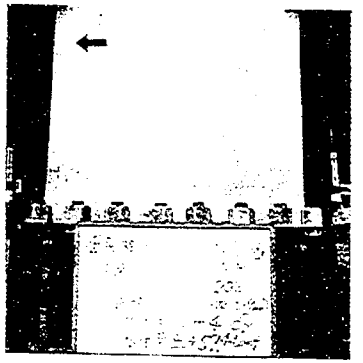
Fig. 11(a) Process of Failure of Rectangular Section (No.2 : the same as No.20)



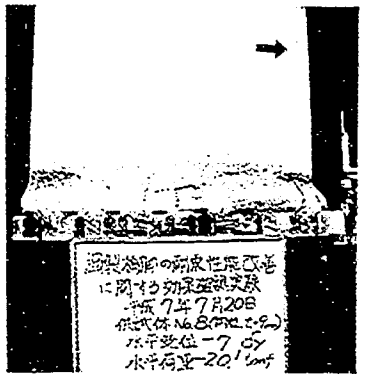
+3 δy



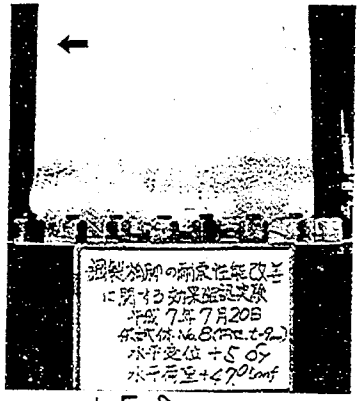
+7 δy



+4 δy Around Peak Load

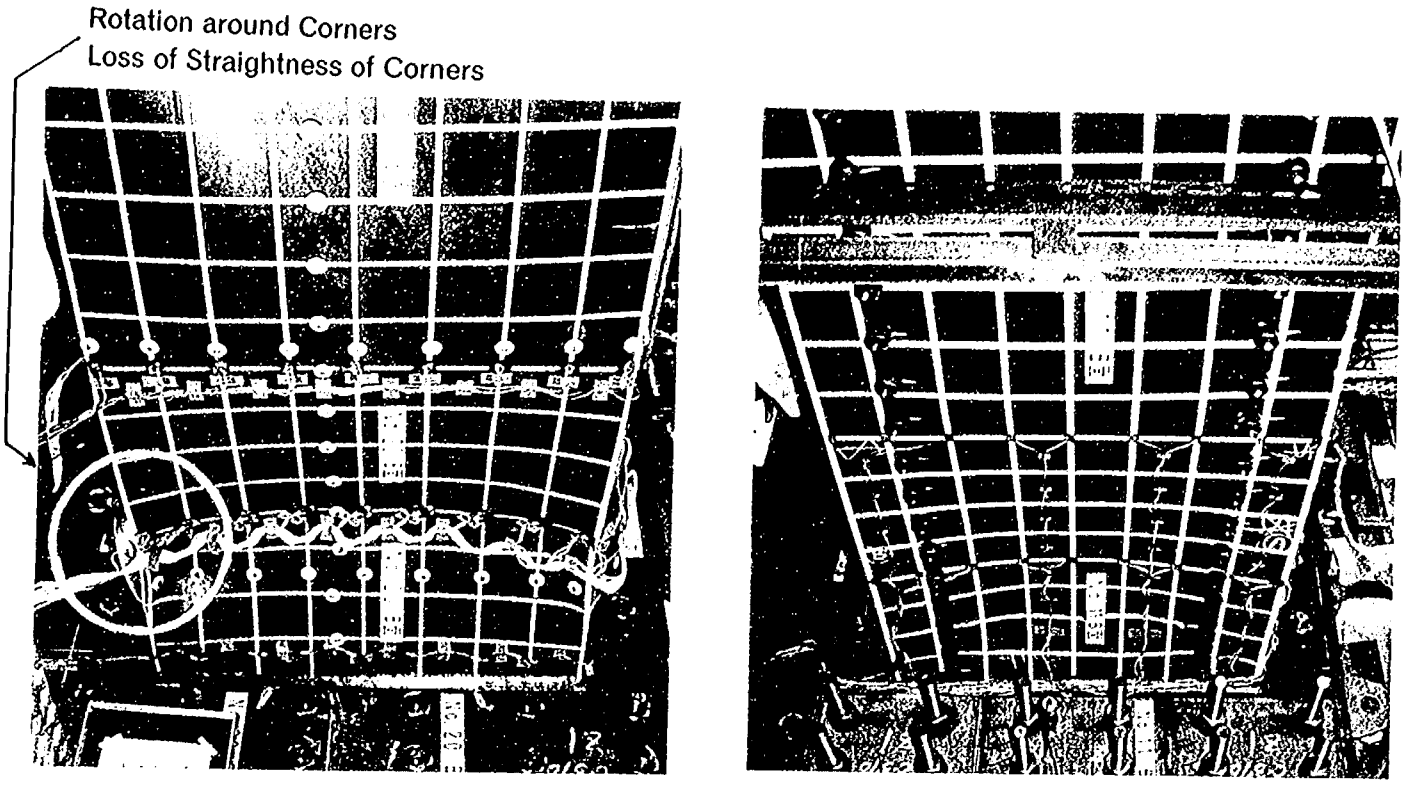


−7 δy Occurrence of Elephant Buckling



+5 δy

Fig. 11(b) Process of Failure of Circular Section (No. 8)



No. 20 $-5\delta y$

(a) As-Built Type

No. 11 $-6\delta y$

(b) Retrofit Type by Corner Plates

Fig. 12 Effect of Coner Plates

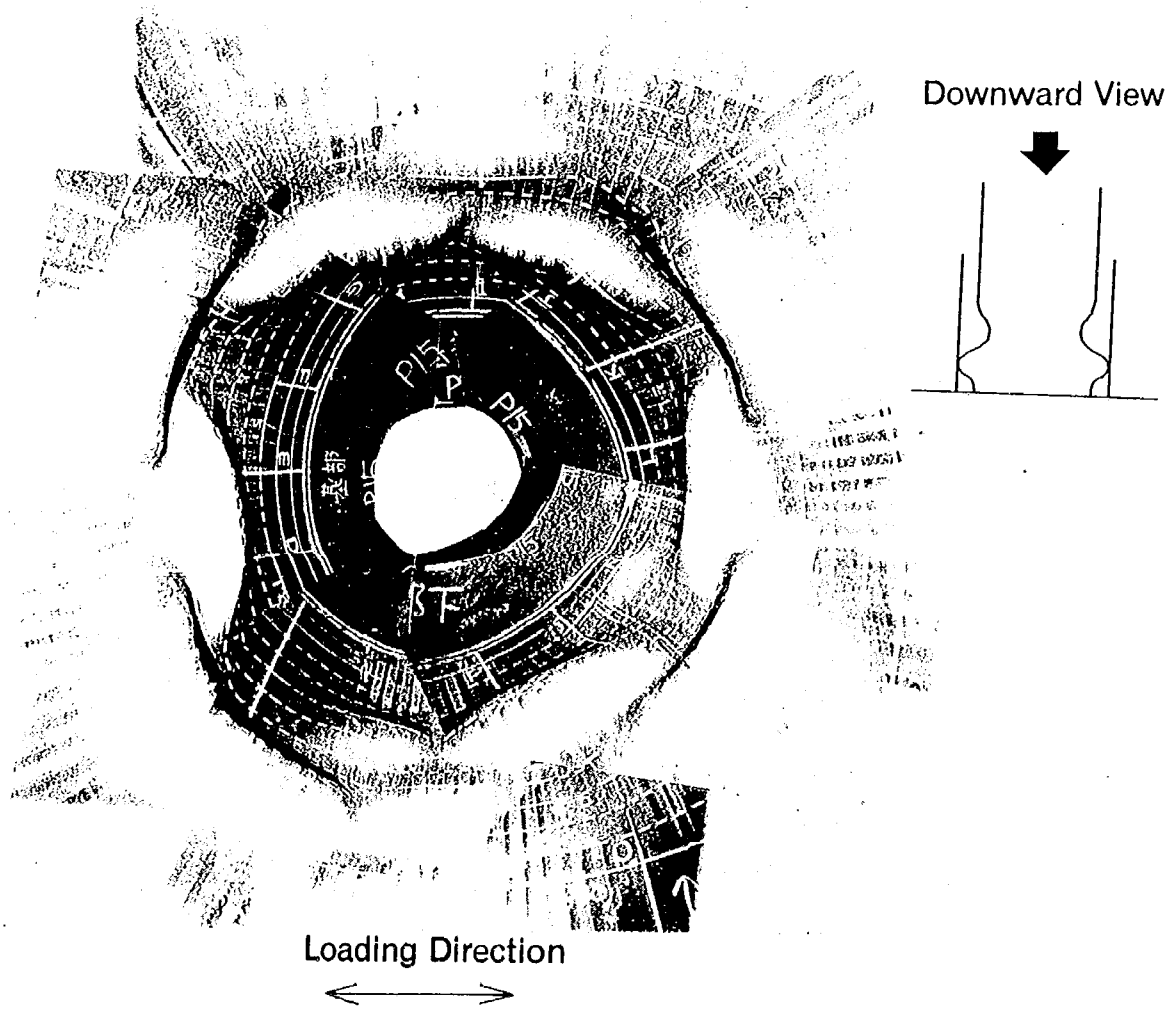
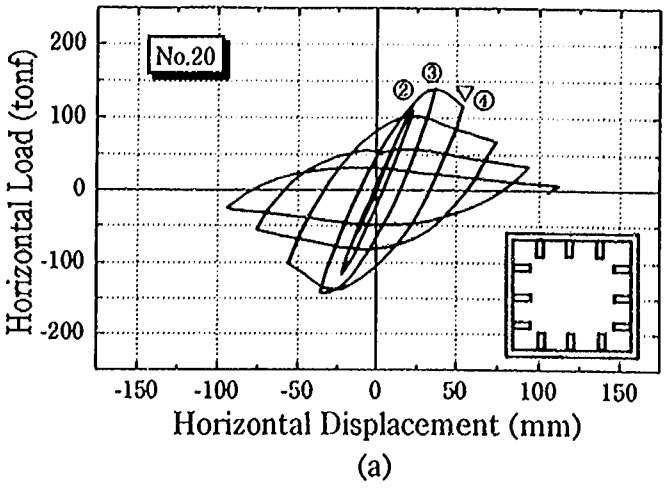
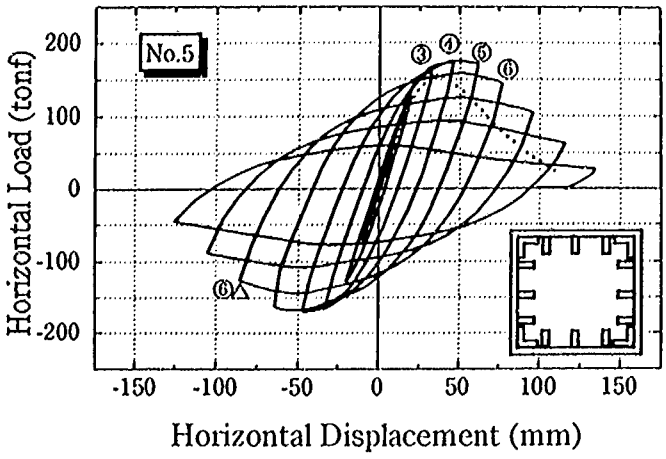


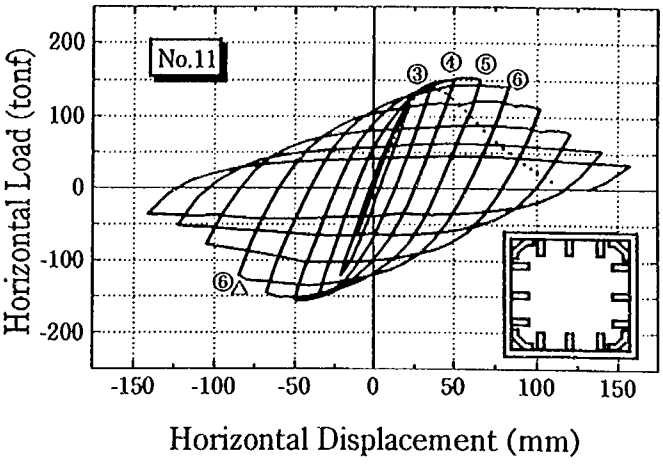
Fig.13 View of the Inside of Retrofit Specimen After the Test



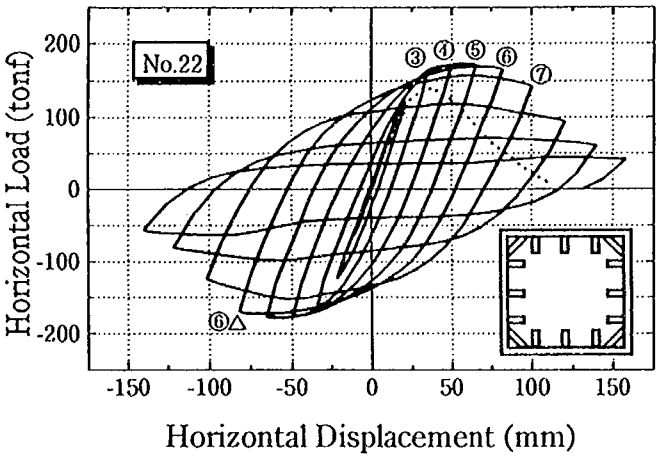
(a)



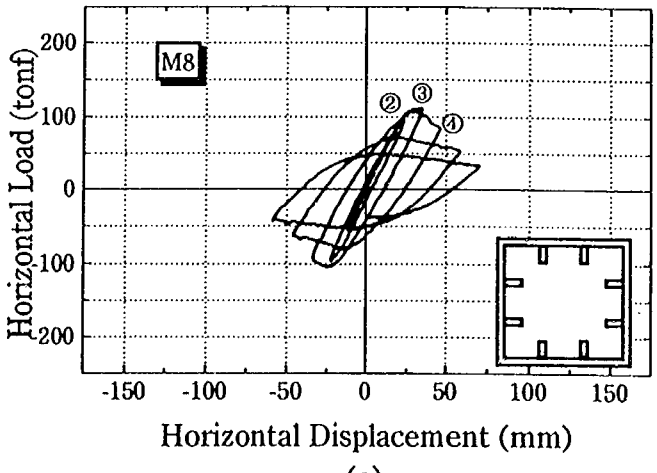
(b)



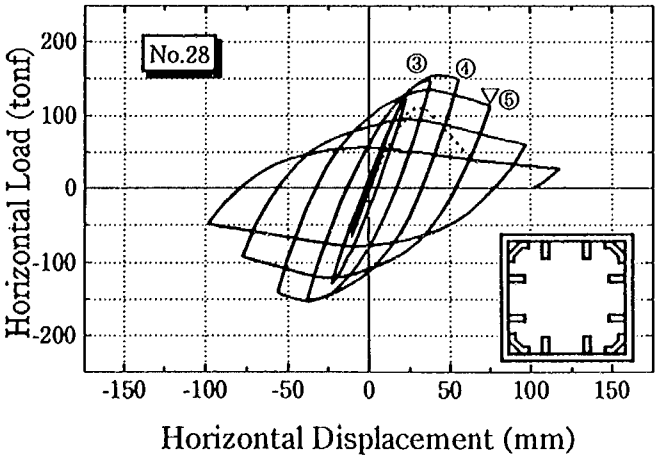
(c)



(d)



(e)



(f)

Fig. 14 Relation between Horizontal Load and Horizontal Displacement (Rectangular Section)

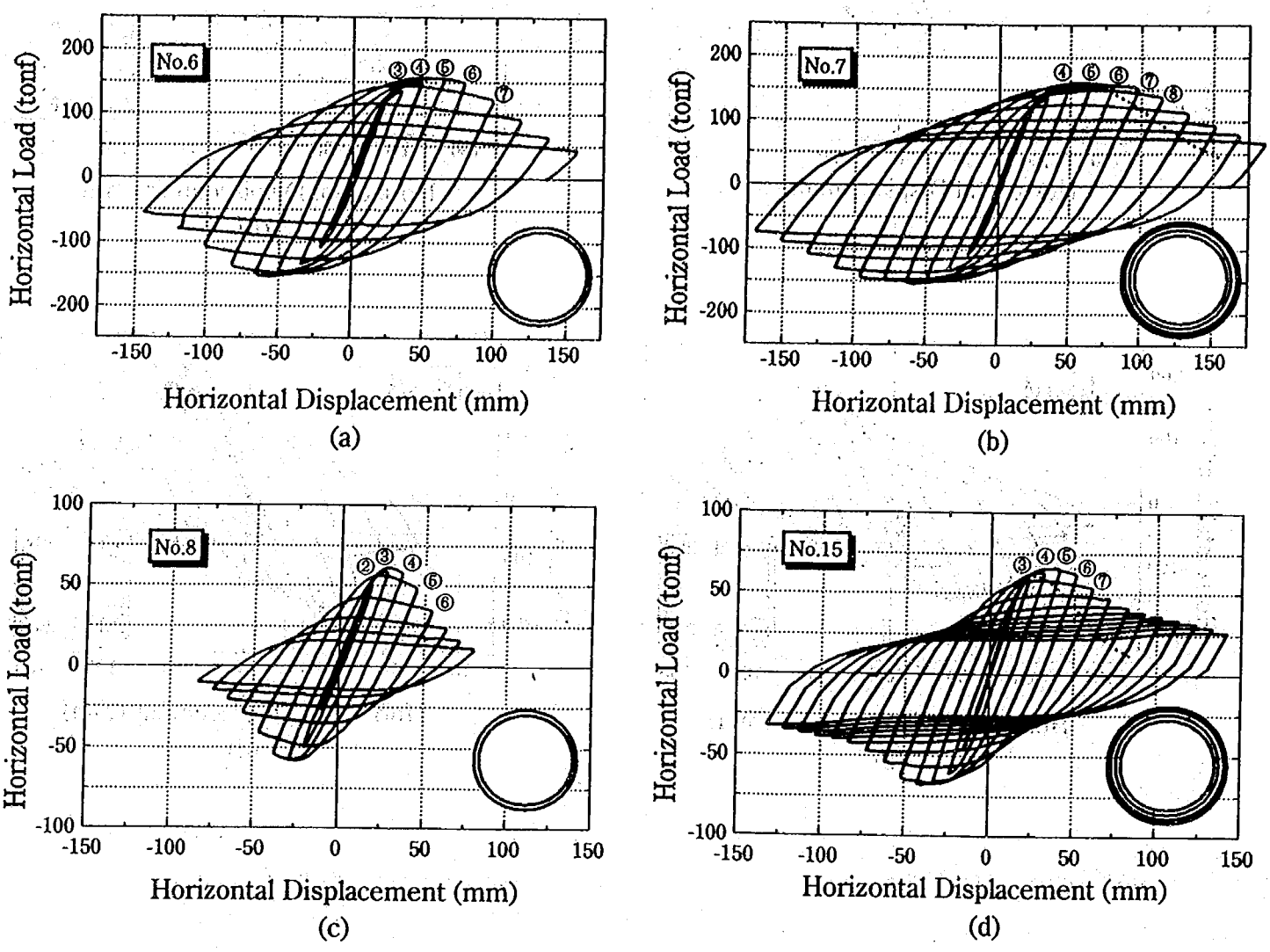
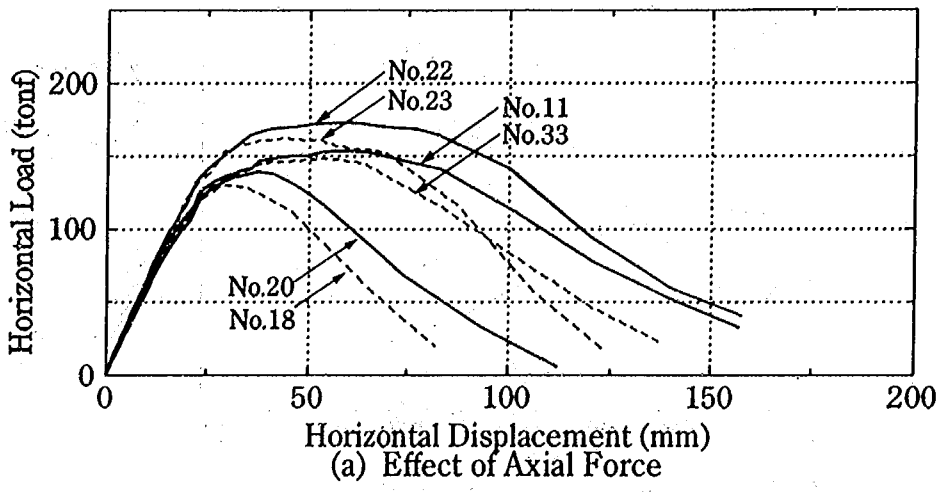
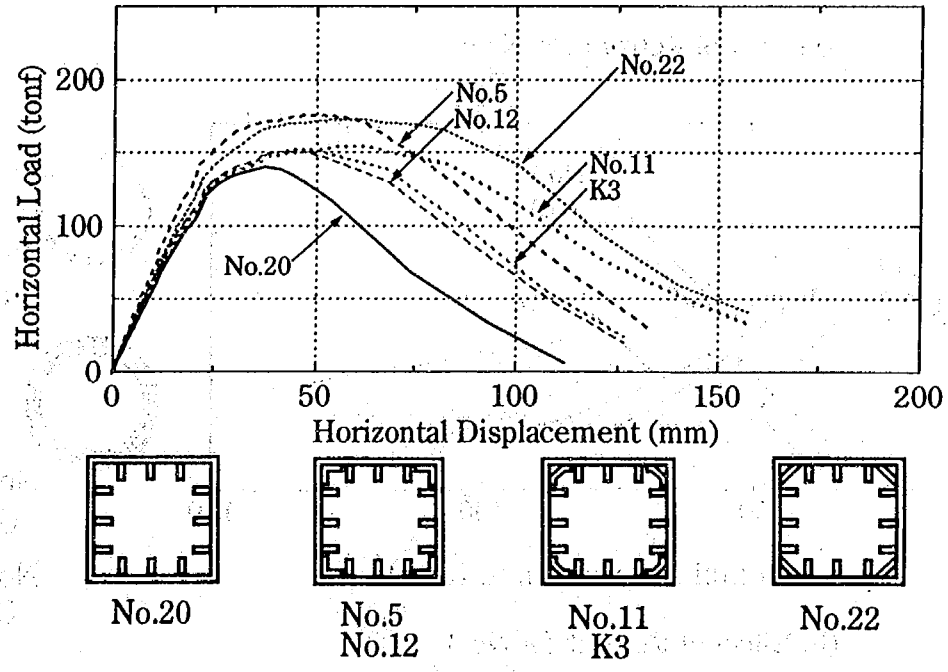


Fig.15 Relation between Horizontal Load and Horizontal Displacement (Circular Section)

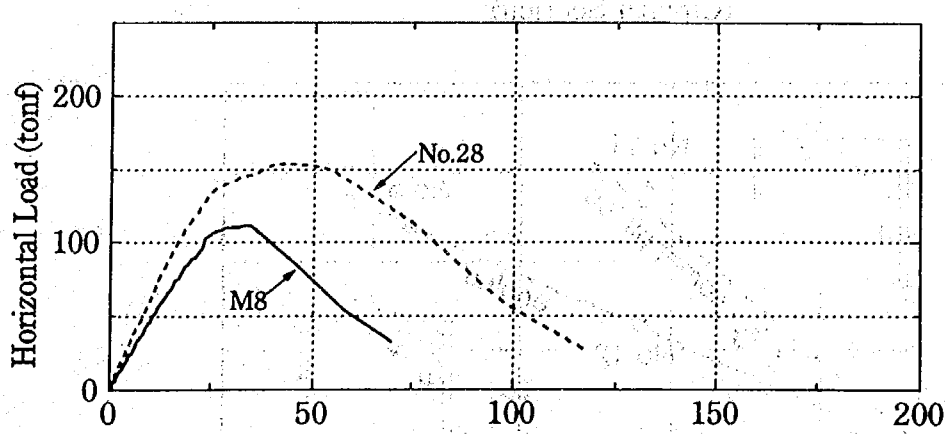


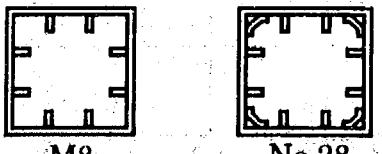
(a) Effect of Axial Force



No.20 | No.5 No.12 | No.11 K3 | No.22

(b) Effect of Retrofit for No.20

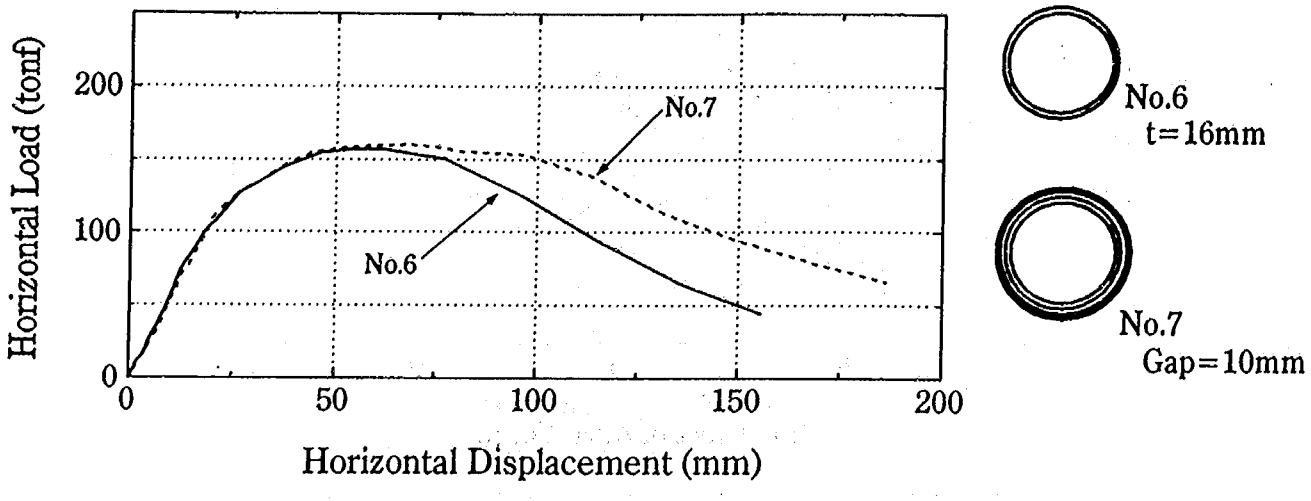




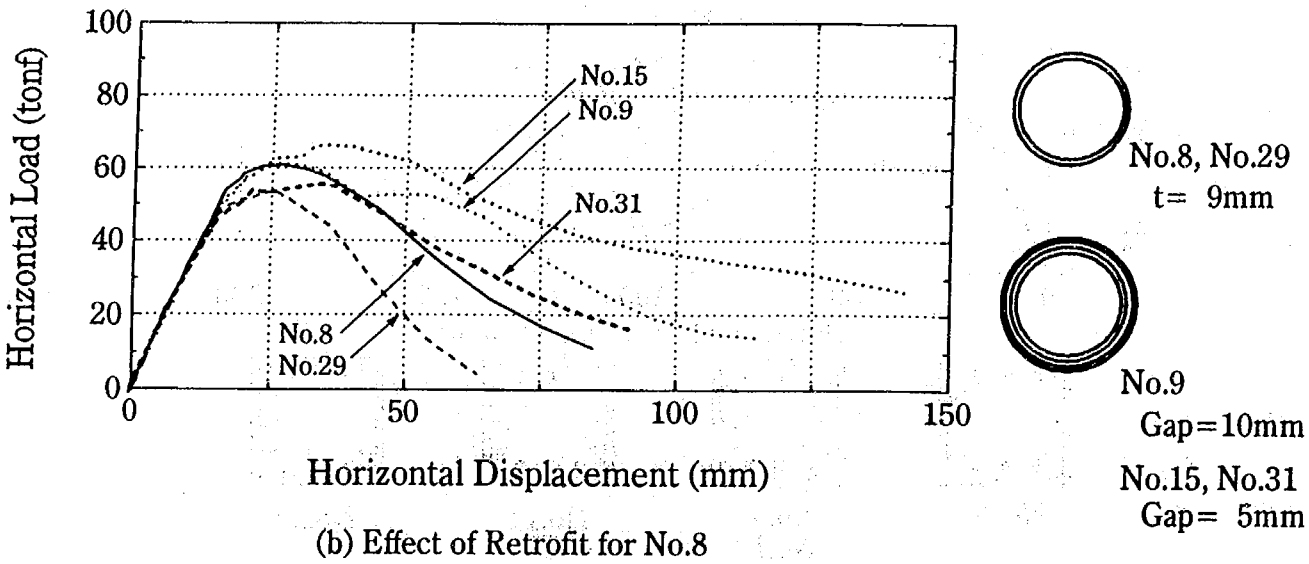
M8 | No.28

(c) Effect of Retrofit for M8

Fig. 16 Horizontal Load - Horizontal Displacement Envelope (Rectangular Section)



(a) Effect of Retrofit for No.6



(b) Effect of Retrofit for No.8

Fig. 17 Horizontal Load - Horizontal Displacement Envelope (Circular Section)

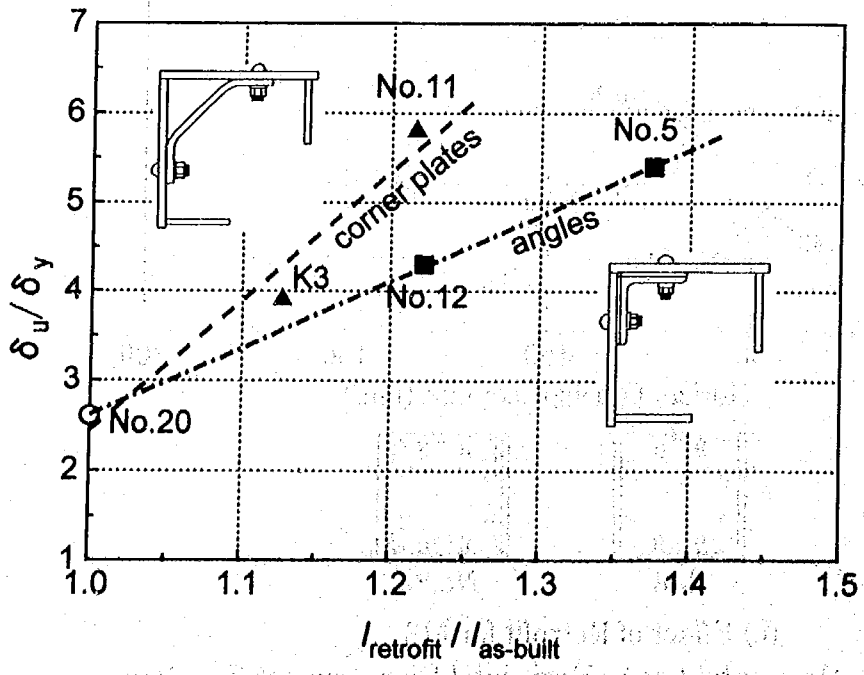


Fig. 18 Effect of Corner Plates on Ductility

Intermediate Hinge Restrainers for Bridges: Performance, Design, and Retrofit

Reginald DesRoches and Gregory L. Fenves

Earthquake Engineering Research Center
University of California, Berkeley

1 Introduction

The dynamic response of multiple-frame bridges and viaducts subjected to earthquake ground motion is affected by many factors: varying properties of frames, yielding of frames, opening and pounding of adjacent frames at intermediate hinges, spatially varying ground motion, and soil-structure interaction. In particular, the opening and closing of hinges and engagement of hinge restrainers produces discontinuities that change the load path and alter the response compared with a continuous structure.

The current design procedures for restrainers and hinge seats (AASHTO and Caltrans) are approximate and may not adequately represent the actual behavior nor do the resulting designs necessarily provide the desired performance during an earthquake. The restrainer design procedure used by Caltrans implies that hinge openings will be limited to the yield displacement of the restrainer. Recent studies have shown that for many cases the restrainers will not meet this performance objective (Saiidi et al., 1996; Yang et al., 1994).

This paper first summarizes the performance of intermediate hinge restrainers in recent earthquakes. Recognizing that restrainer and hinge performance may not be adequate, the paper then presents rational design procedures for restrainers and hinge seat widths for multiple-frame bridges that are appropriate for bridge retrofit and new construction. The results of a parameter study and case studies using nonlinear time history analyses show that the proposed restrainer design procedure is more effective than current procedures for determining the number of restrainers required to limit hinge displacement. The proposed procedure considers only the effects due to longitudinal bridge response. However, extensions to consider effects of transverse response and plan curvature are possible.

2 Background

Following the 1971 San Fernando Earthquake the California Department of Transportation pursued a seismic retrofit program for bridges in the state. The 1971 earthquake showed that bridges are vulnerable to collapse due to unseating at their intermediate hinges (Jennings,

1971). To prevent unseating, spans where tied together with cable restrainers at their hinges. In addition, for new bridges hinge seat widths were increased to 24 inches. In the retrofit of older bridges, the function of restrainers is to avoid excessive relative movement at hinges. As a result, restrainers are designed to avoid yielding even under maximum credible earthquakes. The purpose of restrainers in new bridges is to provide overall integrity for the superstructure. Yielding of restrainers can result in large hinge movements but, because the seats are wide, the movement may not necessarily lead to collapse.

There have been several studies of hinge restrainers. Researchers at the University of Nevada Reno found that the effectiveness of restrainers depends on many factors including intensity of ground motion and stiffness of frames (Saiidi et al., 1996). They recommend that time history analyses need to be performed to predict the number of restrainers required to limit hinge displacement. Singh and Fenves studied the effects of hinge restrainers on the response of two-level viaducts (Singh and Fenves, 1994). They found that hinge openings reached 30 inches, and a large number of restrainers may be needed to reduce the displacement, for cases where non-uniform soil properties causes non-uniform input motion to a viaduct.

A recent study focused on broader range of parameters for hinge restrainers (Yang et al., 1994). This study showed that the current Caltrans procedures could not adequately predict the relative hinge displacement. Furthermore, it was found that unless the restrainer stiffness was comparable to that of the more flexible frame, restrainers had little influence in reducing the relative hinge displacement.

Researchers at the University of Washington (Trochalakis et al., 1995) found similar results, stating that the most important parameters governing the response of hinges are the restrainer stiffness, restrainer gap, frame period ratio, and frame stiffness ratio. It was determined that the Caltrans procedure cannot adequately predict the required restrainer stiffness to limit hinge displacement. From the results of a parameter study, the authors recommended a procedure to estimate the relative hinge displacement. They recommended that the estimated hinge displacement be used in the current Caltrans procedure to calculate the required restrainer stiffness.

3 Restrainer Performance in Recent Earthquakes

Recent earthquakes in the US and Japan have provided an opportunity to study the performance of hinge restrainers. A common cause of damage and collapse in three recent earthquakes was large hinge movements which led to unseating at the hinges. This section briefly summerizes the the performance of hinge restrainers of bridges in the Loma Prieta, Northridge, and Kobe earthquakes.

Loma Prieta, 1989

The Caltrans Maintenance Division reported that 23 bridges which had hinge restrainers suffered damage during the Loma Prieta earthquake. Field observations indicated that restrainers were activated in many instances, but failed in only two cases (Saiidi et al., 1993). The Richardson Bay Bridge and Separation is a 21-span bridge built in 1957 and retrofitted

with cable restrainers in 1973. Restrainer failure and damage due to pounding was evident at several hinges. The Oakland Overcrossing (West Grand Avenue Viaduct) is a steel girder bridge built in 1937 and retrofitted in 1976. The retrofit consisted of longitudinal restrainers at each joint connected by steel brackets to the bottom girder flange or web. During the earthquake, many cables fractured or were overstresed. Many other structures sustained moderate damage to hinge restrainer units. Yielding of restrainers occurred in the China Basin Viaduct and the Route 92/101 Separation. There were several other bridges in which restrainers were engaged and performed adequately.

Northridge, 1994

The epicentral region contained several bridges which had been retrofitted with hinge restrainers. Most of the retrofitted bridges performed well although, in some cases, hinge restrainers did not perform adequately. The Gavin Canyon Undercrossing is a concrete box-girder bridge which had been retrofitted in 1974 with restrainer cables and diaphragm bolsters across the in-span hinges. The bridge collapsed due to unseating and failure of restrainers (Moehle, 1994; Priestley et al., 1994). The Interstate 5/State Road 14 Interchange and the South Connector Overcrossing are concrete box-girder bridges located approximately 12 km from the epicenter. It had also been retrofitted with cable restrainers following the 1971 San Fernando earthquake. Although the collapse of a frame was caused by shear failure in columns, spans in other frames that did not collapse were barely supported on hinge seats. Other structures in the interchange showed evidence of hinge and restrainer damage.

Hyogo-Ken Nanbu (Kobe), 1995

The Hanshin Expressway, which is the major traffic artery through the city of Kobe, sustained extensive damage in the Kobe earthquake. Inadequate seat widths and insufficient restrainers ("falling-off prevention devices") caused many spans to fall off their bearings and bents (Comartin et al., 1995). The eastern portion of the Hanshin expressway is nearly normal to the propagation of the fault and the movement was mainly longitudinal. The Harbour Freeway also sustained significant damage. In particular, almost every expansion joint along the freeway was damaged. There were signs of restrainer damage and failure.

4 Current Design Approach

The Caltrans Bridge Design Specifications uses an equivalent static procedure to design hinge restrainers for multiple frame bridges. The procedure simplifies the problem by replacing the coupled two degree-of-freedom system representing the longitudinal behavior of two adjacent frames with two uncoupled single degree-of-freedom systems. Using the frame with smaller displacement, restrainers are provided until the frame displacement is less than the maximum permissible restrainer displacement, D_r.

One of the problems with the Caltrans procedure is estimating the relative displacement at the hinge between the two frames, D_{eq}, during an earthquake. The Caltrans procedure

calculates the displacement on each side of a hinge and uses the smaller one as the controlling case. This tends to give unconservative results because the procedure would predict a small displacement for a very flexible frame next to a very stiff frame and ultimately the use of minimum restrainers. In this study, the effect of using the larger displacement as the controlling case is investigated (termed the modified Caltrans procedure in this paper). Another problem with the Caltrans procedure is determining the number of restrainers necessary to limit the hinge displacement to the target value. The current procedure uses the stiffness of one frame instead of the combined flexibility of both frames in the calculation for the restrainer stiffness. The use of only one frame stiffness can lead to a large number of restrainers because the flexibility of the two frames is underestimated.

5 Proposed Restrainer Design Approach

The proposed design procedure is based on a simplified two degree-of-freedom linear analytical model for longitudinal earthquake response of two adjacent frames, as illustrated in Figure 1. In the simplified model, the restrainers resist both tension and compression. Because the model is linear, modal combination rules and optimization theory can be used. The restrainer design problem can be seen as having two parts: (1) estimate the relative opening between frames (D_{eq}), and (2) estimate the restrainer stiffness (K_r) required to reduce the relative opening to the target displacement (D_r). The estimate of the maximum relative displacement is achieved by a modal analysis of the two DOF linear system. The modal responses are combined using the CQC combination rule (Kiureghian, 1980). The number of restrainers required to reduce relative hinge displacements to the target displacement are calculated based upon a sensitivity analysis of the system.

Calculation of Relative Hinge Displacement

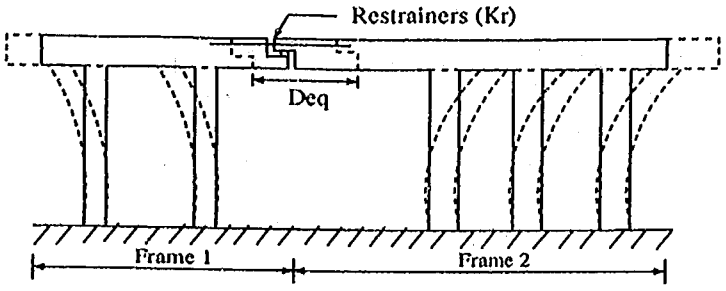
The relative hinge displacement is determined by a modal analysis of the two DOF system representing the longitudinal response of two adjacent frames:

$$D_{eq} = \sqrt{r_1^2 + r_2^2 + 2\rho_{12} r_1 r_2} \tag{1}$$

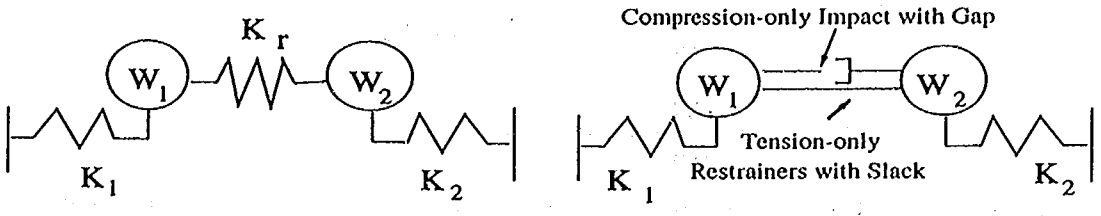
where the correlation coefficient between the response of the two frames is:

$$\rho_{12} = \frac{8\xi^2(1+\beta)(\beta)^{3/2}}{(1-\beta^2)^2 + 4\xi^2(1+\beta)^2(\beta)} \tag{2}$$

with $\beta = \frac{T_2}{T_1}$, where T_1 and T_2 are the periods for the first and second modes of the system, respectively, and $\xi = \xi_i$ is the assumed equal damping ratio for the two modes. The modal response for relative hinge displacement, r_i, of mode i=1 or 2 is given by the pseudo-acceleration response spectrum:



Typical Straight 2-Frame Bridge With Intermediate Hinge



Linear Analytical Model

Nonlinear Analytical Model

Figure 1 : Linear and Nonlinear Analytical Model Used in Study.

$$r_i = P_i S_{ai}(T_i, \xi_i) \tag{3}$$

and the participation factor, P_i, is

$$P_i = \frac{\mathbf{R}^T \mathbf{M} \phi_i}{\omega_i^2 (\phi_i{}^T \mathbf{M} \phi_i)} (\mathbf{a}^T \phi_i) \tag{4}$$

in which $\mathbf{a}^T$=[-1 1], and $\mathbf{R}$ = [1 1]. For the special case with no restrainers (K_r=0), equation 1 reduces to

$$D_{eq_o} = \sqrt{D_1^2 + D_2^2 - 2\rho_{12} D_1 D_2} \tag{5}$$

where $D_i = S_d(T_i, \xi_i)$ are the SDOF maximum displacements.

Calculation of Required Restrainer Stiffness

Once an estimate of the relative hinge displacement, D_{eq}, is obtained from equation 1, the restrainer stiffness needed to reduce the displacement to D_r is determined from a sensitivity analysis. For a linear elastic system subjected to a load, $\mathbf{P}$, the equations of equilibrium are

$$\mathbf{KU} = \mathbf{P} \tag{6}$$

where $\mathbf{K}$, $\mathbf{U}$, and $\mathbf{P}$ are the stiffness, displacement, and external load, respectively. Partial differentiation with respect to K_r gives

$$\frac{\partial \mathbf{K}}{\partial K_r}(\mathbf{U}) + \mathbf{K}\frac{\partial \mathbf{U}}{\partial K_r} = \mathbf{0} \tag{7}$$

which for the two DOF system is

$$\begin{bmatrix} 1 & -1 \\ -1 & 1 \end{bmatrix} \begin{Bmatrix} U_1 \\ U_2 \end{Bmatrix} + \begin{bmatrix} K_1 + K_r & -K_r \\ -K_r & K_2 + K_r \end{bmatrix} \begin{Bmatrix} \frac{\partial U_1}{\partial K_r} \\ \frac{\partial U_2}{\partial K_r} \end{Bmatrix} = \begin{Bmatrix} 0 \\ 0 \end{Bmatrix} \tag{8}$$

Letting $D_{eq} = U_2\text{-}U_1 = \mathbf{a}^T\mathbf{U}$ where $\mathbf{a}^T$ = [-1 1], equation 8 becomes:

$$\mathbf{a}D_{eq} = -\mathbf{K}\frac{\partial \mathbf{U}}{\partial K_r} \tag{9}$$

Multiplying both sides by $\mathbf{K}^{-1}$ and substituting $D_{eq} = \mathbf{a}^T\mathbf{U}$ gives

$$\frac{\partial D_{eq}}{\partial K_r} = -(\mathbf{a}^T\mathbf{K}^{-1}\mathbf{a})D_{eq} \tag{10}$$

$$\frac{\partial D_{eq}}{\partial K_r} = -\frac{1}{K_{mod} + K_r}D_{eq} \tag{11}$$

where $K_{mod} = \frac{K_1 K_2}{K_1 + K_2}$. Using a first order Taylor expansion for hinge displacement about the current restrainer stiffness, K_{r_i}, gives,

$$D_{eq_{i+1}} = D_{eq_i} + \frac{\partial D_{eq}}{\partial K_r}(K_{r_{i+1}} - K_{r_i}) \tag{12}$$

or written in terms of the restrainer stiffness, K_r, the new estimate is

$$K_{r_{i+1}} = K_{r_i} + (K_{mod} + K_{r_i})\frac{(D_{eq} - D_r)}{D_{eq}} \tag{13}$$

Equation 13, gives the updated restrainer stiffness, $K_{r_{i+1}}$, from the current stiffness K_{r_i}, the hinge displacement, D_{eq}, from equation 1 and the target displacement, D_r.

Analytical Model

A nonlinear analytical model is developed to represent the longitudinal response of the bridge structure to strong ground motion. The model represents a straight, two frame bridge supported by an intermediate hinge (Figure 1). Each frame is modeled as a single degree-of-freedom. To simplify the model, abutments are not included because previous studies have shown that the effects of abutments on the relative hinge displacements are small (Trochalakis et al., 1995).

The nonlinear hinge model consist of three spring components. The first component is a nonlinear tension-only spring with slack used to model the restrainers. The second is a friction element, modeled by a bilinear elastic spring. The kinematic coefficient of friction between the bearing and the concrete is taken as 0.20. Based on a normal force at the hinge of 500 kips, the sliding frictional force is 100 kips. Pounding of adjacent masses is accounted for by explicitly correcting for velocities after impact. Energy loss at the hinge through pounding is accounted for by the coefficient of restitution, $e = 0.80$. Previous studies have shown that the relative hinge displacement between interacting frames is not sensitive to the coefficient of restitution in this range (Athanassiadou et al., 1994).

Inelastic Response

It is recognized that typical bridge frames are intended to undergo inelastic deformation during a major earthquake. The nonlinearity of the frames will be accounted for in the restrainer design procedure by determining equivalent stiffnesses and damping ratios based on the maximum displacement of the frames. In this procedure, known as the substitute structure method (Gulkan and Sozen, 1974), the inelastic response is represented by a linear elastic system with equivalent stiffness and damping properties. The effective system stiffness and effective damping ratio are adjusted such that the displacement of the inelastic system is equal to that of the substitute structure model.

The two parameters needed for the substitute structure method are the effective stiffness, K_{eff}, and effective damping, ξ_{eff}. For idealized elastic-perfectly plastic hysteresis, the effective stiffness decreases with increasing ductility to reach the same displacement. Various relationships of effective damping versus ductility factor have been developed (Gulkan and Sozen, 1974). For this study, the relationship based on the Takeda degrading stiffness model is used for all cases (M. J. Kowalsky et al., 1994):

$$K_{eff} = \frac{1}{\mu} K \tag{14}$$

$$\xi_{eff} = \xi + \frac{1}{\pi}(1 - 0.95/\sqrt{\mu} - 0.05\sqrt{\mu}) \tag{15}$$

The restrainer design procedure uses the effective stiffness and damping based on an estimate of the target ductility.

The results of the design procedure, including frame yielding, will be compared with an analytical model. To represent the yielding of the frames, the force- displacement relationship for each frame is modeled as a stiffness degrading element. The frame elements are combines with the nonlinear hinge model in the two DOF system for the frames.

Hinge Seat Widths

Inadequate hinge seat widths cause spans to fall off their supports if the hinge opening displacement is greater than the hinge seat width. Current procedures to estimate required hinge seat widths are based on factors which do not directly consider the level of excitation or the phasing between the frames. Currently the hinge seat width requirements are based on following equations:

$$N = 12 + .03L + .12H(1 + S^2/8000) \text{ N} > 24 \text{ (Caltrans)}$$
$$N = 12 + .02L + .08H(1 + S^2/8000) \qquad \text{(AASHTO)}$$

where L is the frame length (feet), H is the average height of the two adjacent frames (feet), S is the skew angle of the hinge, and N is the hinge seat width (inches). The proposed procedure for hinge seat width is based on estimating the maximum relative hinge displacement without restrainers ($K_r = 0$). This expression is provided in equation 5.

6 Design Procedure

Using the framework described in the previous section, a new design procedure is proposed, as listed in Table 1.

Table 1: Proposed Restrainer Design Procedure

Step		Notes
1	Calculate the maximum restrainer deflection, D_r $D_r = D_y + D_g$, where D_y=yield displacement, and D_g=restrainer slack	
2	Calculate displacement of each frame, D_1, and D_2 where $D_i = S_d(T_i, \xi_i)$ T_i and ξ_i are functions of displacement ductility, μ from eq. 14 and 15.	
3	Estimate D_{eq_o}, the maximum relative hinge displacement where $D_{eq_o} = \sqrt{D_1^2 + D_2^2 - 2\rho_{12}D_1D_2}$ If $D_{eq_o} < D_r$, use the minimum number of restrainers	Eq. 5
4	Determine the restrainer stiffness required to reduce D_{eq_o} to target $K_r = \frac{K_{mod}(D_{eq_o} - D_r)}{D_{eq}}$ where $K_{mod} = \frac{K_{1eff}K_{2eff}}{K_{1eff}+K_{2eff}}$	Eq. 13
5	Perform 2 DOF modal analysis to determine D_{eq} using CQC combination rule, $D_{eq} = \sqrt{r_1^2 + r_2^2 + 2\rho_{12}r_1r_2}$ If $D_{eq} > D_r$ continue to step 6, else Stop with number of restrainers to provide K_r	Eq. 1 - 4
6	Calculate required additional restrainer stiffness, ΔK_r where $\Delta K_r = (K_{mod} + K_r)\frac{(D_{eq} - D_r)}{D_{eq}}$ The new estimate for restrainer stiffness is $K_r = K_r + \Delta K_r$ Go to step 5	Eq. 13

[a]Step 3 may be used to determine hinge seat width

7 Preliminary Results

The proposed procedure is verified by a parameter study for a range of typical cases. The effect of the frame period ratio, (T_2/T_1), on the response of bridges is investigated, which has been shown to be an important factor in the response of the hinges (Yang et al., 1994; Trochalakis et al., 1995). For a range of parameters presented in Table 2, the proposed procedure is compared with the current Caltrans procedure. The number of restrainers predicted by each procedure is used in the nonlinear analytical model to determined the accuracy of the procedure. Following current guidelines, hinge displacements are to be limited to the yield displacement of the restrainers. For 20 ft long restrainers the yield displacement is 4.2 inches. The effectiveness of the procedure is presented in terms of a normalized displacement ratio, which is the ratio of the actual maximum hinge displacements (from the nonlinear model) to the target displacement ($D_r = 4.2$ in).

Four ground motions were selected to represent a range of soil types and earthquake peak ground accelerations. The ground motions used in the study are: Northridge - Arleta (PGA=.32g), Loma Prieta - Corralitas (PGA=.53g), El Centro (scaled by two to PGA=.70), and Northridge - Sylmar (PGA=.82g). With the exception of the El Centro record, all ground motions are along the major axis based on the two components. Each ground motion is applied in both longitudinal directions to account for directionality effects.

Table 2: Parameters Used in Validation Study

Parameter	Values
Frame 1 and 2 Weight (W_1 and W_2)	5000 kips
Frame 2 Stiffness (K_2)	510 kips/in (T_2 = 1.0 sec)
Frame 1 Stiffness (K_1)	102 kips/in - 5100 kips/in (T_1 = 0.32 - 2.23 sec)
Restrainer Gap	0.5 inches
Restrainer Slack	0.5 inches
Hinge Frictional Force	100 kips
Coefficient of Restitution (e)	0.80

Elastic Results

Figures 2 presents a series of plots showing the number of restrainers to limit displacements to yield along with the normalized displacement for the Caltrans, modified Caltrans, and the proposed procedure. For the four earthquakes studied, the Caltrans procedure is unconservative for large frame period ratios, illustrated by large normalized displacement ratios for the large frame period ratios. The Caltrans procedure assumes that the system with the smallest displacement will be the controlling case, but for large frame period ratios T_1 is small and the displacement of frame 1 approaches zero. This implies that restrainers are not required. For frame period ratios approaching unity, the Caltrans procedure is overconservative. This is primarily due to the fact that the Caltrans procedure cannot account for coupling between the restrained frames. As the frame period ratio approaches unity, the frames vibrate in-phase and the relative displacement approaches zero.

The modified Caltrans procedure performs much better than the Caltrans procedure. For two ground motions (El Centro and Sylmar), the modified Caltrans procedure is overconservative in the low frame period ratio range. For these cases, the procedure predicts over three times as many restrainers as necessary and has normalized displacements around 0.40. Similarly, for frame period ratios near unity, the modified Caltrans procedure overestimates the number of restrainers required.

The AASHTO procedure requires that restrainers should be designed for a minimum force of the acceleration coefficient times the weight of the lighter of the two adjoining spans of the structure. The number of restrainers predicted by the AASHTO procedure is shown in Figure 2. In general, the AASHTO procedure is conservative in the short and medium frame period ratio range and unconservative in the large frame period ratio range.

The proposed procedure gives a better estimate of the number of restrainers than the Caltrans, modified Caltrans, or AASHTO methods. For the Arleta record, the proposed

procedure is slightly conservative. For most of the frame period ratio range, the normalized displacement is approximately 0.75 (relative hinge displacement 25% less than target). For the Corralitos record, similar trends are observed. However, for large frame period ratios, the proposed procedure is unconservative. At a frame period ratio of 3.14, the normalized displacement is 1.70. The large normalized displacement ratios at large frame period ratios are due to the pounding effect. Highly out-of-phase frames pound, transferring momentum and producing large displacements. The proposed procedure, which is based on a linear model, does not account for pounding. The same effect is evident in the El Centro and Sylmar studies. For frame period ranges near one, the proposed procedure is overconservative. For frame period ranges near unity, pounding between frames reduces the buildup of dynamic response. Overall, the proposed procedure works well, underestimating required restrainers in only a few cases.

Inelastic Results

A similar parameter study is performed on systems with yielding frames. In the study, the procedure is applied to individual frames with displacement ductility factors of $\mu =$ 2, 4, and 6. The yield force, F_y, for a frame is the maximum strength required to limit the displacement ductility ratio demand to the target ductility, μ_i. In addition to required restrainers and normalized displacement ratios, the displacement ductility demands of the restrained frames are investigated.

Figure 3(a) shows the required number of restrainer for various ductilities over a range of frame period ratios for the Northridge Earthquake (Sylmar). For the entire range of frame period ratios, an increase in ductility demand produces a decrease in required number of restrainers. This can be expected because of the increased effective damping and the decreased effective stiffness of the yielding system. The proposed procedure performs well in predicting required hinge restrainers to limit the hinge displacement of yielding frames. Except for frame period ratios of 0.33 and 3.33, the proposed procedure predicts the relative hinge displacement well. The increased normalized displacement near the frame period ratios of 0.33 and 3.33 is due to the pounding effects of frames with greatly different periods and out-of-phase motion, which increases the ductility demand from the value for individual frames. The normalized displacement for the frame period ratio of 0.33 increases from 1.5 to 2.0 as the ductility increases from 4 to 6. The low normalized displacement at frame period ratios approaching unity is also due to pounding. As mentioned earlier, for frame period ratios near unity, pounding has the beneficial effect of decreasing the response of interacting frames. Figure 3(b) shows the effect of the restrainers on the distribution of ductility in the columns. The restrainers generally increases the ductility demand on the stiffer frame while decreasing the ductility demand on the more flexible frame relative to the target ductility factor for the individual frames.

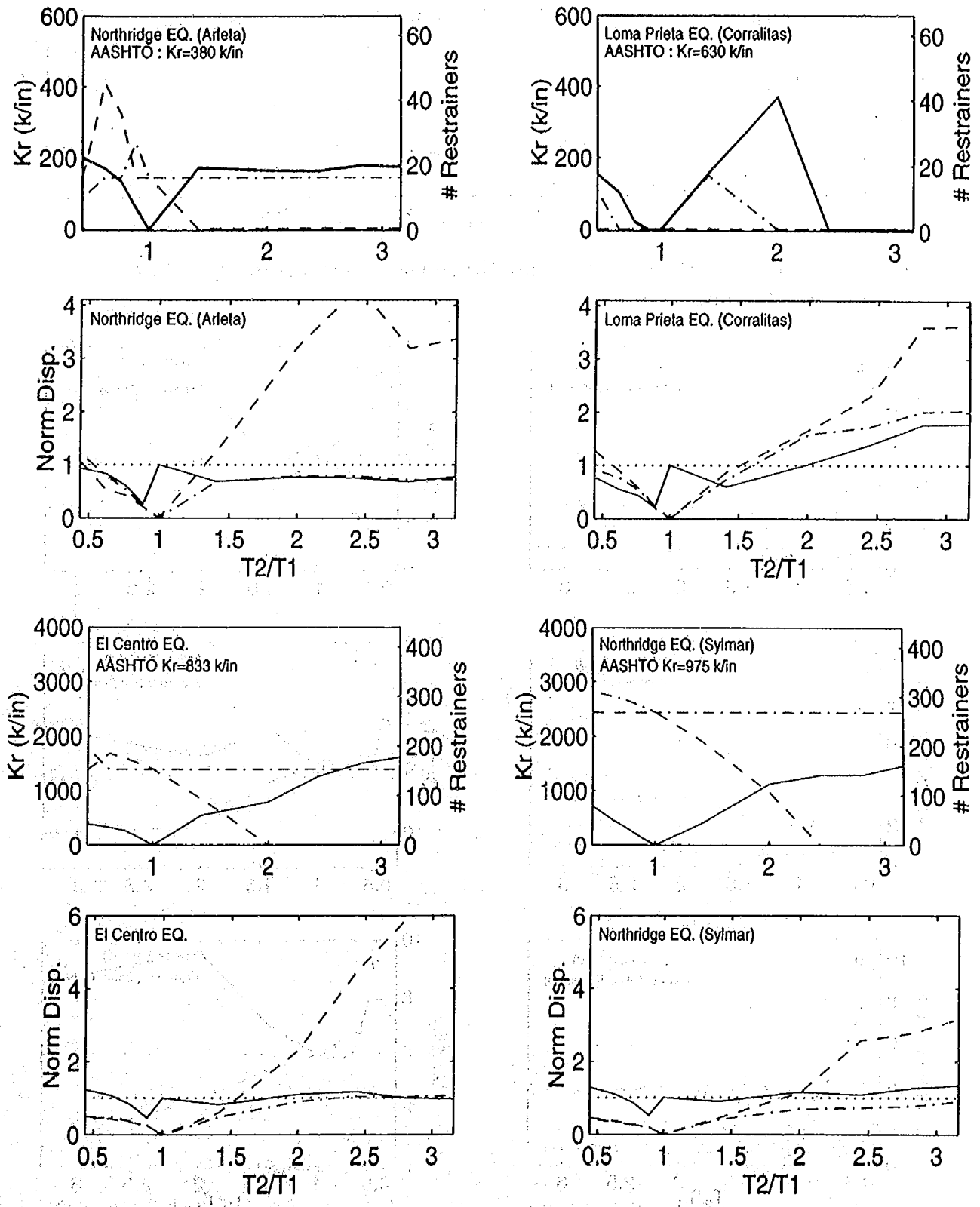
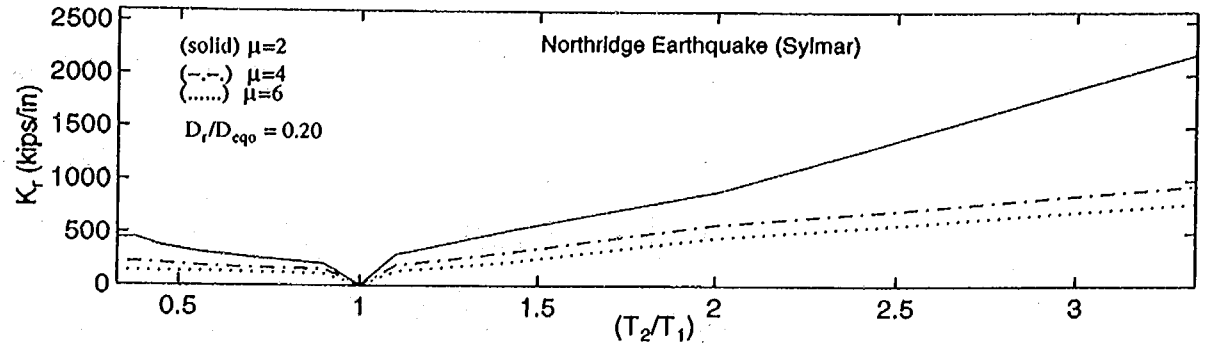
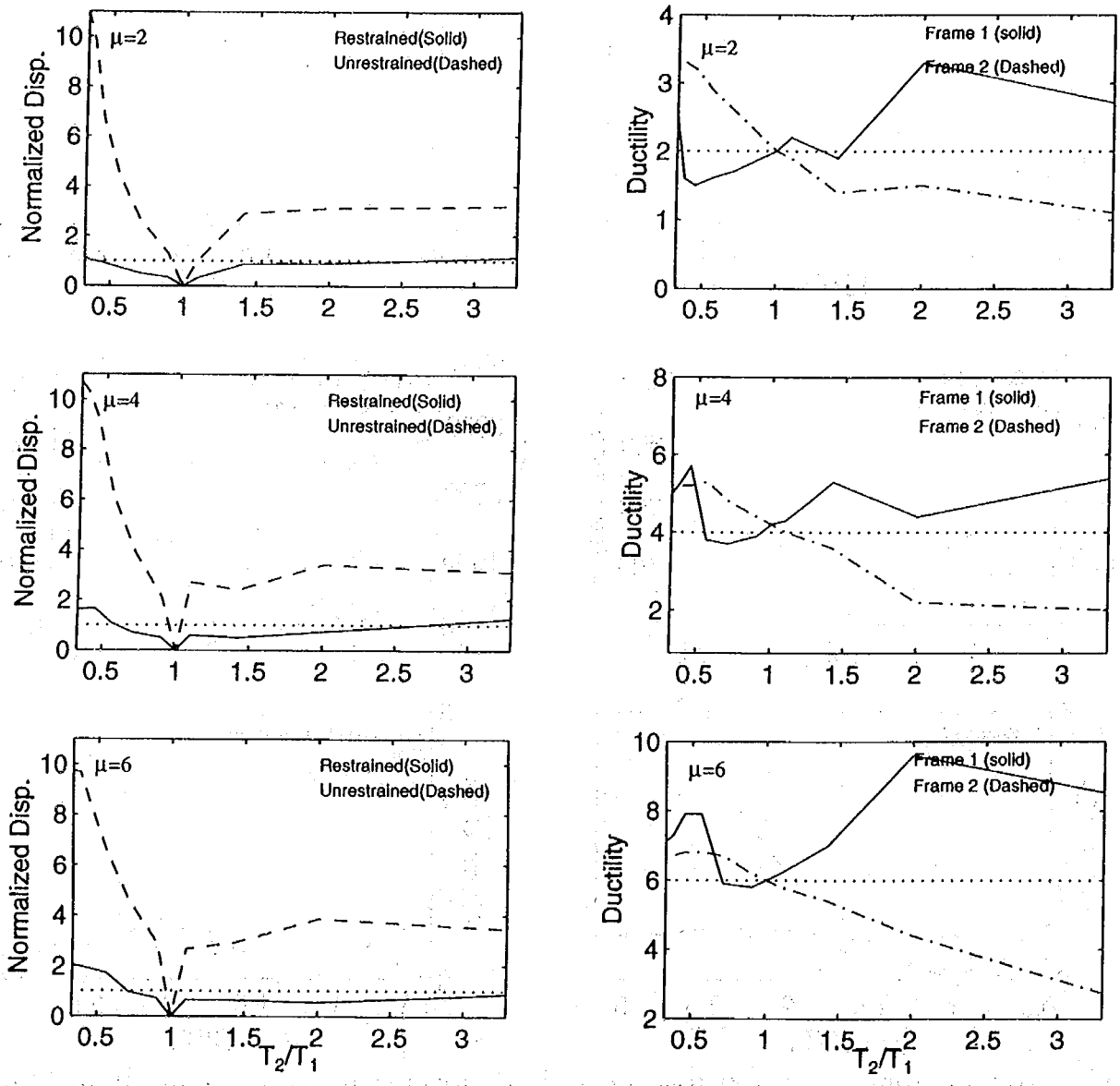


Figure 2 :Restrainer Stiffness using Caltrans (- - -), Modified Caltrans (-.-.-) and Proposed(——) Procedure to Limit Hinge Displacement to 4.2 inches.



(a): Restrainer Stiffness Required to Limit Hinge Displacements to $D_r = .20D_{eq_o}$ for Yielding Frames.



(b) : Normalized Displacement and Frame Ductility Factors for Yielding Frames.

Figure 3 : Required Restrainer Stiffness and the Effect on Frame Ductility Factors for Northridge Earthquake (Sylmar) to Limit Hinge Displacement to $D_r = .20D_{eq_o}$.

Hinge Seat Width

Figure 4 shows the proposed hinge seat width for four earthquakes, along with the normalized displacement. The proposed hinge seat width is much less than the minimum allowable required by Caltrans for nearly all cases. The normalized displacements are near or below unity except for large frame period ratios, where pounding effects control the response.

Based on the results of the parameter study, the proposed design recommendations for hinge seat widths is $N = 1.5D_{eq_o} \geq 24$ inches where D_{eq_o} is based on step 3 of Table 1. The 50% increase factor applied to D_{eq_o} accounts for the uncertainty in displacement predictions and the increased response of out-of-phase frames due to pounding.

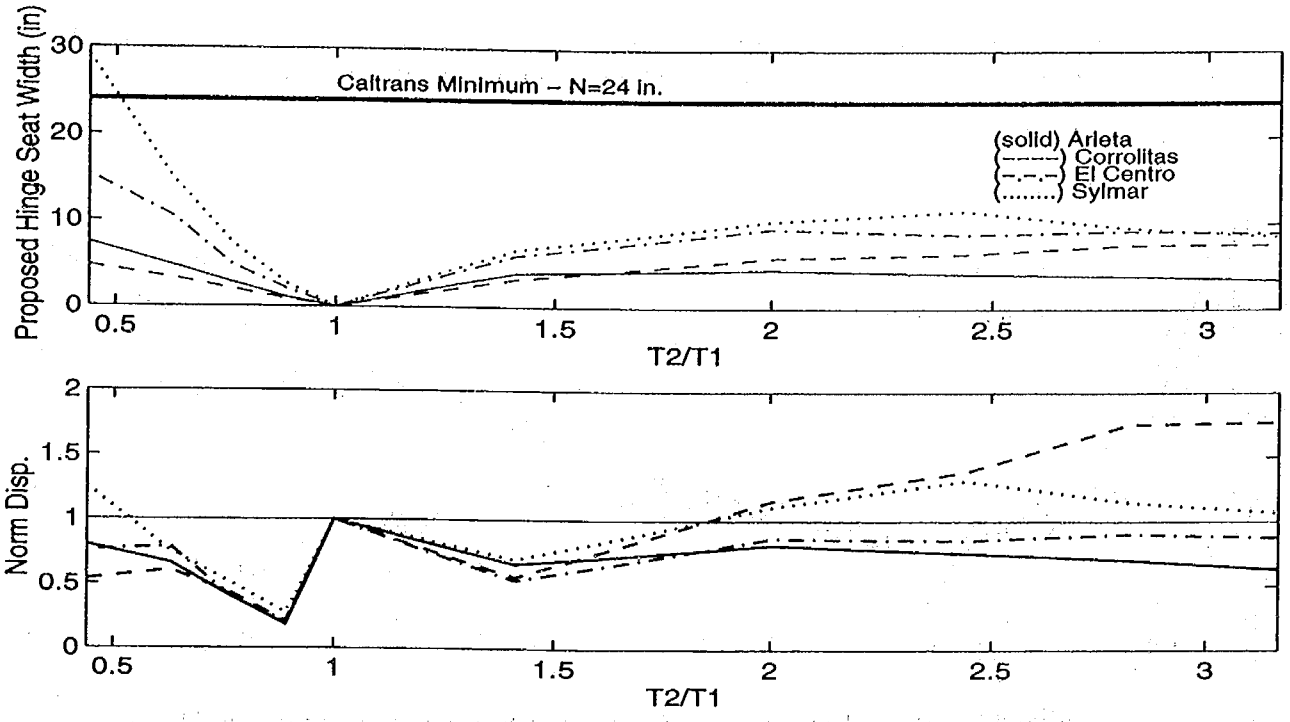


Figure 4 : Proposed Hinge Seat Width Requirements and Normalized Displacements for Multiple-Frame Bridges.

Normalization of Required Restrainer Stiffness

The required restrainer stiffness can be stated in a non-dimensional form that reduces the scatter for a wide range of cases. The non-dimensional stiffness ratio can be stated as:

$$\frac{K_r \mu}{K_{mod}} \frac{1}{(\frac{D_{eq_o}}{D_r} - 1)} \tag{16}$$

where K_r and D_r are the required restrainer stiffness and displacement, μ is the frame design displacement ductility, K_{mod} is the modified stiffness with elastic properties, and D_{eq_o} is the estimate of the hinge opening without restrainers (from equation 5). Equation 16 may also be written as $K_r D_r \mu / K_{mod}(D_{eq_o} - D_r)$. The term $K_r D_r$ is the restrainer force required to

limit the hinge displacement to D_r, and the quantity $K_{mod}(D_{eq_o} - D_r)/\mu$ is the static force required to reduce hinge opening from D_{eq_o} to D_r. This normalization has the advantage that it eliminates the ground motion amplitude as a factor for a linear system. The normalized stiffness is only a function of the frame period ratio (T_2/T_1), D_r/D_{eq_o}, and the shape of the response spectrum.

Figure 5 shows the effect of frame period ratio on the normalized stiffness ratio. For period ratios near one, the normalized stiffness ratio approaches one (except of course for the limit of a period ratio of one for which $D_{eq_o} = 0$ exactly). A normalized stiffness ratio of one indicates that the force required to limit hinge displacement is equal to the static force required to reduce hinge displacement from D_{eq_o} to D_r. For very large and very small period ratios the normalized stiffness ratio increases to values near 3 and 4 because of out-of-phase motion. This highlights the increase in force required to reduce hinge displacements for out-of-phase frames compared with frames which are in-phase. The plot shown is for $D_r/D_{eq_o} = 0.20$, however, plots for different D_r/D_{eq_o} show similar trends.

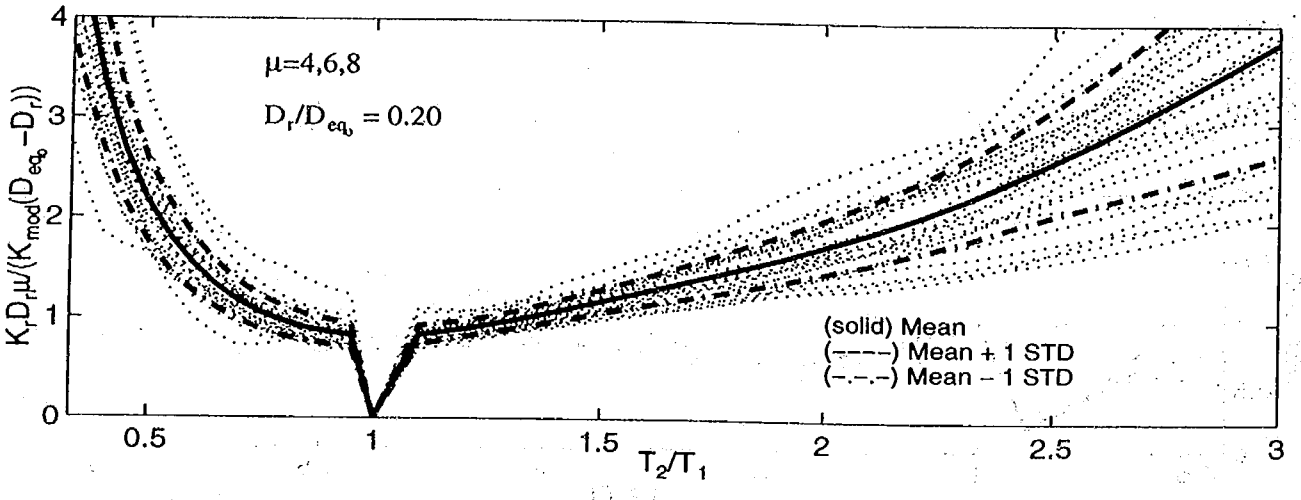


Figure 5 : Normalized Stiffness Required to Restrain Hinge Displacement for Multiple-Frame Bridges (Thirty Earthquake Ground Motions)

8 Example

The design procedure is applied to a typical four-frame bridge used in the Caltrans Bridge Design Specifications (Caltrans, 1990). The properties of the bridge are shown in Figure 6. The restrainer slack considered is 1/4-in., and the gap is 3/4-in. The ground motion record is the El Centro S00E component, scaled by two (PGA=.70g). The design procedure is applied to hinges 1 and 2 (because the bridge is symmetric about center), and the input motion is applied in both longitudinal directions to account for directionality effects. The design at each hinge is accomplished by considering several possibilities of frame motion. For example, hinge 1 is designed by first considering two cases. Case 1 evaluates frame 1 (moving left) and frame 2 (moving right). Case 2 evaluates frame 1 (moving left) and frame 2+3 (moving right).

Table 3: Application of Proposed Procedure to Typical 3-Span Bridge

Hinge	Case 1 Using 7' Restrainers			Case 2 Using 20' Restrainers		
	D_r (in)	K_r (k/in) (N)[b]	D_{eq} (in)	D_r (in)	K_r (k/in) (N)	D^a_{eq} (in)
H1	1.50	3000 (115)	1.73	4.20	900 (100)	3.65
H2	1.50	1650 (63)	1.00	4.20	725 (84)	4.66
H3	1.50	3000 (115)	1.73	4.20	900 (100)	3.65

[a]Hinge displacement determined from Nonlinear Time History Analysis with K_r for El Centro Earthquake, scaled to 0.70g.

[b]Number of Hinge Restrainers

Similiar the cases considered for hinge 2 are frame 2 (moving left) and frame 3 (moving right), frames 1+2 (moving left) and frame 3 (moving right), and frames 1+2 (moving left) and frames 3+4 (moving right). The target displacement, required restrainer stiffness (or number of restrainers), and the actual hinge displacement obtained from nonlinear time history analyses are listed in Table 3. For the 7 ft restrainers, the procedure slightly underestimates the required restrainer stiffness to reduce hinge displacement for hinges 1 and 3. For 20 ft restrainers, the procedure slightly underestimates the required restrainer stiffness for hinge 2. In general the proposed procedure does a good job in predicting the proper number of restrainers required to limit the hinge displacement to D_r. The Caltrans procedure applied to this example performs adequately for hinge 1. However for hinge 2, the Caltrans procedure gives over twice as many restrainers as the proposed procedure.

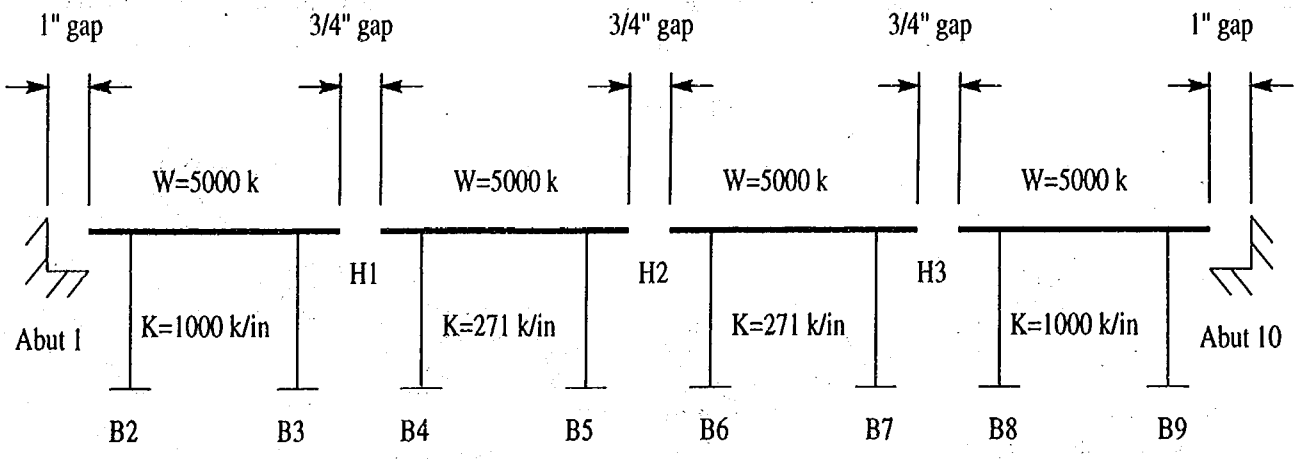


Figure 6: Bridge Model Used for Example Case

9 Case Study

In this section the proposed procedure is applied to the Northwest Connector bridge at the I10/215 interchange in Colton, California. The Northwest Connector is a 2540 ft long, curved, concrete box girder bridge with sixteen spans supported by single column bents and diaphragm abutments (Figure 7). Extensive instrumentation of the bridge prior to the 1992

Landers and Big Bear earthquakes has led to studies on the response of the curved bridge as well as the response of the intermediate hinges (Fenves and Desroches, 1994). For this study frame elements are modeled as elastic and nonlinear compression-only and tension-only elements are used at the intermediate hinges.

The proposed procedure is applied to the Northwest Connector subjected to the Landers earthquake, scaled by a factor of two (PGA=.30g). The Caltrans, modified Caltrans, and proposed procedure are applied to the frames to determine the number of restrainers required to keep relative displacements less than 4.2 in. Table 3 shows the results of the Caltrans, modified Caltrans and the proposed procedures along with results from nonlinear time history analyses. The results for the required restrainer stiffness vary greatly between the three procedures. The Caltrans procedure determines that restrainers are not required at any of the hinges because a stiff frame is usually next to a more flexible frame. According to the procedure, the stiff frame has a displacement less than the permissible hinge opening, resulting in the use of no restrainers. The lack of restrainers at hinges 3 and 7 allow displacements that exceed 4.2 in. The modified Caltrans procedure produces slightly better results although they are too conservative. The proposed procedure predicts as much as 50% fewer restrainers than the modified Caltrans procedure, while still limiting the relative hinge displacement. These results are consistent with the results from the parameter study which showed that for a wide range of frame period ratios, pounding reduces the relative hinge displacements.

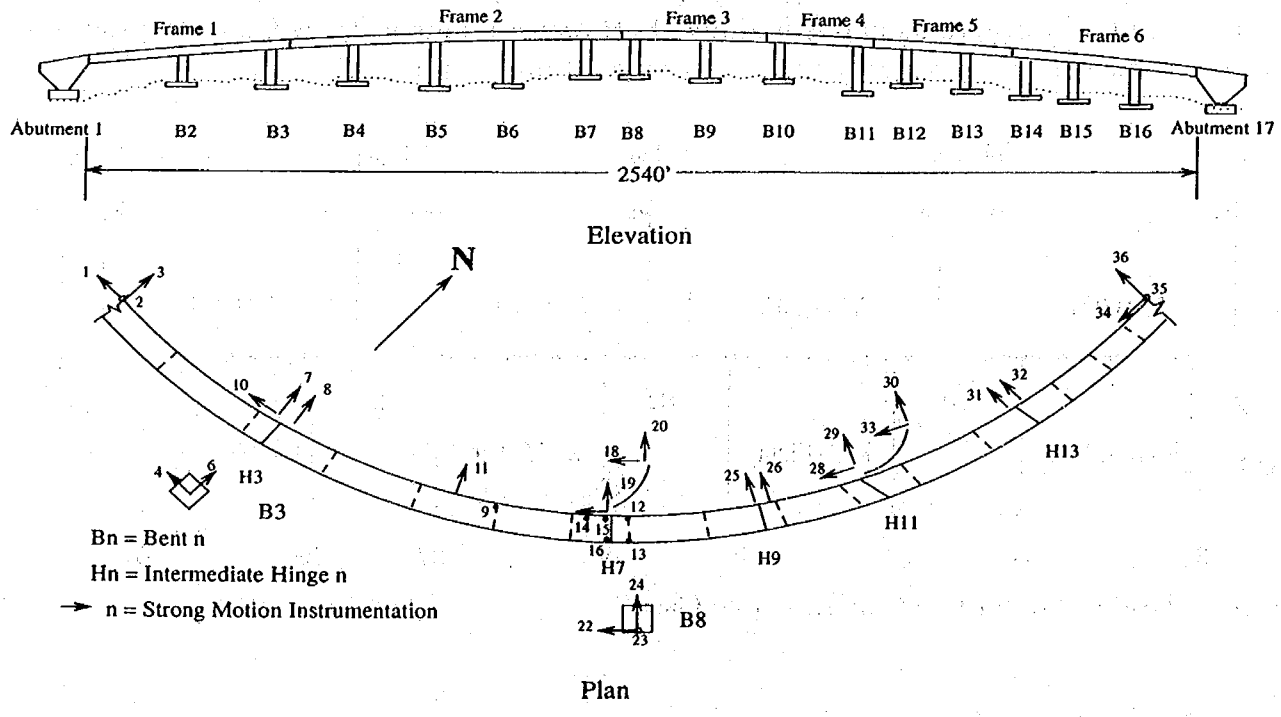


Figure 7 : General Plan and Seismic Instrumentation for Northwest Connector at Interstate 10/215 Interchange in Colton, CA.

Table 4: Application of Proposed Procedure to Northwest Connector[a]

Hinge	Caltrans Procedure		Modified Caltrans Procedure		Proposed Procedure	
	K_r (k/in) (N)[b]	D_{eq} (in)	K_r (k/in) (N)	D_{eq} (in)	K_r (k/in) (N)	D_{eq} (in)
H3	0 (0)	6.24	2215 (238)	1.56	888 (95)	2.88
H7	0 (0)	7.92	2215 (238)	0.94	690 (74)	2.64
H9	0 (0)	0.97	0 (0)	1.44	0 (0)	1.20
H11	0 (0)	2.16	159 (17)	1.56	91 (10)	1.80
H13	0 (0)	3.12	159 (17)	3.12	111 (12)	3.24

[a]Landers Earthquake scaled to 0.30g, $D_r = 4.2$ in, D_{eq} determined from Nonlinear Time History Analysis

[b]Number of restrainers

10 Conclusions

- The Caltrans procedure for hinge restrainers is conservative for small frame period ratios (0.45-1.5) and unconservative for large frame period ratios (1.5 - 3.16) when predicting required restrainer stiffnesses. The AASHTO procedure shows a similar trend.
- A new design procedure is proposed for determining the number of restrainers to limit hinge displacement. The proposed procedure accounts for the coupling between frames and intensity of ground motion. Analytical studies show that the proposed procedure accurately predicts required restrainer stiffness to limit hinge displacement.
- Pounding of frames generally decrease the relative hinge displacement and required restrainer stiffness. However, for highly out-of-phase frames, pounding increases hinge displacement.
- Pounding and engaging of restrainers redistribute ductility demands on bridge frames. The more flexible frames have decreased ductility demands and stiffer frames have increased ductility demands.
- A case study of a curved bridge shows that the proposed procedure works well to predict the required number of restrainers to limit hinge displacement to a prescribed value.

The new design procedure should lead to improved performance of intermediate hinge restrainers for new and retrofit construction. Extensions to include transverse motion, skew, and spatial variation of ground motion are possible within the proposed framework.

Acknowledgments

This study has been supported by the California Department of Transportation under Grant RTA-59A131 and the NCEER Highway Project, through the Federal Highway Administra-

tion, as Task 106-F-3.1.

REFERENCES

Athanassiadou, C. J., Penelis, G. G., and Kappos, A. J. (1994). "Seismic Response of Adjacent Buildings With Similiar or Different Characteristics," *Earthquake Spectra*, 10(2), pp. 293–317.

Caltrans (1990). "Bridge Design Specifications Manual," California Department of Transportation.

Comartin, C., Greene, M., and Tubbesing, S. (1995). "The Hyogo-Ken Nanbu Earthquake : Preliminary Reconnaissance Report," Earthquake Engineering Research Institute.

Fenves, G. L. and Desroches, R. (1994). "Response of the Northwest Connector in the Landers and Big Bear Earthquakes," *Report No. UBC/EERC-94/12*, Earthquake Engineering Research Center, University of California, Berkeley.

Gulkan, J. and Sozen, M. (1974). "Inelastic Response of Reinforced Concrete Structures to Earthquake Motion," *ACI Journal of the Structural Engieering*, 71(12), pp. 604–610.

Jennings, P. C. (1971). "Engineering Features of the San Fernando Earthquake of February 9, 1971," *Report No. EERL 71-02*, Earthquake Engineering Research Laboratory, California Institute of Technology, Pasadena, CA.

Kiureghian, A. D. (1980). "A Response Spectrum Method for Random Vibrations," *Report No. UCB/EERC-80/10*, Earthquake Engineering Research Center, University of California, Berkeley.

Kowalsky, M. J., Priestley, M. J. N., and MacRae, G. A. (1994). "Displacement Based Design - A Methodolgy for Seismic Design Applied to Single Degree of Freedom Reinforced Concrete Structures," *Report No. SSRP–94/16* , Dept. of Applied Mechanics and Engineering Sciences, University of California, San Diego, La Jolla, CA.

Moehle, J. P. (1994). "Northridge Earthquake of January 17, 1994: Reconnaissance Report, Volume 1 – Highway Bridges and Traffic Management," *Earthquake Spectra*, 11(3), pp. 287–372.

Priestley, N. M. J., Seible, F., and Uang, C. M. (1994). "The Northridge Earthquake of January 17, 1994: Damage Analysis of Selected Freeway Bridge," *Report No. SSRP–94/06*, Dept. of Applied Mechanics and Engineering Sciences, University of California, San Diego, La Jolla, CA.

Saiidi, M., Maragakis, E., and Feng, S. (1996). "Parameters in Bridge Restrainer Design for Seismic Retrofit," *Journal of Structural Engineering*, 122(1), pp. 55–61.

Saiidi, M., Maragakis, E., S. Abdel-Ghaffar, a. S. F., and O'Connor, D. (1993). "Response of Bridge Hinge Restrainers During Earthquakes – Field Performance, Analysis, and Design," *Report No. CCEER 93/6*, Engineering Research and Development Center, Univeristy of Nevada, Reno.

Singh, S. and Fenves, G. L. (1994). "Earthquake Analysis and Response of Two-level Viaducts," *Report No. UCB/EERC-94/11*, Earthquake Engineering Research Center, University of California, Berkeley.

Trochalakis, P., Eberhard, M., and Stanton, J. (1995). "Evaluation and Design of Seismic Restrainers for In-span Hinges," *Draft Technical Report*, Washington State Department of Transportation, University of Washington, Seattle, Washington.

Yang, Y. S., Priestley, M., and Ricles, J. (1994). "Longitudinal Seismic Response of Bridge Frames Connected by Restrainers," *Report No. SSRP-94/09*, Structural Systems Research Project , Dept of Applied Mechanics and Engineering Sciences, University of California, San Diego, La Jolla.

SEISMIC VULNERABILITY ANALYSIS OF STEEL BRIDGE BEARINGS

J. B. Mander, D-K Kim and I.G. Buckle
State University of New York at Buffalo

ABSTRACT

Due to the absence of any guidelines for the modeling of steel bridge bearings, the bridge analyst often assumes only extremes of elastic or plastic behavior— either rigid or completely free behavior for fixed and expansion bearings, respectively. But laboratory experimental results have demonstrated such an idealization may be unrealistic— expansion bearings do have some resistance to longitudinal movements and fixed bearings have some flexibility to transverse movement. This study presents procedures for analyzing initial elastic stiffness and the ultimate strength of a steel bearing assembly. Furthermore, cyclic force-displacement models for computational transient non-linear dynamic analysis of bridges are developed. The models are validated against experimentally observed force-displacement relationships of various types of steel bearings. Recommendations are given so that the models can be used with elements that exist in a general purpose non-linear time-history analysis computer program. Using this information the results of an analytical study are presented. The effect of variable clearances and strength that may exist in individual steel bearings on the overall performance of bridge structures is investigated. Results of the study show that displacement demands, and thus the propensity for unseating the girders, are highly dependant on the initial clearances and relative strength between bearings in a group.

INTRODUCTION

Many existing bridge structures, especially highway bridges located in the central and eastern U.S., consist of slab-on-girder (SOG) decks, with the steel girders seated on steel bearings. When carrying out a seismic evaluation of an existing bridge structure it is important to have a clear understanding of the role of the steel bearings play in transmitting the loads from the superstructure to the substructure. Realistic modeling of the horizontal force-displacement response of steel bearings is of fundamental importance to the process of analysis and design, but without experimental data the analyst is left to his own judgment in defining these force-displacement relationships for steel bearings. A relatively accurate prediction of the initial elastic stiffness and the ultimate strength of a bearing assembly is important for elastic analyses (including the determination of bridge mode shapes and frequencies) and for plastic analysis (pushover analysis to determine potential collapse mechanisms) of bridges, respectively.

Nowadays, there is much interest in the seismic evaluation of existing bridges, but existing evaluation recommendations (Buckle and Friedland, 1995) do not provide any guidance on how bearings should be modeled. Therefore, this paper presents the results of several typical experiments and based on observed results proposes rational procedures for analyzing:

(i) the initial elastic stiffness,
(ii) ultimate strength of a bearing assembly, including the reinforced concrete pedestal,
(iii) non-linear force-displacement behavior of bearing systems under reversed cyclic loading.

Such models are of interest for studying the transient seismic response of SOG bridges where the steel girders are seated on steel bearings. Therefore, an illustrative analytical study is presented that utilizes these modeling recommendations. The effect of variable clearances and strength that may exist in individual steel bearings on the overall performance of bridge structures is investigated. Conclusions are drawn on the displacement demands that are imposed on bearings and the conditions that may lead to unseating the girders.

CYCLIC FORCE-DEFORMATION MODELING OF BEARING BEHAVIOR

A recent experimental investigation by Mander et al. (1996) showed that the cyclic loading behavior of steel bridge bearings is very nonlinear. Such behavior is difficult to analyze and little guidance is presently available to the analyst wishing to undertake a seismic evaluation (Buckle and Friedland 1995). The relative contributions of the anchor bolts, guide plates, pintles, bedding material, compression of corrosion debris and the effects of surface defects on behavior are not easily distinguished. Local frictional effects, such as at the pintle-socket interface, may also affect behavior in the plastic deformation range. The initial assembly clearances and the widening as a result of the compaction of debris at each cycle of loading also affects overall behavior. It is therefore not surprising that post yield behavior can not be computed a priori based on rational assumptions; it is thus necessary to resort to semi-empirical modeling where values of certain key parameters are based on experimental observations.

In this study the non-linear cyclic force-deformation behavior of steel bridge bearings is modeled using a combination of elements shown in Fig. 1. The initial stiffness and ultimate strength are computed based on rational assumptions derived from the fundamentals of structural mechanics. The determination of stiffness and strength for different bearing types is described in the following sections. Post-yield stiffnesses and frictional coefficients determined from experimental observations are used to calibrate the force-deformation models. Results shown herein are limited to a class of high type fixed and expansion steel bridge bearings. Full details of modeling other bearing types may be found elsewhere (Mander et al., 1996).

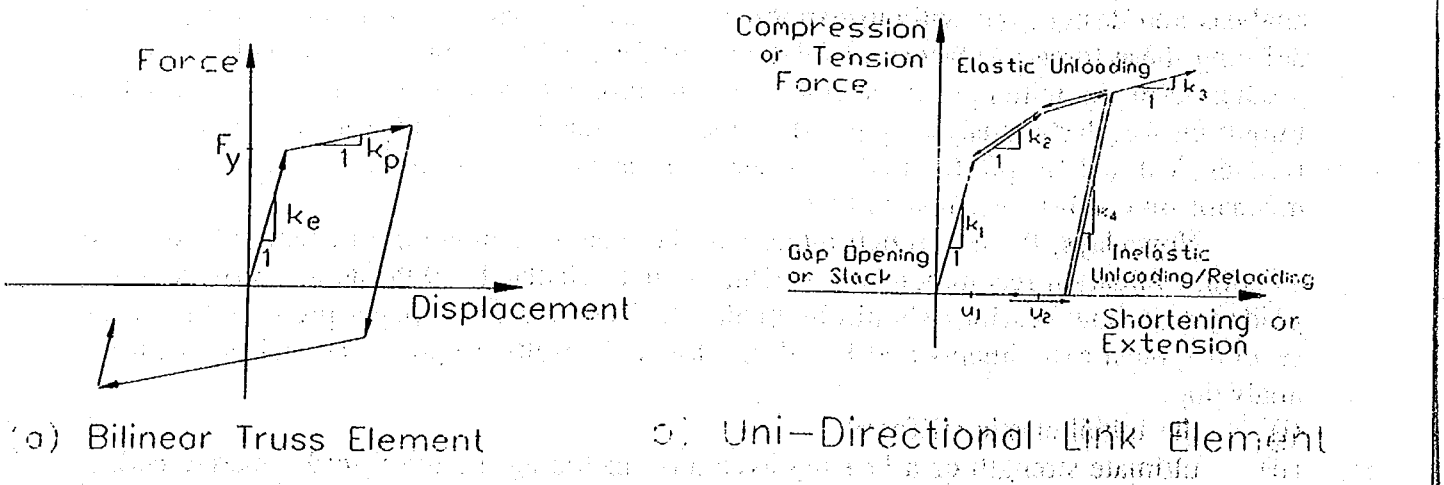


Fig. 1. Nonlinear Elements used for modeling bearings, for the DRAIN-2DX Program these are (a) Element Type 1 and (b) Element Type 9.

The proposed analytical models can be used in conjunction with any appropriate non-linear time history analysis computer programs that possesses elements that conform to the two types shown in Fig. 1. For this study the computer program DRAIN-2DX (Prakash et al. 1992) was used to perform the force-deformation simulations.

For Coulomb friction behavior, an elasto-plastic truss element (element type #1 in DRAIN-2DX) can be used. Inelastic behavior is specified for yielding in both tension and compression (Fig. 1(a)). In Coulomb friction behavior, elastic stiffness (before sliding) k_e is very large and post-elastic stiffness (after sliding) k_p is zero. The yield force F_y is proportional to the normal reaction (or tributary weight, W) with coefficient of sliding friction μ.

Transitions in the behavior from sliding to elastic striking (forceful contact of a movable part against a restraint) and from elastic striking to plastic striking behavior can be represented by combination of truss element and link element (element type #9 in DRAIN-2DX). The link element (Fig. 1(b)) can be specified to act in tension or in compression. A tension element has finite stiffness in tension and goes slack in compression. A compression element has finite stiffness in compression and a gap opens in tension. Thus, three elements are necessary to describe the inelastic behavior of a bearing.

Theoretical Initial Elastic Stiffness of Steel Bearings

Before a horizontal force exceeds the frictional resistance of the bearing parts, the initial elastic flexibility (or by inversion, stiffness) of the bearing can be obtained by summing the components of flexibility. Thus by applying a unit (*1 MN*) force to the sole plate of the bearing, the initial elastic stiffness k_i can be determined from

$$\frac{1}{k_i} = f_f + f_s \tag{1}$$

where f_f=flexural flexibility and f_s=shear flexibility.

The flexural flexibility can be determined by the well-known moment area theorems:

$$f_f = \int \phi y dy \tag{2}$$

in which ϕ=curvature ($\phi = M/EI$ where M=bending moment for a unit lateral load, E=Young's modulus, I=moment of inertia) and y=distance measured down from the sole plate.

The shear flexibility is given by

$$f_s = \int \frac{\alpha_f}{GA_s} dy \tag{3}$$

in which α_f = form factor which may be taken as *1.2, 1.1* and *2* for a rectangular, circular and thin tube section, respectively, A_s = shear area and G = shear modulus determined from the well-known relationship

$$G = \frac{E}{2(1+\nu)} \tag{4}$$

where ν = Poisson's ratio. Much of the flexibility of a bearing assembly arises from the flexibility of the thin rubber pad that bearings are typically seated on. It is frequently assumed that rubber maintains constant volume during all deformation (i.e., $\nu_r = 0.5$). Based on tests of rubber pad retrieved from bearing seats in the field $G_{rubber} = 4\ MPa$, thus from equation (4) $E_{rubber} = 12.4\ MPa$. The apparent modulus in bending (E_r) for the strip rubber pad can be obtained from the following equation (Stanton, 1982).

$$E_r = \left(\frac{4}{3} + \frac{1}{4}S^2\right)E_{rubber} \tag{5}$$

where S = shape factor which is the ratio of the area of one loaded surface to the area free to bulge. Generally bearing seats are rectangular, thus the shape factor is defined by

$$S = \frac{BL}{2(B+L)t} \tag{6}$$

where B, L, and t are the breadth, length, and thickness of the rubber pad, respectively.

Theoretical Ultimate Strength of High Type Rocker Bearings

Longitudinal Direction: Fig. 2(a) shows side elevation of a high rocker (expansion) bearing. The strength limitation for the high type rocker bearing is the rolling of the rocker on the masonry plate. The rolling resistance of the bearing can be obtained $F = C_r W$, in which C_r=coefficient of rolling resistance, where $C_r = 0.04$ observed from tests.

To model the force-deformation behavior of the bearing a bi-linear truss element can be used; the post-yield slope (k_p) being necessary to model the effects of plowing out the debris that may accumulate between the rocker and masonry plate. For the example experimental result shown in Fig. 2(d) a value of $k_p = 0.018\ k_e$ may be used to give an improved simulation as shown by the dotted line in Fig. 2(e).

Transverse Direction: Fig. 3(a) shows an elevation of the high type rocker bearing looking along the axis of the bridge girder. The strength limitation is dependent on either the strength of anchor bolts, the pintles, or the keeper plates.

The strength of the keeper plate may be estimated using yield line theory. Under large deformations of the keeper plate, the applied load changes from being uniformly distributed to being a point load at the upper edge of the rocker. After exploring some failure yield lines to obtain the lowest solution, the yield line pattern shown in Fig. 3(b) was identified as the appropriate upper bound solution. Using the principle of virtual work it can be shown that the strength of the keeper plate is given by

$$F_{kp} = 2(m + m')\left(\frac{L_x}{L_y} + \frac{2L_y}{L_x}\right) \tag{7}$$

in which m=the positive moment capacity of the yield line of the keeper plate given by

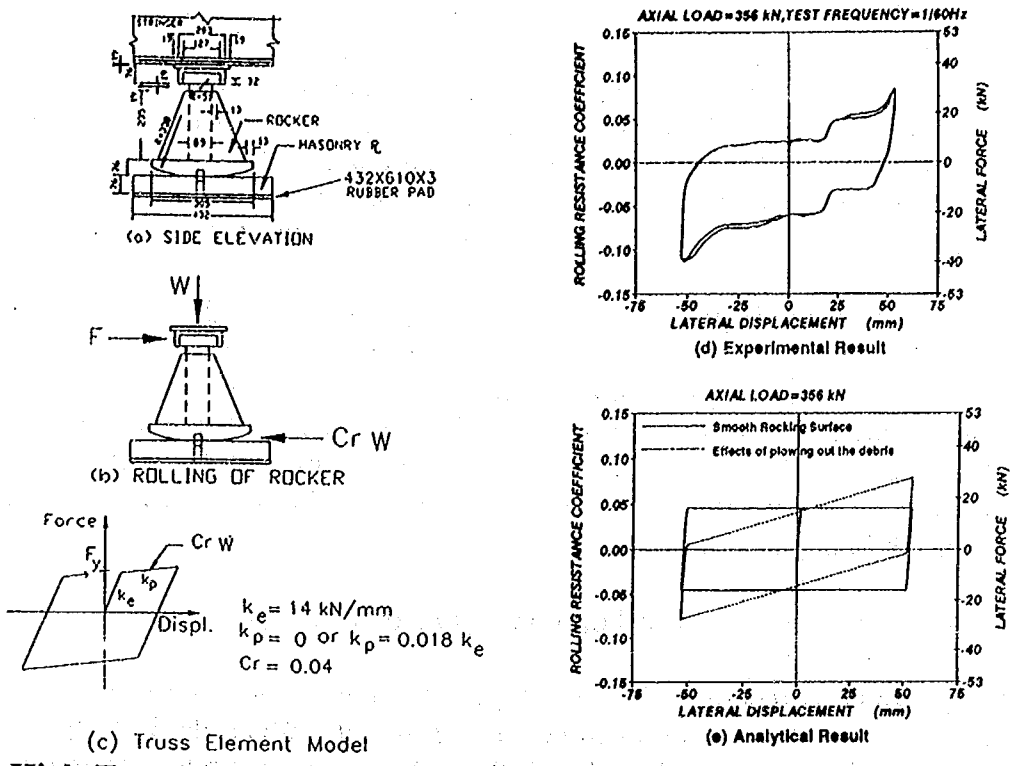


Fig. 2. **High Type Rocker Bearing Tested in the Longitudinal Direction: (a) Side Elevation, (b) Free Body Diagram, (c) Computer Model, (d) Experimental Result, and (e) Analytical Result.**

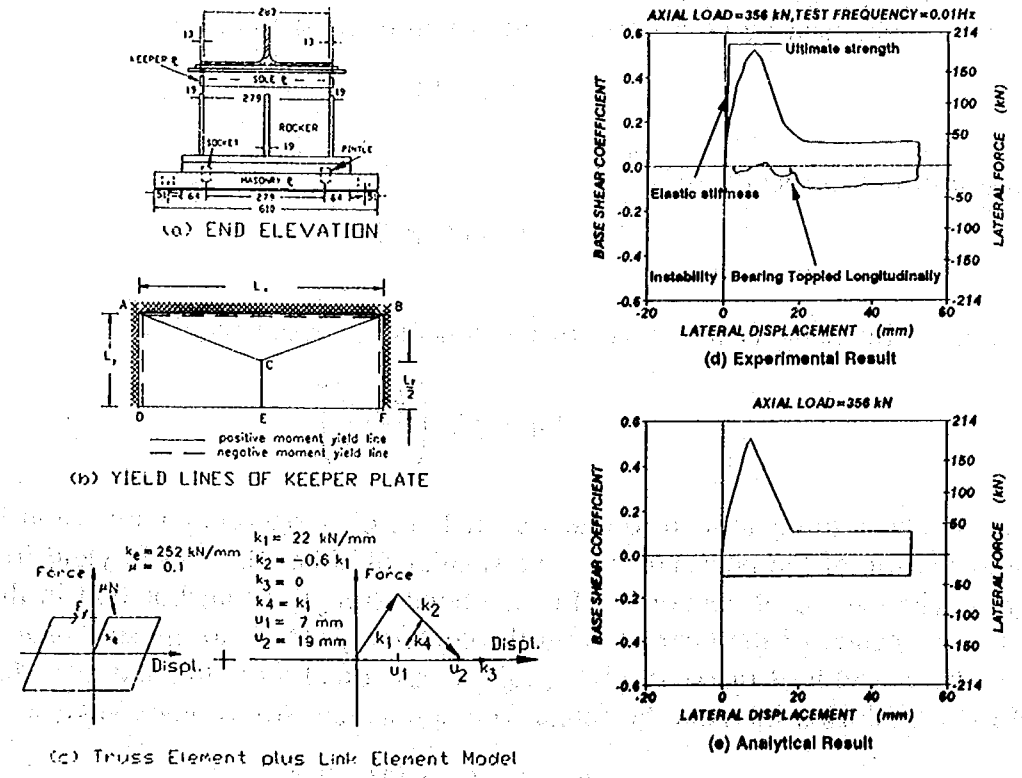


Fig. 3. **High Type Rocker Bearing Tested in the Transverse Direction: (a) End Elevation, (b) Free Body Diagram, (c) Computer Model, (d) Experimental Result, and (e) Analytical Result.**

$m=f_y t^2_p/4$ where f_y=yield strength of the plate, m'=the negative moment capacity of the yield line occurring along the welded edge given by $m'=f_{su}t_w/8$ where t_w=leg length of the weld and f_{su}=the strength of the weld material. The other symbols in equation (7) are defined in Fig. 3(b). Note that the value of F_{kp} in equation (7) is then added to the sliding resistance (μW) to give the total ultimate strength capacity. Based on test results a friction coefficient of $\mu=0.1$ appears reasonable; this lower value resulting from continued polishing of the sole plate-rocker interface under normal service (traffic plus thermal) loads. For the bearing shown in Fig. 3(a), $L_x=127\ mm$, $L_y=51\ mm$, and assuming $f_{su}=f_y=400\ MPa$, then $F_{kp}=159\ kN$.

For analytical modeling of slip between keeper plate and the rocker and the sliding that occurs after the keeper plates fracture can be modeled using an truss element. The increasing stiffness during the keeper plate striking against the rocker and decreasing stiffness due to keeper plate fracture can be modeled using one link element. The combined modeling effect is presented in Fig. 3(c) with the analytical result shown in Fig. 3(e). It will be noted that good agreement can be obtained— except where the bearing toppled in the test, this phenomenon not being accounted for here.

Theoretical Ultimate Strength of High Type Fixed Bearings

Longitudinal Direction Behavior: Fig. 4(a) shows a side elevation of the high type of fixed bearing mounted on a reinforced concrete pedestal. When the bearing is loaded in the longitudinal direction, the lateral load path through to the substructure causes damage to the reinforced concrete pedestal. The failure mode of the combined bearing pedestal assembly results from the rocking of the bearing on the bedding material after bond failure of the anchor bolts due to prying of the masonry plate (Fig. 4(b)). The ultimate lateral strength F of the bearing can be obtained by considering equilibrium of horizontal forces:

$$F=n_b V+\mu_1 C_c \tag{8}$$

and equilibrium of vertical forces:

$$C_c=W+n_b T \tag{9}$$

Equilibrium of moments at the center of the concrete pedestal requires

$$Fh = C_c\left(\frac{b_L-a}{2}\right) \tag{10}$$

in which V=shear force applied to one anchor bolt, C_c=concrete compression force resisting rocking at the top of the pedestal, T = the smaller of either the tensile yield force (= $A_b f_y$ where f_y = yield stress of anchor bolt) or the bond strength of anchor bolt in the concrete pedestal, h = height of the bearing from the concrete pedestal to the sole plate-rocker interface, b_L = width of masonry plate in the longitudinal direction and a = depth of pedestal concrete stress block which can be found from a concrete stress block analysis such that

$$a = C_c / (0.85 f'_c b_T) \tag{11}$$

where b_T = width of masonry plate in the transverse direction.

For the bond stress of the swedged anchor bolt (used for the bearings in the field), T may be estimated from the relationship suggested by Paulay and Priestley (1992), the average bond stress u_a over the length of the anchor bolt being

$$u_a = 1.35\sqrt{f'_c} \quad (MPa) \tag{12}$$

Factors that contribute to bond strength are chemical adhesion, friction and bearing of the bar ribs against the concrete. Unlike reinforcing bars, the surface of the swedged anchor bolts, even though there are irregular dents on the surface, is somewhat more smooth and therefore weaker bearing resistance against the concrete is expected. To apply equation (12) for the swedged anchor bolt case, the following modified equation may be used to estimate the average bond stress u_u of the swedged anchor bolt.

$$u_u = m_f\, u_a \tag{13}$$

where m_f = modification factor that allows for both the reduced bearing capacity of the swedged anchor bolts and the adverse effect of the cyclic loading. Considering only chemical adhesive bond stress as *3.5 MPa* (Giuriani et al., 1991) $m_f = 0.4$ may be assumed.

If bond stresses u_a of constant magnitude are assumed to act uniformly on the anchor bolt's surface (diameter of anchor bolt = d_b) over the embedment length l_{em}, the force in the bar to be anchored can be expressed as follows:

$$T = u_a(\pi\, d_b)\, l_{em} \tag{14}$$

By combining equations (8) through (14), the ultimate lateral strength F of the bearing mounted on the reinforced concrete pedestal with *25 mm* mild steel (f_y=*380 MPa*) swedged anchor bolts can be obtained as follows where T is the smaller of $T = A_b\, f_y$ or equation (14):

$$\frac{F}{W} = 0.5\,\frac{b_L}{h}\left[\left(1+\frac{n_b\,T}{W}\right) - \frac{W}{0.85\,f'_c\,b_L\,b_T}\left(1+\frac{n_b\,T}{W}\right)^2\right] \tag{15}$$

Thus with experimentally obtained concrete strength f'_c = *41 MPa*, u_u = *3.5 MPa*, T = *62 kN* and the ultimate base shear coefficient of *0.67* is obtained from equation (15).

To model the overall force-deformation behavior of the bearing-pedestal assembly, a bilinear truss element and link elements was used to simulate the prying of the masonry plate on the rubber pad and stiffness deterioration and rocking, respectively. Fig. 4(e) shows the analytical result. The initial elastic stiffness was obtained from equation (1), and listed in Table 1. From this table it is evident that the primary source of bearing flexibility arises from the presence of the thin rubber bearing pad located between the masonry plate and the reinforced concrete pedestal.

Table 1. Flexibility analysis of the high type fixed bearing in the longitudinal direction.

Part	Rotation $\int \frac{M}{EI} dy$ (rad/MN-m)	Centroid y^* (mm)	Flexibility Contribution: Flexural f_f (mm/MN)	Flexibility Contribution: Shear f_s (mm/MN)
(A) HIGH TYPE FIXED BEARING ONLY				
Rocker (above Stiffener Plate)	0.232	26	0.006	0.025
Rocker & Stiffener Plate	4.680	236	1.103	0.143
Masonry Plate	0.047	389	0.018	0.005
Rubber Pad	0.096	428	0.041	3.834
		Total Flexibility =	1.168	4.007
		Stiffness $k_i = 1 / (\Sigma f_f + \Sigma f_s) = 1000/(1.168+4.007) = 193$ *kN/mm*		
(B) HIGH TYPE FIXED BEARING ON CRACKED REINFORCED CONCRETE PEDESTAL				
Bearing			1.168	4.007
Cracked Concrete Pedestal	1.435	595	0.853	0.193
		Total Flexibility =	2.021	4.200
		Stiffness $k_i = 1 / (\Sigma f_f + \Sigma f_s) = 1000/(2.021+4.2) = 161$ *kN/mm*		

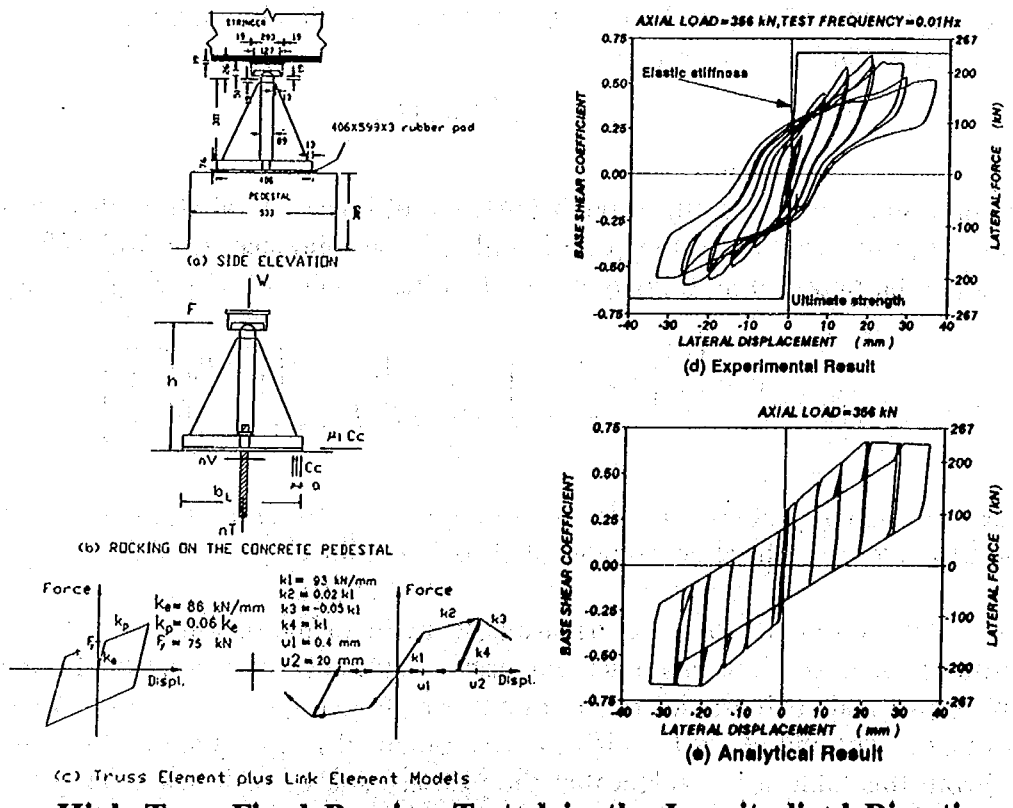


Fig. 4. High Type Fixed Bearing Tested in the Longitudinal Direction: (a) Side Elevation, (b) Free Body Diagram, (c) Computer Model, (d) Experimental Result, and (e) Analytical Result.

ANALYTICAL STUDY OF THE SEISMIC DEMANDS ON STEEL BRIDGE BEARINGS

The seismic demand on high type rocker steel bridge bearings is investigated. A slab-on-girder (SOG) bridge mounted on steel bearings is selected for the purpose of undertaking analytical studies. Transverse restraint of the superstructure is provided at the bearings. When several individual steel bearings with keeper plates are present at a support, the keeper plates may not resist load equally because of slight variations in clearances (Buckle and Friedland, 1995). It is expected that the seismic performance of a bridge will be influenced by its possible variable field conditions, for example where the bearings are not mounted perfectly symmetrically or where some clearances are blocked with debris and/or corroded. This likely scenario is in contrast with "ideal" conditions where the bearings are clean and mounted perfectly symmetrically. Some parametric studies are conducted to investigate impact of imperfection of steel bearings conditions (installation and debris-corrosion related variability of performance) to the transverse direction seismic behavior. Variability may arise in clearances, or the relative strength of bearing at a support line.

For parametric studies, one span of a two-girder bridge with two bearings at each support is selected. This structure is based on a similar configuration of the Rte. 400 bridges recently studied by Wendichansky (1996). The width, length and thickness of concrete deck used are $4.6\,m$, $25.3\,m$ and $0.23\,m$, respectively. Two *W36*×150 steel girders are used as shown in Fig. 5a. The purpose for choosing this simplified deck (rather than a more realistic multi-girder deck) is to provide clear upper and lower bounds to the range of performance when the clearances of steel bearings are symmetrical *vs* unsymmetrical.

Fig. 5b shows the analytical model of the bridge. To focus on the non-linear seismic demand of each type of bearing, only bearing elements exhibit non-linear behavior. Seismic weights ($W=356\text{x}4=1424\,kN$) of *W/4*, *W/2* and *W/4* are lumped at joints *1*, *2* and *3*, respectively.

The natural period of the structure is adjusted by changing the stiffness of the piers. When the period is small the structure may be considered as a single span bridge seated on near-rigid abutments, whereas when the period is long the structure may be thought of as a one span (lollipop) portion of a "long" multiple span bridge with tall piers.

Basically, keeper plates fail in a somewhat brittle manner under horizontal loading. Therefore, the analysis rules shown in Fig. 3 were adopted for modeling the steel bearings. Two cases of bearing clearance are considered in this study, i.e., ***standard clearance case*** and ***variable clearance case***. In the standard clearance case the bearing sole plate is mounted on the rocker exactly symmetrically, thus the clearance between keeper plate and rocker is $3.5\,mm$ each. In the variable clearance case, the bearing sole plate is mounted on the rocker in a completely unsymmetrical fashion. Thus the clearance on one side is already exhausted, while on the other side the clearance is doubled to $7\,mm$. The two different clearance cases are illustrated in Fig. 5c.

The variation in bearing strength has also been considered. This is because the ultimate load capacity of bearings is highly dependent on the strength of the keeper plates.

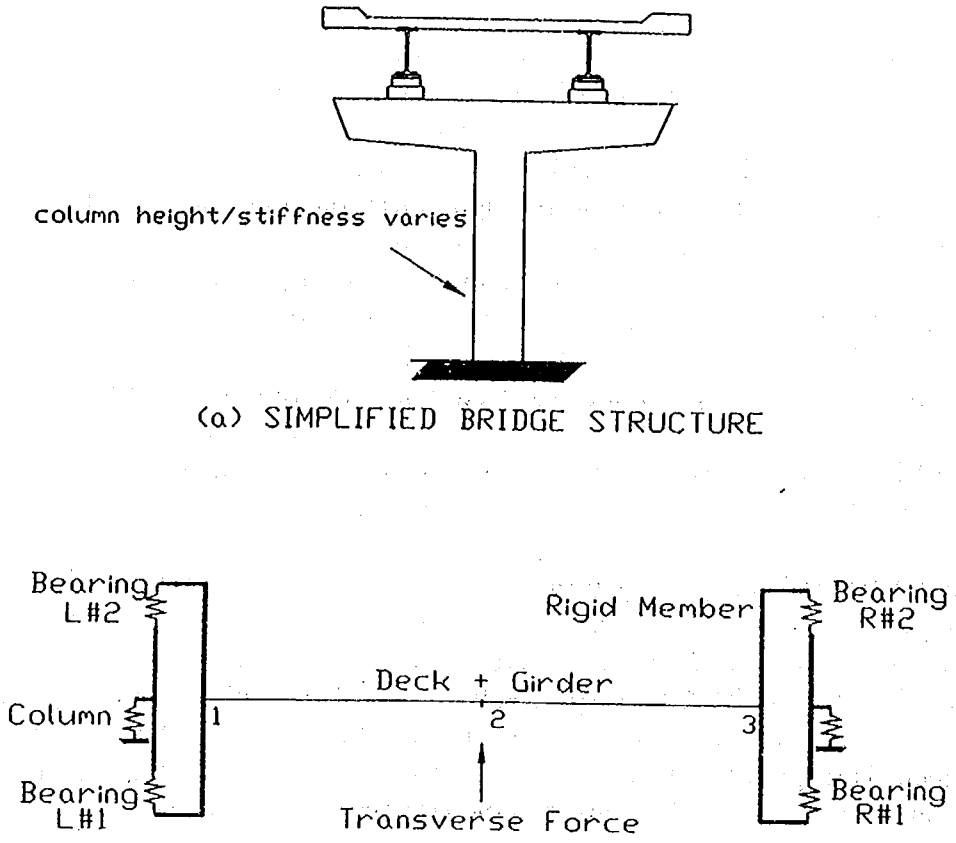


Fig. 5 Configuration of the Bridge Used in the Analytical Study. Also Shown are the Clearances Assumed in the Steel Bearings. Seismic Analyses Were Only Performed in the Direction Transverse to the Bridge Axis.

Therefore, two cases of strength distribution in the bearings are considered in this study — ***standard strength case*** and ***variable strength case***. For the standard strength case all bearings are considered to possess 100% of the normal bearing strength, whereas for the variable strength case the pair of bearings at one support line is assumed to possess 125% of the normal bearing strength while at the other support the strength is assumed to be only 75% of the normal bearing strength. Note that the total lateral strength of the bridge deck for the two cases is the same, but it is expected that torsional response effects may govern the behavior of the bridge with variable strength distribution in the bearings.

Analysis Assumptions and Earthquake Records

The computer program DRAIN-2DX was selected for the purpose of conducting inelastic time history analysis of prototype bridge (Fig. 5a). Several assumptions were made to reduce a complicated engineering problem to a relatively simple problem. The analytical model was developed based on the following assumptions:

(i) All inelastic behavior was assumed to be concentrated in the bearing elements.

(ii) Both mass proportional and stiffness proportional damping where the damping is approximately *5%* of the critical damping for the first two modes was used.

(iii) All the analyses were performed with variable numerical integration time-steps ranging from *0.01 sec* to *0.0001 sec*.

(iv) Ground accelerations are considered only in the transverse horizontal direction.

Nonlinear dynamic analysis of the prototype bridge were performed using four ground acceleration records: El Centro NS ($PGA=0.35g$); Pacoima Dam S74W ($PGA=1.08g$); Northridge, Sylmar Hospital Parking Lot N-S ($PGA=0.6g$); and Kobe, Kobe Station ($PGA=0.83g$).

It can be expected that the adverse effect of variable clearances and strength of the bearings in the field make the seismic response of a bridge somewhat different from the standard case. This effect can be expressed in terms of dynamic magnification factors for bearing force and displacement demands as follows;

Force dynamic magnification is defined as:

$$DM^F = \frac{F^*_{max}}{F_{max}} \tag{16}$$

Displacement dynamic magnification is defined as:

$$DM^D = \frac{D^*_{max}}{D_{max}} \tag{17}$$

where F_{max} and D_{max} are maximum force and displacement of bearings during an earthquake event for the ideal case, and F^*_{max} and D^*_{max} are maximum force and displacement of bearings for the variable clearance/strength case.

Using the computer program DRAIN-2DX non-linear time history analyses were conducted with four selected earthquakes. The analyses were carried out with the first natural period of the bridge (T_1) over the range $0.1 \leq T_1 \leq 4.0$ sec. F_{max}, D_{max}, F^*_{max} and D^*_{max} were sorted from computer output and dynamic magnifications for force and displacement were plotted at each natural period of the bridge.

Analysis Results for the Variable Clearance Case

Bearing force and displacement demands and the resulting dynamic magnifications resulting from clearance variations are shown in Fig. 6. It is observed that when the natural period of bridge is less than *1 sec*, keeper plates either fail or are close to failure during all four earthquake excitations when the clearances of bearing are perfectly symmetric. The same trend is observed with the variable clearances. However, when the clearances of the bearing vary, the keeper plates tend to fail over a wider range of bridge natural period (about up to $T=2.0$ *sec*). Normally the natural period of a SOG bridge is less than *1 sec*. In this range the seismic force demand is large, thus keeper plates tend to fail for most seismic events for all cases regardless of the variation of the bearing clearances. Therefore the force magnification $DM^F=1.0$ (no adverse effect) is obtained for three strong earthquakes. For El Centro earthquake, $DM^F=1.25$ when $T_1=0.8$ *sec* keeper plates fractured for the variable clearance case but survived with a large deformation for the standard clearance case. When the structure (bridge) is flexible ($T > 1$ *sec*), a rare case for real SOG bridges, large force magnification effects are observed. However, this effect is considered to be trivial because the bearing force demands are small.

If the natural period of the bridge is less than about *1 sec*, then the steel bearing displacement demands are almost constant. For longer natural periods, bearing displacements drop sharply due to reduced force demand on the bridge. However, unlike forces, the displacement magnification may be substantial over the natural period range *0.5* to *2.5* sec. The displacement magnification can indeed be sufficient to unseat the bridge girders.

Analysis Results for the Variable Strength Case

Fig. 7 presents the analytical results for the standard and variable strength case. Similar trends to those mentioned above for the variable clearance case are also observed. It should be noted that the keeper plates of the weaker bearings always fail first. This sets up a torsional imbalance in the deck that may cause the end with the bearings with failed keeper plates to slide freely until unseating of those bearings occurs.

CONCLUSIONS

1. Stiffness of bearings in the initial elastic phase may be determined by using classical strength of materials concepts. Bearing stiffness is largely governed by the bedding

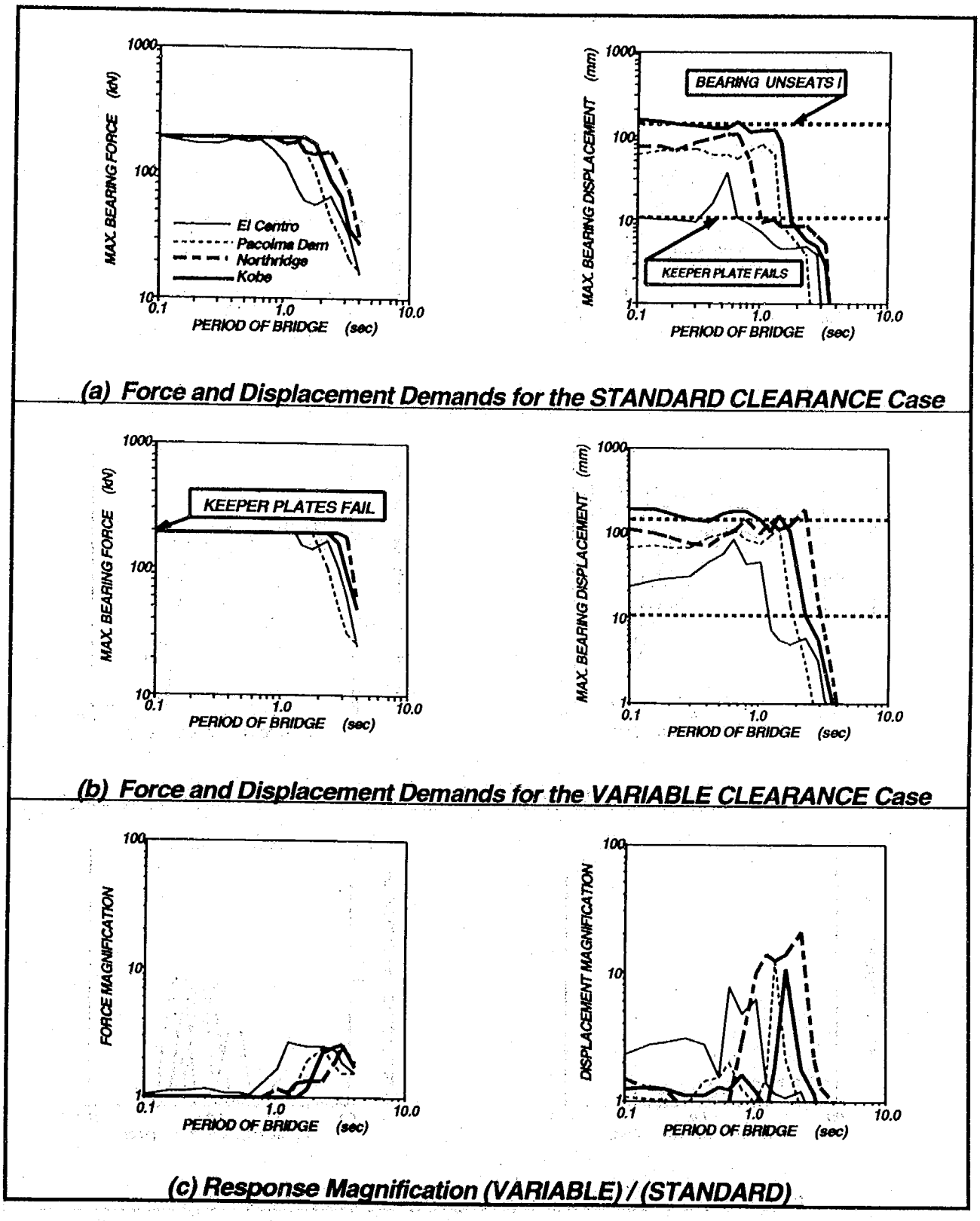


Fig. 6 Effect of Steel Bearing Clearances on Force and Displacement Demands

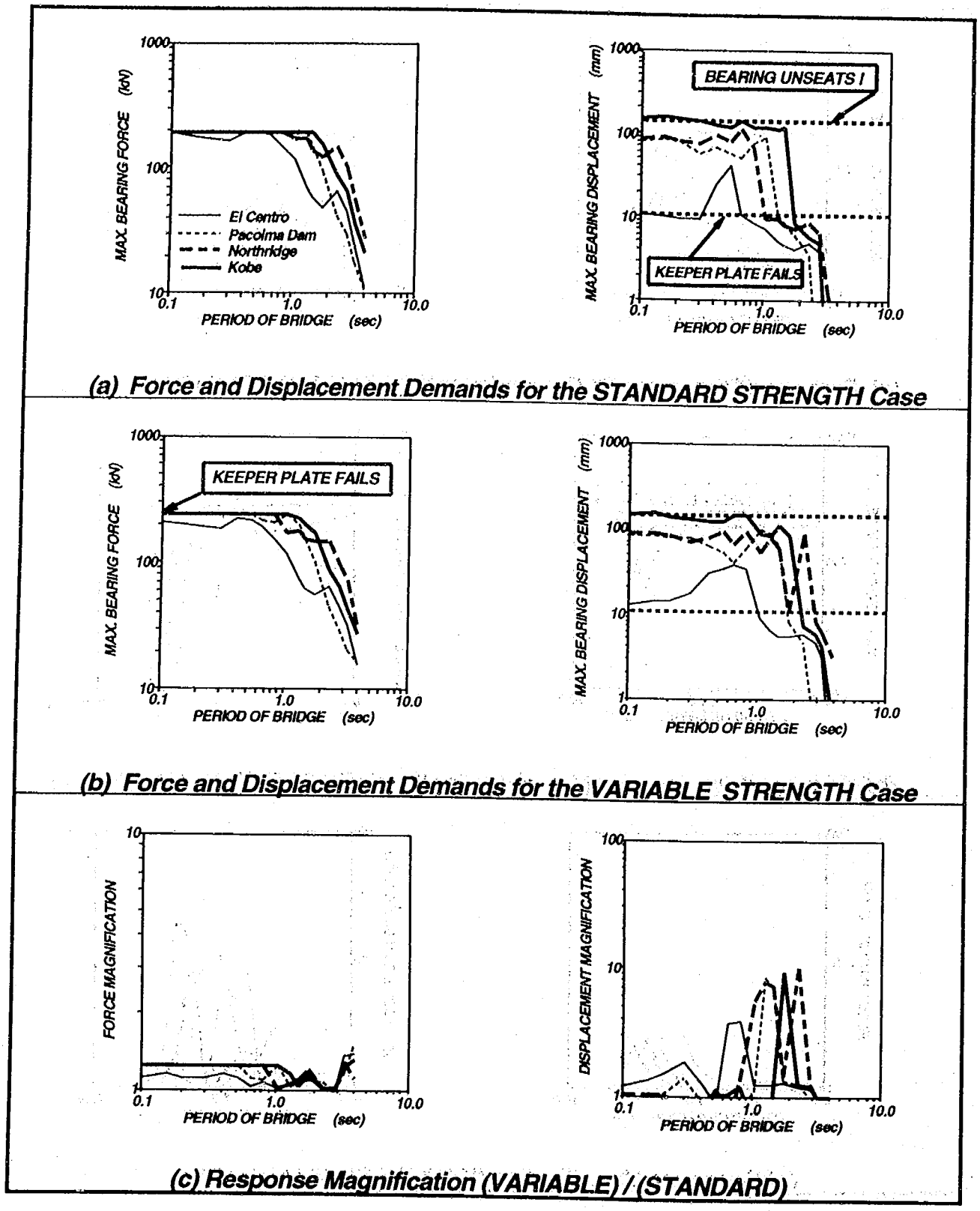


Fig. 7 Effect of Steel Bearing Strength on Force and Displacement Demands

material.

2. Strength of the high type of steel bridge bearings is governed by the keeper plate capacity. Following keeper plate failure, sliding (governed by Coulomb friction) takes place until unseating occurs.

3. For undertaking computational studies using non-linear dynamic analysis, force-displacement relationships for steel bearings can be simulated using the elements that exist in a general purpose computer program. This study has shown that standard macro-models that exist in non-linear dynamic analysis programs such as DRAIN-2DX, are appropriate for representing the non-linear force deformation response of bridge bearing-pedestal assembles.

4. Variations in mounting clearances of bearings, and the relative strength capacity of bearings at different support lines are inevitable in the field. These variations will affect the seismic performance of the bridge. Although the displacement demands on steel bearings largely depend on the characteristics of the seismic excitation, the displacement demands for a given earthquake may be magnified by some 25 times if the clearances or strength of the bearings vary, this is often sufficient to unseat the girders.

ACKNOWLEDGEMENTS

Financial support is acknowledged from the National Center for Earthquake Engineering Research through a contract with the Federal Highway Administration project on Seismic Vulnerability of Existing Highway Construction (FHWA Contract DTFH61-92-C-00106).

REFERENCES

Buckle, I.G., and Friedland, I.M.,(1995) " Seismic Retrofitting Manual for Highway Bridges," U.S. Department of Transportation, Federal Highway Administration, Report No. FHWA-RD-94-052, May, 309 pp.

Giuriani, E., Plizzari, G., and Schumm, C. (1991) "Role of Stirrups and Residual Tensile Strength of Cracked Concrete on Bond," Journal of Structural Engineering, Vol. 117, No. 1, January.

Mander, J.B., Kim, D-K, Chen, S.S., and Premus, G.J., (1996), "Response of Steel Bridge Bearings to Reversed Cyclic Loading," Technical Report NCEER 96-0014, National Center for Earthquake Engineering Research, State University of New York at Buffalo, Yew York.

Paulay, T., and Priestley, M.J.N. (1992), Seismic Design of Reinforced Concrete and Masonry Buildings, John Wiley & Sons, 744 pp.

Prakash, V., Powell, G.H., Campbell, S.D., and Filippou, F.C. (1992), "DRAIN-2DX User Guide", Department of Civil Engineering, University of California Berkeley, California.

Stanton, J.F. and Roeder, C.W. (1982),"Elastomeric Bearings Design, Construction, and Materials," National Cooperative Highway Research Program, Report 248, Transportation Research Board, National Research Council, Washington, D.C., August.

Wendichansky, D.A., (1996)," Experimental Investigation of the Dynamic Response of Two Bridges Before and After Retrofitting with Elastomeric Bearings," Ph D Dissertation, Department of Civil Engineering, State University of New York at Buffalo.

Session 7

Retrofit Methods for Foundations and Geotechnical Considerations

(Co-Chairs: J. Murakoshi, K. Almand)

"Inspection and Restoration of Damaged Foundations due to the Great Hanshin Earthquake 1995"
by H. Ishizaki, A. Nanjoh, J. Kawakami, N. Egawa, Y. Adachi,
Presented by: Yukio Adachi

"Seismic Design of Pile Foundations"
by M. Nakano, Y. Kimura,
Presented by: Yoshitomi Kimura

"Site Remediation and Seismic Response Mechanisms"
by K. Adalier, A. Elgamal
Presented by: Ahmed Elgamal

"Seismic Design Treatment of Liquefaction-Induced Ground Flow"
by K. Tamura, T. Hamada, T.Azuma
Presented by: Kei-ichi Tamura

"A Study on Measures against Ground Flow Using The Finite Element Method"
by M. Ogasawara, H. Tsunoda, T. Makita, S. Gose
Presented by: Hiroshi Tsunoda

Inspection and Restoration of Damaged Foundations due to the Great Hanshin Earthquake 1995

Hiroshi Ishizaki*, Atsushi Nanjo*, , Furitsu Yasuda*, Yoriko Kawakami*, Noriaki Egawa*
*Hanshin Expressway Public Corporation
Yukio Adachi**
**Public Works Research Institute, Ministry of Construction

Introduction

The Hanshin Expressway structures suffered tremendous damage from the Great Hanshin Earthquake in January 1995, especially the Kobe route and the Wangan route shown in Fig 1. The size of the region affected and severity were tremendously extensive. What is most notable in this event is that a lot of damage due to excessive earthquake force was found to the foundations of highway bridges, while foundation damage in the past was limited mainly to scouring. Therefore the foundations of the Kobe route and the Wangan route had to be inspected and restored without sufficient preparation in terms of not only inspection and evaluation methods but also strengthening methods.

The three inspection methods were mainly employed. The most reliable method was direct visual inspection while it was expensive and took time, so indirect visual inspection and nondestructive inspection that require much less time were mostly employed. The overall survey was conducted to investigate residual displacement due to lateral ground flow induced by liquefaction on the Wangan route. The inspection results revealed that the foundations of the Wangan route along the perimetric sections of reclaimed land where the ground underwent liquefaction were severely damaged but that the damage to the foundations of the Kobe route and of the inland areas of the Wangan route was comparatively small so they were reused. The most severely damaged foundations were restored by adding piles to strengthen the seismic resistant capacity.

This paper introduces and explains the investigation methods, the inspection results on the bridge foundations, and retrofit or restoration methods of them with emphasis on the pile foundation, damaged by the Great Hanshin Earthquake.

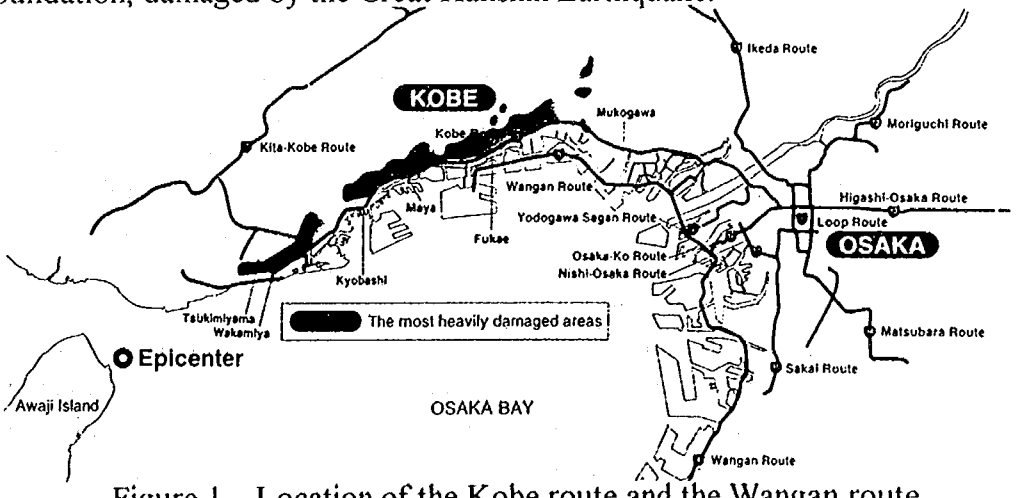


Figure 1 Location of the Kobe route and the Wangan route

Inspection Methods

General

Investigation of pile damage should be conducted from the view point of investigating both damage to pile body itself and ground condition around foundation. The methods listed in table 1 were employed to investigate the damage to the pile body itself, the methods in table 2 were conducted to know the overall information of ground condition.

Table 1. Inspection methods for damage to bridge foundations

Investigation	Inspection Methods
Direct visual inspection (Eye inspection)	Direct visual inspection of surface cracks on a pile body.
Indirect visual inspection (Bored-hole camera inspection)	Indirect visual inspection of inside pile cracks with a small camera inserted into a hole bored in a pile.
Nondestructive inspection (Pile integrity test)	Nondestructive inspection of cracks and defects in piles by analyzing reflected impact wave.

Table 2. Investigation methods for ground condition around piers

Investigation	Inspection Methods
Visual inspection (Eye inspection)	Inspection of cracks and settlement around piers by eye.
GPS survey (Global Positioning System)	Satellite survey of residual displacement in piers located along the sea side or in reclaimed islands.

Direct Visual Inspection

Direct visual inspection was the most direct and reliable way of determining the damage because it allows their direct observation by excavating and exposing the pile top section, though only externally. Orientation and intensity of cracks in the piles can be indispensable in determining the degree of damage. On the other hand, due to the need for excavation, the benefits of this inspection method depend on the labor and equipment available for excavation, and inspection area is only limited to the pile top section, not the entire length. Prevention work for secondary shock disaster by putting temporary bent to girders and pier beams may prevent these inspection work so that it is impossible to check the pile damage of severely damaged piers. It may also be necessary to prevent water ingress near the sea.

Indirect Visual Inspection (Bored-hole Camera Inspection)

An alternative method was an indirect visual method using a bored-hole camera, which allows inexpensive, rapid investigation to piles to a similar extent to direct visual inspection. Borehole cameras have been used to investigate bedrock, mainly to check for joints, cracks and faults prior to dam construction. Here, a hole is bored down the center of the target pile and a small camera is inserted in the hole to allow assessment of the conditions inside. For this inspection, a 66-mm-diameter borehole was made in a pile and a small TV camera was inserted into the hole to look for any cracking in the hole wall. Fig 2 shows the configuration of the inspection equipment. This method evaluates the damage based on the information of a 66mm ϕ hole in a 1000~1500m ϕ piles so that it needs careful consideration to assess the whole pile damage based on observed inside crack width and inside crack density.

Investigation Method for Ground Condition around Piers

The first step in studying the damage to pile foundations is to investigate the ground condition as well as the foundation itself. The ground conditions around piers, such as cracks on pavement, settlement and liquefaction of the ground, and movement of piers, can be checked by eye inspection immediately. Global Positioning System (GPS) survey that is a kind of satellite-based survey is the only method to accurately measure the absolute movement of piers and the ground when the triangulation points were already moved. The results of these inspections are very helpful to estimate the level of damage.

Inspection Result

Typical Inspection Result of the Kobe Route

The Kobe route passes over the solid inland ground, almost no liquefaction was observed along this route after the earthquake. Part of the route showed small-scale cracks and settlement around piers. Photo 1 shows a typical example.



Photo 1 Ground condition just after the quake (the Kobe route)

In the restoration project for the Kobe route, the possibility of reusing the foundation structures was a major subject of discussion. Here, the inspection results of the piltz bridge foundations, an elevated section of which fell down, are introduced. The elevated, 18-span continuous concrete bridge collapsed due to flexural-shear failure of the columns. Photo 2 shows the worst example of the direct visual inspection results. As the foundation was totally exposed, all the pile tops were checked visually. Cracks were found in all the pile tops, the biggest being about 2 mm in width. On the other hand no cover concrete was spalled from any pile, and hammer tests revealed that only normal concrete acoustics were heard. A typical captured crack obtained by bored-hole camera inspection is shown in Photo 3. Fig 4 shows the crack distribution in the direction of the pile axis, indicating that cracks are concentrated in the top section.

This was seen on almost all the piles of the Kobe route, except for a few piles where some cracks were found around bar cut-off sections or where there was a strata change. These inspection results suggest that cracks concentrate near the tops of piles and make

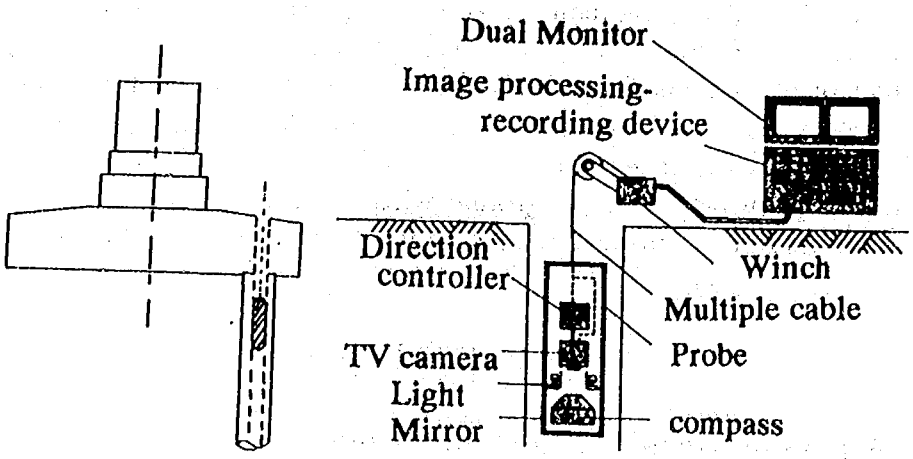


Fig 2 Indirect visual inspection (Bored-hole camera inspection)

Nondestructive Inspection (Pile Integrity Test)

The basic idea of a nondestructive inspection is to analyze a reflected elastic wave, which can be achieved rapidly and at a fairly low cost. It is a very useful, effective way of roughly assessing the damage to a pile. The principle of the pile integrity test is to generate an impact wave with a hammer, and measure the reflected wave with an accelerometer. The wave contains information on changes in the pile cross section and cracks collected while it travels through the pile body. Analyzing disturbances in the wave allows the presence of cracks and other defects to be judged, leading to an estimation of the amount of damage to the pile. The general idea of this method is shown in Fig 3. Besides many advantages of this method, it requires fairly expert knowledge to analyze the inspection results, and it tend to underestimate the number of multiple adjacent cracks.

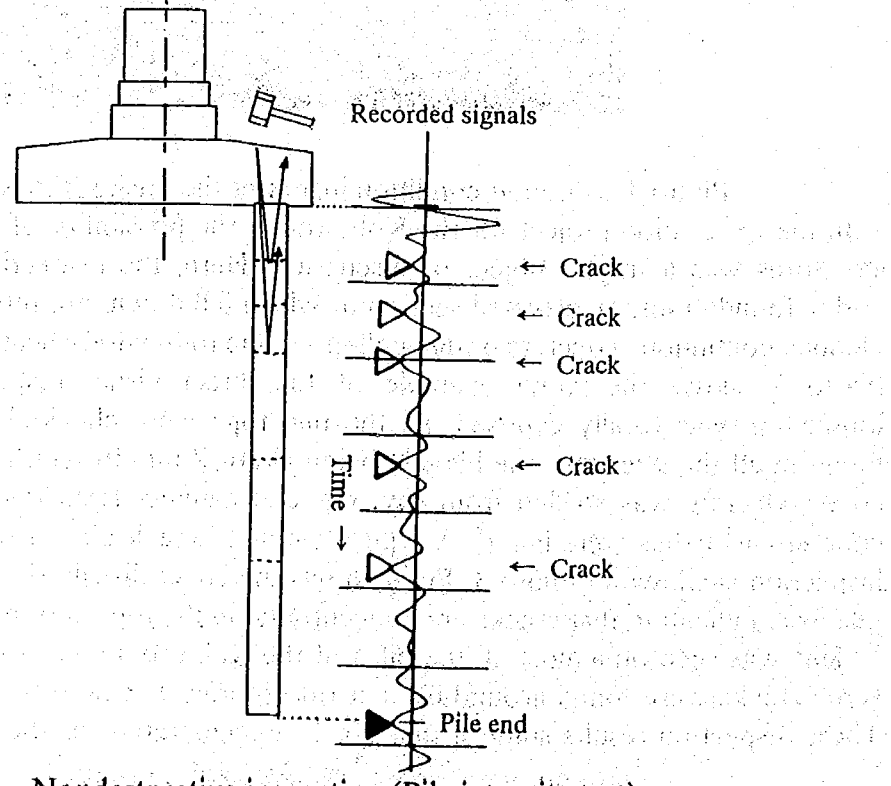


Fig 3 Nondestructive inspection (Pile integrity test)

good sense from a design point of view. No cracks larger than the one mentioned above were found and some of the foundations inspected proved to be completely free of cracks.

The pile damage inspection project of the Kobe route was conducted by two phases. The first phase was carried out for over 50 foundations in consideration of inspection area, and structure type. According to the factor analysis of the results, the damage may seem greater where the settlement and cracks were found, N values in the surface ground were fairly small, the cover depth over the pile cap was comparatively thin, and the damage of column and pier is extremely great or non. It may seem also greater where the foundation located near rivers or former river sites. The secondary phase continues to investigate those in the indicated area mentioned above. In total, 123 pile foundations were checked, resulting that no greater damage found at the piltz bridge site was found in the Kobe route.



Photo 2 The worst damage found on the pile of the collapsed piltz bridge

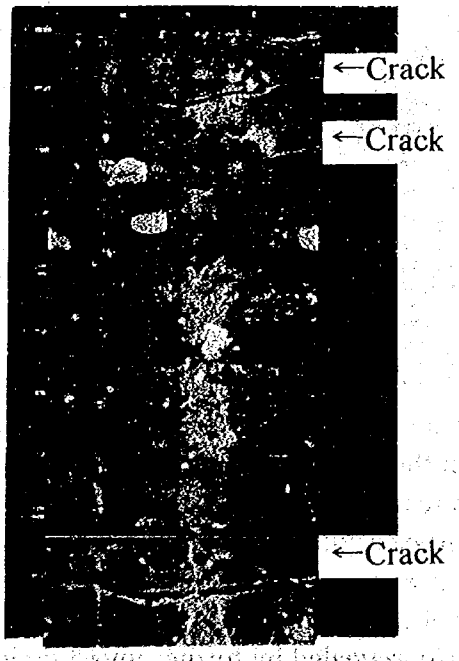


Photo 3 The bored-hole camera inspection result on the pile of the piltz bridge

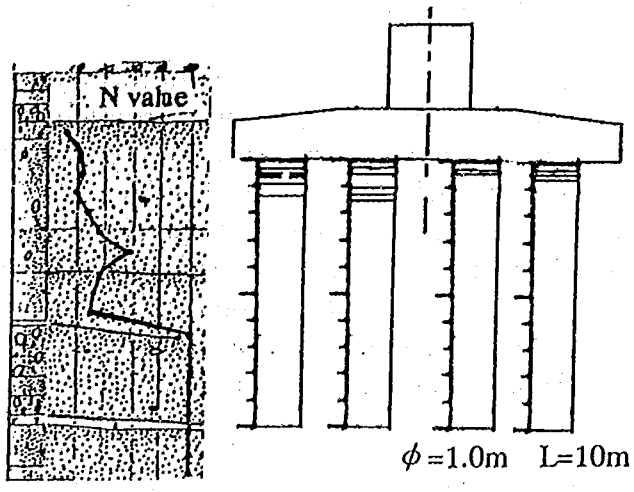


Figure 4 Crack distribution on the pile of the collapsed piltz bridge

Typical Inspection Result of the Wangan Route

Along the Wangan route that connects recently-reclaimed islands, liquefaction occurred after the earthquake, causing big displacements in piers, especially along the waterfront of reclaimed lands(see Photo 4). Many piers near the waterfront had moved horizontally toward the waterfront, and that the ground near the waterfront had settled much around a half meter. The nearer the area was to the seismic epicenter, the greater the settlement. According to the GPS survey result, it can be seen that the movement of the foundations near the waterfront were fairly big in comparison with other areas.

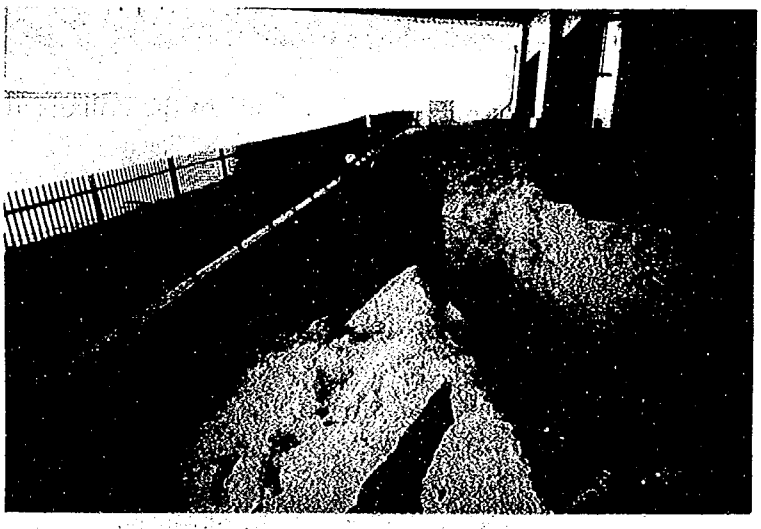


Photo 4 Ground condition just after the quake (the Wangan route)

Primary inspection on the Wangan route was conducted for some foundations that had exhibited by far the greatest amount of shift. Photo 5 shows an example of the inspection results. In spite of the large residual horizontal-displacement measured (about one meter), no major damage such as spalling of concrete, and buckling of reinforcements in the pile top. This is believed to be attributable to the fact that cracks were distributed widely through the piles, that was revealed by further investigation. After the primary inspection, continuing investigation of the Wangan route was carried out using nondestructive and

indirect visual inspections because the underground water level was high and the foundations were large, which would have required large-scale construction to stop water ingress.

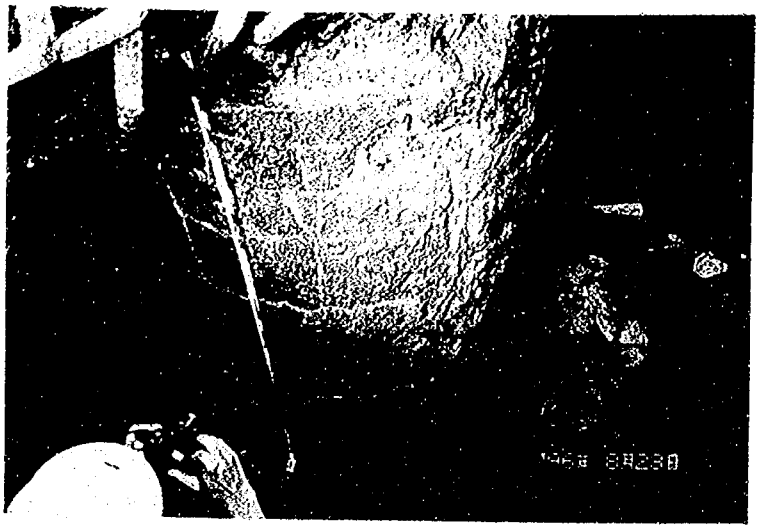


Photo 5 Exposed surface of the pile top that exhibited greater amount of shift

Figure 5 shows the average cracking density of the foundations in the recently reclaimed area obtained by pile integrity tests, and also shows the relative residual displacement obtained by the GPS survey. According to this figure, almost all the piles in the reclaimed land have cracks all through the reclaimed layer. The more amount of relative residual shift is seen, the more amount of cracks can be found.

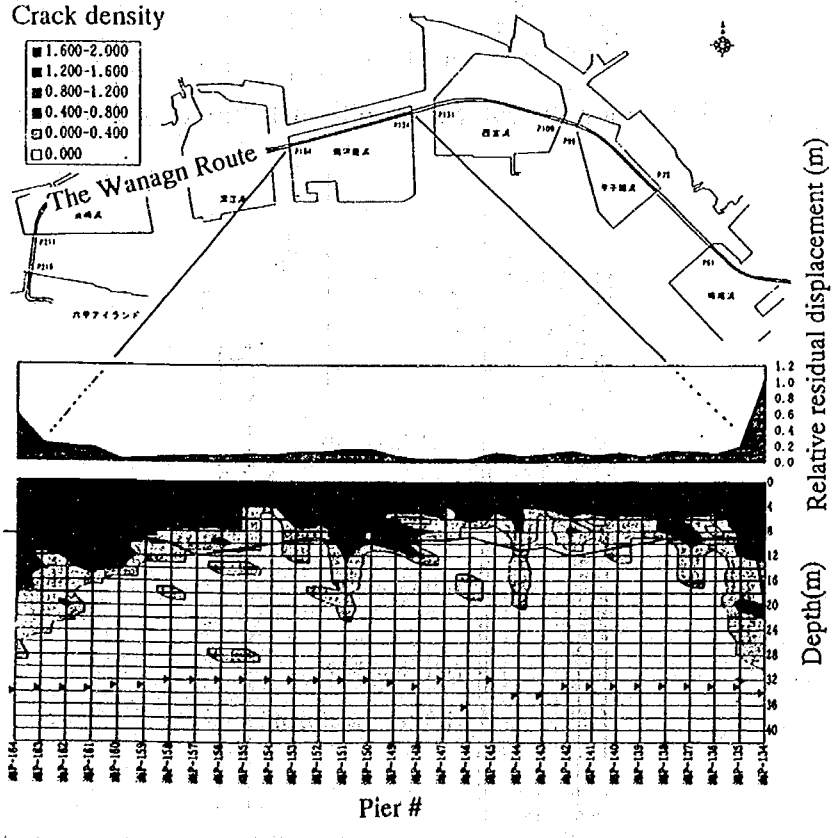


Figure 5 The relation between relative residual shift and crack density.

Figure 6 and 7 show the typical inspection results of the foundations both near the waterfront and inland. The foundations along the waterfront suffered cracks that were distributed evenly along the piles in the reclaimed layer, in alluvial deposits, and even in diluvial deposits. The foundations in inland area also had cracks down to the boundary with the diluvial layer as well as in the reclaimed layer, and in the pile tops; however, the density of cracking was less than that of waterfront area.

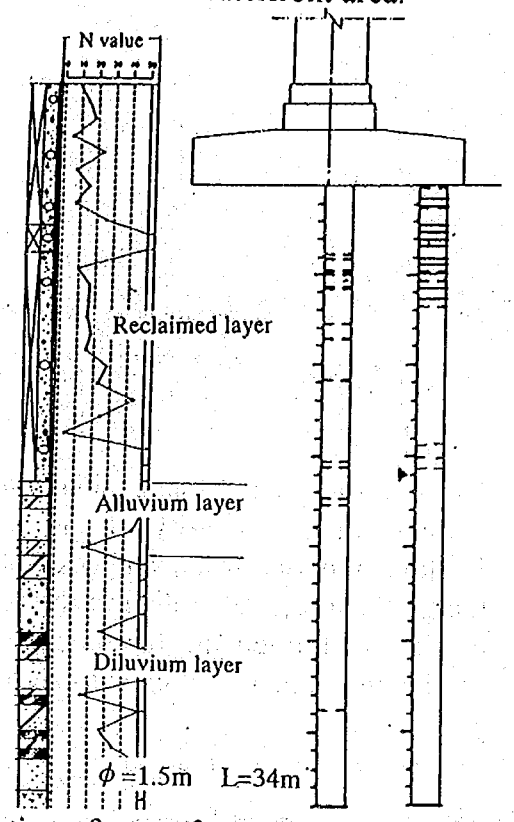


Figure 6 Crack distribution of water front pile that showed greater amount of shift

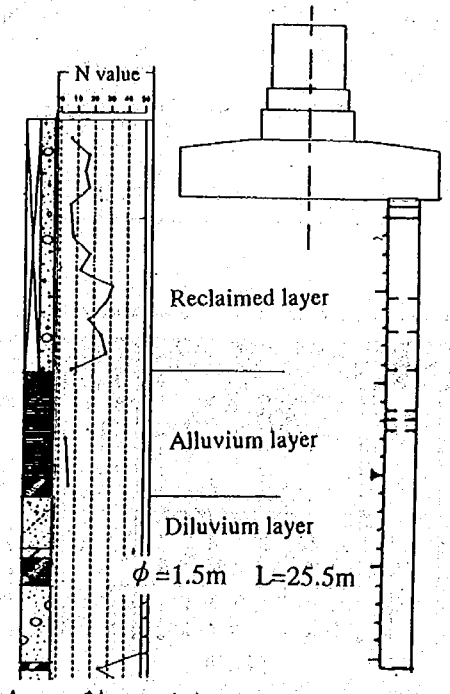


Figure 7 Crack distribution of in reclaimed-land pile that showed relatively no shift

Overall damage assessment results

Overall inspection results were assessed according to the criteria in Table 3. The results are listed in Table 4. This result shows that some foundations of the Kobe route ranked in category c, but the majority of them were ranked d; in general there was little damage to the foundations of the Kobe route. The foundations along the perimetric area of reclaimed on the Wangan route, however, suffered b ranked damage while many on the newly-reclaimed land c. The foundations in areas near the center of the reclaimed land ranked d.

Table 3 Foundation damage evaluation criteria

	Definition
a	Both settlement of the foundation and large residual displacement are found.
b	The foundation has a big residual displacement and piles have flexural cracks.
c	Piles have small flexural cracks.
d	The pile has no damage or has fairly small, negligible flexural cracks.

Table 4 Foundation damage evaluation results (No. of foundations)

Degree of damage	**a**	**b**	**c**	**d**	Total
the Kobe route	0	0	17	92	109
the Wangan route	0	17	57	79	153

Restoration Work

General

The foundations that suffered **b** and **c** ranked damages were given grouting work to increase the durability of reinforcing steels. **c** ranked damaged foundations were essentially thought to have enough safety with respect to its bearing capacity. Installation of additional piles was made only to the foundations with ranked **b** damaged since these foundations were largely affected by lateral ground flow induced by liquefaction.

Checking the Load Bearing Capacity of Damaged Piles

In order to verify the possibility of reusing c-ranked piles, loading tests were conducted for the piles of the piltz bridge where a comparatively high degree of damage was found on the Kobe route. Three kinds of load test (a pile bending test, vertical load test and horizontal load test) were conducted. The pile bending test are discussed here.

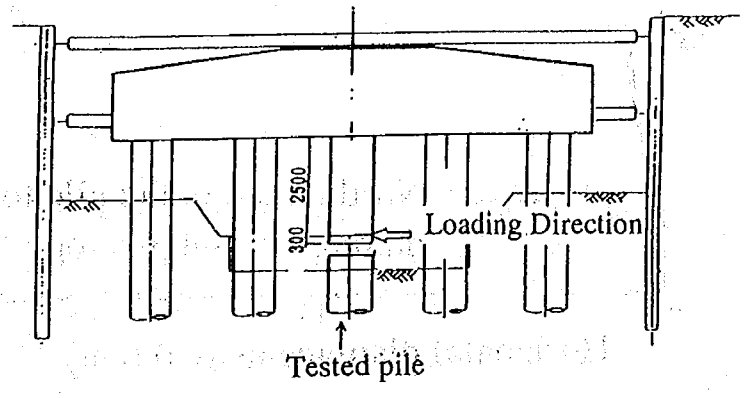


Figure 8 Pile bending test conducted to the pile of the Piltz bridge

The pile bending test was carried out for the pile top section where cracks had developed (see Fig 8). As shown in the figure, the pile was cut off 2.8 m below the pile cap and the top section was used as the test specimen. A horizontal force was applied in one direction at several levels. A maximum applied force was equivalent to about 60% of the calculated yielding bending moment at the pile top section. The observed M-ϕ relation of the pile top section is shown in Fig 9. As can be seen from the figure, no residual curvature but a certain drop in rigidity is observed in the pile top section. This indicates that the steel bars of the pile had experienced just beyond yield stress. The bearing capacity of the entire foundation w/ or w/o damaged top pile section was calculated using the observed pile top rigidity. As shown in Fig 10, the bearing capacity of the entire pile foundation is not affected much w/ or w/o damage at the pile top section. This indicates that the foundations with a similar degree of damage to those shown in Photo 4 can be reused.

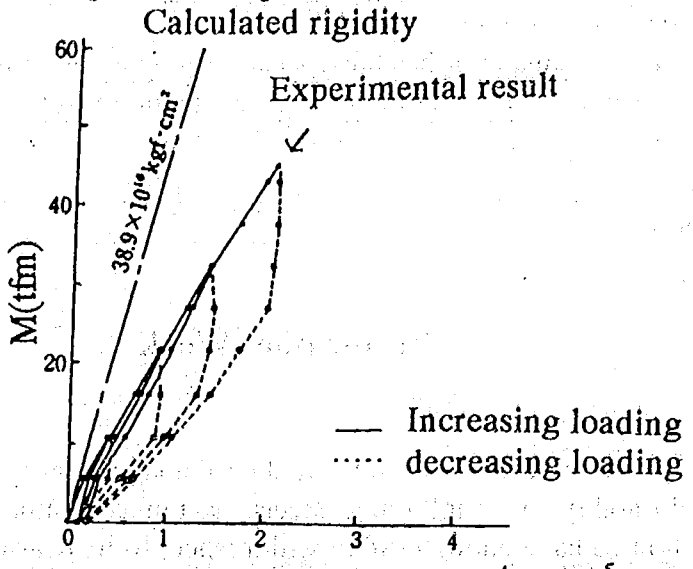


Figure 9 Observed load-curvature relation and calculated result w/o damage

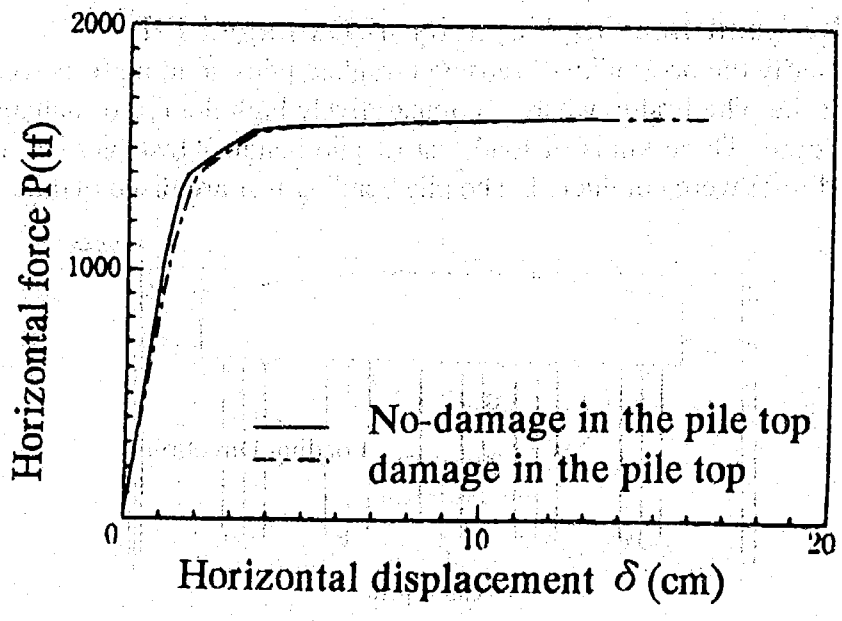


Figure 10 Calculated bearing capacity of the pile of the Piltz bridge

Restoration and Strengthening Work on Damaged Pile Foundation

The foundations with B ranked damage were found only in the areas nearby the shoreline, and therefore these foundations are thought to be affected by the lateral ground flow induced by liquefaction. In order to repair and strengthen the damaged foundation, additional piles were installed around the existing pile cap, and then the pile cap was enlarged to combine the surrounding added piles. Consequently the rigidity of pile foundation as well as the bearing capacity of the pile cap against the lateral soil flow were largely increased.

Here, the design method for adding piles at the north end of the Rokko Island is shown below as an example. The original size of the pile cap was 18m×9.5m×2.5～3 m. It was supported by 14 cast-in-place concrete with 1.5m ϕ and 39m long. The restoration design was made according to the restoration design guideline[1]. The following design considerations were adapted to the 1990 seismic design code.

i)The susceptibility of the ground to liquefaction was checked if the average particle size of soil ranged between 0.02mm and 20mm.

ii)The liquefaction possibility of replaced sand layer beneath the embankment caisson was also checked since some replaced sand layer might have been liquefied according to the site investigation after the quake.

When considering the design force of lateral soil flow force on the foundation, it is very important to know when the lateral flow outbreaks. Studies are made herein by assuming either a) ground flow outbreaks together with the principal motion of earthquake or b) ground flow outbreaks sometime after the principal motion of earthquake. In case of a), the big lateral soil pressure to the foundation should be considered in design as the ground has not reached complete liquefaction and the static characteristics of soil itself still remains. In case of b), the flow pressure to the foundation is much smaller as the ground has reached complete liquefaction.

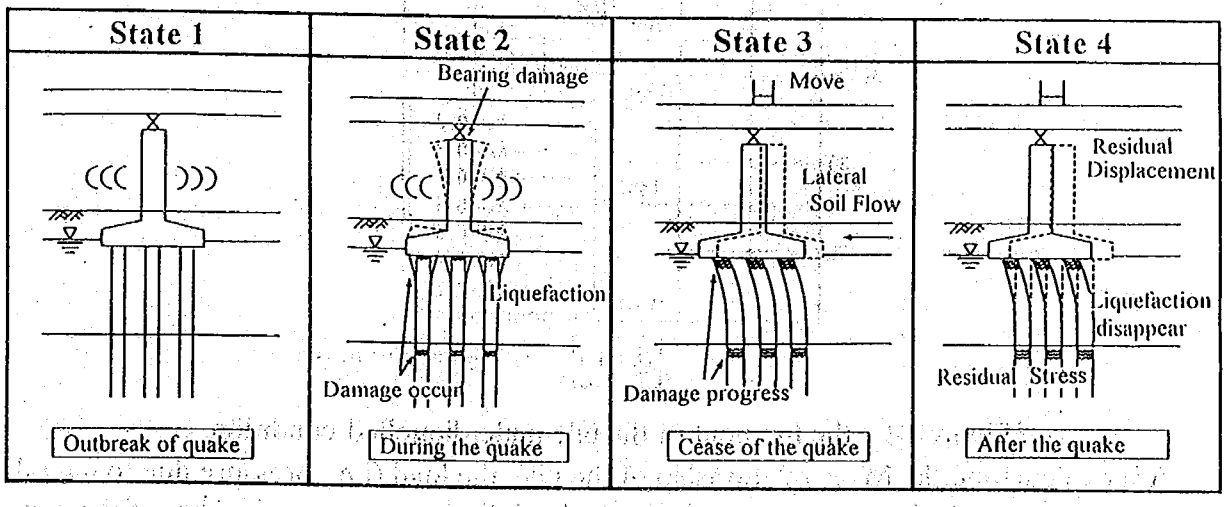


Figure 11 Assumed mechanism of lateral ground flow induced by liquefaction

It is difficult to know which represents the actual mechanism, however, it was concluded that the case ii) is likely to be the actual one because of the following reasons. Case studies of earthquake damages show that lateral soil flow occurs a few minutes after the principal earthquake motion. After examining the damage of the piles, it is difficult to conclude that the horizontal movement of the foundation and cracks found in the piles

were created by one strong stroke of the inertia force of super structure during the principal motion of earthquake because of their location and their amount. As shown in figure 11, the following engineering judgment was made. The liquefaction and the damages to the bridge shoe and piles are induced first during the principal motion of earthquake and then the lateral flow of ground started rapidly after the quay wall failure. Flow pressure is exerted on the foundation as the fissures between the quay wall and the bridge piers are being closed by the flow, and consequently the damage to the piles progressed. Based on this hypothesis, the flow pressure on foundation was estimated by performing a non-linear analysis for the case with the inertia force of bridge and lateral soil flow condition.

Figure 12 shows the moment of the pile calculated by changing seismic coefficient under liquefied condition. According to the result, beyond-yield moment was found at the pile top part and the mid height part of the pile; therefore, the damage to the pile was thought to be induced at these location. When calculating the relationship between lateral soil flow force and displacement of the foundation, the secant stiffness was used for non-damaged pile part and the yield stiffness was used for damaged pile part.

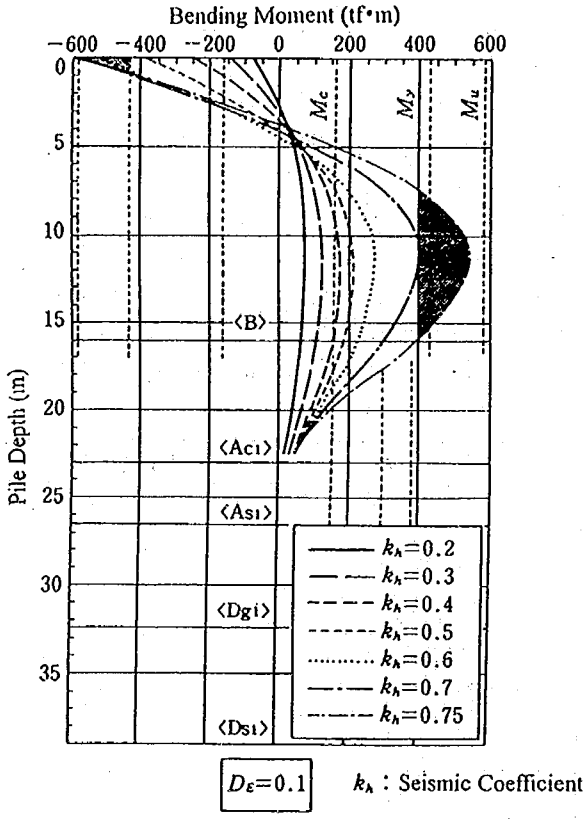


Figure 12 the moment of the pile under liquefied condition

After calculating the M-ϕ relationship of the pile, the load (i.e., pressure due to lateral soil flow) was gradually increased to obtain the load displacement relationship of the pile. The load due to the soil flow was set to act in the longitudinal direction. The soil stiffness between the pile and the liquefied ground was set to zero(i.e., D_E=0) as the amount ground movement exceeds that for the foundation. The soil flow load versus displacement relationship (i.e., P-δ relation) of the pile thus obtained indicated that the lateral soil flow load was about 700tf based on the observed horizontal movement of the foundation.

By considering the available space for construction, and the load carrying capacity, cast-in-place concrete pile with a diameter of 2500mm or 3000mm. The strengthening design was to install additional 12 concrete piles with a diameter of 3000mm to the existing pile foundation. Figure 15 shows the pile design adapted.

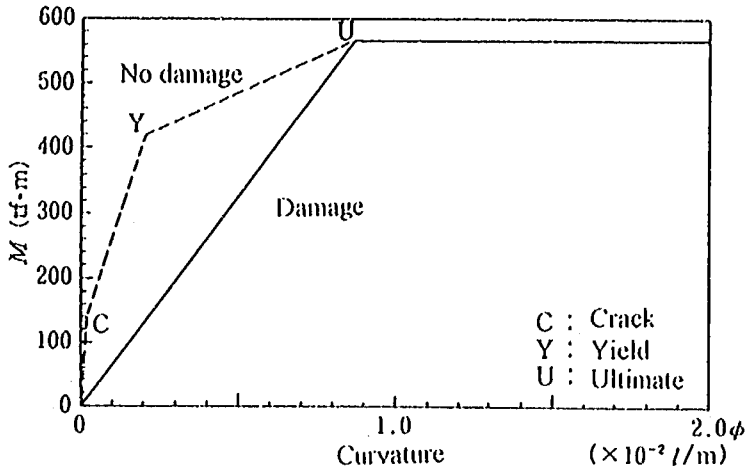


Figure 13 Assumed M-ϕ relation of damaged pile and non-damaged pile

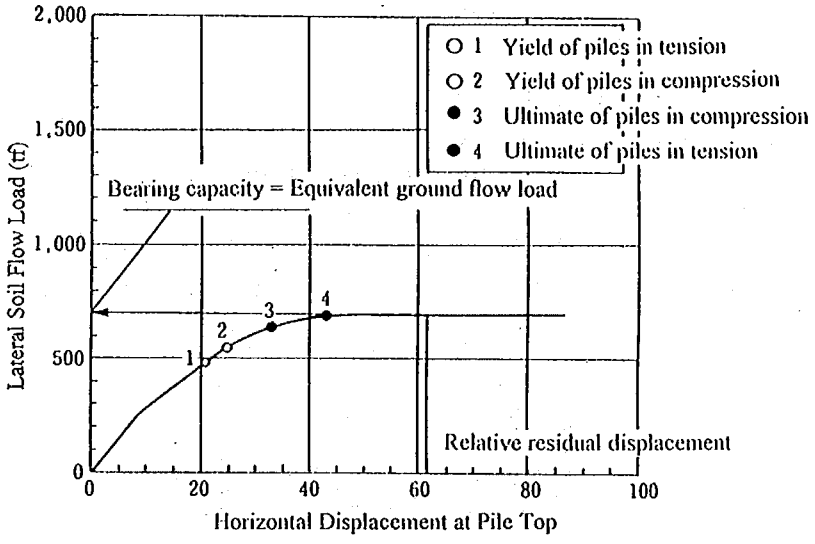


Figure 14 The relation between ground flow force and displacement of the foundation

The vertical stiffness of the existing piles was reduced to a half of the original value to consider the earthquake damage and the design safety. The flexural stiffness of pile was also reduced appropriately according the degree of damage suffered.

Enlargement of existing pile cap was also designed in order to connect the added piles, which are to be install at the perimeter, to the existing pile cap. The strengthening method can be take either extending the pile cap upwards or down words. The downward extension would have problems of exposing the pile and of executing the work beneath the pile cap, the upward extension was adopted. For connecting the reinforcement bar of the added pile to the pile cap, strengthening method with reinforcing bars, not prestressing tendons, was adapted because of uncertainty of the introduced stress by tendons .

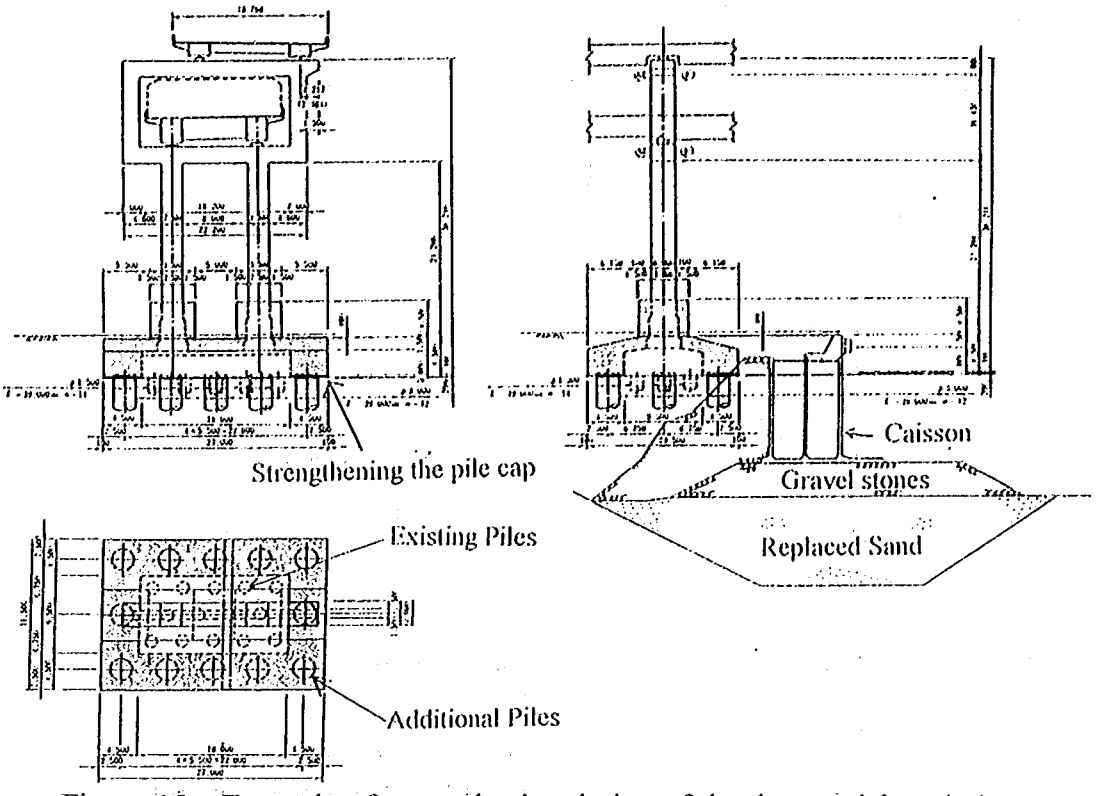


Figure 15 Example of strengthening design of the damaged foundation

The piles added to the existing foundation were 3000mm in diameter that was unusual size (Photo 6). An excavation by rotating casing tube was applied as it has following advantages. The powerful rotational force enables crashing of cobbles in the way, they can be removed by hammer-grab. As casing rotates 360 degree, this method can maintain its verticality, and have better ability of reducing the friction than conventional type.

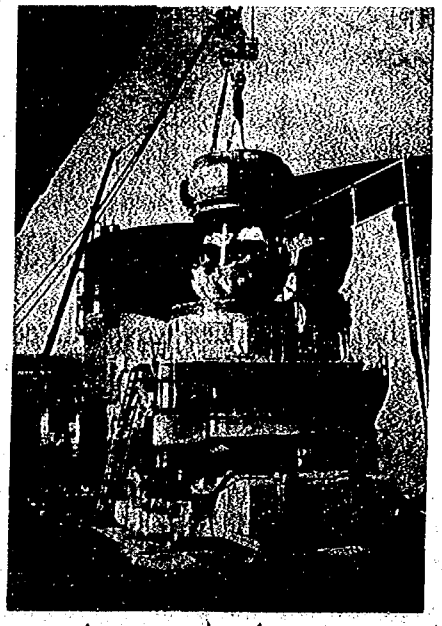


Photo 6 Strengthening work: a cast-in-place concrete pile with 3-2.5m ϕ

Repair Work on Cracked Piles

The foundation with **b** and **c** ranked damage have most of the cracks on pile top. Reinforcing bars inside likely suffer corrosion problems, especially in the Wangan route

that runs along the sea side. In order to prevent water penetration and retain durability, grouting work is made to the piles. Core drilling in the center of a pile is executed as deep as to the location of cracks. A packer unit is then down to the crack location together with a pressuring unit to inject grouting material to the cracks. As grouting material, either cement grouting material or epoxy resign were employed in consideration of hardening time and crack width. Figure 16 shows the configuration of grouting work.

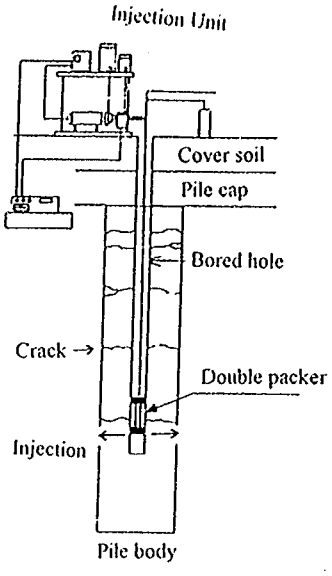


Figure 16 Configuration of grouting work to cracked piles

Concluding Remarks

Inspection work, inspection result of both the Kobe route and the Wangan route, and restoration works are introduced. The damage to foundation due to great earthquake was the first experience so that every works were performed under try and error situation. Many discussion and research were carried out at the same time of the restoration work, resulting in the next coming up code considering lateral ground flow induced by liquefaction.

The authors would like to express sincere appreciation to the Technical committee of Restoration of Hanshin Expressway Damaged by the Great Hanshin Earthquake (Task committee on Foundation chaired by Prof. Matsui) for great comments and efforts.

References

1)Japan Road Association, "The specifications for restoration of the highway bridges damaged by the Great Hanshin Earthquake", Feb. 1995 (In Japanese)

2)Nanjo and Adachi, "Inspection of damage to foundation", *Bridge and foundation* , Aug. 1996 (In Japanese)

3)Seki, Nanjo, and Adachi, "Method of inspection: Foundation", *Proc. of the International seminar on bridge engineering and management*, Jakarta, Sep. 1996

4)Ishizaki, and Egawa, "Restoration of bridge foundation of Hanshin Expressway", *Foundation engineering*, Sep. 1996 (In Japanese)

SEISMIC DESIGN OF PILE FOUNDATIONS

by
Masanori Nakano and Yoshitomi Kimura
Foundation Engineering Division,
Structure and Bridge Department, PWRI, MOC.

ABSTRACT

The check of ductility and dynamic strength for pile foundations has been proposed based on the results of research into the behavior of pile foundations during severe deformation. For this pile foundation analysis method, a rigid frame pile model was made accounting for the non-linear properties of the vertical resistance of piles, horizontal ground resistance, and the bending stiffness of the pile body. Horizontal loading tests of pile foundation model were performed to clarify the foundation ductility factor - degree of pile body damage relationship. These tests confirmed that at less than 4 times the yield displacement, the pile bodies are spared serious damage.

1. INTRODUCTION

The Hyogo-ken Nanbu Earthquake of January 17, 1995 caused severe damage to highway bridges, including collapsed bridge piers and bridge falls at many locations. Shortly after the earthquake, the state of this damage was surveyed by visually examining the bridge piers and other above ground structures and emergency restoration work was performed to prevent secondary damage. Because the foundations are underground, it was impossible to directly assess their damage immediately after the earthquake. Surveys of damage to the foundations conducted in conjunction with the restoration work confirmed that little damage was suffered by the foundations(1).

After the earthquake, the "Committee for Investigation on the Damage of Highway Bridges Caused by the Hyogo-ken Nanbu Earthquake" was formulated in the Ministry of Construction to survey the damage and clarify the factors which contributed to the damage. On February 27, 1995, the Committee approve the "Guide Specifications for Reconstruction and Repair of Highway Bridges Which Suffered Damage due to the Hyogo-ken Nanbu Earthquake(2)", and the Ministry of Construction noticed on the same day that the reconstruction and repair of the highway bridges which suffered damage by the Earthquake shall be made by the Guide Specifications. The design method that accounts for the non-linear behavior of pile foundations based

on the results of research at the Public Works Research Institute and elsewhere was included in the Guide Specifications.

This design method, one based on the fact that a pile foundation provides greater horizontal strength than a bridge pier body, is difficult to apply in a case where the ground around the foundation will liquefy or a case where the bridge pier body has ultimate horizontal strength sufficiently great to withstand the design horizontal seismic coefficient. Thus when the Specifications for Highway Bridges were revised, a model experiment concerning the strength and ductility of pile foundations was carried out to propose an seismic design method for pile foundations.

This paper describes experiments conducted by the Public Works Research Institute and introduces the seismic design method for pile foundations.

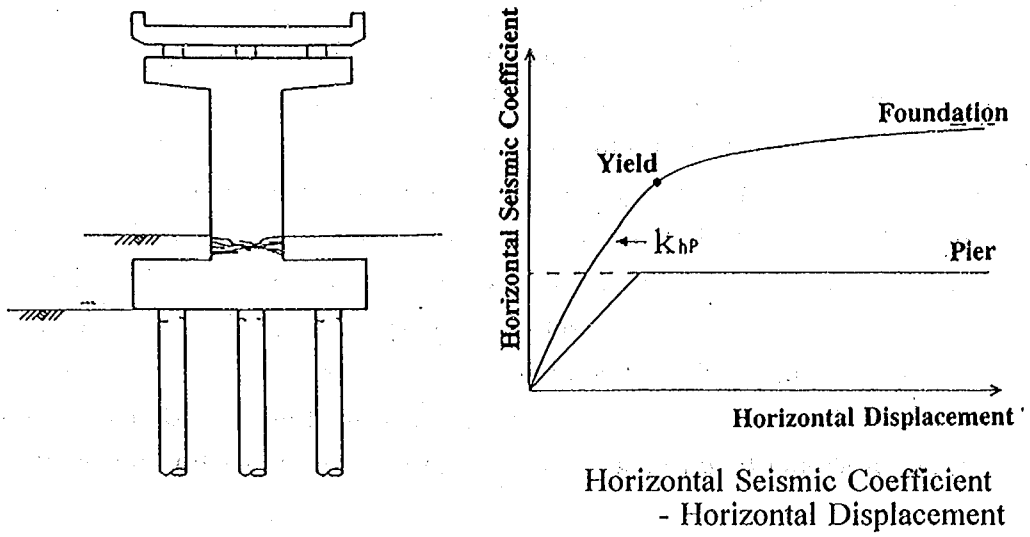
2. FUNDAMENTALS OF THE SEISMIC DESIGN OF FOUNDATIONS

Damage inflicted on foundations of highway bridges by the Hyogo-ken Nanbu Earthquake was relatively minor. In many cases, the damage was not severe because the horizontal strength of the foundation was greater than that of the bridge pier body or because the foundations provided sufficient ductility to withstand the decline in the horizontal strength of the foundation caused by liquefaction. So judging from the state of the damage, the seismic design method in the present Specifications is a satisfactory design method for foundations.

But during the Hyogo-ken Nanbu Earthquake, load greater than the conventional design seismic force acted on these structures, and the balance of the strengths of the various parts of the bridge and the strength of the foundations have come to differ as, for example, bridge pier bodies designed considering this provide greater strength than in the past. And because it is difficult both to survey the damage to underground foundations and to reinforce these foundations, it is necessary to design foundations so they will not suffer severe damage. So when performing the seismic design of foundations, it should be done in conformity with the following guidelines.

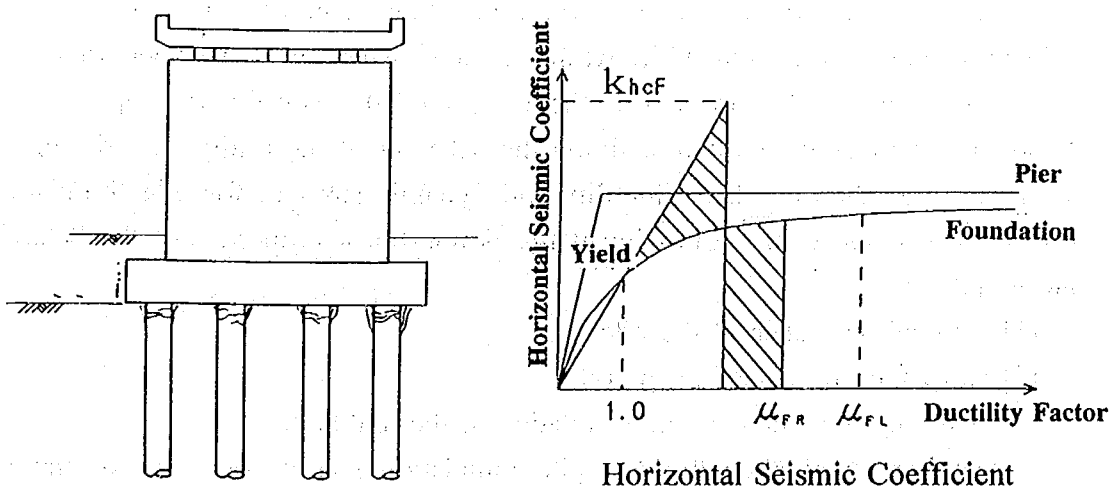
It should be based on the fact that the plastic deformation of the base of a bridge pier body, whose damage can be studied and which can be restored with relative ease, absorbs earthquake energy. For this reason, the horizontal strength of the foundation must be equal to or greater than that of the bridge pier body (See Figure 1 (a)).

In a case where a bridge pier body such as a wall-type bridge pier which has sufficiently great ultimate horizontal strength in the direction at right angles to the bridge axis against the design horizontal seismic coefficient for check of ductility and dynamic strength, it is not necessarily rational to design the horizontal strength of the foundation so that it is equal to or greater than the ultimate horizontal strength of the



Horizontal Seismic Coefficient
- Horizontal Displacement

(a) Case of a Principal Plastic Hinge Formed in the Bridge Pier Base



Horizontal Seismic Coefficient
- Ductility Factor

(b) Case of Principal Non-linear Properties in the Foundation - Ground System

Figure 1. Basic Guidelines for the Design of Foundations Using the Check of Ductility and Dynamic Strength

of the bridge pier. And when liquefaction occurs, the decline in the bearing capacity of the ground around the foundation causes a decline in the strength of the overall foundation, but even in this case, if the horizontal strength of the foundation is greater than the ultimate horizontal strength of the bridge pier body, the structural cross section is excessive, making this an irrational overall bridge design.

Consequently, when designing a foundation in such cases, it is more rational to allow for plasticization at and beyond yield within a range where excessive damage will not be inflicted on the foundation body even when the horizontal strength of the foundation is lower than the ultimate horizontal strength of the bridge pier body. In such cases, the response ductility factor (response horizontal displacement / yield horizontal displacement) of the foundation under the horizontal force corresponding to the design horizontal seismic coefficient for check of ductility and dynamic strength is calculated, and it should be checked to make sure it is below the limiting value (Figure 1(b)).

3. ANALYTICAL MODEL OF A PILE FOUNDATIONS

In order to check of dynamic strength and ductility for pile foundations, it is necessary to calculate the horizontal strength of pile foundations and its behavior during severe deformation. The displacement method stipulated in the present Specifications handles the behavior of the foundation as linear behavior by restricting the displacement of the foundation within a range where it is assumed to be elastic behavior. It is impossible to ignore the effects of the non-linear properties of the behavior of the foundation when studying the behavior of the bridge pier during severe deformation. So when check of ductility and dynamic strength for pile foundations, it is necessary to consider the following items as non-linear properties of the behavior of a pile foundation.

[1] Vertical resistance of the piles

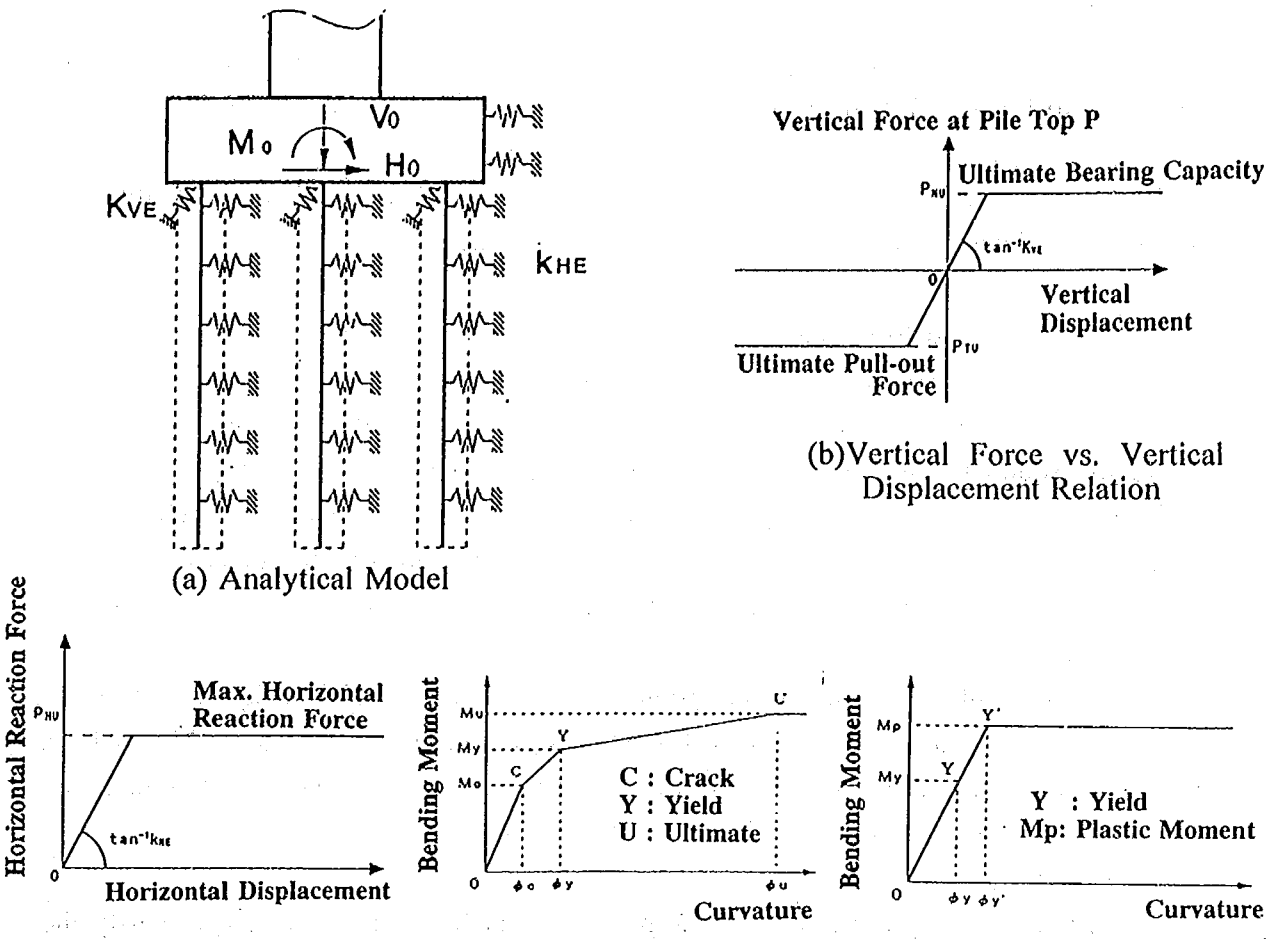
[2] Horizontal resistance of the piles

[3] Bending moment - curvature relation of the pile bodies

The horizontal strength of a pile foundation and its behavior during severe deformation can, as shown in Figure 2, be analyzed by replacing the pile foundation with a rigid frame structure supported by a ground spring and considering this to be non-linear.

(1) Vertical Resistance of the Piles

The vertical force at pile top - vertical displacement relationship for a pile generally reveals non-linear behavior. The following method is considered as a method for modelling this kind of non-linear behavior for design purposes.



(a) Analytical Model

(b)Vertical Force vs. Vertical Displacement Relation

(c) Horizontal Force vs. Horizontal Displacement Relation

(d) Moment vs. Curvature Relation of Reinforced Concrete Piles

(e) Moment vs. Curvature Relation of Steel Pipe Piles

Figure 2. Analytical Models of Pile Foundations

[1] Approximating the vertical force - vertical displacement curve at the top of the piles with a function (Weibull function curve formula for example).

[2] Modelling the pile tip resistance and the pile surface resistance respectively as elasto-plastic forms.

[3] Modelling the vertical force - vertical displacement curve at the top of the piles with a elasto-plastic form.

At the Public Works Research Institute, the results of vertical loading tests of many piles were organized to propose modelling based on the above methods(3). Considering convenience in actual design work and the precision of the design constant estimation, the following model was used for the design calculations.

The resistance properties in the vertical direction of the pile were considered to be elasto-plastic form, with the pile axial direction spring constant K_{VE} considered to be the initial gradient, and the ultimate bearing capacity P_{NU} and the ultimate pull-out bearing capacity P_{TU} treated as the upper limit values.

In this case, the pile's axial direction spring constant K_{VE} was assumed to be

the pile axial direction spring constant K_V calculated as stipulated in the Specifications.

The ultimate bearing capacity P_{NU} and the ultimate pull-out force P_{TU} were considered to be the ultimate bearing capacity of the pile R_U calculated as stipulated in the Specifications and (ultimate pull-out force of the pile P_U) + (effective weight of the pile W). These values did not exceed the ultimate bearing capacity and ultimate pull-out force determined from the stress of the pile body.

(2) Horizontal Ground Resistance

1) Non-linear Properties of the Ground Resistance

The ground reaction force properties should be faithfully modelled so that the horizontal ground reaction force p - horizontal displacement y relationships at varying depths in the ground is the p - y curve used for DNV etc.(4). But when the ground survey precision and the convenience of the calculation in the design task are considered, it is not necessarily appropriate to apply this method to the design of bridge foundations.

Consequently, the horizontal ground resistance was estimated by modelling as a bilinear model of the kind shown in Figure 2 (c). The effectiveness of this analysis method was confirmed and confirming the effectiveness of this analysis method based on an analysis of the results of horizontal loading tests(5).

2) Effects of the Pile Group

Experiments concerning the effects of the pile group have been performed to clarify the horizontal resistance of the pile under various relationships. At the Public Works Research Institute, steel pipe piles with a diameter of 102 mm were arranged as single piles, in straight lines, side by side, and as vertical and batter pile groups in test ground prepared inside a soil tank, then horizontal loading testing was performed on these piles(6). When proposing a design method, the results of horizontal loading tests of pile groups of these kinds are analyzed, and the coefficients η_k of the coefficient of horizontal ground reaction and η_p of maximum value of horizontal ground reaction are introduced.

3) Calculation Method

Based on 1) and 2), the horizontal ground resistance is found as follows.

The horizontal ground resistance properties is considered to be elasto-plastic in form with the coefficient of horizontal ground reaction K_{HE} as the initial gradient, and the maximum value of the horizontal ground reaction force P_{HU} to be the upper limit value (same figure (c)). K_{HE} and P_{HU} can be found from the following formulae.

$$k_{HE} = \eta_k \alpha_k k_H \quad (1)$$

$$p_{HU} = \eta_p \alpha_p p_U \quad (2)$$

Where:

k_{HE} : Coefficient of horizontal ground reaction used for the check of ductility and dynamic strength (kgf/cm ^{3})

p_{HU} : Maximum value of the horizontal ground reaction force (kgf/cm ^{2})

k_H : Coefficient of horizontal ground reaction (kgf/cm ^{2}), found as stipulated in the Specifications.

p_U : Passive earth pressure during an earthquake (kgf/cm ^{2}), found as stipulated in the Specifications. It can account for the weight of the soil up to the ground surface which is stable over a long period around a foundation as the overburden load.

α_k : Coefficient for the coefficient of horizontal ground reaction of a single pile.

α_p : Coefficient for the maximum value of the horizontal ground reaction force for a single pile.

η_k : Coefficient for the coefficient of horizontal ground reaction accounting for the pile group effects.

η_p : Coefficient for the maximum value of the horizontal ground reaction force accounting for the pile group effects.

Table 1 presents the values of the coefficient α_k of the coefficient of horizontal ground reaction and the coefficient α_p of the maximum value of the horizontal ground reaction force of a single pile. This was obtained based on an analysis of the results of the horizontal loading test of a single pile shown in 1).

Table 1 Coefficient

Type of Ground	α_k	α_p
Sandy Ground	1.5	3.0
Cohesive Ground	1.5	1.5

Note: In cohesive ground where N $\leqq$ 2, α_p is assumed to equal 1.0.

The coefficient η_k for the coefficient of horizontal ground reaction accounting for the pile group effects is the following value.

$$\eta_k = 2/3 \tag{3}$$

The coefficient η_p for the maximum value of the horizontal ground reaction force accounting for the pile group effects is the following value.

Cohesive ground: $\eta_p = 1.0$ (4)

Sandy ground : $\eta_p \cdot \alpha_p$ = Interval between the centers of the piles in the direction at right angles to the loading direction / pile diameter ($\leqq \alpha_p$) (5)

In the case of piles other than those in the front pile in sandy ground, the value

is 1/2 of that indicated in (5).

The values of η k, η p are found from the results of the analysis of the loading tests of group piles in 2).

(3) The Bending Moment - Curvature Relationship of a Pile Body

When using the displacement method, a pile body is treated as an elastic body in order to keep the stress of the reinforcing bars etc. of the pile body from exceeding the allowed stress. When calculating the horizontal strength of a pile foundation, it is important to evaluate the behavior of the pile body after yield and the ultimate strength. It is necessary to appropriately model the bending moment - curvature relationship in the pile body.

The points of inflection in the bending moment - curvature relationship when bending moment acts on a concrete pile are usually treated as the cracking time (C), the time when the reinforcing bars begin to yield (Y), and the ultimate time of the section (U). The analytical model was a trilinear model linking these points found for a circular steel reinforced concrete cross section with the axial direction N and subjected to the bending moment M (Figure 2(d)).

Because points of this sort are not clearly revealed on a steel pipe pile, it is modelled as a bilinear model with the point at which the stress of the outermost edge of the steel pipe pile reaches the yield point considered to be the initial gradient, and the plastic moment treated as the maximum value (same figure (e)).

4. LOADING TESTS OF THE LIMITING VALUE OF THE DUCTILITY FACTOR OF A PILE FOUNDATIONS

4.1 Test Objectives

In the case of a wall type bridge pier at right angles to the bridge axis or a case where liquefaction will occur, it is rational to design the bridge so that the energy is absorbed by the foundation. Even in these cases, it is necessary to design the bridge so that the response ductility factor of the foundation is within a certain value in order to prevent excessive damage to the foundation body.

As a limiting value for this ductility factor, the safety coefficient for the ultimate was used to determine the allowed ductility factor for a reinforced concrete bridge pier. Even when a member which is part of the pile body of a pile foundation reaches the ultimate state, this does not result in an immediate conspicuous horizontal strength decline in the overall foundation system. It is difficult to define the ultimate for an entire pile foundation system. For this reason, loading tests of a model pile foundation is done to clarify the ductility factor of the foundation and the state of damage to the pile body. This information is used as reference data when determining

the limiting value of the ductility factor.

Loading tests were performed using PHC, cast-in-place piles, and steel pipe piles which are used for pile foundations of highway bridges. The following section refers to the tests of cast-in-place and PHC piles.

4.2 Test Method

Figure 3 shows an overview of the loading method. This testing, which is done to clarify the state of damage to a pile body when horizontal force acts upon pile groups, requires that moment and horizontal force act on the model simultaneously. The loading was performed by simultaneously controlling three jacks to hold the vertical load at a constant level and performing alternating positive and negative loading of a horizontal force with the horizontal force H/moment M ratio constant at M/H = 2.5 m.

The pile foundation models used were six reinforced concrete piles with a diameter of 30 cm and a length of 180 cm; three set in the loading direction and two at right angles to the loading direction. The interval between their centers was 75 cm, which was 2.5 times their diameters.

The displacement of the horizontal loading position at the level where the axial direction reinforcing bars at the outer edge of the pile bodies of all piles yielded in the previous analysis was set at 1 δ_y, and positive - negative alternating loading was performed while increasing the displacement in increments of 1 δ_y. Three cycles of loading were done for each δ_y. The vertical load was 84 tf.

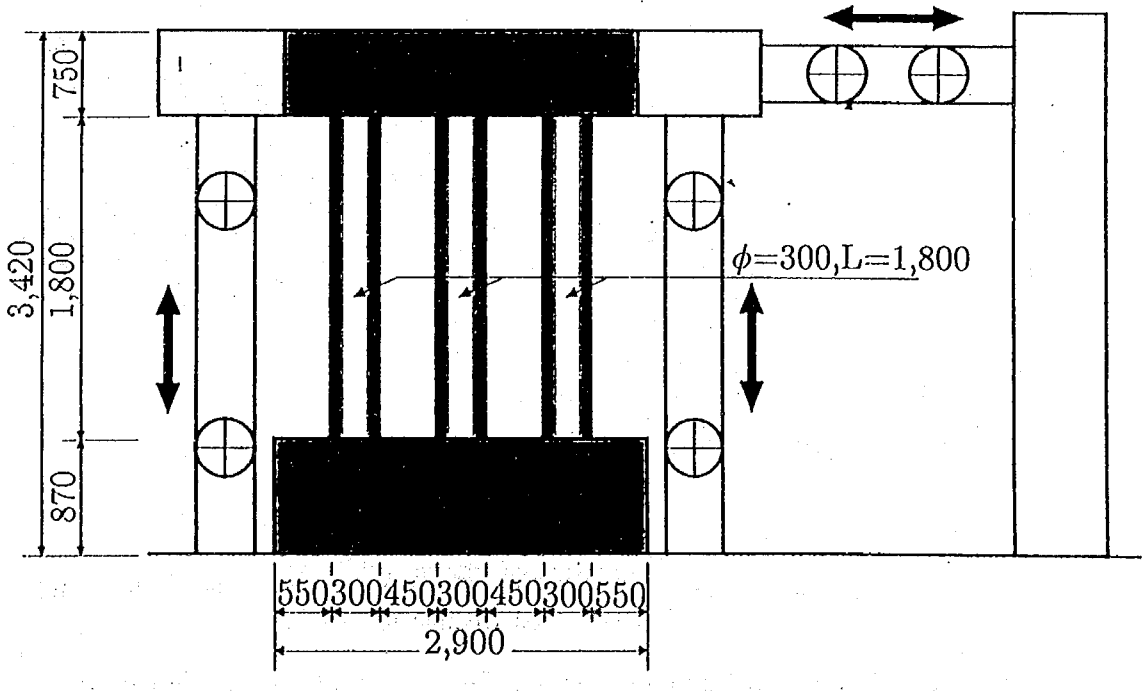


Figure 3. Loading Test

4.3 Test Results

(1) Cast-in-place Piles

The models of cast-in-place piles were made using 16 reinforcing bars of type SD295A, D10 as the axial direction reinforcement. The hoop ties were made of SD295A, D4 installed at 4 cm intervals. The distance from the outer surfaces of the piles to the centers of their axial direction reinforcement was 5 cm. The results of material testing show that the compressive strength of the concrete was 323 kgf/cm ^{2} while the yield point of the steel reinforcing bars was 3,757 kgf/cm ^{2}.

Figure 4 shows the hysteresis curve of the horizontal force and the horizontal displacement of the cast-in-place piles. A description of the state of damage to the piles follows.

At 2 δ_y, signs that the covering concrete would soon collapse appeared at the top and bottom bases of the piles at the ends and in the bottom of the piles in the middle, and maximum load was reached at 3 δ_y. At that time, some of the covering concrete at the bottom of pile 1 separated. At 4 δ_y, covering concrete at the top of pile 1, the top and bottom of pile 3, and the bottom of pile 2 separated, but this did not expose any of the reinforcing steel rods (Photograph 1). At 6 δ_y, steel reinforcing rods were exposed and buckled at the bottom of pile 1 and at the top and bottom of pile 3, and at 7 δ_y, steel reinforcing rods were exposed and buckled even at the top of pile 1. As the cyclic loading continued, the hoop ties and axial direction reinforcement failed reducing the horizontal strength.

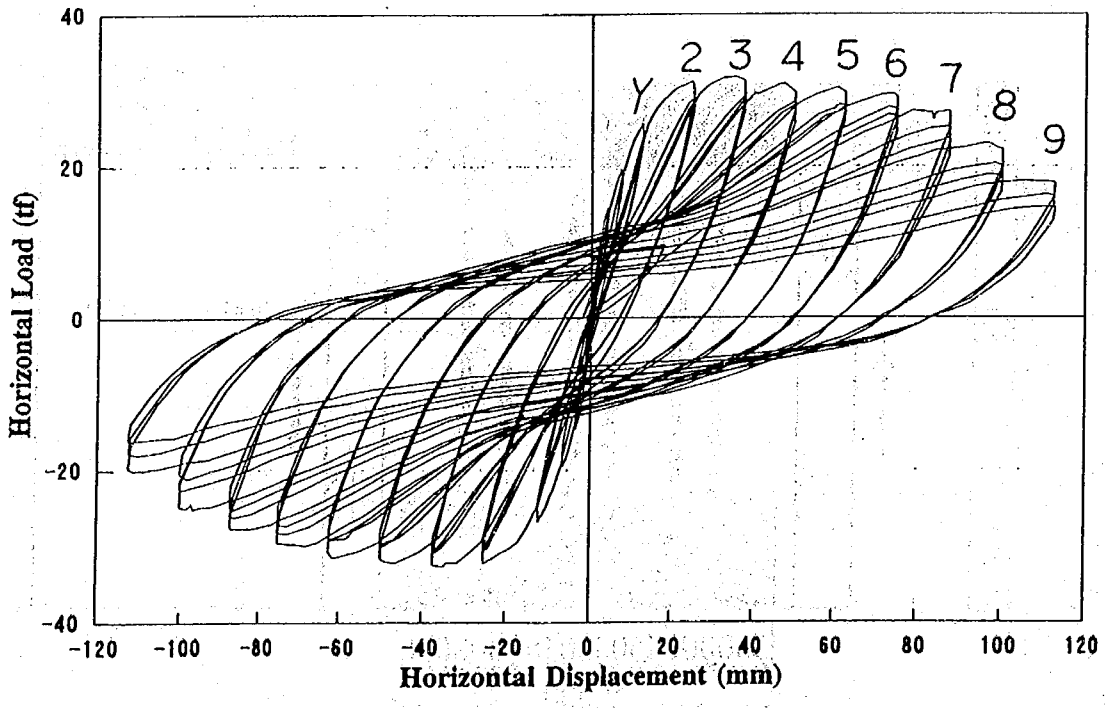
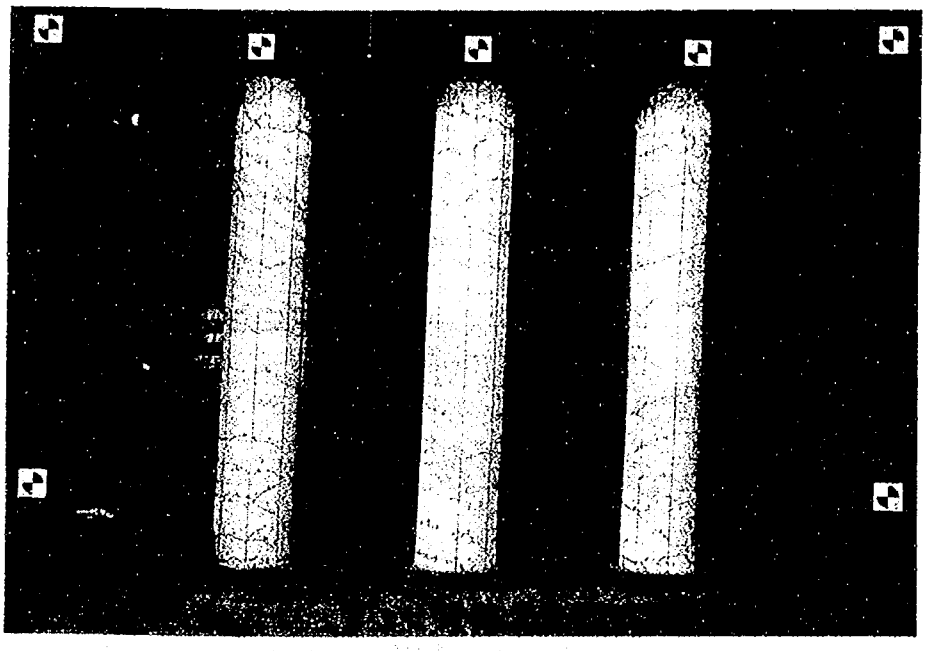


Figure 4. horizontal Load - horizontal Displacement Hysteresis Curve (Cast- in-Place Piles)



Photograph 1. State of Damage to Pile Bodies
(Cast-in-place Piles, + 4 δ_y)

(2) PHC Piles

The PHC piles were type B with a plate thickness of 6 cm. Twelve PC reinforcements with a diameter of 7 mm were installed in the axial direction, while spiral reinforcement material SD295, D6 was installed at intervals of 50 mm. The inside of the pile bodies were plugged with 75 cm layers of concrete at each end. This required an increase in the quantity of spiral reinforcing material in order to raise the shear bearing strength and deformation performance of the piles to conform with long-established JIS standards. Results of material testing indicate that the compressive strength of the concrete in the pile body was 818 kgf/cm ^{2} and the yield point of the PC reinforcing material was 13,140 kgf/cm ^{2}.

Figure 5 shows the hysteresis curve of the horizontal force and horizontal displacement of the PHC piles. Photograph 2 shows the state of the specimens after loading to 4 δ_y. The state of the pile body damage is largely similar to that observed on the cast-in-place piles, confirming that the PHC piles can be counted on for satisfactory deformation performance thanks to the installation of sufficient amounts of spiral steel reinforcing rods and the addition of the plugging concrete. A comparison of the results with those from the cast-in-place pile testing shows that there were fewer cracks in the pile body and the width of cracks formed after overloading were narrower than in the cast-in-place piles.

The area enclosed by the horizontal load - horizontal displacement hysteresis

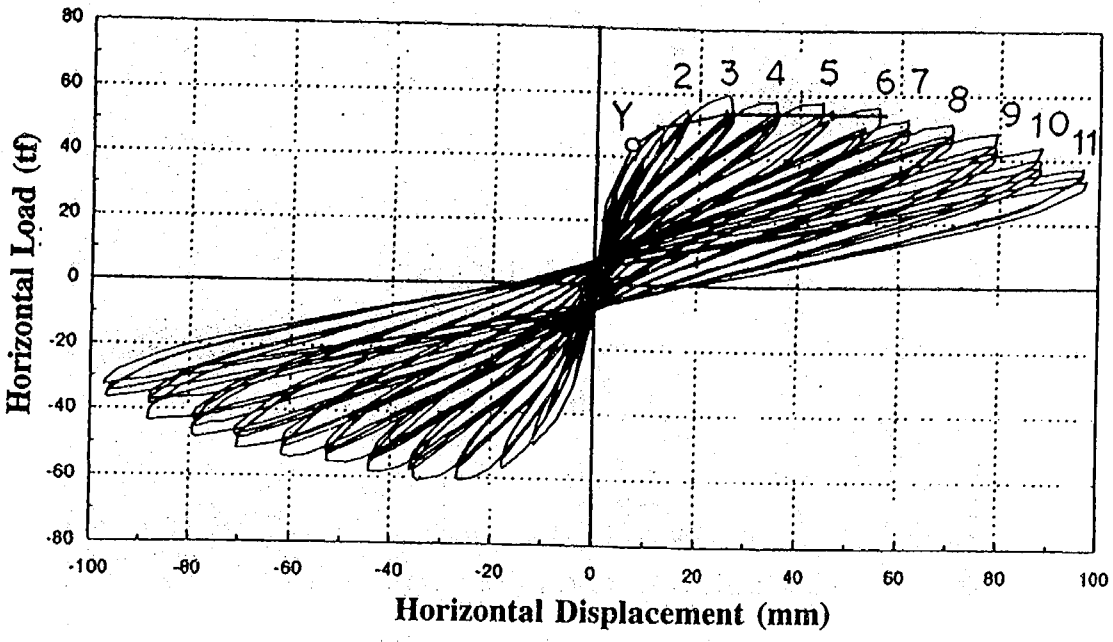
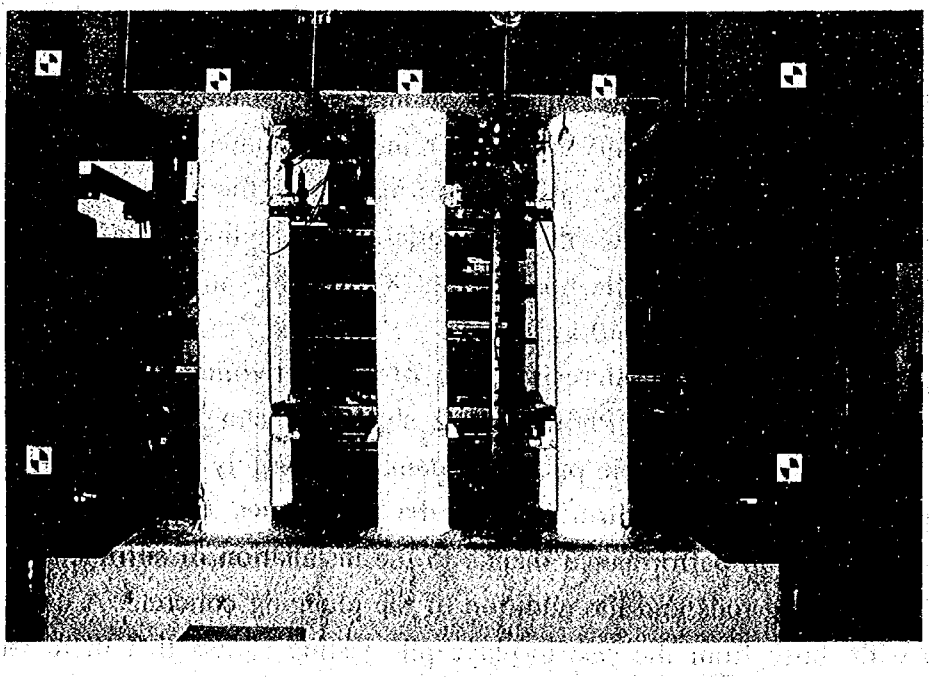


Figure 5 horizontal Load - horizontal Displacement Hysteresis Curve
(PHC Piles)



Photograph 2 State of Damage to Pile Bodies
(PHC Piles, +/- 4 δ_y)

curve was smaller than it was in the results of the test of the cast-in- place piles; a characteristic of prestressed members.

While not described in this report, similar loading testing was performed using a vertical and batter pile group made up of steel pipe piles. Based on the results of this test and calculation results, the limit value for the ductility factor of a pile foundation has been set at 4.

5. CONCLUSION

The check of dynamic strength and ductility for pile foundations has been proposed based on the results of research into the behavior of pile foundations during severe deformation. For this pile foundation analysis method, a rigid frame pile model was made accounting for the non-linear properties of the vertical resistance of piles, horizontal ground resistance, and the bending stiffness of the pile body. Horizontal loading testing of models of pile foundations was performed to clarify the foundation ductility factor - degree of pile body damage relationship. This test confirmed that at less than 4 times the yield displacement, the pile bodies are spared serious damage.

REFERENCES

1) Ministry of Construction : Report on the Damage of Highway Bridges by the Hyogo-ken Nanbu Earthquake, Committee for Investigation on the Damage of Highway Bridges caused by the Hyogo-ken Nanbu Earthquake, 1995.
2) Ministry of Construction : Guide Specifications for Reconsturuction and Repair of Highway Bridges Which Suffered Damage due to the Hyogo-ken Nanbu Earthquake, 1995.
3) Okahara et. al.: Research on the Bearing Capacity of Single Piles and Design Methods for Column-shaped Foundations, Technical Memorandum of Public Works Research Institute No. 2919, 1991.
4) Det Norske Veritas: Rule for Design, Construction, and Inspection of Offshore Structure, 1977.
5) Kimura, Tatsuta, Kasuga: Evaluation of the Non-linear Properties of horizontal Resistance of Piles During Severe Deformation, Papers Presented at the Symposium on Limit State Design Methods for Foundation Structures, 1995.
6) Fujiwara, Okahara, Nakatani, Kimura and TAKAGI: Horizontal Bearing Capacity of Pile Foundations Based on Horizontal Loading Tests, 24th UJNR Joint Panel Meeting,1992.

Site Remediation and Seismic Response Mechanisms

Korhan Adalier
Rensselaer Polytechnic Institute, Dept. of Civil Engineering, Troy, NY 12180 USA

and

Ahmed-W. Elgamal
Columbia University, Dept. of Civil Engr and Engr Mechanics, New York, NY 10027 USA

ABSTRACT

A number of ground improvement techniques are presented within a seismic soil behavior framework. Under earthquake loading conditions, the associated response mechanisms are discussed. These response mechanisms must sustain the soil bearing capacity, and limit ground deformations to low acceptable levels. In view of these demands, the performance of a number of commonly employed seismic site remediation techniques is analyzed. For that purpose, results of a recent centrifuge testing program are employed to illustrate advantages and limitations.

INTRODUCTION

Numerous techniques have been developed to increase ground stiffness and strength (Hausmann 1990). A few of these techniques have been employed to increase dynamic ground bearing capacity (Yoshimi 1990, Mitchell and Wentz 1991, Jakura and Abghari 1994). Within a simplified framework, the underlying response mechanisms associated with these techniques will be presented. Attention will be primarily dedicated to site liquefaction (Fig. 1) countermeasures.

A brief summary of liquefaction countermeasures and associated response mechanisms will be presented below. In addition, the results of a recent centrifuge testing study (Adalier 1996) will be discussed. This centrifuge study compared four different techniques for remediation of a liquefiable foundation layer underlying an earth embankement.

LIQUEFACTION COUNTERMEASURES

The soil improvement techniques presented below will be divided into four main categories: 1) densification, 2) drainage, 3) solidification, and 4) inclusions (Adalier 1996). A brief description of each with a number of relevant references follows.

Densification Methods

Densification (see mechanisms in Fig. 2) increases liquefaction resistance due to the associated decrease in void ratio or increase in relative density, and mean effective stress (increase in lateral stresses). Densification can be achieved using several methods such as vibro-compaction, vibro-replacement, deep dynamic compaction, deep blasting, compaction grouting, and displacement piles. A comprehensive description of these methods can be found in (ASCE 1977), in a state-of-the-art paper by Mitchell (1981), and in Broms (1991). Densification of loose soils has been the most popular method of reducing earthquake related liquefaction potential. However, most densification techniques (e.g., vibro-densification) have limited application to existing structures because of settlement and damage concerns.

Vibro-techniques: These methods involve driving a vibratory probe into the soil, and densifying the soil surrounding the probe during driving and withdrawal (Fig. 3). Gravel or crushed stones maybe introduced into the hole created by a vibro-probe, and compacted (stone column technique or vibro-replacement). Mitchell (1970, 1981), Welsh (1987), Moseley (1993), Xanthakos et al. (1994), and Adalier (1996) provide good summaries of vibro densification techniques.

Deep Dynamic Compaction: This technique involves repeated dropping of heavy weights from heights of up to 40 m onto the ground surface. Shock waves created by the impact densify the soil. Deep dynamic compaction can improve all soils except for cohesive soils below the groundwater table. The main limitation of this method is its potential to damage surrounding structures due to large vibrations, noise, and flying debris. Leonards et al. (1980), Lukas (1986), and Slocombe (1993) give very comprehensive discussions about the general uses of this method. Important theoretical aspects are given by Menard and Broise (1975), Scott and Pierce (1975), and Hansbo (1978).

Deep Blasting: This method involves detonation of charges at some specified depth. The shock waves created by blasting densify the saturated soil layer. Blasting is effective only in saturated soils, and is especially effective in saturated cohesionless soils with low fines content (less than around 20%). It is the least expensive and quickest among all densification methods. However due to environmental dangers, it is mostly used at isolated sites. A comprehensive discussion about this method is also given by Prugh (1963), Mitchell (1970), Ivanov (1980), and Jeffries (1991).

Compaction Grouting: This procedure involves pumping a low slump thick grout (Fig. 4) under high pressures (usually ranging between 100 to 400 psi) to displace and compact the surrounding soil (producing an increased confinement effect such as that shown in Fig. 5). This technique can be applied in granular soils with high fines content, giving it an advantage over other densification methods. The major advantage of grouting is that it can be used in small, difficult-to-access areas and as a remedial measure beneath or adjacent to an existing structure. Warner (1982) reports an overall history of this technique. Graf (1992) gives an overview on current practice, and Rubright and Welsh (1993) describe the method comprehensively.

Displacement Piles: Piles of timber, steel or prestressed concrete are driven compacting the surrounding soil by displacement as well as by vibration. Detailed information about this method is given by Iyengar (1981), and Solymar and Reed (1986).

Drainage Techniques

Use of relief wells (Fig. 5) such as gravel drains (stone columns) or prefabricated drains are typical examples for increasing drainage in the soil system (Fig. 6). It is believed that the proper installation of stone columns (gravel drains) by vibro-replacement mitigates the potential for liquefaction by increasing the density of surrounding soil, providing drainage for the control of pore pressures, and introducing a stiff element (stone columns) which can potentially carry higher stress levels and restrict deformations (Priebe 1991; Baez and Martin 1993, Adalier 1996). Among the comprehensive studies on drainage are Seed and Booker (1977), Tokimatsu and Yoshimi (1980), Iai (1988), and Onoue et al. (1991).

Solidification Methods

These methods (see mechanism in Fig. 7) involve introducing stabilizing chemicals (e.g., cement, bentonite, and sodium silicates) by either injection (e.g., injection grouting) or physically mixing (e.g., jet grouting and deep-soil-mixing). These methods are relatively expensive, and are generally only considered for limited areas for construction of stabilized zones or cells within a larger soil mass (improved grid shape); or for situations where other soil improvement techniques cannot be used (e.g., small, difficult-to-access areas, or under existing structures). Comprehensive information regarding different solidification methods is reported in Mitchell (1981), and Winterkorn and Pamukcu (1991), and Adalier (1996).

In general, injection grouting can be effective in sands with less than 20% fine material (silt and clay). On the other hand, jet grouting which involves mixing with grout by cutting and fracturing the soil with high pressure water or air jets can be effective in any type of inorganic soil. More detailed information about grouting techniques is given by Mitchell (1981), Welsh (1987), Moseley (1993), Xanthakos et al. (1994), and Adalier (1996).

The deep-soil-mixing technique whereby soil is physically mixed with cementing material via mixing augers, can be used for any type of soil. Taki and Yang (1991) and Jasperse and Ryan (1992) give an overview of the deep-soil-mixing technique. A complete discussion about the deep-soil-mixing technique is given by Toth (1993).

Inclusions

This method involves forming of inclusions in the soil such as concrete, timber, or steel piles, and sheet piles. Inclusion techniques usually rely on the ability of inclusions to reduce shear stress and restrict shear straining in the soil. Also, depending on the installation method (i.e., driving or placing technique), it can densify the surrounding soil and enhance liquefaction resistance. In general, these techniques have enjoyed little popularity as liquefaction countermeasure methods. More thorough information about these methods may be found in Kramer and Holtz (1991), and Adalier (1996).

CENTRIFUGE STUDY

A series of model tests (Adalier 1996) were conducted at the Rensselaer Polytechnic Institute (RPI) Centrifuge Research Center. The RPI centrifuge is an Acutronic 100g-ton machine. On the centrifuge, uniaxial base shaking may be imparted by available servo-hydraulic centrifuge shake tables. In addition to the 1 ton actuator shake table used in this study, a new large shaker 1m in length with a 14 ton double actuator system is now available (Van Laak 1996). Dynamic testing was conducted at a centrifugal acceleration of 75g.

The seismic response of a cohesive highway embankement overlying a layer of loose saturated clean sand was studied (Adalier 1996), with and without liquefaction countermeasures (Fig. 8). In this series of tests, the models were heavily instrumented with accelerometers, pore-pressure transducers, and LVDTs. Each model was subjected to three consecutive shaking events. Sufficient time was allowed between shaking events to allow for full excess pore pressure dissipation. In each event, shaking was about 6 seconds in duration. Input motion consisted of a 1.6 Hz sinusoidal signal with a peak amplitude of about 0.1g (first shaking event), 0.2g (second shaking event), and 0.3g (third shaking event).

After dynamic excitation, large deformations and cracks were observed in the benchmark model with no liquefaction countermeasures (Model 1 of Fig. 8). Along the embankement crest, a settlement of 0.75m was measured. In Model 2 with the densified soil columns, settlement was reduced by about 50%. Nevertheless, the level of deformations was still excessive. In model 3, an unexpected outward movement of the remediated cement walls was observed. This movement led to settlements of the embankement and unsatisfactory overall response. The berm (surcharge effect, see mechanism of Fig. 7) of Model 4 was found quite effective, particularly in preserving the embankement integrity. Finally, in Model 5, the liquefied foundation soils were contained below the embankment with no lateral deformations. Additionally, the embankement further preserved its integrity, ironically due to liquefaction of its underlying foundation, which produced an effective base isolation mechanism.

SUMMARY AND CONCLUSIONS

The response mechanisms associated with site remediation were briefly presented within a simplified comparative framework. Attention was focused on liquefaction countermeasure techniques. The performance of four such techniques was reviewed based on results of a recent centrifuge testing program. In this program, the underlying remediation mechanisms included stiffening, increased confinement, and containment of a loose liquefiable stratum, underlying a cohesive earth embankement. All remediation techniques resulted in improved overall dynamic response. Containment and increased confinement were found to be especially effective in preserving the embankement integrity.

ACKNOWLEDGEMENTS

This research was supported by the National Center for Earthquake Engineering Research, the National Science Foundation, and Hayward Baker Construction Company.

REFERENCES

Adalier, K. (1996). "Mitigation of Earthquake Induced Liquefaction Hazards." Ph.D. Thesis, Rensselaer Polytechnic Institute, Troy, NY.

ASCE (1977). Soil Improvement, History, Capabilities, and Outlook. ASCE Committee on Placement and Improvement of Soils, Geotechnical Engineering Division, New York.

Baez, J. I., and Martin, G. R. (1993). "Advances in the design of vibro systems for the improvement of liquefaction resistance." Symposium of Ground Improvement, Vancouver Geotechnical Society, Vancouver, B.C.

Broms, B. B. (1991). "Deep Compaction of granular soils." Foundation Engineering Handbook, 2nd Edition, Von Nostrand Reinhold, NY, NY, pp. 814-832.

Graf, E. D. (1992). "Compaction Grout; 1992." in Grouting, Soil Improvement, and Geosynthetics, Proc. of the Conference, New Orleans, R. H. Borden, R. D. Holtz and I. Juran (eds.), Geotechnical Special Publication No. 30, ASCE, Vol. 1, pp. 257-287.

Hansbo, S. (1978). "Dynamic consolidation of soil by falling weight." Ground Engineering, 11, 5, pp. 27-31.

Hausmann, M. R. (1990). Engineering Principles of Ground Modification, McGraw-Hill.

Iai, S. (1988). "Large scale model tests and analysis of gravel drains." Report of the Port and Harbor Research Institute, Vol. 27, No.3, Sept.

Ivanov, P. L. (1980). "Consolidation of saturated soils by explosions." Proc. Int. Conf. on Compaction, ENPC, Paris, 1, pp. 331-337.

Iyengar, M. (1981). "Improvement of characteristics of a liquefiable soil deposit by pile driving operations." Inter. Conf. on Recent Advances in Geotechnical Earthquake Eng. and Soil Dynamics, St. Louis, Mo.

Jakura, K., and Abghari, A. (1994). "Mitigation of liquefaction hazards at three California bridge sites." 5th US-Japan Workshop, Snowbird, Utah, October.

Jasperse, B. H., and Ryan, C. R. (1992). "Stabilization and fixation using soil mixing." Grouting, Soil Improvement and Geosynthetics, ASCE Geotech. Spec. Pub. No. 30, pp. 1273-1284.

Jeffries, M. G. (1991). "Explosive Compaction." Geotechnical News, pp. 29-31.

Kramer, S. L., and Holtz, R. D. (1991). Soil Improvement and Foundation Remediation with Emphasis on Seismic Hazards. A Report of a workshop sponsored by the National Science Foundation and held at the University of Washington, Dept. of Civil Eng., Seattle, Washington, Aug. 19-21.

Leonards, G. A., Cutter, W. A., and Holtz, R. D. (1980). "Dynamic compaction of granular soils." J. Geotech. Eng., ASCE, Vol. 106, GTI, pp. 35-44.

Lukas, R. G. (1986) "Dynamic compaction for highway construction." Vol. 1, Design and Construction Guidelines, Federal Highway Administration, Office of Research and Development, U.S. D.O.T., Washington, D.C., Report No. FHWA/RD-86/133, July.

Menard, L., and Broise, Y. (1975). "Theoretical and practical aspects of Dynamic Consolidation." Geotechnique, Vol. 15, No. 1, March, pp. 3-18.

Mitchell, J. K. (1970). "In place treatment of foundation soils." J. of Soil Mech. and Found. Div., ASCE, Vol. 96, No. SM1, pp. 73-110.

Mitchell, J. K. (1981). "Soil Improvement State-of the-Art Report." Session 12, Proc. of the 10th Int. Conf. on soil Mech. and Found. Eng., Stockholm, Vol. 4, pp. 506-565.

Mitchell, J. K., and Wentz, F. J. (1991). "Performance of improved ground during the Loma Prieta earthquake." UCB/EERC Report 91/12.

Moseley, M. P. (1993). Ground Improvement. Chapman & Hall, Pub. by CRC Press Inc., Florida, 218pp.

Onoué, A., Ting, N., Germaine, J. T., Whitman, R. V., and Mori N. (1991). "Smear zone around a drain pile and well resistance of drains." Geo-Coast' 91, 3-6 Sept., Yokohoma, Japan.

Priebe, H. J. (1991). "Vibro Replacement - design criteria and quality control." Deep Foundation Improvements: Design, Construction, and Testing, ASTM STP 1089, M. I. Esrig and R. C. Bachus (eds.), ATSM, Philadelphia, pp. 62-72.

Prugh, B. J. (1963) "Densification of soils by explosive vibrations." Proc. ASCE, J. of Construction Division, ASCE, Vol. 89, No. CO1, pp. 79-100.

Rubright, R., and Welsh, J. (1993). "Compaction Grouting." Ch. 6, In Ground Improvement, Moseley M. P. (ed.), Chapman & Hall (Pub.).

Scott, R. A., and Pierce R. W. (1975). "Soil compaction by impacts." Geotechnique, 25, 1, pp. 19-30.

Seed, H. B., and Booker, J. R. (1977). "Stabilization of potentially liquefiable sand deposits using gravel drains." J. of Geotechnical Eng. Div., ASCE, Vol. 103, No. GT7, July, pp. 757-768.

Slocombe, B. C. (1993). "Dynamic Compaction." Ch. 2, In Ground Improvement, Moseley M. P. (ed.), Chapman & Hall (Pub.).

Solymar, Z. V., and Reed, D. J. (1986). "A comparison of foundation compaction techniques." Canadian Geotechnical Journal, 23, No. 3, pp.271-280.

Taki, D, and Yang, D. S. (1991). "Soil-Cement mixed wall techniques." Geot. Eng. Congress 1991, Boulder, F. G. McLean, D. A. Campbell and D. W. Harris (eds.), Geot. Spec. Pub. No. 27, ASCE, Vol. 1, pp. 289-309.

Tokimatsu, K., and Yoshimi, Y. (1980). "Effects of vertical drains on the bearing capacity of saturated sand during earthquakes." Proc. of Int. Conf. on Eng. for Protection from Natural Disasters, Asian Institute of Technology, Jan., pp. 643-655.

Toth, P. S. (1993). "In Situ soil mixing." Chapter 9 in Ground Improvement, Moseley M. P. (ed.), Pub. by Chapman & Hall, London, 218 pages.

Van Laak, P. (1996). "Development of Dynamic Capability for Geotechnical Centrifuge Model Studies." Ph.D. Thesis, Rensselaer Polytechnic Institute, Dept. of Civil Engineering, Troy, NY.

Warner, J. (1982). "Compaction Grouting - the first thirty years." ASCE Specialty Conf. on Grouting in Geotechnical Engineering, New Orleans.

Welsh, J. P. (1986). "In situ testing for ground modification techniques." Use of In Situ Tests in Geotechnical Engineering, Proc. In Situ' 86, Blacksburg, VA, S. P. Clemence, ed., Geotechnical Special Publication No. 6, ASCE, pp. 322- 335.

Welsh, J. P. (ed.) (1987). Soil Improvement - A Ten Year Update. Geotechnical Special Publication No. 12, ASCE, NY, NY.

Winterkorn, H. F., and Pamukcu, S. (1991). Soil Stabilization and Grouting. Chapter 9 in Foundation Engineering Handbook, Hsai-Yang Fang (ed.), 2nd Ed., Pub. by Van Nostrand Reinhold, NY, NY.

Xanthakos, P. P., Abramson, L. W., and Bruce, D A. (1994). Ground Control and Improvement. A Wiley-Interscience Publication, John Wiley & Sons Inc., New York, NY, 910 pages.

Yoshimi, Y. (1990). "Soil improvement methods for liquefaction remediation with emphasis on Japanese experience." Symposium on Recent Developments in Ground Improvement Techniques, Bangkok, 29 Nov. - 3 Dec., Seismic Workshop, World Port, Los Angeles.

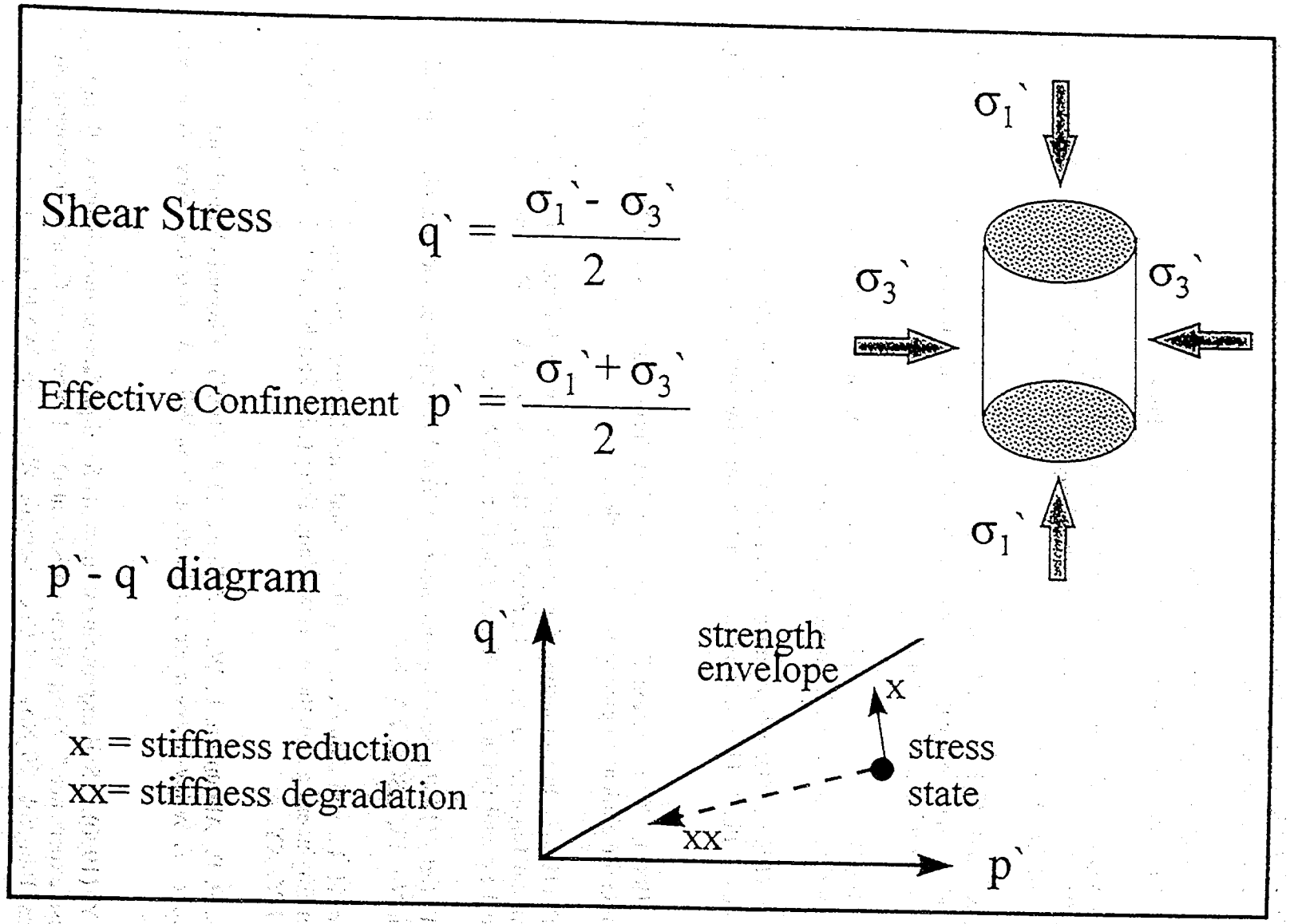


Figure 1: Schematic showing p-q diagram, typical soil stress-state, and liquefaction mechanism (xx).

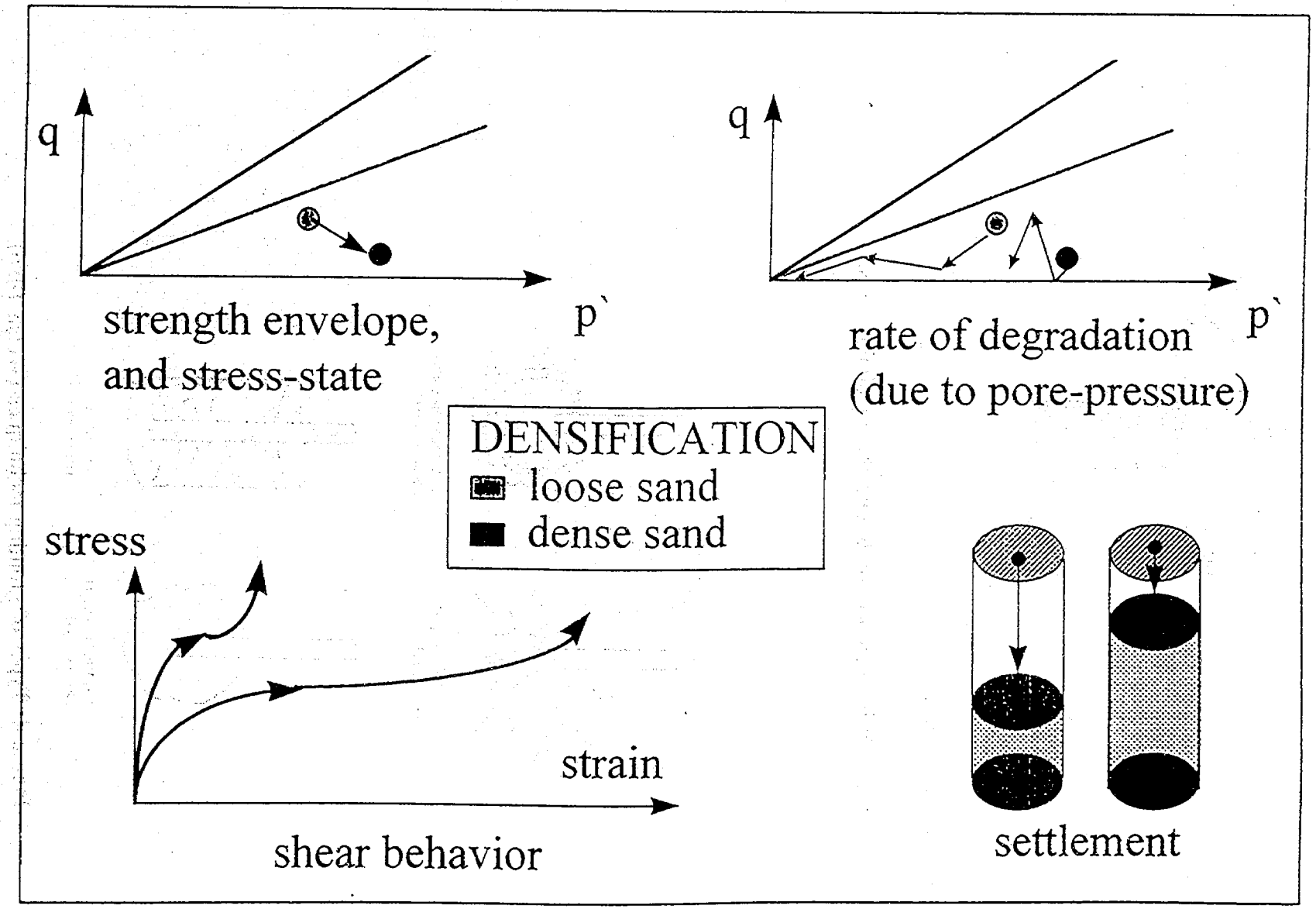


Figure 2: Schematic diagram showing mechanisms associated with increase in sand relative density.

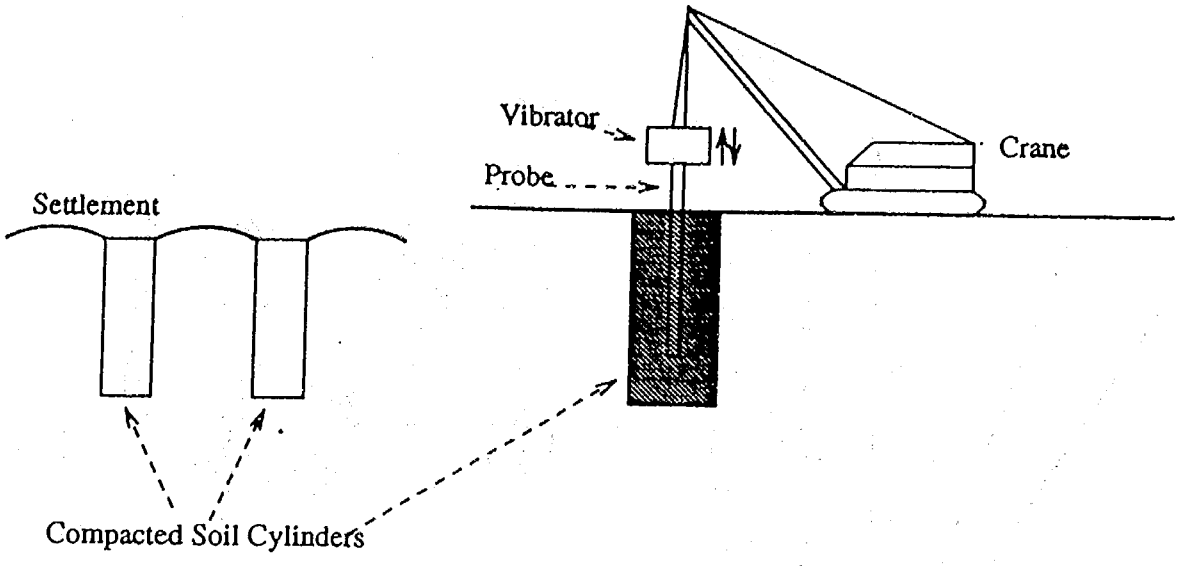


Figure 3: Vibro-compaction to densify liquefiable soils.

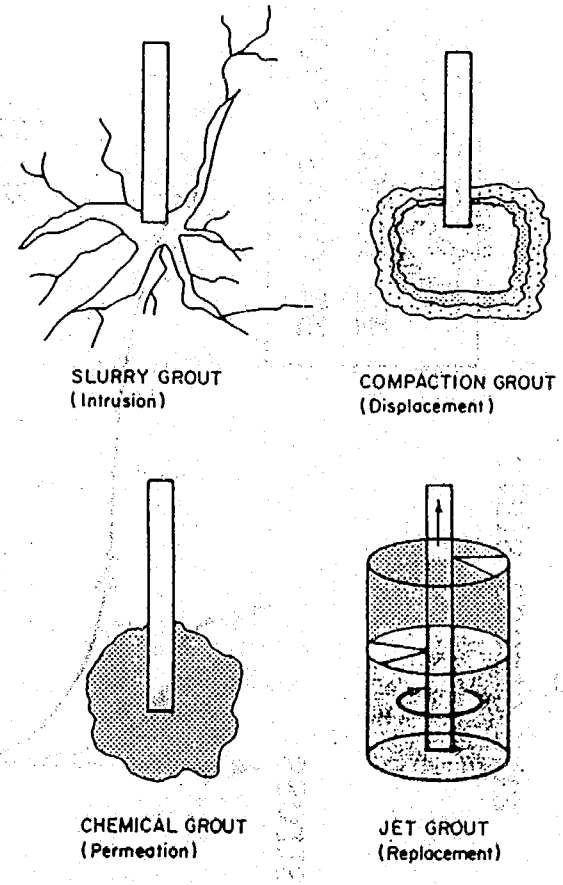
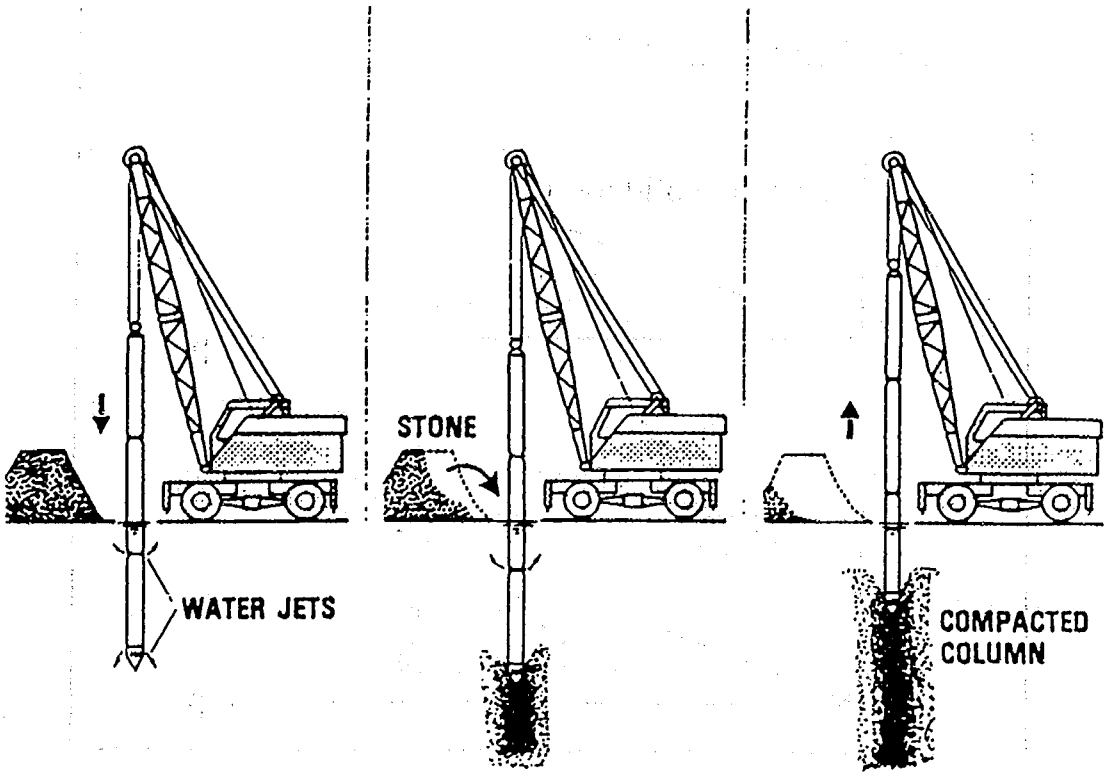


Figure 4: Types of grouting techniques (Welsh 1986).



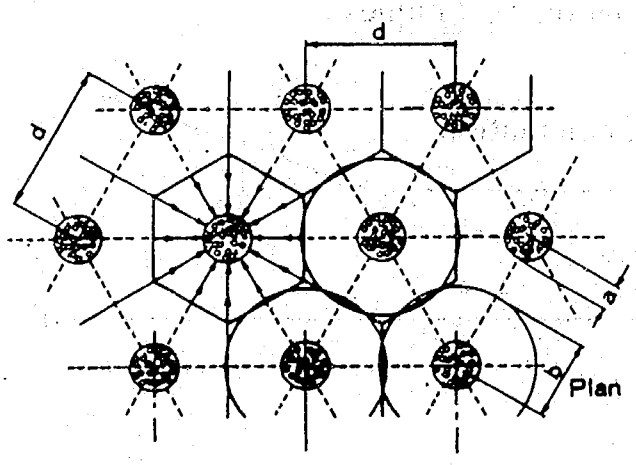


Figure 5: Gravel drain construction.

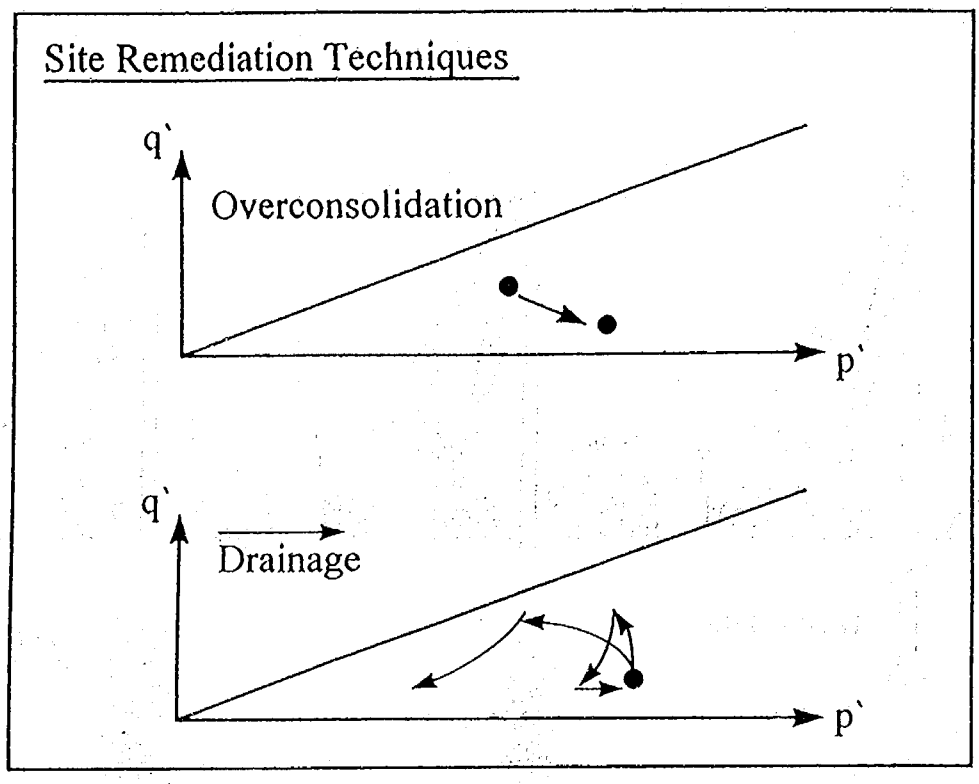


Figure 6: Mechanisms associated with increased confinement and increased drainage.

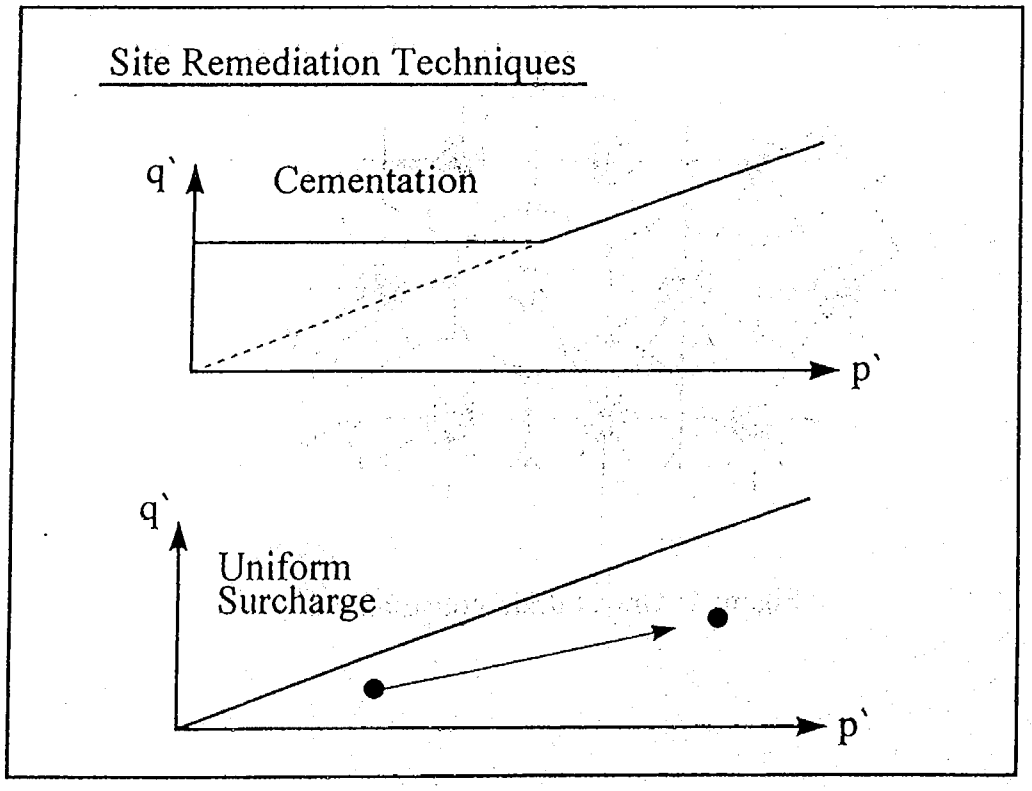
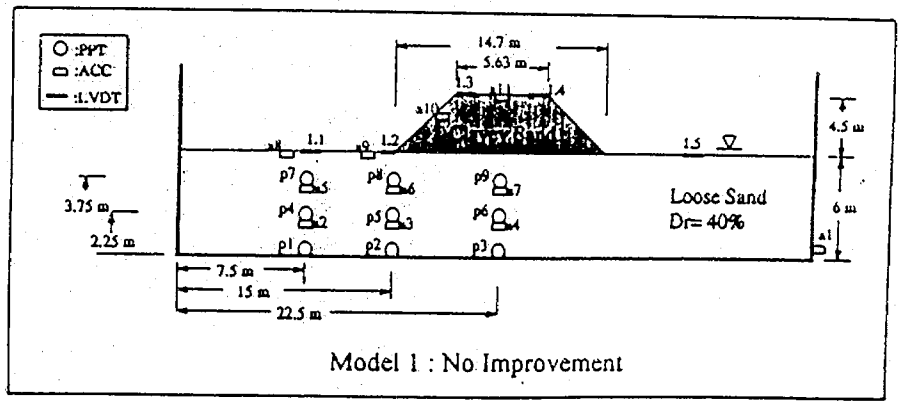
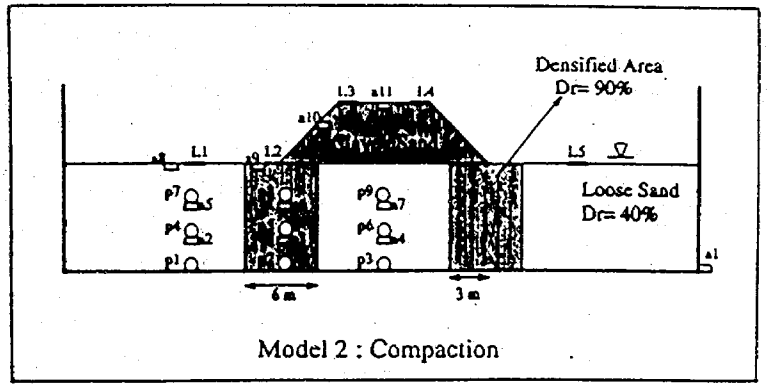


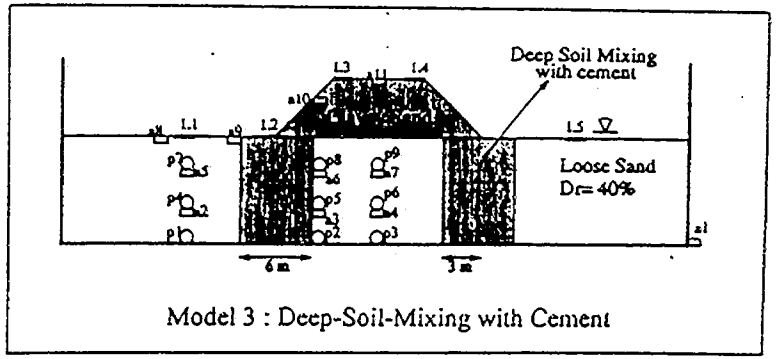
Figure 7: Mechanisms associated with solidification (cementation), and surcharge loading.



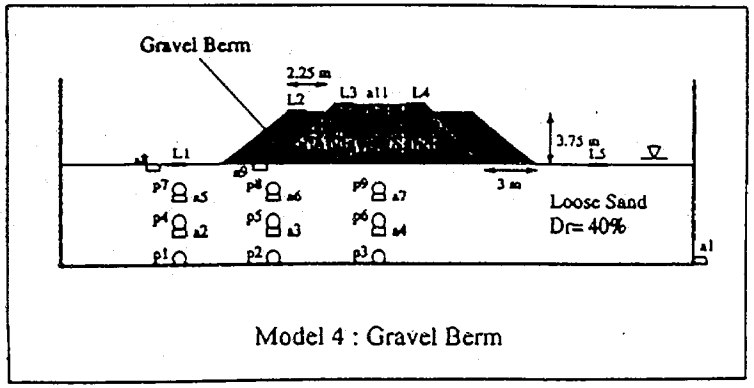
Model 1 : No Improvement



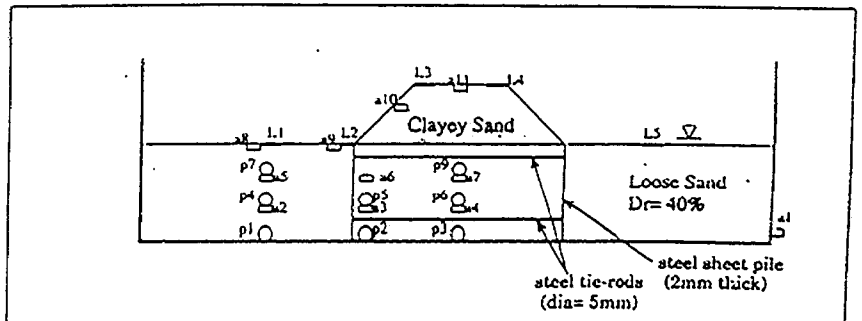
Model 2 : Compaction



Model 3 : Deep-Soil-Mixing with Cement

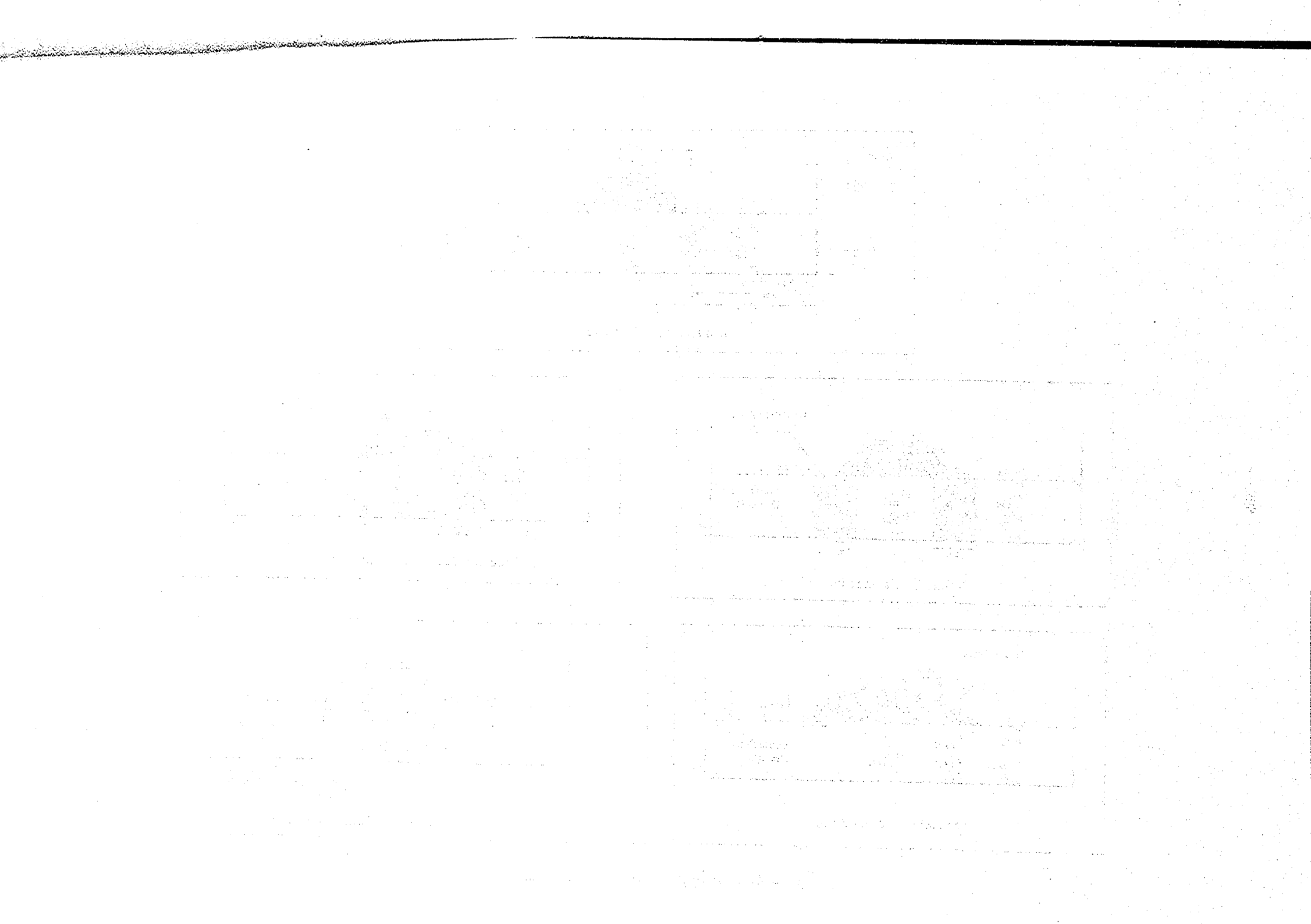


Model 4 : Gravel Berm



Model 5: Sheet Pile Enclosure

Figure 8: Configurations of centrifuge models 1 to 5.



SEISMIC DESIGN TREATMENT OF LIQUEFACTION-INDUCED GROUND FLOW

Keiichi Tamura [1], Tadashi Hamada [2] and Takuo Azuma [3]

1 Head, Ground Vibration Division, Public Works Research Institute, Ministry of Construction, 1 Asahi, Tsukuba-shi, Ibaraki-ken 305 Japan
2 Research Engineer, Earthquake Disaster Prevention Technology Division, ditto
3 Research Engineer, Ground Vibration Division, ditto

ABSTRACT

The Hyogo-ken Nanbu Earthquake of January 1995 caused liquefaction in wide area. Especially, liquefaction induced the ground flow with the movement of sea walls at the waterfront, and this ground flow caused damage to various structures behind sea walls. This paper summarizes a feature of the liquefaction-induced ground flow, its influence on highway bridges and an outline of seismic design treatment of the liquefaction-induced ground flow for highway bridges.

INTRODUCTION

When the soft ground undergoes liquefaction, the strength and the bearing capacity of the ground decreases, and the ground subsides. Besides that, near the water's edge, liquefaction may yield the ground flow with the movement of a sea wall or revetment, which causes damage to the structures behind it. The Hyogo-ken Nanbu Earthquake of January 1995 caused widespread liquefaction in the reclaimed land. Furthermore, liquefaction induced the ground flow with the movement of sea walls, and this ground flow caused large deformation of highway bridge foundations. In Japan, the liquefaction-induced ground flow has been recognized since the Niigata Earthquake of 1964 from an engineering point of view [1], however it was the first time that the ground flow caused the extensive damage to the newly constructed highway bridges.

This paper presents a feature of the liquefaction-induced ground flow in the Hyogo-ken Nanbu Earthquake, its influence on highway bridges which includes an estimation of ground flow force acting on a bridge foundation and an outline of seismic design treatment of the liquefaction-induced ground flow in the newly revised "Specifications for Highway Bridges".

DAMAGE TO HIGHWAY BRIDGES DUE TO LIQUEFACTION-INDUCED GROUND FLOW

No highway bridge suffered serious damage such as collapse of a superstructure directly due to the liquefaction-induced ground flow in the 1995 Hyogo-ken Nanbu Earthquake, however, the ground flow yielded large deformation of bridge foundations and related damage. As an example of damage to a highway bridge, the case of Shin- Shukugawa Bridge on Route 5, Bay Shore Line of the Hanshin Expressway is here presented [2].

The Shin-Shukugawa Bridge completed in 1993 is a 3-span cantilever box girder bridge which crosses a watercourse between reclaimed lands, i.e., Nishinomiya-hama and Minami Ashiya-hama. An overview of the damage to this bridge is shown in Figure 1. Since a toll gate is located on the P-134 pier on Minami Ashiya-hama, the width of the bridge varies from 28m to 69m. The bridge is supported by movable supports at its both ends on reclaimed lands, and by fixed supports on intermediate piers.

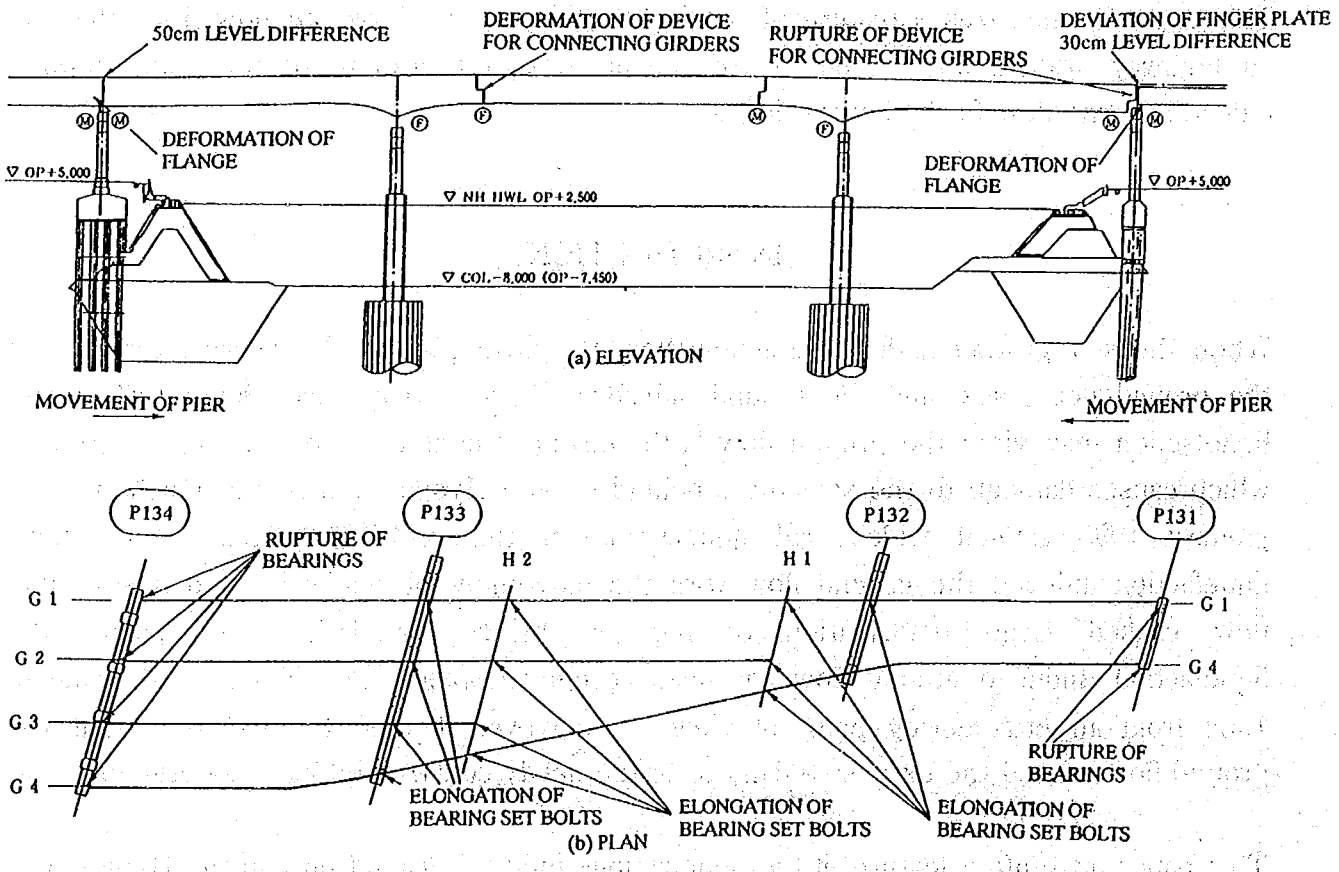


Figure 1 Overview of Damage to the Shin-Shukugawa Bridge

The P−131 pier on Nishinomiya−hama was a 2−column RC rigid frame pier with two caisson foundations, 6m in diameter. The P−134 pier on Minami Ashiya−hama was a 4−column steel rigid frame pier and was supported by cast−in−place concrete piles, 1.5m in diameter. The foundations were constructed in the reclaimed soil and supported by a diluvial sandy layer.



Photo 1 Ground Failure near the Shin−Shukugawa Bridge



Photo 2 Damage to Bearing Support of the Shin−Shukugawa Bridge

Extensive liquefaction occurred around the bridge as shown in Photo 1, and both P−131 and P−134 piers moved toward the watercourse with the movement of sea walls. The damage was concentrated to the end piers on reclaimed lands. The piers were installed

with pivot roller supports, whose upper and lower shoes diverged as shown in Photo 2, which caused the difference in level between adjacent girders. A device for connecting girders on the P−131 pier was ruptured. A device for connecting girders was deformed at a cantilever hinge.

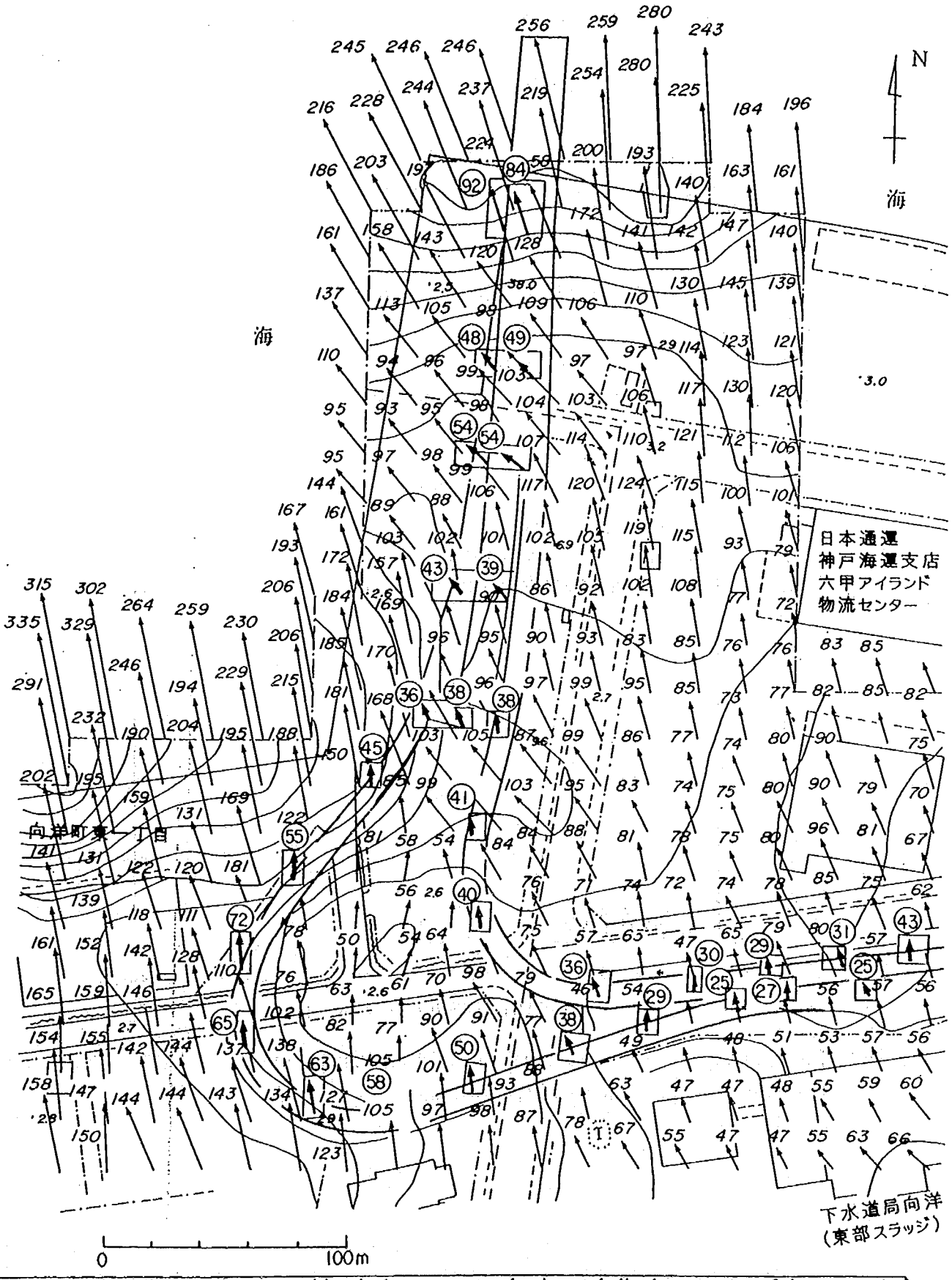
ESTIMATION OF GROUND MOVEMENT DUE TO GROUND FLOW

The aerial photogrammetry was employed to estimate the ground movement vectors by comparing aerial photos taken before and after the earthquake [3] . The result of aerial photogrammetry conducted by Hamada et al. [4] was referred in this study. The main modifications from their study are as follows:

1) Hamada et al. used three survey points on Rokko Island as reference points for aerial photogrammetry, while six points established for surveying the bridge pier locations of the Route 5, Bay Shore Line of the Hanshin Expressway were used as reference points in this study.
2) Hamada et al. found displacement vectors of fixed objects on the ground surface such as manhole covers. In addition to this, displacement vectors at intersection points of 20m interval grids were found in the present study. The residual horizontal displacements of bridge piers at the height of 1m above the ground level were also estimated in this study by another survey conducted after the earthquake.

The horizontal displacement vectors of the ground and bridge piers were found to include uniformly about 20cm component for the south−west direction. In addition to this, triangulation points near the Route 5 of the Hanshin Expressway shifted the same amount for the south−west direction. This displacement may be attributed to the base ground movement caused by fault movement or wide area ground movement. In the present study, this displacement is excluded from the result of aerial photogrammetry of the ground displacement and the residual displacement of bridge piers. The displacement vectors found may include a certain degree of error because of the errors associated with aerial survey and photographic interpretation. The accuracy of measurement is estimated as ± 30cm for the ground displacement and ± 10cm for residual displacement of bridge piers, respectively [3] .

Figure 2 shows the vectors of the ground displacement and residual displacement of bridge piers near the north shore of Rokko Island. The sea walls moved toward the watercourse and the ground flow occurred, which caused the movement of the ground and bridge piers behind the walls. At the edge of the water, the ground moved more than 2m, and a bridge pier moved approximately 0.9m. The movements of the ground and bridge piers generally decrease as the distance from the watercourse increases.



NOTE: Number at arrows and in circles represent horizontal displacements of the ground and residual horizontal displacements of bridge piers, respectively. (Unit : cm)

Figure 2 Horizontal Displacements of the Ground and Residual Displacements of Bridge Piers at Rokko Island

Figure 3 shows the relationship between the residual horizontal displacements of bridge piers and the horizontal displacements of the ground on the Route 5 of the Hanshin Expressway. Although the considerable scatters exist, the residual displacements of bridge piers tend to increase as the ground displacements increase, in general. The residual displacements of piers with rigid foundations, i.e., caisson and diaphragm wall foundations, are smaller than those with pile foundations for a certain amount of ground displacement.

The relationship between the residual horizontal displacements of bridge piers and the distance from the water's edge is shown in Figure 4. The residual displacement rapidly decreases with the increase of distance from the edge of the water. The range in which prominent residual displacement occurred is limited to approximately 100m from the water's edge.

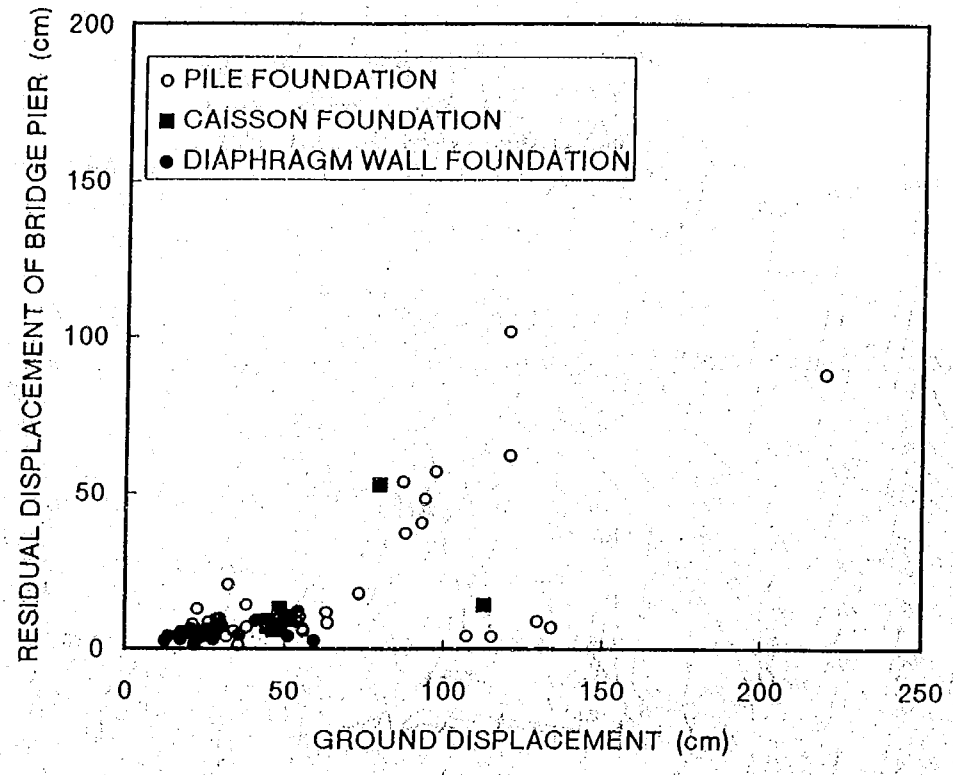


Figure 3 Relationship between Residual Horizontal Displacements of Bridge Piers and Horizontal Displacements of the Ground

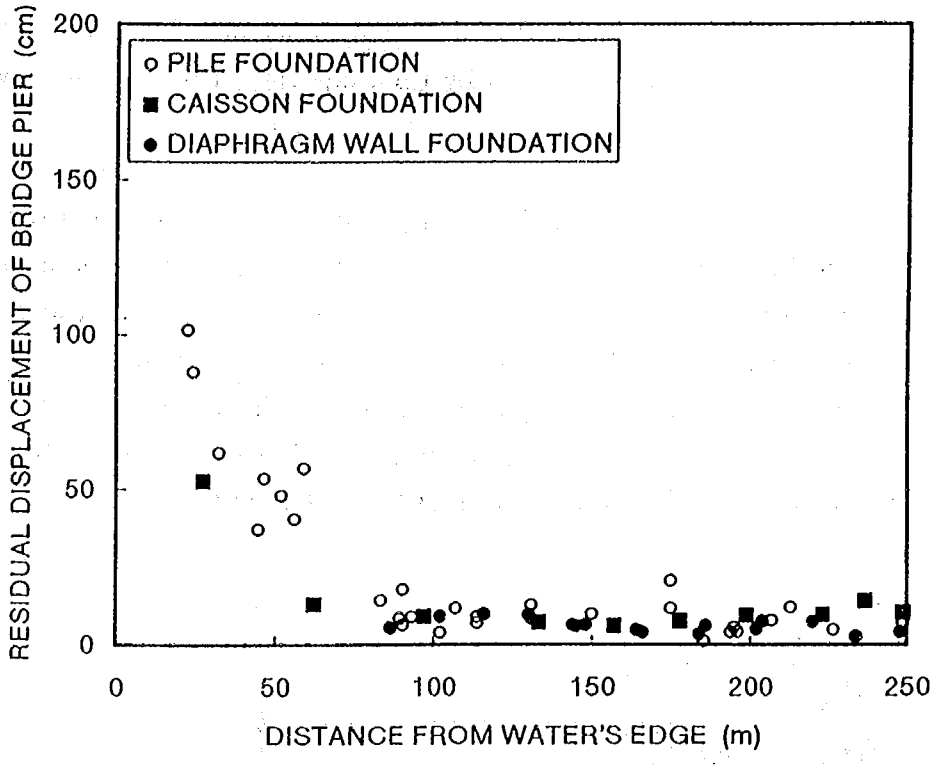


Figure 4 Relationship between Residual Horizontal Displacements of Bridge Piers and Distance from Water's Edge

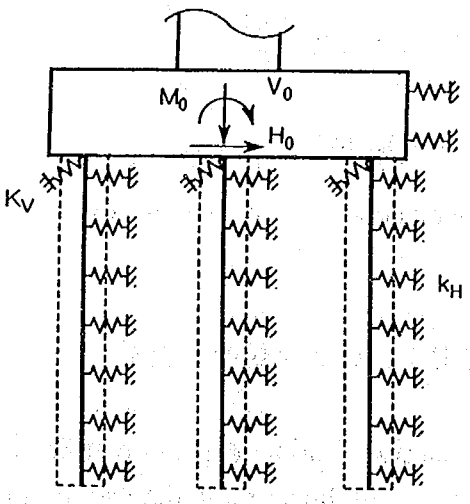
ESTIMATION OF GROUND FLOW FORCE BY BACK ANALYSIS

The force acted on a bridge foundation due to the liquefaction–induced ground flow was estimated by back analysis of bridges which suffered residual horizontal displacements. The result for P–216 pier, which is located at the north edge of Rokko Island, is here presented. The P–216 pier was a 2–story steel rigid frame pier and was supported by cast–in–place concrete piles, 1.5m in diameter. The bearings on this pier are fixed for a watercourse–side girder and movable for a inland–side girder. The soils are composed of sandy artificial fill, alluvial clay and alternation of diluvial sand and clay. The residual horizontal displacement of this pier was 0.9m, as shown in Figure 2. The ground water level of the site was 3.3m below the ground surface, and the liquefaction was judged to occur in the sandy artificial fill below the ground water level [5)]

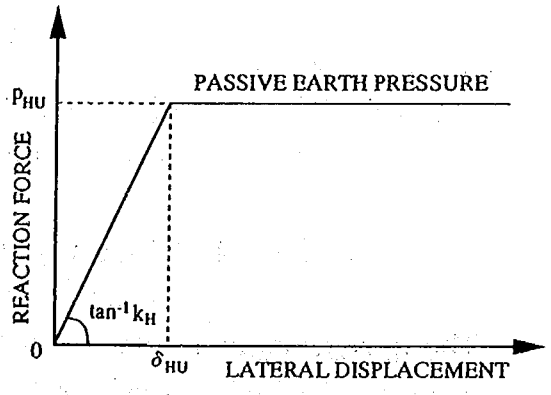
In the estimation of the force acted on a bridge foundation due to the ground flow, it was assumed that the layer near the ground surface which did not liquefy (non–liquefied layer) moved with the layer which liquefied (liquefied layer), and both layers caused force to a bridge foundation [6)] . Since the non–liquefied layer was considered to move toward the structure and exert force on it, the force equivalent to the passive earth pressure was assumed to act on a bridge foundation in the non–liquefied layer. The liquefied layer

was considered to move fluidly around the structure, and the force corresponding to a certain portion of overburden pressure was assumed to act on a bridge foundation in the liquefied layer. This portion was estimated by back analysis of bridge piers with residual displacements.

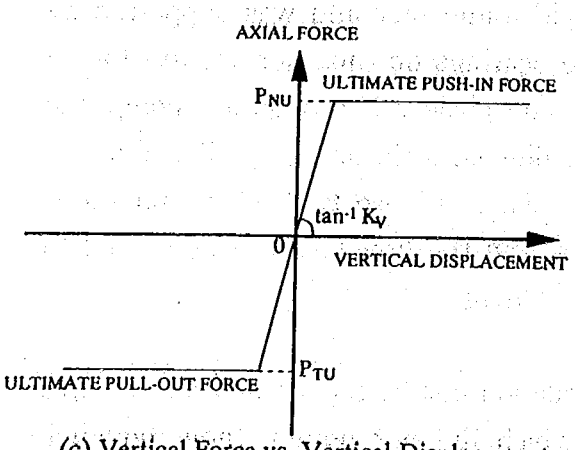
In the analysis, as shown in Figure 5, the bridge foundation was so idealized that a rigid footing is supported by piles that are supported by soils, considering nonlinear properties of pile bodies and the ground [7] . The soil resistance were ignored for the non-liquefied and liquefied layers that were considered to move when the ground flow occurred. The width for which the ground flow force applied was set as the width of structure for a pier and footing, and the projected width between the end piles for pile bodies. Figure 6 shows an overview of the analyzed foundation and the applied force.



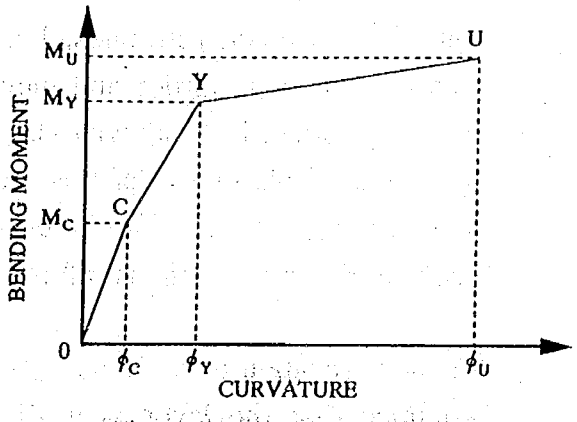
(a) Analytical Model



(b) Lateral Force vs. Lateral Displacement



(c) Vertical Force vs. Vertical Displacement



(d) Bending Moment vs. Curvature

Figure 5 Idealization of Pile Foundation for Nonlinear Analysis

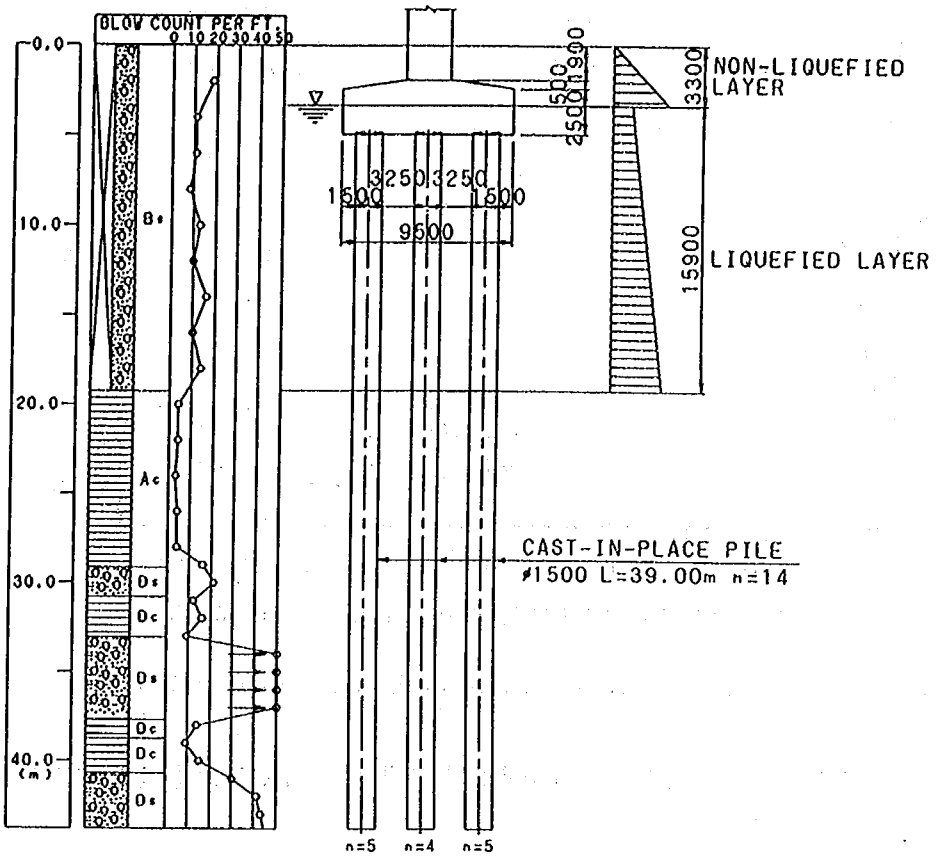


Figure 6 Overview of Analyzed Foundation and Applied Force

Since how much portion of the overburden pressure of the liquefied layer acted on a bridge foundation is unknown, varying this portion parametrically and calculating the relationship between lateral force and displacement, the amount of force that was consistent with the residual displacement was estimated. The result is shown in Figure 7. The total force which caused the residual displacement of 0.9m to the P−216 pier was estimated as 2,256tf; 578tf for non−liquefied layer and 1,678tf for liquefied layer. The ratio of the force applied in the liquefied layer to the overburden pressure was calculated as 0.32 for this pier. Similar analysis was conducted for the four bridge piers on the Route 5 of the Hanshin Expressway, and the contribution factor of overburden pressure was estimated approximately as 0.3.

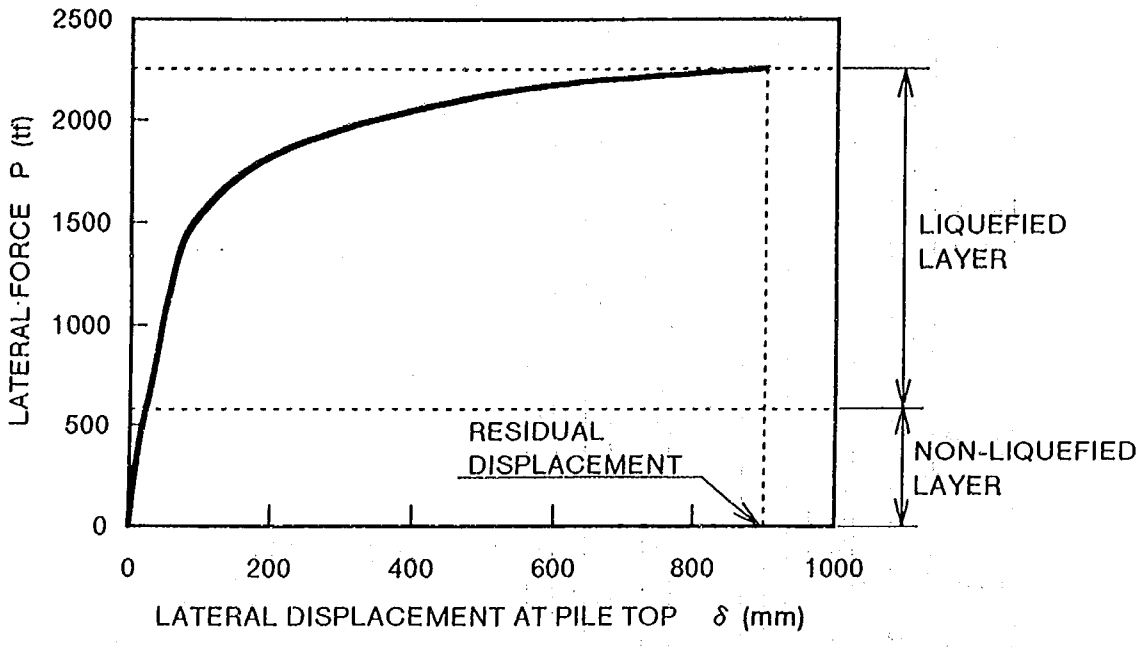


Figure 7 Relationship between Lateral Force and Displacement at Pile Top

SEISMIC DESIGN TREATMENT OF GROUND FLOW

Based on the above-mentioned facts, when the liquefaction-induced ground flow that may affect bridge seismicity is likely to occur, this influence has become to be considered in the newly revised "Specifications for Highway Bridges" [5] . The case in which the ground flow that may affect bridge seismicity is likely to occur is generally that the ground is judged to be liquefiable and is exposed to biased earth pressure, e.g., the ground behind a sea wall. The effect of liquefaction-induced ground flow is considered as the force acting on structure. This method premises that the surface soil is of the non-liquefiable and liquefiable layers, and the forces equivalent to the passive earth pressure and 30% of the overburden pressure are applied to the structure in the non-liquefiable layer and liquefiable layer, respectively. As seen from Figure 4, since the magnitude of ground flow decreases as the distance from the water's edge increases, modification by distance is incorporated in the estimation of the ground flow force. Modification by the degree of liquefaction is also established.

The seismic safety of a foundation is checked by confirming the displacement at the top of foundation caused by ground flow does not exceed an allowable value, in which a foundation and the ground are idealized as shown in Figure 5. In this process, the inertia force of structure is not necessary to be considered simultaneously, because the liquefaction-induced ground flow may take place after the principal ground motion ends.

CONCLUSIONS

A feature of the liquefaction-induced ground flow and its influence on highway bridges were presented. The ground movement caused by the ground flow was estimated by comparing aerial photos taken before and after the earthquake, and the ground flow force acted on a bridge foundation was estimated by back analysis using a nonlinear foundation model. From the analysis of this study, the ground flow force may be estimated as the sum of the passive earth pressure of the non-liquefied layer and 30% of the overburden pressure of the liquefied layer. An outline of seismic design treatment of liquefaction-induced ground flow for highway bridges was also presented.

REFERENCES

1) Masanori Hamada, Susumu Yasuda, Ryoji Isoyama and Katsutoshi Enomoto: Observation of Permanent Ground Displacements Induced by Soil Liquefaction, Proc. of Japan Society of Civil ENgineers, No.376, 1986 (in Japanese)

2) Hisanori Otsuka et al.: Report on the Disaster Caused by the 1995 Hyogoken Nanbu Earthquake, Chapter 5, Damage to Highway Bridges, Report of PWRI, No.196, 1996

3) Committee for Investigation on the Damage of Highway Bridges by the Hyogo-ken Nanbu Earthquake, 1995: Report on the Damage of Highway Bridges by the Hyogo-ken Nanbu Earthquake, 1995 (in Japanese)

4) Masanori Hamada, Ryoji Isoyama and Kazue Wakamatsu: The 1995 Hyogoken-Nanbu (Kobe) Earthquake, Liquefaction, Ground Displacement and Soil condition in Hanshin Area, Association for Development of Earthquake Prediction, 1995

5) Japan Road Association: Specifications for Highway Bridges, Part 5 Seismic Design, 1996 (in Japanese)

6) Keiichi Tamura, Yoshio Ninomiya and Tadashi Hamada: Estimation of Effects of Liquefaction-Induced Ground Flow on Bridge Foundations, 28th Joint Meeting, U.S.-Japan Panel on Wind and Seismic Effects, UJNR, 1996

7) Japan Road Association: Reference for Applying the Guide Specifications for Reconstruction and Repair of Highway Bridges Suffered Damage from the Hyogo-ken Nanbu Earthquake of 1995, 1995 (in Japanese)

A Study on Measures Against Ground Flow Using The Finite Element Method

By M. Ogasawara,[1] H. Tsunoda,[1]T.Makita [1], and S. Gose [2]

Abstract

It is assumed that ground flow accompanying liquefaction occurs when the ground becomes unbalanced under the effects of deformation of a revetment. This paper reports on the use of FEM analysis to estimate the state of imbalance of ground caused by liquefaction, and describes ground flow protection measures which treat the ground displacement estimated in this way as an external force. The FEM analysis of the imbalanced state includes an assessment performed by varying the stiffness of the ground before and after liquefaction. A study was performed to develop a method of protecting structures from this problem by installing steel pipe sheet-piles between revetments and the structures. When considering measures for dealing with ground flow, it is necessary to understand its mechanism. Consequently, ground flow mechanism was considered, and based on this mechanism, two evaluation methods were studied. One assesses ground displacement as an external force as described above and another treats the ground flow as shearing deformation. Finally the ways the two methods handle a sample disaster were studied.

Introduction

During the Hyogo-ken Nanbu Earthquake (January 17, 1995), liquefaction in landfill near revetments along the harbor shoreline caused ground flow (movement) accompanied by the movement of structures. A report from the Hyogo-ken Nanbu Earthquake Road Bridge Earthquake Damage Counter-measures Committee (1995) reports bridge pier movement as great as about 1.0 m.

1: Engineer, Metropolitan Expressway Public Corp., Tokyo, Japan
2: Consultant Engineer, CTI Engineering Co., Ltd., Tokyo Japan

This ground flow did not occur only as a result of liquefaction in horizontal ground. It is induced by plastic flow occured in the surrounding groun after that nearby revetments subside and move as result of liquefaction. Consequently, ground deformation was greatest near the revetments, but declined as the distance from the revetments increased. In other words, the ground flow force declined as the distance rose. For this reason, it has been concluded that one effective way to prevent ground flow would be to locate ground flow protection work between the revetment and the structure to be protected, and as far as possible from the revetment (close to the structure).

The horizontal motion of ground accompanying the deformation of a revetment is assumed to be the sum of the motion during and after the earthquake. Little is known about the percentage accounted for by the two motions, it is difficult to analytically clarify this factor, and it is difficult to believe that doing so would provide practical benefits. So the method employed involved varying the stiffness of the liquefied stratum before and after liquefaction and treating the resulting difference between the ground displacements calclated from the dead weight analyses performed with the FEM method as the total horizontal motion of the ground. The revised Road Bridge Guidelines state that it is appropriate to apply this method when the ground condition is complex.

Two methods of assessing the external force acting on a structure from the ground displacement have been considered. One is the response displacement method which applies ground displacement to a structure. The other method assumes that the deformation of the ground is shear deformation and treats the shear force which causes this shear deformation as an external force. Based on the results of analyses of a sample disaster using these two methods, the response displacement method has been judged to be effective and was used as the external force for the counter-measure work.

The results of a study of measures to protect bridge piers in the area under the jurisdiction of the Metropolitan Expressway Public

Corporation performed using the above method show that the installation of steel pipe sheet-piles with a diameter of 1.2 m and a sheet thickness of 19 mm in front of a line of piers can be counted on to provide a certain level of effectiveness.

Mechanism of Ground Flow Induced by Liquefaction

Figure 1 is a schematic diagram of the effect of ground flow on bridge piers. In this figure, it is hypothesized that there is no

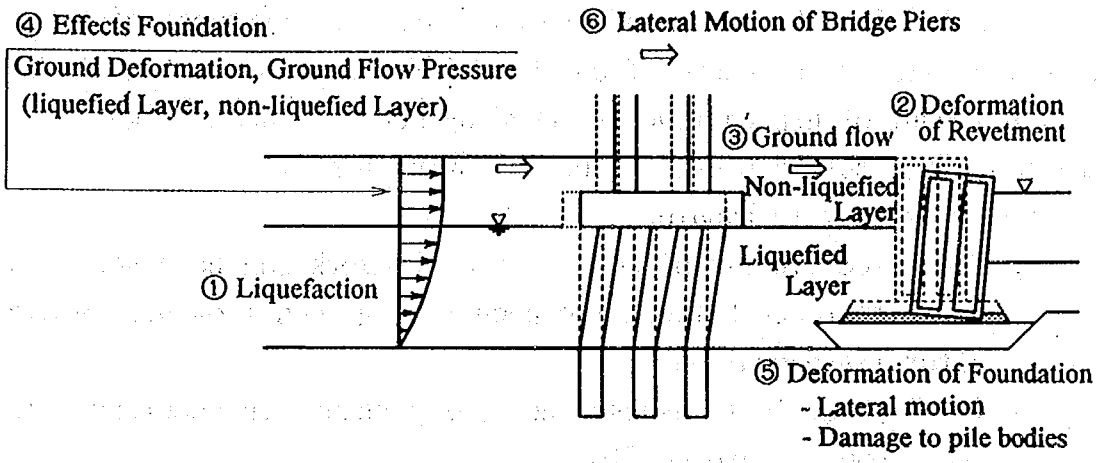


Figure 1. Concept on the Mechanism of the Effect of Ground flow on Bridge Pier Foundations

liquefaction from the ground surface to the bottom of the footing (non-liquefied stratum), but that liquefaction occurs deeper than the bottom of the footing (liquefied stratum). The numbers inside the circles signify the sequence of phenomena up to the point that horizontal displacement of the bridge piers occurs. ① Liquefaction: The liquified stratum in the diagram is liquefied by the earthquake. ② Deformation of the revetment: The revetment inclines towards the ocean, subsides, and moves horizontally under the effects of increasing soil pressure and a decline in the bearing force of the foundation ground caused by the liquefaction. ③ Ground flow: As the revetment is deformed, the ground behind it moves a long distance horizontally towards the ocean as it subsides. ④ Effect on the foundation: The horizontal motion of the ground applies flow pressure on the structure. ⑤ & ⑥: Deformation of the foundation and lateral

motion of the bridge piers: The bridge piers are moved horizontally by the flow pressure.

This mechanism shows that the deformation of the revetment is transmitted to the bridge piers through the ground. As a result, it has been concluded that the implementation of measures to block this transmission process will be effective (a measure taken between the revetment and structure).

Estimation of Ground Flow Displacement

The amount of ground flow is estimated based on a static elastic FEM analysis. To find the amount of ground flow, the stiffness of the liquefied stratum is reduced from the stiffness prior to liquefaction and the amount of ground flow is found by means of dead weight analyses. This method provides the following benefits.

① It is easy to handle.

② The effectiveness of counter-measure work can be assessed as the difference between the amount of ground flow before and after its execution.

③ It is possible to assess the flow pressure in accordance with the amount of ground flow.

④ The effects of the thickness of the flow stratum, the distance from the revetment, the inclination of the ground, etc. can be reflected in the amount of ground flow.

Figure 2 is a flow chart of this study process. The non-liquefied stratum above the liquefied stratum is reduced in order to mitigate resistance caused by cracking of the ground surface during liquefaction and tensile force generated analytically.

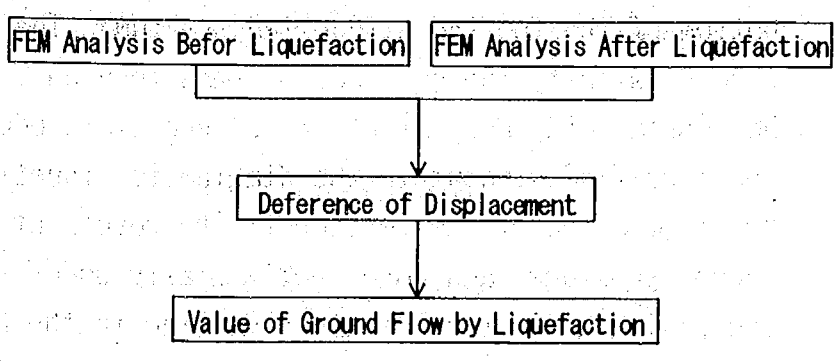


Fig.2 Estimation on Displacement of Ground Flow

The amount of ground flow was calculated for a case where there are neither bridge piers nor protective work, in order to account for the

joint element with an upper limit value for tension and slippage between the revetment and the ground.

Ground Flow Force Estimation Procedure

Procedure Considering Ground Flow Force as Displacement

A method of providing the displacement of the ground at the location of the structure, the flow pressure P is assessed using formula (1).

$$p = k \times (\delta_g - \delta_f) \leq p_p \quad \cdots\cdots\cdots\cdots \quad (1)$$

Where, p : Flow pressure (tf/m^2), δ_g : Ground displacement (m), δ_f : Foundation displacement (m), k : Ground spring constant of the flow stratum (tf/m^3), Pp: Passive soil pressure (tf/m^2). Figure 3 is a schematic diagram illustrating this concept. k_{II} in the figure is the resistance spring constant of the ground in which the piles are placed, and the passive soil pressure is treated as the upper limit. The spring constant of the liquefied stratum is the value obtained by multiplying the coefficient of subgrade reaction used for the design by the reduction rate of the ground stiffness after liquefaction obtained when calculating the ground flow. The ground depth direction displacement distribution treats the displacement at the ground surface as the maximum value and assumes that it is a cosin distribution with the displacement at the bottom surface of the liquefaction stratum equal to zero. The structure is assumed to be non-linear material using M (bending moment) ~ (curvature).

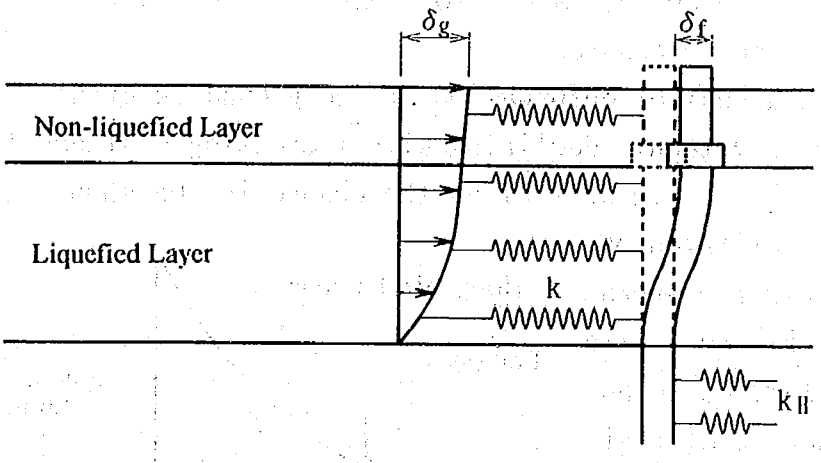


Figure 3. Concept of Ground Displacement as the Flow Pressure

Procedure Considering Ground Flow Force as Shearing Deformation

Using this method, it is assumed that the horizontal direction displacement accompanying the ground flow is an inverted triangular shear deformation as shown in Figure 4, the shear strain is found by reducing the ground surface displacement (δ_g) by the flow stratum thickness (H), and the assessment is performed treating the shear force equivalent to shear deformation within a certain range as the flow pressure.

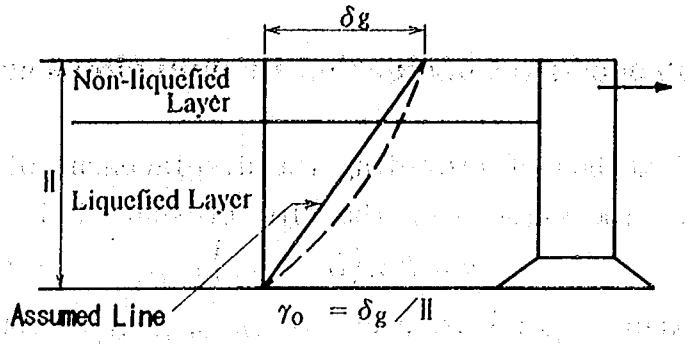


Figure 4. Shear Deformation Concept

The amount of deformation of the ground is greatest at the location of the revetment, declining with increasing distance from the revetment. If this is thought of as the change in the shear strain, it can be approximated by the curve shown in Figure 5 with reference to an example of past deformation. In this figure, the vertical axis is the shear strain while the horizontal axis is the distance from the revetment. γ_0 is the shear strain at the center of the bridge pier, and it is hypothesized that the shear force which corresponds to the shear deformation of the ground behind this location is the flow pressure. In this study, it is assumed that there is action by a shear force (S) generated in an imaginary soil column in a range α times the liquefied

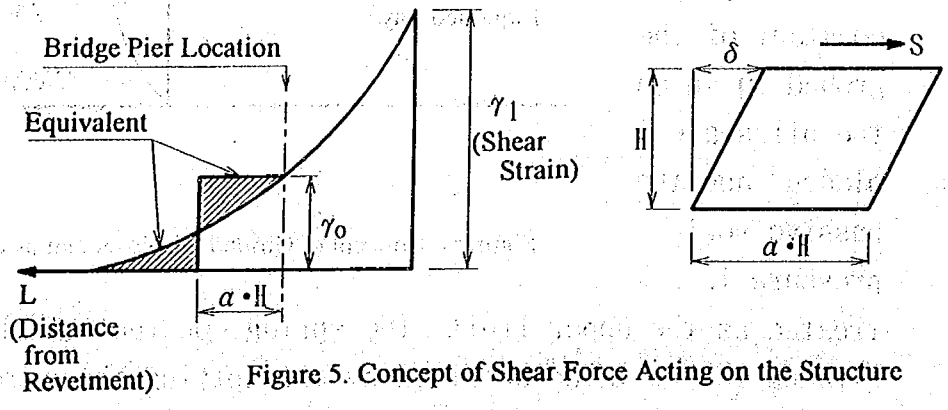


Figure 5. Concept of Shear Force Acting on the Structure

stratum thickness (H) as shown in Figure 5. This shear force acts on the structure as a uniform load in the stratum thickness direction. Consequently, the size of the flow pressure (p) is found from formula (2).

$$p = S/H = G \cdot \gamma_0 \cdot \alpha \cdot H/H = G \cdot \gamma_0 \cdot \alpha \quad \cdots\cdots\cdots (2)$$

Where G is the shear stiffness of the flow stratum, and the value after liquefaction obtained through FEM analysis is used. Figure 6 shows an analytical model.

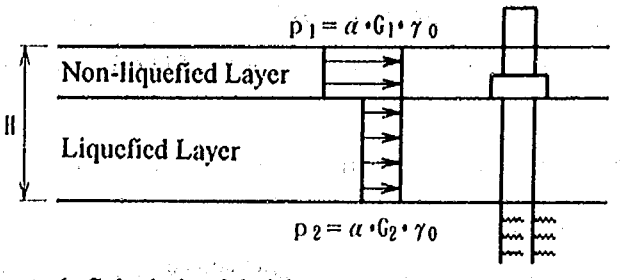


Figure 6. Calculation Model for the Method Which Treats Shear Force as the Flow Pressure

Test of the Procedures Based on an Example of Past Deformation

Estimation of Ground Flow Displacement

Using measured amounts of movement of the ground surface caused by liquefaction observed after the Hyogo-ken Nanbu Earthquake, the methods were verified by varying the ground stiffness before and after liquefaction. Because there is no detailed data concerning the physical properties of the ground, the following hypotheses were established. Because with this method, the difference between the relative displacements is assumed to be the amount of ground flow, the important points are the hypothetical stiffness reduction rate and Poisson's ratio of the liquefied stratum after liquefaction. The modulus of deformation of the ground before liquefaction (Eo) was 28 · N (N: standard penetration test value), while Poisson's ratio (ν) was 0.33. The unit weight used was the weight in water. The modulus of deformation of the liquified stratum after liquefaction was 1/100 of that before liquefaction. This reduction rate was set based on parametric analysis for an actual example with reference to the results of research by Yasuda et al (1994). The modulus of deformation of the non-liquefied stratum above the liquefied stratum was set at

about 1/10 of that before liquefaction. This was done to mitigate the resistance caused by the tensile stress, which is a shortcoming of elastic analysis. And the boundaries of the ground were set 500 m inland from the back of the revetment and 100 m on the ocean side. The horizontal displacement was fixed and the vertical displacement was free.

Figures 7 to 9 show comparisons of the observed values and analytic values of the horizontal displacement of the ground surface. These are examples of Minami Ashiya Beach, Uozaki Beach (See the model in Figure 10), and Port Island. These figures demonstrate that it is possible to estimate the approximate amount of displacement of ground using this method.

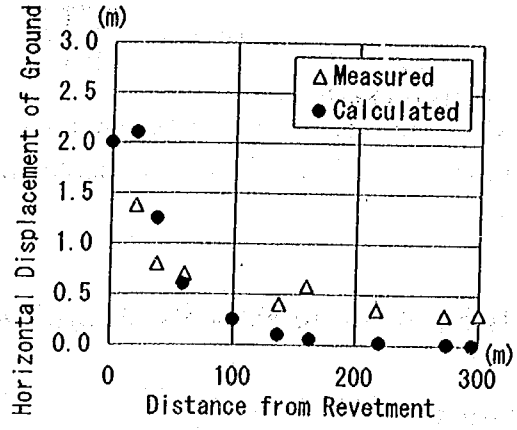


Fig. 7 Distance from Revetment-Displacement Relationship(Minami Asiya Beach)

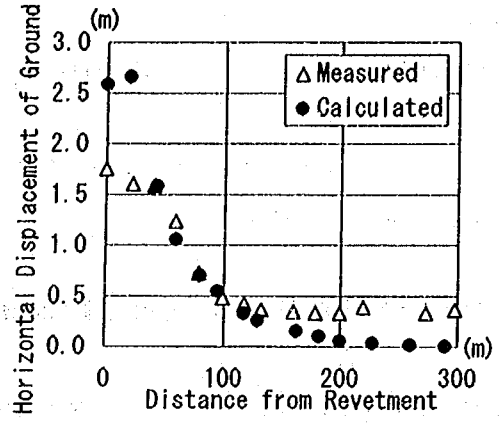


Fig. 8 Distance from Revetment-Displacement Relationship(UOSAKI Beach)

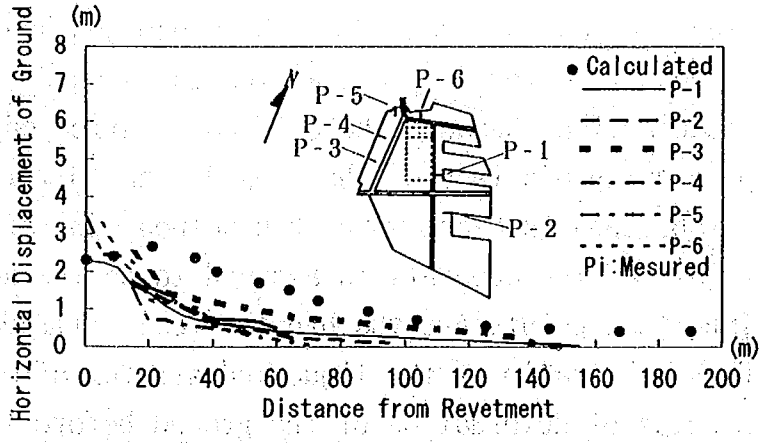


Fig. 9 Distance From Revetment-Displacement Relationship (Port Island:Measured Displacement Based on Reference Source No. 2)

Ground Flow Force Estimation Procedure

The ground flow force is estimated based on the ground displacement found as described above. It is found for deformed bridge piers at

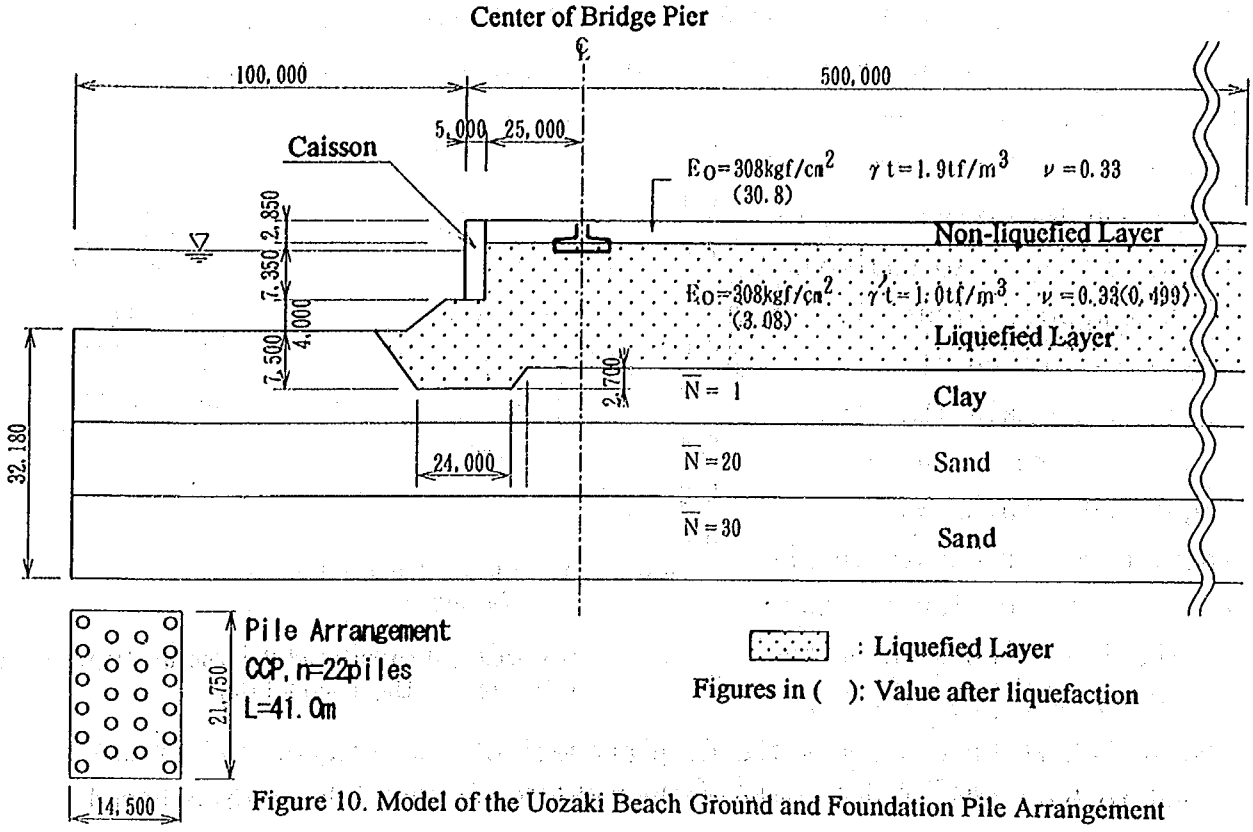


Figure 10. Model of the Uozaki Beach Ground and Foundation Pile Arrangement

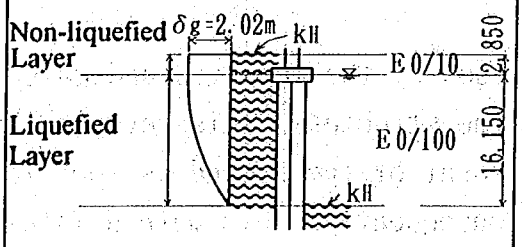
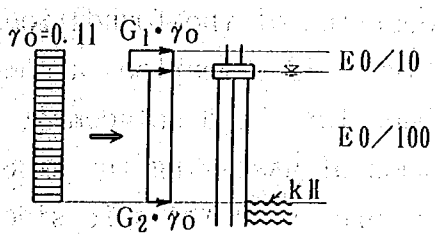
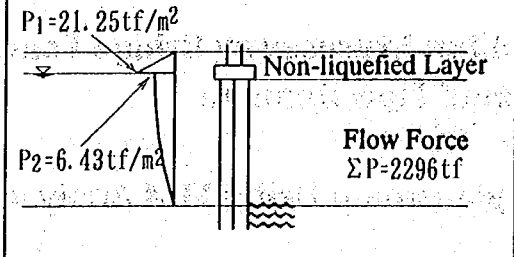
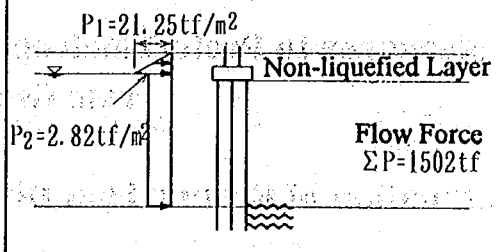
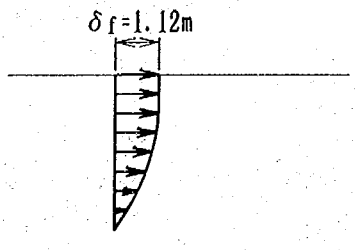
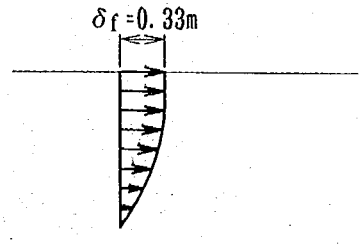
	(1) Calculating the Flow Pressure From the Horizontal Displacement of the Ground	(2) Calculating the Flow Pressure From the Shear Deformation of the Ground
Analytical Model of Foundation (Schematic Diagram)		
Flow Pressure		
Foundation Displacement Distribution (Schematic Diagram)		

Figure 11. Comparison of Calculated Values (Uozaki Beach)

Minami Ashiya Beach, Uozaki Beach, and near Rokko Island. In all cases, they were cast-in-place concrete piles with a diameter of 1.5 m.

Figure 10 presents the ground model for Uozaki Beach and the arrangement of its bridge pier foundations as an example. Figure 11, an example of calculation results, reveals that the flow pressure in the non-liquefied stratum was passive soil pressure in all cases, but the flow pressure in the liquefied stratum was found to be 2,296 tf using the method which considers the displacement of the ground, and it was found to be 1,502 tf using the method which assesses this force based on shear deformation; the flow pressure is smaller in the latter case. The size of the flow pressure in the liquefied stratum varies by about 35%, but the amount of displacement of the foundation varies by more than three times. This difference is a result of the non-linear properties of the foundation.

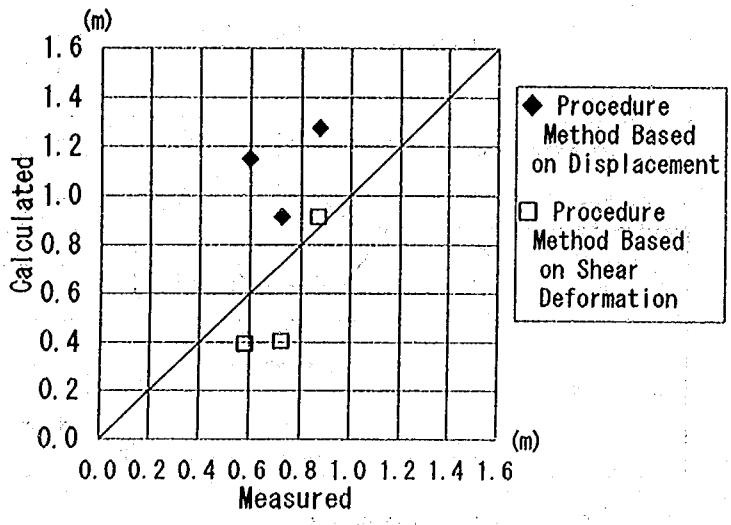


Fig. 12 Measured and Calculated Horizontal Displacement Relation of the Foundation

Figure 12 summarizes a comparison of the measured and calculated values for the displacement of the structure. This reveals that the method of assessing the displacement of the ground as the flow pressure is on the safe side. Consequently, this method is used to study counter measures.

Measures to Protect Metropolitan Expressway Bridge Foundations From Ground Flow Damage

Estimation of Ground Flow Displacement Using FEM Analysis

Figure 13 is a general drawing of the structure of the bridge piers studied. Their foundations are cast-in-place concrete piles with a diameter of 1.5 m. The amount of flow of the foundation is analyzed without a structure. The revetment, which is a steel sheet-pile Type

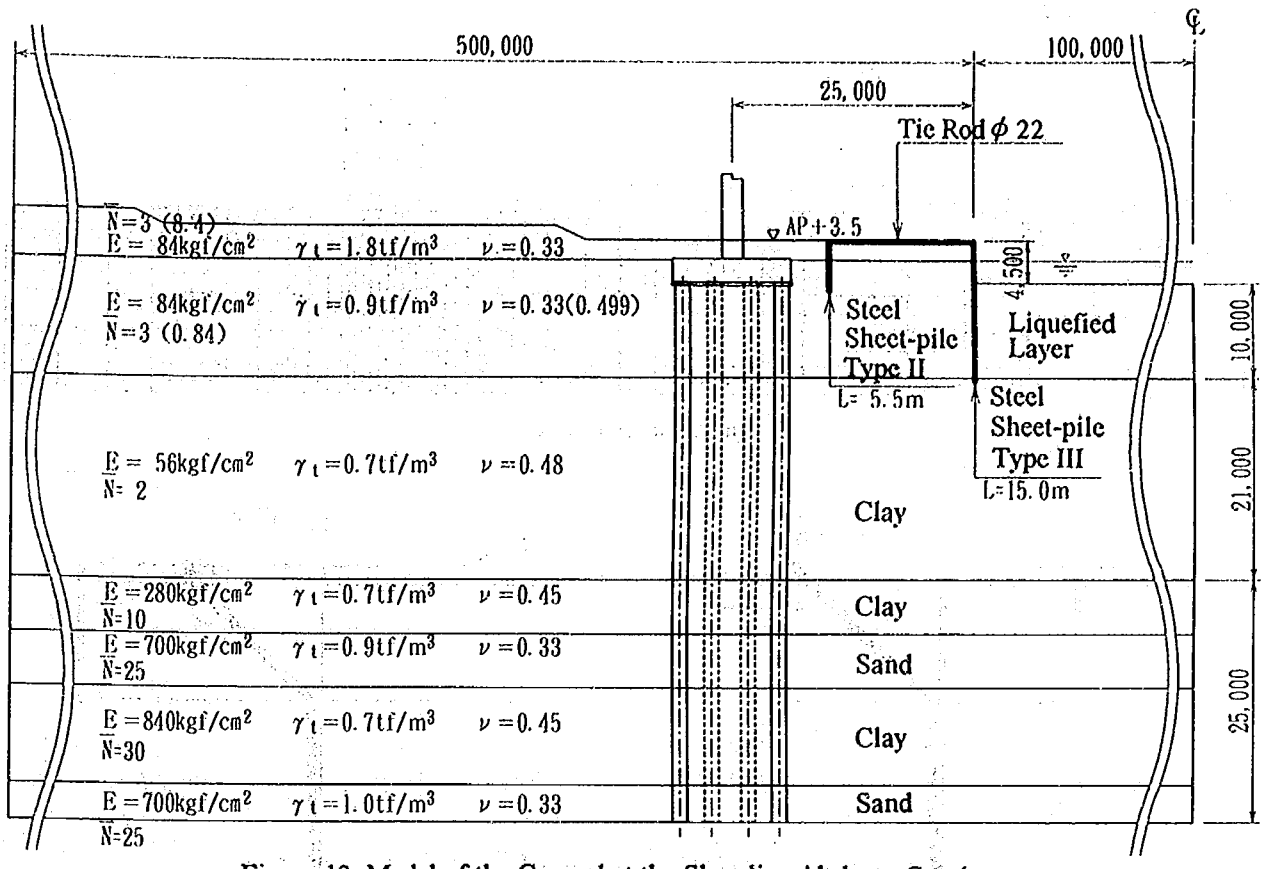
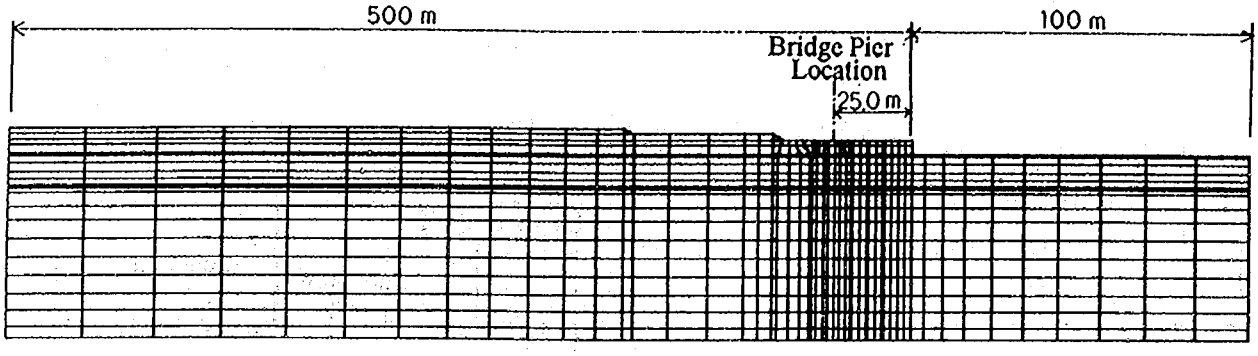


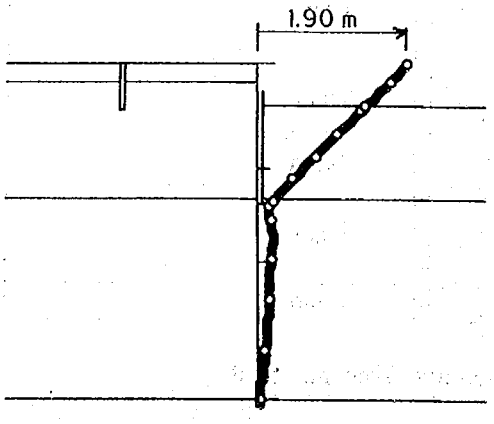
Figure 13. Model of the Ground at the Shoreline Akebono Canal

III (length: 15 m), is linked by tie rods to and supported by a steel sheet-pile Type II with a length of 5.5 m. The liquefied stratum is assumed to extend from the top surface of the footing to a depth of about 12.4 m. The modulus of deformation prior to liquefaction is shown in the same figure. The modulus of deformation was 84 kgf/cm2 for both the non-liquefied stratum above the liquefied stratum and for the liquefied stratum, but after liquefaction, these fell to 1/10 and 1/100 respectively and FEM analysis was used to perform dead weight analysis. Figure 14 shows the depth direction distribution of the ground displacement in the mesh diagram and at various locations. At

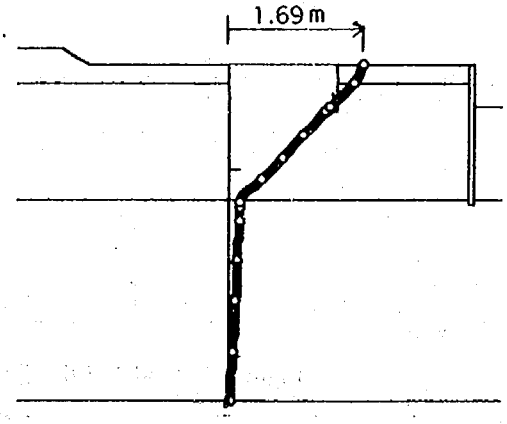
the revetment location, it is inclined towards the sea and the ground is deformed in the shape of an inverted triangle, but as the distance from the revetment increases, the deformation comes to resemble cosin distribution. At the foundation location, ground displacement of 1.69 m is forecast.



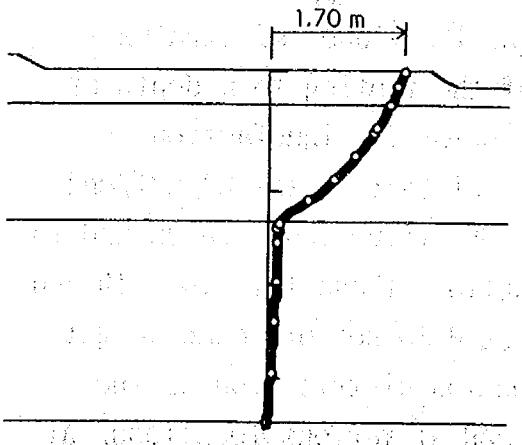
(a) Mesh Diagram



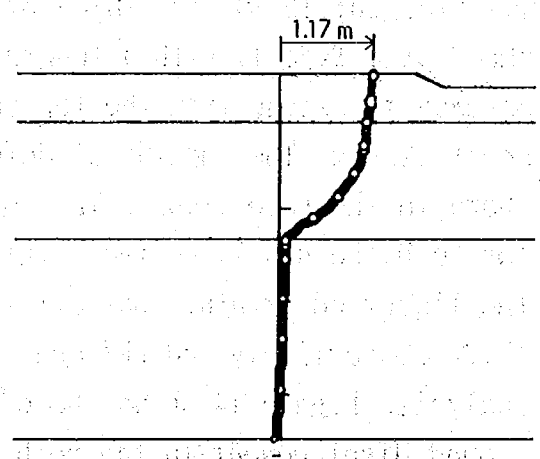
(b) Revetment Location



(c) Foundation Location + (25 m from Revetment)



(d) Location 60 m from Revetment



(e) Location 100 m from Revetment

Figure 14. Analytical Processing of Ground Displacement

Check on the Safety of Pile Foundations

Figure 15 shows the bending moment distribution obtained by allowing the ground displacement found by means of FEM analysis to act on the structure. Based on this, it is forecast that the horizontal displacement of the foundation will be 83.1 cm and the maximum bending moment will exceed the failure moment for all piles.

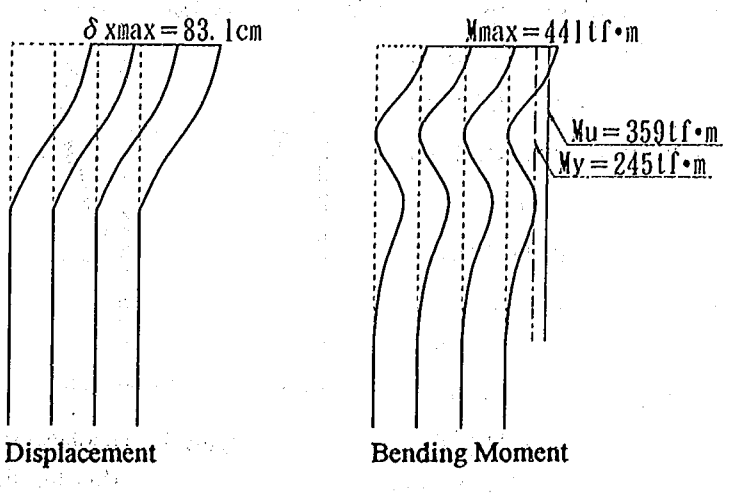


Figure 15. Results of Non-linear Analysis of Piles (Method Considering Ground Displacement)

Design of Ground Flow Damage Protection Measures

A study was performed to propose a measure involving the installation of steel pipe sheet-piles in front of the bridge piers. Figure 16 shows the calculation model. It shows a proposed case in which the tops of the steel pipe sheet-piles are installed close to the boundary between the liquefied and non-liquefied strata. This approach was proposed because it is believed that it will permit a big reduction of the ground displacement by restricting the displacement of the liquefied stratum,

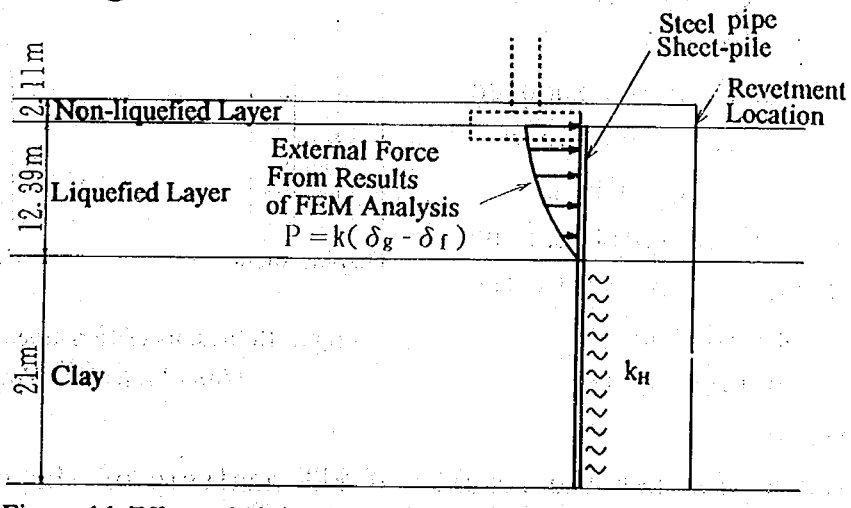
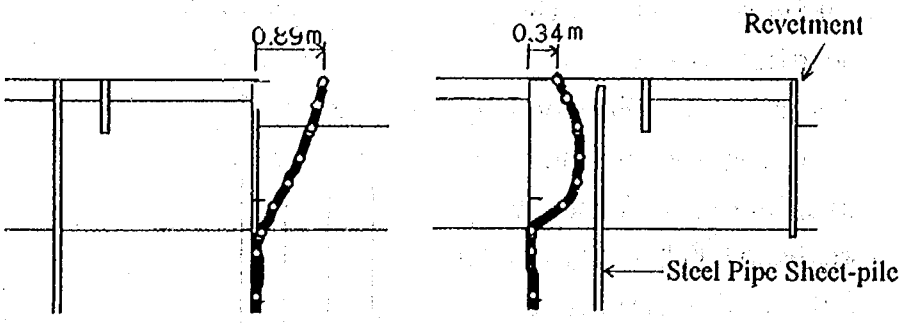


Figure 16. Effects of Sheet-pile Based on the Method Accounting for Ground Displacement (Calculation Model)

and that by preventing large flow pressure in the non-liquefied stratum, it will be possible to design economic protection work. The displacement as external force which was used was the ground displacement at the foundation location. As a result, it was possible to reduce the steel pipe sheet-pile's maximum bending moment (214.8 tf-m/m) to a level below the yield bending moment (355.2 tf-m/m) by installing a row of steel pipe sheet-piles with a diameter of 1.2 m and a sheet thickness of 19 mm. In cases where it is not possible to execute the large diameter steel pipe sheet-piles adopted in this case, multiple rows of steel pipe sheet-piles which can be placed will be installed to control the deformation of the ground.



(a) Revetment Location (b) Foundation Location

Figure 17. Displacement of the Ground After Installation of the Protective Work

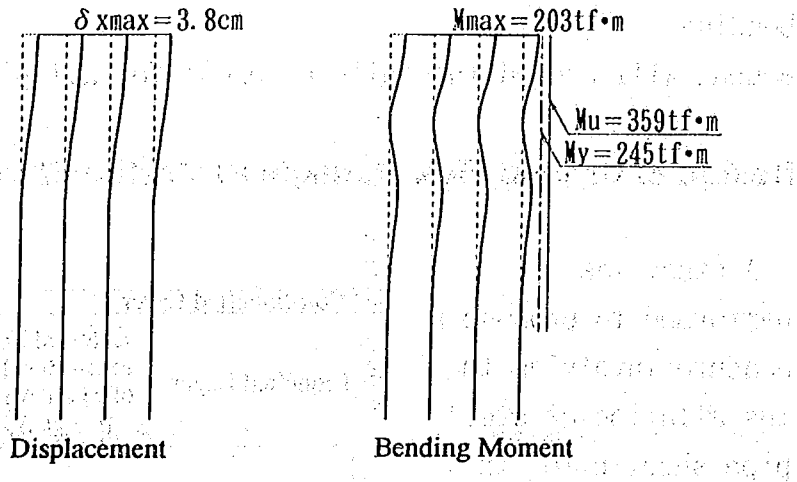


Figure 18. Results of Non-linear Analysis of Piles (After Protective Work)

Figure 17 shows the results of FEM analysis of the displacement of the ground at the revetment location and at the foundation locations when the above steel pipe sheet-piles have been installed. The foundation location displacement is cut sharply to 0.34 m. Figure 18 shows the results of an analysis of the action of this displacement on a bridge pier foundation as an external force. As this figure shows, the displacement of the foundation is cut from 83.1 cm to 3.8 cm and the

maximum bending moment is lower than the yield bending moment, confirming that the safety of the structure is guaranteed by this measure.

Acknowledgements

This report is a summary of details of deliberations now being conducted by the Survey and Research Committee On the Effect of Ground Flow on Viaducts (Committee Chairman: Shioi Yukitaka, Professor at Hachinohe Institute of Technology) at the Technology Research Center for National Land Development. The authors wish to express their gratitude to all the members of the committee for their work.

References

1) Hyogo-ken Nanbu Earthquake Road Bridge Earthquake Damage Countermeasures Committee (1995): Report on a Survey of Damage to Road Bridges by the Hyogo-ken Nanbu Earthquake, pp 55.
2) Ishihara, K. (1995): Soil Properties and Ground Deformation, Report on Hanshin Earthquake, The Japanease Geotechnical Society.
3) Yasuda, S. Masuda, S. Nagase, H. Oda, S. (1994): Dynamic Modulus of Deformation in Undisturbed Material Taken Continuously in the Depth Direction, 9th Japan Earthquake Engineering Symposium, pp. 835 - 840.
4) Kiku, H. Yasuda, S. Masuda, T. Itafuji, S. Mine, K. (1994): Torsional Shear Testing of the Strength and Deformation of Liquefied Sand, 9th Japan Earthquake Engineering Symposium, pp. 871 - 876.

Special Session

Effects of Loading History

(Co-Chairs: K. Kawashima, A. Whittaker)

"Effect of Loading Hysteresis on Ductility of Reinforced Concrete Columns"
by J. Hoshikuma, S. Unjoh, K. Nagaya
Presented by: Jun-ichi Hoshikuma

"Testing Methodologies for the Seismic Performance of Reinforced Concrete Bridge Piers"
by A. Taylor
Presented by: Andrew Taylor

EFFECT OF LOADING HYSTERESIS ON DUCTILITY OF REINFORCED CONCRETE COLUMNS

Jun-ichi Hoshikuma[1], Shigeki Unjoh[2] and Kazuhiro Nagaya[3]

1) Research Engineer, Earthquake Engineering Division, Public Works Research Institute
2) Head, Earthquake Engineering Division, Public Works Research Institute
3) Research Engineer, Earthquake Engineering Division, Public Works Research Institute

ABSTRACT

A controlled cyclic lateral displacement pattern with gradually increasing amplitude has been classically applied to test specimens. In such cyclic loading test, a definition of cyclic number is very important, because it affects the ductility of reinforced concrete columns significantly. In this paper, a series of four identical reinforced concrete bridge columns were loaded with various cyclic number, and the differences in observed damage were studied. The skeleton model of strength-displacement relation for reinforced concrete bridge columns was idealized, and the ultimate point was determined to be applicable to seismic design. Furthermore, the evaluation method of the ultimate curvature/displacement taking account into effect of cyclic number was proposed. It is found from a comparison with test results that calculated ultimate displacements correspond well to observed ultimate displacements when cover concrete initiates spalling-off.

INTRODUCTION

Characteristics of ground motion during the Hyogo-ken Nanbu Earthquake were significantly different from one in past earthquakes. In the Hyogo-ken Nanbu Earthquake, the elastic acceleration response spectrum was recorded as approximately 2.0G, although the current design elastic acceleration response spectrum is 0.7G to 1.0G. On the other hand, the duration time of the ground motion is so short that cyclic number of seismic response in columns is small as compared with response during past recorded ground motions in Japan.

In studies of the ductility evaluation of reinforced concrete columns, a controlled 10-cyclic lateral displacement pattern with gradually increasing amplitude has been classically applied to test specimens. This is because the ductility factor is used for the seismic design supposing an earthquake with long duration time so that large cyclic number of response will be expected. On the other hand, it has been found that the effect of loading hysteresis on the ductility of reinforced concrete columns is significant. Consequently, in the seismic design sopposing ground motion such as the Hyogo-ken Nanbu Earthquake, the ductility factor should be evaluated based on the loading test by small cyclic number.

In this paper, four identical reinforced concrete column specimens were loaded with various cyclic number, and the effect of loading hysteresis was examined. A skeleton of lateral force-displacement relation was idealized, and evaluation method of the ductility was proposed to be applicable to the seismic design based on the test results.

CYCLIC LOADING TESTS OF REINFORCED CONCRETE BRIDGE COLUMNS WITH VARIOUS CYCLIC NUMBER

Test Specimens

To examine the effect of cyclic number on response, four identical specimens shown in Fig. 1 were constructed. A cross section is square with 60cm dimension, and a column height is 3.01m so that an aspect ratio is 5.0. There are forty-eight longitudinal reinforcing bars of SD295/D10 in the section, and square hoops of SD295/D6 with 75mm spacing. The ratio of longitudinal reinforcing bar to cross sectional area is 0.95%, and the volumetric ratio of hoops is 0.3%. Curvature of sections were measured through the section from the base to 520mm column height by LVDTs as shown in Fig. 1.

Test Setup and Loading Pattern

The footing of test specimens were fixed to the reaction wall, and a controlled lateral displacement was supplied to the column top by a dynamic actuator. A static axial loading of 353kN was also given, which corresponded to 0.98MPa in a uniaxial stress.
A first-yield displacement 1 δ_{yo} was determined here as a displacement at the top of column when the longitudinal reinforcing bars yielded at the base section. The lateral cyclic displacement was applied with gradually increasing amplitude under the displacement control. Based on observed strain of longitudinal reinforcing bars at the base section, the first-yield displacement was defined here as 11mm.
The displacement hysteresis histories applied to specimens were shown in Fig. 2. The cyclic numbers in each loading step for P-1, P-2 and P-3 were one, three and ten, respectively. In P-4, the loading pattern ($\pm$ 1 δ_{yo}, $\pm$ 3 δ_{yo}, $\pm$ 5 δ_{yo}, $\pm$ 15 δ_{yo}) was different from others.

Observed Hysteresis Curves and Damage Mode

Fig. 3 shows the observed lateral force-displacement hysteresis curve. The peak strength of every specimen was approximately 150kN, so that the effect of cyclic number on the strength was less significant. It can be, however, observed that the cyclic number affected the ductility, and a displacement when the lateral force deteriorated was large as the cyclic number was small. Damages developed on the transversal face of specimens are illustrated in Fig. 4. As compared the damage after 5 δ_{yo} loading step, cover concrete spalled and longitudinal reinforcing bars buckled in P-3, on the other hand, only the horizontal cracks were developed in other specimens. This means that the damage propagation accelerates as the cyclic number becomes large.

DUCTILITY EVALUATION

Skeleton Model for Lateral Force-Displacement Relation of Reinforced Concrete Columns

A lateral response of reinforced concrete column can be approximated by elasto-plastic curve as shown in Fig. 5. A yield curvature and a yield displacement are calculated as

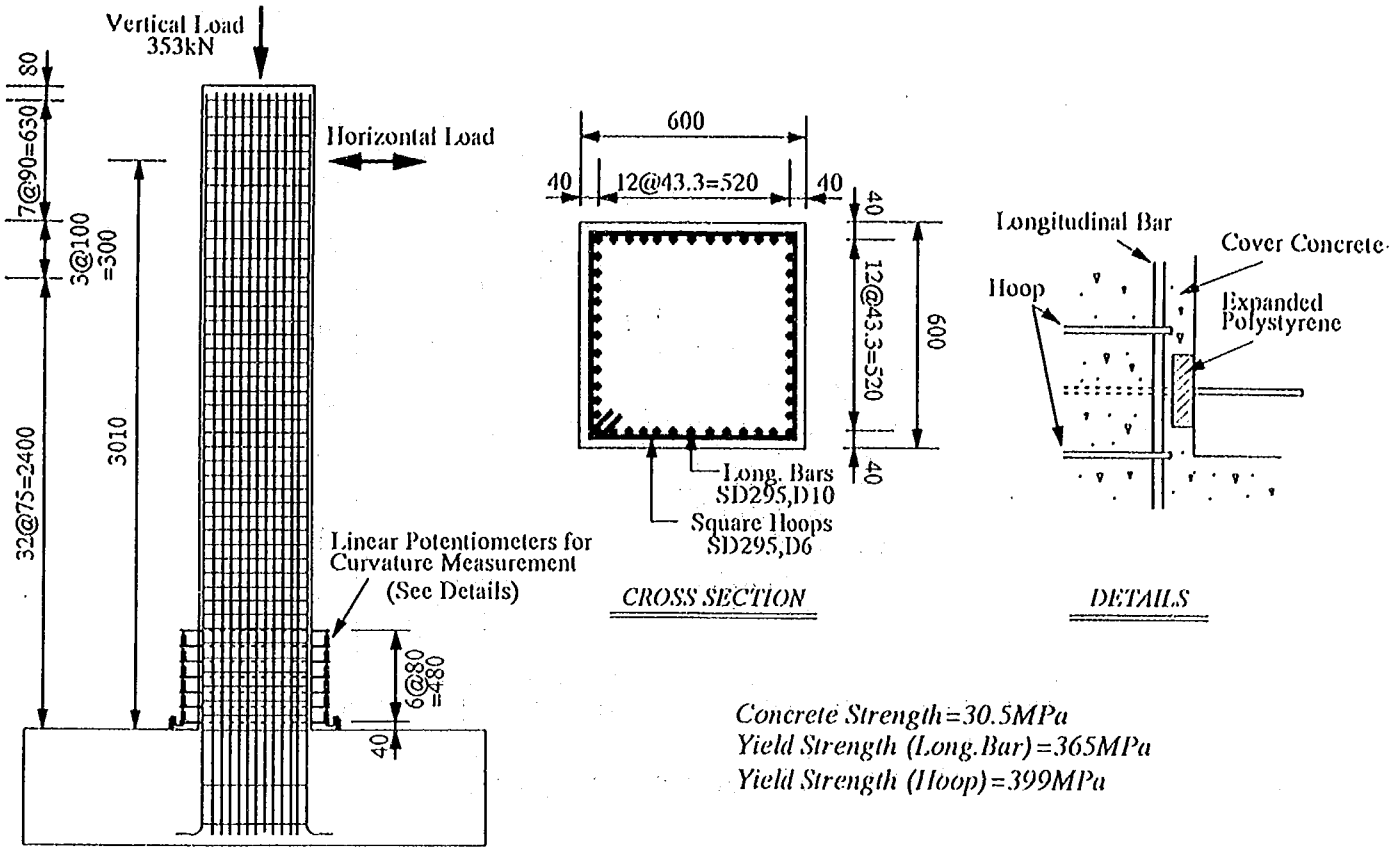


Fig. 1 Test Specimen

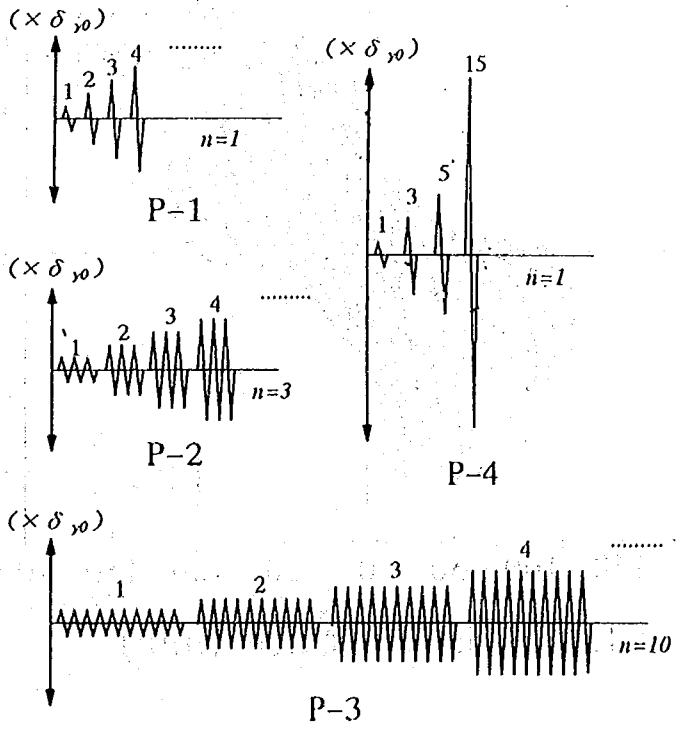
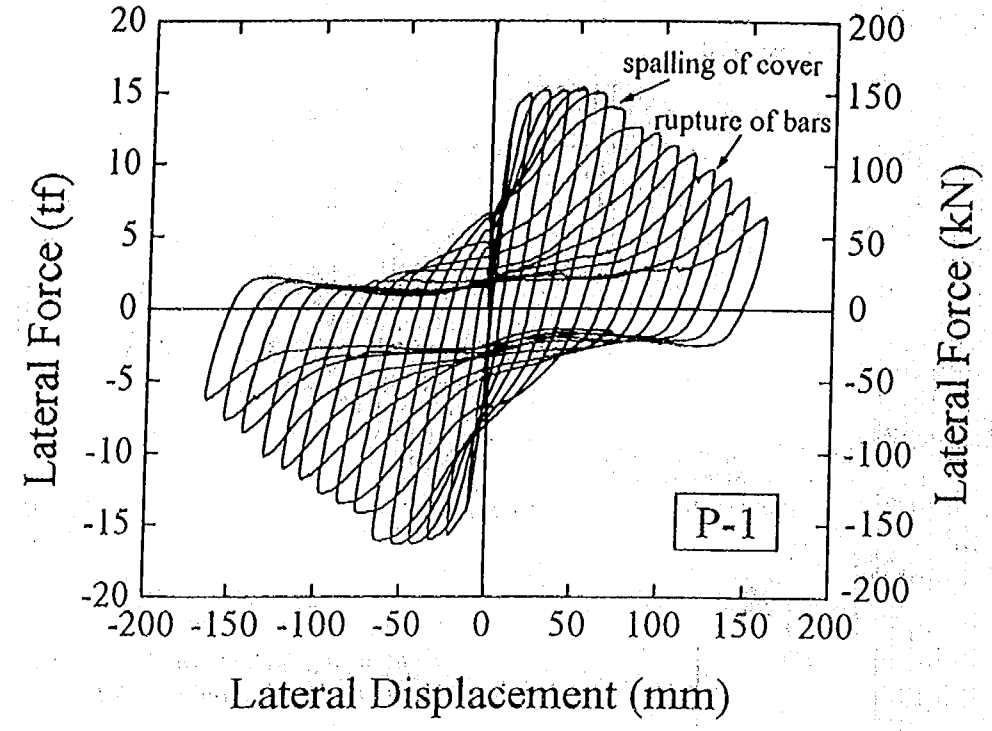
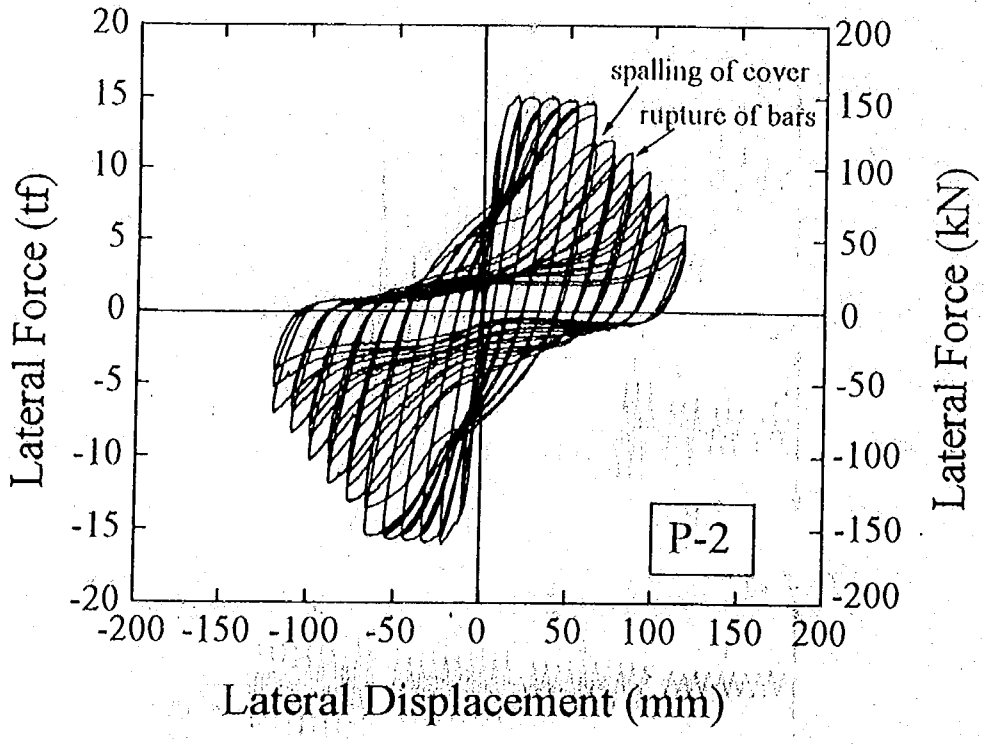


Fig. 2 Loading History

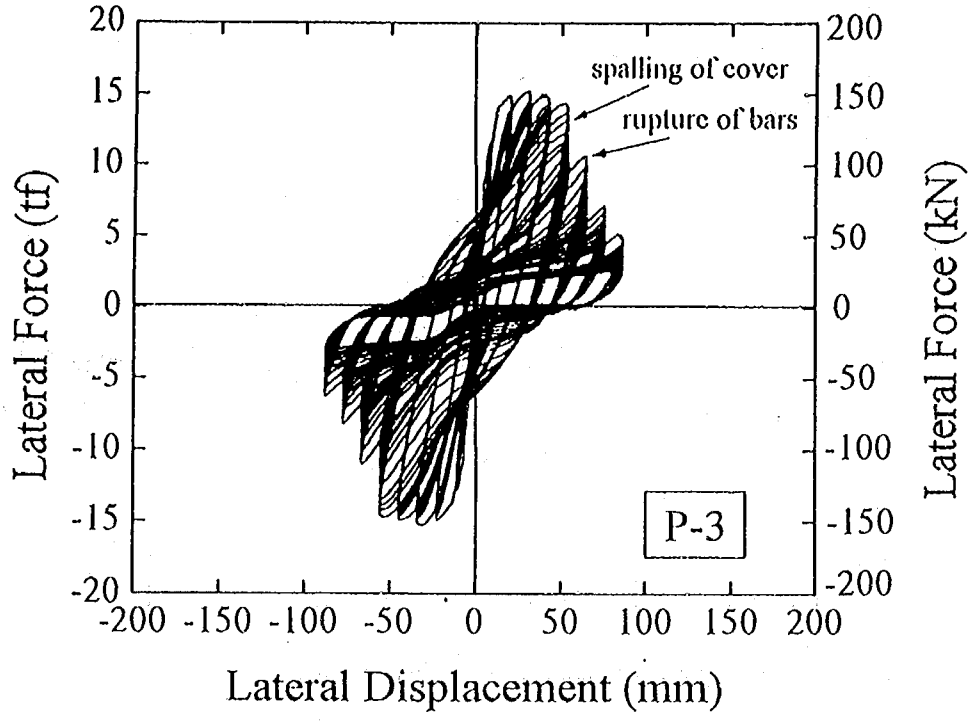


(a) P-1 Specimen (1-Cycle in Each Step)

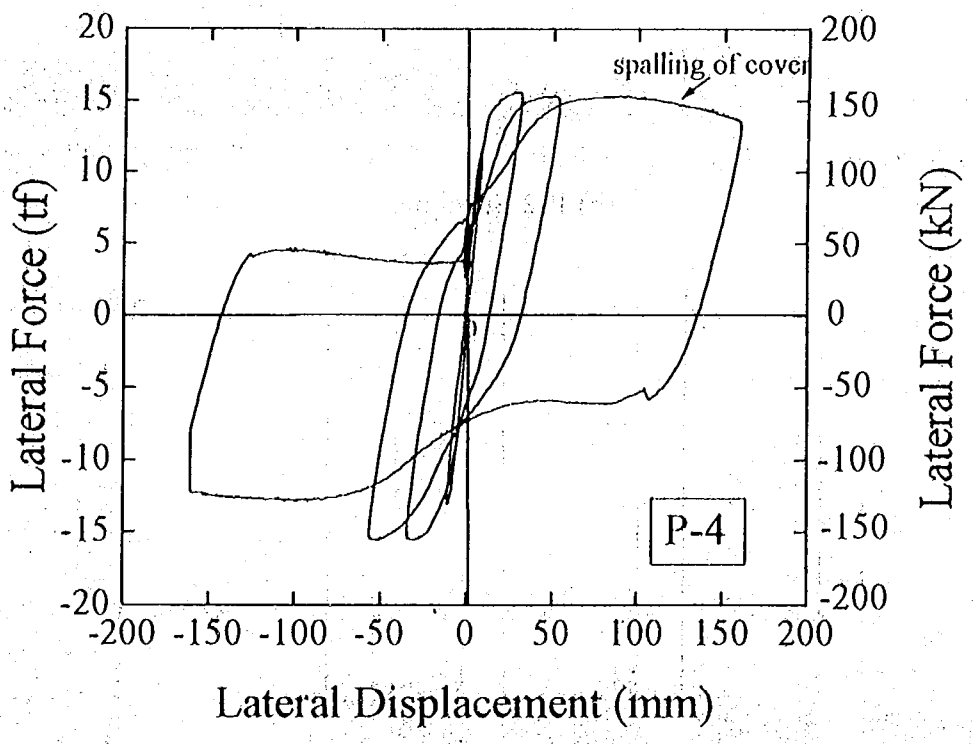


(b) P-2 Specimen (3-Cycle in Each Step)

Fig. 3 Observed Hysteresis Curves

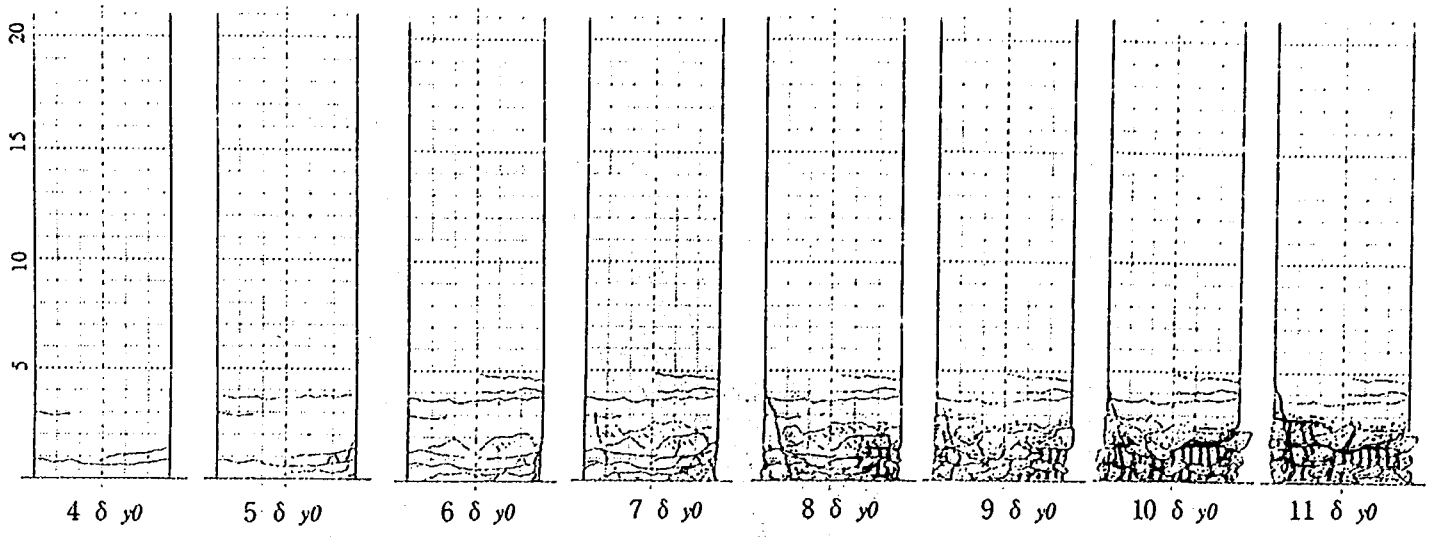


(c) P-3 Specimen (10-Cycle in Each Step)

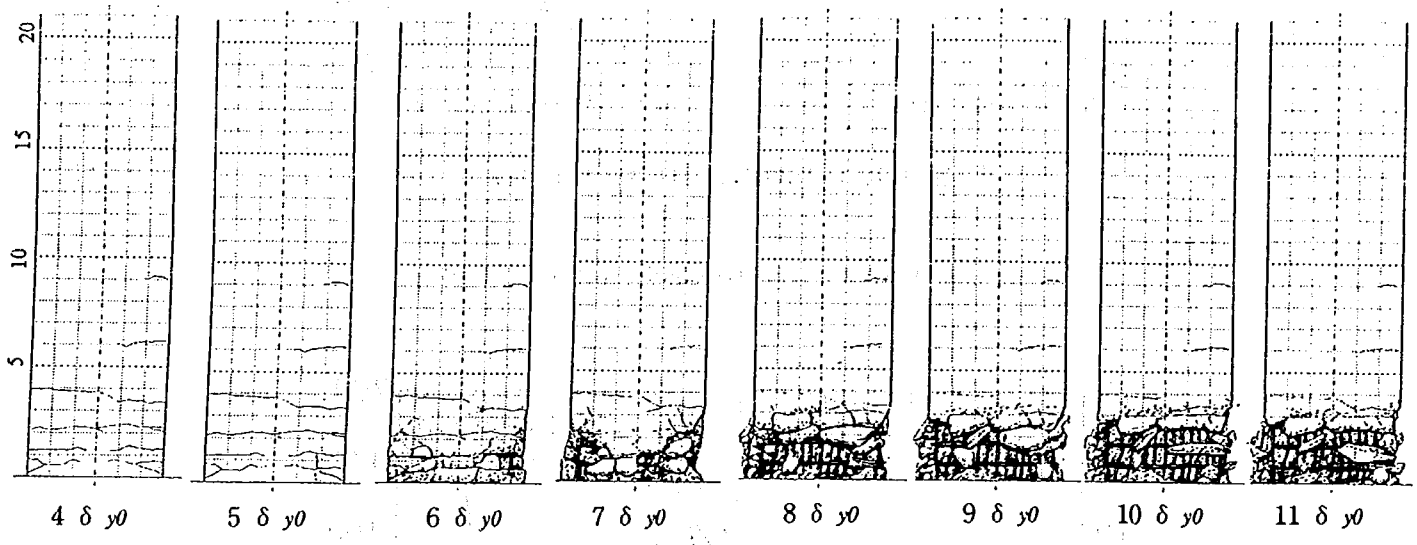


(d) P-4 Specimen (1-Cycle)

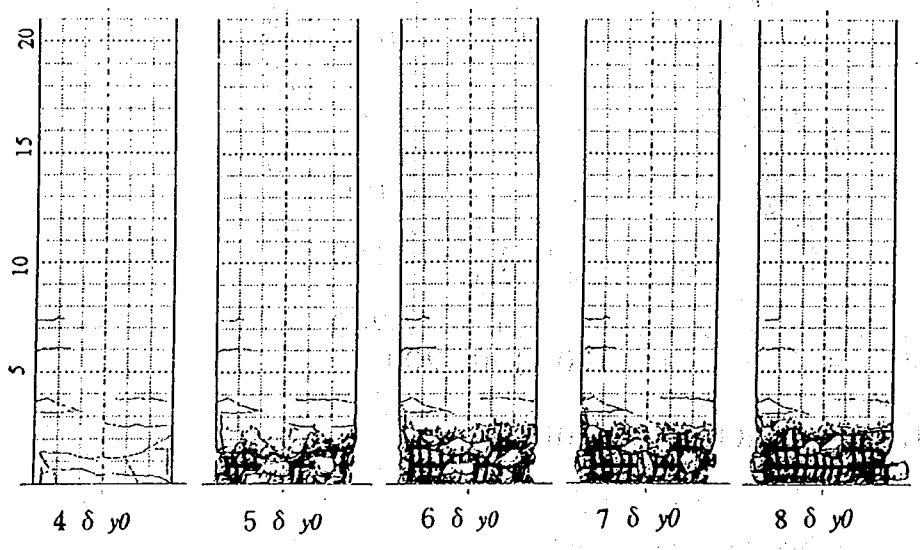
Fig. 3 Observed Hysteresis Curves



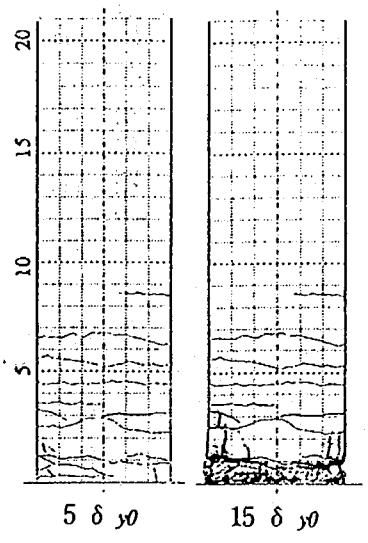
(a) P-1 Specimen



(b) P-2 Specimen



(c) P-3 Specimen



(d) P-4 Specimen

Fig. 4 Damage Propagation

$$\phi_y = (M_u / M_{yo})\,\phi_{yo} \quad (1)$$

$$\delta_y = (M_u / M_{yo})\,\delta_{yo} \quad (2)$$

where, ϕ_y, δ_y: yield curvature and yield displacement,
ϕ_{yo}, δ_{yo}: first-yield curvature and first-yield displacement, and
M_{yo}, M_u: first-yield moment and ultimate moment.

In the skeleton curve, an idealization is not made for the lateral force deteriorating branch, in which the lateral force-displacement hysteresis response is unstable due to failure of core concrete section following buckling of longitudinal reinforcing bars as shown in Fig. 3.

Some definitions of the ultimate condition have ever been proposed as the lateral force deteriorates to 80% of the peak lateral strength or to the first-yield strength. However, it should be noted how a displacement ductility factor is applied to the seismic design by an equal-energy approach, in which the lateral design force is reduced according to the displacement ductility factor. Applicability of the equal-energy approach to seismic design of fixed-base cantilever columns has been examined by Kawashima et al. In their studies, it is concluded that equal-energy approach would be applicable to a prediction of inelastic response of reinforced concrete columns as long as hysteresis curves can be idealized by Mutou model. It can be observed in Fig. 3 that response hysteresis tends to be unstable after cover concrete is spalling-off. The event of spalling-off of cover concrete indicates that longitudinal reinforcing bars buckle and damage has developed to a core section, which results in the unstable response. The ultimate point, therefore, would be theoretically determined as cover concrete spalls-off, for seismic design by the equal-energy approach.

Ultimate Strain of Confined Concrete and Moment-Curvature Analysis

A moment-curvature relation of sections was calculated based on stress-strain curve of the confined concrete. In the analysis, a model of Hoshikuma et al. shown in Fig. 6 was used for the stress-strain model of confined concrete, because their model was developed for reinforced concrete columns with structural details specific in Japanese design codes. To evaluate the effect of cyclic characteristic of response, two ultimate strains of concrete are defined for small cyclic number loading (Loading Type-I) and large one (Loading Type-II) as

$$\varepsilon_{cu} = \begin{cases} \varepsilon_{cc} & \text{for Type-I Loading} \\ \varepsilon_{cc} + 0.8\,\sigma_{cc} / E_{des} & \text{for Type-II Loading} \end{cases} \quad (3)$$

where, σ_{cc} is a peak stress of confined concrete, ε_{cc} is a strain at peak stress, and E_{des} is a deteriorating rate.

The strain distributions at the first-yield and ultimate conditions were assumed here as shown in Fig. 7. It should be noted that the ultimate strain is given at the outermost confined point, where longitudinal reinforcing bars are placed on the section. The compressive stress developed at cover concrete is assumed to be zero because cover concrete is expected to crash at the ultimate stage.

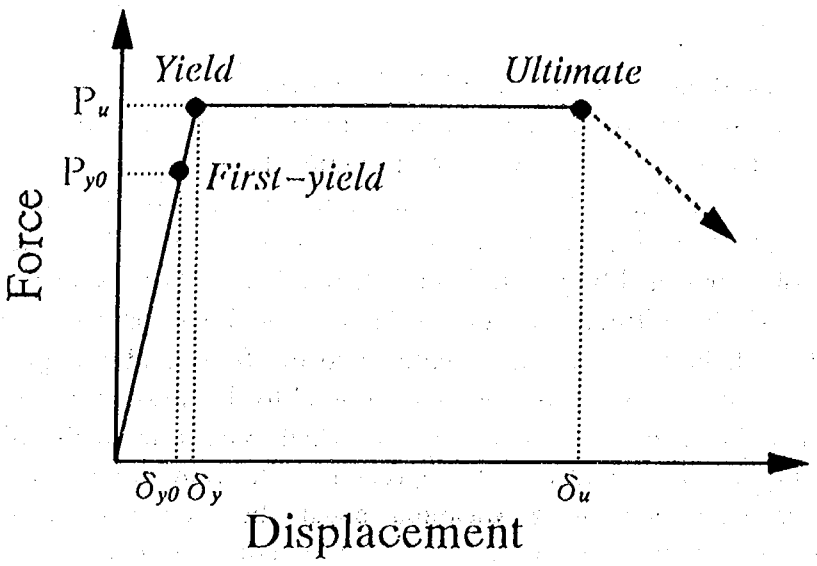


Fig.5 Skeleton Model of Lateral Force-Displacement Relation for Seismic Design

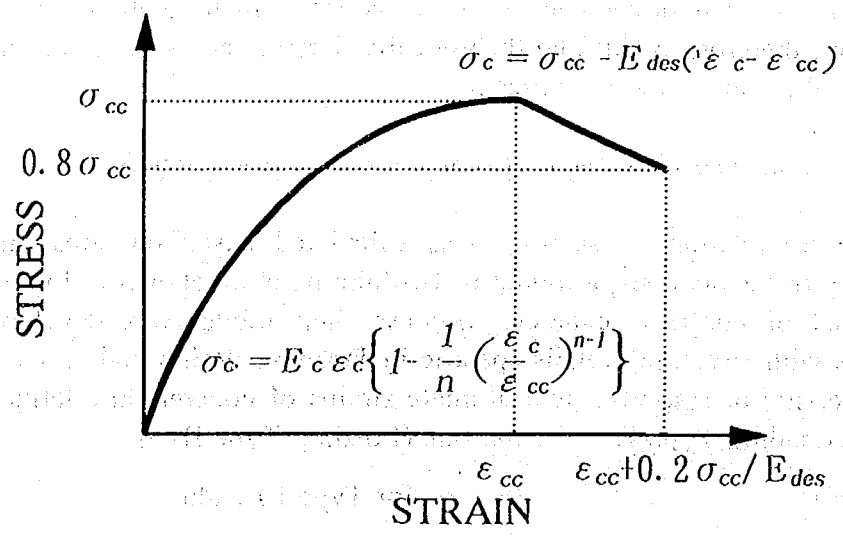


Fig.6 Stress-strain Model of Confined Concrete

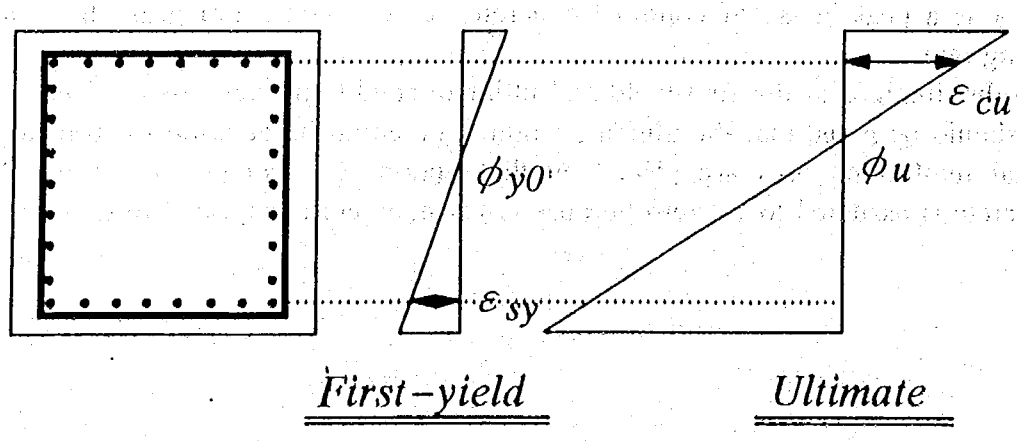


Fig.7 Strain Distributions at First-yield and Ultimate Conditions

Lateral Displacement

The first-yield displacement is calculated by integrating curvature developed in whole section through the column height when the base moment reaches a first-yield moment M_{yo}, and written as

$$\delta_{yo} = \frac{H^2}{6}\{(\phi_c + 2\phi_{yo}) - (\phi_{yo} - \phi_c)\frac{M_c}{M_{yo}} - \phi_{yo}\frac{M_c^2}{M_{yo}^2}\} \quad (4)$$

where, M_c and ϕ_c are cracking moment and cracking curvature, respectively. The yield displacement is calculated by substituting Eq. (4) to Eq. (2).
The ultimate displacement is given by the yield curvature of section and the yield displacement defined in Eqs (1) and (2), and described by

$$\delta_u = \delta_y + (\phi_u - \phi_y) L_p (H - L_p / 2) \quad (5)$$

where, L_p is an equivalent plastic hinge length.

ANALYSIS FOR SPECIMENS AND COMPARISON WITH TEST RESULTS

Curvature Distributions and Equivalent Plastic Hinge Length

Fig. 8 shows measured plastic curvature distributions at the determined ultimate displacements which are 6.5 δ_{yo} for P-1, 6 δ_{yo} for P-2, and 5 δ_{yo} for P-3. The plastic curvature is calculated by subtracting the yield curvature given in Eq. (1) from measured ultimate curvature. Note that the curvature developed at section from base to 40mm height is assumed to be caused by yield penetration of longitudinal reinforcing bars to footing, so that no indicator is drawn in the chart, to distinguish the elasto-plastic column deformation from the rotation due to the yield penetration. The plastic curvature was measured through the section from bottom to 440mm column height in any specimens.
Table 1 shows the moment-curvature relations of test specimens calculated by above analytical model. It was supposed in Eq. (3) that the 10-cyclic loading be Type-I Loading and the 1- or 3-cyclic loading be Type-II Loading. An equivalent plastic hinge length was given by the distribution of measured plastic curvature ϕ_{EXP} and the calculated ultimate plastic curvature ϕ_{CAL}, and written as

$$L_p = (\int \phi_{EXP}\, dh) / \phi_{CAL}$$
$$= (\Sigma \phi_{EXP} \triangle h) / \phi_{CAL} \quad (6)$$

where, $\triangle h$ is a gauge length for curvature measurement, and is 80mm in the test. It can be found that the equivalent plastic hinge length was estimated as 300mm to 330mm in test specimens with 600mm cross sectional dimension.

Lateral Strength and Displacement Ductility

The lateral force-displacement relations of specimens were calculated by Eqs. (4) and (5) based on the moment-curvature analysis, and compared with measured hysteresis envelopes as shown in Fig. 9. The measured rotational displacements due to yield penetration of longitudinal

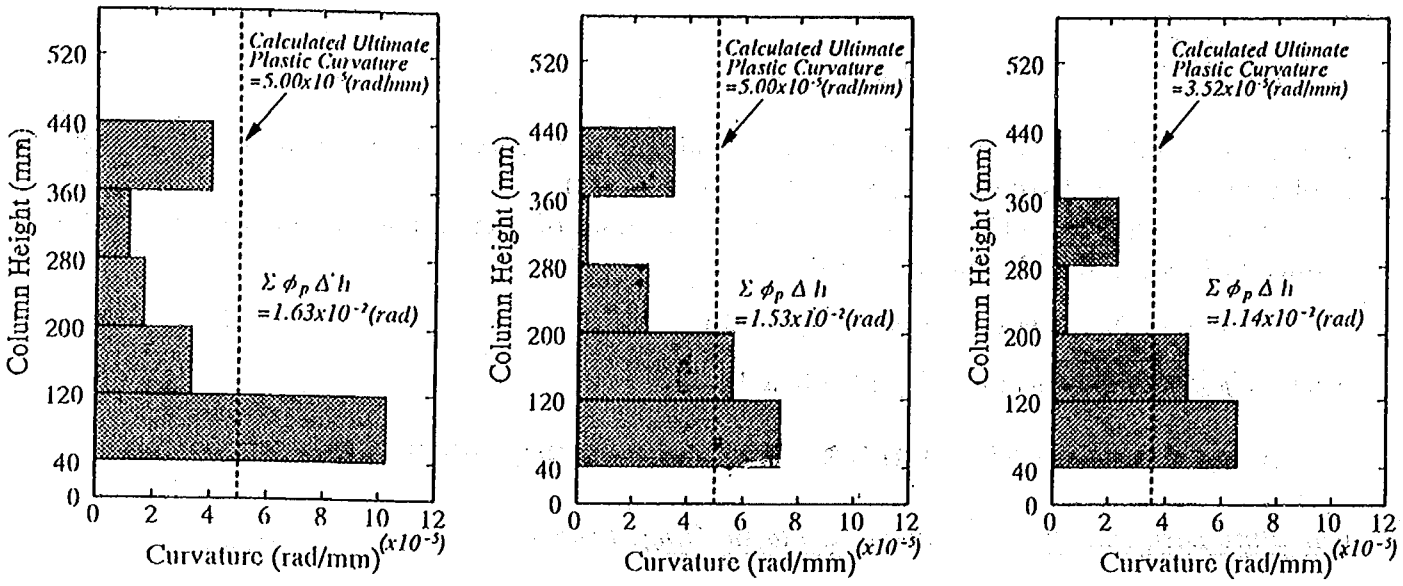
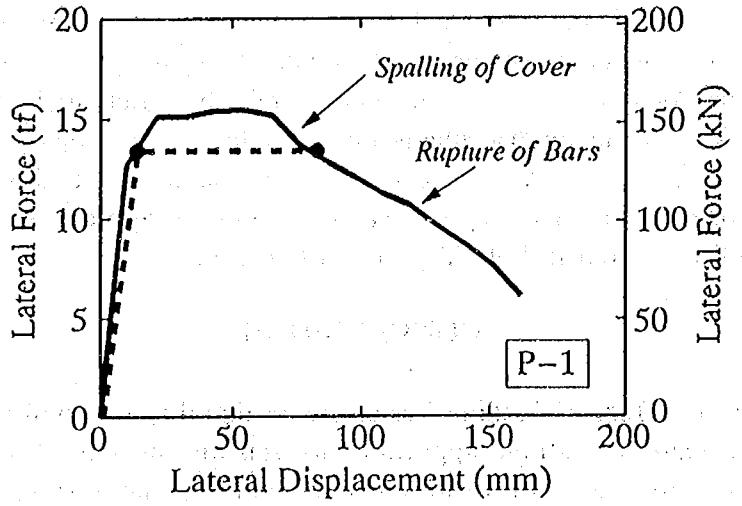


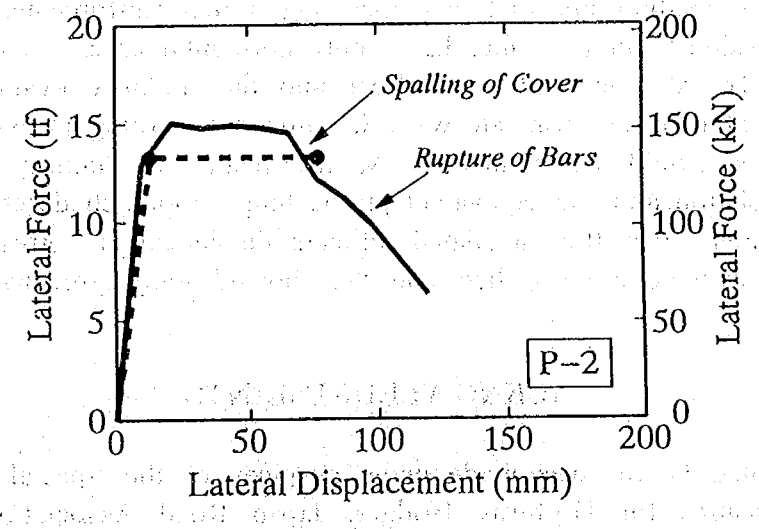
Fig. 8 Plastic Curvature Distributions at Potential Plastic Hinge Region

Table 1 Calculated Moment-Curvature Relation and Equivalent Plastic Hinge Length

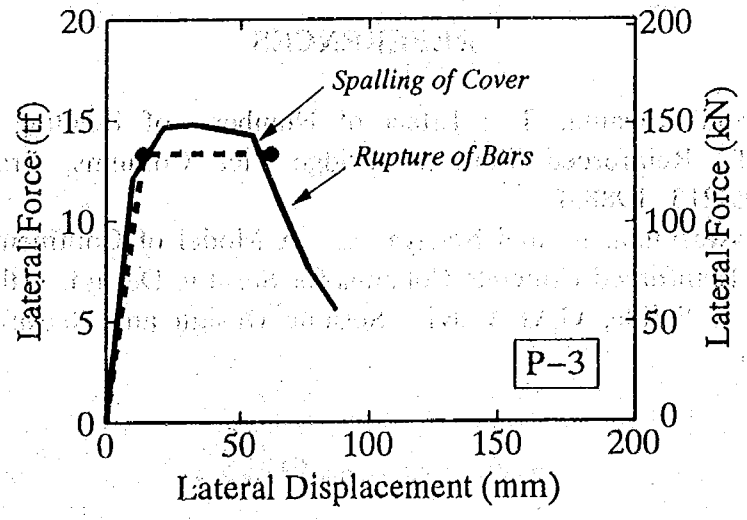
Specimen		P-1	P-2	P-3
Loading Type		Type II		Type I
First-yield	Flexural Strength M_{y0} (kJ)	337.8		337.8
	Curvature ϕ_{y0} (rad/mm)	4.44×10^{-6}		4.44×10^{-6}
Yield	Flexural Strength M_y (kJ)	392.3		392.3
	Curvature ϕ_y (rad/mm)	5.16×10^{-6}		5.16×10^{-6}
Ultimate	Flexural Strength M_u (kJ)	392.3		392.3
	Curvature ϕ_u (rad/mm)	5.52×10^{-5}		4.04×10^{-5}
Plastic Curvature ϕ_p (rad/mm)		5.00×10^{-5}		3.52×10^{-5}
$\Sigma \phi_p \Delta$ h (rad)		1.63×10^{-2}	1.53×10^{-2}	1.14×10^{-2}
Equivalent Plastic Hinge Length L_p (mm)		326	306	324



(a) P-1 Specimen



(b) P-2 Specimen



(c) P-3 Specimen

Fig. 9 Observed Envelopes of Lateral Force-Displacement Relation and Calculated Skeleton Curves

reinforcement were included in calculated displacements. The estimated lateral strength is equivalent to the strength when cover concrete initiates to spall-off, which corresponds well to assumption of the analytical model. On the other hand, the calculated ultimate displacements show good agreement with the displacements just after the cover concrete spalls, which is just ultimate condition determined in above section. It can be also found that tentative ultimate strains of confined concrete given in Eq. (3) would be roughly appropriate, because the ultimate displacements are well predicted in both Type-I and II loadings.

CONCLUSIONS

This paper presented the effect of loading hysteresis on ductility of reinforced concrete columns and proposed its evaluation method applicable to seismic design. The identical reinforced concrete columns were loaded with various cyclic number, and test results showed that the controlled displacement history given to top of columns affected the ductility significantly. In case of column with the volumetric ratio of lateral steel bars of 0.3%, it was observed from comparison during the loading step of 5 δ_{yo} that longitudinal reinforcements buckled seriously in P-3 (10-cyclic loading), on the other hand, only horizontal cracks were developed in P-1 (1-cyclic loading). To take account such effect into the ductility evaluation, two ultimate compression strains of confined concrete were determined according to cyclic number, so that two ductility factors would be estimated. At the result of ductility analysis based on moment-curvature relation and the equivalent plastic hinge approach described here, it can be found in any specimens that the calculated ultimate displacement corresponded well to the displacement when cover concrete spalled, and also showed good agreement with the proposed ultimate condition.

ACKNOWLEDGEMENTS

The research presented herein was made under auspices of the Special Sub-Committee for Seismic Countermeasures for Highway Bridges, Japan Road Association (Chair: Prof. K. Kawashima, Tokyo Institute of Technology). The authors extend their sincere appreciation to the strong support of Prof. K. Kawashima.

REFERENCES

1) Kawashima, K. and Koyama, T. : Effect of Number of Loading Cycles on Dynamic Characteristics of Reinforced Concrete Bridge Pier Columns, Proceed-ings of JSCE, No.392/I-9, pp.205-213, 1988.4
2) Hoshikuma, J., Kawashima, K. and Nagaya, K. : A Model of Confinement Effect on Stress-strain Relation of Reinforced Concrete Columns for Seismic Design, 11th WCEE, 1996.6
3) M.J.N. Priestley, F. Seible, G.M. Calvi : Seismic Design and Retrofit of Bridges, Wiley-Interscience, 1996

TESTING METHODOLOGIES FOR THE SEISMIC PERFORMANCE OF REINFORCED CONCRETE BRIDGE PIERS

Andrew W. Taylor, Ph.D., P.E.
Building and Fire Research Laboratory
National Institute of Standards and Technology
Gaithersburg, Maryland

ABSTRACT

Standards for seismic testing of reinforced concrete bridge piers are discussed. Because there are no commonly accepted testing protocols or reporting requirements for tests of bridge piers, it is often difficult to compare data obtained from different research programs. If certain basic data were recorded in all tests of bridge piers, and if this data were reported in a uniform format, much more could be learned from the collective body of data obtained in research programs around the world. The purpose of this paper is to provide a basis for development of international standards for testing bridge piers. The main issues discussed are test configuration; scaling; force and displacement variables; axial stress level; symbols and units; and load path.

INTRODUCTION

The purpose of this paper is to discuss several of the primary issues related to development of protocols for testing reinforced concrete bridge piers and for reporting test results. Because there are no commonly accepted testing protocols or reporting requirements for tests of reinforced concrete bridge piers, it is often difficult to compare data obtained from different research programs. If certain basic data were recorded in all tests of bridge piers, and if this data were reported in a uniform format, much more could be learned from the collective body of data obtained in research programs around the world.

While standard testing and reporting protocols have been developed in the United States for steel structures (Applied Technology Council, 1992), similar standards do not exist for reinforced concrete structures. It is hoped that the discussions in this paper will serve as a catalyst for development of standardized testing and reporting procedures for the seismic performance of reinforced concrete bridge piers. Several issues are raised and discussed, and in some cases possible approaches to developing protocols are presented. The issues discussed are test configuration; scaling; force and displacement variables; axial stress level; symbols and units; and load path.

ISSUES IN THE DEVELOPMENT OF PROTOCOLS FOR TESTING AND REPORTING

Test Configuration

A variety of specimen types have been employed in bridge pier testing programs. However, most of these specimens are minor variations of three basic configurations: cantilever specimens (Figure 1a); double ended specimens (Figure 1b); and double curvature specimens (Figure 1c). In the United States, cantilever specimens have been most common, although other types of specimens have also been tested. Double-ended specimens and cantilever specimens have been the most common in New Zealand. Double curvature specimens have been used widely in Japan, as well as cantilever specimens.

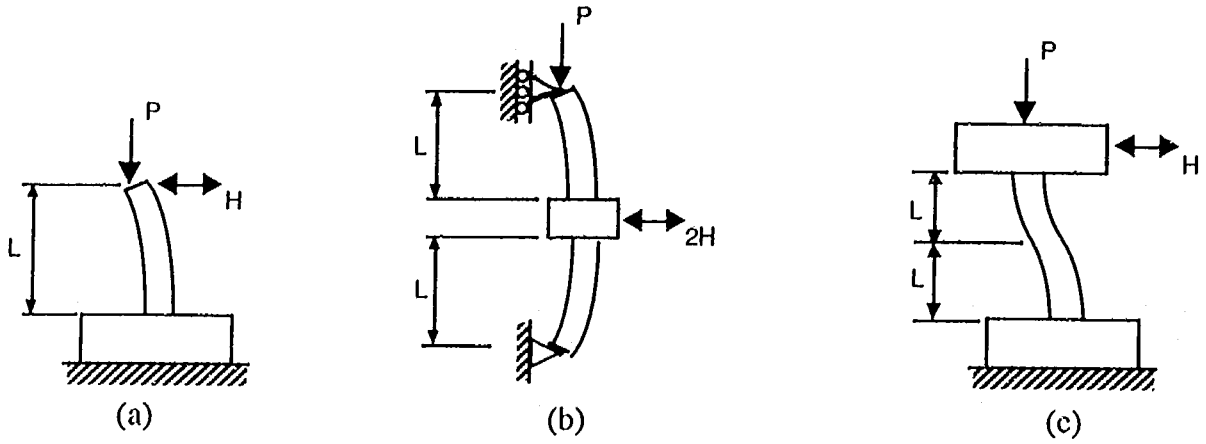


Figure 1. Common bridge pier test configurations: (a) cantilever specimen; (b) double ended specimen; (c) double curvature specimen

The choice of test specimen configuration usually depends on two factors: the test apparatus available; and the configuration of the prototype bridge pier being investigated (e.g. tall flexure-dominated cantilever piers; or short, shear-dominated piers fixed at both ends). While it may not be necessary to establish standardized test specimen configurations, it is important to establish standardized terminology and data reporting formats. For example, the length of the specimen "L" might be defined as the length of an equivalent cantilever specimen, as shown in Figure 1(a), (b) and (c). Similarly, the displacement reported could be defined as the displacement of the equivalent cantilever: this would be simply the displacement of the pier tip in figure 1(a); the displacement of the center stub in figure 1(b); and one-half the relative lateral displacement of the top and bottom transfer beams in figure 1(c).

Scaling

Relatively few full-scale bridge piers have been tested, primarily because of the high forces and displacements required. Most laboratory tests of bridge piers are carried out on reduced scale specimens with scale factors in the range 1/6 to 2/3. In evaluating results from such tests, the effects of scaling must be considered.

A comparative study of full-scale and 1/6-scale bridge pier tests was conducted at the National Institute of Standards and Technology (Stone and Cheok, 1989). In this study two full-scale (1.5 m diameter) cantilever bridge piers were subjected to cyclic lateral loads in the inelastic range, and simultaneous constant axial load. The height-to-diameter ratios of the two full scale piers were 6 and 3. In another phase of the study, geometrically similar specimens were constructed at 1/6 scale and tested under the same loading regimen as the full scale specimens. Two types of concrete were used in the 1/6 scale specimens: a "microconcrete", in which both coarse aggregate (gravel) and fine aggregate (sand) were scaled geometrically, and an approximately scaled concrete in which the coarse aggregate was scaled geometrically and the fine aggregate was not scaled. It was found that the performance of the model piers made with the approximately scaled concrete were very close to the performance of the full scale piers. On the other hand, some aspects of the performance of the model piers made with "microconcrete" were not close to the performance of the full scale piers. Specifically, the microconcrete models were more flexible than the full scale piers, strength degradation was more rapid, and ultimate ductility was lower. Thus, it was concluded that the 1/6 scale specimens with approximately scaled aggregate could adequately represent the behavior of the full scale piers.

Based on the NIST study described above, model specimens with scale factors as low as 1/6, and constructed of concrete with geometrically scaled coarse aggregate, appear to be

representative of full scale specimens. However, opinions vary on the lowest feasible scale factor for bridge pier test specimens. Some researchers take a more conservative approach and limit scale factors to no less than 1/2. There is a need for more definitive guidance on scaling of bridge pier test specimens so that proper interpretations may be made of results from tests on small scale specimens.

Force and Displacement Variables

The most important variables reported in tests of bridge piers are the measures of forces and displacement applied to the specimens. In past research programs a number of different variables have been recorded and reported. Force-type variables have included lateral force; axial force; and moment at fixed ends of the specimen. Displacement-type variables have included lateral displacement; displacement ductility; curvature; curvature ductility; and lateral drift (lateral displacement divided by specimen height). In addition, some researchers have reported the energy dissipated by the specimen, calculated as the area bounded by lateral load-displacement hysteresis loops. Researchers have measured and reported the force and displacement variables which best serve the objectives of their test program. However, the use of different force and displacement variables makes it difficult to compare data from independent test programs.

One of the most commonly reported variables has been ductility (either displacement or curvature ductility). The most difficult aspect of calculating ductility prior to a test, or measuring ductility during a test, is determining the yield displacement of the specimen. Yield displacement has been defined in various ways by different researchers. Some have defined yield displacement as the displacement at onset of first yielding of any longitudinal reinforcing bar. However, this is usually not the point at which the lateral load vs. lateral deflection curve first begins to exhibit a change of slope. Normally, yielding must have occurred in several longitudinal bars before the load-deflection plot changes shape. Furthermore, *a priori* calculations of the point at which yielding first occurs in a longitudinal bar are usually inaccurate. In a study by Konwinski (1996), calculated yield displacements were compared with measured yield displacements for two different test programs, containing 60 bridge pier test specimens. It was found that the ratio of measured to calculated yield displacement varied from 0.75 to 2.5, with an average value of 1.6, as shown in Figure 2. So, it appears that it is difficult to obtain a consistent definition of displacement at first yield. Analytical predictions and experimental observations are usually not in agreement.

An alternative to the use of ductility (i.e. yield displacement) as a measure of pier behavior, some researchers have used lateral drift. Lateral drift is simply the measured lateral displacement of the pier divided by the pier length. While this quantity is not tied directly to the inelastic behavior of the specimen, it does have the advantage of being an unambiguous quantity, not clouded by the determination of yield displacement. The use of lateral drift as a primary performance measure does not exclude consideration of yielding and other inelastic material behavior in interpretation of the behavior of the bridge pier specimen. However, it does remove the ambiguities associated with calculation and measurement of the yield displacement.

Another useful measure of pier performance is the energy dissipated by the specimen during each cycle of lateral displacement. Energy dissipation is not always reported by researchers, and it is usually difficult to calculate at a later date without access to the original numerical load-deflection data. Therefore, even if a research program is not focused on energy dissipation as a measure of pier performance, it would helpful to later researchers if the original researchers would calculate energy dissipated per cycle and include this data as part of the test report.

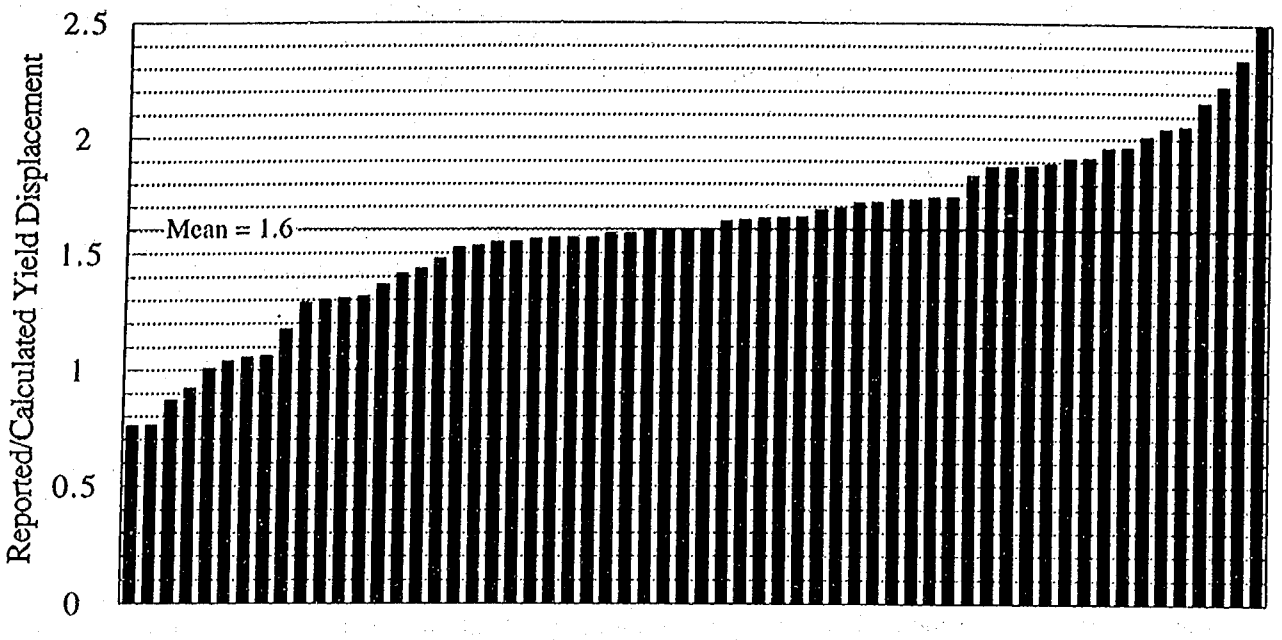


Figure 2. Reported/Calculated yield displacements for piers tested by Ang (1985), Wong (1990) and Wight (1973). (After data by Konwinski, 1996)

Axial Stress Level

Typical axial stress levels on bridge piers vary from country to country, depending on the prevailing seismic design philosophy and practices. Thus, bridge pier test results from a particular country tend to focus on the typical axial stress level for that country. For example, in the United States axial stresses in bridge piers due to the self weight of the bridge superstructure are normally on the order of 10 percent of the gross cross section capacity[1] for piers designed to resist seismic loads. As a result, bridge pier tests in the United States have often been conducted at approximately this axial stress level. Axial stress levels in tests conducted in New Zealand have tended to be higher - on the average about 20 percent of the gross cross section capacity.

When comparing test results from different countries, and from different test programs, the effects of the axial stress level must be considered. To facilitate these comparisons, a definition of axial stress level should be adopted. Axial stress level can be calculated several ways: based on the gross cross section area, or the area of the confined core; and the cross section capacity may include or exclude the strength contributions of longitudinal reinforcement.

Symbols and Units

Although the choice of the symbols used to represent variables such as geometric dimensions, stresses and strains in test specimens may at first appear to be a trivial issue, it is in fact a rather important one. Direct comparison of data from different research programs is hindered by the use of different symbols for the same quantity, or the same symbol for different quantities. Mistakes in interpretation of the data often result. This problem is only further compounded when different measurement systems, (e.g. SI and traditional American units) are used. Therefore, it is proposed that definitions of common quantities encountered in testing of bridge piers should be

[1] i.e. $0.1P/\left(f_c' A_g\right)$, where P is the axial load, f_c' is the concrete compressive strength, and A_g is the gross cross section area of the pier

developed, that standard symbols should be assigned to these quantities, and that the quantities should be defined in terms of SI units. Consistent use of symbols and measurement systems will greatly facilitate comparisons of data from different research programs.

Load Path

Recent studies at the National Institute of Standards and Technology (NIST) have highlighted the importance of the sequence of lateral loading, or "load path", in determining the type and degree of damage exhibited by a bridge pier (Taylor, et al., 1996a, 1996b). In the NIST test program twelve identical 1/4 scale cantilever bridge piers with circular cross sections were subjected to cyclic lateral load patterns and constant axial load. The loading apparatus and a typical test specimen are shown in Figures 3 and 4. The piers were geometrically scaled models of a prototype bridge pier designed according to California Department of Transportation (Caltrans) seismic design specifications (Caltrans 1992).

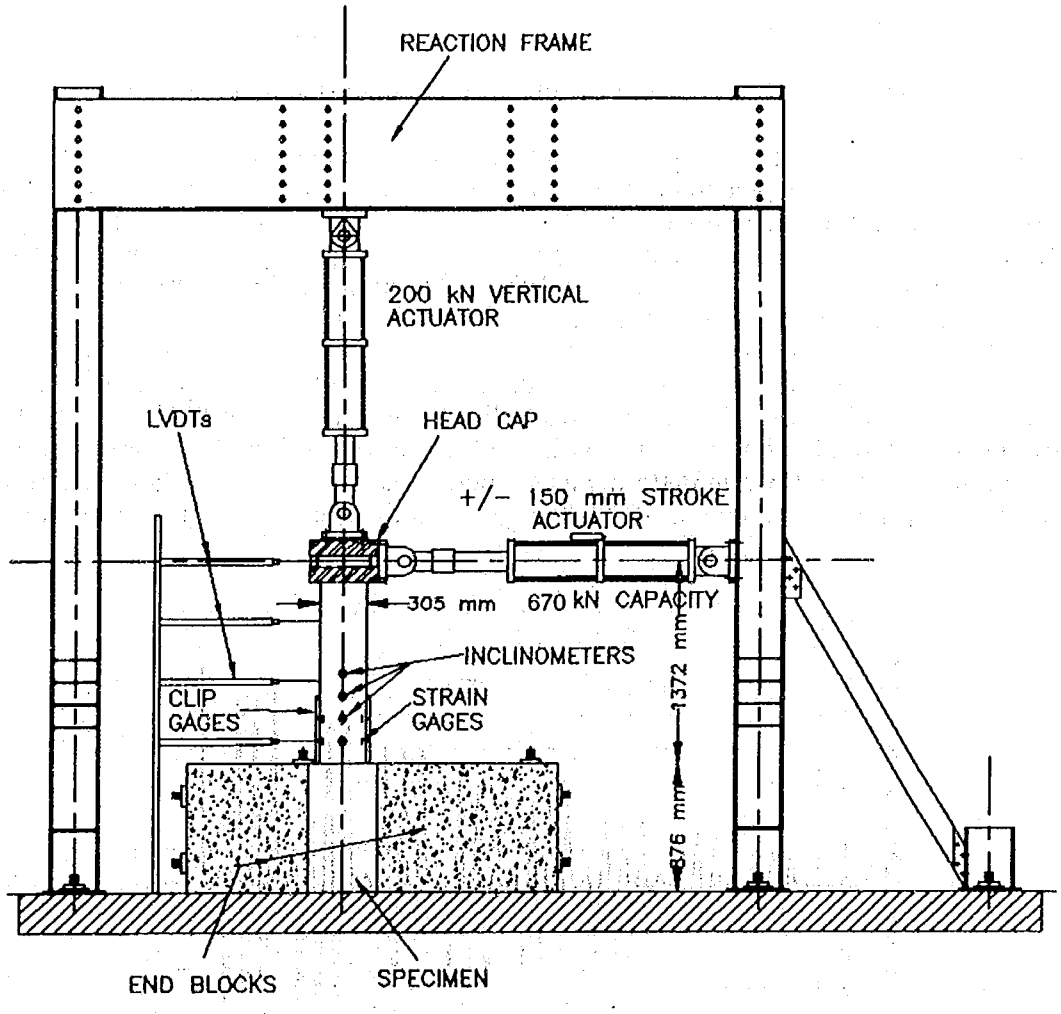


Figure 3. Load frame and instrumentation for cyclic lateral load tests

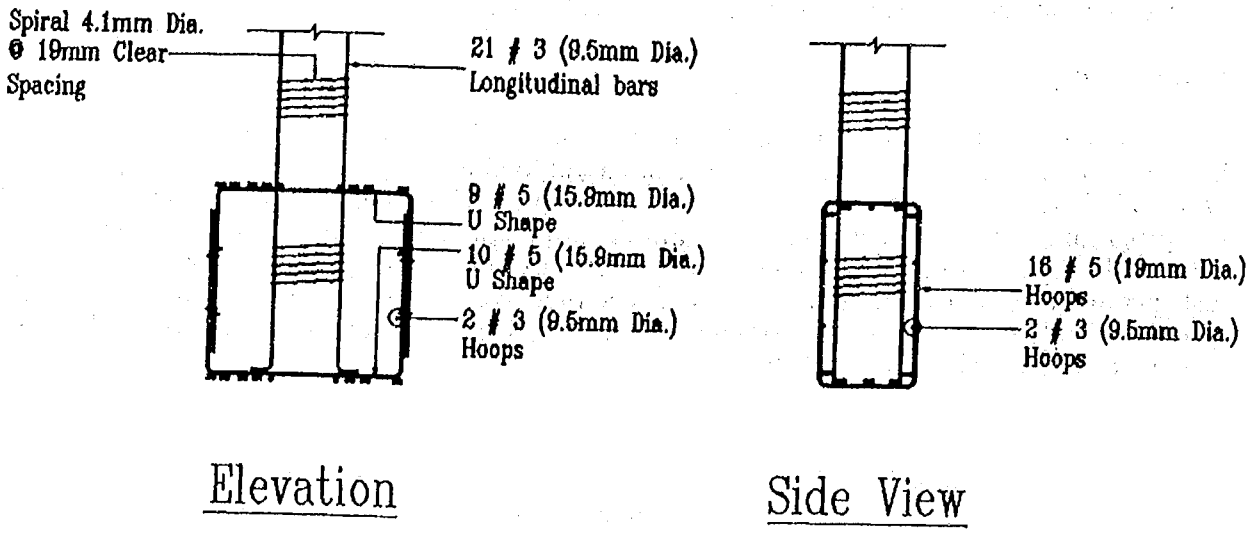


Figure 4. Reinforcement details for pier specimen and base block

The main variable in the test program was the lateral displacement pattern applied at the tip of the cantilever pier. All displacement patterns were applied at a slow rate. The first six specimens were subject to "benchmark" displacement patterns, which were intended to provide information on the strength, stiffness and fatigue resistance of the pier. The applied displacement patterns for specimens 1 to 6 are described in Table 1. Specimen 1 was a simple "pushover" test, which determined the strength and stiffness envelope for the pier. A *de facto* standard displacement pattern, similar to patterns used by many researchers in past experimental programs, was applied to specimen 2, and is shown in Figure 5. This displacement pattern, which consists of a sawtooth wave with gradually increasing amplitude, was later compared with results of tests in which simulated earthquake loading was applied to the pier (tests 7 to 12). For specimens 3 to 6 a constant amplitude sawtooth wave pattern was applied to each specimen. These specimens were used to study the fatigue resistance of the bridge pier, and to calibrate fatigue-based damage models.

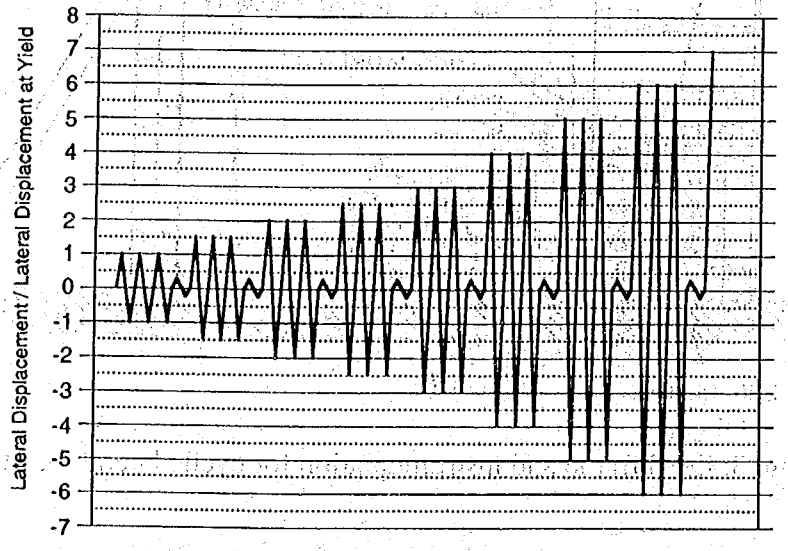


Figure 5: Typical laboratory displacement history, applied to Specimen 2

Table 1. Displacement patterns applied to specimens 1 to 6

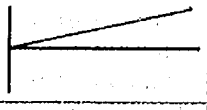
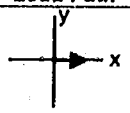
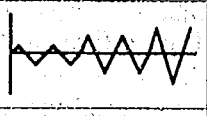
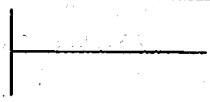
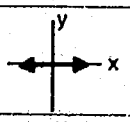
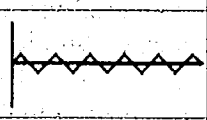
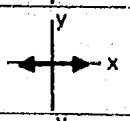
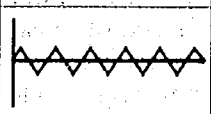
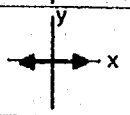
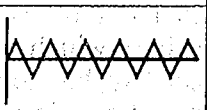
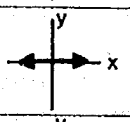
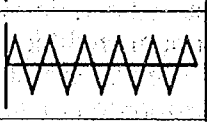
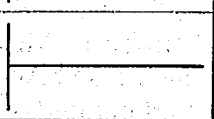
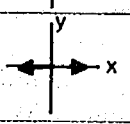
No.	Load Regimen	X-Direction Load History	Y-Direction Load History	Plan view of Load Path
1	Monotonic "Pushover" Test			
2	"Standard" displacement pattern			
3	2Δy			
4	3Δy			
5	4Δy			
6	5Δy			

Table 2. Earthquake records applied to Specimens 7 to 12

Spec. No.	Event No.	Description: Event Severity and Number	Purpose of Applying Event to Pier	Earthquake Record	Scale Factor	Scaled PGA g's
7	1	Damaging No. 1	Significant damage	Loma Prieta 1989, Presidio	12.0	1.20
	2	Minor No. 1	Aftershock	Imperial Valley 1979, Superstition Mtn.	1.8	0.34
	3	Minor No. 2	Second aftershock	San Fernando 1971, 2011 Zonal Avenue	1.2	0.10
	4	Damaging No. 2	Failure of pier	San Fernando 1971, 455 S. Figueroa St.	3.6	0.54
8	1	Minor No. 1	Minor damage	Imperial Valley 1979, Superstition Mtn.	1.8	0.34
	2	Minor No. 2	Minor damage	San Fernando 1971, 2011 Zonal Avenue	1.2	0.10
	3	Damaging No. 1	Significant damage	Loma Prieta 1989, Presidio	12.0	1.20
	4	Damaging No. 2	Failure of pier	San Fernando 1971, 455 S. Figueroa St.	3.6	0.54
9	1	Damaging No. 3	Significant damage	San Fernando 1971, Orion Boulevard	3.25	1.43
	2	Minor No. 2	Aftershock	San Fernando 1971, 2011 Zonal Avenue	1.2	0.10
	3	Damaging No. 4	Moderate damage	El Centro 1940	1.0	0.35
	4	Minor No. 3	Aftershock	San Fernando 1971, 455 S. Figueroa St.	1.0	0.15
	5	Damaging No. 3	Failure of pier	San Fernando 1971, Orion Boulevard	3.25	1.43
10	1	Minor No. 2	Minor damage	San Fernando 1971, 2011 Zonal Avenue	1.2	0.10
	2	Damaging No. 4	Moderate damage	El Centro 1940	1.0	0.35
	3	Minor No. 3	Aftershock	San Fernando 1971, 455 S. Figueroa St.	1.0	0.15
	4	Damaging No. 3	Significant damage	San Fernando 1971, Orion Boulevard	3.25	1.43
	5	Damaging No. 3	Failure of pier	San Fernando 1971, Orion Boulevard	3.25	1.43
11	1	Damaging No. 4	Significant damage	Northridge 1994, VA Hospital	1.0	0.42
	2	Minor No. 4	Aftershock	Northridge 1994, Griffith Observatory	1.0	0.26
	3	Minor No. 5	Minor damage	Taft 1952	1.0	0.36
	4	Damaging No. 5	Failure of pier	Mexico City 1985, SCT	1.0	0.17
12	1	Minor No. 4	Minor damage	Northridge 1994, Griffith Observatory	1.0	0.26
	2	Minor No. 5	Minor damage	Taft 1952	1.0	0.36
	3	Damaging No. 4	Significant damage	Northridge 1994, VA Hospital	1.0	0.42
	4	Damaging No. 5	Failure of pier	Mexico City 1985, SCT	1.0	0.17

A typical displacement history for Specimens 7 to 12 is shown in Figure 6. The details of the displacement histories for these specimens are shown in Table 2. These last six specimens were used to study the effects of real earthquake displacement histories on accumulation of damage, particularly over a series of events of varying intensity. The displacement patterns applied to Specimens 7 to 12 were derived from measured earthquake acceleration records, using the following process. Given an earthquake acceleration record, the deformation history at the top of the pier was computed using the inelastic dynamic analysis program IDARC (Kunnath et al. 1992). The earthquake records used in tests 7 to 12 were selected from a pool of available strong ground motion records recorded at bedrock sites in the state of California, and one record from Mexico City. Each specimen was subjected to a series of up to five earthquakes. Table 2 shows that earthquakes of a range of intensities were applied, and the order in which they were applied was varied. The pool of available earthquake records was subdivided into two main categories: minor events and major events. Minor events were intended to simulate either isolated low-intensity earthquakes, or low intensity aftershocks following a major earthquake. Minor events would cause little or no damage to the specimens in this test program, as determined from the results of the constant amplitude tests (Specimens 3 to 6). Based on observations from these tests, minor events were defined as those which caused three to five excursions into the inelastic range, with ductility demands no greater than $3\Delta y$. Major events were divided into two types: damaging earthquakes and maximum credible events. Again, based on the results of the earlier constant-amplitude tests, damaging events were defined as those which caused multiple excursions into the inelastic range, with ductility demands greater than $3\Delta y$, but generally less than $5\Delta y$. The earlier tests showed that this level of ductility demand caused deterioration of the pier, but that the pier retained much of its strength and stiffness. Maximum credible events were those which caused cycles with ductility demands greater than $5\Delta y$. The earlier tests also showed that just a few excursions greater than $5\Delta y$ resulted in rapid deterioration of strength and stiffness. In some cases, where acceleration records were not available which met the desired criteria, the records were modified by simple amplitude scaling. These scale factors are reported in Table 2.

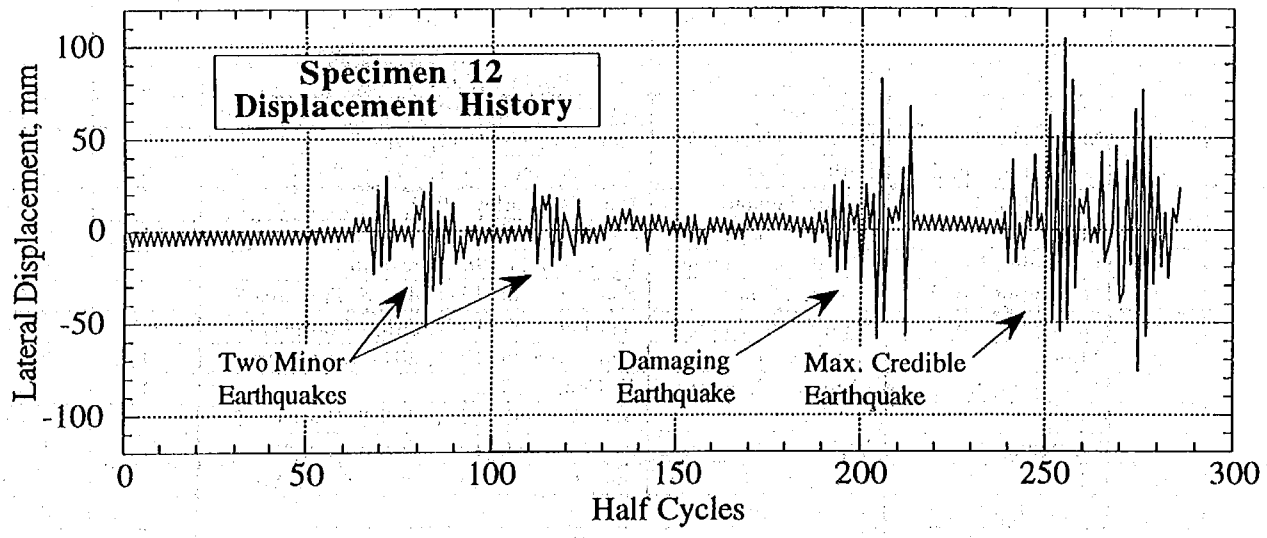


Figure 6: Typical earthquake displacement histories, applied to Specimen 12

At this time the results of the NIST test program on the 12 identical model bridge piers are still being interpreted. However, the following preliminary conclusions can be stated.

1) There appears to be a threshold ductility level for well-confined, circular, flexure-dominated piers above which degradation of stiffness and strength is rapid. For the piers tested in this study this threshold ductility level was about $4\Delta y$. Below this threshold

degradation was more gradual, and for ductility demands of 2Δy or less degradation was minimal. The difference in response when the bridge pier was cycled at ±5Δy and ±4Δy is illustrated in figure 7.

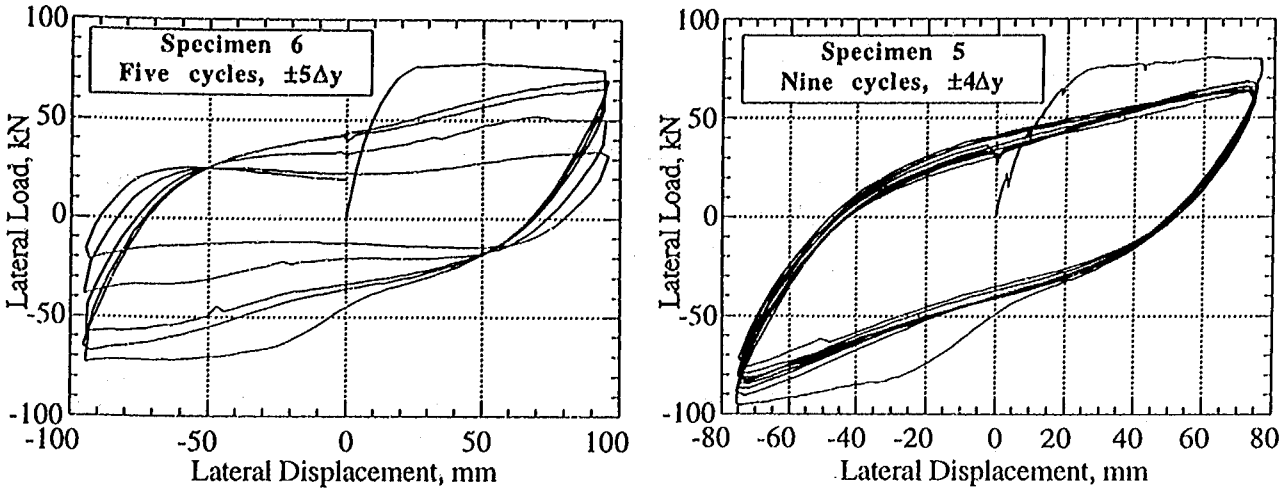


Figure 7: Lateral load-displacement plots at ±5Δy and ±4Δy

2) The constant amplitude tests in this study confirm that cumulative dissipated energy at failure is strongly path dependent. This effect is illustrated in figure 8. Therefore cumulative energy by itself is not a reliable measure of pier damage.

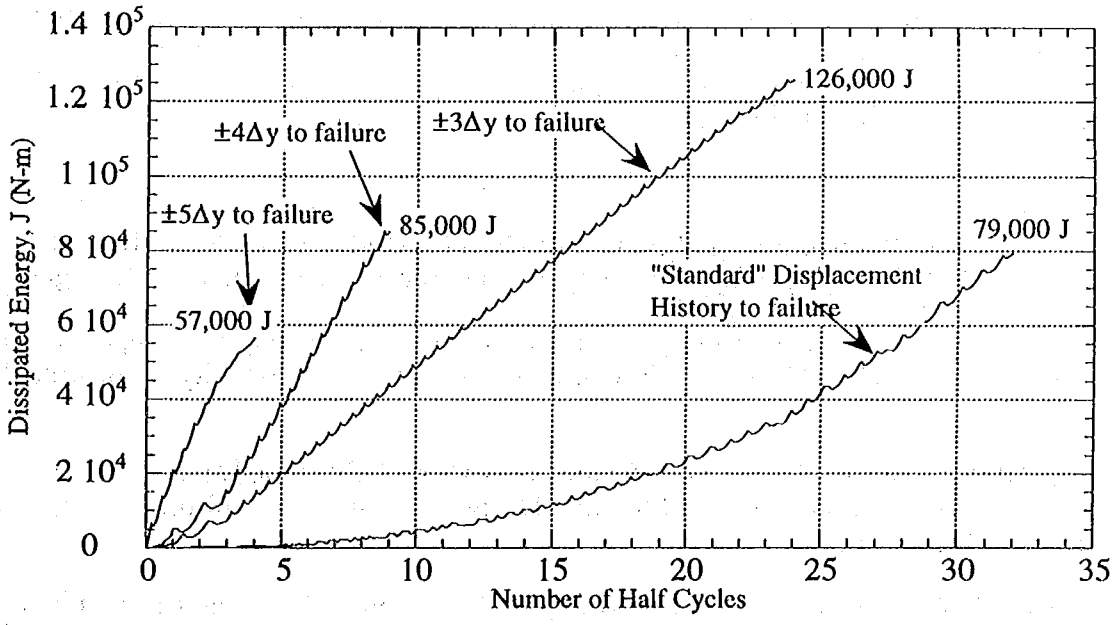


Figure 8: Cumulative energy to failure for Specimens 2, 4, 5 and 6

3) Minor earthquakes appear to have very little influence on the damage exhibited by well-confined, circular, flexure-dominated bridge piers in subsequent major events. While the precise definition of a "minor" event is open to interpretation, this study indicates that the strength and stiffness of a well-confined, circular, flexure-dominated bridge pier should not be discounted because the pier has been subjected to minor events.

4) The random loading tests indicate that failure mode is path dependent. Nominally identical piers failed either due to low-cycle fatigue of longitudinal reinforcement, or due to rupture of confining reinforcement. The only variable between tests was the load path. The relationship between load path and failure mode is currently under study.

5) Cumulative fatigue methods, based on Miner's rule (Miner, 1945) for fatigue of metals, appear to predict well the progress of damage in piers which failed due to low cycle fatigue of longitudinal bars. However, Miner's rule does not apply to those piers which failed due to rupture of the confining reinforcement. Other damage models are being investigated which may apply to confinement failure. Furthermore, the findings of this study apply only to well-confined, circular, flexure-dominated piers. A future study is planned to investigate well-confined, circular, shear-dominated piers.

SUMMARY

Six issues related to the development of standard testing and reporting methods for tests of reinforced concrete bridge piers have been discussed. These issues are test configuration; scaling; force and displacement variables; axial stress level; symbols and units; and load path. It is hoped that this paper will lead to dialogue on these issues, and ultimately to the development of international protocols for tests of the seismic performance of reinforced concrete bridge piers

ACKNOWLEDGMENTS

I would like to thank the following colleagues for their helpful suggestions and ideas: Dr. William C. Stone (National Institute of Standards and Technology); Prof. John Mander (State University of New York at Buffalo); Prof. Julio Ramirez (Purdue University); and Prof. Sashi Kunnath (University of Central Florida). I also gratefully acknowledge the financial support of the National Center for Earthquake Engineering Research (NCEER), the California Department of Transportation (Caltrans), and the Federal Highway Administration (FHWA) for the NIST bridge pier test programs described in this paper.

REFERENCES

Ang, B.G. (1985), "Seismic Shear Strength of Circular Bridge Piers, Ph.D. Report, Department of Civil Engineering, University of Canterbury, New Zealand, 407 pages.

Applied Technology Council (1992), "Guidelines for Seismic Testing of Components of Steel Structures," report ATC-24, Applied Technology Council, Redwood City, California, 57 pages.

Caltrans (1992), "Bridge Design Specifications," State of California, Department of Transportation (Caltrans), Office of Structure Design, Sacramento, California, August 1986 (revisions to December 1992).

Konwinski, Colleen M. (1996), "Shear Strength of Reinforced Concrete Bridge Piers Subjected to Earthquake Loading," Master of Science Thesis, Department of Civil Engineering, Purdue University, West Lafayette, Indiana, April.

Kunnath, S.K., Reinhorn, A.M., and Lobo, R.F. (1992), "IDARC Version 3.0; A Program for the Inelastic Damage Analysis of Reinforced Concrete Structures," Report NCEER-92-0022, National Center for Earthquake Engineering Research, State University of New York at Buffalo, August 1992.

Miner, M.A. (1945), "Cumulative Damage in Fatigue," *Journal of Applied Mechanics*, Vol. 12, 1945, p. A-159.

Stone, W.C., and Cheok, G.S. (1989), "Inelastic Behavior of Full-Scale Bridge Columns Subjected to Cyclic Loading," Building Science Series No. 166, National Institute of Standards and Technology, Gaithersburg, Maryland, January, 252 pages.

Taylor, A.W.; El-Bahy, A.; Stone, W.C.; and Kunnath, S. (1996a), "Effect of Load Path on Seismic Damage to RC Bridge Columns," *Proceedings*, 11th World Conference on Earthquake Engineering, Acapulco, Mexico, June 1996, paper No. 1897, 8 pages.

Taylor, A.W.; El-Bahy, A.; Stone, W.C.; and Kunnath, S. (1996b), "Effect of Load Path on Damage to Concrete Bridge Piers," *Proceedings*, 28th Joint Panel Meeting on Wind and Seismic Effects, Gaithersburg, Maryland, May 14-17, 1996.

Wight, J.K., and Sozen, M.A. (1973), "Shear Strength Decay in Reinforced Concrete Columns Subjected to Large Deflection Reversals," Structural Research Series No. 403, University of Illinois at Urbana-Champaign, Civil Engineering Studies, 290 pages.

Wong, Y.L. (1990), "Squat Circular Bridge Piers Under Multi-Directional Seismic Attack," Ph.D. Report, Department of Civil Engineering, University of Canterbury, New Zealand, 264 pages.

Resolutions

Third US-Japan Workshop on Seismic Retrofit of Bridges

Resolutions

General

The third U.S.-Japan Workshop on Seismic Retrofit of Bridges was held at Osaka, Japan on December 10 and 11, 1996, under the auspices of Task Committee J on "Wind and Earthquake Engineering for Transportation Systems" of the UJNR Panel on Wind and Seismic Effects. The workshop was attended by 20 U.S. and 66 Japanese participants. For the Japan side, the Public Works Research Institute, the Ministry of Construction sponsored and organized the workshop. The workshop was sponsored on the U.S. side by the Federal Highway Administration and the National Science Foundation. Participation of the U.S. delegates was coordinated by the National Center for Earthquake Engineering Research.

Recent earthquakes have caused significant damage to bridges in both Japan and the U.S. This was evidenced in the U.S. during the 1989 Loma Prieta and 1994 Northridge earthquakes. In Japan, bridge distress and failures were observed during the 1995 Hyogo-ken-Nanbu earthquake. These and other earthquakes point out the urgent need for reliable methods for evaluating the earthquake vulnerability of bridges and for effective and practical methods for seismic retrofit.

This workshop comprised the presentation and discussion of 11 U.S. and 15 Japanese papers, which covered a wide range of topics including screening and prioritizing procedures, retrofit technologies for reinforced concrete and steel columns, and retrofit methods for foundations. A special session was devoted to testing procedures and their effects on test results. Fruitful discussions on many issues of common concern took place. The participants also showed great interest in actual applications of retrofit methods, and retrofit technologies using new materials.

The participants agree that the workshop was successful and led to greater understanding of the issues related to seismic hazard mitigation for existing bridges. While much information has been developed on these important issues, it is

recognized that many problems remain unresolved and that additional studies and research are needed. The participants expressed interest in technology and applications related to new materials, new construction procedures, verification tests in the field and laboratory, and development of reliable and efficient tools for analysis.

Resolutions

1. There are many topics of common interest related to the development and implementation of seismic retrofit of bridges. It is therefore resolved that continued cooperation between researchers and bridge engineers in both countries is strongly encouraged. The active exchange of research and design experience, in both the laboratory and field, will facilitate the advancement of seismic retrofit technology and its practical implementation in both countries.

2. Because of the rapid rate at which new information on seismic retrofit technology and applications is produced and implemented, the participants recommend that the fourth U.S.-Japan workshop on seismic retrofit of bridges be held in the U.S. within two years.

3. It is recommended that one or more example bridge structures be identified for the purpose of comparing analysis and retrofit procedures, standards, and guidelines used by investigators and practitioners in both countries.

4. The participants recognized the importance of testing methodology, test interpretation, and test reporting, for conducting testing protocols and meaningful comparison of research results. This workshop encouraged holding a joint workshop on testing methodology, test interpretation, and test reporting in the near future.

5. Cooperative activities between the U.S. and Japan should be encouraged to address problems of mutual concern. The participants recommended that opportunities should be explored for exchange of personnel as well as available laboratory and testing facilities.

Appendices

"The 4th WS on Earthquake Protective Systems for Bridges"

December 9, Monday

8:30-9:00 **Registration**

9:00-9:30 **Opening Session (Co-Chairs: T. Terayama, I. Friedland)**

Opening Remarks (Japan) Dr. Koichi Yokoyama
Opening Remarks (Japan) Dr. Shigeki Unjoh
Opening Remarks (U.S.A.) Dr. Ian G. Buckle

9:30-10:10 **Session 1: State of the Art**

(Co-Chairs: S. Unjoh, G. Fenves)

"Menshin Design of Highway Bridges"
by K. Kawashima, S. Unjoh
Presented by: Kazuhiko. Kawashima

"Update on the Proposed AASHTO Guide Specification for Seismic Isolation Design"
by R. Lacalle
Presented by: Roberto Lacalle

10:10-10:30 Break

10:30-11:50 **Session 2: Passive/Hybrid Protective Systems**

(Co-Chairs: H. Iemura, A. Kiremidjian)

"Development of High Damping Systems for Long Span Bridges"
by S. Unjoh, H. Otsuka, Y. Goto, I. Shimoda, Y. Maehara, T. Takeda
Presented by: Shigeki. Unjoh

"Development of High Damping Devices for Long Span Bridges and the Design Method"
by S. Unjoh, Y. Goto, I. Shimoda, Y. Maehara
Presented by: Yozo Goto

"Aging Studies of High-Damping Rubber and Lead-Rubber Seismic Isolators"
by P. Clark, J. Kelly, I. Aiken
Presented by: Peter Clark

"Development of Super High Damping Rubber Damper for the Seismic Response Control of Long Span Bridges"
by K. Goda, S. Suzuki, Y. Suitsu, S. Unjoh, H.Otsuka, K. Nagaya
Presented by: Kengo Goda

11:50-13:30 Lunch

13:30-14:30 **Session 3: Hybrid/Semi-active Systems and Smart Materials**

(Co-Chairs: A. Igarashi, A. Itani)

"Modeling of a Variable Damper and its Application"
by T. Sato, M. Sato, S. Tanaka, K. Toki
Presented by: Tadanobu Sato

"Seismic Response Control of PC Cable-Stayed Bridge under Construction by Active Mass Damper"
by M. Tsunomoto, H. Otsuka, S. Unjoh, K. Nagaya
Presented by: Meguru Tsunomoto

"Thermo-visco-elasto-plastic Modeling of Elastomeric and Lead-Rubber Bridge Bearings"
by J. Mander, D-K Kim, S. Chen
Presented by: John Mander

14:30-14:50 Break

14:50-16:30 **Session 4: Experimental and Field Observations 1**

(Co-Chairs: T. Sato, S. Arzoumanidis)

"Analysis of Seismic Response of Yamaage-Bridge"
by S. Unjoh
Presented by: Shigeki Unjoh

"Seismic Isolation and Energy Dissipation Technologies: a Test and Evaluation Program for Highway Bridge Applications"
by K. Almand
Presented by: Kathleen Almand

"The Restoring Force Characteristics of LRB under the Influence of Variable Axial Loads and Rotational deformation
by H. Iemura, A. Igarashi, Y. Chen, H. Nakajima
Presented by: Akira Igarashi

"Field Testing of a Four-span Seismically Isolated Bridge"
by A. Gilani, S. Mahin, G. Fenves, J. Chavez, I. Aiken
Presented by: Gregory Fenves

"Enhancement of Lateral Seismic Load Distribution in Continuous Girder Bridges : Test of Stiffening and Damping Components of a New Device"
by W. Tanzo, J. Hernandez Jr., H. Mutsuyoshi, A. Tsuzuki
Presented by: J. Hernandez Jr.

18:00 **Reception Hosted by Japan Side**

December 10, Tuesday

8:30-9:30 **Session 5: Experimental and Field Observations 2**
(Co-Chairs: M. Abe, A. Elgamal)

"Design of the 19-Span Continuous Rigid Frame Bridge with Seismic Isolator"
by H. Hayashi, S. Kawakita,
Presented by: Shiro Kawakita

"Testing of Protective Systems and Hardware for Bridge Applications"
by A. Whittaker, I. Aiken, P. Clark, G. Fenves, N. Makris, S. Mahin
Presented by: Andrew Whittaker

"The Analysis of Seismic Response of the Bridge with Menshin Bearings during the Hyogo-ken Nanbu Earthquake"
by T. Naganuma, Y. Horie, H. Kobayashi, N. Sasaki
Presented by: Toshihiko Naganuma

9:30-9:50 Break

9:50-10:50 **Session 6: Methods/Issues and Applications**
(Co-Chairs: H. Otsuka, A. Taylor)

"Use of Visco-Elastic Dampers to Suppress Seismic Vibration of Bridges"
by M. Shinozuka, J-M Kim, R. Purasinghe
Presented by: Masanobu Shinozuka

"Effectiveness of Unseating Prevention Devices with Energy Dissipation"
by K. Kawashima, M. Yabe,
Presented by: Masaaki Yabe

"Seismic Protection of Bridges with Fluid Dampers and the Issue of Viscous Heating"
by N. Makris, S. McMahon
Presented by: Nicos Makris

10:50-11:10 Break

11:10-11:40 **Resolutions and Closure**
(Co-Chairs: S. Unjoh, I. Buckle)

11:40-11:50 Group Photo

11:50-13:20 Lunch

"The 3rd WS on Seismic Retrofit of Bridges"

13:20-13:50 **Opening Session**

(Co-Chairs: T. Terayama, I. Friedland)

Opening Remarks (Japan) Mr. Yasuyuki Fujishiro

Opening Remarks (U.S.A.) Dr. H. S. Lew

13:50-14:30 **Session 1: State of the Art**

(Co-Chairs: S. Unjoh, M. Shinozuka)

"Damage to Highway Bridges by the 1995 Hyogoken Nanbu Earthquake And the Retrofit of Highway Bridges in Japan"
by H. Otsuka, T. Terayama, J. Hoshikuma, K. Kosa
Presented by: Hisanori Otsuka

"Innovative Seismic Retrofit of California Highway Structures"
by S. El-Azazy
Presented by: Saad El-Azazy

14:30-14:50 Break

14:50-15:30 **Session 2: Screening and Prioritization of Bridges for Retrofitting**

(Co-Chairs: H. Mutsuyoshi, J. Mander)

"Seismic Retrofitting Manuals for Highway Systems: System Assessment, Screening, Evaluation, and Retrofitting"
by I. Buckle, I. Friedland
Presented by: Ian Friedland

"Use of Transportation Network Systems for Bridge Retrofit Prioritization and Emergency Response"
by A. Kiremidjian, N. Basöz
Presented by: Anne Kiremidjian

15:30-15:50 Break

15:50-16:50 **Session 3: Evaluation of Existing Bridges**

(Co-Chairs: J. Hoshikuma, N. Makris)

"Analytical Methods for the Seismic Evaluation of Existing Bridges"
by R. Imbsen, F. Nobari
Presented by: Roy Imbsen

"Seismic Evaluation and Retrofit of Existing Multi-column Bents"
by T. Terayama, H. Otsuka
Presented by: Toru Terayama

"Queensboro Bridge: Seismic Condition Assessment and Retrofit of a Landmark Bridge"
by S. Arzoumanidis, R. Gajer, A. Malik
Presented by: Serafim Arzoumanidis

16:50-17:10 Break

17:10-18:10 **Session 4: Retrofit Methods for RC Columns 1**

(Co-Chairs: Y. Kimura, R. Imbsen)

"Seismic Retrofit of Square RC Columns by Steel Jacketing"
by J. Hoshikuma, H. Otsuka, K. Nagaya
Presented by: Jun-ichi Hoshikuma

"An Experimental Study on Seismic Retrofit of Reinforced Concrete Bridge Piers"
by H. Ikeda, N. Wada, K. Osada, Y. Igase, Y. Tamura
Presented by: Yoshinori Igase

"Retrofits of Reinforced Concrete Bridge Columns with Prestressing Steel Ties"

by T. Yoshioka
Presented by: Tamio Yoshioka

December 11, Wednesday

8:40-10:20 **Session 5: Retrofit Methods for RC Columns 2**
(Co-Chairs: Y. Adachi, P. Clark)

"Development of Base Isolation System of Existing Bridges"
by Y. Hishiki, T. Takeda, H. Nagumo, T. Ichinomiya, Y. Okimi
Presented by: Hiroyuki Nagumo

"An Experimental Study on Ductility of RC Pier Models Winded with FRP Tape"
by H. Mikami, M. Sato, H. Konno, N. Kishi
Presented by: Hiroshi Mikami

"Seismic Retrofit of Bridge Columnsing Prefabricated Composite Jackets"
by Y. Xiao
Presented by: Yan Xiao

"Seismic Retrofit of Reinforced Concrete Bridge Piers by Carbon Fiber Sheet"
by M. Hosotani, K. Kawashima, J. Hoshikuma
Presented by: Manabu Hosotani

"Experimental Study Concerning Retrofit of RC Column by CFRP Sheet"
by F. Hakamada, Y. Maekawa, J. Hoshikuma
Presented by: Fumio Hakamada

10:20-10:40 Break

10:40-12:00 **Session 6: Retrofit Methods for Steel Columns, Superstructure and Restrainers**
(Co-Chairs: K. Tamura, Y. Xiao)

"Cyclic Behavior of Shear Links in Retrofitted Richmond-San Rafael Bridge Towers"
by A. Itani
Presented by: Ahmad Itani

"An Experimental Study on Seismic Retrofit of Steel Bridge Piers"
by K. Nishikawa, J. Murakoshi, Y. Josen, M. Takahashi
Presented by: Jun Murakoshi

"Intermediate Hinge Restrainers for Bridges: Performance, Design, and Retrofit"
by R.DesRoches, G. Fenves
Presented by: Gregory Fenves

"Seismic Vulnerability Analysis of Steel Bridge Bearings"
by J. Mander, D-K Kim, I. Buckle
Presented by: John Mander

12:00-13:30 Lunch

13:30-15:10 **Session 7: Retrofit Methods for Foundations and Geotechnical Considerations**
(Co-Chairs: J. Murakoshi, K. Almand)

"Inspection and Restoration of Damaged Foundations due to the Great Hanshin Earthquake 1995"
by H. Ishizaki, A. Nanjoh, J. Kawakami,N. Egawa, Y. Adachi,
Presented by: Yukio Adachi

"Seismic Design of Pile Foundations"
by M. Nakano, Y. Kimura,
Presented by: Yoshitomi Kimura

"Site Remediation and Seismis Response Meshanisns"
by K. Adalier, A. Elgamal
Presented by: Ahmed Elgamal

"Seismic Design Treatment of Liquefaction-Induced Ground Flow"

by K. Tamura, T. Hamada, T. Azuma
Presented by: Kei-ichi Tamura

"A Study on Measures against Ground Flow Using The Finite Element Method"
by M. Ogasawara, H. Tsunoda, T. Makita, S. Gose
Presented by: Hiroshi Tsunoda

15:10-15:30 Break

15:30-16:10 **Special Session: Effects of Loading History**
(Co-Chairs: K. Kawashima, A. Whittaker)

"Effect of Loading Hysteresis on Ductility of Reinforced Concrete Columns"
by J. Hoshikuma, S. Unjoh, K. Nagaya
Presented by: Jun-ichi Hoshikuma

"Testing Methodologies for the Seismic Performance of Reinforced Concrete Bridge Piers"
by A. Taylor
Presented by: Andrew Taylor

16:10-16:30 Break

16:30-17:00 **Resolutions and Closure**
(Co-Chairs: S. Unjoh, H. S. Lew)

Participants

Participants from The U.S. Side

Kathleen Almand
HITEC
1015 15th Street. NW. Suite 600
Washington, D.C. 20005-2605
Tel. 202-842-0555
Fax. 202-789-5345
E-mail kalmand@cerf.asce.org

Serafim G. Arzoumanidis
Steinman, Boyton, Gronquist &Birdsall
110 William Street
New York, NY 10038
Tel. 212-266-8370
Fax. 212-266-8540

Ian G. Buckle
National Center for Earthquake Engineering Research
State University of NY at Buffalo
105 Red Jacket Quadrangle
Buffalo, NY 14261
Tel. 716-645-3391
Fax. 716-645-3399
E-mail igb@acsu.buffalo.edu

Peter Clark
Earthquake Engineering Research Center
University of California, Berkeley
1301 South 46th Street
Richmond, CA 94804-4698
Tel. 510-231-9556
Fax. 510-231-5696
E-mail sacsteel@eerc.berkeley.edu

Saad El-Azazy
Senior Bridge Engineer
California Dept. of Transportation
Division of Structures
1801 30th Street, West Bldg. P.O. Box 942874
Sacramento, CA 94274-0001
Tel. 916-227-8124
Fax. 916-227-8898

Ahmed-W. Elgamal
Columbia University
Department of Civil Engineering
610 Mudd Building
New York, NY 10027
Tel. 212-854-1203
Fax. 212-854-6267

Gregory Fenves
Professor
University of California, Berkeley
Department of Civil Engineering
729 Davis Hall
Berkeley, CA 94720-1710
Tel. 510-643-8543
Fax. 510-643-8928
E-mail fenves@ce.berkeley.edu

Ian Friedland
National Center for Earthquake Engineering Research
State University of NY at Buffalo
102 Red Jacket Quadrangle
Buffalo, NY 15261-0025
Tel. 716-645-3391
Fax. 716-645-3399
E-mail imf@acsu.buffalo.edu

Roy A. Imbsen
Imbsen&Associates, Inc.
9912 Business Park Drive, Suite 130
Sacramento, CA 95827
Tel. 916-366-0632
Fax. 916-366-1501
E-mail raimbsen@imbsen.com

Ahmad M. Itani
Assistant Professor
University of Nevada, Reno
Department of Civil Engineering
258 Reno, NV 89557-0152
Tel. 702-784-4379
Fax. 702-784-4466
E-mail itani@scs.unr.edu

Anne S. Kiremidjian
Professor and Direstor
Stanford University
Department of Civil Engineering
Terman 238
Stanford, CA 94305-4042
Tel. 415-723-4164
Fax. 415-725-9755
E-mail ask@ce.stanford.edu

Roberto Lacalle
California Dept. of Transportation
Division of Structures, MS-9
P.O. Box 942874
Sacramento, CA 94274-0001
Tel. 916-227-8070
Fax. 916-227-8245

H.S. Lew
Chief
Structural Division
National Institute of Standards and Technology
Building 226, Rm. 168
Gaithersburg, MD 20899
Tel. 301-975-6060
Fax. 301-869-6275

Nicos Makris
University of California, Berkeley
Department of Civil and Environmental Engineering
711 Davis Hall
Berkeley, CA 94702-1710
Tel. 510-643-2682
Fax. 510-643-8928
E-mail makris@ce.berkeley.edu

John B. Mander
State University of New York at Buffalo
Department of Civil Engineering
230 Ketter Hall
Buffalo, NY 14260
Tel. 716-645-2114
Fax. 716-645-3733
E-mail jmander@ubvms.cc.buffalo.edu

Masanobu Shinozuka
Profrssor
University of Southern California
Department of Civil Engineering
3620 South Vermont Avenue, KAP254
Los Angeles, CA 90089-2531
Tel. 213-740-9528
Fax. 213-740-9529

Andrew W. Taylor
Research Structural Engineer
National Institute of Standards and Technology
Structures Division
Bldg. 226, Room B158
Gaithersburg, MD 20899
Tel. 301-975-6078
Fax. 301-869-6275
E-mail ataylor@nist.gov

Andrew S. Whittaker
Associate Director
Earthquake Engineering Research Center
University of California, Berkeley
1301 South 46th Street
Richmond, CA 94804-4698
Tel. 510-231-9554
Fax. 510-231-9471

Yan Xiao
Assistant Professeor
University of Southern California
Dept. of Civil Engineering
Kaprielian Hall, 224B
Los Angeles, CA 90089-2531
Tel. 213-740-6130
Fax. 213-744-1426
E-mail yanxiao@rcf.usc.edu

Lalliana Mualchin
California Dept. of Transportation
Division of Structures, MS-9
(Carrently Visiting Kyoto Univ.)
P.O. Box 942874
Sacramento, CA 94274-0001
Tel. 916-227-8735
Fax. 916-227-8898
E-mail tslmual@ts1.dot.ca.gov

Participants from The Japan Side

Masato Abe
Assistant Professor
Department of Civil Engineering
University of Tokyo
Hongo 7-3-1, Bunkyo-ku,
Tokyo, 113
Tel. 03-5802-3312
Fax. 03-5689-7292
E-mail masato@kyouryou.t.u-tokyo.ac.jp

Yukio Adachi
Senior Research Engineer
Earthquake Engineering Division,
Earthquake Disaster Prevention Research Center
Public Works Research Institute,
Ministry of Construction
1, Asahi, Tsukuba-shi,
Ibaraki, 305
Tel. 0298-64-4966
Fax. 0298-64-4424
E-mail y-adachi@pwri.go.jp

Yoshihiko Akao
Chief Engineer
Isolation Design Section,
MB Development Department
Yokohama Rubber Co., Ltd.
Tel. 0463-35-9703
Fax. 0463-35-9765

Haruki Akiyama
Manager
First Design Division,
Design Department
Honshu Shikoku Bridge Authority
5-1-5, Toranomon, Minato-ku,
Tokyo, 105
Tel. 03-3434-7281
Fax. 03-3578-9298

Noriaki Egawa
Engineer
Second Kobe Construction Department
Hanshin Expressway Public Corp.
1-3-3, Higashikawasaki-cho, Chuo-ku, Kobe-shi,
Hyogo, 650
Tel. 078-360-8144
Fax. 078-360-8158

Yasuyuki Fujishiro
Director
Structure and Bridge Department
Public Works Research Institute,
Ministry of Construction
1, Asahi, Tsukuba-shi,
Ibaraki, 305
Tel. 0298-64-2835
Fax. 0298-64-0565
E-mail fujisiro@pwri.go.jp

Kengo Goda
Seismic Isolation Technology Development Department
Bridgestone Co., Ltd.
1, Kashio-cho, Tozuka-ku, Yokohama-shi,
Kanagawa, 244
Tel. 045-825-7589
Fax. 045-825-7676

Shingo Gose
Deputy Manager
Traffic Structure Division,
Road and Traffic Department
CTI Engineering Co., Ltd.
9th Chuo Bldg., 4-9-11, Honcho Nihonbashi, Chuo-ku,
Tokyo, 103
Tel. 03-3668-0451
Fax. 03-5695-1847

Yozo Goto
General Manager
Civil Engineering Department No.5
Obayashi Corp.,
Technical Research Institute
640, Shimokiyoto 4-chome, Kiyose-shi,
Tokyo, 204
Tel. 0424-95-0951
Fax. 0424-95-0903

Fumio Hakamada
Senior Engineer
Maintenance Department
Hanshin Expressway Public Corp.
4-1-3, Kyutaro-machi, Chuo-ku,
Osaka, 541
Tel. 06-252-8121
Fax. 06-252-4583

Masahiro Hayashi
Third Design Division,
Design Department
Honshu-Shikoku Bridge Authority
45 Mori Bldg., 5-1-5, Toranomon, Minato-ku,
Tokyo, 105
Tel. 03-3434-7281
Fax. 03-3578-9298

Hidenao Hayashi
Manager
Kobe Maintenance Department
Hanshin Expressway Public Corp.
16-1, Shinko-cho, Chuo-ku, Kobe-shi,
Hyogo, 650

Mituhiro Hayashida
Engineer
Maintenance and Facility Section
Hanshin Expressway Public Corp.
2-3 D2-105 Shin-senri-Nisimachi, Toyonaka-shi,
Osaka, 565

Jaime Y. Hemandez Jr.
Master of Engineering Student
Graduate School of Science and Engineering
Saitama University
Rm. 3209, 645 Shimo-Okubo, Urawa-shi,
Saitama, 338
Tel. 048-859-4218

Yasuhisa Hishijima
Director
General Manager of Technical Department
Kawaguchi Metal Industries Co,. Ltd.
3-6-107, Sakurada Washinomiya-machi,
Kitakatsushika-gun,
Saitama, 340-02
Tel. 048-259-1118
Fax. 048-259-1139

Yoshihiro Hishiki
Chief
Structural Engineering Section,
Civil Engineering Department 1
Kajima Corp.,
Kajima Technical Research Institute
19-1, Tobitakyu 2-chome, Chofu-shi,
Tokyo, 182
Tel. 0424-89-7076
Fax. 0424-89-7078

Riki Honda
Research Engineer
Ground Vibration Division,
Earthquake Disaster Prevention Research Center
Public Works Research Institute,
Ministry of Construction
Tel. 0298-64-2211
Fax. 0298-64-0598
E-mail rhonda@pwri.go.jp

Yoshihei Horie
Senior Engineer
Engineering Department
Hanshin Expressway Public Corp.
Tel. 06-252-8121
Fax. 06-252-4583

Jun-ichi Hoshikuma
Research Engineer
Earthquake Engineering Division,
Earthquake Disaster Prevention Research Center
Public Works Research Institute,
Ministry of Construction
Tel. 0298-64-4966
Fax. 0298-64-4424
E-mail hosikuma@pwri.go.jp

Manabu Hosotani
Research Student
Department of Civil Engineering
Tokyo Institute of Technology
2-12-1, O-okayama, Meguro-ku,
Tokyo, 152
Tel. 03-5734-2922
Fax. 03-3729-0728

Hirokazu Iemura
Professor
Life Line Engineering Lab,
Graduate School of Civil Engineering,
Kyoto University
Yoshida Honmachi, Sakyo-ku,
Kyoto, 606-01
Tel. 075-753-5087
Fax. 075-753-5926

Akira Igarashi
Associate Professor
Department of Civil Engineering Systems
Kyoto University
Yoshida Honmachi, Sakyo-ku,
Kyoto, 606-01
Tel. 075-753-5088
Fax. 075-753-5926
E-mail igarashi@catfish.kuciv.kyoto-u.ac.jp

Yoshinori Igase
Deputy Head
Bridge Section
Japan highway Public Corp.,
Research Institute
4-1, 1Chome, Tadao, Machida-Shi,
Tokyo, 194
Tel. 0427-91-1621
Fax. 0427-92-8650

Hiroshi Ishizaki
Manager
Second Kobe Construction Department
Hanshin Expressway Public Corp.
1-3-1, Higashi Kawasaki-cho, Chuo-ku, Kobe-shi,
Hyougo 650

Touta Katsukawa
Technical Research & Development Institute.
Kumagai Gumi Co., Ltd.
1043 Onigakubo, Tsukuba-shi,
Ibaraki, 300-22
Tel. 0298-47-7501
Fax. 0298-47-7480

Yoriko Kawakami
Engineer
First Kobe Construction Department
Hanshin Expressway Public Corp.
17-1 Aza-Higashimukai, Shimotanigaami,
Yamada-cho, Kita-ku, Kobe-shi,
Hyogo, 651-12
Tel. 078-582-0345
Fax. 078-582-0348

Shiro Kawakita
Chief Engineer
Specified Planning Office
Planning Division
Hanshin Expressway Public Corp.
4-1-3, Kyutaro-machi, Chuo-ku,
Osaka, 541
Tel. 06-252-8121
Fax. 06-252-4583

Kazuhiko Kawashima
Professor
Department of Civil Engineering
Tokyo Institute of Technology
2-12-1, O-okayama, Meguro-ku,
Tokyo, 152
Tel. 03-5734-2922
Fax. 03-3729-0728
E-mail kawasima@cv.titech.ac.jp

Masaharu Kawashima
Deputy Director-General
Road Department
Kyushu Regional Construction Bureau,
Ministry of Construction
2chome 10-7, Hakatacki higashi, Hakata-ku,
Fukuoka-shi,
Fukuoka, 812
Tel. 092-471-6331
Fax. 092-476-3494

Yoshitomi Kimura
Senior Research Engineer
Foundation Engineering Division,
Structure and Bridge Department
Public Works Research Institute,
Ministry of Construction
1, Asahi, Tsukuba-Shi
Ibaraki, 305
Tel. 0298-64-4916
Fax. 0298-64-0565

Kenji Kohsa
Senior Engineer
Kobe Reconstruction Division
Hanshin Expressway Public Corp.
Tel. 078-331-9801
Fax. 078-331-9733
E-mail GCH06310@niftyserve.or.jp

Hisashi Kon-no
Head
Structures Section,
Structures Division
Civil Engineering Research Institute,
Hokkaido Development Agency
1-3, Hiragishi, Toyohira, Sapporo,
Hokkaido, 062
Tel. 011-841-1111
Fax. 011-824-1226

Shin-ichiro Kumagai
Deputy General Manager
Construction & Engineering Division,
Civil Engineering Department,
Civil Engineering Operations
Sumitomo Construction Co., Ltd.
13-4, Araki-Cho, Shinjuku-ku,
Tokyo, 160
Tel. 03-3225-5132
Fax. 03-3353-6656

Hiroshi Mikami
Senior Research Engineer
Technical Research Institute
Mitsui Construction Co., Ltd.
518-1, Komaki, Nagareyama-shi,
Chiba, 270-01
Tel. 0471-40-5202
Fax. 0471-40-5216

Yoshihiro Morioka
Development Section
Engineering Development Department,
Civil Engineering Design Division
Kajima Corp.
Tel. 03-5561-2111
Fax. 03-5561-2152

Kazuhiko Murai
Visiting Researcher
Earthquake Engineering Division,
Earthquake Disaster Prevention Research Center
Public Works Research Institute,
Ministry of Construction
1, Asahi, Tsukuba-shi,
Ibaraki, 305
Tel. 0298-64-4966
Fax. 0298-64-4424
E-mail murai@pwri.go.jp

Jun Murakoshi
Senior Research Engineer
Bridge Division,
Structure and Bridge Department
Public Works Research Institute,
Ministry of Construction
1, Asahi, Tsukuba-shi,
Ibaraki, 305
Tel. 0298-64-4919
Fax. 0298-64-0565
E-mail murakosi@pwri.go.jp

Hiroshi Mutsuyoshi
Professor and Head of Foreign Student Office in Graduate
Program Department of Civil and Environmental Engineering
Saitama University
225 Shimo-okubo Urawa-shi,
Saitama, 338
Tel. 048-858-3553
Fax. 048-855-9361

Toshihiko Naganuma
Chief
First Research and Development Section,
Research and Development Division
Hanshin Expressway Management Technology Center
Toa Bldg., 4-5-7, Minami-Honmachi, Chuo-ku,
Osaka, 541
Tel. 06-244-6043
Fax. 06-244-9612

Kazuhiro Nagaya
Research Engineer
Earthquake Engineering Division,
Earthquake Disaster Prevention Research Center
Public Works Research Institute,
Ministry of Construction
1, Asahi, Tsukuba-shi,
Ibaraki, 305
Tel. 0298-64-4966
Fax. 0298-64-4424
E-mail nagaya@pwri.go.jp

Hiroyuki Nagumo
Engineer
Civil Engineering Design Division,
2nd Design Department
Kajima Corp.
5-30, Akasaka 6-chome, Minato-ku,
Tokyo, 107
Tel. 03-5561-2111
Fax. 03-5561-2156

Yuji Nakai
Sumitomo Construction Co., Ltd.
13-4, Araki-Cho, Shinjuku-ku,
Tokyo, 160
Tel. 03-3225-5132
Fax. 03-3353-6656

Sachio Nakamura
Chief Research Engineer
Computational Analysis Lab.,
R&D Department
Yokohama Rubber Co., Ltd.
2-1 Oiwake, Hiratsuka-shi,
Kanagawa, 254
Tel. 0463-35-9588
Fax. 0463-35-9758

Atsushi Nanjo
Senior Engineer
Engineering Department,
Design Division
Hanshin Expressway Public Corp.
4-3-1, Kyutaro-machi, Chuo-ku,
Osaka, 541
Tel. 06-252-8121
Fax. 06-252-4583

Hajime Ohuchi
Chief Research Engineer
Structural Engineer Department
Obayashi Corp.,
Technical Research Institute
640, Shimokiyoto 4-chome, Kiyose-shi,
Tokyo, 204
Tel. 0424-95-0995
Fax. 0424-95-0904

Hiroaki Okamoto
Senior Engineer
Civil Engineering Design Division,
2nd Design Department
Kajima Corp.
5-30, Akasaka 6-chome, Minato-ku,
Tokyo, 107
Tel. 03-5561-2111
Fax. 03-5561-2156

Koji Osada
Engineer
Tokyo 1st Operation Bureau
Japan Highway Public Corp.
1-1, Nanpeidai, Miyamae-ku, Kawasaki-shi,
Kanagawa, 216
Tel. 044-865-8247
Fax. 044-866-3521

Hisanori Otsuka
Professor
Department of Civil Engineering
Kyushu University
6-10-1, Hakozaki, Higashi-ku,
Fukuoka, 812
Tel. 092-642-3266
Fax. 092-642-3266
E-mail otsuka@civil.doc.kyushu-u.ac.jp

Kai Qi
Researcher
Division of Earthquake Disaster
Kyoto University,
Disaster Prevention research Institute
Gokasho, Uji,
Kyoto, 611
Tel. 0774-38-4070
Fax. 0774-38-4070

Haruyuki Sakoda
Senior Manager
Steel Structure Division,
Bridge Engineering Department
Kawasaki Heavy Industries, Ltd.
8, Niijima, Harima-cho, Kako-gun,
Hyogo, 675-01
Tel. 0794-35-8413
Fax. 0794-35-0249

Tadanobu Sato
Professor
Section of Dynamics of foundation Structures,
Division of Earthquake Disaster Prevention
Kyoto University,
Disaster Prevention research Institute
Gokasho, Uji,
Kyoto, 611
Tel. 0774-38-4065
Fax. 0774-38-4070
E-mail sato@catfish.dpri.kyoto-u.ac.jp

Chiaki Sudo
Section Manager Seismic Isolation,
Technology Development Department
Bridgestone Co., Ltd.
1, Kashio-cho, Tozuka-ku, Yokohama-shi,
Kanagawa, 244
Tel. 045-825-7589
Fax. 045-825-7676

Shigenobu Suzuki
Seismic Isolation Technology Development Department
Bridgestone Co., Ltd.
1, Kashio-cho, Totsuka-ku, Yokohama-shi,
Kanagawa, 244
Tel. 045-825-7589
Fax. 045-825-7676

Yoshinori Tachibana
Manager
Infrastructure Engineering Department
Oriental Consultants Co., Ltd.
3-5-7, Hisamoto, Takatsu-ku, Kawasaki-shi,
Kanagawa, 213
Tel. 044-812-8815
Fax. 044-812-8825

Mitsunori Takahashi
Visiting Researcher
Earthquake Engineering Division,
Earthquake Disaster Prevention Research Center
Public Works Research Institute,
Ministry of Construction
1, Asahi, Tsukuba-shi,
Ibaraki, 305
Tel. 0298-64-4966
Fax. 0298-64-4424
E-mail m-takahs@pwri.go.jp

Isao Takatori
General Manager
Planing Division
Public Works Research Center
Takara Bldg., 1-6-4, Taito, Taito-ku,
Tokyo, 110
Tel. 03-3835-3609
Fax. 03-3832-7397

Keiichi Tamura
Head
Ground Vibration Division,
Earthquake Disaster Prevention Research Center
Public Works Research Institute,
Ministry of Construction
1, Asahi, Tsukuba-shi,
Ibaraki, 305
Tel. 0298-64-2926
Fax. 0298-64-0598
E-mail tamura@pwri.go.jp

Yoji Tamura
Bridge Section
Japan highway Public Corp..
Research Institute
4-1, 1-Chome, Tadao. Machida-Shi.
Tokyo, 194
Tel. 0427-91-1621
Fax. 0427-92-8650

William Tanzo
Associate Professor
Civil and Environmental Engineering Department.
Faculty of Engineering
Saitama University
225 Shimo-okubo Urawa-shi.
Saitama, 338
Tel. 048-858-3556
Fax. 048-858-3556

Kenji Tasaki
Visiting Researcher
Earthquake Engineering Division.
Earthquake Disaster Prevention Research Center
Public Works Research Institute.
Ministry of Construction
1, Asahi, Tsukuba-shi.
Ibaraki, 305
Tel. 0298-64-4966
Fax. 0298-64-4424
E-mail k-tasaki@pwri.go.jp

Toru Terayama
Senior Research Engineer
Earthquake Engineering Division,
Earthquake Disaster Prevention Research Center
Public Works Research Institute,
Ministry of Construction
1, Asahi, Tsukuba-shi.
Ibaraki, 305
Tel. 0298-64-4966
Fax. 0298-64-4424
E-mail terayama@pwri.go.jp

Hiroshi Tsunoda
Engineer
Design and Research Division.
Engineering Department
Metropolitan Expressway Public Corp.
1-4-1, Kasumigaseki, Chiyoda-ku,
Tokyo, 100
Tel. 03-3502-7311
Fax. 03-3502-2411

Meguru Tsunomoto
Senior Research Engineer
Technical Division
Oriental Construction Co., Ltd.
1-2, 2-Chome Hirakawa-cho, Chiyoda-ku,
Tokyo, 102
Tel. 03-3261-1176
Fax. 03-3261-1139
E-mail LDX04457@niftyserve.or.jp

Shigeki Unjoh
Head
Earthquake Engineering Division,
Earthquake Disaster Prevention Research Center
Public Works Research Institute,
Ministry of Construction
1, Asahi, Tsukuba-shi,
Ibaraki, 305
Tel. 0298-64-2932
Fax. 0298-64-4424
E-mail unjoh@pwri.go.jp

Sadafumi Uno
Chief Manager
Technical Development Room
Kawaguchi Metal Industries Co., Ltd.
2-25-1, Kizawa, Toda-shi,
Saitama, 335
Tel. 048-259-1118
Fax. 048-259-1139

Masaaki Yabe
Graduate Student
Department of Civil Engineering
Tokyo Institute of Technology
2-12-1, O-okayama, Meguro-ku,
Tokyo, 152
Tel. 03-5734-2922
Fax. 03-3729-0728

Furitsu Yasuda
Chief Engineer
Engineering Division, Design Section
Hanshin Expressway Public Corp.
1-3, 4-chome, Kyutaro-machi, Chuo-ku,
Osaka, 541
Tel. 06-252-8121
Fax. 06-252-4583

Koichi Yokoyama
Director
Earthquake Disaster Prevention Research Center
Public Works Research Institute,
Ministry of Construction
1, Asahi, Tsukuba-shi,
Ibaraki, 305
Tel. 0298-64-2829
Fax. 0298-64-0598
E-mail yokoyama@pwri.go.jp

Tamio Yoshioka
Director
Research Laboratory
Oriental Construction Co., Ltd.
5, Kinugaoka, Moka-shi,
Tochigi, 321-43
Tel. 0285-83-7921
Fax. 0285-83-0021
E-mail KYL06022@niftyserve.or.jp